# Sustainable cultivated land use and management

**Edited by**
Yongsheng Wang, David Lopez-Carr, Jianzhou Gong vand Jinlong Gao

**Published in**
Frontiers in Environmental Science

## About Frontiers

Frontiers is more than just an open access publisher of scholarly articles: it is a pioneering approach to the world of academia, radically improving the way scholarly research is managed. The grand vision of Frontiers is a world where all people have an equal opportunity to seek, share and generate knowledge. Frontiers provides immediate and permanent online open access to all its publications, but this alone is not enough to realize our grand goals.

## Frontiers journal series

The Frontiers journal series is a multi-tier and interdisciplinary set of open-access, online journals, promising a paradigm shift from the current review, selection and dissemination processes in academic publishing. All Frontiers journals are driven by researchers for researchers; therefore, they constitute a service to the scholarly community. At the same time, the *Frontiers journal series* operates on a revolutionary invention, the tiered publishing system, initially addressing specific communities of scholars, and gradually climbing up to broader public understanding, thus serving the interests of the lay society, too.

## Dedication to quality

Each Frontiers article is a landmark of the highest quality, thanks to genuinely collaborative interactions between authors and review editors, who include some of the world's best academicians. Research must be certified by peers before entering a stream of knowledge that may eventually reach the public - and shape society; therefore, Frontiers only applies the most rigorous and unbiased reviews. Frontiers revolutionizes research publishing by freely delivering the most outstanding research, evaluated with no bias from both the academic and social point of view. By applying the most advanced information technologies, Frontiers is catapulting scholarly publishing into a new generation.

## What are Frontiers Research Topics?

Frontiers Research Topics are very popular trademarks of the *Frontiers journals series*: they are collections of at least ten articles, all centered on a particular subject. With their unique mix of varied contributions from Original Research to Review Articles, Frontiers Research Topics unify the most influential researchers, the latest key findings and historical advances in a hot research area.

Find out more on how to host your own Frontiers Research Topic or contribute to one as an author by contacting the Frontiers editorial office: frontiersin.org/about/contact

# Sustainable cultivated land use and management

# Table of contents

frontiers | Frontiers in Environmental Science

# Editorial: Sustainable cultivated land use and management

Yongsheng Wang[1]*, David Lopez-Carr[2], Jianzhou Gong[3] and Jinlong Gao[4]

[1]Key Laboratory of Regional Sustainable Development Modeling, Institute of Geographic Sciences and Natural Resources Research, Chinese Academy of Sciences, Beijing, China, [2]University of California, Santa Barbara Santa Barbara, Santa Barbara, CA, United States, [3]Guangzhou University, Guangzhou, China, [4]Nanjing Institute of Geography and Limnology, Chinese Academy of Sciences, Nanjing, China

Editorial on the Research Topic
Sustainable cultivated land use and management

## Introduction

Cultivated land is an important resource for human survival and development, making its protection one of the highest global priorities. Healthy, ecological, and highly efficient cultivated lands form the basis of modern agriculture and thus the foundation of food security. In recent decades, rapid urbanization and industrialization have promoted economic development and improved livelihoods worldwide, leading to diversified food and commodity production and consumption. Notwithstanding, land degradation problems including abandonment, pollution, and erosion have emerged during the land-use transition, posing challenges to both the ecosystem service supply and Sustainable Development Goals (SDGs). In particular, intensive cultivated land use and the overwhelming dependence on fertilizers and pesticides have led to agricultural non-point source pollution and greenhouse gas emissions, which further challenge the ecological environment and sustainable development.

Within this Research Topic, we aimed to present a collection of original articles that address the theories, practices, and models for sustainable cultivated land use and management. This Research Topic collected a total of 17 papers, which can be largely divided into the following three areas.

(1) Land use and ecosystem service—a total of six papers, including land-use transitions and their influence on spatiotemporal patterns of the ecosystem service and their contribution to the Sustainable Development Goals.
(2) Cultivated land use—a total of five papers, including spatiotemporal changes and driving forces, vulnerability, and planting pattern change.

(3) Cultivated land management—a total of six papers, including fragmentation identification, productivity, optimization, and fertilization management.

## Land use and ecosystem services

Jian et al. identified the dominant morphology of land-use change and explored the recessive morphology and driving mechanisms in Baiyun District, Guangzhou city, China. The results improved the methods for reconstructing the three-dimensional space of land and provided paths for solving the problems of limited land resources and mixed land-use space in China's urban suburbs. Wei et al. calculated the evolutionary process of production–living–ecological space and analyzed the ecoenvironmental effects on typical industrial bases using the integrated ecoenvironmental quality index with a land-use transfer matrix and ecological contribution rate. Ma et al. studied the multidimensional gradient spatial differentiation characteristics of rural ecological land and clarified the impact of natural and human factors on ecological land under different gradients.

Xiang et al. predicted the land-use pattern and evaluated the ecosystem services in the Western Sichuan Plateau, China. This study suggested adjustments of the land-use structure and the management decisions regarding ecological environment protection. Wen et al. revealed the supply and demand patterns of ecosystem services, and they found that population attractiveness, industrial structure, and the NDVI are the main contributors to the coordination of the supply of and demand for ecosystem services. Hu et al. assessed the spatial–temporal changes of ecosystem service values and the SDGs scores in the Beijing–Tianjin–Hebei region (BTH). This study suggested that SDG6, SDG11, and SDG12 should be prioritized to advance the synergistic development of the SDGs in the BTH.

## Cultivated land use

Li et al. revealed that significantly increased cultivated land area was to be found in underdeveloped areas in China. Complex interaction between social, economic, agricultural, and natural factors caused the change in cultivated land area in China between 1996 and 2019. Ou and Wang investigated the varied spatiotemporal expansion of greenhouse-led cultivated land in Shandong province, China, from 1989 to 2018. Internal budget expenditures for rural development, local retail sales, the average earnings of local farmers, and external vegetable supply and consumption were the driving forces of greenhouse-led cultivated land expansion. Niu et al. assessed the cultivated land system vulnerability in Sanmenxia city, China. They concluded that vulnerability was affected by the sensitivity and adaptive capacity of human social and economic

activities and the capacity of the farmland system to cope with stress. Feng and Wang detected the spatial mismatch of water resources and grain planting pattern changes in China. The depletion of grain production potential in the water-limited regions was suggested to balance the agricultural development between the north and south regions. Lastly, Du et al. analyzed the evolution of cropping patterns based on remote sensing identification and provided a practical basis for establishing high-yield and efficient planting models in the "black soil" region of China.

## Cultivated land management

Su et al. improved a land fragmentation measurement model based on natural surface elements and road networks. The new model provides a more reliable and robust measurement of land fragmentation than the existing indices. Xu et al. created a new approach for the identification of irregular fragmented cultivated land with unclear characteristics in sandy areas. The results suggest that scale transformation can be used to improve the accurate and efficient identification of fragmented cultivated land. Lin et al. designed a new method to predict the spatial layout of citrus production in Sichuan province of China in 2025. They provided the polices of stabilized citrus areas and optimized production space for the local government. Liu et al. revealed the positive effect of agricultural machinery services on cultivated land productivity based on a case study in north China. The authors show that increasing smallholders' access to various types of agricultural machinery services can improve the productivity of cultivated land in regions dominated by smallholders. Zhang et al. constructed an optimal land allocation method based on soil moisture characteristics and provided valuable sustainable land optimization solutions for the efficient, sustainable use and protection of land resources in semiarid regions. Wang et al. explored the effects of different fertilizer combinations on the soil organic carbon pool and *L. barbarum* yield under drip fertigation in Ningxia, northwestern China. The results suggest that drip fertigation with $60 \text{ mg L}^{-1}$ nitrogen plus $30 \text{ mg L}^{-1}$ phosphorus is the optimal practice for carbon sequestration and the sustainable production of *L. barbarum* in arid regions.

The 17 papers in this Research Topic use field experiments, regional investigations, and model simulation and prediction, and they provide interesting and meaningful results and thought-provoking discussions on land use and ecosystem services, cultivated land use, and cultivated land management. We express our thanks to all the authors and reviewers who contributed to this Research Topic. Together, these articles provide a valuable insight into the discussion of sustainable cultivated land use and management and create an exciting impetus for future research. More attention should be dedicated to meet the ever-growing needs of people for a

better life by cultivated land quantity and quality and ecological protection. An ecological environmental impact assessment of cultivated land use is conducive to the coupling of the sustainable use of cultivated land and the sustainable development of human society.

## Author contributions

More attentions should be addressed to meet the people's ever-growing needs for a better life by cultivated land quantity, quality and ecological protection. Ecological environmental impact assessment of cultivated land use is conducive to the coupling of cultivated land sustainable use and human society sustainable development.

## Conflict of interest

The authors declare that the research was conducted in the absence of any commercial or financial relationships that could be construed as a potential conflict of interest.

## Publisher's note

All claims expressed in this article are solely those of the authors and do not necessarily represent those of their affiliated organizations, or those of the publisher, the editors and the reviewers. Any product that may be evaluated in this article, or claim that may be made by its manufacturer, is not guaranteed or endorsed by the publisher.

# Application of Spatiotemporal Pattern Mining Methods for Land Use Transition Research: A Case Study of Baiyun District in Guangzhou

Yuqing Jian[1], Yuangong Chen[2], Jianzhou Gong[1]*, Chen Wenli[3] and Kanglin Chen[1]

[1]Guangzhou University, Guangzhou, China, [2]Hong Kong Polytechnic University, Kowloon, Hong Kong SAR, China, [3]Guangdong Party Institute of Chinese Communist Party, Guangzhou, China

The use of spatio-temporal statistical combination method to explore the land use transition in urban suburbs provides an essential resource for promoting urban-rural integration and management of further urbanization. A combination of Space Time Cube and Geodetector methods was used to quantitatively identify the dominant morphology of land use change, and explore the recessive morphology and driving mechanism in Baiyun District, a suburb of Guangzhou from 1980 to 2020. Between these years, the land use changes were dominated by the expansion of built-up land and the shrinkage of cropland. The expansion took place in southern (1990-2000) to central (2000-2005) areas of the jurisdiction, followed by large-scale decentralization (2005-2010). Land use activities showed a downward trend. A continuous cold spot was mainly distributed in the southeast and remote areas near the urban center, whereas a continuous hot spot was spatially characterized by a multinuclear pattern, mainly concentrated in the center and south. Socioeconomic factors significantly affected the spatial pattern of land use activities. The trend turning in land use morphology of land use change can be divided into four stages: land primitivation from 1980 to 1990, land fragmentation from 1990 to 2000, land overflow from 2000 to 2010, and land intensification from 2010 to the present. Baiyun District is at the forefront of China's development and has typical "suburban" characteristics, which can provide a reference for other suburbs in China to develop in stages. Today, urban suburbs in China face the problems of limited land resources and mixed land use space. Taking advantage of the new national strategic environment could effectively solve these land use issues in urban suburbs and achieve sustainable development. New trends in land use morphology research, also considering land use effects and land use change mechanisms in an integrated manner, are conducive to further deepening the understanding of land use transitions. Moreover, spatiotemporal statistical methods have innovated the field of mining the spatiotemporal characteristics of land use. Based on a scientific method for spatiotemporal analysis, we were able to reconstruct the three-dimensional space of land and improve the methods applied for research into land use change.

**Keywords: land use transition, trend turning, space time cube, geodetector, urban suburb**

# 1 INTRODUCTION

Transformation refers to the process of fundamental changes in the structural form of things, their mode of operation and people's perceptions (Asquith et al., 2018). In 1995, geographer Grainer, inspired by the Forest Transformation Hypothesis, extended the Nation-al Land Use Morphology theory to the National Land Use Transition process theory, which focuses on forestry. This theory states that most countries that have forestry as a significant component of their economy show varying degrees of change in land use morphology over time. This is caused by a range of underlying socio-economic factors that are ultimately controlled through policy measures and lead to a new equilibrium in land use morphology (Grainger, 1995a; Grainger, 1995b). As human-driven changes to the Earth's surface generate dramatic land use change, global environmental change and socio-economic sustainability require integrated management (Turner et al., 2007). Several scholars have developed land use transition theories on the basis of Grainer's process theory, focusing on the current land use change and major issues of land use management. For example, Long Hualou proposed the "land use morphology transition" based on the theory that land use morphology includes the dominant morphology of land use type structure and the recessive morphology, which is dependent on the dominant morphology and has multiple attributes such as quality and property rights. The land use morphology transition refers to the transition of regional land use morphology caused by each land use type transfer within a specific period of time (Long and Qu, 2018). DeFries pointed out that the transition of land use functions has gradually changed from purely natural ecology to intensive human use (DeFries et al., 2004). Lambin stated that the mechanism behind land use transition are mainly endogenous socio-ecological forces and exogenous socio-economic factors (Lambin and Meyfroid, 2010). During the period, international research on land use transition came to the following consensus: 1) the loss of cropland and the expansion of built-up land are the most typical forms of land use transition; 2) land use transition is non-linear and evolves in accordance with the socio-economic development stage of a country or region (DeFries et al., 2004; Foley et al., 2005; Lambin and Meyfroid, 2010; Long and Qu, 2018). Correspondingly, the concept of land use transition has been deepened and defined as the trend turning of land use morphology in a certain region in long-term changes under socio-economic development. This includes the trend turning of specific land use types such as cropland, forest, built-up land, rural land, and also in the overall land use morphology of the region (Song, 2017). "Trend turning" is often used in climatology, for example, when long time series are analyzed, two temporally close periods may show significantly different trends (Zuo et al., 2019). Land use transition focuses on trend turning in land use morphology, defined as the development of land use change to a certain stage, resulting in a land use morphology with a set of typical stage characteristics corresponding to a certain stage of socio-economic development (Li, 2021).

Trend turning of land use transition could improve the explanation of the various stage characteristics of the transition of dominant morphology and the analysis of the land use problems indicated by the transition of recessive morphology. This information can then be used to identify suitable response strategies for the regulation of the transition (Yang et al., 2018; Li, 2021). Internationally, scholars have focused on the trend turning of land use morphology from different perspectives, such as long time series of area change (Hailu et al., 2020); spatiotemporal pattern of a certain land type (Li et al., 2020); spatial expression of landscape features accompanying land use changes (Asabere et al., 2020), the "ecological-social-economic" benefits of land use change (Chen et al., 2021), and the factors of land phase change (Qu et al., 2020), have been studied in stages. Existing studies generally focus on the geographic patterns, processes, change rules and mechanisms, and have researched land use morphological (dominant and recessive) transition, land use functional transition, land use transition mechanisms. However, these approaches should be strengthened with tools and further methodological improvements to visualize the research findings.

In recent years, the rise of Spatiotemporal statistics has brought new ideas and methods to geographical research. Spatiotemporal statistics procedures use computers to visualize complex and abstract spatiotemporal data interactively. By reconstructing and analyzing the change process of spatial position and attribute of the geographical phenomenon over time, we can identify the specific relationships and detect anomalies. Furthermore, the mathematical model of spatiotemporal processes can be established to identify the driving factors behind geographical phenomena. Spatial correlation analysis tools such as Kriging, Moran's I, LISA, GWR, Bayes have been widely used for these purposes (Spöck and Pilz, 2015). Therefore, with reference to spatiotemporal statistical research, this study proposed the combined application of the Space Time Cube and Geodetector methods for identifying land use morphology changes. Space Time Cube measures trends in the values of each spatial location across time, identifying emerging hot and cold spots and outliers (Esri, 2021). Geodetector is then used to detect the spatial heterogeneity of different geographical phenomena and their driving forces (Wang et al., 2010). The combined application has the potential to quickly and intuitively obtain the spatiotemporal characteristics of the dominant land use morphology and analyze the recessive land use morphology changes under the potential mechanism.

As a result of urbanization in recent decades, rural production elements in China have become concentrated towards cities, leading to considerable transformation of urban and rural boundaries (Liu and Li, 2017). In this process, the traditional rural core periphery has gradually evolved into a transitional space of urban elements based on a dualistic structure such as the urban suburbs (also known as urban fringe, edge cities and urban-rural transition zone, etc.) (Gu, 2020). Similar to the natural ecotone (Hansen et al., 1988), the suburban territorial space also has the unique heterogeneous characteristics of adjacent areas, forming a unique land use transition problem. For example, the dominant morphology of land use, such as the rapid non-agriculturalization of cropland and the disorderly expansion of built-up land (Ma et al., 2020);
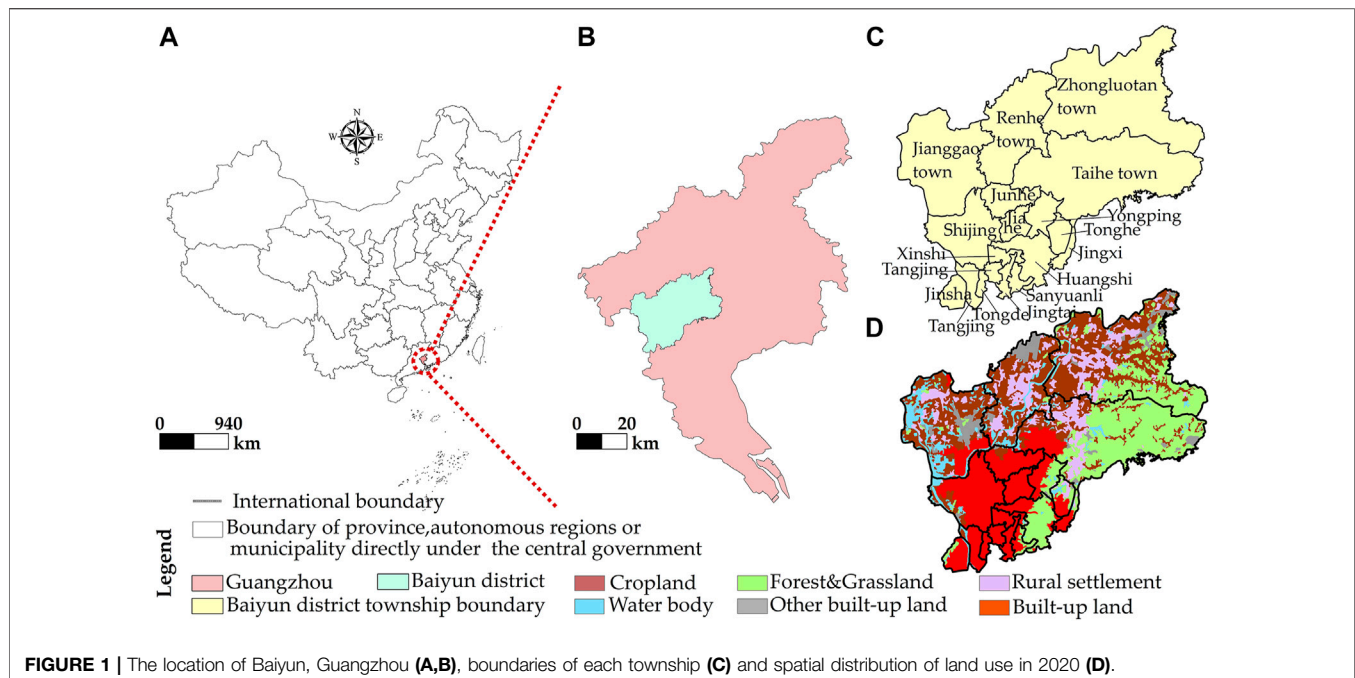
**FIGURE 1 |** The location of Baiyun, Guangzhou **(A,B)**, boundaries of each township **(C)** and spatial distribution of land use in 2020 **(D)**.

There are particular problems associated with land use recessive morphology, such as "village in city," and the related issues of mixed ownership and the pollution of "production-living-ecology" space(Yao and Tian, 2020); The development problems associated with land use stage, such as resource and environmental constraints (Cao et al., 2021; Elahi et al., 2022a), the conception lag behind of natives (Elahi et al., 2022b), backward industrial technology and uncontrollable extreme weather (Elahi et al., 2021; Nath et al., 2022). The dominant morphology dominated by the land structure and the recessive morphology have gradually become projected in the suburban space (Yanbo et al., 2021). Suburbs in China have quietly undergone an irreversible and difficult land use transition. However, there has been relatively little research on the growth and characteristics of these suburban areas. For example, research is usually based on a comparative analysis of the dominant morphologies of each period in terms of both "quantity" and "spatial structure," and research on the trend transition of land use morphology in suburban comprehensive period is currently lacking. These omissions are not conducive to revealing the transitional and phased spatial characteristics of suburban land use change and the transitional and periodic characteristics of associated land use change. Moreover, it is not easy to excavate the hybridity of its characteristics in the vertical direction. This study takes Baiyun District, Guangzhou, a suburb in a developing metropolis in China, as the study area. A three-module quantitative study of land use transition paths (**Section 3.1**), spatiotemporal evolution morphology (**Section 3.2**) and master control factors (**Section 3.3**) was conducted through the integrated application of the Space Time Cube and Geodetector methods. Based on these results, the trending transitional development of land use morphology in the study area was analyzed in local development history (**Section 3.4**). The study's contributions are specifically addressed: 1) enrich the theories related to land use transition in suburbs, 2) couple spatio-temporal statistics and land system science through spatiotemporal pattern mining methods, 3)provide a scientific basis for strategic decisions to promote urban-rural integration.

# 2 MATERIALS AND METHODS

## 2.1 Study Area
Baiyun District is located in the central and western part of Guangzhou City (**Figure 1**). It is in the transition zone between the low mountains of central Guangdong and the plains of the Pearl River Delta, high topography in the north and northeast and low in the west and south. It belongs to the southern subtropical monsoon climate zone, with high precipitation and temperatures occurring in the same period and an average annual temperature of 21.8 °C and annual rainfall of 1,694 mm. It contains the Baiyun Mountain Scenic Area and the Maofeng Mountain Forest Park, and is thus considered a region of Guangzhou with a good natural environment (Baiyun District Information Database in Guangzhou, 2021).

In the 1980s, the study area was officially renamed "Baiyun District" from its original name of "Suburban District" and was included in the urban area of Guangzhou. In 2010, Baiyun District had 14 streets and four towns under its jurisdiction, making it the largest administrative district in Guangzhou's central urban area with the largest external population (Guangzhou Statistic Bureau, 2021). The complexity and diversity of diverse administrative jurisdictions and the frequent mixing of resource flows have resulted in Baiyun

District having considerable urban suburban characteristics, and its land use activities are typical of urban areas.

## 2.2 Data Sources

This study used eight periods of land use raster data for 1980, 1990, 1995, 2000, 2005, 2010, 2015 and 2020 with a spatial resolution of 30 m (http://www.resdc.cn/) provided by the Resource and Environment Science Data Center of the Chinese Academy of Sciences. With reference to the Classification of Land Use Status (GB/T21010-2007) and taking into account the actual situation of the study area, the land use types in the study area were subdivided into six categories: cropland, forest and grassland, water body, built-up land, rural settlement, and other built-up land.

The geographical detector data were obtained from NASA SRTM3 elevation at a spatial resolution of 90 m. The annual average precipitation and temperature data were spatially interpolated datasets with a spatial resolution of 1 km in 2000 and 2015 from the Data Center for Resource and Environmental Sciences of the Chinese Academy of Sciences (http://www.resdc. cn/data.aspx?DATAID=264). The road network data were obtained from Open Street Map for 2000 and 2020 vector data obtained from Open Street Map (https://www.openstreetmap. org/). Socioeconomic data were taken from the information database of Baiyun District, Guangzhou and the website of Baiyun District People's Government, Guangzhou. In addition, the 2010 administrative boundaries were used as the standard to maintain the integrity of statistical data and the consistency of administrative divisions.

## 2.3 Space Time Pattern Mining Methods

This paper visualizes the land-transfer paths at different stages with the help of the Sankey energy shunt map. The Space Time Cube and the spatiotemporal hotspot analysis method were combined to visualize the spatial trends and temporal characteristics of cold and hot spots of land activities. The geographical detector method was used to detect the attribution of land change within each township. Finally, the historical evolutionary process behind different land use development stages was considered with local development history.

### 2.3.1 Land Transfer Path Analysis

The land use transfer matrix approach obtains a two-dimensional matrix through the generation of a land use transfer path, and explains this path concerning the structural characteristics of land use change and the direction of transfer between types (Li C et al., 2021). In particular, the different land use types are identified by codes in a fixed order (1, 2 and 3). For example, the change path of cropland to "forest and grassland" and "forest and grassland" can be expressed as 1-2-2. Finally, a Sankey diagram was created to visualize different land transfer paths from 1980 to 2020.

### 2.3.2 Trend Analysis of Cold and Hot Spots Based on Space Time Cube

The Space Time cube is a three-dimensional cube proposed by Hagerstrand (1968). A two-dimensional plane is used to express

the spatial location and region, and another dimensional time axis expresses the temporal change in the location of the two-dimensional plane (**Figure 2**) (https://desktop.arcgis.com/). The analysis process includes the identification of land use cold spots and hot spots in two dimensions, the creation of a Space Time Cube, and a statistical test for cold and hot spots, as follows:

1) Land Use Hotspot Identification. The accuracy of the land use data, the size of the study area and the visualization of the data were all taken into account in this study. After a preliminary test to identify the most suitable scale (data not presented), a 600 m * 600 m grid was selected as the study unit. The area of land use change at different times within each unit was first obtained, and then the Getis-Ord Gi* tool was used to calculate and compare the local sum of adjacent elements within each grid with the sum of all elements, thus allowing the analysis of the local spatial aggregation of area change at different times.
2) Space Time Cube. The Space Time Cube was constructed as a NetCDF data structure by calculating point counts and aggregating specified attributes using stereograms (bars). All bar location count trends and aggregated field values were then further evaluated to identify the evolution of a geographical phenome-non or scalar with a location attribute over a time series.
3) Statistical analysis. The Mann–Kendall statistical method was used to analyze the spatiotemporal change trend of land activity. The change trend of cold and hot spots was evaluated for each land activity location with data and presented on the map (**Figure 3**) (https://desktop.arcgis. com/). The analysis results of spatiotemporal cold and hot spots included 17 patterns, such as new hot spots and continuous hot spots, and the basis for the classification is shown with reference to the official website.

All trend analysis operations were completed in ArcGis 10.7.

### 2.3.3 Factor Detector

The Geodetector method (http://www.geodetector.org/) is based on statistical principles for spatial variance analysis. It represents a set of statistical methods to detect spatial variance and its mechanisms. This method is mainly applied to detect the spatial variance and to what extent factor explains the spatial variance of attribute.

$$q = 1 - \frac{1}{N\sigma^2}\sum_{h=1}^{L} N_h \sigma_h^2$$

Where $q$ is the spatial variance of a factor indicator, which is used to detect the factor's influence on land use activities. N is the sample size of the whole region. $\sigma^2$ is the variance of land change in the whole region. $h$ is the identification partition, $h = 1, 2, ..., L$, where L denotes the number of partitions. $0 \leq q \leq 1$, the larger the value of q, the stronger the factor's influence on land activities. Conversely, the smaller the value of $q$, the weaker the influence. A $q$ of 0 indicates no spatial variance in the study area and the spatial distribution of land use is random.

**FIGURE 2 |** Space Time cube.



**FIGURE 3 |** The process of spatiotemporal cold and hot spot analysis.
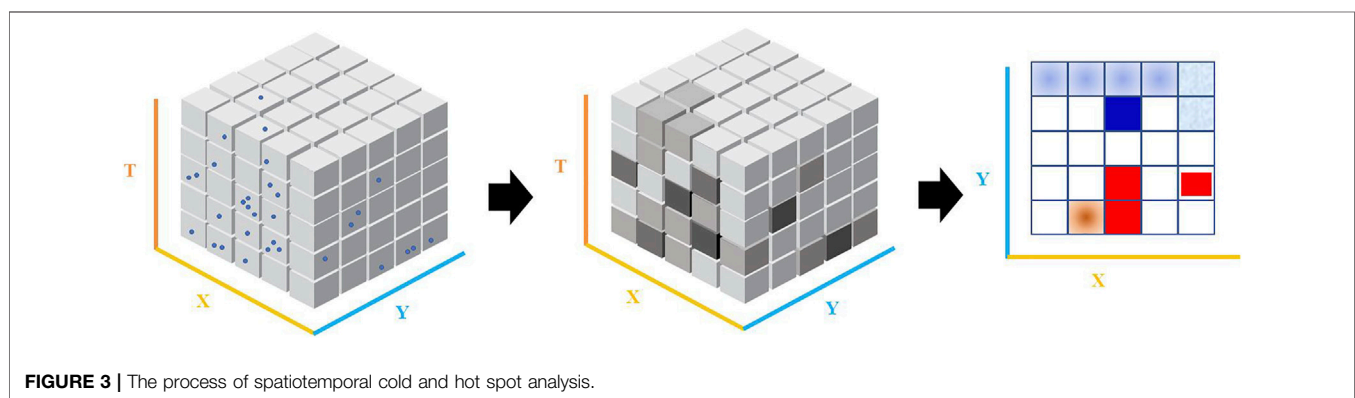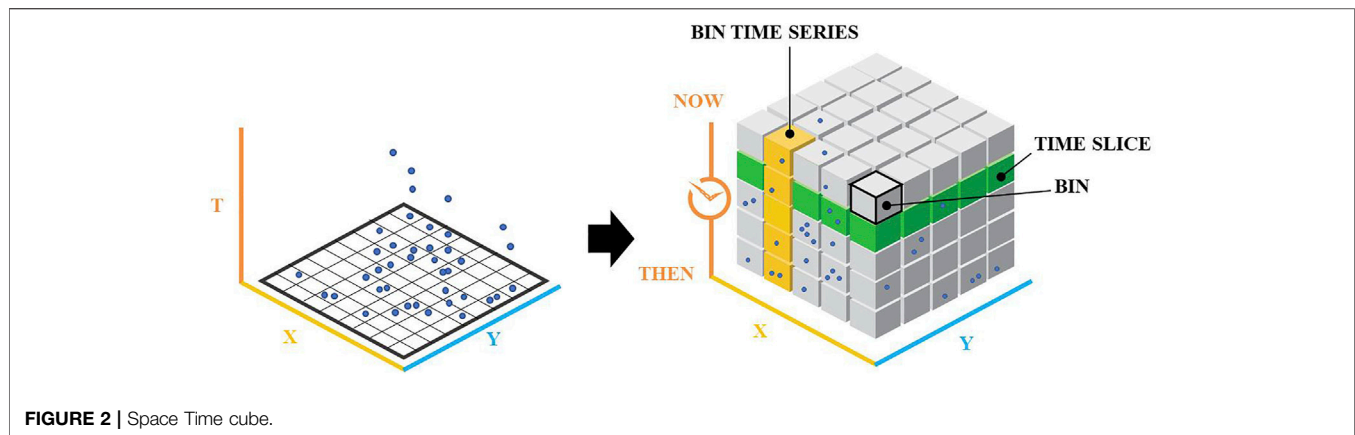
**TABLE 1 |** Land-use changes in Baiyun District.

| Land use type | 1980 | | 1990 | | 2000 | | 2010 | | 2020 | |
|---|---|---|---|---|---|---|---|---|---|---|
| | km$^2$ | % | km$^2$ | % | km$^2$ | % | km$^2$ | % | km$^2$ | % |
| Cropland | 340.1 | 51 | 326.9 | 49 | 272.6 | 41 | 200.0 | 30 | 187.9 | 28 |
| Forest&Grassland | 185.1 | 28 | 185.3 | 28 | 183.0 | 28 | 174.8 | 26 | 173.7 | 26 |
| Water body | 34.5 | 5 | 39.8 | 6 | 50.2 | 8 | 54.5 | 8 | 54.7 | 8 |
| Built-up land | 26.1 | 4 | 29.3 | 4 | 74.4 | 11 | 163.3 | 25 | 164.3 | 25 |
| Rural area | 71.5 | 11 | 75.2 | 11 | 74.1 | 11 | 46.0 | 7 | 46.1 | 7 |
| Other built-up land | 5.3 | 1 | 5.9 | 1 | 8.1 | 1 | 23.7 | 4 | 35.7 | 6 |

In this paper, 18 townships were used as detection areas. Based on the existing studies and data accessibility, the accumulated area of land change in each township between 2000 and 2020 as a proportion of its administrative area was $Y$. The socioeconomic factors (change in GDP $X1$, change in the agricultural output value $X2$, change in the gross industrial output value $X3$, and change in the road network density $X4$) and natural environment (DEM $X5$, slope $X6$, average annual temperature change $X7$, and average annual precipitation change $X8$), for a total of eight factors. Since the statistical objects of socioeconomic data changed considerably from 1980 to 2000, this study also took the local development history into account to provide a context for the identified land activity mechanisms.

## 3 RESULTS

### 3.1 Land Use Change and Transfer Path

As shown in **Table 1**, from 1980 to 2020, the land use changes in Baiyun District of Guangzhou were dominated by urbanization. The built-up land area increased from 26.1 km$^2$ (1980) to 164.3 km$^2$ (2020), an expansion of 138.2 km$^2$. The growth rate was as high as 529.6%. From 1990 to 2000, the new built-up land was mainly distributed in the southern part of Baiyun District (the southern part of Shijing, Jiahe, the western part of Yongping, the eastern part of Songzhou, the southern part of Tonghe, the western part of Huangshi and the central part of Jingxi). From 2000 to 2005, it was mainly distributed in the central part of

**FIGURE 4 |** Spatial distribution of new land in each township at different times **(A–G)**.



**FIGURE 5 |** Land-transfer paths within different time periods, 1980-2020.
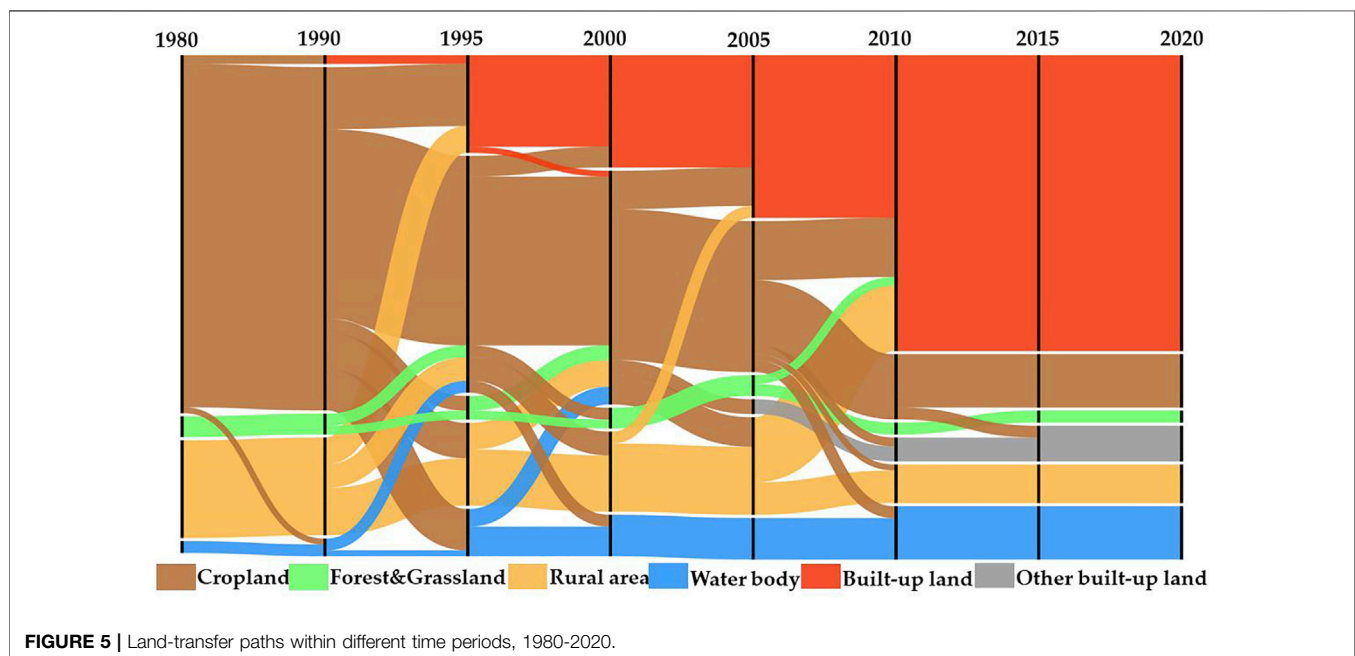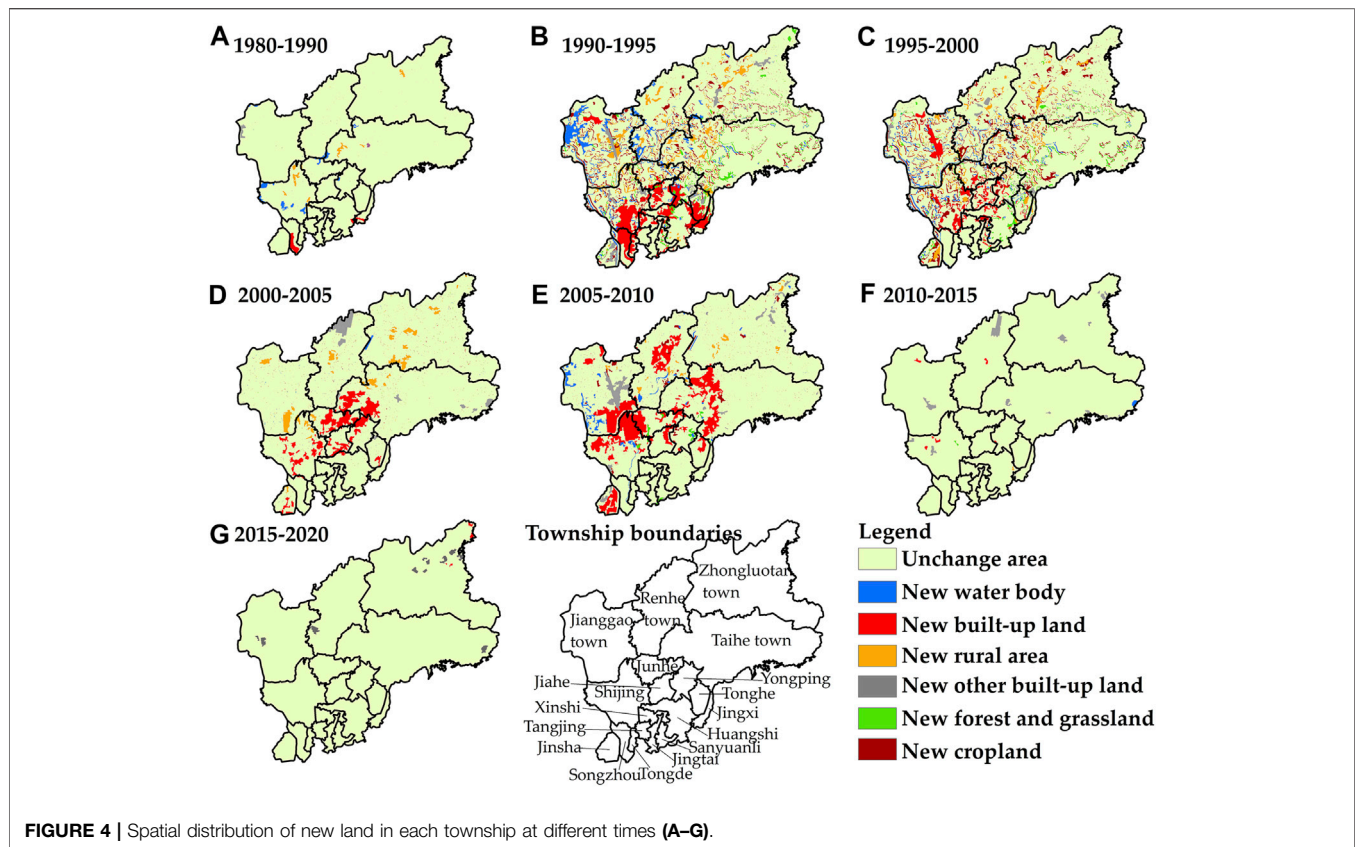
Baiyun District (the western parts of Taihe, Junhe and Yong-ping). From 2005–2010, it showed a large-scale scattered expansion in the study area (Taihe, Jinsha, bordering Shijing, Junhe and Jianggao, and the central part of Renhe) (**Figure 4**).

**Table 1** shows that the cropland area decreased from 340.1 km$^2$ (1980) to 193.3 km$^2$ (2020), a reduction of 146.8 km$^2$ (43.2%). During this process, the percentage change in the area of forest and grassland, water body, rural settlement and other built-up

**TABLE 2 |** Quantities of different land-transfer paths in 1980–2020.

| Land-transfer paths | Area(km$^2$) | Land-transfer paths | Area(km$^2$) |
|---|---|---|---|
| C-Unchange | 159.2 | C(80-90)-F&G(95)-C(00-20) | 5.1 |
| F&G-Unchange | 154.4 | F&G(80-90)-C(95)-F&G(00-20) | 4.6 |
| R-Unchange | 21.4 | R(80-00)-B(05-20) | 4.5 |
| B-Unchange | 20.6 | C(80-10)-O(15-20) | 4.5 |
| W-Unchange | 20.4 | R(80-90)-C(95)-R(00-20) | 4.5 |
| O-Unchange | 1.4 | W(80-90)-C(95)-W(00-20) | 4.5 |
| C(80-90)-B(95-20) | 20.2 | C(80-00)-R(05-20) | 4.1 |
| C(80-05)-B(10-20) | 19.1 | C(80-05)-W(10-20) | 3.9 |
| C(80-05)-B(10-20) | 12.9 | R(80-90)-C(95)-R(00-05)-B(10-20) | 3.7 |
| C(80-00)-B(05-20) | 12.0 | C(80-90)-R(95-20) | 3.2 |
| C(80-90)-B(95-20) | 9.4 | C(80)-B(90-20) | 3.2 |
| C(80-90)-W(95-20) | 8.2 | C(80-00)-O(10-20) | 3.0 |
| C(80-95)-B(00-20) | 7.1 | F&G(80-05)-B(10-20) | 2.9 |
| C(80-90)-R(95)-C(00-20) | 7.0 | C(80-90)-B(95)-C(00)-B(05-20) | 2.4 |
| C(80-90)-W(95)-C(00-20) | 6.3 | C(80)-W(90-20) | 2.4 |
| C(80-00)-R(05)-C(10-20) | 5.9 | C(80-90)-R(95)-C(00-05)-B(10-20) | 2.4 |
| C(80-00)-O(05-20) | 5.2 | C(80-05)-R(10-20) | 2.4 |

Note: C represents cropland, F&G represents forest and grassland, R represents rural area, W represents water body, B represents built-up land and O represents other built-up land. C (80–90)–B (95–20), indicates a land transfer path in which land use is converted from cropland in 1980–1990 to built-up land in 1995–2020. The other pathways are expressed similarly.

land relative to built-up and cropland was only a maximum of 4%, and the overall land activity was stable. This indicates that the new built-up land was mainly transferred from cropland.

There were 936 land transfer paths from 1980 to 2020, so this paper only considers the land transfer paths with the amount of 2 km$^2$ (**Figure 5**). In terms of transfer amount, land use change in Baiyun District was dominated by the invariance of each land type. The largest areas were 159.2 km$^2$ of cropland and 154.4 km$^2$ of forest and grassland (**Table 2**). The Sankey diagram shows that the period of 1990–2010 was the most diverse and active in land transfer paths, mainly in the form of transfers out of cropland into built-up land. Among these, the land transfer paths involving land between cropland and built-up land were cropland (1980–1990) to built-up land (1995–2020), cropland (1980–2005) to built-up land (2010–2020), cropland (1980–2000) to built-up land (2005–2020) and cropland (1980) to built-up land (1990–2020), with a transfer amount of 61.4 km$^2$. The amount of land transfer of rural settlement was also significant and was mainly converted to built-up land and cropland. The total amount of rural settlements transferred to built-up land in different periods was 26.9 km$^2$. The transfer of built-up land to cropland was the most notable, with all of it being transferred from cropland first and then back to cropland.

In general, during 1980–2020, the main trend in land use change in Baiyun District was a large-scale decrease in cropland, which was mainly transformed into built-up land. Built-up land expanded massively by transforming large amounts of cropland and rural settlements. Although this land use change was dramatic, land transfer paths were dominated by the invariance of each land use type.

## 3.2 Spatiotemporal Cold and Hot Spots Distribution of Land Activity
The temporal distribution trend analysis of land activities in the cell grid was analyzed, and the Z-score was −2.44 with a $p$-value of

0.01. The land activity showed a decreasing trend throughout the study period. As shown in **Figure 6**, land activity in Baiyun District was dominated by continuous cold spots from 1980 to 2020, covering an area of up to 190.6 km$^2$, accounting for 29% of the entire study area. It was mainly concentrated in the southeast near the urban center (Sanyuanli, Huangshi, Xinshi, Tangjing and Jingtai), and widely distributed in remote areas (Zhongluotan and the forest-dominated eastern part of Taihe). The second most prominent pattern was the Oscillating Cold Spot pattern, adjacent to or interconnected with the Consecutive Cold Spot and New Cold Spot areas. A multinuclear pattern spatially characterizes the Consecutive Hot Spot pattern. The most prominent areas showing this pattern were those bordering Jianggao, Shijing and Junhe, followed by the central part of Jinsha, the north-central part of Renhe and the local area of Taihe township (**Figure 6**).

The number and location of hot and cold hotspots of land activity in Baiyun District from 1980–2020 varied over time. The non-statistically significant cold or hot spots pattern was dominant in each period, but there were still obvious stable hot spots (**Figure 7**). During 1980–2010, a multinuclear pattern of land activity hotspots was very prominent and was mainly concentrated in the central and southern parts of the study area. Since 2010, however, the pattern of hotspots has rapidly weakened. It is noteworthy that the cold spot pattern, relative to land activity by period, only appeared for 1990–1995 and 1995–2000. Its main distribution is consistent with the spatiotemporal trends described above.

## 3.3 Mechanisms Driving Spatial Heterogeneity of Land Activities
Based on a combination of expert experience and the Natural Breaks (Jenks) method, the classification method uniformly discretizes numerical quantities into type quantities. Natural environmental and socioeconomic factors were classified into
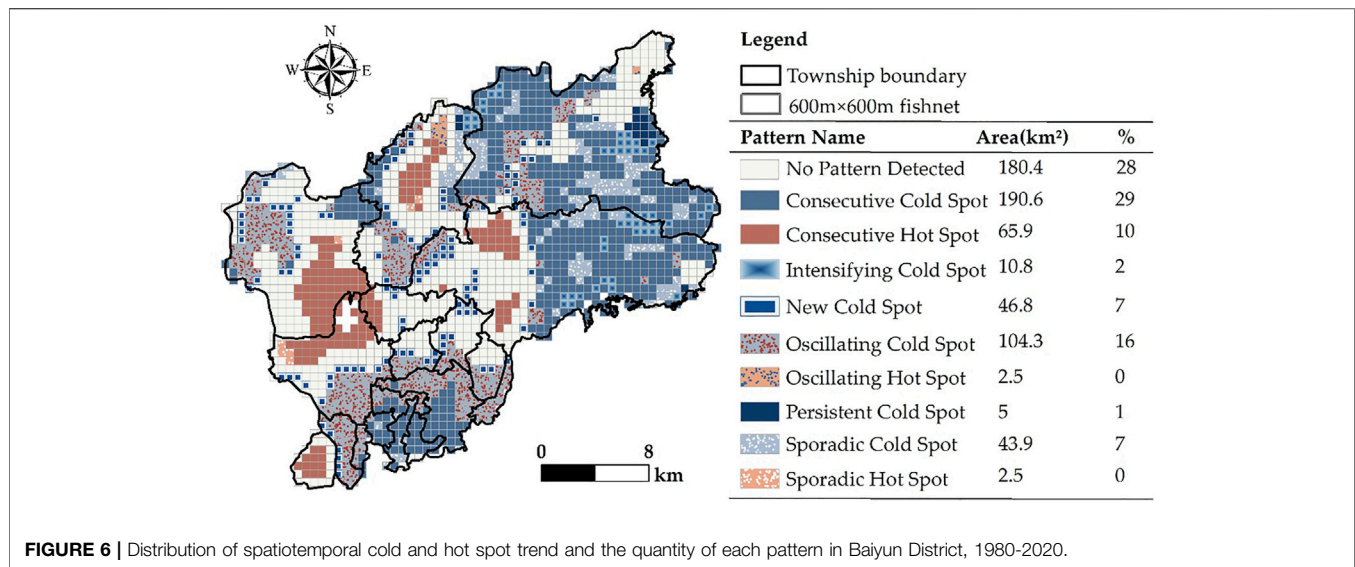
**FIGURE 6 |** Distribution of spatiotemporal cold and hot spot trend and the quantity of each pattern in Baiyun District, 1980-2020.
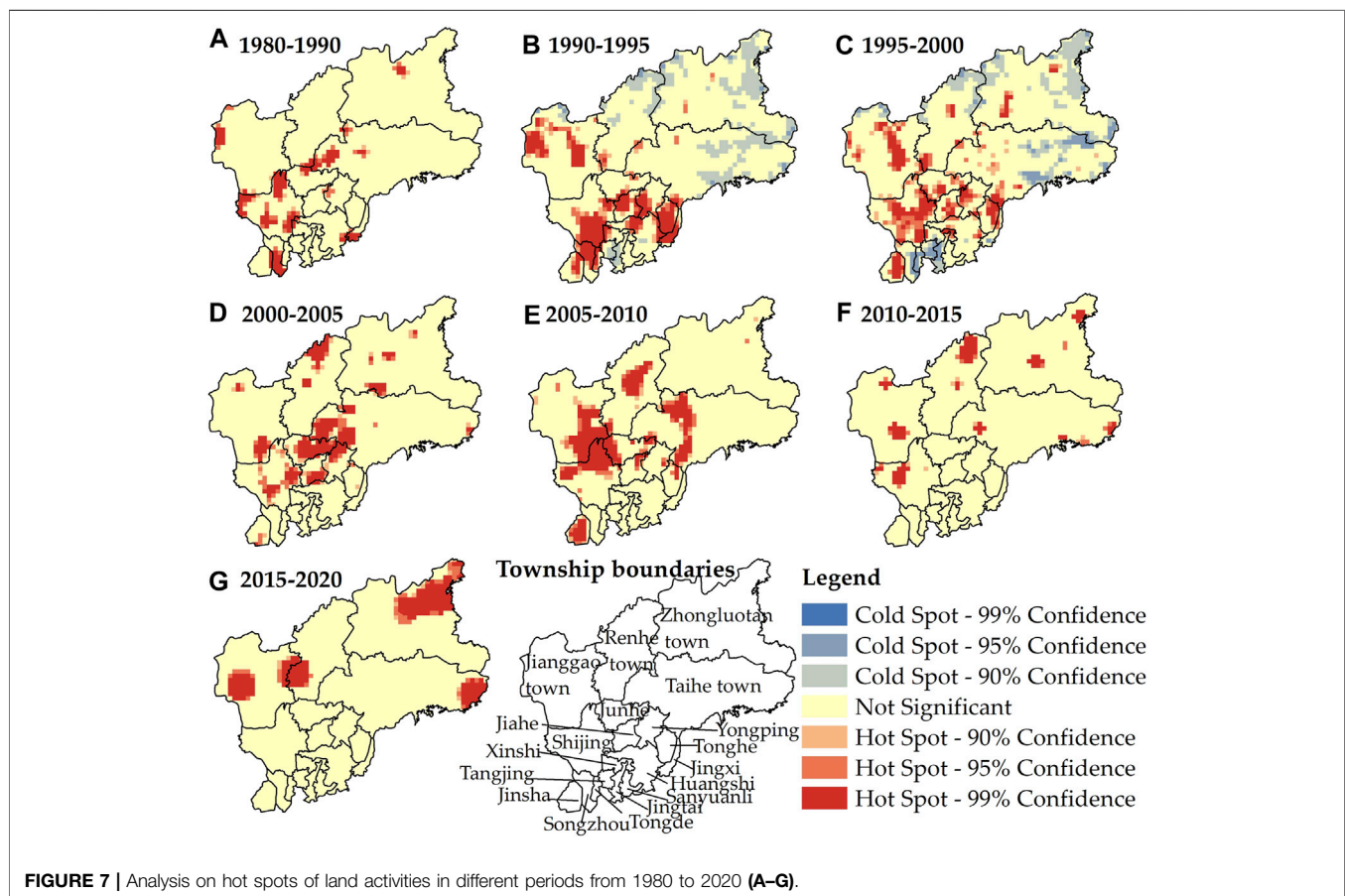


**FIGURE 7 |** Analysis on hot spots of land activities in different periods from 1980 to 2020 **(A–G)**.

2 and 5 categories, respectively, using the Natural Breaks (Jenks) method (**Table 3**). The results show that over the past 20 years, socioeconomic factors significantly impacted the spatial pattern of land activities in Baiyun District, whereas the influence of natural environmental factors was relatively insignificant. In

descending order of intensity, the main influencing factors (all having passed the significance test) were as follows: $X_1$ (0.47) for change in GDP, $X_3$ (0.44) for change in the gross industrial output value, $X_7$ (0.35) for change in the average annual temperature, $X_5$ (0.27) for DEM, $X_6$ (0.27) for slope, $X_2$ (0.26) for change in the

**TABLE 3** | The influencing factors and detection results of land-use change in Baiyun District, 2000-2020.

| Factors | Class 1 | Class 2 | Class 3 | Class 4 | Class 5 | q statistic |
|---------|---------|---------|---------|---------|---------|-------------|
| $X_1$(million) | <2868 | 2868–7005 | 7005–11,189 | 11,189–14,910 | >14,910 | 0.47** |
| $X_2$(million) | <−488 | −488–1744 | 1744–4994 | 4994–13,256 | >13,256 | 0.44** |
| $X_3$(million) | <−235 | −235~−37 | −37~14 | 14–204 | >204 | 0.26** |
| $X_4$(km/km$^2$) | <4.35 | 4.35–7.44 | 7.44–10.21 | 10.21–12.06 | >12.06 | 0.21** |
| $X_5$(m) | <13.12 | 13.12–105.7 | | | | 0.27** |
| $X_6$(°) | <6.17 | 6.17–11.59 | | | | 0.27** |
| $X_7$(mm) | <177.9 | 177.9–259.6 | | | | 0.35** |
| $X_8$(°C) | <-0.27 | −0.27–0 | | | | 0.07** |

*Note: **indicates significant at the 5% level.*

**TABLE 4** | Interactive detection results of regional differentiation of land-use change in Baiyun District, 2000-2020.

| q | $X_1$ | $X_2$ | $X_3$ | $X_4$ | $X_5$ | $X_6$ | $X_7$ | $X_8$ |
|---|-------|-------|-------|-------|-------|-------|-------|-------|
| $X_1$ | 0.47 | | | | | | | |
| $X_2$ | 0.59 | 0.44 | | | | | | |
| $X_3$ | 0.62 | 0.55 | 0.26 | | | | | |
| $X_4$ | 0.74 | 0.77 | 0.39 | 0.21 | | | | |
| $X_5$ | 0.55 | 0.55 | 0.31 | 0.56 | 0.27 | | | |
| $X_6$ | 0.55 | 0.55 | 0.31 | 0.56 | 0.27 | 0.27 | | |
| $X_7$ | 0.77 | 0.82 | 0.67 | 0.68 | 0.35 | 0.35 | 0.35 | |
| $X_8$ | 0.49 | 0.44 | 0.40 | 0.43 | 0.28 | 0.28 | 0.37 | 0.07 |

*Note: Interact result-Gray fill (factor detector); Light orange (Enhance,bi-); Light blue (Enhace,nonlinear).*

agricultural output value, $X_4$ (0.21) for change in the road network density and $X_8$ (0.07) for change in average annual precipitation.

The interactions of different factors on the impact of land activity positively reinforce a single factor's influence. The interaction detection results show that a two-factor enhancement dominated the interaction type. Compared with the single factor, the q-values of each factor increased to different degrees (**Table 4**). The changes in the average annual precipitation $X_7$ had the most substantial influence on the interaction of socio-economic factors. The next most prominent performance was the interaction of road network density change $X_4$ on GDP change $X_1$ and agricultural output value change $X_2$, which increased several times compared with its individual effects. The socioeconomic factors were bi-factorially enhanced in terms of the type of interaction. The exception was road network density change $X_4$, which was non-linearly enhanced with GDP change $X_1$ and agricultural output value change $X_2$. It is worth noting that the interaction type between the change of road network density $X_4$ and the natural environment factors was a nonlinear enhancement.

## 3.4 The Trend Turning of Land Use Morphology Process in Baiyun District Guangzhou From 1980 to 2020

The trend turning of land use morphology is the core of land use transition re-search, since regional land use morphology often changes in accordance with changes in the economic and social development stage. During the studied period, the land conversion caused conflicts in land use morphology, which were subsequently alleviated through corresponding policy measures. This process of land use conflict mitigation is known as land use transition. By combining the characteristics of the spatial heterogeneity mechanisms described in the previous section and local development history, we considered the changes in land use morphology, the conflicts, and alleviation methods in the development process of land use transition in Baiyun District. The land use transition process was divided into the following three stages and then applied to explore further the mechanism of the long-term land use transition (**Figure 8**).

### 3.4.1 Land Primitivation in 1980–1990
Baiyun District is located in the transition zone between the low mountains of central Guangdong Province and the Pearl River Delta Plain. The north and northeast of Baiyun District are characterized by large hills and mountains, preserving large areas of pristine ecological forest. In the west and south, there are flat, broad alluvial plains with fertile soil and various soil types and genera, providing favorable conditions for a number of plantations (rice, vegetables, drought-tolerant cereals, peanuts, forestry). Therefore, since the reform and opening up, industrialization and urbanization were delayed in Baiyun District compared with the main urban area of Guangzhou. Traditional agricultural activities still dominate the study area, forming a stable spatial pattern of natural spaces and large-scale agricultural production. In the early stage, under the premise of not changing land use, the farmer families contracted the land to the collective and enjoyed full management autonomy as the primary production unit. As a result, the rural economy grew rapidly and provided sufficient labor and land for subsequent industrialization (Baiyun District Information Database in Guangzhou, China, 2021).

### 3.4.2 Land Fragmentation in 1990–2000
Since 1990, with the second wave of global industrial transfer and the promotion of the second round of the contract management responsibility system, low-end industries have become the target of foreign investment, and a large amount of rural collective land has been expropriated or illegally occupied (Long, 2012; Gong et al., 2019). At the same time, industrial production has also created a large number of employment opportunities. Local farmers have entered the workforce, and migrants from the surrounding cities and counties around Guangzhou have moved in to work (Yang, 2019). This has led to a boom in the informal expansion of self-housing and external leasing in remote areas. The real estate

**FIGURE 8 |** Suburban development patterns in different period of Baiyun District. Note: "Three old reform" refers to the transformation mode unique to Guangdong Province: old town, old factory, and old village transformation. "HCRS" refers to the Household contract responsibility system, a form of agricultural production responsibility system in which farmers contract land and other means of production and production tasks from collective economic organizations (mainly villages and groups) on a household basis. "GBA" refers to Guangdong-Hong Kong-Macao Greater Bay Area.

planned economy (1990-1995) and the real estate market economy (1996-2000) directly contributed to the large-scale construction of commercial housing in the southern part of Baiyun District (Su et al., 2005). Therefore, the 1990-2000 presented in **Figure 4** also verifies the construction development in the north and south of Baiyun District. In addition, The "rural land capitalization" of Baiyun District has led to the rapid shrinkage of cropland area. However, the shortage of cropland in the urban area of Guangzhou and the timely open policy of purchasing and selling agricultural products caused Baiyun District to become the main grain supply source area for urban Guangzhou. At the same time, Baiyun District also became prominent in the northern transportation and export of agricultural products. As a result, the agricultural production space gradually shifted from the suburbs to the middle and outer suburban agricultural areas (Baiyun District Information Database in Guangzhou, China, 2021). The land space dominated by traditional agriculture in Baiyun District reduced rapidly, and the fragmentation of land development intensified. Spatially, there was a large area of built-up land in the south and fragmentation of land in the center and north.

### 3.4.3 Land Overflow in 2000–2010
Since the turn of the 21st century, the global economy has been developing in an integrated way, with industrial adjustment and

upgrading and international transfer occurring in parallel (Yang et al., 2020). Baiyun District, which used to rely on traditional agriculture and low-end industries, was facing unprecedented challenges. Under the government's leadership, there was a massive transfer of agricultural production space to urban residential and public built-up land in 2000–2010 relative to previous periods. The built-up land expanded from the south to the center of the district, and the urban villages formed in a low-cost way, outside of the modern urban management, and the land uses were highly mixed (Yang, 2019; Yao and Tian, 2020). Driven by the "Strong Industrial Zone," "Modern Logistics Development Plan" and "Optimized Northern Development" polices, a large number of professional markets, logistics parks or industrial agglomeration areas were built the central and western regions and the northern part of remote areas. Thus, as shown in **Figure 4**, the expansion of other construction land (industrial land) from 2000 to 2010 was particularly significant relative to other periods. This also validates the significant role of gross industrial output as the second influencing factor on land use change. This construction was reliant on the transfer of rural collective land, which had the advantage of cheaper prices than urban areas (Baiyun District Information Database in Guangzhou, China, 2021). As a result, a large number of laborers from the surrounding inland provinces of Guangdong

Province were absorbed. Since 2000, in response to the requirements of the tenth Five-Year Plan for developing the national economy, the north of Renhe Town in Baiyun District developed large-scale infrastructure land to construct the new Baiyun International Airport (Yang et al., 2020). In general, under the government's coordination, the land activities during this period showed a significant trend of spatially pushed development from the middle to the north.

### 3.4.4 Land Intensification in 2010 to Present

The rapid population growth and urban expansion in the first decade of the 21st century led to the shortage of new built-up land and reserve land for further development (Gong et al., 2018a). In 2009, Baiyun District government mapped idle land, low-utility land, old factories and hillsides to supplement cropland (Baiyun District Information Database in Guangzhou, China, 2021). Under the premise of maintaining the current land use, the southern part of Baiyun District carried out the reconstruction of urban villages, evacuation of villages to build houses or revitalization of the stock of built-up land (Li et al., 2019). Thanks to better transport facilities and lower land rents, the central and northern parts took over the urban capital from the south (Gong et al., 2018b). In central Baiyun District, the old factories and historical sites were rebuilt into a fine chemical industrial zone, innovation industrial zone or science and technology park in the process of the "Exit the secondary industry and enter the tertiary industry" policy, and develop an "industrial clustering" regional model (Lin et al., 2019). The northern part focused on implementation as a land reserve planning region. Since 2010, Baiyun District has seen a decrease in the overall land-use changes under the land-intensive approach of limiting incremental land and excavating stock land. However, under the guidance of local and national planning divisions, the land functions have diversified, leading to a spatial pattern of ecological tourism in the east, Baiyun New City in the south, a creative industry gathering area in the middle, an industrial logistics area in the west, and an airport economic zone in the north of the district (People's Government of Baiyun District, Guangzhou City, 2022a; People's Government of Baiyun District, Guangzhou City, 2022b).

## 3.5 Discussion

### 3.5.1 The Trend Turning of Land Use Morphology in Urban Suburb

Our research results confirm that the trend turning of land use morphology can integrate land use morphology, use function, land use effect and the mechanism of land use change, and systematically sort out land use transition. Meanwhile, this study innovatively combines the history, policy measures and socio-economic development of the study area for a time-phased refinement analysis, which further confirms that land use transition in urban suburbs is a spatiotemporal evolution process of a complex man-land relationship. It is also the most direct result of multiple forces such as physical geography and socioeconomic conditions on land use morphology (Gong et al., 2019; Yao and Tian, 2020; Cao et al., 2021). The unique natural environment has shaped the original farming style, and the continuous improvement of the agricultural business system after the founding of New China has

injected continuous momentum into agricultural production (Li H et al., 2021; Zhou et al., 2021). Since the reform and opening up, the original dual/dualistic structure has collapsed/subsequently disintegrated, and the urban suburbs have gradually developed on the periphery of the traditional rural core (Yang, 2019). The combination of foreign capital and local resource liberalization has contributed to the conversion of land use morphology from hybridization to large-scale development. The limited land resources are gradually formed into the regional space of specific function positioning types under the rational allocation planning (Gong et al., 2018a). However, urban suburbs continue to be faced with the problem of limited land resources. Even under the multiple constraints of the "Controlling growth and forcing storage" policy, the problems of mixed tenure, spatial fragmentation, poor living environment and industrial inefficiency continue to persist (Gong et al., 2019; Yang, 2019; Yao and Tian, 2020; Cao et al., 2021). The recent construction of the Guangdong-Hong Kong-Macao Bay Area and the national strategy of rural revitalization have brought new opportunities and challenges to the urban suburbs of the Pearl River Delta (Gong, et al., 2019). However, it remains unclear how the new circumstances could help to solve the problem of land use transition and stimulate the vitality of land use development in the urban suburbs. In addition, the reshaping of the position of urban suburbs in the urban-rural relationship and consideration of how the urban suburbs should act as a bridge between urban and rural area need to be topics of further research.

### 3.5.2 Reliability of Land Use Transition Method

With the accumulation of spatiotemporal data and the advent of the big data era, feature mining of spatiotemporal data with geology as the object of analysis with statistical methodology has brought a new opportunity for land use research. For example, it can solve the problems of massive data analysis and visualization on different spatial units and in different periods (Wang et al., 2014). Moreover, it can also meet the needs of attribute diversification, function differentiation and mechanism diversification, and realize long time series of evolutionary laws, interactive dynamics and prediction research. The spatiotemporal feature mining method selected in the current study is an effective coupling of spatiotemporal statistics and land system science. The method focuses on the breakthrough of land use research from traditional two-dimensional plane space to the realization of three-dimensional spatial visualization, which is a fundamental attempt to study the mono-temporal land use morphology to long-temporal land use transition (Esri, 2021; Wang et al., 2010). As in this study, the cold hotspot analysis of land activities breaks through the traditional two-dimensional land transfer, effectively visualizing the multidimensional land use morphology and revealing the dominant land use morphology. Based on this approach, we deeply explored the changes of recessive land use morphology, for example, to reveal the process of land substitution caused by the changes of socioeconomic development stages (such as industrial transfer, infrastructure projects) and the real problems derived from it. However, this study considered a combination of existing spatiotemporal data analysis methods, which continue to have

associated problems such as the scale disunity of the source data, the lack of data attributes and the required improvement to the detection factor system. In addition, the uneven distribution of data acquisition at large spatial scales leads to a lack of spatiotemporal slice information, and the type data generation is biased (Wang et al., 2014; Zhou et al., 2020). Therefore, it remains necessary to conduct considerable spatiotemporal data analysis practice alongside the further innovation and development of spatiotemporal statistical methods and theoretical systems.

## CONCLUSION

This study explores the land use transition path of a typical suburb using a spatio-temporal statistical combination approach. The combination of Space Time Cube and Geodetector methods revealed that land use in Baiyun District, a suburb of Guangzhou, has been dominated by the expansion of built-up land and the shrinking of cropland since 1980. Over the same period of land activity showed a continuous cold spot pattern, followed by an oscillating cold spot pattern. The overall land activity showed a downward trend. In the context of local history, we found that socioeconomic factors significantly affected the conversion of land use types in different development periods, leading to different conflict patterns. The land use transition in the urban suburb was transformed from morphology to quality, mainly through policy measures and continuous spatial transfer. Combined with the variability of spatiotemporal characteristics of land use, the study region was divided into four stages of land development: Land Primitivation from 1980 to 1990, Land

Fragmentation from 1990 to 2000, Land Overflow from 2000 to 2010 and Land Intensification from 2010 to the present. The study region is at the forefront of China's development, and its "urban suburb" identity is typical. So the results of this paper can provide a reference for the development of other urban suburbs in China. In addition, this study confirms that the introduced spatio-temporal statistical methods can be used to assist further research on land use transition. However, the factors influencing this paper still need to be further refined, especially those closely related to those areas with intensive land use activities.

## DATA AVAILABILITY STATEMENT

The raw data supporting the conclusion of this article will be made available by the authors, without undue reservation.

## AUTHOR CONTRIBUTIONS

YJ and JG: substantial contributions to conception and design, acquisition of data, analysis and interpretation of data; YC and CW: drafting the article and revising it critically for important intellectual content; CW: collecting the data.

## FUNDING

## REFERENCES

Asabere, S. B., Acheampong, R. A., Ashiagbor, G., Beckers, S. C., Keck, M., Erasmi, S., et al. (2020). Urbanization, Land Use Transformation and Spatio-Environmental Impacts: Analyses of Trends and Implications in Major Metropolitan Regions of Ghana. *Land Use Policy* 96, 104707. doi:10.1016/j.landusepol.2020.104707

Asquith, M., Backhaus, J., Geels, F., Golland, A., Hof, A., Kemp, R., et al. (2018). *Perspectives on Transitions to Sustainability*. Kongens, Denmark: European Environment Agency. ISSN 1725-9177. doi:10.2800/332443

Baiyun District Information Database in Guangzhou, China (2021). *Baiyun District People's Government*. Available at: http://www.by.gov.cn/ (Accessed March 30th, 2022).

Cao, W., Zhou, S., and Zhou, M. (2021). Operational Pattern of Urban-Rural Integration Regulated by Land Use in Metropolitan Fringe of China. *Land* 10 (5), 515. doi:10.3390/land10050515

Chen, Z., Zhang, Q., Li, F., and Shi, J. (2021). Comprehensive Evaluation of Land Use Benefit in the Yellow River Basin from 1995 to 2018. *Land* 10, 643. doi:10.3390/land10060643

DeFries, R. S., Foley, J. A., and Asner, G. P. (2004). Land-use Choices: Balancing Human Needs and Ecosystem Function. *Front. Ecol. Environ.* 2 (5), 249–257. doi:10.1890/1540-9295(2004)002[0249:lcbhna]2.0.co;2

Elahi, E., Khalid, Z., Tauni, M. Z., Zhang, H., and Lirong, X. (2021). Extreme Weather Events Risk to Crop-Production and the Adaptation of Innovative Management Strategies to Mitigate the Risk: A Retrospective Survey of Rural Punjab, Pakistan. *Technovation* [in press], 102255. doi:10.1016/j.technovation.2021.102255

Elahi, E., Khalid, Z., and Zhang, Z. (2022b). Understanding Farmers' Intention and Willingness to Install Renewable Energy Technology: A Solution to Reduce the Environmental Emissions of Agriculture. *Appl. Energ.* 309, 118459. doi:10.1016/j.apenergy.2021.118459

Elahi, E., Zhang, Z., Khalid, Z., and Xu, H. (2022a). Application of an Artificial Neural Network to Optimise Energy Inputs: An Energy- and Cost-Saving Strategy for Commercial Poultry Farms. *Energy* 244, 123169. doi:10.1016/j.energy.2022.123169

Esri.(2021). Arcgis 10.3 for Desktop Web Help: Create Space Time Cube. Available at: Http://Desktop.Arcgis.Com/En/Arcmap/10.3ltools/Space-Time-Pattern-Mining-Toolbox/Create-Space-Time-Cube.Htm (Accessed March 30, 2022).

Foley, J. A., DeFries, R., Asner, G. P., Barford, C., Bonan, G., Carpenter, S. R., et al. (2005). Global Consequences of Land Use. *Science* 309 (5734), 570–574. doi:10.1126/science.1111772

Gong, J., Hu, Z., Chen, W., Liu, Y., and Wang, J. (2018a). Urban Expansion Dynamics and Modes in Metropolitan Guangzhou, China. *Land Use Policy* 72, 100–109. doi:10.1016/j.landusepol.2017.12.025

Gong, J., Jian, Y., Chen, W., Liu, Y., and Hu, Y. (2019). Transitions in Rural Settlements and Implications for Rural Revitalization in Guangdong Province. *J. Rural Stud.* [in press]. doi:10.1016/j.jrurstud.2019.10.037

Gong, J., Jiang, C., Chen, W., Chen, X., and Liu, Y. (2018b). Spatiotemporal Dynamics in the Cultivated and Built-Up Land of Guangzhou: Insights from Zoning. *Habitat Int.* 82, 104–112. doi:10.1016/j.habitatint.2018.10.004

Grainger, A. (1995a). National Land Use Morphology: Patterns and Possibilities. *Geography* 80 (3), 235–245. Available at: https://www.jstor.org/stable/40572668.

Grainger, A. (1995b). The Forest Transition: An Alternative Approach. *Area* 27 (3), 242–251. Available at: https://www.jstor.org/stable/20003580.

Gu, C. L. (2020). "Urbanization," in *International Encyclopedia of Human Geography*. 2nd Edn. Elsevier, 141–153. ISBN: 9780081022955.

Guangzhou Statistic Bureau (2021). *Information Database in Guangzhou, China.* Available at: http://tjj.gz.gov.cn/?msclkid= 724e5938b02b11ec901d076de0a5227a (Accessed March 30th, 2021).

Hagerstrand, T. (1982). Diorama, Path and Project. *Tijd voor Econ. Soc. Geog* 73 (6), 323–339. doi:10.1111/j.1467-9663.1982.tb01647.x

Hailu, A., Mammo, S., and Kidane, M. (2020). Dynamics of Land Use, Land Cover Change Trend and its Drivers in Jimma Geneti District, Western Ethiopia. *Land Use Policy* 99, 105011. doi:10.1016/j.landusepol.2020.105011

Hansen, A. J., Castri, F. D., and Naiman, R. J. (1988). Ecotones: what and Why? in a New Look at Ecotones: Emerging International Projects on Landscape Boundaries. *Biol. Int.* 17, 9–16.

Lambin, E. F., and Meyfroidt, P. (2010). Land Use Transitions: Socio-Ecological Feedback versus Socio-Economic Change. *Land Use Policy* 27 (2), 108–118. doi:10.1016/j.landusepol.2009.09.003

Li, C. (2021). Analysis Path of Diagnosis and Regulation of Regional Land Use Transition. *Geographical Res.* 40 (5), 1464–1477. doi:10.11821/dlyj020200457

Li, C., Wu, Y., Gao, B., Zheng, K., Wu, Y., and Li, C. (2021). Multi-scenario Simulation of Ecosystem Service Value for Optimization of Land Use in the Sichuan-Yunnan Ecological Barrier, China. *Ecol. Indicators* 132, 108328. doi:10.1016/j.ecolind.2021.108328

Li, H., Wang, L., Gong, J., Zhu, A.-X., and Hu, Y. (2021). Land-Use Modes of the Dike-Pond System in the Pearl River Delta of China and Implications for Rural Revitalization. *Land* 10 (5), 455. doi:10.3390/land10050455

Li, X., Hui, E. C. M., Chen, T., Lang, W., and Guo, Y. (2019). From Habitat III to the New Urbanization Agenda in China: Seeing through the Practices of the "three Old Renewals" in Guangzhou. *Land Use Policy* 81, 513–522. doi:10.1016/j.landusepol.2018.11.021

Li, Y., Li, Y., Karácsonyi, D., Liu, Z., Wang, Y., and Wang, J. (2020). Spatio-temporal Pattern and Driving Forces of Construction Land Change in a Poverty-Stricken County of China and Implications for Poverty-Alleviation-Oriented Land Use Policies. *Land Use Policy* 91, 104267. doi:10.1016/j.landusepol.2019.104267

Lin, X., Huang, B., Wu, J., Ge, M., and Lin, J. (2019). Industrial Upgrading with Innovation Production Service System: Evidence from Guangzhou, China. *Proced. CIRP* 83, 351–357. doi:10.1016/j.procir.2019.04.083

Liu, Y., and Li, Y. (2017). Revitalize the World's Countryside. *Nature* 548, 275–277. doi:10.1038/548275a

Long, H. L. (2012). Land Use Transition and Rural Transformation Development. *Prog. Geogr.* 31 (2), 131–138. doi:10.11820/dlkxjz.2012.02.001

Long, H., and Qu, Y. (2018). Land Use Transitions and Land Management: A Mutual Feedback Perspective. *Land Use Policy* 74, 111–120. doi:10.1016/j.landusepol.2017.03.021

Ma, L., Long, H., Tu, S., Zhang, Y., and Zheng, Y. (2020). Farmland Transition in China and its Policy Implications. *Land Use Policy* 92, 104470. doi:10.1016/j.landusepol.2020.104470

Nath, S., Shams, J., vanLaerhoven, F., and Driessen, P. (2022). The Impact of Decision-Making on Conflict: Rethinking the Roles of Technocrats and Residents during Tidal River Management in Coastal Bangladesh. *Land Use Policy* 117, 106103. doi:10.1016/j.landusepol.2022.106103

People's Government of Baiyun District, Guangzhou City (2022a). Baiyun District Functional Area Land Use Master Plan (2013-2020). Available at: http://www. by.gov.cn/gzjg/sghhzrzyjbyqfj/cxgh/content/post_4686258.html (Accessed March 30th, 2022a).

People's Government of Baiyun District, Guangzhou City (2022b). General Land Use Plan of Baiyun District, Guangzhou City (2010-2020). Available at: http:// www.by.gov.cn/gzjg/sghhzrzyjbyqfj/cxgh/content/post_4671580. html(Accessed March 30th, 2022b).

Qu, S. J., Hu, S. G., Li, W. D., Wang, H., Zhang, C. R., and Li, Q. F. (2020). Interaction Between Urban Land Expansion and Land Use Policy: An Analysis Using the DPSIR Framework. *Land Use Pol.* 99, 104856. doi:10.1016/j.landusepol.2020.104856

Song, X. Q. (2017). Discussion on Land Use Transition Research Framework. *Acta Geographica Sinica* 72 (3), 471–487. doi:10.11821/dlxb201703009

Spöck, G., and Pilz, J. (2015). Incorporating Covariance Estimation Uncertainty in Spatial Sampling Design for Prediction with Trans-gaussian Random fields. *Front. Environ. Sci.* 3 (39), 1–22. doi:10.3389/fenvs.2015.00039

Su, J. Z., Wei, Q. Q., and Guo, H. L. (2005). The Mechanism and Adjustment of Urban Sprawl of Guangzhou. *Acta Geographica Sinica* 60 (4), 626–636. doi:10.11821/xb200504011

Turner, B. L., Lambin, E. F., and Reenberg, A. (2007). The Emergence of Land Change Science for Global Environmental Change and Sustainability. *Proc. Natl. Acad. Sci. U.S.A.* 104 (52), 20666–20671. doi:10.1073/pnas.0704119104

Wang, J. F., Ge, Y., Li, L. F., Meng, B., Wu, J. L., Bo, Y. C., et al. (2014). Spatiotemporal Data Analysis in Geography. *Acta Geographoca Sinica* 69 (9), 1326–1345. doi:10.11821/dlxb201409007

Wang, J. F., Li, X. H., Christakos, G., Liao, Y. L., Zhang, T., Gu, X., et al. (2010). Geographical Detectors-Based Health Risk Assessment and its Application in the Neural Tube Defects Study of the Heshun Region, China. *Int. J. Geographical Inf. Sci.* 24 (1), 107–127. doi:10.1080/13658810802443457

Yanbo, Q., Guanghui, J., Wenqiu, M., and Zitong, L. (2021). How Does the Rural Settlement Transition Contribute to Shaping Sustainable Rural Development? Evidence from Shandong, China. *J. Rural Stud.* 82, 279–293. doi:10.1016/j.jrurstud.2021.01.027

Yang, Q. K., Duan, X. J., Wang, L., and Jin, Z. (2018). Land Use Transformation Based on Ecological-Production-Living Spaces and Associated Eco-Environmental Effects: A Case Study in the Yangtze River delta. *Scientia Geographica Sinica* 38, 97–106. doi:10.13249/j.cnki.sgs.2018.01.011

Yang, R. (2019). Spatial Differentiation and Mechanisms of Typical Rural Areas in the Suburbs of a metropolis: A Case Study of Beicun Village, Baiyun District, Guangzhou. *Acta Geographica Sinica* 74 (8), 1622–1636. doi:10.11821/dlxb201908010

Yang, R., Zhang, J., Xu, Q., and Luo, X. (2020). Urban-rural Spatial Transformation Process and Influences from the Perspective of Land Use: A Case Study of the Pearl River Delta Region. *Habitat Int.* 104, 102234. doi:10.1016/j.habitatint.2020.102234

Yao, Z., and Tian, L. (2020). How Did Collectivity Retention Affect Land Use Transformation in Peri-Urban Areas of China? A Case of Panyu, Guangzhou. *J. Rural Stud.* 79, 1–10. doi:10.1016/j.jrurstud.2020.08.009

Zhou, C. H., Sun, J. L., Su, F. Z., Yang, X. M., Pei, T., Ge, Y., et al. (2020). Geographic Information Science Development and Technological Application. *Acta Geographoca Sinica* 75 (12), 2593–2609. doi:10.11821/dlxb202012004

Zhou, Y., Li, X., and Liu, Y. (2021). Cultivated Land protection and Rational Use in China. *Land Use Policy* 106, 105454. doi:10.1016/j.landusepol.2021.105454

Zuo, B., Li, J., Sun, C., and Zhou, X. (2019). A New Statistical Method for Detecting Trend Turning. *Theor. Appl. Climatol.* 138, 201–213. doi:10.1007/s00704-019-02817-9

# Spatiotemporal Evolution and Simulation Prediction of Ecosystem Service Function in the Western Sichuan Plateau Based on Land Use Changes

Mingshun Xiang[1,2†], Jin Yang[1,2*], Wenheng Li[1], Yueting Song[3], Chunjian Wang[1,2], Yan Liu[1,2], Mengli Liu[1] and Yuxiang Tan[1]

[1]College of Tourism and Urban-Rural Planning, Chengdu University of Technology, Chengdu, China, [2]Research Center for Human Geography of Tibetan Plateau and its Eastern Slope, Chengdu University of Technology, Chengdu, China, [3]School of Earth Sciences, China University of Geosciences, Wuhan, China

Being closely related to ecosystem services, land use changes can affect ecosystem service functions by acting on ecosystem patterns and its processes, thus having impact on regional sustainable development. Taking the Western Sichuan Plateau as the study area based on land use data from 1990 to 2020, the CA-Markov model was employed to predict the land use pattern under natural change scenarios, and the improved InVEST model and equivalent method were used to evaluate the ecosystem services in the study area from two different perspectives, as to analyze the evolution trend. The results show that: 1) From 1990 to 2020, the carbon storage in the Western Sichuan Plateau showed a fluctuating increase, with an average annual increase of $3.17 \times 10^7$ t, of which the total contribution rate of woodland and grassland to the total carbon storage exceeded 95%. In recent 30 years, the carbon storage of the Western Sichuan Plateau has little spatial variation, with the increase and decrease regions accounting for less than 5% with overall sporadically dots-like distribution. 2) Ecosystem Service Value (ESV) increased by $1.36 \times 10^{10}$ yuan in the past 30 years, which was similar to carbon storage and showed a wave-like increase; the contribution rate of woodland to the total ESV of the study area was more than 68%, occupying the dominant position. ESV was generally stable in the past 30 years, and the area with significant changes accounted for less than 9%, mainly located in the northeast and southwest of the study area. 3) In the next 10 years, under the current ecological protection measures, the carbon storage and ESV of the Western Sichuan Plateau will increase by $5.3980 \times 10^7$ t and $2.4087 \times 10^9$ yuan compared with that of 2020, indicating a positive development of ecosystem service function. This study results provides a scientific basis for the adjustment of land use structure and the management decision of ecological environment protection in the Western Sichuan Plateau.

**Keywords: land use change, CA-Markov model, Western Sichuan Plateau, carbon storage, ecosystem service value**

# 1 INTRODUCTION

Land is the material foundation of human production and life, and is the closest part between human and nature (Ye and Zhang, 2008; Zhang et al., 2021). As an important component and driving factor of global ecological environment change (Zhang et al., 2021), land use change comprehensively reflects the interaction process of various factors within the terrestrial ecosystem, has great significance in regional ecosystem service function, and is one of the important factors affecting human survival and development. With the continuous change of land use pattern, regional ecosystem service function will also change accordingly.

Ecosystem service function, which refers to the benefits that people get from the ecosystem through material flow and energy flow, is an important function of the ecosystem on the external environment (Costanza et al., 2014). Costanza et al. (1997) are the first to identify the theory and method of calculating ESV globally. In recent years, Xie et al. (2015) modified the estimation method proposed by Costanza based on the reality of China, put forward the ESV evaluation equivalence system, and constructed a dynamic evaluation method of terrestrial ecosystem value in China based on the equivalent factor approach of unit area value. The equivalent factor approach of unit area value has been greatly applied in the dynamic monitoring and evaluation of ecosystems such as urban ecosystem (Dai et al., 2021), wetland ecosystem (Zhou et al., 2020), watershed ecosystem (Temesgen et al., 2018), and farmland ecosystem (Fang et al., 2017).

At the same time, the carbon sink capacity of terrestrial ecosystems plays a leading role in the global carbon cycle, atmospheric $CO_2$ absorption and global climate change (Houghton, 2003). There is a response relationship between carbon storage and land use change, and land use change is usually accompanied by a large amount of carbon exchange (Vizaino-Brawvo et al., 2020). Therefore, studying ecosystem service function from carbon storage has become a new perspective. Until now, the research method of ecosystem service carbon storage based on InVEST model and the ecosystem service function evaluation method combined with the CA-Markov model have also been widely used (He et al., 2016; Jiang et al., 2017; Li et al., 2021). Its research fields mainly include the relationship between land use change and carbon density in watershed (Zhao et al., 2019), carbon storage change caused by urban expansion and simulation prediction (Firozjaei et al., 2019), ESV change and ecological function improvement model in mountainous areas (He et al., 2021), and spatiotemporal change characteristics of ecological restoration projects and carbon storage in plateau areas (Li et al., 2021). According to relevant research results, the InVEST model requires little data and runs fast. It can master the spatial distribution and dynamic change of carbon storage from spatiotemporal scale, reflect the relationship between land use change and carbon storage, and realize the dynamic evaluation of ecological service function (Hou et al., 2018).

As early studies on ecosystem service function are mostly focused on the present and the past, there are fewer simulation predictions for the future (Liu et al., 2021), which provided insufficient support for ecological environmental protection and management. The artificial neural network (Li and Yeh, 2005; Lei et al., 2012), CLUE-S (Zhang et al., 2014; Tian and Ren, 2012), SLEUTH (Nigussie and Altunkaynak, 2016; Nigussie and Altunkaynak, 2019), CA-Markov (Liu et al., 2019; Wang et al., 2020; Matlhodi et al., 2021) and other prediction models is applied in the study of land use evolution, especially CA-Markov model that predicts the change trend of land use in the future based on land use transfer matrix and land use data. The CA-Markov model can not only effectively simulate spatial change in land use, but also improve the prediction accuracy of land use type transformation, which overcomes the shortcomings of traditional land evolution simulation models (Zhang et al., 2017) and greatly promotes the prediction study of ecosystem service function evolution. Gaglio et al. (2019) evaluated the ecosystem service function of Paul do Boquilobo in 1967, 1990 and 2015, and further simulated and evaluated the ecosystem service function under two different situations of "high productivity agriculture" and "complete natural vegetation coverage" in 2050. Liu et al. (2021) used InVEST model and CA-Markov model to predict and analyze the spatiotemporal change and evolution trends of carbon storage in Shule River Basin, and considered that the growth of grassland, cropland and woodland area was the main reason for the increase of regional carbon storage. Gao et al. (2021) estimated the change of ESV based on the land use data of Shijiazhuang City in 1988, 1998, 2008 and 2018, and simulated the change of ESV in 2030 under three different situations by using CA-Markov, so as to provide scientific guidance for the construction of urban network. Gashaw et al. (2018) estimated land use land cover (LULC) change and its impact on ESV of Andassa Watershed of the Upper Blue Nile Basin, and predicted ESV change from 2018 to 2045, which provides a basis for the decision-making of regional ecological protection.

In recent years, great importance was attached to ecosystem service researches which yielded solid outcomes. However, a majority of researches was only evaluated from ESV, lacking effective comparison of multiple methods, resulting in relatively single outcomes, and significantly fewer researches on the ecological service function of alpine plateau area. The Western Sichuan Plateau is Located at the southeastern edge of Qinghai-Tibet Plateau, which is a typically eco-environment fragile and climatically sensitive area in China. It is also an important ecological barrier and water conservation area in the upper reaches of Yangtze River and Yellow River, and has a significant ecological status (Wu et al., 2021; Zhong et al., 2021). Facing the combined impact of climate change, natural disasters and human activities, ecosystem service function in the Western Sichuan Plateau have changed significantly, but the temporal and spatial differences are still unclear. In this context, this paper chooses the Western Sichuan Plateau as the study area and introduces CA-Markov model to predict the land use types in 2030. Based on the improvement of the unit area value equivalent factor method and InVEST model, the temporal and spatial evolution characteristics of the ecological service function in the study area were compared and analyzed from
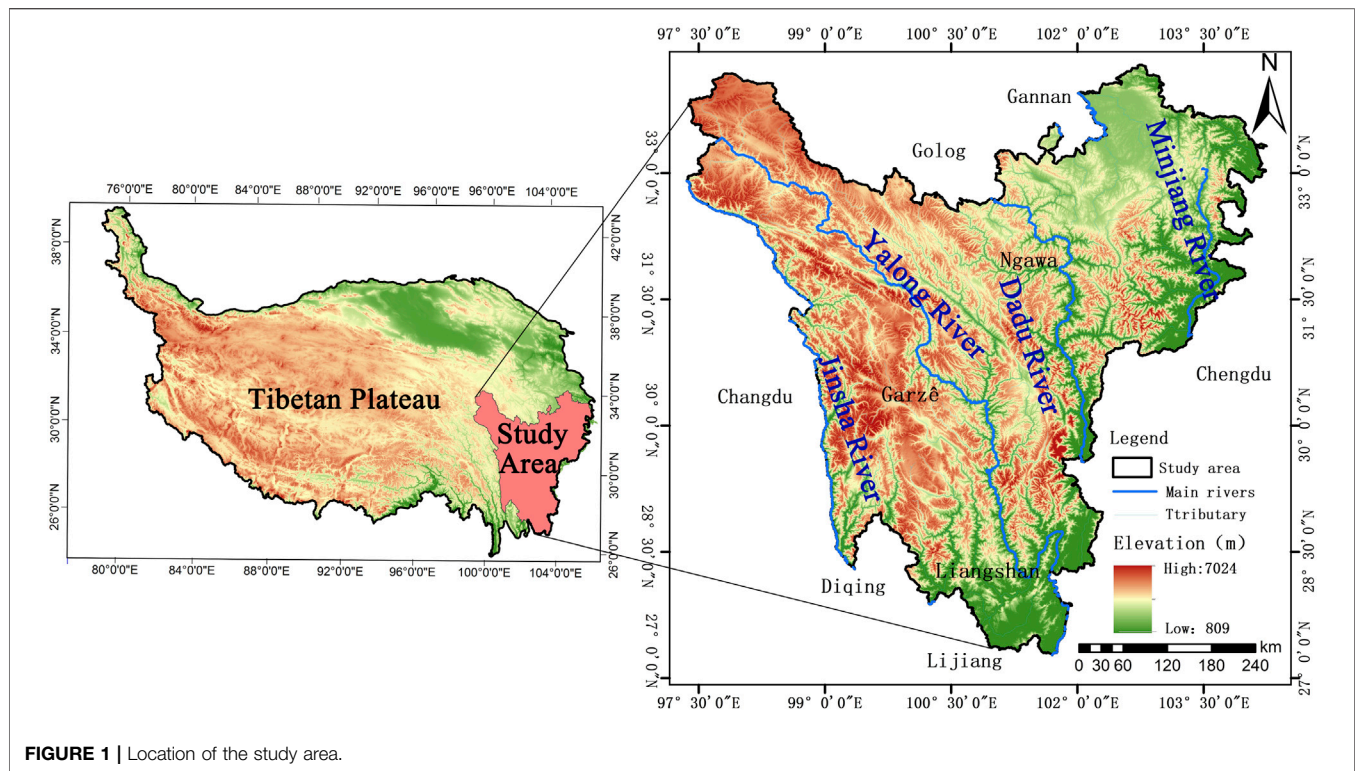
**FIGURE 1 |** Location of the study area.

the perspectives of ESV and carbon storage, as to analyze the possible future ecological environment issues and find the key prevention and control area. The research results are conducive to understand the evolution characteristics and future development trend of the ecosystem in the Western Sichuan Plateau, provide theoretical basis for the rational utilization of land resources and the protection of ecological environment, and promote ecological protection and regional high-quality development in ecologically fragile areas.

## 2 OVERVIEW AND RESEARCH METHODS OF THE STUDY AREA

### 2.1 Overview of the Study Area

With an area of about $2.59 \times 10^5 \, km^2$, the Western Sichuan Plateau (27.11°–34.31°N and 97.36°–104.62°E) is located in the transition zone between Qinghai-Tibet Plateau and Sichuan Basin, including 31 counties under the jurisdiction of Garze Tibetan Autonomous Prefecture and Aba Tibetan and Qiang Autonomous Prefecture, and Muli County, Yanyuan County, and part of Mianning County of Liangshan Yi Autonomous Prefecture. As a part of the ecological barrier of the Qinghai-Tibet Plateau, the Western Sichuan Plateau has outstanding ecological functions such as water conservation, soil and water conservation, biodiversity maintenance and climate regulation, so it is also one of the hotspots of biodiversity protection in the world. With the elevation ranging from 780 to 7556 m and large topographic fluctuations, the study area is dominated by high mountain valleys and high mountain plateaus. With annual

precipitation about 556.8–730 mm and temperature about 9.01–10.5°C, the climate in the study area is subtropical plateau monsoon climate with obvious geographical differences. The study area is rich in water resources, including the Yalong River, Dadu River, Min River, and other important river systems in the upper reaches of the Yangtze River, and the Baihe River, Heihe river and other river systems of the Yellow River (**Figure 1**). The main vegetation types are alpine meadow, shrub, coniferous forest, broad-leaved forest, etc., which makes the study area the most coniferous forest types in China. The main types of soil are plateau meadow soil, dark brown soil, brown soil, cold frozen soil, and cinnamon soil, and these five types account for more than 85% of the total area of the study area.

### 2.2 Data Sources and Processing

The land use remote sensing monitoring data, administrative boundary data and geological disaster vector data were obtained from Resources and Environmental Science and Data Center (http://www.resdc.cn/). The spatial resolution of land use remote sensing monitoring data is 30 m × 30 m, including six first-level classification and 26 second-level classification. The first-level classification includes cropland, woodland, grassland, water body, built-up land, and unused land. The accuracy of remote sensing classification is not less than 95% for cropland and built-up land, not less than 90% for grassland, woodland, and water body, and not less than 85% for unused land, which meets the need of the research. After pre-processing such as merging, cropping and reclassification, the land use classification maps for seven periods of 1990, 1995, 2000, 2005, 2010, 2015 and 2020 were obtained. The geological

**TABLE 1 |** Average ESV of per—hectare of land in the Western Sichuan plateau (yuan·hm$^{-2}$).

| First category | Second category | Cropland | Woodland | Grassland | Water body | Built-up land | Unused land |
|---|---|---|---|---|---|---|---|
| Provisioning service | Food production | 1,109.63 | 404.69 | 130.55 | 1,044.36 | 0.00 | 0.00 |
| | Raw materials | 522.18 | 926.87 | 182.76 | 300.25 | 0.00 | 0.00 |
| | Water supply | 26.11 | 483.02 | 104.44 | 10,822.18 | 0.00 | 104.85 |
| Regulating service | Gas regulation | 874.65 | 3,067.81 | 665.78 | 1,005.20 | 0.00 | 33.88 |
| | Climate regulation | 469.96 | 9,177.31 | 1749.30 | 2,989.48 | 0.00 | 26.21 |
| | Waste treatment | 130.55 | 2,597.85 | 574.40 | 7,245.25 | 0.00 | 133.46 |
| | Hydrological regulation | 352.47 | 4,582.13 | 1,279.34 | 133,,469.21 | 0.00 | 383.80 |
| Supporting service | Soil conservation | 1,344.61 | 3,733.59 | 809.38 | 1,214.07 | 0.00 | 25.14 |
| | Maintain nutrient cycle | 156.65 | 287.20 | 65.27 | 91.38 | 0.00 | 0.00 |
| | Biodiversity conservation | 169.71 | 3,394.17 | 731.05 | 3,328.90 | 0.00 | 25.62 |
| Cultural service | Entertainment | 78.33 | 1,488.21 | 326.36 | 2,467.30 | 0.00 | 16.94 |

disaster data with 12,192 geological disasters in number covered the period from 1990 to 2020. By making combined analysis with both ESV and carbon storage layers, the impact of geological disasters on ecosystem service function was estimated.

The DEM data were obtained from the Geospatial Data Cloud (http://www.gscloud.cn/) with a spatial resolution of 30 m × 30 m. The Qinghai-Tibetan Plateau boundary data were collected from the Global Change Research Data Publishing and Repository (http://www.geodoi.ac.cn/WebCn/Default.aspx). Data of carbon density of different land types were obtained from Chinese Ecosystem Research Network Data Center (http://www.nesdc.org.cn/). Meteorological data such as rainfall and temperature came from China Climate Bulletin (http://zwgk.cma.gov.cn/). Social and economic data such as grain output per unit area and sown area of crops mainly came from China Statistical Yearbook and Sichuan Statistical Yearbook, while grain price came from Sichuan Grain Network (http://www.scgrain.com/). All the data were entered into GIS geodatabase after preprocessing.

## 2.3 Research Method
### 2.3.1 Evaluation of Ecosystem Service
Costanza et al. (1997) clarified the principles and methods of evaluating the value of ecosystem service, and then Xie et al. (2003) proposed the Chinese Ecological Service Value Equivalent Factor Approach based on the research of Costanza. This study is based on the ESV equivalent table per unit area proposed by Xie et al. (2015). China's average grain output per unit area in 2020 was kg·hm$^{-2}$, while the average grain output in the Western Sichuan Plateau was 3,422.53 kg·hm$^{-2}$, and the average price of grain crops was 2,670 yuan·hm$^{-2}$. Since the economic value provided by the natural ecosystem is one seventh of the economic value of food output service provided by the existing cropland per unit area, the economic value of the ESV equivalent factor of the Western Sichuan Plateau after modified is determined as 1,305.45 yuan·hm$^{-2}$, and then the ESV per unit area of the Western Sichuan Plateau was obtained (**Table 1**).

The formula for calculating the value of ecosystem services in the study area is:

$$\text{ESV} = \sum_{i=1}^{n} S_i \times VC_j \quad (i = 1, 2, \ldots n), \tag{1}$$

Where ESV represents the ESV (yuan); $S$ represents the area (hectares) of land use type $i$ in the study area, and $VC$ represents the ESV coefficient (yuan·hm$^{-2}$) per unit area of the ecosystem type $i$.

### 2.3.2 Carbon Storage Evaluation Based on InVEST Model
The carbon storage model of the InVEST model divides the carbon storage of the ecosystem into four basic carbon pools, namely above-ground carbon, underground carbon, soil carbon, dead organic matter carbon. The carbon exchange between different carbon pools in terrestrial ecosystems and the atmosphere is shown in **Figure 2** (InVEST 3.2.0 User's guide).

The calculation formula of total carbon storage in the Western Sichuan Plateau is as follows:

$$C_{total} = C_{above} + C_{below} + C_{soil} + C_{dead}, \tag{2}$$

Where $C_{total}$ is the total carbon storage; $C_{above}$ is the above-ground carbon storage; $C_{below}$ is the underground carbon storage; $C_{soil}$ is the soil carbon storage, and $C_{dead}$ is the dead organic matter carbon storage.

Based on the carbon density and land use data of different land use type, the carbon storage of each land use type in the Western Sichuan Plateau is calculated by the formula:

$$C_{totali} = (C_{above} + C_{below} + C_{soil} + C_{dead}) \times A_i, \tag{3}$$

Where $i$ is the average carbon density of each land use, and $A_i$ is the area of this land used.

The carbon density data of different land use types in this study were obtained from the shared date of the National Ecological Science Data Center and some documents (Chen et al., 2002; Li et al., 2003; Xie et al., 2004; Chuai et al., 2013; Zhang et al., 2018). Since the carbon density data were collected from the results of studies in different parts of China, the selected documents should be close to or be similar to the study area as far as possible to avoid excessive data gap. At the same time, the carbon density varies with climate, soil properties and land use (Fu et al., 2019), so the carbon density should be modified according to the climate characteristics and land use types of the Western Sichuan Plateau. Existing research results show that the carbon density is positively correlated with annual precipitation and weakly correlated with annual average
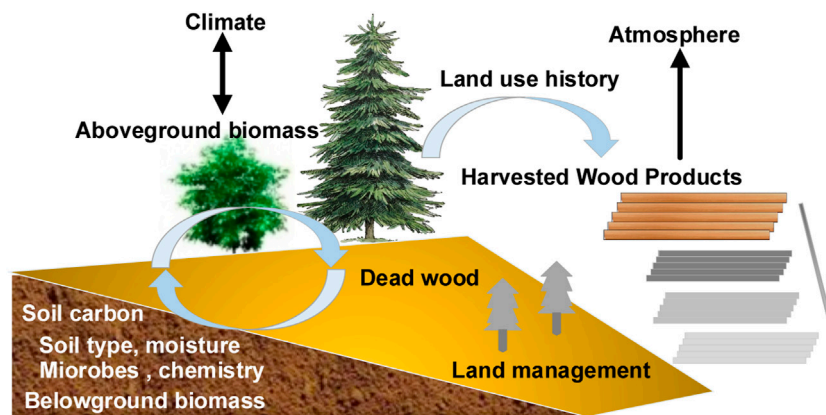
**FIGURE 2 |** Carbon exchange between carbon pool and the atmosphere.

**TABLE 2 |** Carbon density values of different land use types in the Western Sichuan plateau (t·hm$^{-2}$).

| Land use type | $C_{above}$ | $C_{below}$ | $C_{soil}$ | $C_{dead}$ |
|---|---|---|---|---|
| Cropland | 1.241 | 17.574 | 11.847 | 2.138 |
| Woodland | 9.233 | 33.670 | 17.355 | 3.073 |
| Grassland | 7.687 | 25.130 | 10.918 | 1.585 |
| Water body | 0.653 | 0.000 | 0.000 | 0.000 |
| Built-up land | 0.544 | 7.990 | 0.000 | 0.000 |
| Unused land | 0.283 | 0.000 | 2.361 | 0.000 |

temperature. The quantitative expression of the relationship between carbon density and temperature and precipitation is as follows (Raich and Nadelhoffer, 1989; Giardina and Ryan., 2000; Chen et al., 2007; Alam et al., 2013).

$$C_{SP} = 3.3968 \times P + 3996.1 \quad (R^2 = 0.11), \tag{4}$$

$$C_{BP} = 6.7981e^{0.00541P} \quad (R^2 = 0.70), \tag{5}$$

$$C_{BT} = 28 \times T + 398 \quad (R^2 = 0.47, P < 0.01), \tag{6}$$

Where $C_{SP}$ is the soil carbon density (kg.m$^{-2}$) based on the annual precipitation; $C_{BP}$ is the biomass carbon density (kg.m$^{-2}$) based on the annual precipitation; $C_{BT}$ is the biomass carbon density (kg.m$^{-2}$) based on annual average temperature; $P$ is the average annual precipitation (mm), and $T$ is the annual average temperature (°C). In the past 30 years, the average annual temperature of China and the Western Sichuan Plateau was 9.0 and 6.3 °C, and the average annual precipitation was 643.50 and 812.65 mm respectively. The product of the carbon density data of the reference documents and the modified indices is the carbon density data of the Western Sichuan Plateau.

The modified formula of carbon density in the Western Sichuan Plateau is as follows:

$$K_{BP} = \frac{C'_{BP}}{C''_{BP}}, \tag{7}$$

$$K_{BT} = \frac{C'_{BT}}{C''_{BT}}, \tag{8}$$

$$K_B = K_{BT} \times K_{BP}, \tag{9}$$

$$K_S = \frac{C'_{SP}}{C'''_{SP}}, \tag{10}$$

Where $K_{BP}$ is the modified indices of precipitation factor in biomass carbon density; $K_{BT}$ is the modified indices of temperature factor; $C'_{BP}$ and $C''_{BP}$ are the biomass carbon density obtained from annual precipitation in the Western Sichuan Plateau and the whole country respectively. $C'_{BT}$ and $C''_{BT}$ are the biomass carbon density obtained from annual average temperature; $C'_{SP}$ and $C''_{SP}$ are the soil carbon density data obtained from annual average temperature; $K_B$ and $K_S$ are the biomass carbon density modified indices and soil carbon density modified indices respectively. The carbon density values of each land use type after modified in the Western Sichuan Plateau are shown in **Table 2**.

### 2.3.3 CA-Markov Model

CA-Markov model, the main tool to simulate Land-Use and Land-Cover Change (LUCC) (Sang et al., 2010), combines Cellular Automata (CA) and Markov model and uses transition probability matrix to simulate the change of land use over time. Markov model simulates the matrix of land use change over time by calculating the probability of land use transfer in the first and second phases for predicting the subsequent changes on this basis (Zhao et al., 2019). The calculation formula is as follows (Nasehi et al., 2019):

$$P_{ij} = \begin{bmatrix} P_{11} & P_{12} & ... & P_{1n} \\ P_{21} & P_{22} & ... & P_{2n} \\ ... & ... & ... & ... \\ P_{n1} & P_{n2} & ... & P_{nn} \end{bmatrix}, \text{ and } \sum_{j=1}^{n} P_{ij} = 1 \, (i, j = 1, 2, ..., n),$$

$$\tag{11}$$

$$St + 1 = P_{ij} * S, \tag{12}$$

Where $S_t$, and $S_{t+1}$ is the land use state during $t$ and $t + 1$ respectively; $P_{ij}$ is the transition probability matrix, and $n$ is the land use type.

CA model can simulate the spatiotemporal evolution of land use, can reflect the local interaction of system evolutionary

dynamics (Wang et al., 2021) and simulate random, nonlinear, and spatial change trends. This makes up for the failure of Markov model to identify the spatial variability of land use (Wickramasuriya et al., 2009). CA model is represented as follows:

$$S(t, t + 1) = f[S(t), N], \tag{13}$$

Where $s$ is the set of finite and discrete states of the cell; $f$ is the conversion rule function of the cell state; $N$ is the neighborhood of each cell; $t$ and $t + 1$ are two different moments.

The year 2010 was taken as the starting timefor prediction to simulate the land use situation in the study area in 2030, and Kappa coefficients were used to test the simulation results. Using CROSSTAB model IDRISR 17.0, the Kappa coefficients of 2010 are 0.929, indicating good simulation effect (Liu et al., 2021; Yang et al., 2021) and the verified CA-Markov can be used to predict land use in 2030.

Combined with The Regional Ecological Construction and Environmental Protection Plan of The Qinghai-Tibet Plateau (2011–2030), we took the year 2010 as the starting time for prediction, thus the data to land use in 2020 was calculated. By comparison the prediction results and the actual data to land use in 2020, we concluded that the Kappa coefficients were 0.929, indicating that the simulation result was working well (Liu et al., 2021; Yang et al., 2021). On this basis, the data to land use in 2030 was worked out with taking the year 2020 as the starting time for prediction. All predictions conducted are based on natural variation scenarios, without limiting factors.

### 2.3.4 Analysis Method for Changes in Ecological Service Functions

This study uses exploratory spatial analysis to reveal the spatial agglomeration types and autocorrelation of ecosystem service function changes in the Western Sichuan Plateau. The global Moran's I is used for global autocorrelation measurement and examination, and its calculation formula is as follows (Lei et al., 2020):

$$Moran'I = \frac{n\sum\limits_{i=1}^{n}\sum\limits_{j=1}^{n} w_{ij}(x_i - x)(x_j - x)}{\sum\limits_{i=1}^{n}(x_i - x)\sum\limits_{i=1}^{n}\sum\limits_{j=1}^{n} w_{ij}}, \tag{14}$$

Where $n$ is the number of grids; $x_i$ and $x_j$ are the attribute values of grid $i$ and $j$ respectively; $x$ is the average value of attributes; $w_{ij}$ is the spatial weight matrix. If Moran's I is significantly positive, it indicates that there is a spatial positive correlation of ESV; otherwise, there is a spatial negative correlation; when Moran's I is 0, it indicates random distribution.

Kernel density was used to estimate the spatial clustering of ecological service change in different periods. The higher the kernel density value, the greater the intensity of regional changes and the more obvious the clustering characteristics (Liu et al., 2015).

$$fn(x) = \frac{1}{nh}\sum\limits_{i=1}^{n} k\left(\frac{x - X_i}{h}\right), \tag{15}$$

Where $f(x,y)$ is the density estimation at the location $(x, y)$; $n$ is the number of ecological service function change points; $x - X_i$ is the distance between the location and the $i$-th observation location, and $h$ is the bandwidth.

## 3 RESULTS AND ANALYSIS

### 3.1 Change Characteristics of Land Use in the Study Area From 1990 to 2020

The data to land use in western Sichuan Plateau from 1990 to 2020 was shown in **Figure 3**.

From 1990 to 2020, grassland occupied more than 55% of the study area. While woodland area followed, accounting for about 44%. The coverage rate of unused land, cropland, water body and built-up land was relatively low, accounting for less than 10% of the study area. Throughout the past three decades years, the area of each region changed to varying degrees, with the biggest change in the area of the built-up land which increased by 141.38%. Then, the water body area continued to rise, with a cumulative increase of 44.11%. Woodland and unused land reflected a fluctuating rise, with the largest increase occurring from 2005 to 2010. The area of cropland and grassland decreased by 1.17 and 2.06%, respectively. Cropland area dropped significantly from 1990 to 1995, and grassland area from 2005 to 2010. In general, the continuous increase area of built-up land and water body was witnessed as the result of population growth and extensive human activities. By implementing policy of returning farmland to forest and protecting natural forest, the area of woodland continued to rise. At the same time, geological disasters and human activities led to some grassland degradation, and increased area of unused land.

### 3.2 Spatiotemporal Change Characteristics of Carbon Storage in the Study Area From 1990 to 2020

#### 3.2.1 Overall Change Characteristics of Carbon Storage

The carbon storage of the Western Sichuan Plateau from 1990 to 2020 were calculated respectively, and the carbon storage of different land use types and total carbon storage of the study area in each year are shown in **Table 3**.

As shown in **Table 3**, the carbon storage of the Western Sichuan Plateau from 1990 to 2020 is $1.2445 \times 10^{10}$ t, $1.2453 \times 10^{10}$ t, $1.2438 \times 10^{10}$ t, $1.2438 \times 10^{10}$ t, $1.2465 \times 10^{10}$ t, $1.2461 \times 10^{10}$ t, $1.2455 \times 10^{10}$ t respectively, increased $3.1666 \times 10^{7}$ t per year on average. Among them, the carbon storage slowly increased from 1990 to 1995, slightly decreased from 1995 to 2005, increased relatively more from 2005 to 2010, and slowly decreased from 2010 to 2020, showing a fluctuating increasing trend of "increase-decrease-increase-decrease".

From the perspective of land use types, the carbon storage of different land use types in different periods of the Western Sichuan Plateau has little change. In general, the carbon storage of woodland, water body, built-up land and unused land increased, among which the carbon storage of water body and built-up land increased significantly; the carbon storage of
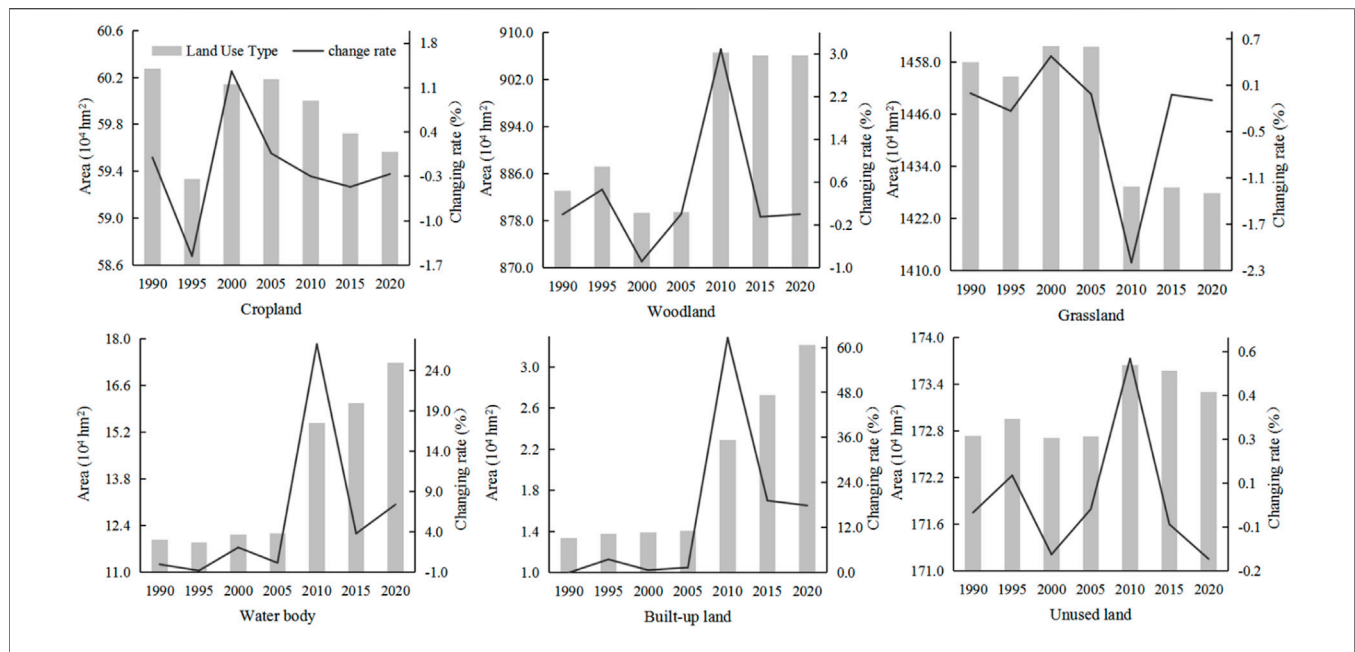
**FIGURE 3 |** Land use of the Western Sichuan Plateau from 1990 to 2020.

**TABLE 3 |** Carbon storage of the Western Sichuan Plateau from 1990 to 2020.

| Types | Year | Cropland | Woodland | Grassland | Water body | Built-up land | Unused land | Total |
|---|---|---|---|---|---|---|---|---|
| Carbon storage/ | 1990 | 197.71 | 5,592.72 | 6,607.43 | 0.78 | 1.14 | 45.67 | 12,445.45 |
| (106 t) | 1995 | 194.63 | 5,618.66 | 6,592.33 | 0.78 | 1.18 | 45.73 | 12,453.3 |
| | 2000 | 197.27 | 5,569.24 | 6,623.99 | 0.79 | 1.19 | 45.66 | 12,438.15 |
| | 2005 | 197.4 | 5,569.63 | 6,623.25 | 0.79 | 1.2 | 45.67 | 12,437.95 |
| | 2010 | 196.81 | 5,741.26 | 6,478.07 | 1.01 | 1.95 | 45.91 | 12,465.02 |
| | 2015 | 195.9 | 5,738.58 | 6,476.89 | 1.05 | 2.33 | 45.89 | 12,460.64 |
| | 2020 | 195.39 | 5,738.8 | 6,471.07 | 1.13 | 2.75 | 45.82 | 12,454.95 |
| Changing rate/(%) | 1990–1995 | −1.56 | 0.46 | −0.23 | 0.00 | 3.51 | 0.13 | 0.06 |
| | 1995–2000 | 1.36 | −0.88 | 0.48 | 1.28 | 0.85 | −0.15 | −0.12 |
| | 2000–2005 | 0.07 | 0.01 | −0.01 | 0.00 | 0.84 | 0.02 | 0.00 |
| | 2005–2010 | −0.30 | 3.08 | −2.19 | 27.85 | 62.50 | 0.53 | 0.22 |
| | 2010–2015 | −0.46 | −0.05 | −0.02 | 3.96 | 19.49 | −0.04 | −0.04 |
| | 2015–2020 | −0.26 | 0.00 | −0.09 | 7.62 | 18.03 | −0.15 | −0.05 |
| | 1990–2020 | −1.17 | 2.61 | −2.06 | 44.87 | 141.23 | 0.33 | 0.08 |

cropland and grassland decreased by 1.17 and 2.06% respectively in 2020 compared with 1990. In terms of the contribution of different land use types to the total carbon storage, the contribution rate is grassland, woodland, cropland, unused land, built-up land and water in a descending order. Woodland and grassland account for 34 and 56% of the total area of the study area respectively, and their carbon storage accounts for 45 and 53% of the total carbon storage, which are the main carbon pools in the study area.

From **Table 3**, it can be seen that the correlation between the total carbon storage and above-ground biological carbon storage is not significant in the Western Sichuan plateau.

The main reason is that this area is dominated by grassland and woodland, and the high altitude, cold climate and relatively low precipitation prevent crops and forest grasses from fixing carbon on the ground for a long time due to withering and dying, resulting in insignificant correlation between above-ground carbon storage and total carbon due to depletion. The underground biological carbon storage, soil carbon storage and dead organic matter carbon are all significant positive correlation with total carbon stock. In conclusion, woodland and grassland represent the main carbon pools. That to say, the increase and decrease in the coverage of the two types of land serve as the main reason for the changes of regional carbon storage.

**FIGURE 4 |** Temporal and spatial distribution of carbon storage during 1990–2020.



**FIGURE 5 |** Spatial distribution changes of carbon storage during 1990–2020.
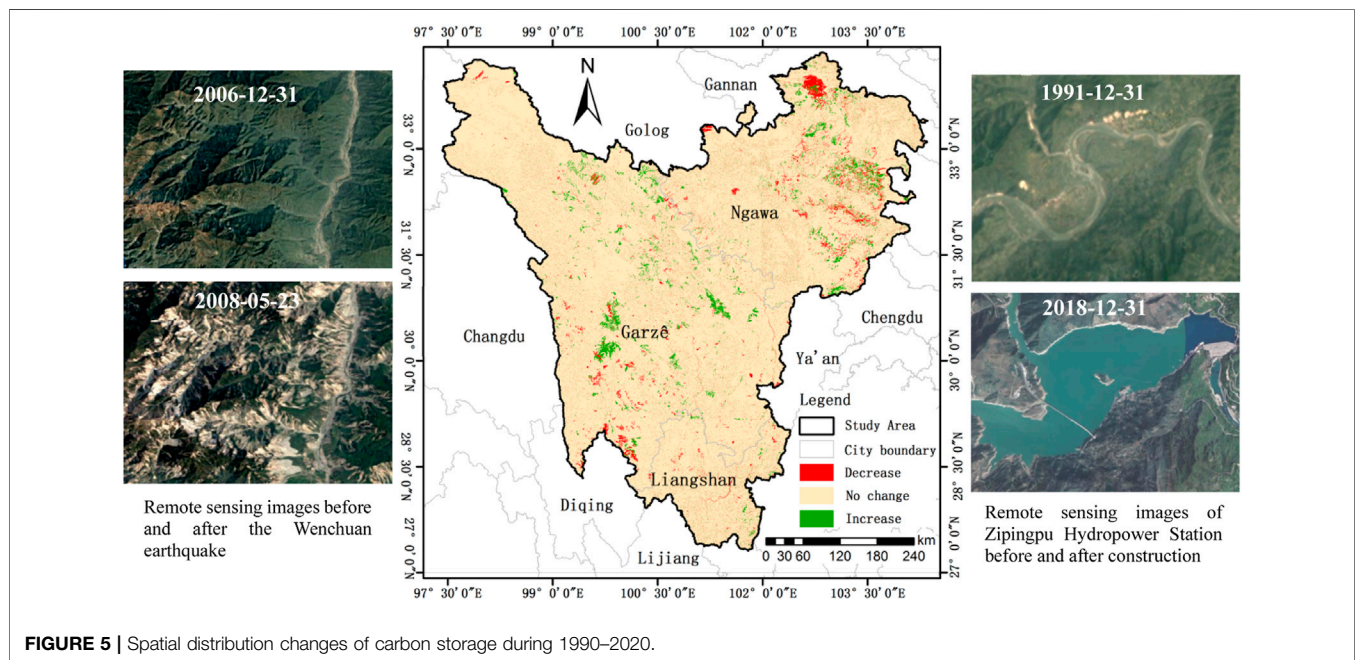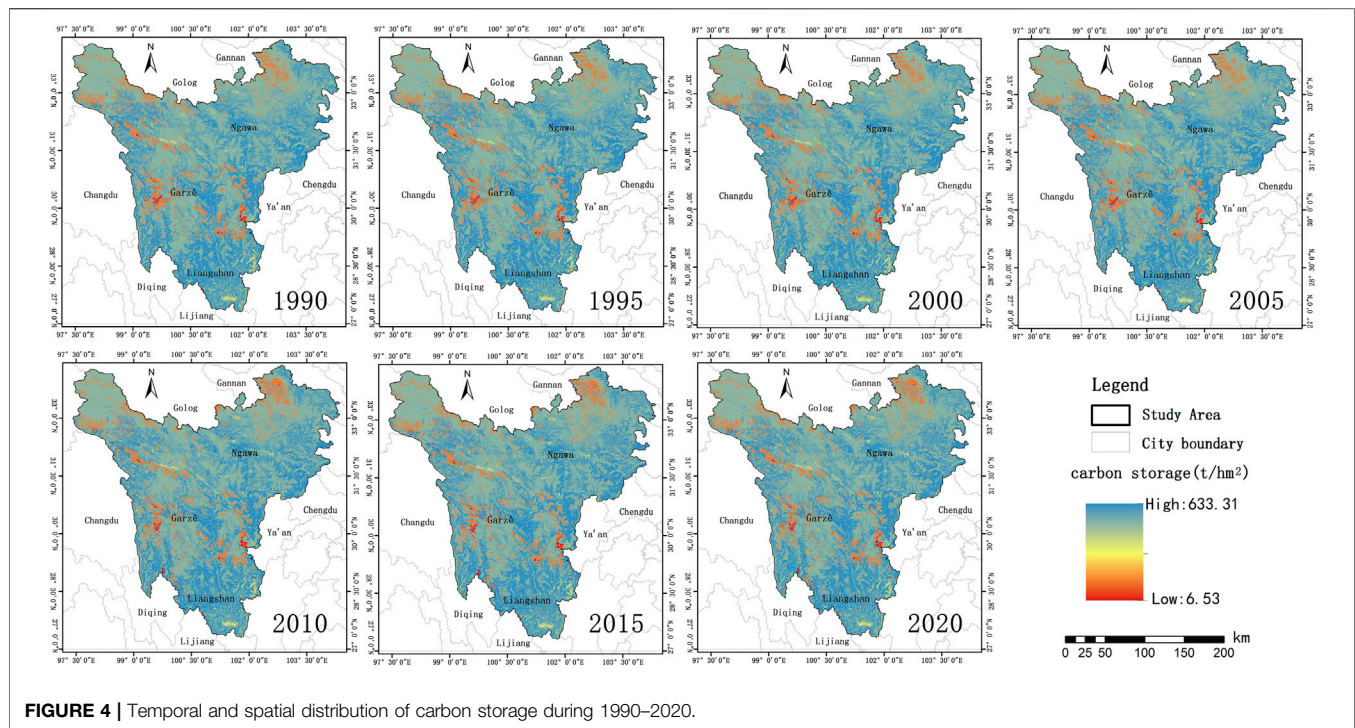
## 3.2.2 Spatiotemporal Change Characteristics of Carbon Storage

From the perspective of the spatial pattern of carbon storage in the Western Sichuan Plateau (**Figure 4**), there is no obvious difference in the spatial distribution of carbon storage from 1990 to 2020, and high carbon storage is distributed throughout the whole area. The carbon storage of the Yalong River, Dadu River and Min River is obviously high, which is closely related to the rich water resources and high forest coverage in this area. Areas with low carbon storage are sporadically distributed in the

**TABLE 4 |** ESV change of the Western Sichuan Plateau during 1990–2020.

| Types | Year | Cropland | Woodland | Grassland | Water body | Unused land | Total |
|---|---|---|---|---|---|---|---|
| ESV/(108 yuan) | 1990 | 31.5534 | 2,661.8907 | 964.9541 | 196.4838 | 12.9536 | 3,867.8356 |
| | 1995 | 31.0625 | 2,674.2378 | 962.7486 | 194.9501 | 12.9701 | 3,875.9691 |
| | 2000 | 31.4845 | 2,650.7155 | 967.3723 | 199.0429 | 12.9515 | 3,861.5667 |
| | 2005 | 31.5051 | 2,650.8996 | 967.2645 | 199.4129 | 12.9531 | 3,862.0352 |
| | 2010 | 31.4112 | 2,732.5903 | 946.0621 | 253.8747 | 13.0214 | 3,976.9597 |
| | 2015 | 31.2653 | 2,731.3146 | 945.8894 | 263.5875 | 13.0162 | 3,985.0731 |
| | 2020 | 31.1835 | 2,731.4168 | 945.0399 | 283.1463 | 12.9943 | 4,003.7864 |
| Changing rate/(%) | 1990–1995 | −1.56 | 0.46 | −0.23 | −0.78 | 0.13 | 0.21 |
| | 1995–2000 | 1.36 | −0.88 | 0.48 | 2.10 | −0.14 | −0.37 |
| | 2000–2005 | 0.07 | 0.01 | −0.01 | 0.19 | 0.01 | 0.01 |
| | 2005–2010 | −0.30 | 3.08 | −2.19 | 27.31 | 0.53 | 2.98 |
| | 2010–2015 | −0.46 | −0.05 | −0.02 | 3.83 | −0.04 | 0.20 |
| | 2015–2020 | −0.24 | 0.00 | −0.09 | 7.42 | −0.17 | 0.47 |
| | 1990–2020 | −1.15 | 2.61 | −2.06 | 44.11 | 0.31 | 3.51 |

middle, west and north of the study area in the shape of dot and strip, mainly because water body and unused land occupy a relatively high proportion.

In order to further reflect the spatial change of carbon storage in the Western Sichuan Plateau from 1990 to 2020, the two periods of carbon storage distribution map in 2020 and 1990 were raster processed, with a raster size of 30 × 30 m. The Map Algebra tool of Arcgis was used to calculate the change of each raster. The carbon storage change value greater than 5% is defined as the increase region, the carbon storage change value less than −5% is defined as the decrease region, and the carbon storage change value between −5 and 5% is defined as no change region.

From **Figure 5**, it can be seen that the carbon storage in most areas of the Western Sichuan Plateau remained basically unchanged from 1990 to 2020. Statistics showed that the no change region is $2.3617 \times 10^7 \, hm^2$, accounting for 91.28% of the total area; the decrease region is $1.0439 \times 10^6 \, hm^2$, accounting for 4.03% of the total area; the increased area is $1.2131 \times 10^6 \, hm^2$, accounting for 4.69% of the total area. From the perspective of spatial distribution, the decrease and increase regions are scattered. The decrease regions are relatively concentrated in 10 counties such as Zoige County, Hongyuan County, Songpan County, Wenchuan County and Xiangcheng County, mainly because the carbon storage is reduced due to grassland degradation caused by climate change, mountain disasters and human activities (Liu et al., 2020). Areas with relatively concentrated increase of carbon storage are mainly located in Litang County, Daofu County, Sertar County and other counties, which are closely related to the benefits generated by the natural forest protection project.

## 3.3 Spatiotemporal Change Characteristics of ESV in the Study Area From 1990 to 2020
### 3.3.1 Overall Change Characteristics of Ecological Service Value
Combining the land use data of the Western Sichuan Plateau, the ESV was calculated, and the ESV of different land use types from 1990 to 2020 were obtained (**Table 4**).
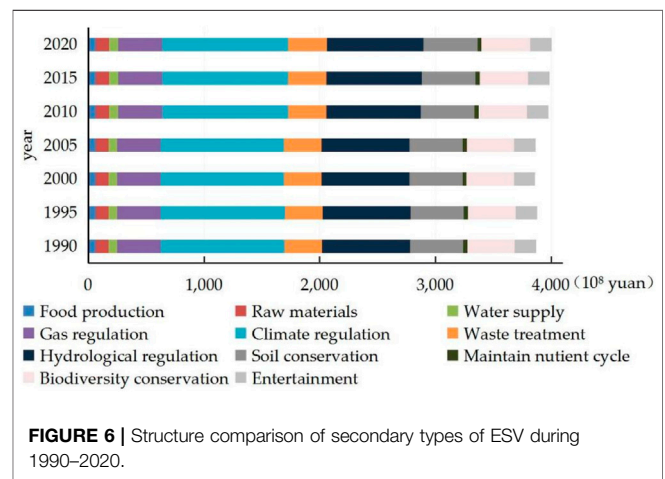


**FIGURE 6 |** Structure comparison of secondary types of ESV during 1990–2020.

From **Table 4**, it can be seen that the ESV of the Western Sichuan Plateau from 1990 to 2020 is 3,867.8356 × $10^8$ yuan, 3,875.9691 × $10^8$ yuan, 3,861.5667 × $10^8$ yuan, 3,862.0352 × $10^8$ yuan, 3,976.9597 × $10^8$ yuan, 3,985.0731 × $10^8$ yuan, 4,003.7864 × $10^8$ yuan. With an increase of 135.9509 × $10^8$ yuan (3.29%) and an average annual increase of 4.5317 × $10^8$ yuan, the overall change of carbon storage in the Western Sichuan Plateau during the 30 years is not significant. From the trend of ESV changes, ESV increased slowly from 1990 to 1995, decreased slowly from 1995 to 2005, increased significantly from 2005 to 2010, and slowed down the increase trend from 2010 to 2020, presenting a fluctuation of "increase-decrease-increase" fluctuation state on the whole.

In terms of land use types, the ESV of different land use types in the Western Sichuan Plateau changed little in different periods. In general, the ESV of woodland, water body and unused land increased, and the increase trend of water body was the most obvious. The ESV of water body increased by 44.11% during the 30 years, which is partly related to the hydropower plant construction activities carried out in the Min River, Yalong River and Dadu River during the period. The ESV of cropland and grassland decreased slightly, decreasing by 1.15 and 2.06%

**FIGURE 7 |** The spatial distribution of ESV during 2006–2020.
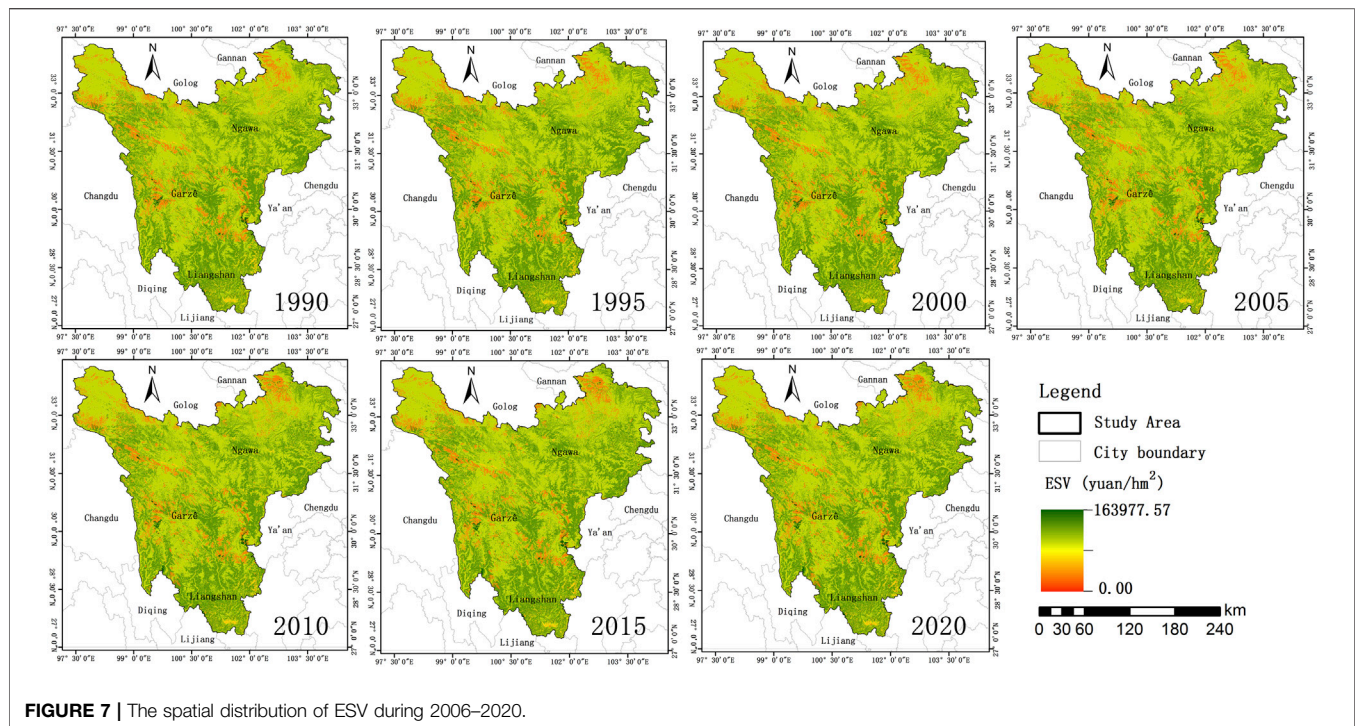
respectively, which is related to the continuous expansion of built-up land during the period. From the perspective of the contribution of different land use types to regional ESV, the contribution rate of different land use types is woodland, grassland, water body, cropland and unused land in descending order, of which the woodland with a contribution rate of more than 68% is the main component of ESV in the study area. In summary, the service structure of the Western Sichuan Plateau remained generally stable. The varying coverage of water body and woodland is the most important cause for the change of regional ESV and spatial difference.

Among the second-level ecological service function value, the ecological service function value per unit area from low to high is nutrient cycle maintenance, raw material production, food production, aesthetic landscape, gas regulation, soil conservation, biodiversity, environmental purification, water supply, climate regulation and hydrological regulation, and the value of the following function from low to high is: nutrient cycle maintenance, food production, water supply, raw material production, aesthetic landscape, environmental purification, gas regulation, biodiversity, soil conservation, hydrological regulation and climate regulation. The structure of various service functions is basically stable from 1990 to 2020 (**Figure 6**). Among the first-level ecological service function value, the value of provisioning service is 16,161.8836 yuan/hm$^2$; the value of regulating service is 170,808.0298 yuan/hm$^2$; the value of supporting service is 15,376.7448 yuan/hm$^2$, and the value of cultural service is 4,377.1408 yuan/hm$^2$. The total value ratio of the four first-level ecological service functions was basically maintained at 6: 65: 23: 5, and the regulation service

took an obvious advantage, indicating that ecological protection is the focus of the study area.

### 3.3.2 Spatial Change Characteristics of Ecological Service Value

From the perspective of spatial pattern of ESV (**Figure 7**), the spatial distribution characteristics of ESV are similar to carbon storage, showing the characteristics of "high in the south and low in the north" and "high in the east and low in the west". The main reasons for the overall low ESV are the high altitude and cold climate in the north, and the main land use types are grassland and unused land. While in the east and south, the climate is relatively warm and humid and the main land use types are woodland and cropland. At the same time, the Min River, Dadu River, Yalong River and Jinshajiang River are the main rivers within the territory, which flow from north to south or southeast, so the ESV in the south and east is relatively high. From the perspective of time dimension, there is no significant difference in ESV between 1990 and 2020. The ecological advantages in the south and east still persist, and the regulating capacity of the ecosystem continues to be enhanced, indicating that the conservation and management of public welfare forests, natural forests and grassland resources implemented over the years show good ecological effects. In order to further identify the spatial differentiation characteristics of ESV in the Western Sichuan Plateau from 1990 to 2020, the distribution maps of ESV in 2020 and 1990 were raster processed and the raster size was 30 × 30 m to calculate the changes of ESV in each raster. The ESV change value greater than 5% is defined as the increase region, less than −5% is defined as the decrease region, and the
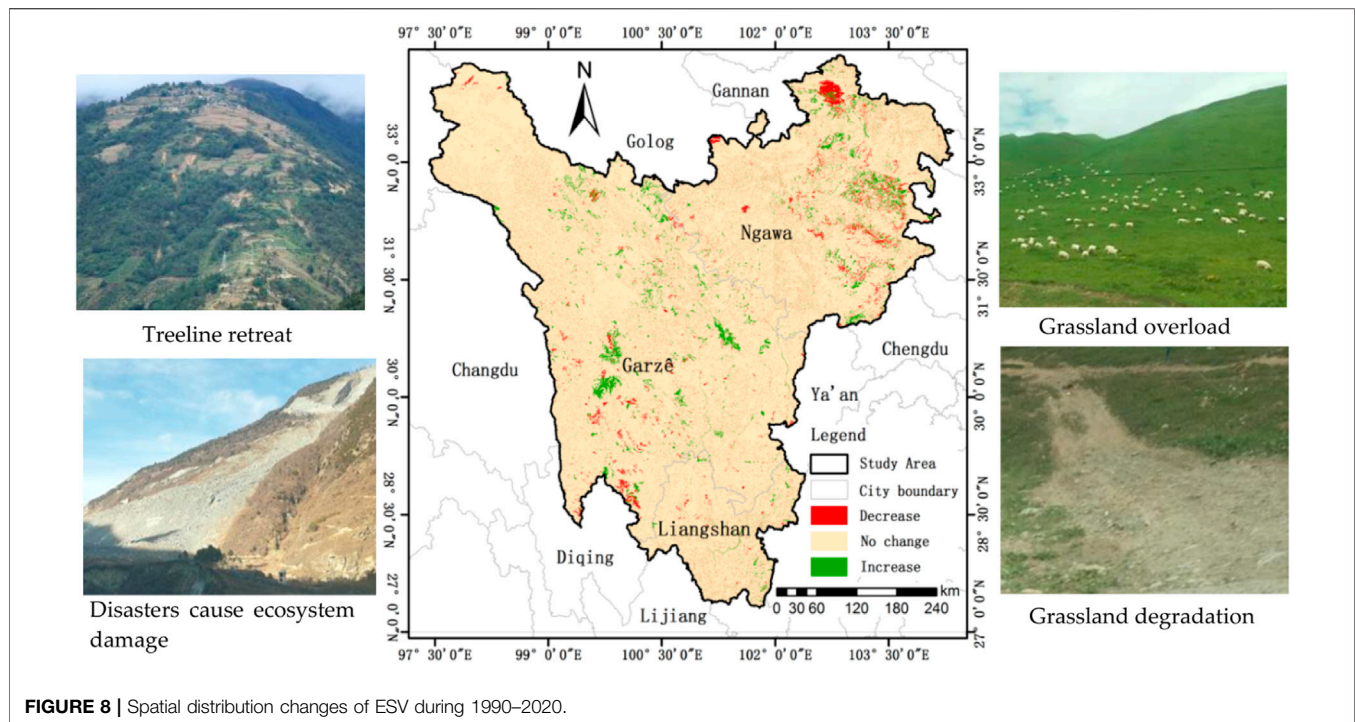
**FIGURE 8 |** Spatial distribution changes of ESV during 1990–2020.

**TABLE 5 |** Land use of the western Sichuan plateau from 2020 to 2030.

| Types | Cropland | Woodland | Grassland | Water body | Built-up land | Unused land |
|---|---|---|---|---|---|---|
| Area/($10^4$ hm$^2$) | 59.1137 | 930.4460 | 1,406.2724 | 17.1306 | 3.2258 | 171.1685 |
| Changing rate/(%) | −0.76 | 2.68 | −1.51 | −0.79 | 0.26 | −1.23 |

ESV change value between −5 and 5% is defined as no change region.

From **Figure 8**, it can be seen that there is no change of ESV in most areas of the Western Sichuan Plateau from 1990 to 2020, indicating that the Western Sichuan Plateau ecosystem is generally stable.

Statistics show that the no change region is $2.3617 \times 10^7$ hm$^2$, accounting for 91.28% of the total area; the decrease region is $9.9269 \times 10^5$ hm$^2$, accounting for 3.84% of the total area; and the increase region is $1.2644 \times 10^6$ hm$^2$, accounting for 4.89% of the total area. Areas in decrease region are sporadically distributed like dots, and the relatively concentrated areas are mainly located in the northeast and southwest of the study area. The main reason for the decrease of ESV in the northeast is that the over-loading rate of grassland was high before 2016, and the ecological function of some wetland and plateau lakes was degraded due to overgrazing. At the same time, the Min River Basin is densely covered with deep-cut alpine landforms, ravines and frequent natural disasters, especially the Wenchuan earthquake has caused serious damage to the regional ecological environment. The main reason for the decrease in the southwest is the early woodland degradation. Although major ecological projects such as returning farmland to forest and natural forest protection were actively implemented in the early stage, the problems such as low

quality of forest system and low efficiency of forest ecological function were still prominent. Other sporadic reduction areas are mainly caused by the expansion of built-up land and human activities. The areas where ESV increases are mainly located in Litang County in the East and Daofu County in the middle, which is closely related to the increasing woodland area in these areas.

## 3.4 Simulation and Prediction of Ecosystem Service Function in the Western Sichuan Plateau in 2030
### 3.4.1 Land Use Changes of the Western Sichuan Plateau in 2030

Using the CA-Markov model in IDRISSI 17.0 to predict the land use of the western Sichuan plateau in 2030 under natural change scenario, and conclude the changes of different land use from 2020 to 2030. The result was displayed in **Table 5**.

From **Table 5**, under the natural change scenario, the area of woodland and built-up land will be further increased from 2020 to 2030, by 2.68 and 0.26% respectively. However, area of cropland, grassland, water body and unused land decreased to varying degrees, particularly the area of grassland and unused land, all of which covered more than 1% of the study area. In terms of transformation, the increased area of built-up land

**TABLE 6 |** Carbon storage of the western Sichuan plateau from 2020 to 2030.

| Types | Cropland | Woodland | Grassland | Water body | Built-up land | Unused land | Total |
|---|---|---|---|---|---|---|---|
| Carbon storage/(106 t) | 193.90 | 5,892.62 | 6,373.29 | 1.12 | 2.75 | 45.25 | 12,508.93 |
| Changing rate/(%) | −0.76 | 2.68 | −1.51 | −0.88 | 0.00 | −1.24 | 0.43 |
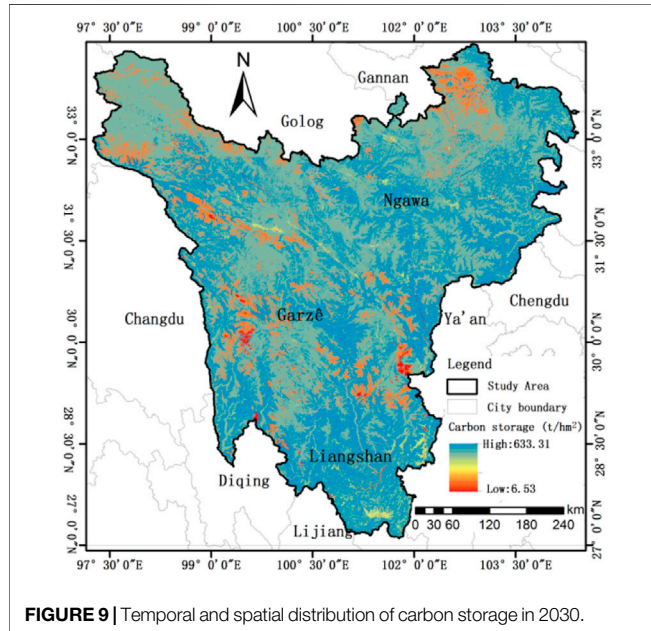


**FIGURE 9 |** Temporal and spatial distribution of carbon storage in 2030.
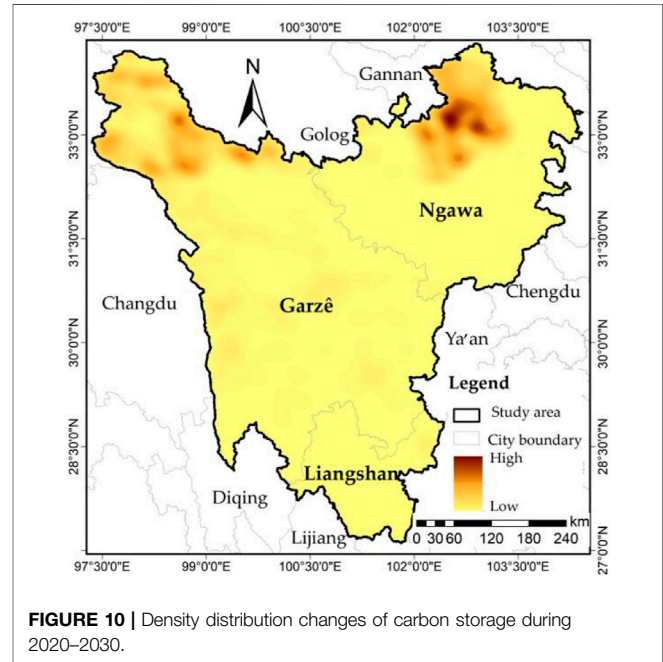


**FIGURE 10 |** Density distribution changes of carbon storage during 2020–2030.

mainly came from cropland, while grassland, water body and unused land were mainly transformed into woodland.

### 3.4.2 Carbon Storage Changes of the Western Sichuan Plateau in 2030

The carbon storage of the Western Sichuan Plateau in 2030 was calculated respectively. Different land use types, the total carbon storage of the study area and the change rate of carbon storage from 2020 to 2030 are shown in **Table 6**.

From **Table 6**, it can be seen that the carbon storage of the Western Sichuan Plateau in 2030 is $1.2509 \times 10^{10}$ t, and the carbon storage increases by $5.2895 \times 10^{7}$ t in 10 years, with an average increase of $5.2895 \times 10^{6}$ t per year, indicating that the carbon storage of the Western Sichuan Plateau is increasing under the background of natural change. In terms of land use types, the carbon storage of cropland, grassland, water body and unused land decreased slightly, while the carbon storage change of built-up land was not obvious, and the carbon storage of woodland increased significantly, which is the main reason for the increase of total carbon storage in the study area from 2020 to 2030.

From the carbon storage spatial distribution of the Western Sichuan Plateau (**Figure 9**), the spatial pattern of carbon storage in 2030 does not change much compared with the period from 1990 to 2020. The high carbon storage areas are still distributed throughout the whole area, while the low carbon storage areas are

distributed in the central, western and northern parts of the study area in a dotted and banded pattern.

The carbon storage distribution map in 2030 was raster processed to calculate the change of each raster from 2020 to 2030. The carbon storage change value greater than 5% is defined as the increase region, less than −5% is defined as the decrease region, and the carbon storage change value between −5 and 5% is defined as no change region. From 2020 to 2030, the decrease region of carbon storage in the Western Sichuan Plateau will be 291.19 ha; the increase region will be 21,518.12 ha and no region will be 25,851,760.68 ha. The Moran's I for calculating the spatial change of carbon storage in the Western Sichuan Plateau at the grid scale is 0.3423 and the value of $p < 0.001$, indicating that there is a positive correlation in the spatial change of carbon storage and a certain regional distribution in space.

From the perspective of the spatial pattern of carbon storage change (**Figure 10**), the increase region of carbon storage is concentrated in Ruoergai County and Hongyuan County in the northeast, and a small amount distributed in Seda County and Shiqu County in the northwest. The decrease region is relatively few and the agglomeration characteristic is not obvious. The main reason lies in that with the conducted desertification control project and the implementation of ecological conservation policy in the

**TABLE 7 |** Ecological service value and changes of the Western Sichuan Plateau in 2030.

| Types | Cropland | Woodland | Grassland | Water body | Built-up land | Unused land | Total |
|---|---|---|---|---|---|---|---|
| ESV/($10^8$ yuan) | 31.0004 | 2,735.7332 | 943.2192 | 304.9363 | 0.0000 | 12.9841 | 4,027.8733 |
| Changing rate/(%) | −0.59 | 0.16 | −0.19 | 7.70 | 0.00 | −0.08 | 0.60 |
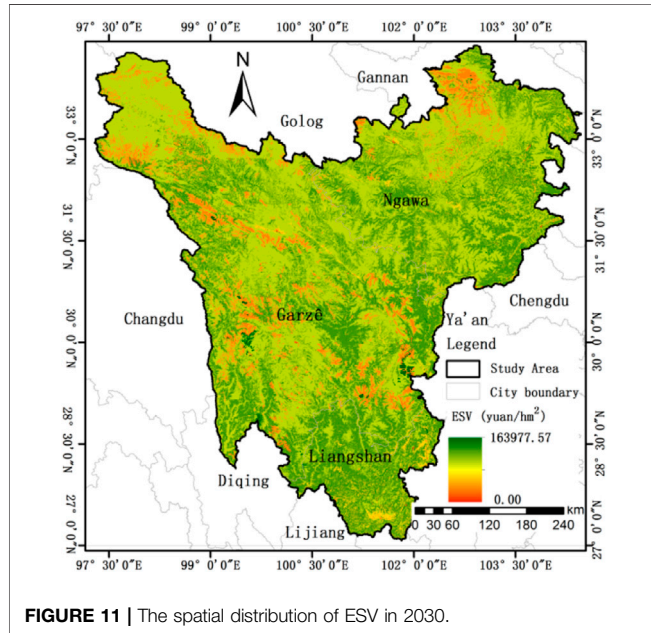


**FIGURE 11 |** The spatial distribution of ESV in 2030.
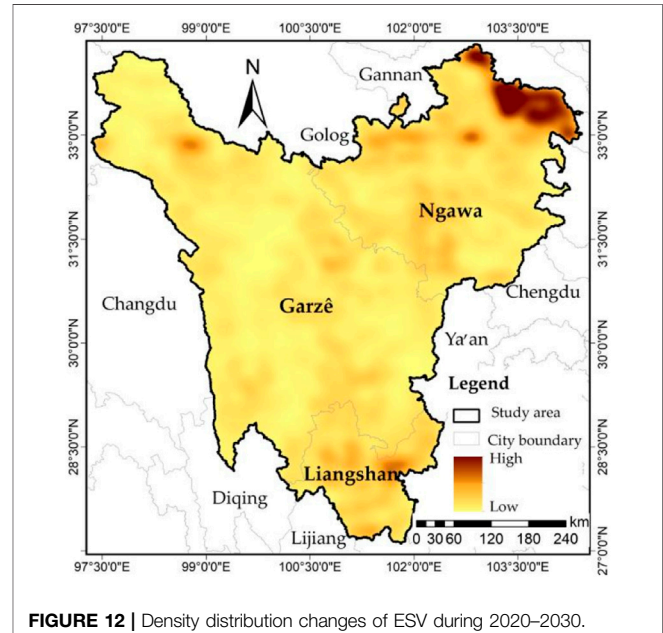


**FIGURE 12 |** Density distribution changes of ESV during 2020–2030.

study area, the desertification issue in Ruoergai County, Hongyuan County, Shiqu County and other key control areas has been significantly addressed. Going forward, the carbon storage capacity of the study area will continue to be enhanced in the future because of the current policies and treatment measures.

### 3.4.3 ESV Change of the Western Sichuan Plateau in 2030

The ESV of the Western Sichuan Plateau in 2030 was calculated respectively. For different land use types, the total ESV of the study area and the change rate of ESV from 2020 to 2030 are shown in **Table 7**.

From **Table 7**, it can be seen that the ESV of the Western Sichuan Plateau in 2030 is 4,027.8733 × $10^8$ yuan, and the ESV increased by 24.0869 × $10^8$ yuan during the period from 2020 to 2030, with an increase of 0.43% and an average annual increase of 2.4087 × $10^8$ yuan, indicating that the ESV in the Western Sichuan Plateau shows an increasing trend under the natural change situation.

From the perspective of the spatial distribution of ESV in the Western Sichuan Plateau (**Figure 11**), the spatial pattern of ESV in 2030 has little change compared with the period from 1990 to 2020. Areas with high ESV is still distributed in the whole region, while areas with low ESV are distributed in the central, western and northeastern part of the study area in a pattern of block and band.

The ESV distribution map in 2030 was raster processed to calculate the change of each raster from 2020 to 2030. The ESV change value greater than 5% is defined as the increase region, less than −5% is defined as the decrease region, and the ESV change value between −5 and 5% is defined as the no change region. From 2020 to 2030, the decrease region of ESV in the Western Sichuan Plateau will be 293.56 ha, while the increase region will be 263,085.13 ha, and no change region will be 25,610,191.3 ha. The Moran's I for calculating the spatial change of ESV in the Western Sichuan Plateau at the grid scale is 0.3779, the value of $p < 0.001$, indicating that there is a positive correlation in the spatial change of ESV and a certain regional distribution in space. From the perspective of the spatial pattern of ESV change (**Figure 12**), the increase region of ESV is concentrated in Ruoergai County and Jiuzhaigou County in the northeast, Shiqu County in the in the northwest and Mianning County, Muli County and Yanyuan County in the south. The decrease area is relatively low, with a point distribution and not obvious agglomeration characteristics. From 2020 to 2030, the increased area of woodland in Jiuzhaigou County, Ruoergai County, Shiqu County and other regions is relatively large. While the contribution from woodland to ESV is much greater than that to carbon storage, which serves as the main reason for the slight difference between the regional spatial pattern of ESV and carbon storage.

# 4 DISCUSSION

Unlike previous works, this study is based on the improved InVEST model and the ESV equivalent factor model of Xie Gaodi to study the ecosystem service function of the Western Sichuan Plateau from carbon storage and ESV and predict their change trends, which will be helpful to improve the accuracy of evaluation results and the practicality of the research results.

From 1990 to 2020, the carbon storage of the Western Sichuan Plateau showed a fluctuating trend of "slow increase-rapid decrease-rapid increase-slow decrease", including two periods of dramatic changes from 1995 to 2000 and from 2005 to 2010. From 1995 to 2000, the carbon storage decreased by $3.0315 \times 10^6$ t annually, which was related to the decrease of forest area and the continuous increase of bare land area caused by long-term logging activities. According to relevant studies, more than $3.5 \times 10^7$ m of timber was cut in the Dadu River and Yalong River basins of the study area between 1958 and the end of the 20th century (Zhou, 2000). From 2005 to 2010, the average annual increase of carbon storage was $5.4150 \times 10^6$ t. Thanks to the implementation of Natural Forest Protection Regulations of Sichuan Province and the Natural Forest Protection Project in 2000, the interference and destruction of ecological system caused by human activities were reduced and forest resources were protected (Lai and Yang, 2018), so that the period from 2005 to 2010 has shown good ecological benefits. It shows that the ecological environmental protection measures, such as close hillsides to facilitate afforestation and return the grain plots to forestry and grass, can effectively promote the restoration and rehabilitation of the regional ecological environment by reducing the disturbance of human activities to the study area.

From 1990 to 2020, the overall trend of ESV is increasing, which can be divided into four stages: "slow increase—slow decrease—rapid increase—slow increase". Similar to the trend of carbon storage change, the two time periods with large changes are 1995–2000 and 2005–2010, but the trend is different after 2010. The overall increase of ESV in the study area from 1990 to 2020 is consistent with the conclusion of relevant studies. Jiang et al. (2020) found that ESV of the Qinghai-Tibet Plateau increased by 2.26% in the past 25 years, mainly due to the large expansion of rivers and lakes and the reduction of bare land and glacier snow cover. The increase of rivers and plateau lakes contributes greatly to the increase of regional ESV, but the carbon storage capacity of water body is very weak, which is one of the reasons for the inconsistent development trend of carbon storage and ESV after 2010.

From 1990 to 2020, the spatial change of carbon storage and ESV in the study area is consistent. The increase region is mainly located in the middle and east of the study area, while the decrease region is mainly located in the northeast and southwest, which are mainly affected by land cover change. Relevant studies have shown that the land use type and degree in the Western Sichuan Plateau have a great impact on carbon storage and ESV (Gascogine et al., 2011; Yang et al., 2014). Over the past few decades, cover changes in Ruoergai County, Jiuzhaigou County and Maoxian County in the northeast and

Litang County in the southwest of the Western Sichuan Plateau have shown an overall decreasing trend (Zheng et al., 2020). At the same time, from 1990 to 2020, the population of the study area increased by 714,600 human settlements continued to expand, and production activities such as grazing intensified. As a result, the area of built-up land and water body (mainly the increase in water storage area caused by power stations) increased by 141.38 and 44.11% respectively. Centralized grazing near the settlement intensifies grassland degradation, while the West Sichuan Plateau has a low temperature, low accumulated temperature and long recovery cycle after the destruction of grassland and woodland (Zhang et al., 2020).

The CA-Markov model was used to predict the land use of the Western Sichuan Plateau in 2030. In line with the current development trend, the carbon storage and ESV in the study area will increase by $2.4807 \times 10^6$ t and $5.3980 \times 10^9$ yuan respectively in the next decade, indicating an overall positive development of ecological environment. The main reason for the enhancement of ecosystem services was that land was developed to woodland. It indicates that strengthening the construction of key ecological function areas and biodiversity protection in the Western Sichuan Plateau, enhancing the protection and management of public welfare forests, natural forests and grassland resources, promoting the rehabilitation of sandy land, degraded alpine wetlands and river wetlands and the restoration degraded grasslands will consolidate and enhance the functional benefits of the ecosystem in the Western Sichuan Plateau.

# 5 CONCLUSION

In this study, the CA-Markov model was employed to predict the land use pattern under natural change scenarios, and the improved InVEST model and equivalent method were used to evaluate the ecosystem services in the study area from two different perspectives. From 1990 to 2020, the carbon stock of the western Sichuan Plateau showed an overall fluctuating increase. While it reflected relatively dramatic during 1995–2000 and 2005–2010. The contribution rate to total carbon storage in the study area arranged from high to low: grassland, woodland, cropland, unused land, built-up land and water body. The spatial carbon storage change in the past three decades hasn't changed much in Western Sichuan Plateau. The changed areas are scattered and dotted in general, and relatively concentrated in the east and southwest.

In the past three decades, the ESV increases are similar to carbon stocks, showing an overall wave-like increase trend. The ESV in 2005–2010 and 2015–2020 showed relatively dramatic changes due to water body, and was slightly different from the change trend of carbon storage. The contribution to regional ESV arranges from high to low: woodland, grassland, water body, cropland, unused land and built-up land. Woodland is the land with the highest contribution rate. From the spatial distribution of ESV, the overall spatial characteristics are "high in the south and the east but low in the north and the west". Areas with

relatively obvious changes, mainly located in the northeast and southwest of the study area, are caused by human activities and natural disasters.

Ecosystem services in the western Sichuan plateau present positive growth under current ecological conservation measures. To pursue a high-standard regional development, efforts must be intensified to stay regional ecological conservation above the red line, reasonably control the coverage area of built-up land and keep ecosystem stable.

This paper discussed the changing characteristics of ecosystem services in the Western Sichuan Plateau from two perspectives, further investigation is necessary. The simulation accuracy of LUCC needs to be further enhanced in light of the actual conditions and limiting factors in the study area. The carbon density value should also be verified with measured data to provide data basis for accurate estimation of carbon storage.

## DATA AVAILABILITY STATEMENT

The original contributions presented in the study are included in the article/Supplementary Material, further inquiries can be directed to the corresponding author.

## AUTHOR CONTRIBUTIONS

Research design and analysis: MX and JY; Experiment: WL; Manuscript: MX and YS; Investigation and validation: CW; Data curation: YL; Supported the data preparation: ML; Interpretation of the results: YT. All authors have read and agreed to the published version of the manuscript.

## REFERENCES

Alam, S. A., Starr, M., and Clark, B. J. F. (2013). Tree Biomass and Soil Organic Carbon Densities across the Sudanese woodland savannah: A Regional Carbon Sequestration Study. *J. Arid Environments* 89, 67–76. doi:10.1016/j.jaridenv.2012.10.002

Chen, L., Liu, G., and Li, H. (2002). Estimating Net Primary Productivity of Terrestrial Vegetation in China Using Remote Sensing. *Natl. Remote Sensing Bull.* 6 (2), 129–135. doi:10.1088/1009-1963/11/5/313

Chen, G., Yang, Y., Liu, L., Li, X., Zhao, Y., and Yuan, Y. (2007). Research Review on Total below Ground Carbon Allocation in Forest Ecosystems. *J. Subtropical Resour. Environ.* 2 (01), 34–42. doi:10.1007/s11461-007-0044-x

Chuai, X., Huang, X., Lai, L., Wang, W., Peng, J., and Zhao, R. (2013). Land Use Structure Optimization Based on Carbon Storage in Several Regional Terrestrial Ecosystems across China. *Environ. Sci. Pol.* 25, 50–61. doi:10.1016/j.envsci.2012.05.005

Costanza, R., d'Arge, R., de Groot, R., Farber, S., Grasso, M., Hannon, B., et al. (1997). The Value of the World's Ecosystem Services and Natural Capital. *Nature* 387 (6630), 253–260. doi:10.1038/387253a0

Costanza, R., de Groot, R., Sutton, P., van der Ploeg, S., Anderson, S. J., Kubiszewski, I., et al. (2014). Changes in the Global Value of Ecosystem Services. *Glob. Environ. Change* 26, 152–158. doi:10.1016/j.gloenvcha.2014.04.002

Dai, X., Johnson, B. A., Luo, P., Yang, K., Dong, L., Wang, Q., et al. (2021). Estimation of Urban Ecosystem Services Value: A Case Study of Chengdu, Southwestern China. *Remote Sensing* 13 (2), 207. doi:10.3390/RS13020207

Fang, F., Feng, J., Li, F., and Peng, S. (2017). Impacts of the north Migration of China's rice Production on its Ecosystem Service Value during the Last Three Decades (1980-2014). *J. Integr. Agric.* 16 (01), 76–84. CNKI:SUN: ZGNX.0.2017-01-009. doi:10.1016/s2095-3119(16)61360-6

Firozjaei, M. K., Sedighi, A., Argany, M., Jelokhani-Niaraki, M., and Arsanjani, J. J. (2019). A Geographical Direction-Based Approach for Capturing the Local Variation of Urban Expansion in the Application of CA-Markov Model. *Cities* 93, 120–135. doi:10.1016/j.cities.2019.05.001

Fu, Q., Xu, L., Zheng, H., and Chen, J. (2019). Spatiotemporal Dynamics of Carbon Storage in Response to Urbanization: A Case Study in the Su-Xi-Chang Region, China. *Processes* 7 (11), 836–854. doi:10.3390/pr7110836

Gaglio, M., Aschonitis, V., Pieretti, L., Santos, L., Gissi, E., Castaldelli, G., et al. (2019). Modelling Past, Present and Future Ecosystem Services Supply in a

Protected Floodplain under Land Use and Climate Changes. *Ecol. Model.* 403, 23–34. doi:10.1016/j.ecolmodel.2019.04.019

Gao, X., Wang, J., Li, C., Shen, W., Song, Z., Nie, C., et al. (2021). Land Use Change Simulation and Spatial Analysis of Ecosystem Service Value in Shijiazhuang under Multi-Scenarios. *Environ. Sci. Pollut. Res.* 28 (24), 31043–31058. doi:10.1007/s11356-021-12826-9

Gascoigne, W. R., Hoag, D., Koontz, L., Tangen, B. A., Shaffer, T. L., and Gleason, R. A. (2011). Valuing Ecosystem and Economic Services across Land-Use Scenarios in the Prairie Pothole Region of the Dakotas, USA. *Ecol. Econ.* 70 (10), 1715–1725. doi:10.1016/j.ecolecon.2011.04.010

Gashaw, T., Tulu, T., Argaw, M., Worqlul, A. W., Tolessa, T., and Kindu, M. (2018). Estimating the Impacts of Land Use/land Cover Changes on Ecosystem Service Values: The Case of the Andassa Watershed in the Upper Blue Nile basin of Ethiopia. *Ecosystem Serv.* 31, 219–228. doi:10.1016/j.ecoser.2018.05.001

Giardina, C. P., and Ryan, M. G. (2000). Evidence that Decomposition Rates of Organic Carbon in mineral Soil Do Not Vary with Temperature. *Nature* 404 (6780), 858–861. doi:10.1038/35009076

He, C., Zhang, D., Huang, Q., and Zhao, Y. (2016). Assessing the Potential Impacts of Urban Expansion on Regional Carbon Storage by Linking the LUSD-Urban and InVEST Models. *Environ. Model. Softw.* 75, 44–58. doi:10.1016/j.envsoft.2015.09.015

He, C., Jin, J., Zhang, H., and Yuan, J. (2021). The Change of Ecological Service Value and the Promotion Mode of Ecological Function in Mountain Development Using InVEST Model. *Arab J. Geosci.* 14 (6), 510. doi:10.1007/s12517-021-06869-y

Hou, H., Dai, E., and Zhang, M. (2018). A Review on InVEST Model for the Evaluation of Ecosystem Service Function. *J. Capital Normal Univ. (Natural Sci. Edition)* 39 (4), 62–67. doi:10.19789/j.1004-9398.2018.04.012

Houghton, R. A. (2003). Revised Estimates of the Annual Net Flux of Carbon to the Atmosphere from Changes in Land Use and Land Management 1850-2000. *Tellus B* 55 (2), 378–390. doi:10.1034/j.1600-0889.2003.01450.x

Jiang, W., Deng, Y., Tang, Z., Lei, X., and Chen, Z. (2017). Modelling the Potential Impacts of Urban Ecosystem Changes on Carbon Storage under Different Scenarios by Linking the CLUE-S and the InVEST Models. *Ecol. Model.* 345, 30–40. doi:10.1016/j.ecolmodel.2016.12.002

Jiang, W., Lü, Y., Liu, Y., and Gao, W. (2020). Ecosystem Service Value of the Qinghai-Tibet Plateau Significantly Increased during 25 Years. *Ecosystem Serv.* 44, 101146. doi:10.1016/j.ecoser.2020.101146

Lai, J., and Yang, W. (2018). Dynamic Changes of Vegetation Cover in Natural forest Area of Western Sichuan in Recent 29 Years Based on RS. *Remote Sensing Land Resour.* 30 (4), 132–138. doi:10.6046/gtzyyg.2018.04.20

Lei, W., Yang, W., and University, P. (2012). An ANN-CA Modeling Method for Land Cover Change in the Karst Area of China: A Case Study of Maotiao River Basin. *Acta Scientiarum Naturalium Universitatis Pekinensis* 48 (1), 111–122. doi:10.13209/j.0479-8023.2012.015

Lei, J., Chen, Z., Chen, X., Li, Y., and Wu, T. (2020). Spatio-temporal Changes of Land Use and Ecosystem Services Value in Hainan Island from 1980 to 2018. *Acta Ecologica Sinica* 40 (14), 4760–4773. doi:10.1111/j.1538-4632.1995.tb00338.x

Li, X., and Yeh, A. (2005). Cellular Automata for Simulating Complex Land Use Systems Using Neural Networks. *Geographical Res.* 24 (1), 19–27. doi:10.3321/j.issn:1000-0585.2005.01.003

Li, K., Wang, S., and Cao, M. (2003). Carbon Stocks of Soil and Vegetation in China. *Scientia Sinica(Terrae).* 33 (1), 72–80. CNKI:SUN:JDXK.0.2003-01-007.

Li, K., Cao, J., Adamowski, J. F., Biswas, A., Zhou, J., Liu, Y., et al. (2021). Assessing the Effects of Ecological Engineering on Spatiotemporal Dynamics of Carbon Storage from 2000 to 2016 in the Loess Plateau Area Using the InVEST Model: A Case Study in Huining County, China. *Environ. Dev.* 39, 100641. doi:10.1016/j.envdev.2021.100641

Liu, Y., Wang, Y., Peng, J., Yuan, Y., Ma, J., and Wei, H. (2015). Selection of Different Clustering Algorithms for Settlement Landscape Aggregation in Suburb. *Scientla Geogr. Aphica Sinica* 35 (6), 674–682. doi:10.1016/j.chnaes.2015.06.005

Liu, J., Ren, H., Wang, X., Shirazi, Z., and Quan, B. (2019). Measuring and Predicting Urban Expansion in the Angkor Region of Cambodia. *Remote Sensing* 11 (17), 2064–2084. doi:10.3390/rs11172064

Liu, M., Zhang, Z., Sun, J., Wang, Y., Wang, J., Tsunekawa, A., et al. (2020). One-year Grazing Exclusion Remarkably Restores Degraded alpine Meadow at Zoige, Eastern Tibetan Plateau. *Glob. Ecol. Conservation* 22, e00951. doi:10.1016/j.gecco.2020.e00951

Liu, Y., Zhang, J., Zhou, D., Ma, J., Dang, R., Ma, J., et al. (2021). Temporal and Spatial Variation of Carbon Storage in the Shule River Basin Based on InVEST Model. *Acta Eco Sin* 41 (10), 4052–4065. doi:10.5846/stxb201911152452

Matlhodi, B., Kenabatho, P. K., Parida, B. P., and Maphanyane, J. G. (2021). Analysis of the Future Land Use Land Cover Changes in the Gaborone Dam Catchment Using CA-Markov Model: Implications on Water Resources. *Remote Sensing* 13 (13), 2427. doi:10.3390/RS13132427

Nasehi, S., Imanpour namin, A., and Salehi, E. (2019). Simulation of Land Cover Changes in Urban Area Using CA-MARKOV Model (Case Study: Zone 2 in Tehran, Iran). *Model. Earth Syst. Environ.* 5 (1), 193–202. doi:10.1007/s40808-018-0527-9

Nigussie, T. A., and Altunkaynak, A. (2016). Assessing the Hydrological Response of Ayamama Watershed from Urbanization Predicted under Various Landuse Policy Scenarios. *Water Resour. Manage.* 30 (10), 3427–3441. doi:10.1007/s11269-016-1360-4

Nigussie, T. A., and Altunkaynak, A. (2019). Modeling the Effect of Urbanization on Flood Risk in Ayamama Watershed, Istanbul, Turkey, Using the MIKE 21 FM Model. *Nat. Hazards* 99 (2), 1031–1047. doi:10.1007/s11069-019-03794-y

Raich, J. W., and Nadelhoffer, K. J. (1989). Belowground Carbon Allocation in Forest Ecosystems: Global Trends. *Ecology* 70 (5), 1346–1354. doi:10.2307/1938194

Sang, L., Zhang, C., Yang, J., Zhu, D., and Yun, W. (2010). Simulation of Land Use Spatial Pattern of Towns and Villages Based on CA–Markov Model. *Math. Comp. Model.* 54 (3), 938–943. doi:10.1016/j.mcm.2010.11.019

Temesgen, H., Wu, W., Shi, X., Yirsaw, E., Bekele, B., and Kindu, M. (2018). Variation in Ecosystem Service Values in an Agroforestry Dominated Landscape in Ethiopia: Implications for Land Use and Conservation Policy. *Sustainability* 10 (4), 1126. doi:10.3390/su10041126

Tian, Y., and Ren, Z. (2012). Land Use Change Simulations in Loess Hilly Areas Based on CLUE-S Model: A Case Study in Xianyang Loess Tableland Areas of Shaanxi Province. *Prog. Geog.* 31 (9), 1224–1234. doi:10.11820/dlkxjz.2012.09.014

Vizcaíno-Bravo, Q., Williams-Linera, G., and Asbjornsen, H. (2020). Biodiversity and Carbon Storage Are Correlated along a Land Use Intensity Gradient in a Tropical Montane forest Watershed, Mexico. *Basic Appl. Ecol.* 44, 24–34. doi:10.1016/j.baae.2019.12.004

Wang, R., Hou, H., Murayama, Y., and Derdouri, A. (2020). Spatiotemporal Analysis of Land Use/Cover Patterns and Their Relationship with Land Surface Temperature in Nanjing, China. *Remote Sensing* 12 (3), 440. doi:10.3390/rs12030440

Wang, Q. H., Kalantar-Zadeh, K., Kis, A., Coleman, J. N., and Strano, M. S. (2021). Electronics and Optoelectronics of Two-Dimensional Transition Metal Dichalcogenides. *Nat. Nanotechnol* 7 (11), 699–712. doi:10.1038/nnano.2012.193

Wickramasuriya, R. C., Bregt, A. K., van Delden, H., and Hagen-Zanker, A. (2009). The Dynamics of Shifting Cultivation Captured in an Extended Constrained Cellular Automata Land Use Model. *Ecol. Model.* 220 (18), 2302–2309. doi:10.1016/j.ecolmodel.2009.05.021

Wu, L., Wang, H., Shao, H., and Zhou, S. (2021). Spatiotemporal Pattern of Vegetation and its Response to Climate Change in the Western Sichuan Plateau. *Res. Soil Water Conservation* 28 (1), 171–178. doi:10.13869/j.cnki.rswc.20200722.001

Xie, G., Lu, C., Leng, Y., Zheng, D., and Li, S. (2003). Ecological Assets Valuation of the Tibetan Plateau. *J. Nat. Resour.* 18 (2), 189–196. doi:10.11849/zrzyxb.2003.02.010

Xie, X., Sun, B., Zhou, H., Li, Z., and Li, A. (2004). Estimation and Spatial Distribution of Soil Organic Carbon Density and Content in China. *Acta Pedologica Sinica* 41 (1), 35–43. doi:10.11766/trxb200301140106

Xie, G., Zhang, C., Zhang, L., Chen, W., and Li, S. (2015). Improvement of the Evaluation Method for Ecosystem Service Value Based on Per Unit Area. *J. Nat. Resour.* 30 (08), 1243–1254. doi:10.11849/zrzyxb.2015.08.001

Yang, S., Li, T., Gan, Y., Wang, Y., Ji, L., Song, Z., et al. (2014). Impact of Different Use Patterns and Degrees of Grassland Use on Vegetation Carbon Storage in the Aba Grassl and Pastoral Area. *Acta Prataculturae Sinica* 23 (3), 325–332. doi:10.11686/cyxb20140338

Yang, J., Xie, B., and Zhang, D. (2021). Spatio-temporal Evolution of Carbon Stocks in the Yellow River Basin Based on in VEST and CA-Markov Models. *Chin. J. Eco-Agriculture* 29 (6), 1018–1029. doi:10.13930/j.cnki.cjea.200746

Ye, Y., and Zhang, J. (2008). Impact of Land-Use Changes on the Ecosystem Service Value in Guangzhou City. *Ecologic Sci.* 27 (02), 119–123. CNKI:SUN:STKX.0.2008-02-014.

Zhang, G., Guhathakurta, S., Lee, S., Moore, A., and Yan, L. (2014). Grid-Based Land-Use Composition and Configuration Optimization for Watershed Stormwater Management. *Water Resour. Manage.* 28 (10), 2867–2883. doi:10.1007/s11269-014-0642-y

Zhang, X., Zhou, Q., Wang, Z., and Wang, F. (2017). Simulation and Prediction of Land Use Change in Three Gorges Reservoir Area Based on MCE-CA-Markov. *Trans. Chin. Soc. Agric. Eng.* 33 (19), 268–277. doi:10.11975/j.issn.1002-6819.2017.19.035

Zhang, J., Li, M., Ao, Z., Deng, M., Yang, C., and Wu, Y. (2018). Estimation of Soil Organic Carbon Storage of Terrestrial Ecosystem in Arid Western China. *J. Arid Land Resour. Enviroment* 32 (09), 132–137. doi:10.13448/j.cnki.jalre.2018.280

Zhang, J., Cui, X., Wang, Y., Gongbuzeren Zhuang, M., and Ji, B. (2020). Ecological Consequence of Nomad Settlement Policy in the Pasture Area of Qinghai-Tibetan Plateau: From Plant and Soil Perspectives. *J. Environ. Manage.* 260, 110114. doi:10.1016/j.jenvman.2020.110114

Zhang, J., Li, Q., Wu, X., Zhang, C., Wang, J., and Wu, G. (2021). Evolution of the Ecosystem Services Value and Carrying Capacity in the Guangdong-Hong Kong-Macao Greater Bay Area Based on Land Use Changes. *Acta Eco Sin* 41 (21), 1–12. doi:10.5846/stxb202007141841

Zhao, M., He, Z., Du, J., Chen, L., Lin, P., and Fang, S. (2019). Assessing the Effects of Ecological Engineering on Carbon Storage by Linking the CA-Markov and InVEST Models. *Ecol. Indicators* 98, 29–38. doi:10.1016/j.ecolind.2018.10.052

Zheng, Y., Yang, W., and Liu, C. (2020). Dynamic Monitoring and Driving Force Analysis of Vegetation Cover Change in Western Sichuan Plateau in Recent 20 Years. *Remote Sensing Tech. Appl.* 35 (6), 1447–1456. doi:10.11873/j.issn.1004-0323.2020.6.1447

Zhong, D., Sun, M., Zhang, Y., Yu, W., and Yang, C. (2021). Spatio - Temporal Variation and Influencing Factors of Snow Cover in WestSichuan Plateau from 2001 to 2020. *J. Arid Land Resour. Environ.* 35 (11), 111–118. doi:10.13448/j.cnki.jalre.2021.305

Zhou, J., Wu, J., and Gong, Y. (2020). Valuing Wetland Ecosystem Services Based on Benefit Transfer: A Meta-Analysis of China Wetland Studies. *J. Clean. Prod.* 276, 122988. doi:10.1016/j.jclepro.2020.122988

Zhou, X. (2000). Policy Choices for Backward Development—Investigation and Thinking on the Economic and Social Conditions After the Implementation of the Natural Forest Logging Ban in Ganzi Prefecture, Sichuan Province (Part 2). *J. Southwest Univ. Nationalities (Philosophy Soc. Sciences)* 21 (8), 1–7.

**Conflict of Interest:** The authors declare that the research was conducted in the absence of any commercial or financial relationships that could be construed as a potential conflict of interest.

Check for updates

# Integrating Ecosystem Services Into Assessments of Sustainable Development Goals: A Case Study of the Beijing-Tianjin-Hebei Region, China

Siwei Hu[1,2†], Yanying Yang[1,3*†], Ang Li[1,2], Kai Liu[1,2], Changhong Mi[1] and Rongguang Shi[1,3*]

[1]Agro-Environmental Protection Institute, Ministry of Agriculture and Rural Affairs, Tianjin, China, [2]Graduate School of Chinese Academy of Agricultural Sciences, Beijing, China, [3]Key Laboratory for Environmental Factors Control of Agro-Product Quality Safety, Ministry of Agriculture and Rural Affairs, Tianjin, China

Trade-offs between eco-environment protection and socioeconomic development hinder the success of sustainable development goals (SDGs). Solutions based on ecosystem services (ESs) provide the co-benefits and pathways for fulfilling the SDGs. However, assessing the progress towards SDGs based on the contribution of ESs to SDGs is lacking. Here we assessed the **s**patial-temporal changes of ecosystem service values (ESV) and the SDG scores in the Beijing-Tianjin-Hebei region (BTH) over the past 20 years using "ES-SDG linkages." The total ESV and ES-SDG Index score in the BTH showed a spatial pattern of high values in the northern plateau and low values in the southern plain. The total ESV increased from 25,335 yuan ha$^{-1}$ in 2000 to 27,344 yuan ha$^{-1}$ in 2020, mainly attributed to water provision and water regulation. The decrease of cropland, grassland, and wetland in the BTH between 2000 and 2010 caused a decrease in the value of nine ESs, whereas the increase of forestland, waterbodies and wetland between 2010 and 2020 contributed to an increase in the value of seven ESs. The ES-SDG Index score decreased slightly from 36.8 in 2000 to 35.5 in 2010, and then increased to 36.0 in 2020 due to the control of rapid urbanization and strengthen of ecological restoration. Our study indicates that the changes of ES-SDG Index score mainly depended on food provision, water provision, climate regulation, nutrient cycling, habitat & biodiversity, and cultural services. The assessment of SDGs suggests that SDG6, SDG11, and SDG12 should be prioritized to advance the synergistic development of SDGs in the BTH, which will also enhance the understanding of stakeholders about the progress of achieving SDGs.

**Keywords: ecosystem service values, sustainable development goals, urbanization, ecological restoration, land-use management**

# 1 INTRODUCTION

Ecosystem services (ESs) are the foundation of human well-being and sustainable development (Costanza et al., 2016; Geijzendorffer et al., 2017; Wood et al., 2018). The interactions among ESs, human well-being, and sustainable development have become one of the core issues in sustainability science (Wu, 2013; Guerry et al., 2015; Fu, 2020). Since 17 sustainable development goals (SDGs) and 169 targets incorporating economic, social, and environmental dimensions of sustainability were proposed by the United Nations in 2015, most countries have made considerable progress towards achieving those SDGs, especially in terms of the elements of socioeconomic development (Sachs et al., 2021). However, much progress made in socioeconomic development was based on the unsustainable exploitation of nature. Approximately 60% of ESs have been degraded globally (MA, 2005). Fourteen of the 18 categories of nature's contributions to people (NCP) have declined (IPBES, 2019). Biodiversity loss and ecosystem fragmentation have threatened the realization of 80% of the SDG targets (UNEP, 2021). Despite human activities having created substantial wealth by exploiting ecosystems intensively, it is difficult to compensate for the lost benefits caused by eco-environment deterioration (Wood et al., 2018; Yin et al., 2021). Achieving the SDGs was hindered by trade-offs between eco-environmental protection and human well-being (Yang et al., 2020).

Numerous studies have quantitatively evaluated the performance of SDGs through environmental and socioeconomic indicators (Schmidt-Traub et al., 2017; Xu et al., 2020; Huan et al., 2021; Zhang et al., 2022b). However, ES indicators were rarely considered in SDG assessment (Cochran et al., 2020; Pires et al., 2021). ES-based solutions with comprehensive consideration of land management, ecological restoration, and human well-being can offer co-benefits and pathways for the fulfillment of the SDGs (Keesstra et al., 2018; Johnson et al., 2019; Yang et al., 2020; Liu et al., 2022). Existing studies have linked ESs with SDGs systematically mainly through expert survey and network analysis. A science-policy tool using a Delphi process was developed to prioritize NCP-SDG bundles (Anderson et al., 2019). Online surveys that gather expert views on the importance of ESs to achieving the SDGs were conducted to evaluate the strengths of the SDG-ES relations (Wood et al., 2018; Yang et al., 2020). Network analysis was used to unravel the relationship between cryosphere services and SDGs based on the chain of causal effects and cascading effects (Zhang et al., 2022a). Additionally, bibliometric network analysis was also applied to explore the connections between ESs and SDGs (Hawken et al., 2021).

Twelve SDGs and 41 targets were identified to be closely related to 16 ESs (Wood et al., 2018). Food provision, water provision, carbon storage, and habitat & biodiversity were recognized as critical services contributing to >14 SDG targets, especially in SDG6 (Clean Water and Sanitation), SDG13 (Climate Action), SDG14 (Life Below Water), and SDG15 (Life on Land) (Wood et al., 2018; Yang et al., 2020). Water

provision, water regulation, climate regulation and research & education among the cryosphere services were found to have strong contributions to SDG1 (No Poverty), SDG 2 (Zero Hunger), SDG 6 (Clean Water), SDG11 (Sustainable Cities and Communities), SDG12 (Responsible Production and Consumption) and SDG15 (Life on Land) (Zhang et al., 2022a). Different types of ESs contribute different amounts to SDGs. Even a single ES may benefit multiple SDGs, e.g. soil conservation is perceived to benefit SDG6 (Clean Water and Sanitation), SDG13 (Climate Action), and SDG15 (Life on Land) (Yin et al., 2022). Improved food provision contributed to SDG1 (No Poverty), SDG2 (Zero Hunger), and SDG13 (Climate Action), whereas, under scenarios tested in the Volta basin, losses in other ESs such as erosion control had negative consequences toward SDG15 (Life on Land), SDG6 (Clean Water), and SDG3 (Good Health) (Johnson et al., 2019). These all showed strong linkages between ESs and SDGs. However, few studies have assessed the progress of SDGs through the ES-SDG linkages. Therefore, it is vital to integrate ESs into the assessment of SDGs in order to identify critical ESs and SDGs for decision-making.

The Beijing-Tianjin-Hebei region (BTH) is one of the most developed areas in Northern China (Zhou et al., 2018). Socioeconomic development progressed considerably in the BTH over recent decades. The proportion of urban population has grown from 39% to 69%, the area of construction land has grown 57%, and GDP has grown 8-fold between 2000 and 2020 (National Bureau of Statistics of China, 2001; National Bureau of Statistics of China, 2021). However, environmental problems such as sandstorms, air pollution, water pollution, and soil erosion have also placed considerable pressure on the BTH (Yang et al., 2019b). Eco-environment protection has been strengthened since 2010. The rate of land urbanization has been controlled (Tian et al., 2020). Previous studies found that some important ESs such as sandstorm prevention and water retention have been improved in the BTH, and the SDG Index score continuously increased over this period (Ouyang et al., 2016; Wang et al., 2019; Xu et al., 2020). However, how the changes in ESV affect the achievement of SDGs in the BTH is still unclear. Here we analyzed the spatial-temporal changes of the value of 11 ESs and the ESV in the BTH at the county level from 2000 to 2020. Twelve SDG and ES-SDG Index scores were assessed based on the "ES-SDG linkages" (Wood et al., 2018). Critical ESs and SDGs were identified to inform land-use management and sustainable development in the BTH and other regions.

# 2 MATERIALS AND METHODS

## 2.1 Study Area
BTH is located in northeastern China between 36°05′–42°40′N and 113°27′–119°50′E (**Figure 1**). It comprises 13 cities and covers an area of about 218,000 km². BTH has a population of 110.37 million and a gross domestic product (GDP) of 8,639.32 billion yuan, accounting for 7.8% and 8.5% of the total Chinese population and GDP, respectively, in 2020. The
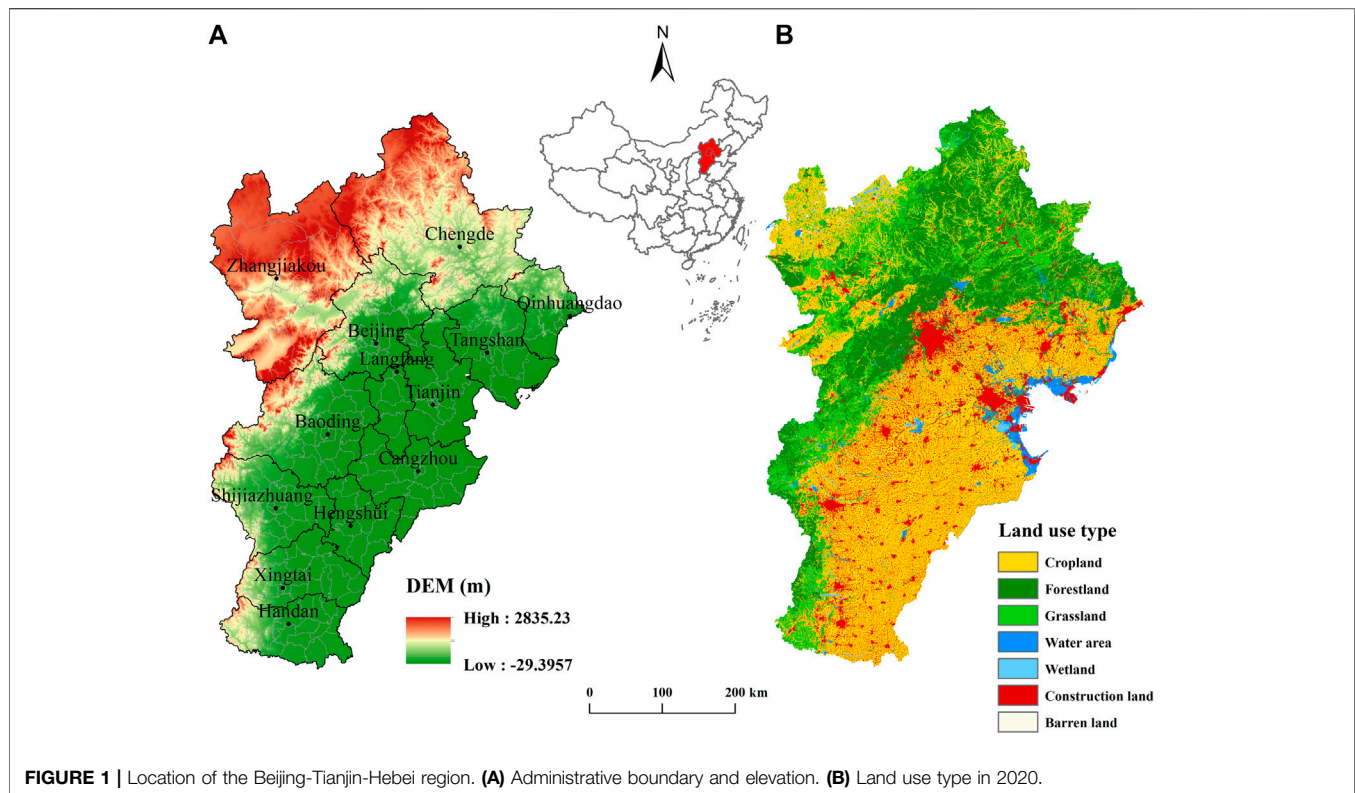
**FIGURE 1** | Location of the Beijing-Tianjin-Hebei region. **(A)** Administrative boundary and elevation. **(B)** Land use type in 2020.

geographical elevation descends from the northwest to the southeast. A variety of ecosystem types can be found in the BTH. Forestland and grassland, accounting for 21% and 16% of the total land area of BTH, respectively, are mainly distributed in the north and west where there is the Bashang Plateau, and the Yanshan and Taihang Mountains. The southeast is a wide plain where cropland (46%) predominates, whereas water areas and wetlands (4%) are mainly distributed in the alluvial coastal plain near the Bohai Sea. The study area was determined to be 153 counties (districts) excluding municipal district in the BTH.

## 2.2 Quantifying and Mapping ESV

Many studies have been performed on the evaluation of ESV (Costanza et al., 1997; de Groot et al., 2012; Gashaw et al., 2018). The equivalent factor method (Xie et al., 2003; Xie et al., 2017), based on a survey of 500 Chinese ecological experts, is widely used in ESV evaluations in China (Jiang et al., 2021). The method classifies ESs into 11 types: food provision (FP), raw material (RM), water provision (WP), air quality regulation (AQR), climate regulation (CR), waste treatment (WT), water regulation (WR), erosion prevention (EP), nutrient cycling (NC), habitat & biodiversity (HB), and cultural services (CS). The economic value of the standard equivalent factor for ESV is equal to 1/7th of the market value of national average food crops output per unit area (Hu et al., 2021). The area, yield, and price of the crops in 2020 were selected to calculate the economic value of the standard equivalent factor. The equation is as follows:

$$VC_0 = \frac{1}{7} \sum_{i=1}^{n} \frac{p_i q_i}{m} \ (n = 1, 2, 3) \tag{1}$$

where $VC_0$ is the economic value of the standard equivalent factor for ESV per unit area, n is the different crops (rice, wheat, and corn), $p_i$ is the yield of different crops, $q_i$ is the price of different crops, and m is the total area of all crops.

The calculation result of $VC_0$ in the BTH was 2406.5 yuan ha$^{-1}$. The value of individual ESs and the total ESV were calculated based on the following equation and mapped using ArcGIS10.7.

$$AESV_f = \frac{\sum \left( A_k \times VC_0 \times EC_{fk} \right)}{S} \tag{2}$$

$$AESV = \sum_{f=1}^{n} AESV_f \ (n = 1, 2, \ldots, 11) \tag{3}$$

where $AESV_f$ and AESV refer to the value of ES type "f" and the total ESV per unit area, $A_k$ is the area for the land-use "k," $EC_{fk}$ is the equivalent coefficient for land-use "k" and ES type "f," and S is the total land-use area. Given the different land-use types in the BTH, the equivalent coefficients for each ESV per unit area were listed in **Table 1** (Xie et al., 2017).

## 2.3 Scoring ES-SDG Index

The ESV were standardized on a scale of 0–100 using min-max normalization.

$$AESV'_f = \frac{AESV_f - min\left(AESV_f\right)}{max\left(AESV_f\right) - min\left(AESV_f\right)} \times 100 \tag{4}$$

TABLE 1 | The equivalent coefficients for ecosystem service value per unit area in the Beijing-Tianjin-Hebei region.

| Ecosystem classification | Farmland | | Forest | | Grassland | | Wetland | Barren land | | Water area |
|---|---|---|---|---|---|---|---|---|---|---|
| | Dry land | Paddy field | Broad-leaved | Bush | Prairie | Meadow | Wetland | Desert | Barren | Water |
| Food provision | 0.85 | 1.36 | 0.29 | 0.19 | 0.10 | 0.22 | 0.51 | 0.01 | 0.00 | 0.80 |
| Raw material | 0.40 | 0.09 | 0.66 | 0.43 | 0.14 | 0.33 | 0.50 | 0.03 | 0.00 | 0.23 |
| Water provision | 0.02 | −2.63 | 0.34 | 0.22 | 0.08 | 0.18 | 2.59 | 0.02 | 0.00 | 8.29 |
| Air quality regulation | 0.67 | 1.11 | 2.17 | 1.41 | 0.51 | 1.14 | 1.90 | 0.11 | 0.02 | 0.77 |
| Climate regulation | 0.36 | 0.57 | 6.50 | 4.23 | 1.34 | 3.02 | 3.60 | 0.10 | 0.00 | 2.29 |
| Waste treatment | 0.10 | 0.17 | 1.93 | 1.28 | 0.44 | 1.00 | 3.60 | 0.31 | 0.10 | 5.55 |
| Water regulation | 0.27 | 2.72 | 4.74 | 3.35 | 0.98 | 2.21 | 24.23 | 0.21 | 0.03 | 102.24 |
| Erosion prevention | 1.03 | 0.01 | 2.65 | 1.72 | 0.62 | 1.39 | 2.31 | 0.13 | 0.02 | 0.93 |
| Nutrient cycling | 0.12 | 0.19 | 0.20 | 0.13 | 0.05 | 0.11 | 0.18 | 0.01 | 0.00 | 0.07 |
| Habitat and biodiversity | 0.13 | 0.21 | 2.41 | 1.57 | 0.56 | 1.27 | 7.87 | 0.12 | 0.02 | 2.55 |
| Cultural services | 0.06 | 0.09 | 1.06 | 0.69 | 0.25 | 0.56 | 4.73 | 0.05 | 0.01 | 1.89 |
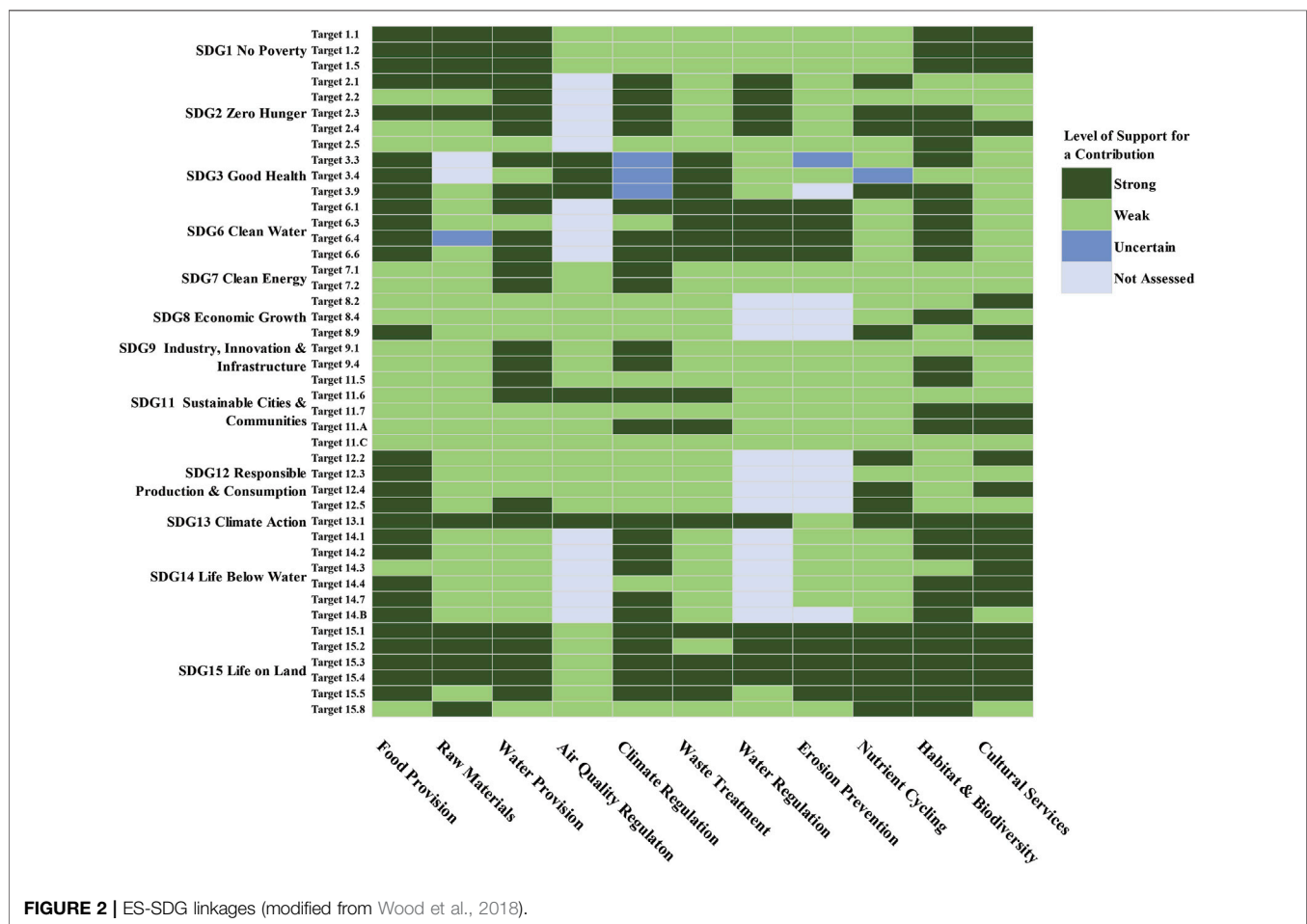


FIGURE 2 | ES-SDG linkages (modified from Wood et al., 2018).

Referring to the results of an expert survey on the contributions of 16 ESs to 44 targets across 12 SDGs conducted by Wood et al., 2018, we revised the contribution of 11 ESs to 12 SDGs: SDG1 (No Poverty), SDG2 (Zero Hunger), SDG3 (Good Health and Well-Being), SDG6 (Clean Water and Sanitation), SDG7 (Affordable and Clean Energy), SDG8 (Decent Work and Economic Growth), SDG9 (Industry, Innovation and Infrastructure), SDG11 (Sustainable Cities and Communities), SDG12 (Responsible Production and Consumption), SDG13 (Climate Action), SDG14 (Life Below Water), SDG15 (Life on Land) (**Figure 2**). SDG4
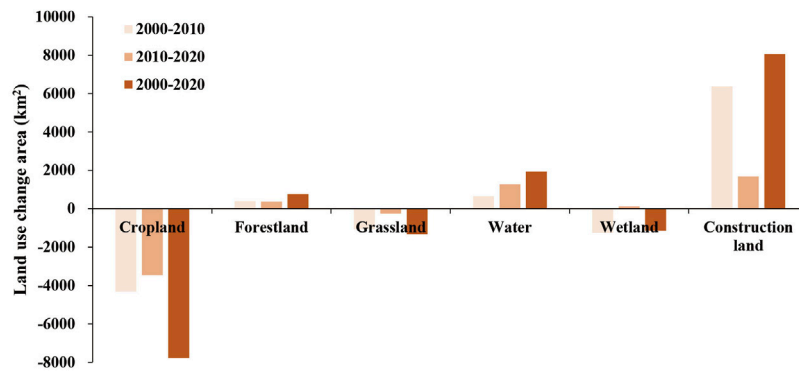
**FIGURE 3 |** Land use changes between 2000 and 2020 in the Beijing-Tianjin-Hebei region.

(Quality Education), SDG5 (Gender Equity), SDG10 (Reduced inequalities), SDG16 (Peace, justice and strong institution), SDG17 (Partnerships for the goals) and the other 125 targets were excluded since there was no clear environmental connection. Based on the "ES-SDG linkages", the SDG score was calculated as follows (Chen et al., 2022):

$$SDG_j = \frac{\sum_{f=1}^{n} \left( AESV'_f \times x_f \times T_{f,j} \times y_j \right)}{\sum_{f=1}^{n} \left( T_{f,j} \right)} \tag{5}$$

where $SDG_j$ is the SDG j score, $T_{f,j}$ is the number of ES-SDG target linkages under the SDG j, and $x_f$ and $y_j$ are the weights of $ES_j$ and targets within the SDG j, respectively. In assuming that every ES and target has the same priority within each SDG, x and y were set to 1. For example, there were three targets (1.1, 1.2, and 1.5) under SDG1, which were strongly supported by the five ESs (food provision, raw materials, water provision, habitat & biodiversity, and cultural services) (**Figure 2**). Consequently, the SDG1 score could be expressed as $[(ES_{food\ provision} \times 3) + (ES_{raw\ materials} \times 3) + (ES_{water\ provision} \times 3) + (ES_{habitat\ \&\ biodiversity} \times 3) + (ES_{cultural\ services} \times 3)]/(3 + 3 + 3 + 3 + 3)$.

The integrated ES-SDG Index score was calculated as follows:

$$ES - SDG\ Index = \frac{\sum_{j=1}^{m} SDG_j}{m} \tag{6}$$

where m is the number of all evaluated SDGs.

## 2.4 Data Resources
Land-use data in 2000, 2010, and 2020 with a resolution of 30 m were obtained from the Resource and Environmental Science and Data Center of the Chinese Academy of Sciences (https://www.resdc.cn/). It was generated by manual visual interpretation from Landsat TM remote sensing images. The crop areas and crop yields were collected from the China Statistical Yearbook. The crop prices were collected from the Ministry of Agriculture and Rural Affairs of China (http://www.moa.gov.cn/).

# 3 RESULTS

## 3.1 Changes of Land Use
The land use of the BTH changed dramatically in terms of the cropland and construction land from 2000 to 2020 (**Figure 3**). Cropland decreased the most (7,775 km²), followed by grassland (1,323 km²) and wetland (1,143 km²). Construction land increased the most (8,058 km²), followed by water (1,927 km²) and forestland (765 km²). However, the construction land increased much less in the 2010s than 2000s. The decrease of cropland and grassland also slowed in the 2010s. The wetland increased from 2010 to 2020.

## 3.2 Spatial-Temporal Changes of ESV
### 3.2.1 Spatial-Temporal Changes of Individual ESV
The value of 11 ESs in the BTH showed different spatial variation (**Figure 4**). WR had the largest ESV in the BTH among the 11 ESs, followed by CR and EP, whereas the WP and NC had low ESV. The high-value areas of FP were concentrated in the southeastern BTH and the northwest of Zhangjiakou with dense cropland. The high-value areas of WP and WR were distributed in the eastern and northern BTH with large waters and wetlands. The high-value areas of the other eight ESs such as CR, EP, and HB were gathered in the north and western BTH with abundant forestland.

The value of four ESs increased, whereas the value of seven ESs decreased from 2000 to 2020 (**Figure 5**). The value of WP, WR, WT, and CR increased by 56.86%, 24.59%, 4.94%, and 0.55%, respectively. The value of FP, RM, AQR, and NC have continuously declined between 2000 and 2020, with decreased rates of 6.51%, 2.23%, 3.00%, and 4.56%, respectively. During 2000–2020, the Bohai Rim of the eastern BTH and Yanshan Mountain of the northern BTH improved the value of WT and WR significantly, whereas the southeastern BTH, especially the suburbs of Baoding, Shijiazhuang, and Handan decreased the value of FP, RM, and NC significantly. Additionally, the value of AQR in the suburbs of Beijing and Tianjin decreased (**Figure 4**).

### 3.2.2 Spatial-Temporal Changes of the Total ESV
The high-value areas of the total ESV in the BTH were mainly found in Yanshan Mountain, Bashang Plateau, and Bohai Rim

**FIGURE 4 |** Spatial patterns of the individual ecosystem service values in the Beijing-Tianjin-Hebei region.
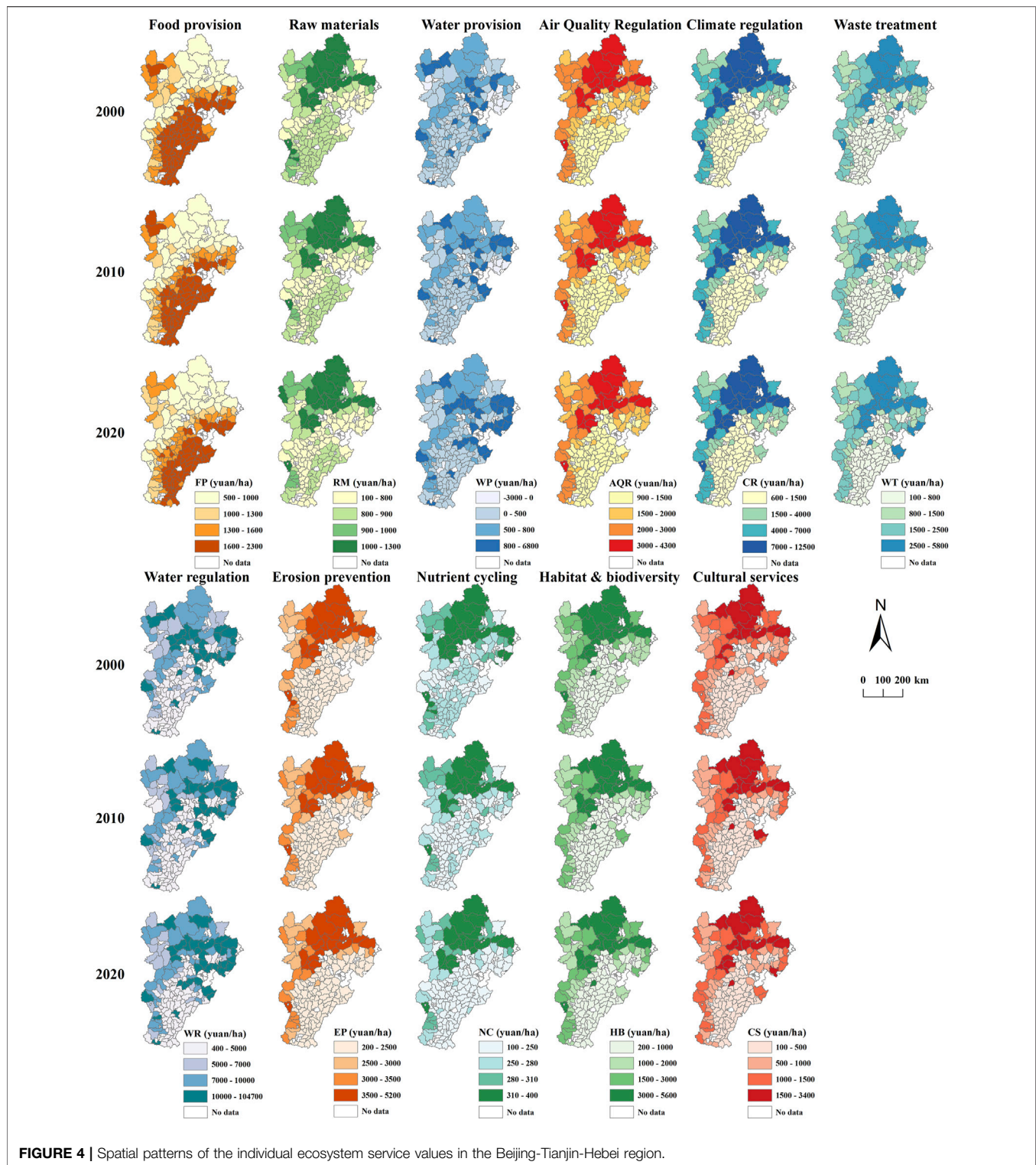
plain, where there were rich forests or wetlands, whereas low-value areas were distributed in the southern plain where most areas were cropland (**Figure 6**). 53% of counties increased the ESV notably from 2000 to 2020, especially counties in the Bohai Rim region. In contrast, some counties in the northwestern

mountains such as Zhangjiakou and on the southern plain such as Hengshui experienced a decreased ESV. The Shenze county of Shijiazhuang had the maximum decline, of 37%. The ESV in different areas showed different changes between the 2 decades. The ESV in most areas of the BTH decreased from
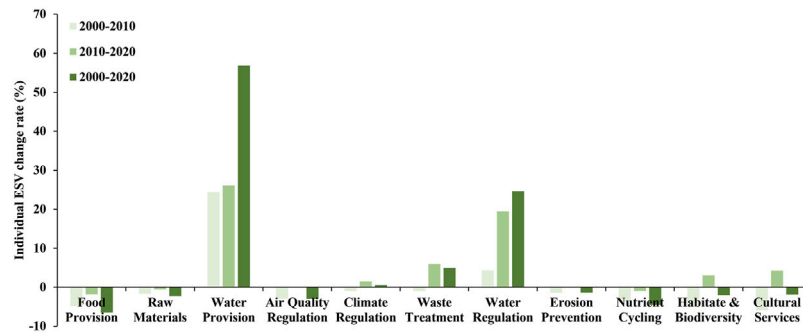
**FIGURE 5 |** Temporal changes in individual ecosystem service values in the Beijing-Tianjin-Hebei region.
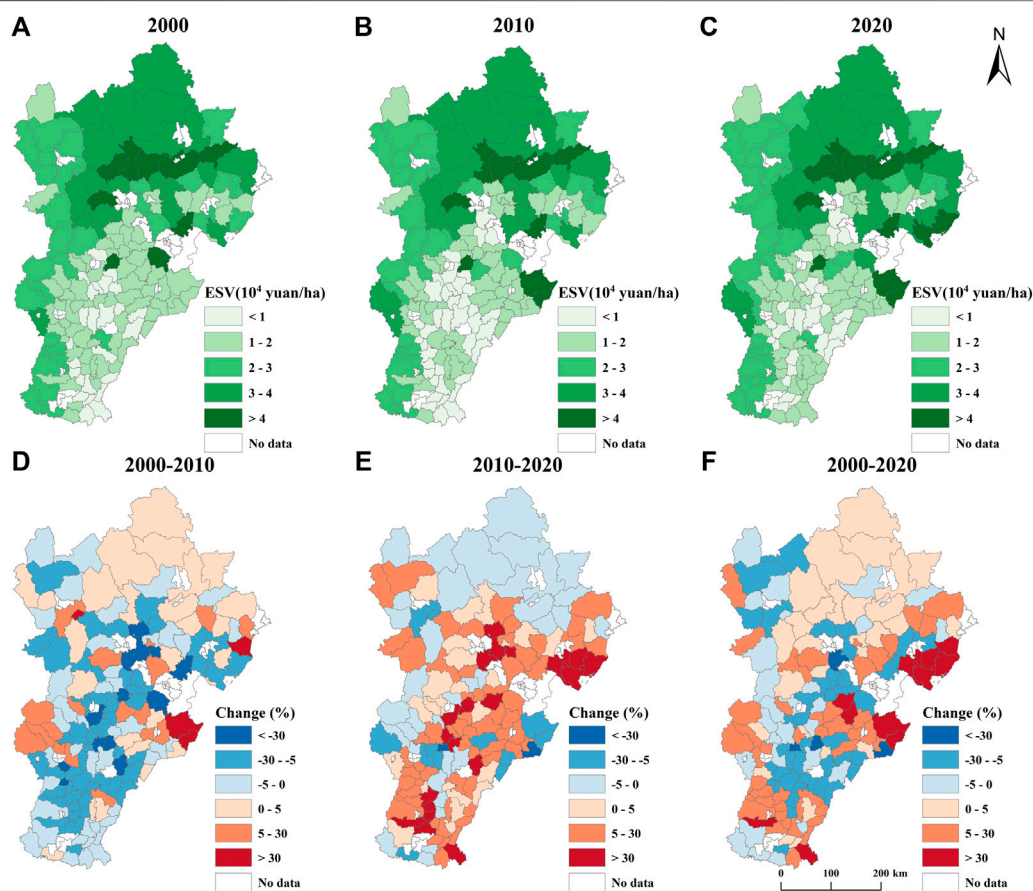


**FIGURE 6 |** Spatial-temporal changes in total ecosystem service values in the Beijing-Tianjin-Hebei region.

2000 to 2010, especially the southern plain and suburbs of big cities, whereas the ESV in the southern plain and central BTH increased from 2010 to 2020. However, the northern plateau experienced a decreased ESV between 2010 and 2020. Overall, the total ESV of the BTH increased from 25,335 yuan ha$^{-1}$ in 2000 to 27,344 yuan ha$^{-1}$ in 2020, representing a growth of 7.93%.

## 3.3 Spatial-Temporal Changes of ES-SDG Index Scores

### 3.3.1 Spatial-Temporal Changes of Individual SDG Scores

The scores of 11 SDGs (excluding SDG12) in the BTH showed a similar spatial pattern of high in the north and western

**FIGURE 7 |** Spatial patterns of individual SDG scores in the Beijing-Tianjin-Hebei region.
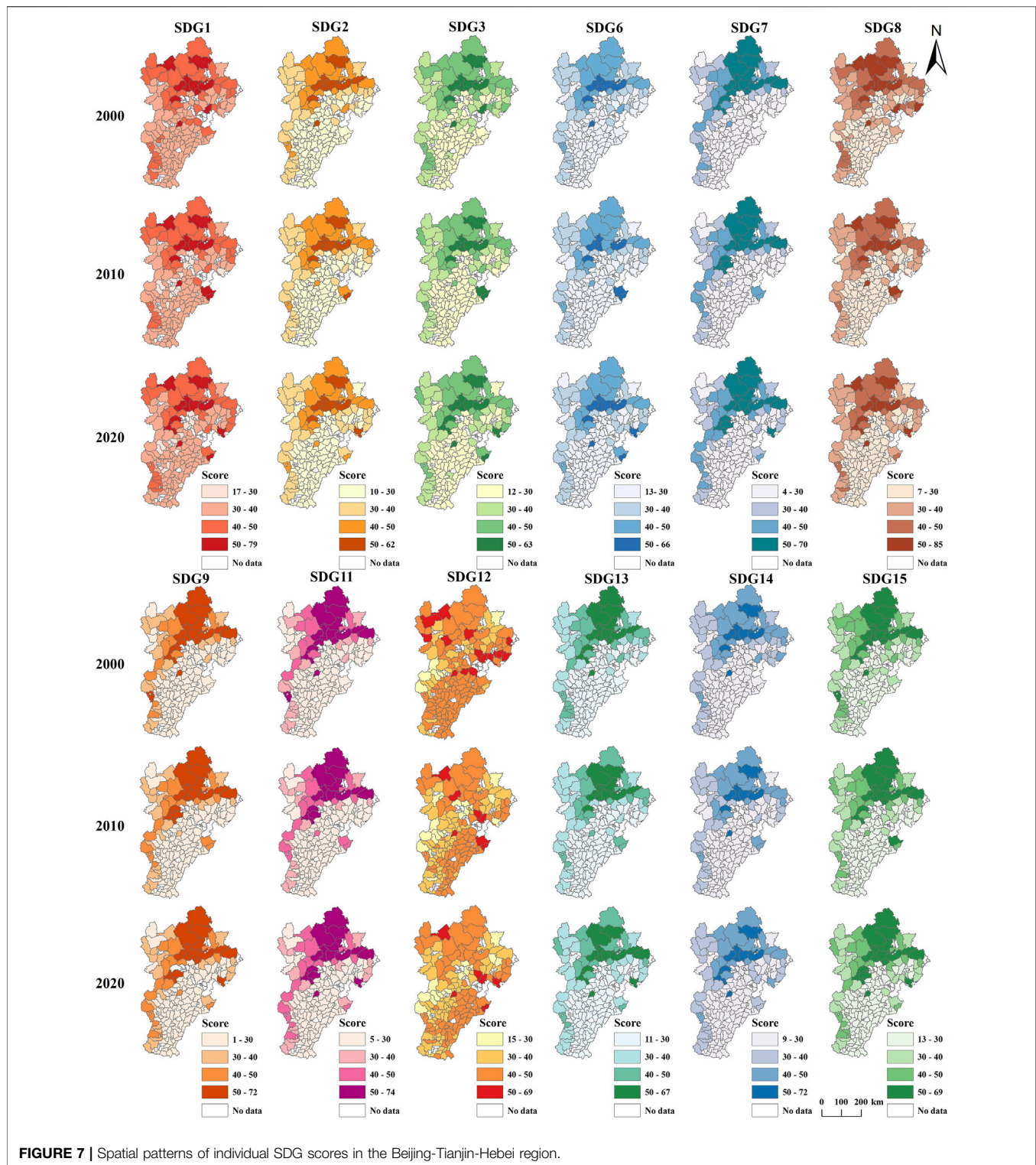
mountains and low in the south (**Figure 7**). SDG1, SDG12, and SDG15 had the best performance in the BTH, whereas SDG6 and SDG11 performed poorly. The individual SDG scores in most of the counties in the southern BTH decreased from 2000 to 2010, whereas 30 counties, mainly located in Beijing, Shijiazhuang,

Xingtai and Baoding increased all individual SDG scores from 2010 to 2020.

SDG7, SDG9, and SDG11 scores increased, whereas the other eight SDG scores, especially SDG12, SDG8, and SDG14, decreased between 2000 and 2020 (**Figure 8**). The SDG7 score
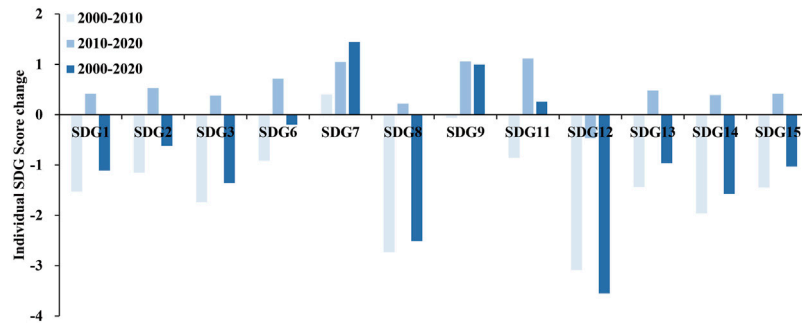
**FIGURE 8 |** Temporal changes in individual SDG scores in the Beijing-Tianjin-Hebei region.
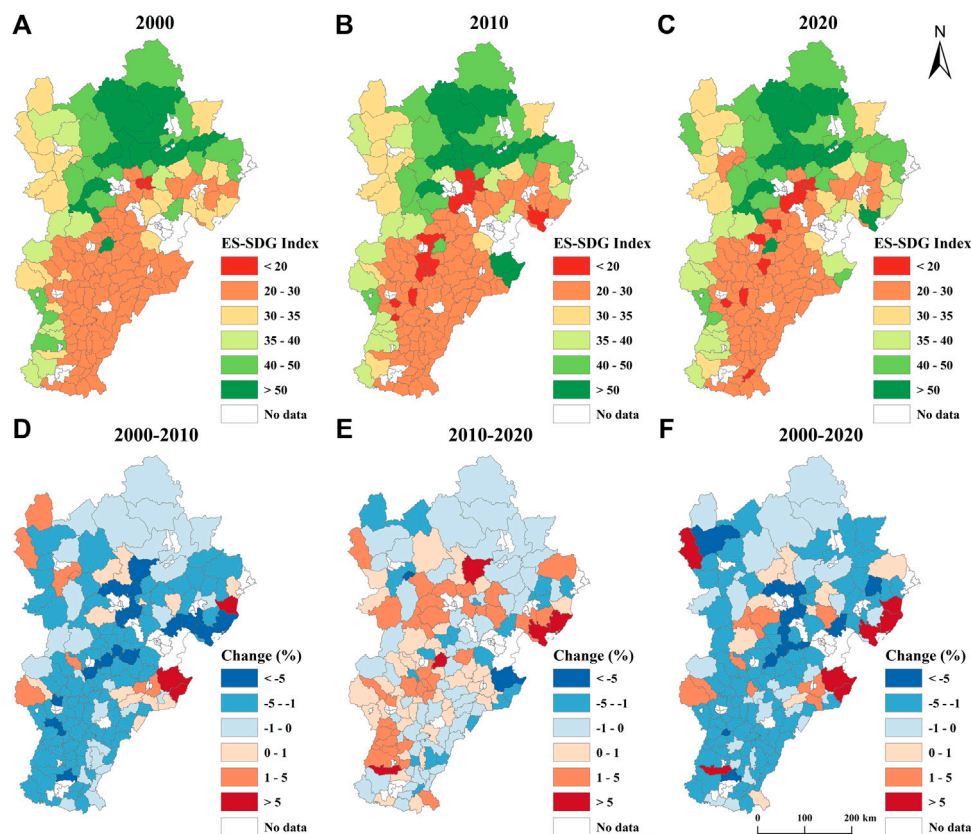


**FIGURE 9 |** Spatial-temporal changes in ES-SDG Index scores in the Beijing-Tianjin-Hebei region.

increased steadily and SDG12 score decreased continuously from 2000 to 2020. Ten SDG scores showed a trend of decline between 2000 and 2010 and a rise between 2010 and 2020 in the BTH.

### 3.3.2 Spatial-Temporal Changes of ES-SDG Index Scores

The ES-SDG Index score of counties in the northern plateau were high and the counties in the southern plain were low (**Figure 9**). The

ES-SDG Index score of the entire BTH decreased slightly from 36.8 in 2000 to 35.5 in 2010, and then increased to 36.0 in 2020. 84% of counties exhibited a decrease in the ES-SDG Index score between 2000 and 2020. The areas that declined most notably were mainly found in the suburbs of big cities, of which Daxing District of Beijing declined the most (48.7%). Conversely, the counties near the Bohai Sea increased their ES-SDG Index scores substantially, with Caofeidian District increasing the most (86.7%). ES-SDG Index scores in most of the BTH decreased from 2000 to 2010, whereas

50% of counties, especially counties in Beijing, Baoding, Shijiazhuang, and Tangshan increased from 2010 to 2020.

# 4 DISCUSSION

## 4.1 Impacts of Land Use Change on ESV and ES-SDG Index Scores

Land use change alters the ESV and ES-SDG Index scores through the cascade process of "structure-process-function-service-sustainability" (Chen et al., 2022). The decrease of cropland, grassland, and wetland in the BTH between 2000 and 2010 caused a decrease in the value of nine ESs, such as food provision, air quality regulation and nutrient cycling, whereas the increase of forestland, waterbodies and wetland between 2010 and 2020 contributed to an increase in the value of seven ESs, such as water provision, water regulation, waste treatment, and climate regulation. Although the value of seven ESs declined between 2000 and 2020, the total ESV of the BTH increased by 7.93% due to the increase in waterbodies and forestland that have very high equivalent coefficients (Zhang et al., 2015; Xie et al., 2017).

The ES-SDG Index score in the BTH showed a downward trend between 2000 and 2010 and an upward trend between 2010 and 2020, attributed to the urbanization and eco-environment protection policies. Rapid urbanization led to a large amount of cropland being converted to construction land, which resulted in the continuous decline of the value of food provision (Zhou et al., 2018; Wang et al., 2019). Expansion of construction land was controlled from 2010 for "New-Type Urbanization" (Zhao et al., 2018). Forestland and waterbodies were continuously expanded as a result of the implementation of the "Grain to Green Program" and "Beijing-Tianjin Sandstorm Source Control Project" since 2000 in the BTH (Bryan et al., 2018; Yang et al., 2019b). Increase of climate regulation, waste treatment, and erosion prevention were also found in another study in the BTH for growth of forestland (Tian et al., 2020). Water provision, waste treatment, and water regulation increased notably in the coastal areas due to wetland conservation and conversion of paddy fields to dry land (Ma et al., 2019; Zhang et al., 2019). Meanwhile, the restoration of forestland and waterbodies in rural areas has rapidly increased the ESV, offsetting the reduction of ESV caused by the expansion of urban construction land (Zhou et al., 2018).

Except for the improvement of SDG7, SDG9, and SDG11 scores between 2000 and 2020, the remaining 9 SDG scores declined, of which SDG8, SDG12, and SDG14 declined the most. According to "ES-SDG linkages," water provision and climate regulation made strong contributions to SDG7, SDG9, and SDG11. Therefore, the increasing value of water provision and climate regulation in the BTH contributed to the improvement of SDG7, SDG9, and SDG11. Food provision, nutrient cycling, habitat & biodiversity, and cultural services made strong contributions to SDG8, SDG12, and SDG14. Therefore, the decrease of food provision, nutrient cycling, habitat & biodiversity, and cultural services caused the decrease of SDG8, SDG12 and SDG14. Overall, the changes of individual SDG and ES-SDG Index scores in the BTH was mainly due to food provision, water provision, climate regulation, nutrient cycling, habitat & biodiversity, and cultural services. The study in the Yangtze River Economic Belt also showed that the increase of SDG Index score was mainly attributed to the improvement of food and water provision (Chen et al., 2022).

## 4.2 Implications for Sustainable Development Management

ESs directly affected the performance of SDGs in the BTH. The trade-offs between provisioning services and regulating services, and the synergies between regulating services and supporting services, indicated that sound land-use management is required to enhance the synergies among multiple ESs (Yang et al., 2019a; Shen et al., 2020). Although the total ESV in the BTH increased from 2000 to 2020, seven of 11 ESs still decreased and 47% of areas experienced a decline in their ESV, especially the value of food provision and nutrient cycling in the southern plain and suburbs of big cities. Urbanization provides a driving force for socioeconomic development. However, it may have negative impacts on the realization of SDGs by occupying prime cropland and destroying ecological land (Zhang D. et al., 2017; Qiu et al., 2021). It is necessary to control the disorderly expansion of construction land. Land consolidation can release cropland for large-scale farming and promote food production in the southern BTH (Duan et al., 2021; Wang et al., 2021). The northern plateau and western mountains are important ecological barriers in the BTH which also achieved high scores in SDGs. However, the ESV of the north and west decreased from 2010 to 2020. Ecosystem conservation and restoration in the Yanshan-Taihang Mountains and Bashang Plateau should be strengthened through gross ecosystem product (GEP) accounting and transregional compensation payment for ecosystem services (Zhang L. et al., 2017; Ouyang et al., 2020). Additionally, lessons can learned from the "Paddy Land-to-Dry Land" program successfully conducted in Miyun Reservoir Watershed, Beijing to protect water quantity and quality in the BTH (Zheng et al., 2013).

The big cities such as Beijing have boosted its economy at the overuse of ESs and greatly increased demand for food, water and energy (Cumming et al., 2014). Advanced technologies and cleaner production facilities need to be deployed to improve water and nutrient use efficiency for SDG6 implementation (Wang et al., 2022). It is suggested to raise investment in ecological infrastructure, such as rehabilitating wetlands, to resist natural disasters and reduce environmental pollution for SDG11 implementation (Cumming et al., 2017). The score of SDG7 has increased steadily whereas the score of SDG12 has decreased continuously over the past 20 years, which was consistent with the findings at the provincial level in China (Zhang et al., 2022b). SDG6, SDG11, and SDG12 should be prioritized to advance the synergistic development of SDGs in the BTH.

## 4.3 Limitations

This study attempts to integrate ESs into SDGs assessment. However, the equivalent factor method based on land-use structure to quantify ESs has certain limitations due to the dynamic and complex nature of ecosystems (Zhang et al., 2020). Furthermore, the ES-SDG Index score based on the environmental indicators cannot fully reflect the progress of SDGs, especially in terms of socioeconomics.

## 5 CONCLUSIONS

Progress towards the SDGs was evaluated based on the "ES-SDG linkages" to detect the impact of ES change on SDGs in the BTH between 2000 and 2020. The total ESV and ES-SDG Index score in the BTH showed a spatial pattern of high in the north and western mountains, and low in the south. The total ESV increased from 25,335 yuan ha$^{-1}$ in 2000 to 27,344 yuan ha$^{-1}$ in 2020, and the improvement of ESV was mainly attributed to water provision and water regulation. However, the ES-SDG Index score decreased slightly from 36.8 in 2000 to 35.5 in 2010, and increased to 36.0 in 2020. Both ESV and ES-SDG Index scores showed obvious stage differences. In most counties, the ESV and ES-SDG Index scores decreased in the first 10 years and increased in the latter 10 years due to the phased differences in BTH's urbanization and environmental protection policies. SDG1, SDG12, and SDG15 had the best performance, whereas SDG6 and SDG11 performed poorly. Ten SDG scores showed a trend of decline between 2000 and 2010 and a rise between 2000 and 2020 in the BTH. SDG7 scores increased steadily, attributed to the increase of water provision and climate regulation, whereas the SDG12 score declined continuously, attributed to the decrease of

food provision and nutrient cycling. Our study indicated that regulating services are the core function of ESs in the BTH, and the changes of SDG and ES-SDG Index scores mainly depended on food provision, water provision, climate regulation, nutrient cycling, habitat & biodiversity, and cultural services. The assessment of SDGs suggests that SDG6, SDG11, and SDG12 should be prioritized to advance the synergistic development of SDGs in the BTH.

## DATA AVAILABILITY STATEMENT

The raw data supporting the conclusion of this article will be made available by the authors, without undue reservation.

## AUTHOR CONTRIBUTIONS

## FUNDING

## REFERENCES

Anderson, C. B., Seixas, C. S., Barbosa, O., Fennessy, M. S., Díaz-José, J., and Herrera-F., B. (2019). Determining Nature's Contributions to Achieve the Sustainable Development Goals. *Sustain. Sci.* 14 (2), 543–547. doi:10.1007/s11625-018-0643-5

Bryan, B. A., Gao, L., Ye, Y., Sun, X., Connor, J. D., Crossman, N. D., et al. (2018). China's Response to a National Land-System Sustainability Emergency. *Nature* 559 (7713), 193–204. doi:10.1038/s41586-018-0280-2

Chen, D., Zhao, Q., Jiang, P., and Li, M. (2022). Incorporating Ecosystem Services to Assess Progress towards Sustainable Development Goals: A Case Study of the Yangtze River Economic Belt, China. *Sci. Total Environ.* 806, 151277. doi:10.1016/j.scitotenv.2021.151277

Cochran, F., Daniel, J., Jackson, L., and Neale, A. (2020). Earth Observation-Based Ecosystem Services Indicators for National and Subnational Reporting of the Sustainable Development Goals. *Remote Sens. Environ.* 244, 111796. doi:10.1016/j.rse.2020.111796

Costanza, R., d'Arge, R., de Groot, R., Farber, S., Grasso, M., Hannon, B., et al. (1997). The Value of the World's Ecosystem Services and Natural Capital. *Nature* 387 (6630), 253–260. doi:10.1038/387253a0

Costanza, R., Daly, L., Fioramonti, L., Giovannini, E., Kubiszewski, I., Mortensen, L. F., et al. (2016). Modelling and Measuring Sustainable Wellbeing in Connection with the UN Sustainable Development Goals. *Ecol. Econ.* 130, 350–355. doi:10.1016/j.ecolecon.2016.07.009

Cumming, G. S., Buerkert, A., Hoffmann, E. M., Schlecht, E., von Cramon-Taubadel, S., and Tscharntke, T. (2014). Implications of Agricultural

Transitions and Urbanization for Ecosystem Services. *Nature* 515 (7525), 50–57. doi:10.1038/nature13945

Cumming, T. L., Shackleton, R. T., Förster, J., Dini, J., Khan, A., Gumula, M., et al. (2017). Achieving the National Development Agenda and the Sustainable Development Goals (SDGs) through Investment in Ecological Infrastructure: A Case Study of South Africa. *Ecosyst. Serv.* 27, 253–260. doi:10.1016/j.ecoser.2017.05.005

de Groot, R., Brander, L., van der Ploeg, S., Costanza, R., Bernard, F., Braat, L., et al. (2012). Global Estimates of the Value of Ecosystems and Their Services in Monetary Units. *Ecosyst. Serv.* 1 (1), 50–61. doi:10.1016/j.ecoser.2012.07.005

Duan, J., Ren, C., Wang, S., Zhang, X., Reis, S., Xu, J., et al. (2021). Consolidation of Agricultural Land Can Contribute to Agricultural Sustainability in China. *Nat. Food* 2 (12), 1014–1022. doi:10.1038/s43016-021-00415-5

Fu, B. (2020). Promoting Geography for Sustainability. *Geogr. Sustain.* 1 (1), 1–7. doi:10.1016/j.geosus.2020.02.003

Gashaw, T., Tulu, T., Argaw, M., Worqlul, A. W., Tolessa, T., and Kindu, M. (2018). Estimating the Impacts of Land Use/land Cover Changes on Ecosystem Service Values: The Case of the Andassa Watershed in the Upper Blue Nile Basin of Ethiopia. *Ecosyst. Serv.* 31, 219–228. doi:10.1016/j.ecoser.2018.05.001

Geijzendorffer, I. R., Cohen-Shacham, E., Cord, A. F., Cramer, W., Guerra, C., and Martín-López, B. (2017). Ecosystem Services in Global Sustainability Policies. *Environ. Sci. Policy* 74, 40–48. doi:10.1016/j.envsci.2017.04.017

Guerry, A. D., Polasky, S., Lubchenco, J., Chaplin-Kramer, R., Daily, G. C., Griffin, R., et al. (2015). Natural Capital and Ecosystem Services Informing Decisions: From Promise to Practice. *Proc. Natl. Acad. Sci. U.S.A.* 112 (24), 7348–7355. doi:10.1073/pnas.1503751112

Hawken, S., Rahmat, H., Sepasgozar, S. M. E., and Zhang, K. (2021). The SDGs, Ecosystem Services and Cities: A Network Analysis of Current Research Innovation for Implementing Urban Sustainability. *Sustainability* 13 (24), 14057. doi:10.3390/su132414057

Hu, Z., Yang, X., Yang, J., Yuan, J., and Zhang, Z. (2021). Linking Landscape Pattern, Ecosystem Service Value, and Human Well-Being in Xishuangbanna, Southwest China: Insights from a Coupling Coordination Model. *Glob. Ecol. Conservation* 27, e01583. doi:10.1016/j.gecco.2021.e01583

Huan, Y., Liang, T., Li, H., and Zhang, C. (2021). A Systematic Method for Assessing Progress of Achieving Sustainable Development Goals: A Case Study of 15 Countries. *Sci. Total Environ.* 752, 141875. doi:10.1016/j.scitotenv.2020.141875

IPBES (2019). *Global Assessment Report on Biodiversity and Ecosystem Services of the Intergovernmental Science-Policy Platform on Biodiversity and Ecosystem Services*. Bonn, Germany: IPBES secretariat.

Jiang, W., Wu, T., and Fu, B. (2021). The Value of Ecosystem Services in China: A Systematic Review for Twenty Years. *Ecosyst. Serv.* 52, 101365. doi:10.1016/j.ecoser.2021.101365

Johnson, J. A., Jones, S. K., Wood, S. L. R., Chaplin-Kramer, R., Hawthorne, P. L., Mulligan, M., et al. (2019). Mapping Ecosystem Services to Human Well-being: a Toolkit to Support Integrated Landscape Management for the SDGs. *Ecol. Appl.* 29 (8). doi:10.1002/eap.1985

Keesstra, S., Nunes, J., Novara, A., Finger, D., Avelar, D., Kalantari, Z., et al. (2018). The Superior Effect of Nature Based Solutions in Land Management for Enhancing Ecosystem Services. *Sci. Total Environ.* 610-611, 997–1009. doi:10.1016/j.scitotenv.2017.08.077

Liu, X., Zhao, W., Liu, Y., Hua, T., Hu, X., and Cherubini, F. (2022). Contributions of Ecological Programs to Sustainable Development Goals in Linzhi, over the Tibetan Plateau: A Mental Map Perspective. *Ecol. Eng.* 176. doi:10.1016/j.ecoleng.2021.106532

MA (2005). *Ecosystems and Human Well-Being: Synthesis*. Washington, DC: Island Press.

Ma, T., Li, X., Bai, J., Ding, S., Zhou, F., and Cui, B. (2019). Four Decades' Dynamics of Coastal Blue Carbon Storage Driven by Land Use/land Cover Transformation under Natural and Anthropogenic Processes in the Yellow River Delta, China. *Sci. Total Environ.* 655, 741–750. doi:10.1016/j.scitotenv.2018.11.287

National Bureau of Statistics of China (2001). *China Statistical Yearbook 2001*. Beijing: China Statistical Press.

National Bureau of Statistics of China (2021). *China Statistical Yearbook 2021*. Beijing: China Statistical Press.

Ouyang, Z., Song, C., Zheng, H., Polasky, S., Xiao, Y., Bateman, I. J., et al. (2020). Using Gross Ecosystem Product (GEP) to Value Nature in Decision Making. *Proc. Natl. Acad. Sci. U.S.A.* 117 (25), 14593–14601. doi:10.1073/pnas.1911439117

Ouyang, Z., Zheng, H., Xiao, Y., Polasky, S., Liu, J., Xu, W., et al. (2016). Improvements in Ecosystem Services from Investments in Natural Capital. *Science* 352 (6292), 1455–1459. doi:10.1126/science.aaf2295

Pires, A. P. F., Rodriguez Soto, C., and Scarano, F. R. (2021). Strategies to Reach Global Sustainability Should Take Better Account of Ecosystem Services. *Ecosyst. Serv.* 49, 101292. doi:10.1016/j.ecoser.2021.101292

Qiu, H., Hu, B., and Zhang, Z. (2021). Impacts of Land Use Change on Ecosystem Service Value Based on SDGs Report--Taking Guangxi as an Example. *Ecol. Indic.* 133, 108366. doi:10.1016/j.ecolind.2021.108366

Sachs, J., Kroll, C., Lafortune, G., Fuller, G., and Woelm, F. (2021). *Sustainable Development Report 2021*. Cambridge: Cambridge University Press.

Schmidt-Traub, G., Kroll, C., Teksoz, K., Durand-Delacre, D., and Sachs, J. D. (2017). National Baselines for the Sustainable Development Goals Assessed in the SDG Index and Dashboards. *Nat. Geosci.* 10 (8), 547–555. doi:10.1038/ngeo2985

Shen, J., Li, S., Liang, Z., Liu, L., Li, D., and Wu, S. (2020). Exploring the Heterogeneity and Nonlinearity of Trade-Offs and Synergies Among Ecosystem Services Bundles in the Beijing-Tianjin-Hebei Urban Agglomeration. *Ecosyst. Serv.* 43, 101103. doi:10.1016/j.ecoser.2020.101103

Tian, Y., Zhou, D., and Jiang, G. (2020). Conflict or Coordination? Multiscale Assessment of the Spatio-Temporal Coupling Relationship between Urbanization and Ecosystem Services: The Case of the Jingjinji Region, China. *Ecol. Indic.* 117, 106543. doi:10.1016/j.ecolind.2020.106543

UNEP (2021). *Making Peace with Nature—A Scientific Blueprint to Tackle the Climate, Biodiversity and Pollution Emergencies*. Nairobi: UNEP Secretariat.

Wang, J., Zhou, W., Pickett, S. T. A., Yu, W., and Li, W. (2019). A Multiscale Analysis of Urbanization Effects on Ecosystem Services Supply in an Urban Megaregion. *Sci. Total Environ.* 662, 824–833. doi:10.1016/j.scitotenv.2019.01.260

Wang, M., Janssen, A. B. G., Bazin, J., Strokal, M., Ma, L., and Kroeze, C. (2022). Accounting for Interactions between Sustainable Development Goals Is Essential for Water Pollution Control in China. *Nat. Commun.* 13 (1). doi:10.1038/s41467-022-28351-3

Wang, S., Bai, X., Zhang, X., Reis, S., Chen, D., Xu, J., et al. (2021). Urbanization Can Benefit Agricultural Production with Large-Scale Farming in China. *Nat. Food* 2 (3), 183–191. doi:10.1038/s43016-021-00228-6

Wood, S. L. R., Jones, S. K., Johnson, J. A., Brauman, K. A., Chaplin-Kramer, R., Fremier, A., et al. (2018). Distilling the Role of Ecosystem Services in the Sustainable Development Goals. *Ecosyst. Serv.* 29, 70–82. doi:10.1016/j.ecoser.2017.10.010

Wu, J. (2013). Landscape Sustainability Science: Ecosystem Services and Human Well-Being in Changing Landscapes. *Landsc. Ecol.* 28 (6), 999–1023. doi:10.1007/s10980-013-9894-9

Xie, G., Lu, C., Leng, Y., Zheng, d., and Li, S. (2003). Ecological Assets Valuation of the Tibetan Plateau. *J. Nat. Resour.* 18 (2), 189–196.

Xie, G., Zhang, C., Zhen, L., and Zhang, L. (2017). Dynamic Changes in the Value of China's Ecosystem Services. *Ecosyst. Serv.* 26, 146–154. doi:10.1016/j.ecoser.2017.06.010

Xu, Z., Chau, S. N., Chen, X., Zhang, J., Li, Y., Dietz, T., et al. (2020). Assessing Progress towards Sustainable Development over Space and Time. *Nature* 577(7788), 74. doi:10.1038/s41586-019-1846-3

Yang, S., Zhao, W., Liu, Y., Cherubini, F., Fu, B., and Pereira, P. (2020). Prioritizing Sustainable Development Goals and Linking Them to Ecosystem Services: A Global Expert's Knowledge Evaluation. *Geogr. Sustain.* 1 (4), 321–330. doi:10.1016/j.geosus.2020.09.004

Yang, Y., Zheng, H., Kong, L., Huang, B., Xu, W., and Ouyang, Z. (2019a). Mapping Ecosystem Services Bundles to Detect High- and Low-Value Ecosystem Services Areas for Land Use Management. *J. Clean. Prod.* 225, 11–17. doi:10.1016/j.jclepro.2019.03.242

Yang, Y., Zheng, H., Xu, W., Zhang, L., and Ouyang, Z. (2019b). Temporal Changes in Multiple Ecosystem Services and Their Bundles Responding to Urbanization and Ecological Restoration in the Beijing-Tianjin-Hebei Metropolitan Area. *Sustainability* 11 (7), 2079. doi:10.3390/su11072079

Yin, C., Zhao, W., Cherubini, F., and Pereira, P. (2021). Integrate Ecosystem Services into Socio-Economic Development to Enhance Achievement of Sustainable Development Goals in the Post-pandemic Era. *Geogr. Sustain.* 2 (1), 68–73. doi:10.1016/j.geosus.2021.03.002

Yin, C., Zhao, W., and Pereira, P. (2022). Soil Conservation Service Underpins Sustainable Development Goals. *Glob. Ecol. Conservation* 33, e01974. doi:10.1016/j.gecco.2021.e01974

Zhang, D., Huang, Q., He, C., and Wu, J. (2017a). Impacts of Urban Expansion on Ecosystem Services in the Beijing-Tianjin-Hebei Urban Agglomeration, China: A Scenario Analysis Based on the Shared Socioeconomic Pathways. *Resour. Conservation Recycl.* 125, 115–130. doi:10.1016/j.resconrec.2017.06.003

Zhang, J., Qu, M., Wang, C., Zhao, J., and Cao, Y. (2020). Quantifying Landscape Pattern and Ecosystem Service Value Changes: A Case Study at the County Level in the Chinese Loess Plateau. *Glob. Ecol. Conservation* 23, e01110. doi:10.1016/j.gecco.2020.e01110

Zhang, J., Wang, S., Zhao, W., Meadows, M. E., and Fu, B. (2022b). Finding Pathways to Synergistic Development of Sustainable Development Goals in China. *Humanit Soc. Sci. Commun.* 9 (1). doi:10.1057/s41599-022-01036-4

Zhang, J., Zhang, W., Liu, S., and Kong, W. (2022a). Cryosphere Services to Support SDGs in High Mountains. *Sustainability* 14 (2), 791. doi:10.3390/su14020791

Zhang, L., Peng, J., Liu, Y., and Wu, J. (2017b). Coupling Ecosystem Services Supply and Human Ecological Demand to Identify Landscape Ecological Security Pattern: A Case Study in Beijing-Tianjin-Hebei Region, China. *Urban Ecosyst.* 20 (3), 701–714. doi:10.1007/s11252-016-0629-y

Zhang, L., Zhen, Q., Cheng, M., and Ouyang, Z. (2019). The Main Drivers of Wetland Changes in the Beijing-Tianjin-Hebei Region. *Ijerph* 16 (14), 2619. doi:10.3390/ijerph16142619

Zhang, Y., Zhao, L., Liu, J., Liu, Y., and Li, C. (2015). The Impact of Land Cover Change on Ecosystem Service Values in Urban Agglomerations along the Coast of the Bohai Rim, China. *Sustainability* 7 (8), 10365–10387. doi:10.3390/su70810365

Zhao, Z., Bai, Y., Wang, G., Chen, J., Yu, J., and Liu, W. (2018). Land Eco-Efficiency for New-type Urbanization in the Beijing-Tianjin-Hebei Region. *Technol. Forecast. Soc. Change* 137, 19–26. doi:10.1016/j.techfore.2018.09.031

Zheng, H., Robinson, B. E., Liang, Y.-C., Polasky, S., Ma, D.-C., Wang, F.-C., et al. (2013). Benefits, Costs, and Livelihood Implications of a Regional Payment for Ecosystem Service Program. *Proc. Natl. Acad. Sci. U.S.A.* 110 (41), 16681–16686. doi:10.1073/pnas.1312324110

Zhou, D., Tian, Y., and Jiang, G. (2018). Spatio-temporal Investigation of the Interactive Relationship between Urbanization and Ecosystem Services: Case Study of the Jingjinji Urban Agglomeration, China. *Ecol. Indic.* 95, 152–164. doi:10.1016/j.ecolind.2018.07.007

**Conflict of Interest:** The authors declare that the research was conducted in the absence of any commercial or financial relationships that could be construed as a potential conflict of interest.

**Publisher's Note:** All claims expressed in this article are solely those of the authors and do not necessarily represent those of their affiliated organizations, or those of the publisher, the editors and the reviewers. Any product that may be evaluated in this article, or claim that may be made by its manufacturer, is not guaranteed or endorsed by the publisher.

Frontiers in Environmental Science

# Spatial Pattern of Rural Ecological Land and Its Multidimensional Gradient Differentiation in a Loess Hilly Region: A Case Study of Longxi County, Gansu Province, China

Libang Ma[1,2,3]*, Yao Yao[1], Tianmin Tao[1] and Yanling Zong[1]

[1]College of Geography and Environmental Science, Northwest Normal University, Lanzhou, China, [2]Key Laboratory of Resource Environment and Sustainable Development of Oasis, Lanzhou, China, [3]Institute of Urban and Rural Development and Collaborative Governance of Northwest, Lanzhou, China

Studying the gradient differentiation of rural ecological land (REL) from a microscopic perspective is conducive to the pattern optimization, scientific control, and protection of REL. This has far-reaching significance for the improvement of village appearance and the delineation of an ecological safety network. Taking Longxi County as an example, this research studied the spatial pattern of REL based on the landscape pattern index and analyzed the multi-dimensional gradient spatial differentiation characteristics of REL. Therefore, we can clarify the impact of natural and human factors on EL under different gradients. The results show 1) the rural ecological background conditions of Longxi County are good, and the area of ecological land (EL) accounts for 90.45% of the total area of the county; 2) there are significant differences between the spatial feature index and spatial pattern of REL in Longxi County. Its diversity, dominance, and shape index were mainly at low and medium levels. The degrees of fragmentation were mainly at low and high levels; and 3) the REL in Longxi County has different evolution laws in different gradients.

Keywords: rural ecological land, spatial pattern, gradient differentiation, loess hilly area in China, Longxi County

## 1 INTRODUCTION

Ecological land (EL) has ecological functions such as water conservation, soil protection, climate regulation, environmental purification, and biodiversity protection. As a "barometer" (Yu et al., 2015) for measuring ecological quality, EL plays an important role in balancing regional and global ecosystems (Colding, 2007; Feng et al., 2021a), ensuring national land ecological security, coping with global climate change, and improving the quality of human life (Guan et al., 2018). However, with the global environmental change and the disturbance of human activities (Song et al., 2015), EL is facing more serious problems of loss and degradation than ever before (Puskás et al., 2021). These problems not only destroy the balance of the ecosystem but also have a serious impact on the quality of life of future generations (Folke et al., 2004). These issues have attracted widespread attention from academia and governments. To solve this problem, the United Nations has implemented a series of initiatives such as the 2030 Agenda for Sustainable Development and the Convention on Biological Diversity [Tóth et al., 2018; UNCCD (United Nations Convention to Combat Desertification), 2017].

As an important part of ecological space, rural ecological land (REL) not only provides ecological support for various production and living activities in rural areas but also plays an important role in guaranteeing the comprehensive and sustainable development of the social economy in rural areas (Yao et al., 2021). The quantity and spatial distribution of REL will have an important impact on rural livability. REL is used as a "buffer zone" for slowing down the destruction of EL in the loess hilly area (Li et al., 2020a). Studying the multi-dimensional gradient differentiation of EL and its influence mechanism has far-reaching significance for the pattern optimization, scientific control and protection of REL, and the maintenance of the ecosystem in arid areas.

In recent years, the spatial pattern of REL has been affected by various factors. In the period of low social productivity, it is mainly affected by the natural environment, such as topography and climate (Sevenant and Antrop, 2007). Since the 20th century, with the acceleration of global industrialization, urbanization, and informatization, both developed and developing countries have faced significant improvements in rural production and living standards, increasing land use intensity, and increasing demand for construction land. Socio-economic factors have gradually become the main factors affecting the spatial pattern of EL use (Li et al., 2020b). EL in developed countries such as Europe and North America is first affected by socio-economic aspects such as traffic conditions and geographic location (Gonzalez-Abraham et al., 2007; Peng et al., 2016; Gong et al., 2018). In China, there is a strong "land grab" phenomenon between ecological protection and economic development (Fei et al., 2020), which seriously affects the regional ecological security and the sustainable development of the rural ecological environment. How to avoid a series of problems such as the encroachment of rural ecological space, ecological destruction, environmental pollution, and disorderly development of land space has become a practical problem that needs to be solved urgently today. Therefore, it is of great significance to study the spatial pattern of EL and analyze the distribution type, fragmentation degree, concentration, and shape complexity of REL under different natural geographical environments and socio-economic backgrounds for guiding future EL protection and promoting the optimization of REL use pattern.

In recent years, with the in-depth study of rural land ecosystems and the concept of EL, the classification system of EL has been further developed. The classification of EL types from the perspective of land use/land cover has become a method recognized by the academic community. Foreign countries pay more attention to ecological attributes in land use classification and land use management (Deng et al., 2009). Most of the classification of EL is carried out according to the natural characteristics and ecological significance of the land (Frondoni et al., 2011; Qu et al., 2019), and the classification results of EL are used in various research. Pickett et al. (2001) applied the EL classification system to the assessment of environmental conditions. Wassmann et al. (2011) used it to estimate ecological functions, and Capotorti et al. (2012) used it to protect regional biodiversity. In 1898, E. Howard et al. put forward the theory of "garden city," changing the structure of urban and suburban land and alleviating the environmental damage, thereby beginning to study the ecological landscape pattern (Zube, 1986). Hietala-Koivu (1999) studied the evolution of agricultural landscape patterns in southwestern Finland by landscape index analysis. Seppelt and Voinov (2002) optimized the spatial structure of watershed land use by constructing an ecological security pattern . L. Pamela used remote sensing technology and ground observation data to study the dynamic changes in the ecological landscape (Nngler et al., 2008). Joppa assessed the effectiveness of nature reserves to protect species diversity (Joppa and Pfaff, 2011). The research on El by early Chinese scholars mostly focused on the definition of EL (Deng et al., 2009; Yu et al., 2015), the identification of EL (Zhou et al., 2015; Fei et al., 2020; Liu et al., 2021), the construction of the classification system (Yu et al., 2015), the analysis based on landscape security pattern (Yu et al., 2009; Li et al., 2011), the identification and protection of ecological space (Li et al., 2016), and the relationship between EL and cities (Wang and Li, 2006; Su et al., 2007). In 2017, after the implementation of China's "Land Use Status Classification System" (GB/T 21010–2017), there was a renewed upsurge in the study of EL. In recent years, the research focus has mainly been on ecosystem service function and value assessment (Guan et al., 2018; Qu et al., 2019), pattern change and differentiation trend (Wei et al., 2021), and protection effectiveness assessment (Gao et al., 2021). Existing research shows that the research on EL has gradually evolved from qualitative to quantitative and specific, and more emphasis has been placed on the optimization and management of EL patterns.

However, there are still some urgent problems to be solved in the current research. For example, the research on REL started late, and the research content mostly focuses on the identification, classification, and protection of EL. The research areas are mostly concentrated in typical key ecological function areas and suburban areas, ignoring the importance of REL as a powerful reserve for the ecological resource in China. In addition, there is currently a lack of research on the differentiation characteristics of the spatial pattern of REL from a gradient perspective. The existing research on the spatial gradient of land is mainly analyzed from the perspective of a single gradient such as topography and economy. With the rapid development of society and economy and the need to revitalize the world's rural areas, the scientific protection and rational utilization of REL are increasingly important (Li et al., 2020b). This is an essential foundation for the comprehensive and sustainable development of rural society and economy and an essential means to supplement and improve urban functions. Therefore, there is an urgent need to carry out research on the differential mechanism of REL and the impact of different gradients on the spatial distribution of REL.

Longxi County is located in the hilly loess area of Longzhong, with complex and fragmented topography and a fragile ecological environment. Ecological space protection and utilization are crucial in northwest China, considering the significant differences in topographic conditions, per capita income, and town development levels in different regions of Longxi County. Based on the topographical, economic, and administrative gradient differences of "ecological land-dimensional space,"
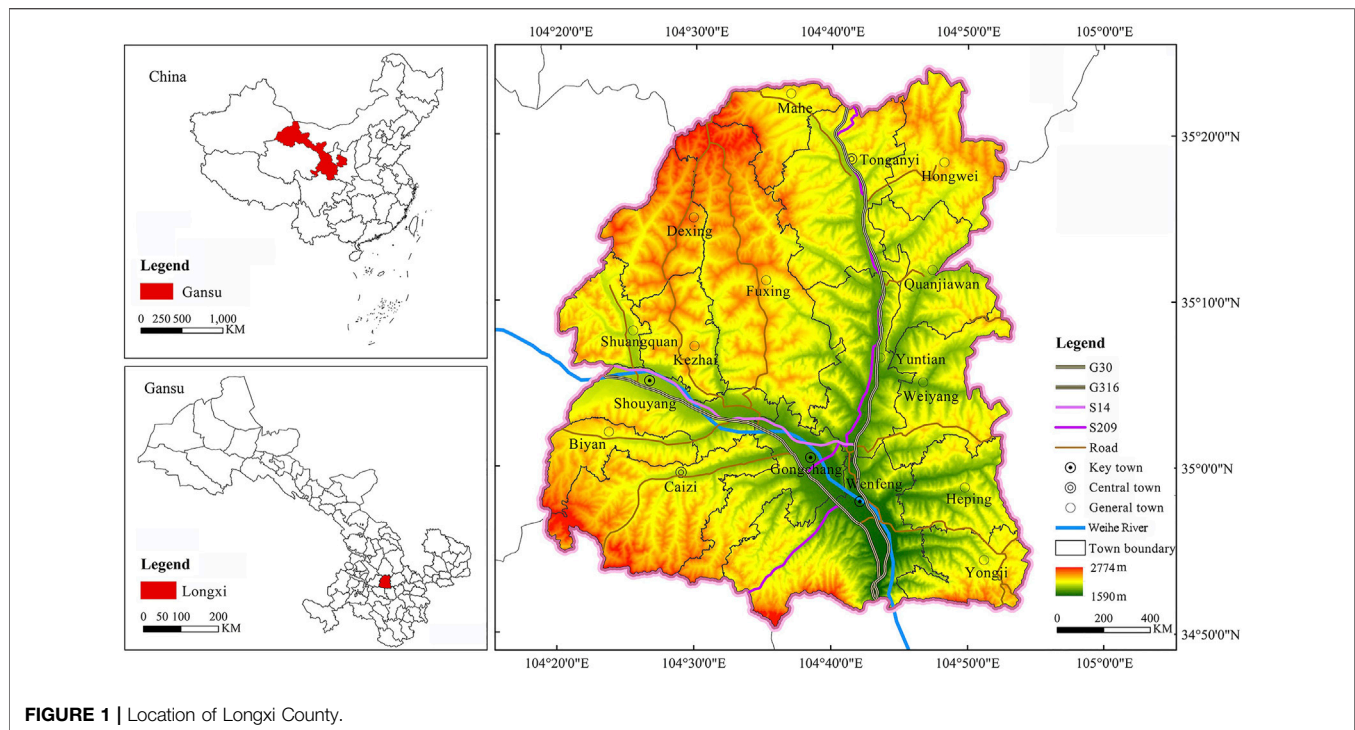
**FIGURE 1 |** Location of Longxi County.

this study comprehensively studied the gradient differences in the spatial structure of REL from multiple dimensions, thereby strengthening the comprehensiveness of geographical gradient research. The main purpose of this study is to explore the gradient differentiation characteristics and laws of REL under different gradients, analyze the impact of different terrains, township development levels, and economic income on the spatial differentiation of REL, and explain its impact mechanism. It is expected to provide a scientific basis for the rational layout, scientific management and control, optimal protection, and sustainable utilization of REL in the loess hilly area of Longzhong. This provides a case reference for the construction of an ecological safety network in the inland areas of northwest China and other places.

The topographic, economic, and administrative gradient differences of "ecological land-dimensional space," take the administrative village as the evaluation unit to reveal the REL structure. The main purpose is to explore the gradient differentiation characteristics and laws of REL under different gradients, analyze the impact of different terrains, township development levels, and economic income on the spatial differentiation of REL, and explain its impact mechanism on EL (Li et al., 2020b). It is expected to provide a scientific basis for the rational layout (Wei et al., 2021), optimal protection, and intensive utilization of REL in the hilly loess area of Longzhong, and provide new ideas and methods for timely adjustment of REL management and improvement of REL management policies, and provide technical support for constructing an ecological safety network in the northwest inland area.

## 2 STUDY AREAS AND DATA

### 2.1 Overview of the Study Areas

Longxi County is located in the southeast of Gansu Province, China, in the middle of Dingxi City (34°50′-35°23′N, 104°18′-104°54′E), with a total area of 2,408 km$^2$ (**Figure 1**). The elevation of Longxi County is between 1, 612–2, 762 m. Since Longxi County is located between the edge of the northwest Loess Plateau and the hilly area of the Qinling Mountain and accompanied by the Wei River flowing from west to east. The loess hills and valleys are high in the northwest and low in the southeast. The northern part of Longxi County is in the loess hills and gully area, the middle part is in the valley plain landform, the south part is in the middle and low hills, the middle and north part is in the temperate arid area, and the south part is in the warm and cold semi-humid area. The geographical environment has significant spatial differences. Longxi County has a temperate continental monsoon climate with four seasons, abundant sunshine, and a mild climate. The average annual temperature is 8.1°C. The annual sunshine hours are 2, 210 h. The annual rainfall is 415 mm, and the annual frost-free period is 160 days.

The superior geographical location and suitable natural environment of Longxi County not only laid a material foundation for early agricultural production but also provided an ideal settlement for the ancestors to thrive. Longxi County governs 12 towns, 5 townships, 213 administrative villages, 11 communities, and 1, 287 villager groups. The total population is 52.48 × 10$^4$, of which the agricultural population is 43.3 × 10$^4$, accounting for 82.51% of the total population (Longxi County Statistical Bulletin 2020). Longxi County has 11.06 × 10$^4$ km$^2$ of

arable land, and the per capita arable land is only 0.25 km$^2$ (Longxi County People's Government, 2020). In recent years, with the acceleration of urbanization and rapid socio-economic development, the flow of population, land, and other elements between urban and rural areas has accelerated, resulting in significant changes in the quantity and structure of rural EL. Longxi County is a typical ecologically sensitive area in the inland northwest China. The fragile ecological environment and unique loess plateau landforms have created a series of ecological and environmental problems such as drought and fragmentation of the surface, ecological severe land loss, and decline in soil quality. This has a significant impact on the quality of the ecological environment and the service functions of the ecosystem. Therefore, it is of great significance to study the spatial distribution and multi-dimensional gradient differentiation characteristics of EL in Longxi County for ecological environment protection and the maintenance of ecosystem stability in the northwest inland region.

## 2.2 Data Source

This study took 213 administrative villages outside the built-up area of Longxi County as the evaluation unit. The data mainly comes from four aspects: 1) basic map: Longxi County Vector Administrative Boundary (1: 250,000), from the National Geomatics Center of China (National Geomatics Center of China, 2021). 2) DEM data: DEM data was from the Geospatial Data Cloud. We obtained elevation and slope data of Longxi County through ArcGIS image correction. 3) Socio-economic statistics: basic data such as the population and economic income of 213 administrative villages in Longxi County were derived from field survey data and the "Statistical Bulletin of National Economic and Social Development of Longxi County in 2020" (Longxi County People's Government, 2020). 4) Land use data: the land use data of Longxi County comes from the 2020 Longxi County Land Use Change Database. The research team conducted a 26-day field survey in Longxi County in May, August, and September 2020. Among them, August-September was a supplementary survey. The survey area is mainly distributed in Quanjiawan Town, Tong'anyi Town, Kezhai Town, Yongji Township, Weiyang Township, and Gongchang Town. The research team learned about the general situation and future development trends of the EL of each township by holding meetings and communicating with the leaders of the township. We cooperated with the Longxi County Land Planning Project Department to know the problematic region of the townships' land rectification and ecological restoration.

In addition, the village profiles, demographic characteristics, basic information on social security, public service facilities, infrastructure, economic conditions, population mobility and employment, industrial conditions, homestead usage, rural development types, and village development intentions or existing problems of 213 administrative villages were obtained through a questionnaire survey. The information related to this research mainly includes village profile, demographic characteristics, economic situation, industrial situation, and type of village development. We collected income data for the division of county economic gradients. The survey showed that

the ecological background conditions of Longxi County are relatively good, and the EL area accounts for 90.45% of the total area of the county. However, there are great differences in the distribution and utilization of EL in different regions, closely related to the local terrain, township level, and income.

## 2.3 Research Methods

### 2.3.1 The Classification of Rural Ecological Land

At present, the "classification of ecological land" is a hot topic in academic research and debate. Scholars have different views and can be roughly classified into two categories. One is to classify land use types on a national scale and according to different theoretical systems. The other is to classify land use types on a local and regional scale and according to specific ecological functions required. Land use status classification is a widely used land use classification system. Different EL types have different ecological functions, and the performance of their ecological functions will be affected by location, physical geography, social economy, and other aspects. Analyzing the gradient differentiation of EL will help the sustainable use of EL and the construction of livable villages in rural revitalization.

In this study, we referred to Li et al. (2020b) classification of EL and follow the national standard for land use classification in the "Land Use Status Classification System" (GB/T 21010–2017) from the government of China (GB/T 21010-2017, 2017). We defined seven types of land use with ecological attributes, including cultivated land, garden land, forest land, grassland, water area, water conservancy facility land, and other lands, as EL. We used the spatial extraction tool of ArcGIS 10.4 to extract EL from the data of the third land use survey in Longxi County in 2020. Since there are few secondary land use types in Longxi County, we divided the extracted EL cover patches into four types: cultivated land, forest land, grassland, and water body (**Table 1**).

### 2.3.2 Gradient Division of Rural Ecological Land

REL is not only a process of natural selection (or adaptation) but also the crystallization of humans' long-term social and economic activities, which contains dual attributes of nature and social economy. The development and transformation of REL run through the whole process of economic and social development of the urban-rural regional system. It is a process of multi-scale, multi-dimensional, multi-level, multi-agent, and multi-factor evolution and reorganization in the evolution of rural human—land relationship regional system (Yang and Luo, 2020). The differentiation of geographical space will inevitably lead to the "gradient" differentiation of nature, society, and economy. It is the existence of this "gradient" that has led to the spatial differences of REL in different gradient areas. In this study, we drew on the previous research on the division of gradients and chose the most classic gradient division method from the three aspects of nature, society, and economy that can mostly affect the spatial layout of REL, that is, from the three aspects of terrain, township level, and economic income. This is the most basic and representative perspective to analyze the gradient differences of EL. The terrain is an important factor affecting landscape patterns and land use. Terrain gradients

**TABLE 1 |** Classification and definition of EL types.

| Type | Content | Definition |
|---|---|---|
| Cultivated land | Dryland, irrigated land | The land where crops (including vegetables) are grown |
| Woodland | Shrubland, other woodlands, arbor woodland, orchard | Land for woody plants such as natural forests, secondary forests, artificial forests, shrubs, and fruit trees in the village |
| Grassland | Artificial pasture, natural pasture, other grasslands | Herbaceous land |
| Waterbody | Reservoir water surface, river water surface, pond water surface, inland tidal flats, main canals, gully, breeding ponds | Land waters, beaches, gully, swamps, and other waters that cover the land |

reflect the spatial differentiation of regional, physical, and geographical conditions. The township level reflects the differences in regional and local policies, fiscal revenue, industrial investment, and social and administrative levels. This will have an impact on the spatial distribution of EL. The township gradient is a specific reflection of the township level. Economic income affects the consumption level, construction scale, industrial investment, and employment status of a region to a certain extent, and the economic gradient reflects the spatial differentiation of regional economic levels.

Based on this, this study analyzes the gradient differences of EL in natural, social, and economic aspects from the three most basic and representative perspectives of terrain, township level, and economic income. The topographic gradient shows the spatial differentiation of the regional natural geographic conditions (Pignatti, 1993; Shi et al., 2021). The township gradient shows the spatial differentiation of regional social administrative levels (Ma et al., 2021a). The economic gradient shows the spatial differentiation of regional economic levels (Qu et al., 2017).

### 2.3.2.1 The Division of Topographic Gradient
The topographic gradient is divided by the topographic position index (Zhou and Chen, 2013; Gong et al., 2014), which comprehensively analyzes the elevation and slope attribute information of any spatial grid. It can integrate the elevation and slope information to reflect the terrain distribution of a certain area. Therefore, we used the topographic position index to quantitatively describe the correlation between the spatial pattern characteristics of EL use and topographic gradients (Zhou et al., 2021). The calculation formula is as follows:

$$T = \ln\left[\left(\frac{E}{E_0} + 1\right) * \left(\frac{S}{S_0} + 1\right)\right], \qquad (1)$$

where $T$ is the topographic position index; $E$ and $E_0$ are the elevations and average elevation of any grid in the space, respectively; $S$ and $S_0$ are the slope and the average slope of any grid in the space, respectively. Generally, a grid with a low elevation and a small slope has a small topographic position index. On the contrary, the larger the topographic position index is, the position with a higher elevation but a small slope or a small elevation with a higher slope will have a middle topographic position index (Xu et al., 2020).

### 2.3.2.2 The Division of Township Gradient
The township gradient dominated the differences in local policies, fiscal economy, and industrial investment. It dramatically impacts

rural ecological land's spatial layout, protection, and use. According to the "Longxi County Urban Overall Planning (2011–2030)", the "Longxi County Urban and Rural Overall Planning (2015–2030)", and the "Notice of the Ministry of Housing and Urban-Rural Development on Announcement of the List of National Key Towns" issued by the Ministry of Housing and Urban-Rural Development of the People's Republic of China in 2014 (Ministry of Housing and Urban-Rural Development of the People's Republic of China, 2014), we divided the 17 townships in Longxi County into three gradients: key towns, central towns, and general towns. The key towns include Gongchang Town, Wenfeng Town, and Shouyang Town, located in the Weihe River Valley. The central towns include Caizi Town and Tonganyi Town, located at the north and south ends of Longxi County. General towns include Yuntian Town, Mahe Town, Fuxing Town, Biyan Town, Heping Township, Weiyang Township, Quanjiawan Township, Hongwei Township, Shuangquan Township, Kezhai Township, Dexing Township, and Yongji Township.

### 2.3.2.3 The Division of Economic Gradient
The economic gradient reflects the differences in the financial economy, industrial input, and consumption levels to some extent (错误!未定义书签。), which in turn affects the number of types, fragmentation, concentration, and complex shapes of REL patches. Referring to relevant research, we took the per capita GDP of each administrative region as the basis for dividing the economic gradient (Qiao and Li, 2008; Liu et al., 2010). Due to the limited availability of data, we took the per capita annual net income of farmers in each administrative village in Longxi County in 2020 as an indicator to measure the rural economic gradient based on raster data and statistical survey data.

### 2.3.3 Spatial Pattern of Rural Ecological Land
The quantity, shape, size, quality, and spatial structure of REL play critical roles in regulating the village's functional structure, ecological balance, suitability of life, and local climate (Zhou and Guo, 2003). In this study, diversity index, fragmentation index, dominance index, and shape index are selected to analyze the spatial differentiation characteristics of EL (**Figure 2**). At the same time, the hot and cold spot analysis method is used to analyze the clustering areas of similar values of different spatial characteristic indices.

### 2.3.3.1 Spatial Characteristic Index of Ecological Land
*2.3.3.1.1 Diversity Index.* Using the Gibbs-Martin diversity index (Zhang et al., 2018) to analyze the spatial diversity of EL, the formula is

$$GM_i = 1 - \frac{\sum_{j=1}^{4} A_{ij}^2}{\left(\sum_{j=1}^{4} A_{ij}\right)^2} \quad (i = 1, 2, \ldots, n; j = 1, 2, 3, 4), \quad (2)$$

where $GM_i$ is the diversity index of the ecological space land use type of the $i$th village. $A_{ij}$ is the area of the $j$th EL in the $i$th village. The value range of $GM_i$ is 0–1. The higher the value of $GM_i$, the higher the degree of diversity. When $GM_i = 0$, there is only one land use type.

### 2.3.3.1.2 Fragmentation Iindex.

The fragmentation index (Chen and Fu, 1996) is often interpreted as the fragmentation degree of the landscape segmentation in landscape ecology. In this study, the total number of EL patches per unit area is used to reflect the fragmentation degree of REL patches. The formula is as follows:

$$C = \frac{\sum N_i}{A}, \quad (3)$$

where $C$ is the fragmentation degree of EL. $\sum N_i$ is the total number of pitches of all EL types in the $i$th village. A is the total area of REL. The higher the $C$ value, the greater the degree of fragmentation.

### 2.3.3.1.3 Dominance Index.

The dominance index (Zhou and Guo, 2003) is the degree of centralization of the dominant land use in REL. The formula is

$$D = H_{max} + \sum_{i=1}^{m} P_{ij} * \ln\left(P_{ij}\right), \quad (4)$$

where $D$ is the ecological dominance degree. $P_{ij}$ is the proportion of the area occupied by the $j$th type of EL in the $i$th village. $m$ is the total number of EL types; $H_{max} = \ln m$.

### 2.3.3.1.4 Shape Index.

The landscape shape index (Chen et al., 2017; Li et al., 2021) is often used to reflect the regularity of patches. We calculated the degree of deviation between the shape of REL and the circle (square) of the same area to show the complexity of the spatial form of REL. The formula is

$$LSI = \frac{e}{4\sqrt{a}}, \quad (5)$$

where $LSI$ is the landscape shape index. $e$ is the perimeter of the EL patch. $a$ is the area of the EL patch. The greater the $LSI$ value, the more complicated the shape and the more irregular the distribution of EL patches.

### 2.3.3.2 Analysis of Hot and Cold Spots

The hot spot method was used to identify the spatial distribution position of the similar value aggregation area of the EL spatial characteristic index in Longxi County to make up for the lack of the global spatial autocorrelation and ArcGIS natural breakpoint method in the analysis of the spatial distribution relationship characteristics.

## 3 RESULT ANALYSIS

## 3.1 Overall Characteristics of Rural Ecological Land

In 2020, the total area of REL in Longxi County will be 2,177.24 km$^2$, accounting for 90.45% of the total area. Among them, the cultivated land area is the largest, reaching 1,497.62 km$^2$, accounting for 68.79% of the REL. The grassland area is 363.24 km$^2$, accounting for 16.68% of the REL. The woodland area is 309.61 km$^2$, accounting for 14.22% of the REL. The water body area is the smallest, 6.76 km$^2$, only accounting for 0.31% of the REL. The EL in Longxi County is mainly cultivated land and forest land. The cultivated land is evenly distributed in the county area (except the central urban area). The forest, grassland, and water bodies are mostly distributed along the Weihe River and in the valley.

In the township distribution of REL, there are significant differences in the distribution of different EL types in each township (**Figure 3**). Cultivated land is the EL type that accounts for the largest proportion of each township. The cultivated land of Wenfeng Town, Caizi Town, and Tonganyi Town accounted for more than 40% cultivated land of the county. The cultivated land of Gongchang Town, where the county government is located, accounts for a relatively small proportion of the county's cultivated land, accounting for only 4.14%. The proportion of forest land is second, Tong'anyi Town's forest land accounts for the highest proportion of the county's forest land, accounting for 10.23%, and Shuangquan Town's forest land accounts for the lowest proportion of the county's forest land, only 2.74%. The proportion of grassland is relatively low. The proportion of grassland in Fuxing Town is the highest in the county, accounting for 17.81%. The proportion of grassland in Biyan Town is the lowest, only 1.54%. The proportion of water bodies in the county is the smallest. The water body in Tong'anyi Town accounts for the most significant proportion of water bodies in the county, accounting for 16.57%. The water bodies of Shouyang Town and Wenfeng Town along the Weihe River account for the following highest proportion of the county's water body, accounting for 15.09% and 14.94%, respectively. In general, Tong'anyi Town takes significant advantages in cultivated land and forest land. Grassland and water resources are poor. Fuxing Town has the largest grassland area. Water bodies are less distributed in the county.

## 3.2 Spatial Characteristics of Rural Ecological Land

### 3.2.1 Spatial Pattern Characteristics of Rural Ecological Land

We calculated the diversity index, fragmentation index, dominance index, and shape index of REL in 213 administrative villages and divided them into five categories, lowest, low, medium, high, and highest through the natural breakpoint method in ArcGIS. (**Figure 4**).

The REL diversity index is between 0.33–0.96 (**Figure 4A**), with an average value of 0.57. The REL diversity indexes of 97 administrative villages are greater than the average value, accounting for 45.54% of the total administrative villages. The diversity of REL is mainly low and medium, including 54 and 67 administrative villages, accounting for 25.35 and 31.46% of the total administrative villages, respectively. Only 15 administrative villages have the highest diversity index, accounting for 7.04% of the total administrative villages. This shows that there are fewer
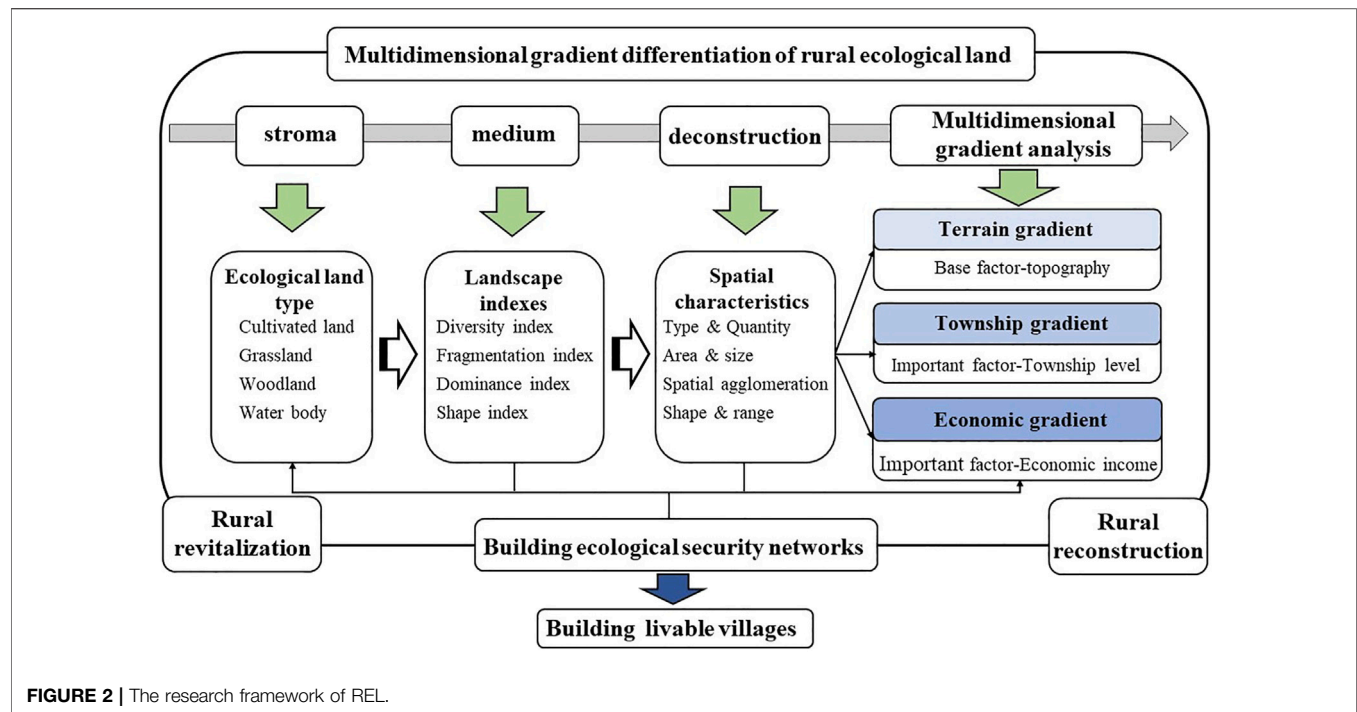
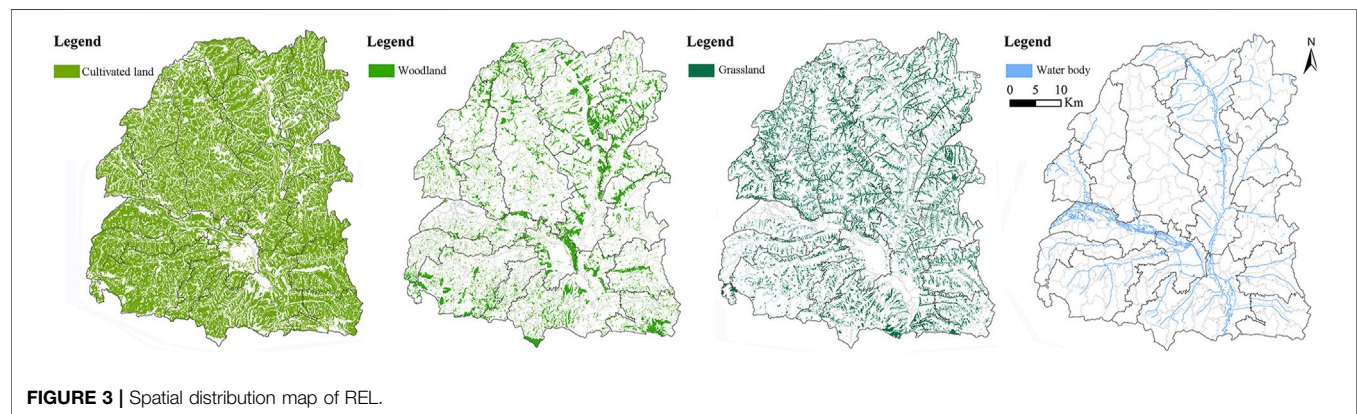FIGURE 2 | The research framework of REL.



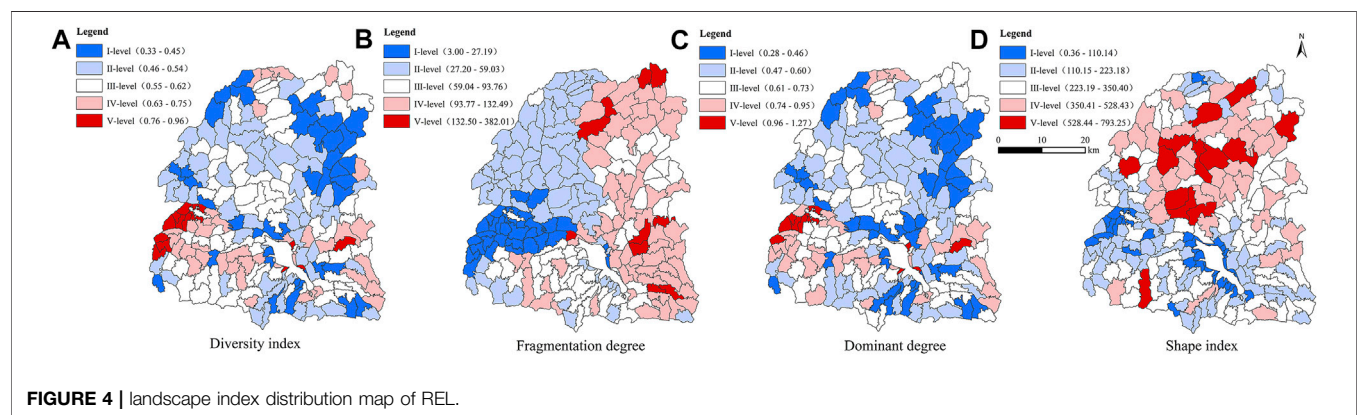FIGURE 3 | Spatial distribution map of REL.



FIGURE 4 | landscape index distribution map of REL.

types of EL in the administrative villages of Longxi County, and the degree of diversity is low. The areas with high and highest values of diversity index are mainly distributed in the south of the Weihe River. The lowest value areas are mainly distributed along the Weihe River and the arid mountainous areas in the north. The low and median areas show a continuous staggered distribution. The central region belongs to the valley terrain, with a high density of population settlements and more diverse types of EL use. Therefore, the high-value area of the diversity index is mainly distributed in the central region.

The REL fragmentation index is between 3.00 and 382.01 (**Figure 4B**), with an average value of 72.15. There are 101 administrative villages with a REL fragmentation index greater than the average value, accounting for 43.72% of the total administrative villages. The fragmentation degree of REL is mainly low and high, including 67 and 60 administrative villages, accounting for 31.46 and 28.17% of the total number of administrative villages, respectively. The number of administrative villages with the highest value is relatively small, only 11, accounting for 5.16% of the total number of administrative villages. There are significant differences in the spatial distribution of REL fragmentation, showing an outward expansion centered on the seat of the county government. The county seat and the east of G30 Lianhuo Expressway are mainly high level, with a relatively high degree of fragmentation. The northwest of the county to the west of the G30 Lianhuo Expressway and the northwest of the Weihe River is dominated by low values, and the degree of fragmentation is relatively low. The inlet of the Weihe River is dominated by the lowest value, and the south is dominated by medium value. The central area is a river valley with a good ecological environment, and the western area is less disturbed by traffic. Therefore, the fragmentation index of EL in the central and western areas is relatively low.

The REL dominance index is between 0.28 and 1.27 (**Figure 4C**), with an average of 0.62. The dominance index of REL for 100 administrative villages is greater than the average value, accounting for 46.95% of the total administrative villages. The dominance index of REL for 126 administrative villages is mainly low and medium value, accounting for 59.15% of the total number of administrative villages. The highest value is only 12, accounting for 5.63% of the total number of administrative villages. The dominance index of the central river valleys and the southern hills and mountains is high. The dominance index of the northern mountainous areas is mainly at the lowest and middle levels. This indicates that the concentration of REL in the central and southern regions is greater than that in the northern mountains. The central part is the river valley, the terrain is relatively flat, and the utilization rate of EL is high.

The REL shape index is between 0.36 and 793.25 (**Figure 4D**), with an average value of 261.92. The shape indexes of REL of 93 administrative villages are greater than the average value, accounting for 43.66% of the total administrative villages. The shape index of REL is mainly of low and medium value, including 63 and 68 administrative villages, accounting for 29.58 and 31.92% of the total number of administrative villages, respectively. There are only 36 administrative villages at a high

level, accounting for 16.90% of the total number of administrative villages. The shape indexes of most of the northern and central regions are significantly greater than that of the southern region. The highest value areas are mainly concentrated in Dexing Township, Fuxing Town, Tonganyi Town, Quanjiawan Town, and Caizi Town. This indicates that the spatial shape of EL patches in the northern and central regions is complex. The northern and central regions belong to the loess hilly and gully region, and the shape of the EL with the ravines vertical and horizontal is more complex and diverse than the topography of the southern river valleys. The northern and central areas belong to the loess hilly and gully area, with the vertical and horizontal gully. The shape of EL is more complex and diverse than that of the southern river valley.

### 3.2.2 Analysis of Hot (Cold) Spots of Rural Ecological Land

We further analyzed hot spots and cold spots in different spaces of REL through the spatial hot spot detection method. In addition, we tested whether there are statistically significant higher- and lower-value areas. The red area in **Figure 5** is the hot spot area, which represents the high-value clusters of the REL diversity index, fragmentation index, dominance index, and shape index. The blue area is cold spots, representing the lower-value areas of the REL diversity index, fragmentation index, dominance index, and shape index. The hot spots and cold spots of different characteristics of REL have significant regional differentiation. The diversity index showed a "hot spot" area in Shouyang Town and Biyan Town at the entrance of the Weihe River, and the "cold spot" area was scattered. On the contrary, the fragmentation index has formed a larger cold spot in Kezhai Town, Shouyang Town, Biyan Town, and Shuangquan Town, where the Wei River flows. Some towns in the north and east of the county have formed four small hot spots. The distribution of hot spots and cold spots in the dominance index is similar to the diversity index, and the area has increased. The shape index forms a large-scale of hot spots in Dexing Township, Fuxing Town, Yuntian Town, Quanjiawan Town, and Tonganyi Town in the central part of the county. Two larger cold spots are formed in Shouyang Town, Biyan Town, Wenfeng Town, and the periphery of the county where the Wei River flows.

## 3.3 Multi-Dimensional Gradient Differentiation of Rural Ecological Land
### 3.3.1 Topographic Gradient Differentiation of Rural Ecological Land

The spatial pattern index of rural ecological land use in different topographic gradients is quite different (**Figure 6**). As the topographic gradient rises, the diversity index and dominance index first decrease and then increase, and the fragmentation index and shape index constantly increase. The average values of the diversity index in low, medium, and high topographic gradients are 0.66, 0.55, and 0.56, respectively. The average values of the fragmentation index are 78.04, 79.73, and 61.23, respectively. The average values of the dominance index are 0.76,

**FIGURE 5 |** analysis of hot spots and cold spots of the landscape index of REL.
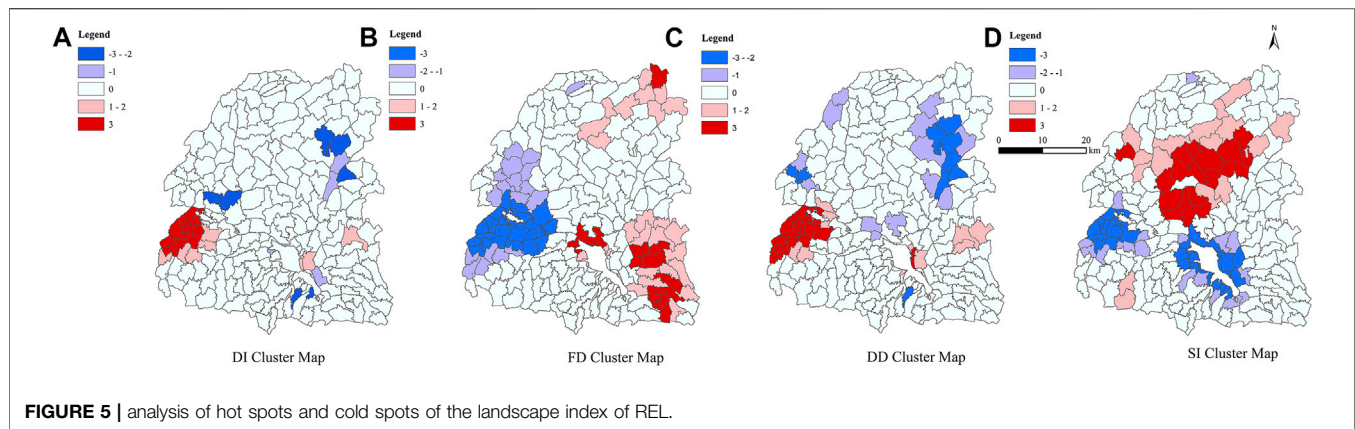
0.59, and 0.62, respectively. The average values of the shape index are 108.67, 260.04, and 309.27, respectively. In the lower-value area of the topographic gradient, the diversity index, fragmentation index, and dominance index fluctuate more significantly with the increase of the topographic level index. In addition, the fluctuation range is large, and the shape index shows a steady rise. The fluctuation trends of the diversity index and the dominance index are similar, and the fragmentation index is the opposite—the greater the diversity index and dominance index, the smaller the fragmentation index. In addition, when the topographic index is between 41 and 50, the diversity and dominance indexes show a sharply downward trend. The shape index and fragmentation index increase slowly. In the median area of the topographic gradient, the diversity index, fragmentation index, and dominance index show a slow rise in fluctuation with the increase of the topographic level index, but it was not significant. The shape index increases rapidly when the topographic position index is between 81 and 130 and then decreases. The fluctuation trends of the diversity index and the dominance index are also similar, and the fragmentation index is the opposite. In the higher-value area of the topographic gradient, the diversity index, fragmentation index, dominance index, and shape index generally show a trend of fluctuation and decline as the topographic level index increases. The diversity index and dominance index increased slightly when the topographic index was between 133 and 150 as well as 171–190 and then decreased rapidly.

### 3.3.2 Township Gradient Differences in Rural Ecological Land

The spatial differentiation characteristics of REL differ significantly in different township gradients (**Figure 7**). As the township level rises, the diversity index and dominance index increase accordingly. The fragmentation index and shape index present a normal distribution, which is relatively high in the central town. The average values of the diversity index in the general town, central town, and key town are 0.55, 0.56, and 0.60, respectively. The average values of the fragmentation index in them are 72.42, 88.69, and 64.65, respectively. The average values of the dominance index in them are 0.59, 0.61, and 0.68, respectively. The average values of the shape index in them are 308.79, 348.59, and 140.64, respectively.

For the general town, the diversity index, fragmentation index, and dominance index show regular fluctuations as the distance from the township government increases. Both the diversity index and the dominance index decrease first and then increase, while the change of the fragmentation index is just the opposite. The shape index shows a steady rise. At a distance of 6–7 km, the diversity index, fragmentation index, dominance index, and shape index all show an increasing trend. In the central town, the diversity index and dominance index show a clear upward trend with increasing distance from the township government. However, the law of change is opposite to that of general town, all of which increase rapidly and then decrease. The change in the fragmentation index is the opposite. The shape index is still showing a steady upward trend. Taking 3–4 km as the boundary, the fluctuation range of the diversity index, fragmentation index, and dominance index show a trend of "large first and then small." The growth rate of the shape index starts to slow down at 4–5 km. In the key town, the diversity index and dominance index show a significant fluctuation and decreasing trend as the distance from the township government increases. The fragmentation index and shape index show an increasing trend, and the shape index increases significantly.

### 3.3.3 Economic Gradient Differences in Rural Ecological Land

The spatial pattern index of REL under different economic gradients is quite different (**Figure 8**). Overall, as the economic gradient increases, the diversity index and dominance index show a slow increase in the average value of the index. The fragmentation index and shape index show a trend of rapid decline at first and then gradually flattening. The average values of the diversity index in low, medium, and high economic gradients are 0.54, 0.56, and 0.59, respectively. The average values of the fragmentation index in them are 79.15, 73.09, and 63.18, respectively. The average values of the dominance index in them are 0.59, 0.61, and 0.66, respectively. The average values of the shape index in them are 307.26, 290.02, and 180.20, respectively. On low economic gradients, although the four types of indexes fluctuate, their amplitudes are relatively small. The diversity index and dominance index rose slowly, while the fragmentation index and shape index declined slowly. In the middle economic

**FIGURE 6 |** Topographic gradient differentiation map of the landscape index of REL.
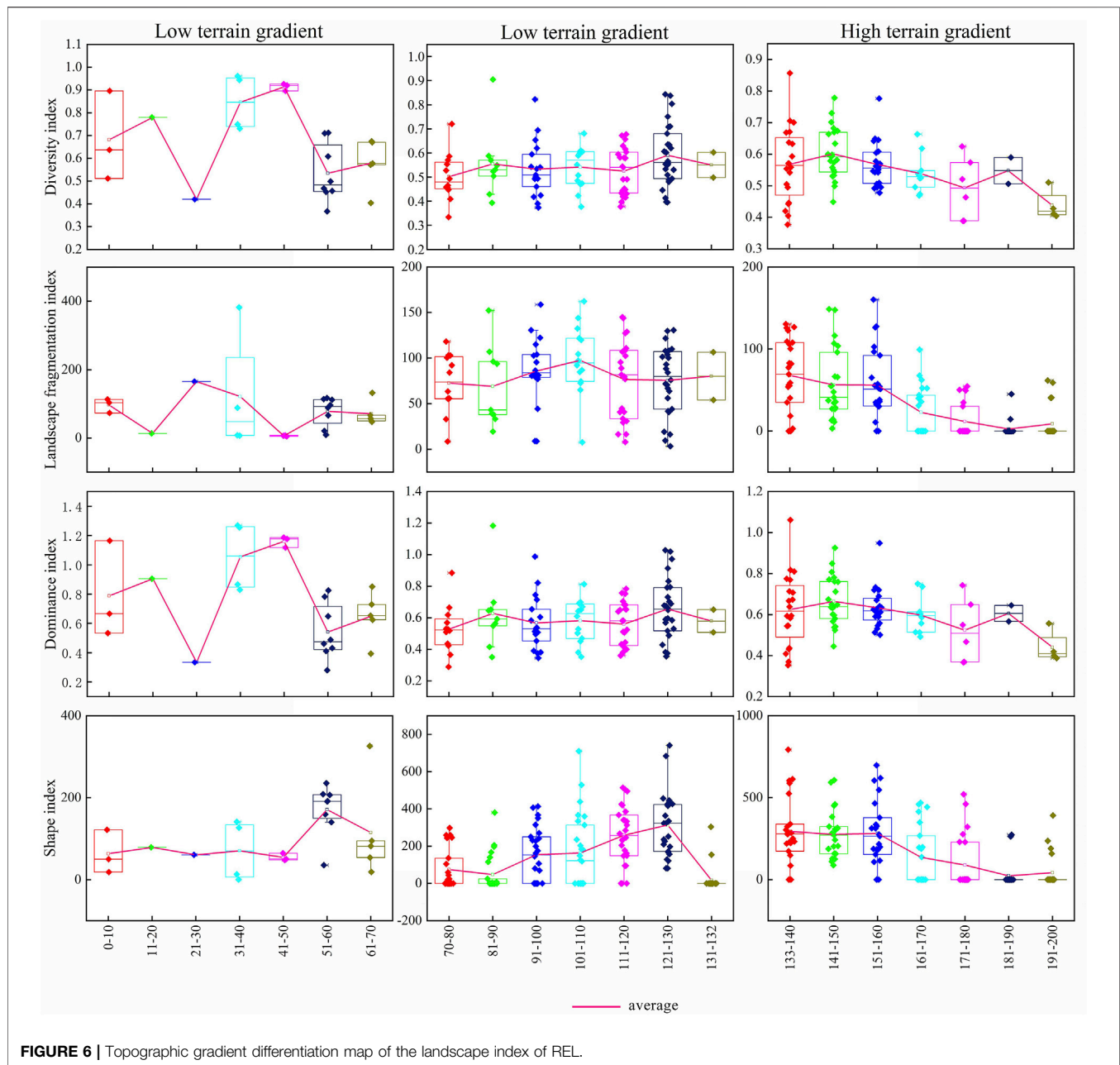
gradient, the fluctuation range of the four types of indexes increased significantly. The turning point is when the per capita annual net income of farmers reaches 7,000–7,500 yuan. The diversity index and dominance index showed a trend of first decreasing and then increasing. The fragmentation index and shape index showed a trend of first increasing and then decreasing. With respect to high economic gradients, the four types of indexes have smaller fluctuations amplitude than the medium economic gradients, and the fluctuation trend is the same as that of the low economic gradients. The diversity index and dominance index maintained a relatively high level of fluctuation. At the same time, the fragmentation index and the shape index are the

opposite. In general, with the increase of the economic gradient, the types of EL used for human development and utilization are more abundant, and the shape of EL is more regular and orderly. Therefore, the diversity index and shape index generally show an increasing trend. In low economic gradient areas, EL is less affected by external factors, and the spatial characteristics do not change significantly. When the economic gradient reaches a certain level, the fragmentation of EL gradually decreases under certain development and planning. However, the dominant type is weakened. However, when developed to a certain extent, the drawbacks of ecological land development and utilization gradually appeared because of the instability of the rural economy. The

**FIGURE 7 |** Township gradient differentiation of the landscape index of REL.
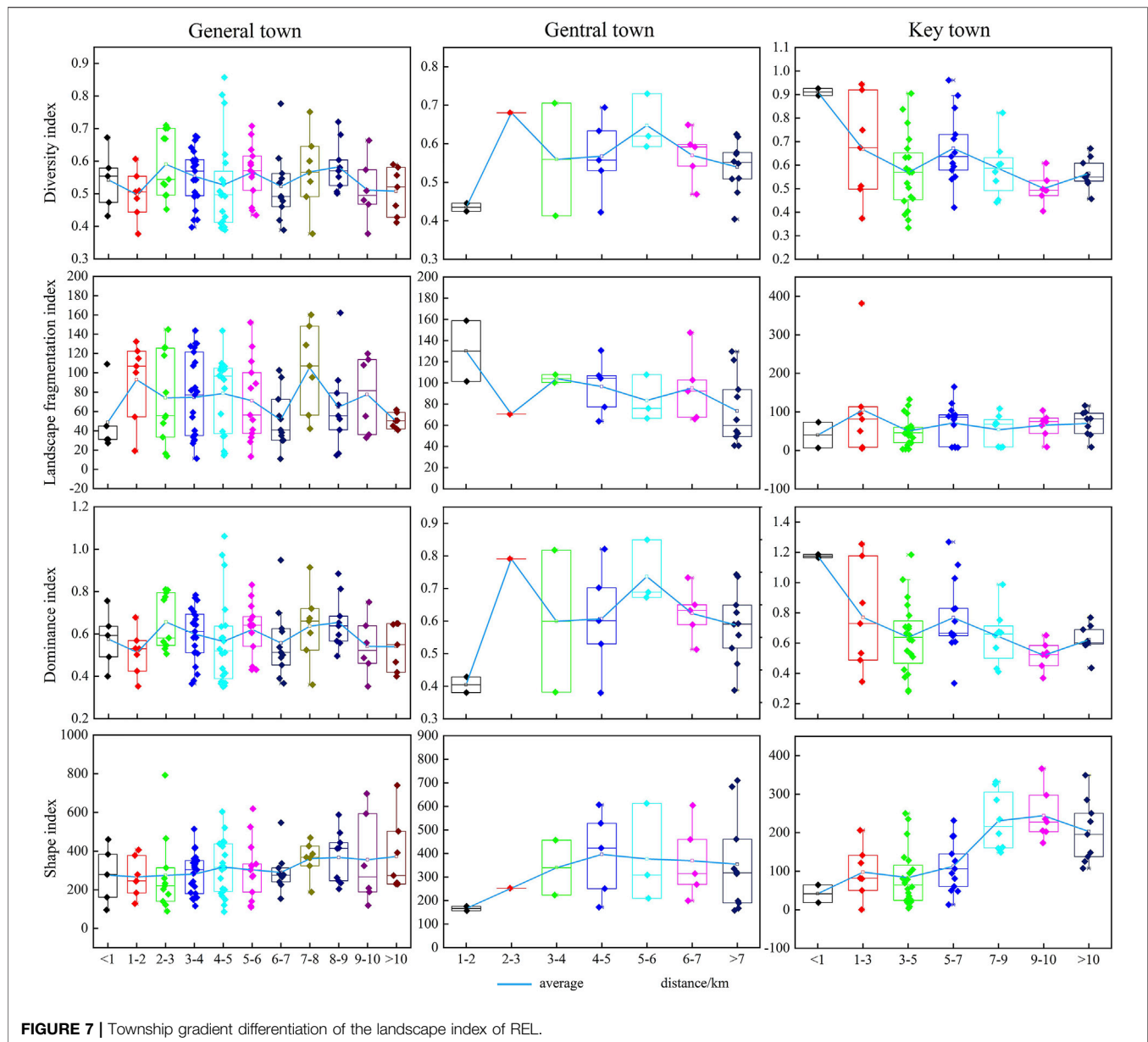
degree of fragmentation and concentration increased and stabilized.

# 4 DISCUSSION

## 4.1 Gradient Differentiation Mechanism of Rural Ecological Land

With the industrialization and urbanization of China, the spatial distribution of rural land use has undergone tremendous changes and reconstruction. Accurately grasping the spatial differentiation characteristics of EL in different dimensions is the key to ecological, environmental protection, and the base of governance and optimization of land space (Han et al., 2021). The spatial distribution of REL

results from the combined effects of multiple factors. It is closely related to the geographical topography, climatic conditions, economic development level, customs, culture, policy control, and other factors (Li et al., 2020b). It has a vital impact on all aspects of the rural ecosystem. Topography is the fundamental driving factor that affects the structure of REL, which will impact the type, scale, and form of the land. The location of towns and their resource endowments determines the rank of towns, and it is an accelerating factor for changes in the structure of REL. Different levels of cities and towns have different effects on REL. As a driving factor of the internal rural land use structure, the level of rural economic development is closely related to the rural industrial structure and land use types. There is a complex interaction mechanism between the two.

**FIGURE 8 |** Economic gradient differentiation of the landscape index of REL.
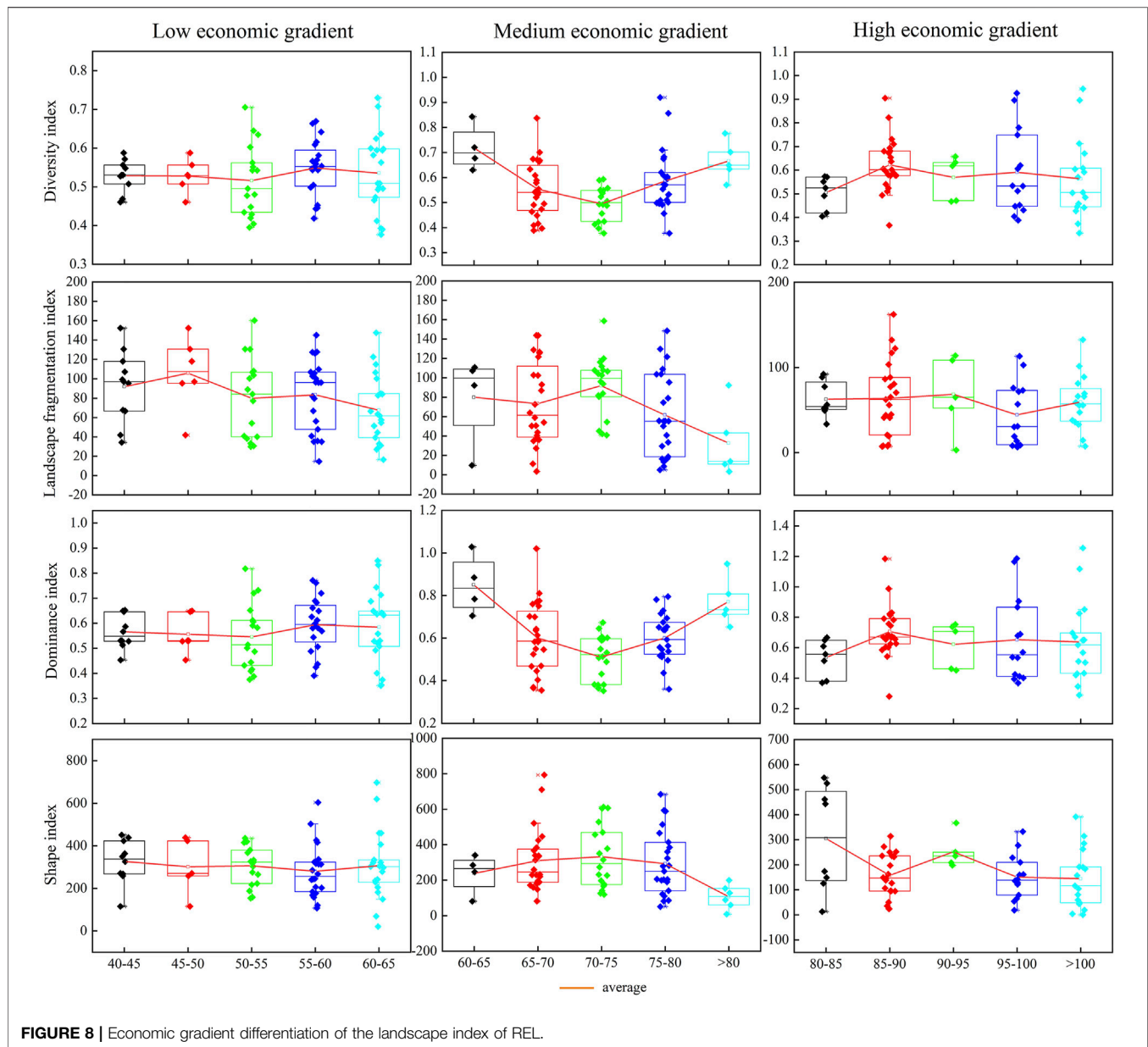
(1) The EL characteristic index varies significantly by changing the topographic gradient level. With the rise of the topographic gradient, the diversity index and fragmentation index of EL decreased overall, while the dominance index and shape complexity increased significantly. In the river valley areas with little difference in altitude and slope, and a small topographic index, there are no prominent regular characteristics in the type of REL, the degree of fragmentation of patches, the degree of land concentration, and the complexity of spatial forms. Its spatial difference depends more on its location and the concentration of human activities. In hilly and mountainous areas where the altitude and slope have increased to a certain extent, and the topographic index is relatively large, the types of REL have increased

significantly—the degree of fragmentation of patches and the degree of centralization of land use increase accordingly. The complexity of the spatial form has also significantly increased. In mountainous areas with high altitudes and slopes and greater topographic index, the topography conditions become relatively complex. The availability of REL has been significantly reduced. The type of land used tends to be single, mostly grassland and woodland, and the patches are well concentrated and contiguous, and the plots are relatively regular.

(2) The EL characteristic index varies significantly by the changes in the township gradient level. With the rise of the township gradient, ecological land's diversity index and dominance index generally increased, while the fragmentation and shape complexity first increased and

then decreased. Due to various factors such as poor soil and a backward economy, the overall geographical environment of general towns is poor. Except for the government seat, most are located in mountainous and hilly areas as the distance from the township government increases, the type of REL, the degree of fragmentation of patches, the degree of concentration of land use, and the degree of complexity of spatial form have no significant change characteristics (Ma et al., 2021a). The overall change range is small, and the influence of the township government is not significant. The township government significantly affects the EL within 3 km outside the central town. The topography in this area is relatively flat, the cultivated land is relatively concentrated, and the degree of concentration is good. As the distance from the township government increases, the types of REL tend to be diversified. However, due to the division of rivers, roads, settlements, and other elements, the land is relatively irregular, and the impact of the township government is not significant beyond 3 km of EL. The key towns are mainly distributed in the river valley areas along the Weihe River. Gongchang Town, Wenfeng Town, and Shouyang Town are arranged along the river, and the layout of EL is greatly affected by the river. The types of EL within 1 km of the periphery of the river are relatively diverse, and the degree of concentration is good. The land patches are concentrated and contiguous, and the degree of fragmentation is low and relatively regular. As the distance from the township government station and the river increases, the types of REL, the degree of centralization of patches were significantly reduced, the degree of fragmentation of patches was increased, and the degree of shape complexity was significantly enhanced.

(3) The EL characteristic index of Longxi County varies greatly due to the changes in economic gradient levels. With the rise of the economic gradient, the diversity index and dominance index of EL generally increased, and the fragmentation and shape complexity showed a downward trend. Villages with low economic gradients are mostly located in mountainous areas, strongly restricted by topography, with poor agricultural production conditions and fragile ecological environments. In addition, they are far away from urban areas and townships, making industrial development difficult, and the number of migrant workers is enormous. The type of land used tends to be single and fragmented. The degree of fragmentation is small, and the patches are relatively regular. The distribution of villages in the middle economic gradient is relatively concentrated, mostly located in hilly areas, with relatively good agricultural production conditions, and are4 close to towns and villages. The types of EL have increased significantly. The land used for agriculture, forestry, water, and the grass is staggered, and the patches of EL tend to be fragmented, centralized, and complex in shape. Most of the villages in the high economic gradient area are located along the Weihe River and the main roads, which are close to the urban area and township area, and the transportation is convenient. The more diverse the use types of EL, the higher the concentration of the dominant EL, and the simpler the shape accordingly.

## 4.2 Suggestions on the Guarantee Policy of Rural Ecological Land

REL directly provides the ecological service guarantee for various production and living activities in rural areas. It is an essential ecological source for absorbing urban life pollution and industrial pollution (Fei et al., 2020). Therefore, scientifically protecting and making good use of REL is an essential foundation for the overall sustainable development of rural society and economy and an essential means to supplement and improve urban functions (Zhou et al., 2016; An, 2018). REL should be classified, optimized, protected, and used based on full consideration of its topographic gradient, township gradient, and economic gradient. First, correctly handle the relationship between man and nature, the relationship between production and ecology, and the relationship between ecology and people's livelihood, scientifically plan the spatial layout of bare, auxiliary, and preservation EL and non-ecological land, and combine the gradient differences of EL in each village. Formulate EL layout and ecological protection goals in different regions, effectively protect the ecological environment and ecological space on which human beings depend, and promote sustainable economic and social development (Qiu et al., 2022). Second, it is necessary to build a county-level ecological security pattern, optimize the county-level grain production and land use pattern, and coordinate the contradiction between regional product development and ecological protection. At the same time, it is actively carrying out the consolidation of agricultural land, tapping the potential of unused land, cultivating or restoring green according to local conditions, increasing the rural ecological space, and improving the rural living environment (Gao, 2017; Yang et al., 2017). Finally, from the perspective of the gradient heterogeneity of EL, we insist on implementing policies based on local conditions and implementing differentiated REL optimization and protection paths (Zhang and Ren, 2016; Zhao et al., 2020).

## 4.3 Prospects for the Future Research on Rural Ecological Land

REL is an important part of territorial space, and it is of great significance for maintaining regional ecological balance and promoting sustainable urban–rural relations. At present, REL has become a hot field of academic research. Existing studies have analyzed the changes and differentiation trends of EL patterns on a long-term scale. Also, they have studied the effectiveness of different ecological spaces on a time scale. Based on the gradient of "important ecological space-surrounding area space," the gradient difference of the protection effect is analyzed. It is concluded that the protective effect of EL in important ecological spaces is better than that of surrounding external areas (Gao et al., 2021). With the development of urbanization, the relationship between urban and rural areas has entered a critical period of strategic transformation. The

development and evolution of regional humanities, nature, society, and other factors will inevitably drive the evolution of the spatial pattern of REL. However, at present, there are few studies on the spatial differentiation and impact mechanism of REL under different gradients from the multi-dimensional gradient of nature, society, and economy. Therefore, this study used the landscape index to explore the differentiation characteristics of the spatial pattern of REL in different dimensions. This not only reflects the spatial pattern characteristics of REL but also reveals the differentiation law of REL under multi-dimensional gradient. This study is of great scientific significance for the adjustment of rural land use structure, the promotion of urban–rural integration construction, the delimitation of regional ecological protection red line (Guan et al., 2018), and the improvement of the ecosystem service function. However, due to the availability of data and the constraints of research perspectives, this study has many uncertainties and limitations. First, according to the traditional land use classification system, this study classifies EL into four categories: woodland, grassland, water body, and cultivated land, without considering the ecological attributes and ecological functions of each land use (Li et al., 2020b). Second, this study attempts to study the spatial differentiation characteristics of REL from a multi-dimensional gradient. This study considers the impacts and differences of multiple factors such as topographical conditions, township development level, and socio-economic conditions on the spatial distribution of REL. However, the interaction of multiple factors on the spatial distribution of EL is not considered (Feng et al., 2021b). In addition, the spatial distribution of REL under different gradients obtained in this study does not mean that the distribution of REL in other areas follows this result. Research on EL in different regions should consider its regional characteristics, local conditions, and socio-economic situations (Ma et al., 2021a).

Ecological civilization has become a national strategy for the construction of a socialist society with Chinese characteristics (Fei et al., 2020). The new situation requires us to accurately identify the spatial differentiation characteristics of REL so as to optimize the reconstruction of rural ecological space, improve the scientific control of rural ecological space, and promote the construction of an ecological safety network (Long et al., 2015; Wen et al., 2017). In the follow-up EL research, we will strengthen the planning and control strategy analysis of EL and the evaluation and analysis of the implementation of institutional mechanisms so that the research results of EL will help to play better a guiding role (Chen et al., 2008; Qi et al., 2016).

# 5 CONCLUSION

The number of REL in Longxi County is relatively large, and the spatial pattern is significantly different. The area of EL accounts for 90.45% of the county's total area. It has an excellent ecological background and is dominated by cultivated land, accounting for 68.79% of the REL. Grassland is second, accounting for 16.68% of REL. The area of water bodies is the least, accounting for only

0.31% of the REL. EL is one of the important types of land use. Accurately grasping the spatial distribution and scale of different types of EL is of great significance for accurately protecting EL and using EL according to local conditions. In the future, Longxi County should focus on protecting the main ecological resource of Cultivated land while taking into account the protection of grassland, forest land, and water bodies.

Second, the spatial characteristic index and spatial pattern of REL in Longxi County are significantly different. The diversity, dominance, and shape index are mainly at low and medium levels, while the fragmentation degree is mainly at low and high levels. In the protection and utilization of EL, we should increase the protection of different types of EL and improve the effectiveness of protection measures according to the spatial characteristics of different types of EL.

The diversity, dominance, fragmentation, and shape index gradients of REL in Longxi County were significantly different. With the increase of the topographic position index, the types of REL increased significantly, the fragmentation degree of patches and the degree of concentration of land use increased, and the complexity of the spatial form also increased significantly. After the local topographic position index reaches a certain level, the availability of REL is significantly reduced. The type of land use tends to be single, the concentration of patches is poor, and the shape of the plot is relatively complex. In addition, REL is also affected by the township level. The higher the level, the more significant the impact, but smaller the impact range. REL of the general township is not significantly affected by the township government, but the township government within 3 km outside the central town is affected significantly. Within 1 km of the key township are significantly affected by the township government. The impact of the economic gradient on REL is closely related to the geographical environment where the village is located. With the rise of the economic gradient, the geographical environment becomes better, the types of land use gradually increase, and the degree of concentration increases, but the fragmentation and morphology show the trend of rising and then falling. Under the division of different gradients, the characteristic indices of EL have different evolution laws. Studying the spatial characteristics of EL from multiple dimensions is conducive to a comprehensive understanding of the internal trends and mechanisms of EL distribution and plays a vital role in national land spatial planning and national land ecological security protection. The protection of REL in Longxi County should fully consider the topography, townships, and economic gradients where it is located, integrate the spatial differentiation characteristics of the diversity, fragmentation, dominance, and shape indexes, and take protection measures according to local conditions. From the aspects of formulating ecological protection goals in different regions, constructing county ecological security patterns, and coordinating the contradiction between regional product development and ecological protection, it proposes differentiated paths for REL optimization and protection to optimize the spatial development pattern of the country and promote the construction of a rural living environment that is livable and suitable for business.

## DATA AVAILABILITY STATEMENT

The raw data supporting the conclusion of this article will be made available by the authors, without undue reservation.

## AUTHOR CONTRIBUTIONS

## FUNDING

## REFERENCES

An, G. (2018). Spatio-temporal Evolution and Conservation Zoning of Ecological Land in Shandong Province Based on EKC & Lorenz Curve. *China Land Sci.* 32, 89–96.

Capotorti, G., Guida, D., Siervo, V., Smiraglia, D., and Blasi, C. (2012). Ecological Classification of Land and Conservation of Biodiversity at the National Level: The Case of Italy. *Biol. Conserv.* 147, 174–183. doi:10.1016/j.biocon.2011.12.028

Chen, L., and Fu, B. (1996). Analysis of Impact of Human Activity on Landscape Structure in Yellow River Delta—A Case Study of Dongying Region. *Acta Ecol. Sin.* 16, 337–344.

Chen, S., Liu, Y., and Peng, L. (2008). Dynamics of Urban Ecological Space Evolution and Policy Responses: A Case Study of Nanjing City. *Acta Ecol. Sin.* 28, 2270–2278. doi:10.3321/j.issn:1000-0933.2008.05.044

Chen, W., Liu, Y., Yin, C., Jing, Y., and Guan, X. K. (2017). Layout Optimization for Rural Settlements Based on Iterative Evaluation Method and its Remediation Strategies. *Trans. Chin. Soc. Agric. Eng.* 33, 255–263. doi:10.11975/j.issn.1002-6819.2017.17.034

Colding, J. (2007). 'Ecological Land Use Complementation' for Building Resilience in Urban Ecosystems. *Landsc. Urban Plan.* 81, 46–55. doi:10.1016/j.landurbplan.2006.10.016

Deng, H., Chen, C., Liu, X., and Wu, G. (2009). Conception and Function Classification of Regional Ecological Land. *Acta Ecol. Sin.* 29, 1519–1524.

Fei, J., Xia, J., Ou, D., Shu, X., and Hu, J. (2020). Integrated Identification and Classification of Rural Ecological Land. *Chin. J. Ecol.* 39, 1045–1055. doi:10.13292/j.1000-4890.202003.031

Feng, R., Wang, F., and Wang, K. (2021). Spatial-temporal Patterns and Influencing Factors of Ecological Land Degradation-Restoration in Guangdong-Hong Kong-Macao Greater Bay Area. *Sci. Total Environ.* 794, 148671. doi:10.1016/j.scitotenv.2021.148671

Feng, R., Wang, F., Wang, K., Wang, H., and Li, L. (2021). Urban Ecological Land and Natural-Anthropogenic Environment Interactively Drive Surface Urban Heat Island: An Urban Agglomeration-Level Study in China. *Environ. Int.* 157, 106857. doi:10.1016/j.envint.2021.106857

Folke, C., Carpenter, S., Walker, B., Scheffer, M., Elmqvist, T., Gunderson, L., et al. (2004). Regime Shifts, Resilience, and Biodiversity in Ecosystem Management. *Annu. Rev. Ecol. Evol. Syst.* 35, 557–581. doi:10.1146/annurev.ecolsys.35.021103.105711

Frondoni, R., Mollo, B., and Capotorti, G. (2011). A Landscape Analysis of Land Cover Change in the Municipality of Rome (Italy): Spatio-Temporal Characteristics and Ecological Implications of Land Cover Transitions from 1954 to 2001. *Landsc. Urban Plan.* 100, 117–128. doi:10.1016/j.landurbplan.2010.12.002

Gao, J., Liu, X., Wang, C., Wang, Y., Fu, Z., Hou, P., et al. (2021). Evaluating Changes in Ecological Land and Effect of Protecting Important Ecological Spaces in China. *Acta Geogr. Sin.* 76, 1708–1721. doi:10.1007/s11442-021-1896-y

Gao, Y. (2017). Strengthen Research on Ecological Space Protection and Use Control. *China Land* 12, 16–18.

Gb/T 21010-2017 (2017). *Current Land Use Classification*. China: standardization administration, State Administration for Market Regulation.

Gong, J., Gao, Y., Zhang, L., Xie, Y., Zhao, C., and Qian, D. (2014). Distribution Characteristics of Ecological Risks in Land Use Based on Terrain Gradient and Landscape Structure: Taking Bailongjiang Watershed as an Example. *J. Lanzhou Univ. Nat. Sci.* 50, 692–698. doi:10.13885/j.issn.0455-2059.2014.05.019

Gong, J., Jiang, C., Chen, W., Chen, X., and Liu, Y. (2018). Spatiotemporal Dynamics in the Cultivated and Built-Up Land of Guangzhou: Insights from Zoning. *Habitat Int.* 82, 104–112. doi:10.1016/j.habitatint.2018.10.004

Gonzalez-Abraham, C. E., Radeloff, V. C., Hawbaker, T. J., Hammer, R. B., Stewart, S. I., and Clayton, M. K. (2007). Patterns of Houses and Habitat Loss from 1937 to 1999 in Northern Wisconsin, USA. *Ecol. Appl.* 17, 2011–2023. doi:10.1890/06-1963.1

Guan, Q., Hao, J., Shi, X., Gao, Y., Wang, H., and Li, M. (2018). Study on the Changes of Ecological Land and Ecosystem Service Value in China. *J. Nat. Resour.* 33, 195–207. doi:10.11849/zrzyxb.20161400

Han, M., Kong, X., Li, Y., Wei, F., Kong, F., and Huang, S. (2021). Eco-environmental Effects and its Spatial Heterogeneity of Ecological-Production-Living' Land Use Transformation in the Yellow River Delta. *Sci. Geogr. Sin.* 41, 1009–1018. doi:10.13249/j.cnki.sgs.2021.06.010

Hietala-Koivu, R. (1999). Agricultural Landscape Change: a Case Study in Yläne, Southwest Finland. *Landsc. Urban Plan.* 46, 103–108. doi:10.1016/s0169-2046(99)00051-1

Joppa, L. N., and Pfaff, A. (2011). Global Protected Area Impacts. *Proc. R. Soc. B* 278, 1633–1638. doi:10.1098/rspb.2010.1713

Li, H., Yi, N., Yao, W., Wang, S., Li, Z., and Yang, S. (2011). Shangri-La County Ecological Land Use Planning Based on Landscape Security Pattern. *Acta Ecol. Sin.* 31, 5928–5936. doi:10.1016/j.chnaes.2010.11.006

Li, M., Tian, F., and Dong, Y. (2016). Space Identification of Ecological Importance and Protection on Urban Ecological Land in Yanji-Longjing-Tumen Area. *Sci. Geogr. Sin.* 36, 1870–1876. doi:10.13249/j.cnki.sgs.2016.12.012

Li, D., Xu, E., and Zhang, H. (2020). Influence of Ecological Land Change on Wind Erosion Prevention Service in Arid Area of Northwest China from 1990 to 2015. *Ecol. Indic.* 117, 106686. doi:10.1016/j.ecolind.2020.106686

Li, G., Jiang, C., Du, J., Jia, Y., and Bai, J. (2020). Spatial Differentiation Characteristics of Internal Ecological Land Structure in Rural Settlements and its Response to Natural and Socio-Economic Conditions in the Central Plains, China. *Sci. Total Environ.* 709, 135932. doi:10.1016/j.scitotenv.2019.135932

Li, J., Zhang, P., and Guo, M. (2021). Spatial Distribution and Optimized Reconstructing Mode of Rural Settlement at the Village Scale of Jilin Province. *Sci. Geogr. Sin.* 41, 842–850. doi:10.13249/j.cnki.sgs.2021.05.012

Liu, L., Lei, D., Ran, Y., and Zhang, Y. (2021). Identification of Critical Ecological Land in Dianchi Watershed Based on the Perspective of Ecosystem Service Function. *Trans. Chin. Soc. Agric. Eng.* 37, 277–284. doi:10.11975/j.issn.1002-6819.2021.11.031

Liu, Y., Liu, Y., and Guo, L. (2010). Spatial Difference Analysis of the Rural Residents'Net- Income along the Bohai Rim in China. *Econ. Geogr.* 30, 992–997.

Long, H., Liu, Y., Li, T., Wang, J., and Liu, A. (2015). A Primary Study on Ecological Land Use Classification. *Ecol. Environ. Sci.* 24, 1–7.

Longxi County People's Government (2020). *Statistical Communiqué on Longxi County's National Economic and Social Development in 2020*. Available online: http://www.cnlongxi.gov.cn/art/2021/7/5/art_10710_1427503.html/November accessed on 10, 2021).

Ma, L., Cui, X., Yao, Y., and Liu, S. (2021a). Gradient Difference of Structure of Rural Construction Land in Loess Hilly Region: A Case Study of Yuzhong County, Gansu Province, China. *Land* 10, 349. doi:10.3390/land10040349

Ministry of Housing and Urban-Rural Development of the People's Republic of China (2014). *Circular of the Ministry of Housing and Urban-Rural Development and Other Departments on Publishing the List of National Key Towns*. Available online: https://www.mohurd.gov.cn/gongkai/fdzdgknr/tzgg/201407/20140731_218612.html (accessed on November 10, 2021).

National Geomatics Center of China (2021). *National Geomatics Center of China*. Available online: http://www.ngcc.cn/ngcc/February accessed on 6, 2021).

Nngler, P., Glenn, E., and Hinojosa-Huerta, O. (2008). Synthesis of Ground and Remote Sensing Data for Monitoring Ecosystem Functions in the Colorado River Delta, Mexico. *Remote Sens. Environ.* 113, 1473–1485. doi:10.1016/j.rse.2008.06.018

Peng, L., Liu, S., and Sun, L. (2016). Spatial-temporal Changes of Rurality Driven by Urbanization and Industrialization: A Case Study of the Three Gorges Reservoir Area in Chongqing, China. *Habitat Int.* 51, 124–132. doi:10.1016/j.habitatint.2015.10.021

Pickett, S. T. A., Cadenasso, M. L., Grove, J. M., Nilon, C. H., Pouyat, R. V., Zipperer, W. C., et al. (2001). Urban Ecological Systems: Linking Terrestrial Ecological, Physical, and Socioeconomic Components of Metropolitan Areas. *Annu. Rev. Ecol. Syst.* 32, 127–157. doi:10.1146/annurev.ecolsys.32.081501.114012

Pignatti, S. (1993). Impact of Tourism on the Mountain Landscape of Central Italy. *Landsc. Urban Plan.* 24, 49–53. doi:10.1016/0169-2046(93)90082-o

Puskás, N., Abunnasr, Y., and Naalbandian, S. (2021). Assessing Deeper Levels of Participation in Nature-Based Solutions in Urban Landscapes – A Literature Review of Real-World Cases. *Landsc. Urban Plan.* 210, 104065. doi:10.1016/j.landurbplan.2021.104065

Qi, F., Li, X., and Liu, K. (2016). System Research of Natural Ecological Space Use Control. *China Land* 12, 21–23.

Qiao, J., and Li, X. (2008). Classification of Rural Henan Economy from the Microscopic Perspective. *Econ. Geogr.* 28, 832–840.

Qiu, S., Peng, J., Zheng, H., Xu, Z., and Meersmans, J. (2022). How Can Massive Ecological Restoration Programs Interplay with Social-Ecological Systems? A Review of Research in the South China Karst Region. *Sci. Total Environ.* 807, 150723. doi:10.1016/j.scitotenv.2021.150723

Qu, Y., Jiang, G., Zhang, B., Li, H., and Wei, S. (2017). Spatial Characteristics of Rural Residential Land Transition and its Economic Gradient Differentiation. *Acta Geogr. Sin.* 72, 1845–1858. doi:10.11821/dlxb201710009

Qu, L., Liu, Y., Zhou, Y., and Li, Y. (2019). Spatio-temporal Evolution of Ecologically-Sustainable Land Use in the Luoxiao Mountains and Responses of its Ecosystem Services: A Case Study of Jinggangshan City in Jiangxi Province. *Acta Ecol. Sin.* 39, 3468–3481. doi:10.5846/stxb201806011223

Seppelt, R., and Voinov, A. (2002). Optimization Methodology for Land Use Patterns Using Spatially Explicit Landscape Models. *Ecol. Model.* 151, 125–142. doi:10.1016/s0304-3800(01)00455-0

Sevenant, M., and Antrop, M. (2007). Settlement Models, Land Use and Visibility in Rural Landscapes: Two Case Studies in Greece. *Landsc. Urban Plan.* 80, 362–374. doi:10.1016/j.landurbplan.2006.09.004

Shi, Y., Han, R., and Guo, L. (2021). Ecosystem Service Value and Is Spatial Response to Urbanization Based on Terrain Gradient in Southern Hilly and Mountainous Region: A Case Study in Northern Guangdong, China. *Acta Ecol. Sin.* 41, 7238–7248. doi:10.5846/stxb202006121526

Song, W., Deng, X., Yuan, Y., Wang, Z., and Li, Z. (2015). Impacts of Land Use Change on Valued Ecosystem Service in Rapidly Urbanized North China Plain. *Ecol. Model.* 318, 245–253. doi:10.1016/j.ecolmodel.2015.01.029

Su, W., Yang, G., and Zhen, F. (2007). Ecological Land Fragmentation and its Connectivity with Urbanization in the Yangtze River Delta. *Acta Geogr. Sin.* 62, 1309–1317. doi:10.11821/xb200712007

Tóth, G., Hermann, T., Ravina da Silva, M., and Montanarella, L. (2018). Monitoring Soil for Sustainable Development and Land Degradation Neutrality. *Environ. Monit. Assess.* 190, 57. doi:10.1007/s10661-017-6415-3

Unccd (United Nations Convention to Combat Desertification) (2017). *Global Land Outlook*. Bonn, Germany: Secretariat of the United Nations Convention to Combat Desertification.

Wang, Z., and Li, R. (2006). Classification, Ecosystem Service, Protection and Utilization of the Urban Ecological Land——A Case Study of Liaocheng City. *Res. Soil Water Conservation* 13, 306–308. doi:10.3969/j.issn.1005-3409.2006.06.098

Wassmann, P., Duarte, C. M., Agustí, S., and Sejr, M. K. (2011). Footprints of climate change in the Arctic marine ecosystem. *Glob. Change Biol.* 17, 1235–1249. doi:10.1111/j.1365-2486.2010.02311.x

Wei, X., Zhang, J., Wang, S., Liu, K., Wang, N., and Liu, Y. (2021). The evolution and differentiation trend of ecological land pattern in the Yellow River Basin from 2000 to 2020. *Chin. J. Ecol.* 40, 3424–3435. doi:10.13292/j.1000-4890.202111.019

Wen, B., Zhu, G., Xia, M., Zhang, K., Liu, Y., and Wang, W. (2017). Ecological land classification protection is based on the landscape security pattern in Yixing City. *Acta Ecol. Sin.* 37, 3881–3891. doi:10.5846/stxb201603170478

Xu, C., Gong, J., Li, Y., Yan, L., and Gao, B. (2020). Spatial distribution characteristics of typical ecosystem services based on terrain gradients of BailongjiangWatershed in Gansu. *Acta Ecol. Sin.* 40, 4291–4301. doi:10.5846/stxb201911152447

Yang, R., and Luo, X. (2020). Progress and Prospects in Rural Space Diversification, Reconstruction, and Governance from a Development Perspective. *Trop. Geogr.* 40, 575–588. doi:10.13284/j.cnki.rddl.003240

Yang, T., Kuang, W., Liu, W., Liu, A., and Pan, T. (2017). Optimizing the layout of eco-spatial structure in Guanzhong urban agglomeration based on the ecological security pattern. *Geogr. Res.* 36, 441–452. doi:10.11821/dlyj201703004

Yao, Y., Ma, L., Che, X., and Dou, H. (2021). Simulation study of urban expansion under ecological constraint-Taking Yuzhong County, China as an example. *Urban For. Urban Green.* 57, 126933. doi:10.1016/j.ufug.2020.126933

Yu, F., Li, X., Zhang, L., Xu, W., Fu, R., and Wang, H. (2015). Study of ecological land in China: Conception, classification. and spatial-temporal pattern. *Acta Ecol. Sin.* 35, 4931–4943. doi:10.5846/stxb201311052672

Yu, K. J., Qiao, Q., Li, D. H., Yuan, H., and Wang, S. S. (2009). Ecological land use in three towns of eastern Beijing: a case study based on landscape security pattern analysis. *Ying Yong Sheng Tai Xue Bao* 20, 1932–1939.

Zhang, J., and Ren, Z. (2016). Spatiotemporal pattern and terrain gradient effect of land use change in Qinling-Bashan mountains. *Trans. Chin. Soc. Agric. Eng.* 32, 250–257. doi:10.11975/j.issn.1002-6819.2016.14.033

Zhang, T., Zhou, J., Zhang, F., Xie, Z., and Zhang, B. (2018). Research on land use evolution in rural residential areas under the background of industrialization and urbanization. *J. China Agric. Univ.* 23, 147–157. doi:10.11841/j.issn.1007-4333.2018.02.18

Zhao, Y., Cao, J., Zhang, X. D., and He, G. (2020). Topographic gradient effect and spatial pattern of land use in Baota District. *Arid. Land Geogr.* 43, 1307–1315. doi:10.12118/j.issn.1000-6060.2020.05.16

Zhou, Q., and Chen, D. (2013). Researched the Topographic Differentiation of Land Use in Chongqing Mountainous Metropolitan Area. *Res. Soil Water Conservation* 20, 86–91.

Zhou, T., and Guo, D. (2003). GIS-based study on the spatial structure of urban greenbelt landscapes: Taking Ningbo City as an example. *Acta Ecol. Sin.* 23, 901–907.

Zhou, R., Wang, X., Su, H., and Lou, Y. (2015). Identification and security pattern of ecological land in Pingdingshan newly developed area. *Acta Ecol. Sin.* 35, 2003–2012. doi:10.5846/stxb201305241169

Zhou, Z., Meng, J., Qi, Y., and Peng, F. (2016). Importance of ecological lands and their pattern optimization in China: A review. *Chin. J. Ecol.* 35, 218–225. doi:10.13292/j.1000-4890.201601.030

Zhou, X., He, Y., Huang, X., and Zhang, M. (2021). Topographic gradient effects of habitat quality and its response to land use change in Hubei Section of the Three Gorges Reservoir. *Trans. Chin. Soc. Agric. Eng.* 37, 259–267. doi:10.11975/j.issn.1002-6819.2021.11.029

Zube, E. (1986). The Advance of Ecology. *Landsc. Archit.* 76(2), 58–67.

# Sustainable Research of Land Optimization in a Semiarid Sandy Area Based on Soil Moisture Characteristics

Hongfei Zhang[1,2], Zhaoyang Cai[1], Jingyuan Chen[1], Yan Xu[1]* and Fengrong Zhang[1]

[1]Land Use and Management Center, China Agricultural University, Beijing, China, [2]Inner Mongolia Autonomous Region Natural Resources Protection and Utilization Research Center, Hohhot, China

Land optimization is a necessary means to improve the land use efficiency and promote the sustainable use of land resources. How to fully consider the regional background conditions and scientifically and comprehensively achieve the sustainable and optimal utilization of land resources is a necessary means to promote the sustainable utilization of land resources, especially in semiarid sandy areas with fragile ecological environments. Therefore, based on the characteristics of a semiarid sandy area and by using existing research, with important water resources as the core, this study constructed an optimal land allocation method in a semiarid sandy area based on the soil moisture characteristics. By taking the Horqin Zuoyihou Banner in the semiarid sandy area of China as a typical case, we explored its soil moisture characteristics and influencing factors and put forward the distribution patterns and suggestions for optimal land use. The results show that it is effective to optimize the land space allocation in semiarid sandy areas based on the soil moisture characteristics, and the corresponding land use activities should be arranged according to the moisture conditions of each region, which is beneficial to achieve sustainable semiarid sandy land use. We hope that this study can provide valuable sustainable land optimization solutions for the efficient, sustainable use and protection of land resources in semiarid regions.

Keywords: semiarid sandy regions, land resources, soil moisture, land optimization, sustainable land

## 1 INTRODUCTION

Sustainable land optimization is a necessary means to improve land use efficiency and promote the sustainable use of land resources (Cao et al., 2012; Song and Chen, 2018). However, the effectiveness of land optimization is affected by many factors, including the development levels of social, economic, ecological, and environmental systems (Li et al., 2020; Gao et al., 2021). Therefore, there are many unreasonable land use schemes in land optimization research, which cause our research on land optimization to lack a certain degree of systematic organization and this work cannot propose practical and effective development schemes for decision-makers (Goldstein et al., 2012; Luo et al., 2019). At present, with the rapid development of industrialization and urbanization, land resources are facing the dual tasks of development and protection, dual contradictions between supply and demand, and the dual pressures of resource utilization and ecological protection are present, especially in semiarid areas with fragile ecological environments (Cui and Shi, 2012; Jiang

et al., 2020; Deng, 2021). Therefore, how to scientifically achieve sustainable optimal utilization of land is not only an important topic in the land science field but is also a necessary means to improve the land use efficiency and promote the sustainable use of land resources (Cotter et al., 2014; Wang et al., 2021).

China's arable land resources are insufficient, and the per capita arable land area is less than 0.1 hm$^2$, which is less than 40% of the world (Lai et al., 2020). Cultivated land for the purpose of ensuring food safety and protecting the red line of cultivated land occupies a supplementary balance, and drought and semiarid areas have become an important replenish area for cultivated land in China (Ghabour et al., 2019). It is difficult to develop only without protection, and the use of land use is difficult to sustain; only the reality of protecting and non-development, the reality of the contradiction between human and land, and the growth of grain demand are not allowed (Song and Chen, 2018; Fan et al., 2020a). Meanwhile, groundwater resources are very valuable resources in drought and semiarid areas, which can determine the scope, scale, and form of land protection and utilization, and it is a necessary factor to meet the growth of non-ground vegetation growth in the semiarid area (Liu et al., 2022). Groundwater has a large impact on surface vegetation, and is also a quantitative relationship between groundwater levels, soil water content and plant ecological types (Maihemuti et al., 2021). Therefore, water resources have become an important condition for sustainable optimization and utilization of land resources in dry and semiarid areas (Jiang et al., 2020).

Fortunately, the existing research has conducted a wealth of research on land optimization, which can be roughly divided into three categories. The first group of methods consider the impacts of natural, economic, social and ecological factors on land space utilization from the perspective of the quantitative structure of land use and uses linear programming models, nonlinear programming, dynamic programming and other methods to calculate the allocation of cultivated land use, and an optimal solution for the macroscopic arable land use quantities and structures is obtained (Verhoeye and Wulf, 2002; Li et al., 2020). The second type of method begins with the spatial land use structure, comprehensively considers the natural conditions, quality conditions, spatial forms, and location conditions of the land, and uses multiple optimization models, cellular automata models, genetic algorithms, multiagent particle swarm optimizations, and water footprints to define constraints (such as the total water resources) and optimization goals (such as the maximum economic benefits) in combination with relevant policies to calculate an optimal allocation scheme for land space utilization in terms of the economic, social, and ecological benefits (Liu et al., 2015; Wang et al., 2020; Rahman and Szabó, 2021; Liao et al., 2022). The third type of method predicts the spatial optimization of different land use types, such as cultivated land, forestland, grassland, garden land, and construction land, under multiple future scenarios from the perspective of land use times, which provides a reasonable and effective sustainable development direction for land use in terms of quantitative structures and spatial distributions (Chakir and Gallo, 2013; Qiu et al., 2022; Rong et al., 2022).

The above analysis shows that the existing land optimization plan achieves the unification of land quantitative structures and spatial structure optimization patterns, can effectively coordinate the contradictions among the individual goals of land use and social goals, and has formed the optimization path of "objective function—numerical constraints - space transformation rules - optimization solution". The research methods and technologies have been improved, which effectively ensure the rational, effective and comprehensive development of the optimal allocation of land space. However, most of the existing research scales are macroscopic, and few scholars have conducted research from the microscopic perspective of the background attribute characteristics of land and have rarely considered the influences of soil moisture characteristics and landform characteristics on the optimal allocation of land, especially in semiarid areas with fragile ecological environments with water shortages and obvious landform differentiation characteristics. Thus, our research on land optimization lacks a certain degree of systematic comprehensiveness and cannot propose practical and effective sustainable land use development measures for decision-makers.

Therefore, to propose a suitable sustainable land optimization scheme for semiarid areas, this study selects the sandy area of the Horqin Zuoyihou Banner, Inner Mongolia Autonomous Region, as the study area. First, we determined the typical year based on the precipitation of the research zone from 1980 to 2019 by using Pearson-III curve. Second, we observe the water dynamics in different soil layers in the soil profile located in the dune depression interphase area in typical years in the study area and clarify the soil water status and its influencing factors in different topographical parts of the growing season by using the time-domain reflectometry method and equidistant layering method. Finally, based on the soil moisture characteristics in the study area, the land use space in the study area is optimally allocated, and corresponding sustainable land optimization suggestions are proposed. We hope that this study can provide valuable sustainable land optimization solutions for the efficient, sustainable use and protection of land resources in semiarid regions.

# 2 MATERIALS AND METHODS

## 2.1 Study Area

The Horqin Zuoyihou Banner is located southeast of Tongliao city, Inner Mongolia Autonomous Region in the central and southern part of the Horqin Sandy Land, between 121°30′-123°42′ E and 42°40′-43°42′N, and the total area is 11,500 km$^2$, which includes 12 towns (**Figure 1**). The elevations in this region gradually decrease from southwest to northeast, and then to the southeast, most of the sandy meadows are interlaced, the dunes are rolling, and the depressions are distributed vertically and horizontally. The annual average temperature in this region is 5.6°C, the annual average precipitation is 428 mm, which is mainly concentrated from June to August. The annual average sunshine amount is 2,837–2,982 h, and the annual average wind speed is 4.6 m/s (Zhou et al., 2019). The eastern plain is a key

**FIGURE 1 |** Study area location.
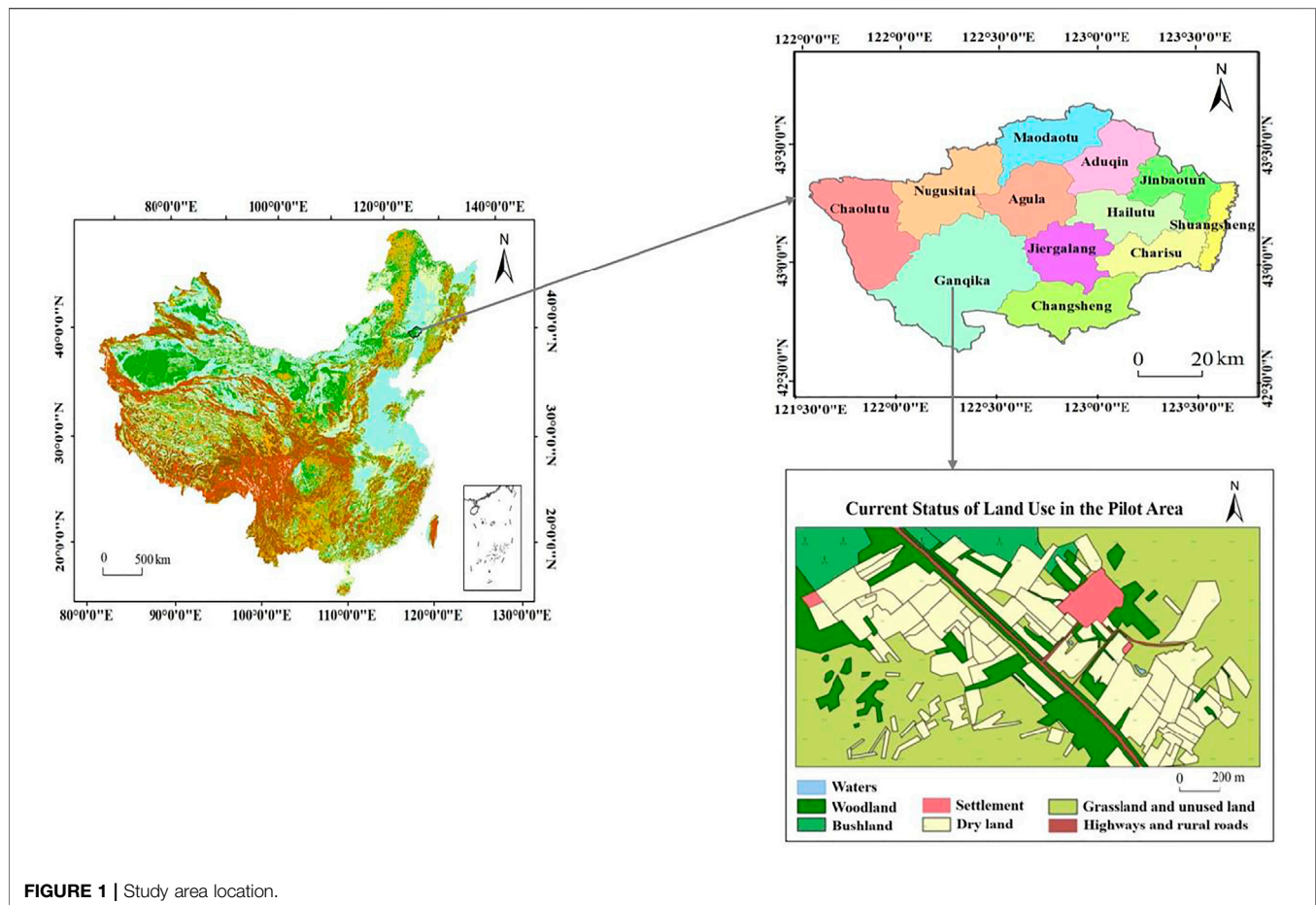
grain-producing area, and most of the central and western areas are key animal husbandry areas, which mainly involve planting corn, rice, wheat, and soybeans, with grain outputs sufficient for approximately 2.2 billion heads of cattle and 1.68 million livestock pens (Zhou et al., 2017). In 2020, the regional GDP was 12.3 billion yuan, the registered population reached 395741, and the per capita disposable income reached 19681 yuan (Statistics Bureau of Inner Mongolia Autonomous Region, 2021).

Because the Horqin Zuoyihou Banner is located in the hinterland of the Horqin Sandy Land (the largest sandy land in China), which belongs to the transition zone between arid and semiarid zones, the ecological environment is fragile, and the contradiction between water supply and demand is sharp, which is typical and representative, so the Horqin Left Front Banner in Inner Mongolia is selected as a typical case for empirical research (Li et al., 2012; Ge et al., 2015). The experimental area selected was the Wudantala Natural Village in Bulagacha, Ganqika Town, which is located in the central part of Kezuohou Banner, which is a typical dune depression area. The relatively flat land near the settlements has been mostly reclaimed as arable land surrounded by dune depressions. The management level of agricultural land is relatively extensive, and field management by farmers is sparse. The experimental area selected was the Wudantala Natural Village in Bulagacha, Ganqika Town, located in the central

part of Kezuohou Banner, which is a typical area with dune depressions. The relatively flat land near the settlements has been reclaimed as arable land surrounded by dune depressions. The management level of agricultural land is relatively extensive, and field management by farmers is sparse. The current land use status in the experimental area is shown in **Figure 1C**.

## 2.2 Data Sources

The topographic data in this study are derived from the surveying and mapping data of the land consolidation project in the pilot area, 1:50,000 contour topographic map of the Horqin Zuoyihou Banner, 30-metre-precision DEM data of the Kezuohou Banner, and wetland GPS positioning data, which are combined with UAV aerial photography images. The geological landform and soil hydrology data are obtained from the land consolidation plan of Tongliao city, soil data of the Horqin Zuoyihou Banner, water resource sustainable development and utilization plan of the Kezuohou Banner, hydrological station data from 1980 to 2019, grid sampling data of the experimental area, and sample point profile sampling data. The meteorological data are obtained from the public meteorological data provided by the national stations. In addition, a small, automated weather station is set up in the test area, which automatically records and counts data such as temperature, wind speed, rainfall, and solar radiation at 30-

**FIGURE 2 |** Research framework for sustainable research of land optimization in a semiarid sandy area based on soil moisture characteristics.
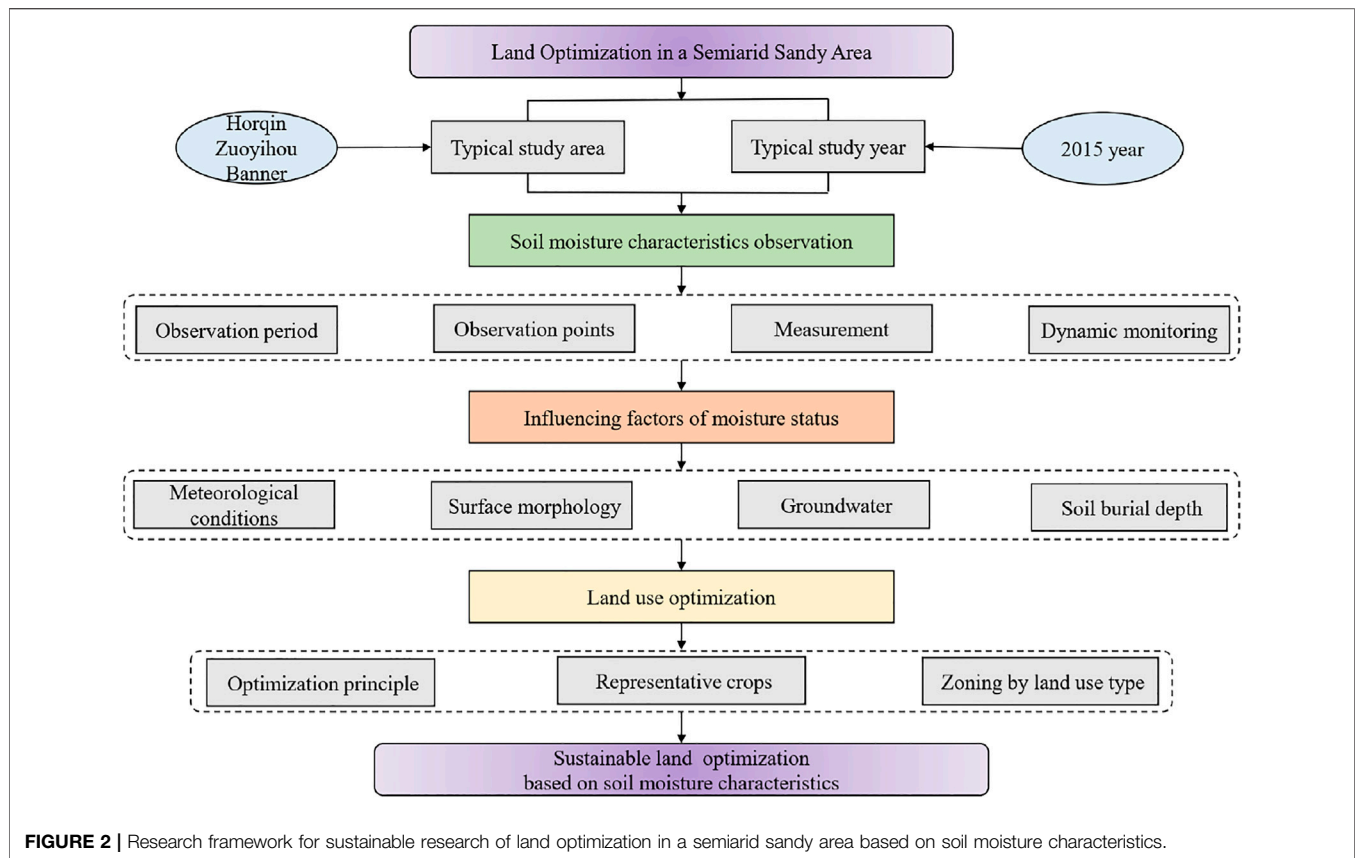
minute intervals. The land use data are obtained from the land remediation plan of the Tongliao Municipal Bureau of Land and Resources and are obtained by visual interpretations combined with remote sensing images and UAV aerial images. The economic and social data are obtained from the 2020 Statistical Yearbook of the Inner Mongolia Bureau of Statistics.

## 2.3 Research Framework

After reviewing the main literature and theories, we divided the research ideas of this article into the following three parts: 1) This study uses Horqin Zuoyihou Banner as a typical case area for semiarid sand, investigating the precipitation of the area from 1980 to 2019, and using Pearson-III curve to determine the typical year for research. 2) Observations of the characteristics and causes of soil moisture differentiation in the dune depression interphase area: The basic landform of the semiarid area-dune depression interphase area was observed to determine the water dynamics of different soil layers in the soil profile and to understand the soil water statuses and their causes in different topographical areas in the growing season. 3) Propose a sustainable land use optimization model: Based on the above two research results, by referring to previous experience and lessons of land use in the region and combined with the regional economic and social development plan, a regional land use optimization plan based on the principles of conservation and sustainability is proposed. The research framework is shown in **Figure 2**.

## 2.4 Research Methods
### 2.4.1 Determination of Typical Research Years
Since the precipitation amounts vary greatly among different years, it is necessary to consider the influence of different hydrological years when analysing the supply and demand characteristics of water resources and water consumption for crop irrigation. In this study, the Pearson-III curve was used to analyse the 30-year hydrological years of the Horqin Zuoyihou Banner from 1980 to 2019, and the representative year of the flat-water year ($p$ = 50%) was determined to be 2015 (Ji et al., 1984).
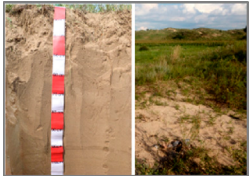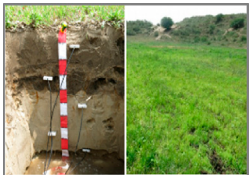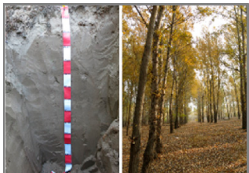
### 2.4.2 Observation Methods to Determine the Soil Moisture Characteristics
#### 2.4.2.1 Moisture Observation Period
The observation period for this research experiment extended from July 7 to October 21, which is divided into a hot and dry period, high temperature and rainy period, and low temperature and low rain period, which not only considers the typical climate in the region but also maintains continuity in time. At the same time, the arithmetic mean values of the data that are measured by most probes are used as the soil water content values of each section and layer, and the water status trends in areas with differing topography in the project area during this period are then summarized.

**TABLE 1 |** Summary table of water observation sampling points.

| Section number | Type | Terrain | Groundwater impact | Cover | Develop and use | Situation |
|---|---|---|---|---|---|---|
| 1–1 | A | Hilltop | No | Very sparse shrub grass | No |  |
| 1–2 | A | Hill middle | No | Sparse shrub grass | No |  |
| 1–3 | A | Hill down | No | Very sparse grass | No |  |
| 2–1 | A | Hilltop | No | Sparse shrub grass | No |  |
| 2–2 | B | Hill middle | Deep | Sparse corn, grass | Fields of corn |  |
| 2–3 | B | Hill down | Deep | Good corn | Fields of corn |  |
| 1–4 | C | Dune land | All | Meadow | Grazing |  |
| 3–1 | A | Hill middle | No | Poplar tree | Shelter forest, woodcutter |  |
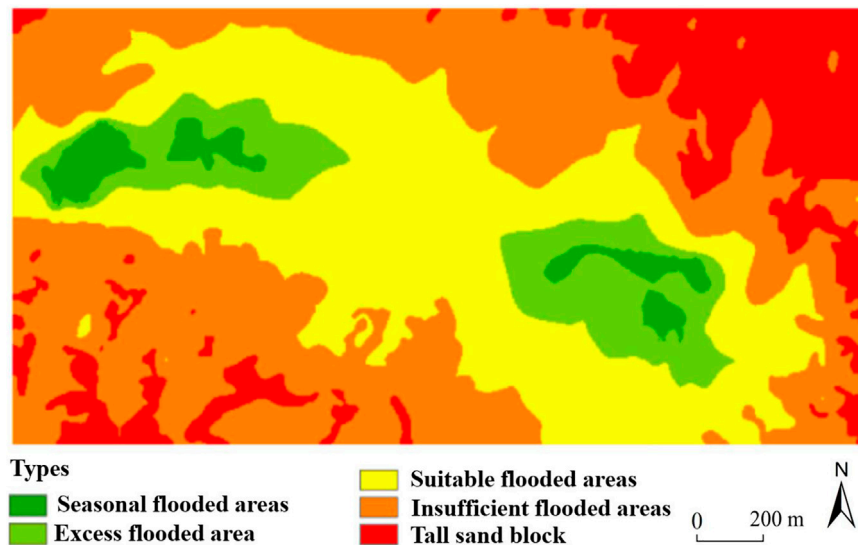
**FIGURE 3 |** Water condition division of the test area.

#### 2.4.2.2 Layout of Moisture Observation Points

Due to the significant differences in the soil moisture conditions in the parts with differing topography in the dune depression interphase area, the distributions and growth of natural vegetation and crops are significantly different. To explore the crop site conditions in areas with differing topography and to then determine a reasonable design, two observational cross-section transects were selected, which are located on an undeveloped natural dune depression slope and on an adjacent slope that has been developed as a farmland dune depression slope. In addition, we extend from the greatest heights of the dune depressions in the two cross-section belts down to the depressions and select sampling points in different parts as the representatives of various dune depression landforms in the project area to measure the soil properties and monitor the water dynamics. See **Table 1** below for a comparison of the sampling points.

According to the results of the initial measurements when the probe is set, the profile sampling points are roughly divided into three categories: "Type A" (the entire body is dry, profiles 1–1, 1–2, 1–3, 2–1, and 3–1); "Type B" (the deep layer is relatively wet, profiles 2–2 and 2–3); and "Type C" (the entire body is wet, profile 1–4).

#### 2.4.2.3 Soil Moisture Measurement Method

To correctly evaluate the water supply capacity of the land, the soil water contents were measured in this experiment by using the time-domain reflectometry method to understand the dynamic change processes of the soil water contents over a long time period. The TDR100 time domain reflectometer host, manufactured by Campbell Scientific, was selected for the experiment, which can obtain automatic continuous measurements based on Datalogger. A specially customized CS630 three-pin probe sensor is used to act as a wave guide. The probe length is 15.0 cm, the probe diameter is 0.318 cm, and the probe dimensions are 5.75*4.0*1.25 cm. The SDI-12 sensor bus communication protocol is used between the probe

and host, and the connection is made with RG-58 coaxial cable and a corresponding standard connector. The water measurement accuracy of the sensor is ±2.5% when measuring dry soils and ±0.6% when measuring saturated soils, which meet the requirements for the measurement accuracy of this experiment. Before burying the probe, the actual probe length is corrected by using the water immersion method to correct the errors that are caused by deformation of the needle. The test adopts a method that involves moving the host computer to obtain point-by-point readings at regular intervals and uses a COM2USB cable to connect a notebook computer with a host computer to form a portable field measurement device. The measurement results are manually read by the PC-TDR program, the waveform diagrams are checked at the same time, and the arithmetic means of the corrected readings of the three waveforms are taken as the results.

#### 2.4.2.4 Dynamic Monitoring Method for Soil Moisture

After selecting the sample points, the section is excavated at each sample point, the equidistant layering method is used to take soil samples at 10, 30, 50, 70, 90, and 110 cm, and TDR probes are embedded to more accurately evaluate the overall conditions along the profile. Dynamic monitoring of the soil moisture in each profile was conducted over a 4-month period, which covered the most important precipitation period and main growing period of crops. The measurements are mainly conducted from approximately 9:00 to 10:00 in the morning, and in the case of rainfall, these are postponed until the next day to obtain a relatively stable moisture distribution trend.

### 2.4.3 Land Use Space Optimization Method
#### 2.4.3.1 Optimization Principle

The sandy area in the Horqin Zuoyihou Banner is vast and sparsely populated, with low production and operation intensity, and the natural ecology of the region is relatively fragile. Large-scale, high-intensity land development can easily
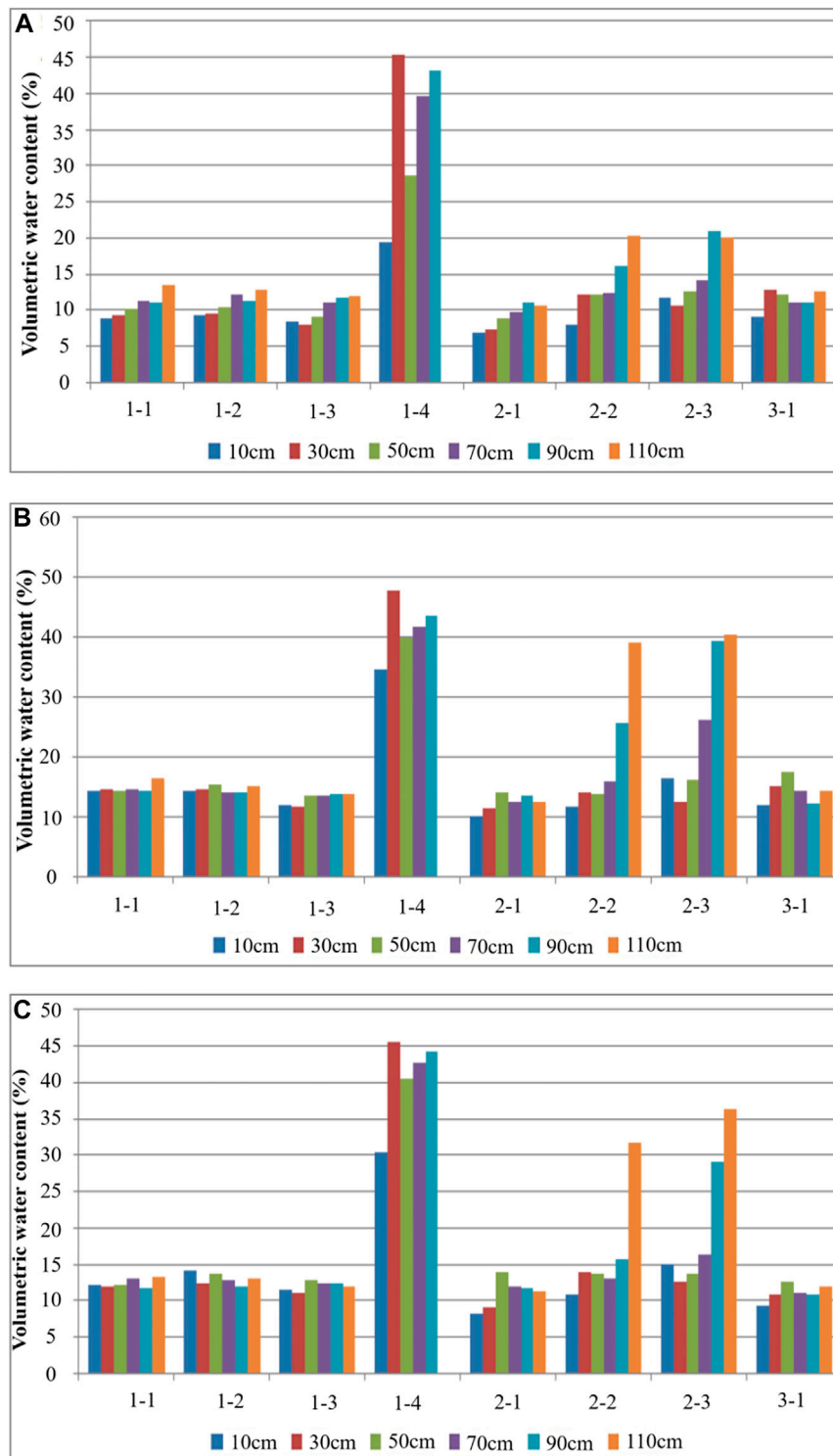
**FIGURE 4 |** Horizontal comparisons of the water content of each section in different periods. **(A)** is the hot, dry period, **(B)** is the high temperature, rainy season, and **(C)** is the low temperature, rainy season.

lead to ecological deterioration (Xu et al., 2018). Therefore, it is necessary to avoid damaging the self-regulating function of the ecosystem, protect and restore the ecological environment and

fully guarantee the production, living and development needs of local residents. This study plans the land use space based on the four principles of adapting measures to local conditions,
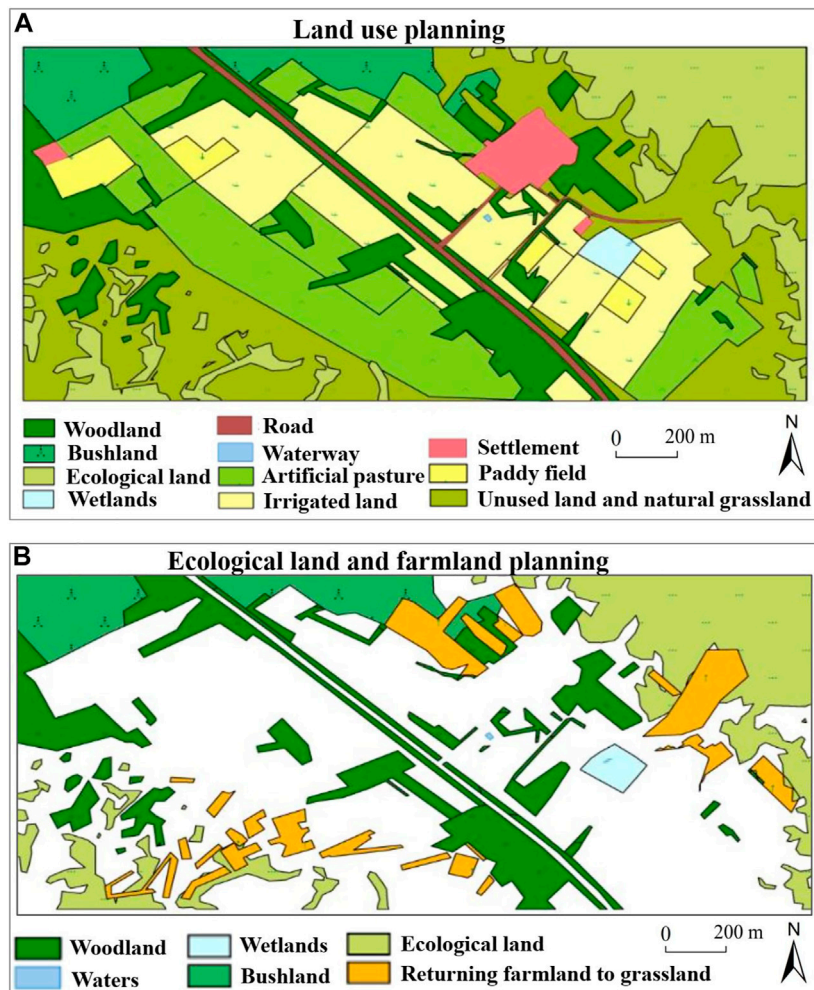
**FIGURE 5 |** Land use planning, ecological land and farmland planning.

setting land with water, minimal disturbance and diversification.

### 2.4.3.2 Selection of Representative Crops
Based on a literature review and field visits and investigations, this study summarizes the main local land use types, determines the main vegetation types that are involved in each land use type, the habitat habits of crops, and the inputs and outputs of various management methods to analyse the needs and adaptations of each land use to the environmental and socioeconomic conditions (Alados et al., 2011; Fan et al., 2020b). The main representative crops that were selected include corn, rice, alfalfa, Leymus chinensis, Cinnamon japonica, Sadawang, reed, and Caragana.

### 2.4.3.3 Zoning by Land use Type
Based on the water condition characteristics mentioned above, the land in the experimental area is divided into the following types (**Figure 3**). The "insufficient flooded areas" with poor moisture conditions consist mainly of those areas with deep groundwater depths (e.g., over 235 m above sea level).

"Suitable flooded areas" with better water conditions consist mainly of those areas with slightly higher terrain, such as low-lying land, that is, distributed in areas with high groundwater levels, and the altitudes are between 233 and 235 m. The "excess flooded area" with good water conditions and low-lying terrain is located mainly at the transition stage between seasonal flooded areas and suitable water areas and is not prone to flooding but does not require year-round irrigation. The "seasonal flooded areas" that are prone to water accumulation during the rainy season include wetlands with year-round water, lakes, seasonal wetlands, and seasonal lakes. The terrain mainly consists of depressions and deserts.

## 3 RESULTS

### 3.1 Analysis of Observation Results of Moisture Status
During the hot, dry period from July to early August, the test area continued to be hot and less rainy, with only a few rainfall events

that were less than 10 mm. The water contents of the A, B, and C profiles were 9%–11%, 9%–20%, and 20–45%, respectively (**Figure 4A**). During the high temperature, rainy period from mid to late August, the rainfall in the experimental area was relatively concentrated, with a cumulative rainfall amount of 195.32 mm. During this period, the soil water contents fluctuated greatly, and the water contents of the A, B, and C profiles were approximately 14%, 15%–40%, and 40%, respectively (**Figure 4B**). In the period with low temperatures and little rainfall occurring after September, the test area entered autumn, with scarce rainfall and rapid temperature decreases. The measured soil moisture contents fluctuated only slightly, and their standard deviation was less than 1%. The water contents of the A, B, and C profiles were approximately 12%, 13%–30%, and 40%, respectively (**Figure 4C**).

## 3.2 Analysis of the Influencing Factors of Moisture Status

Based on the above test results, this study further analysed the influencing factors of soil water contents in the study area under different times and spaces from four aspects, including meteorological conditions, surface morphology, groundwater and soil burial depth. First, in the three stages with hot and dry conditions, high temperature and rainy conditions, and low temperature and little rain with different meteorological conditions, temperature and precipitation have different degrees of influence on the soil water content through water infiltration and water evapotranspiration, respectively. Second, different slope aspects and positive and negative topographies features (e.g., dunes and depressions) affect the soil water content by redistributing solar radiation and surface runoff. Third, groundwater, as a variable with a certain regional consistency, is a direct influencing factor for the water content variations observed in different sections. Finally, the soil in the study area consists mostly of unstructured sandy soil with a uniform top and bottom. The closer it is to the surface, the easier it is for water to evaporate into the atmosphere or be absorbed by the roots of vegetation, which thereby affects the soil water content.

## 3.3 Land Use Optimization Results Based on Soil Moisture Conditions

Based on the observation results and influencing factors of the above-mentioned soil moisture conditions, this study follows the principle of least disturbance and diversification and uses water to determine the land types associated with different soil moisture contents. According to the actual situation of the pilot area types according to local conditions, a corresponding land space utilization planning scheme is formulated. During the planning process, all existing roads, forestland and residential construction land remain unchanged, as shown in **Figure 5A**.

The current patches of arable land in the experimental area are relatively messy, and this distribution is not conducive to large-scale operations. Therefore, it is recommended to carry out land consolidation, rezone the plots, and adjust the planting types according to the water conditions during the land consolidation

process. Specifically (**Figure 5B**), for seasonally flooded areas, their areas, shapes and locations should be adjusted accordingly, and appropriate engineering measures should be adopted to reclaim them as paddy fields or reserve them as wetland reserves. The water-excess area is the main area for grain crop production. In drought years, no irrigation is required to grow corn. Intensive management steps should be carried out to increase the yield per unit of crops. The area, that is, suitable for water is large, but in years with less rain, the cooperation of irrigation measures is needed to ensure the corn output. Therefore, those areas that are far from residential areas are defined as artificial pastures, and relatively drought-tolerant alfalfa, Leymus chinensis, and other crops are planted, while the areas closer to the settlements are still used as dry land, and water-saving irrigation measures such as drip irrigation or sprinkler irrigation are used. All of the cultivated land in the water-deficient area should be converted into artificial pastures, and these could also be enclosed for natural recovery if the conditions are suitable. The sporadic unused land in the settlements can be transformed into village greening, but outside of the settlements, if there is no need for transformation, the status quo can be retained. For road land, it is recommended to build ecological roads in the pilot area; that is, instead of building hardened pavements, shrubs with developed lateral roots and drought resistance should be used to stabilize both sides of the road, and the roads should be fixed through the action of root systems to bind the soil herbs.

## 4 DISCUSSION

### 4.1 Effectiveness of Land Optimization Methods Based on Soil Moisture Characteristics

As a valuable resource type in arid and semiarid areas, groundwater resources determine the scope, scale and form of land protection and utilization to a certain extent (Mitter and Schmid, 2021). The vast, deep, sandy sedimentary layers of the Horqin Sandy Land have good connectivity, and the water infiltrating from various places gathers underground as a whole; even when there is no rainfall, the low-lying desert can still obtain a sufficient water supply. Therefore, groundwater provides a large reservoir in the Horqin Sandy Land. Groundwater is not only the main water source for natural vegetation and field crops but is also the domestic water source for the rural residents in this region (who live in a large number of scattered villages without centralized water supply conditions). However, due to the severe soil desertification in the Horqin Sandy Land, the water retention capacity is extremely poor, and the leakage of natural precipitation is extremely rapid (Zhao et al., 2018). The groundwater depths in this area are very shallow, and the direct supply of groundwater and indirect recharge of water vapour condensation constitute the main and most stable sources of soil moisture. Therefore, it is reasonable and necessary to optimize the land space allocation in semiarid sandy areas based on the soil moisture characteristics.

## 4.2 Limitations of Traditional Optimal Land Utilization

Due to the high population pressure, the pursuit of "the best use of the land" in land use, through highly intensive investments in capital, labour, water and fertilizer, to build a large area of high-yield farmland, that is, concentrated and contiguous, the traditional optimal allocation of land is mainly used in the relatively humid plains area. The core elements of this land optimization method are as follows: large-scale flat farmland constructed through land levelling, filling ditches and ravines, and land rezoning; moisture control by means of well-established irrigation and drainage systems; and high-input artificial methods such as fertilizers and pesticides being used to maintain farmland outputs.

In the Horqin Sandy Land, there are many limitations to this method of utilization (Zhu et al., 2020). 1) The Horqin area is vast and sparsely populated, and the contradiction between man and land is relatively lower. What is more important is the quality of the land rather than the quantity. 2) Large-scale land levelling will be a major blow to the already fragile ecological environment and will also lead to the loss of the only nutrients in the topsoil. 3) Since flood irrigation is difficult to carry out, the significance of land levelling is not great. It is only necessary to meet the requirements of mechanized farming by using simple engineering measures. 4) Since the average precipitation amount over many years is only 450 mm and the sand infiltration intensity is high, the water resource pressure from large-scale farming is very high. 5) The capital and labour inputs are relatively high and do not meet the actual local needs. These special natural characteristics mean that large-scale land levelling should not be carried out in this area, which will further aggravate land desertification (Bao et al., 2019; Duan et al., 2019).

## 4.3 Land Use Optimization Based on Soil Moisture Characteristics

For moisture-deficient areas, due to the harsh conditions, the yields in these areas are low after reclamation and there are even no harvests in drought years, which are the main locations where reclamation-abandonment cycles occur. Therefore, reclamation and planting should be avoided in moisture-deficient areas, and protection should be given priority, or drought-tolerant pastures and shrubs should be planted. For moisture-friendly areas, these areas are usually large, and the deeper layers can be recharged by groundwater, but the water content at the soil surface is slightly lower and the aeration is good. These areas can still support the growth of deep-rooted crops in dry years and will not see decreased crop yields due to stagnant water in wet years.

The suitable water area is the land with the best conditions and is most suitable for agricultural use. It can be used for field farming or for artificial pastures. The excess water area is also the area with low terrain and shallow groundwater depths. In dry years, the region can ensure the water supply of crops, and good harvests can be obtained without irrigation; in rainy years, the groundwater level in the region rises, the soil moisture content is high, the permeability decreases, and deep-rooted crops are susceptible to damage and yield reductions. Therefore, Mesophytes such as corn that are not tolerant to waterlogging

can be planted in dry years, and moisture-loving crops such as rice can be planted in normal years and rainy years. The distribution of seasonally flooded areas is random, and these areas have uneven topography. Most of these areas are occupied by reeds because when these areas are not flooded, the groundwater depths are relatively shallow, and the soil water contents are high. After receiving long-term deposition, the soil is relatively fertile, with strong water and fertilizer retention capabilities. By taking advantage of the seasonal flooding in this area, paddy fields can be reclaimed, and rice can be grown.

## 4.3 Suggestions for Optimal Sustainable Land Use

First, water is the most important limiting factor in the Horqin Sandy Land. By studying the spatial differentiation of the soil moisture conditions and "determining land with water", the corresponding land use activities are arranged according to the moisture conditions of each region, which are the basis for sustainable land use. Specifically, 1) for clumps with poor water conditions, cycles of random reclamation and abandonment will accelerate the degradation of land in the Horqin area, which requires long-term stable management (such as construction land and rotational pastures) to avoid cultivated land becoming the source of desertification. 2) For wetlands that have year-round water, it is necessary to increase the protection efforts to develop seasonally flooded areas to grow rice and to develop dry land with good water conditions to grow corn and other field crops. 3) In view of the two completely different environments that coexist in the small dune and depression areas, the land use activities should be arranged according to the characteristics of the two environments to reduce the damage to the natural landscape, protect biodiversity, and achieve an environmentally friendly and sustainable environment. 4) Based on the soil moisture conditions, the inputs into land use activities according to local conditions are conducive to long-term stable operation and less disturbance to the environment, which are conducive to ecological restoration and sustainable land use.

Second, under the condition that the total amount of water resources is constant and the ecology cannot be destroyed, the limited water resources can be used in those places with higher efficiency (that is, less water can be used to meet the needs of local residents for survival and development) to decrease the impact on the environment. pressure is necessary (Fraser et al., 2013; Dessu et al., 2019). This study believes that adjusting the industrial structure is an important method to develop the semiarid sandy land. If the industrial structure, that is, dominated by agriculture and animal husbandry is to meet the needs of local residents, it will exceed the carrying capacity of the water resources. Non-agricultural land use has a higher level of economic output per unit of water consumption and can meet the survival and development needs of local residents with less land pressure. At present, the primary industry, namely, agriculture and animal husbandry, accounts for a very high proportion of the industrial structure in the study area. Therefore, decreasing the proportion of agriculture in the local economy, increasing the degree of industrialization, creating more non-agricultural employment opportunities, encouraging non-agricultural employment and

urbanization of the agricultural population, and reducing the pressure of agriculture on land are options. development way out.

Finally, in the land use process, care should be taken to protect the groundwater (Mitter and Schmid, 2021). The good connectivity of groundwater bodies will rapidly expand the areas that are affected by pollution, which will cause harm *via* the absorption of natural vegetation, crops, and domestic water intake. More importantly, groundwater is a vital water source in the Horqin area, and groundwater pollution will lead to serious consequences. Therefore, in agricultural production, water-saving irrigation methods should be used to avoid overexploitation while reducing the use of chemical fertilizers and pesticides to avoid pollution (because pollutants are difficult to completely remove once they enter water bodies). For industrial and mining activities, the pressure on groundwater should also be reduced through the selection of water-saving processes and reuse of reclaimed water, and sewage discharges should be strictly controlled.

## 5 CONCLUSION

This study took the sandy area of the Horqin Zuoyihou Banner as the study area, which was combined with the background conditions of the study area, determined the typical years of the study through the Pearson-III curve, observed the soil moisture dynamics, and analysed the influencing factors. Then, we divided the study area into four water characteristic areas and formulated different sustainable land use optimization schemes based on the principle of determining land by water and adapting measures to local conditions. The study found that the C profile has the most water content (45%), and the A profile has the least water content (9%); when the precipitation is relatively concentrated, the soil moisture fluctuation is larger; when the rainfall is less, the soil moisture fluctuation is small. The results show that the topography of the Horqin sandy area has a very high correlation with the spatial differentiation of soil moisture, which will lead to differences in plant community distributions and crop growth conditions in areas with different topographies.

Therefore, this study believes that sustainable land use should be based on the soil moisture conditions, and the corresponding land use activities should be arranged according to the moisture conditions of each region. It is also important to protect wetlands

that have water all year round, develop seasonally flooded areas to grow rice, develop dry land with good water conditions to grow corn and other field crops, use water-deficient lands as construction land and rotational pastures, and take measures to enclose tall sand tusks to assist natural recovery. We hope that this research can provide practical sustainable land optimization methods for China and other parts of the world and can provide policy recommendations for the sustainable utilization of the cultivated land resources in arid sandy areas and regional sustainable development.

## DATA AVAILABILITY STATEMENT

The original contributions presented in the study are included in the article/supplementary material, further inquiries can be directed to the corresponding author.

## AUTHOR CONTRIBUTIONS

YX designed the research; HZ and ZC wrote the main manuscript text; JC performed the data analysis and made figures and tables; FZ provided conceptualization, investigation and methodology. All authors have reviewed the manuscript and approved it for submission.

## FUNDING

## ACKNOWLEDGMENTS

## REFERENCES

Alados, C. L., Puigdefábregas, J., and Martínez-Fernández, J. (2011). Ecological and Socio-Economical Thresholds of Land and Plant-Community Degradation in Semi-arid Mediterranean Areas of Southeastern Spain. *J. Arid Environ.* 75 (12), 1368–1376. doi:10.1016/j.jaridenv.2010.12.004

Bao, Y. Z., Duan, L. M., Liu, T. X., Tong, X., Guo, Q., Wang, H. M., et al. (2019). Simulation of Evapotranspiration and its Components for the Mobile Dune Using an Improved Dual-Source Model in Semi-arid Regions. *J. Hydrol.* 592, 125796. doi:10.1016/j.jhydrol.2020.125796

Cao, K., Huang, B., Wang, S., and Lin, H. (2012). Sustainable Land Use Optimization Using Boundary-Based Fast Genetic Algorithm. *Comput. Environ. Urban Syst.* 36 (3), 257–269. doi:10.1016/j.compenvurbsys.2011.08.001

Chakir, R., and Le Gallo, J. (2013). Predicting Land Use Allocation in France: A Spatial Panel Data Analysis. *Ecol. Econ.* 92, 114–125. doi:10.1016/j.ecolecon.2012.04.009

Cotter, M., Berkhoff, K., Gibreel, T., Ghorbani, A., Golbon, R., Nuppenau, E.-A., et al. (2014). Designing a Sustainable Land Use Scenario Based on a Combination of Ecological Assessments and Economic Optimization. *Ecol. Indic.* 36, 779–787. doi:10.1016/j.ecolind.2013.01.017

Cui, L., and Shi, J. (2012). Urbanization and its Environmental Effects in Shanghai, China. *Urban Clim.* 2, 1–15. doi:10.1016/j.uclim.2012.10.008

Deng, S. (2021). Exploring the Relationship between New-type Urbanization and Sustainable Urban Land Use: Evidence from Prefecture-Level Cities in China. *Sustain. Comput. Inf. Syst.* 30, 100446. doi:10.1016/j.suscom.2020.100446

Dessu, S. B., Melesse, A. M., Bhat, M. G., Price, R. M., Seid, A. H., Debebe, S. A., et al. (2019). Development and Application of a Priority Rated Optimization Model (PROM) for Multi-Sector Water Resource

Management Systems. *Environ. Model. Softw.* 113, 84–97. doi:10.1016/j.envsoft.2018.11.014

Duan, H., Wang, T., Xue, X., and Yan, C. (2019). Dynamic Monitoring of Aeolian Desertification Based on Multiple Indicators in Horqin Sandy Land, China. *Sci. Total Environ.* 650, 2374–2388. doi:10.1016/j.scitotenv.2018.09.374

Fan, J., Wang, L., Qin, J., Zhang, F., and Xu, Y. (2020a). Evaluating Cultivated Land Stability during the Growing Season Based on Precipitation in the Horqin Sandy Land, China. *J. Environ. Manag.* 276, 111269. doi:10.1016/j.jenvman.2020.111269

Fan, J., Xu, Y., Ge, H., and Yang, W. (2020b). Vegetation Growth Variation in Relation to Topography in Horqin Sandy Land. *Ecol. Indic.* 113, 106215. doi:10.1016/j.ecolind.2020.106215

Fraser, E. D. G., Simelton, E., Termansen, M., Gosling, S. N., and South, A. (2013). "Vulnerability Hotspots": Integrating Socio-Economic and Hydrological Models to Identify where Cereal Production May Decline in the Future Due to Climate Change Induced Drought. *Agric. For. Meteorology* 170, 195–205. doi:10.1016/j.agrformet.2012.04.008

Gao, P. P., Li, Y. P., Gong, J. W., and Huang, G. H. (2021). Urban Land-Use Planning under Multi-Uncertainty and Multiobjective Considering Ecosystem Service Value and Economic Benefit - A Case Study of Guangzhou, China. *Ecol. Complex.* 45, 100886. doi:10.1016/j.ecocom.2020.100886

Ge, X., Li, Y., Luloff, A. E., Dong, K., and Xiao, J. (2015). Effect of Agricultural Economic Growth on Sandy Desertification in Horqin Sandy Land. *Ecol. Econ.* 119, 53–63. doi:10.1016/j.ecolecon.2015.08.006

Ghabour, T. K., Ali, R. R., Wahba, M. M., El-Naka, E. A., and Selim, S. A. (2019). Spatial Decision Support System for Land Use Management of Newly Reclaimed Areas in Arid Regions. *Egypt. J. Remote Sens. Space Sci.* 22 (2), 219–225. doi:10.1016/j.ejrs.2018.04.001

Goldstein, J. H., Caldarone, G., Duarte, T. K., Ennaanay, D., Hannahs, N., Mendoza, G., et al. (2012). Integrating Ecosystem-Service Tradeoffs into Land-Use Decisions. *Proc. Natl. Acad. Sci. U.S.A.* 109 (19), 7565–7570. doi:10.1073/pnas.1201040109

Ji, X. W., Ding, J., Shen, H. W., and Salas, J. D. (1984). Plotting Positions for Pearson Type-III Distribution. *J. Hydrol.* 74, 1–29.

Jiang, S., Meng, J., and Zhu, L. (2020). Spatial and Temporal Analyses of Potential Land Use Conflict under the Constraints of Water Resources in the Middle Reaches of the Heihe River. *Land Use Policy* 97, 104773. doi:10.1016/j.landusepol.2020.104773

Lai, Z., Chen, M., and Liu, T. (2020). Changes in and Prospects for Cultivated Land Use since the Reform and Opening up in China. *Land Use Policy* 97, 104781. doi:10.1016/j.landusepol.2020.104781

Li, H. W., Li, Y. P., Huang, G. H., and Gao, P. P. (2020). Identifying Optimal Land-Use Patterns Using a Copula-Based Interval Stochastic Programming Model for Urban Agglomeration under Uncertainty. *Ecol. Eng.* 142, 105616. doi:10.1016/j.ecoleng.2019.105616

Li, M., Fu, Q., Singh, V. P., Liu, D., Li, T., and Zhou, Y. (2020). Managing Agricultural Water and Land Resources with Tradeoff between Economic, Environmental, and Social Considerations: A Multi-Objective Non-linear Optimization Model under Uncertainty. *Agric. Syst.* 178, 102685. doi:10.1016/j.agsy.2019.102685

Li, Y., Awada, T., Zhou, X., Shang, W., Chen, Y., Zuo, X., et al. (2012). Mongolian Pine Plantations Enhance Soil Physico-Chemical Properties and Carbon and Nitrogen Capacities in Semi-arid Degraded Sandy Land in China. *Appl. Soil Ecol.* 56, 1–9. doi:10.1016/j.apsoil.2012.01.007

Liao, S., He, P., Gao, X., Lin, Z., Huang, C., Zhou, W., et al. (2022). Land Use Optimization of Rural Production-Living-Ecological Space at Different Scales Based on the BP–ANN and CLUE-S Models. *Ecol. Indic.* 137, 108710. doi:10.1016/j.ecolind.2022.108710

Liu, X., Cai, Z., Xu, Y., Zheng, H., Wang, K., and Zhang, F. (2022). Suitability Evaluation of Cultivated Land Reserved Resources in Arid Areas Based on Regional Water Balance. *Water Resour. Manage* 36, 1463–1479. doi:10.1007/s11269-022-03093-5

Liu, Y., Tang, W., He, J., Liu, Y., Ai, T., and Liu, D. (2015). A Land-Use Spatial Optimization Model Based on Genetic Optimization and Game Theory. *Comput. Environ. Urban Syst.* 49, 1–14. doi:10.1016/j.compenvurbsys.2014.09.002

Luo, X., Lu, X., Jin, G., Wan, Q., and Zhou, M. (2019). Optimization of Urban Land-Use Structure in China's Rapidly Developing Regions with Eco-Environmental Constraints. *Phys. Chem. Earth, Parts A/B/C* 110, 8–13. doi:10.1016/j.pce.2019.03.001

Maihemuti, B., Simayi, Z., Alifujiang, Y., Aishan, T., Abliz, A., and Aierken, G. (2021). Development and Evaluation of the Soil Water Balance Model in an Inland Arid Delta Oasis: Implications for Sustainable Groundwater Resource Management. *Glob. Ecol. Conservation* 25, e01408. doi:10.1016/j.gecco.2020.e01408

Mitter, H., and Schmid, E. (2021). Informing Groundwater Policies in Semi-arid Agricultural Production Regions under Stochastic Climate Scenario Impacts. *Ecol. Econ.* 180, 106908. doi:10.1016/j.ecolecon.2020.106908

Qiu, J., Huang, T., and Yu, D. (2022). Evaluation and Optimization of Ecosystem Services under Different Land Use Scenarios in a Semiarid Landscape Mosaic. *Ecol. Indic.* 135, 108516. doi:10.1016/j.ecolind.2021.108516

Rahman, M. M., and Szabó, G. (2021). Multi-objective Urban Land Use Optimization Using Spatial Data: A Systematic Review. *Sustain. Cities Soc.* 74, 103214. doi:10.1016/j.scs.2021.103214

Rong, Q., Zeng, J., Su, M., Yue, W., and Cai, Y. (2022). Prediction and Optimization of Regional Land-Use Patterns Considering Nonpoint-Source Pollution Control under Conditions of Uncertainty. *J. Environ. Manag.* 306, 114432. doi:10.1016/j.jenvman.2022.114432

Song, M., and Chen, D. (2018). A Comparison of Three Heuristic Optimization Algorithms for Solving the Multi-Objective Land Allocation (MOLA) Problem. *Ann. GIS* 24, 19–31. doi:10.1080/19475683.2018.1424736

Statistics Bureau of Inner Mongolia Autonomous Region (2021). *Inner Mongolia Statistical Yearbook.* Inner Mongolia: Inner Mongolia Autonomous Region Statistics Press.

Verhoeye, J., and Wulf, R. D. (2002). Land Cover Mapping at Sub-pixel Scales Using Linear Optimization Techniques. *Remote. Sens. Environ.* 79, 96–104. doi:10.1016/s0034-4257(01)00242-5

Wang, G., Han, Q., and de vries, B. (2021). The Multi-Objective Spatial Optimization of Urban Land Use Based on Low-Carbon City Planning. *Ecol. Indic.* 125, 107540. doi:10.1016/j.ecolind.2021.107540

Wang, M., Zhu, C., Wang, F., Li, T., and Zhang, X. (2020). Multi-factor of Path Planning Based on an Ant Colony Optimization Algorithm. *Ann. GIS* 26, 101–112. doi:10.1080/19475683.2020.1755725

Xu, L., Tu, Z., Zhou, Y., and Yu, G. (2018). Profiling Human-Induced Vegetation Change in the Horqin Sandy Land of China Using Time Series Datasets. *Sustainability* 10, 1068. doi:10.3390/su10041068

Zhao, S., Xia, D., Jin, H., Jia, J., and Liu, B. (2018). A Multi-Proxy Late Holocene Climate Record from Aeolian Deposits of the Horqin Sandy Land, Northeast China and its Societal Implications. *Aeolian Res.* 35, 29–38. doi:10.1016/j.aeolia.2018.09.004

Zhou, J., Xu, Y., Gao, Y., and Xie, Z. (2019). Land Use Model Research in Agro-Pastoral Ecotone in Northern China: a Case Study of Horqin Left Back Banner. *J. Environ. Manag.* 237, 139–146. doi:10.1016/j.jenvman.2019.02.046

Zhou, J., Zhang, F., Xu, Y., Gao, Y., and Xie, Z. (2017). Evaluation of Land Reclamation and Implications of Ecological Restoration for Agro-Pastoral Ecotone: Case Study of Horqin Left Back Banner in China. *Chin. Geogr. Sci.* 27, 772–783. doi:10.1007/s11769-017-0907-5

Zhu, W., Gao, Y., Zhang, H., and Liu, L. (2020). Optimization of the Land Use Pattern in Horqin Sandy Land by Using the CLUMondo Model and Bayesian Belief Network. *Sci. Total Environ.* 739, 139929. doi:10.1016/j.scitotenv.2020.139929

# Detecting the Spatial Mismatch of Water Resources and Grain Planting Pattern Changes in China Based on Satellite Data

Yinan Feng and Jieyong Wang *

*Institute of Geographic Sciences and Natural Resources Research, Chinese Academy Sciences, Beijing, China*

China has achieved sustained growth in grain production and significant changes in grain patterns since the early 21st century. Meanwhile, the contradiction between the shortage of water resources and the development of agriculture is becoming more and more severe. This study introduced Gravity Recovery and Climate Experiment (GRACE) gravity satellite Total Water Storage (TWS) Product to indicate total water storage and calculated the Cumulated Normalized Difference Vegetation Index (CNDVI) of cropland as an indicator for grain growth. Based on the continuous satellite data, this paper revealed the spatial mismatch between water resources supply and grain growth pattern in China. The center of gravity of the CNDVI tends to move northwest, while the GRACE TWS data's center of gravity is in the opposite direction. There were different relationships between GRACE-TWS and CNDVI changes in different zones. We calculated the pixel-wise spatial Pearson Correlation coefficients of TWS and CNDVI. The TWS data and CNDVI data show negative correlation trends in the water-limited areas such as the northern arid-semiarid region and northern China plain, while they show a positive correlation in relatively sufficient water resources in southeast China. According to the results, the changing pattern of grain production in China is likely to cause the depletion of grain production potential in the water-limited regions, while the southeastern regions with higher potential still have more capacity for agricultural production.

Keywords: grain production pattern, spatial mismatch, water resource, satellite data, China

## 1 INTRODUCTION

In parallel to the importance of other energy resources for production systems (Elahi et al., 2022a; Elahi et al., 2022b), water is also one of the imperative resources for plant production. Water, which is one of the most fundamental inputs for agricultural production. Irrigation, fertilizer applications or pesticide, water takes part in almost every section of agricultural activities (Elahi et al., 2021a; Elahi et al., 2021b). Accompanied by the rapidly increasing demands on water, the development of China's agriculture leads to severe water stress in some regions where water is the limiting factor in the local

---

**Abbreviations:** CNDVI, Cumulated Normalized Difference Vegetation Index; ESA, European Space Agency; GLR, German Aerospace Center; GRACE, Gravity Recovery and Climate Experiment; TWS, Total Water Storage; LCCS, Land Cover Classification System; NDVI, Normalized Difference Vegetation Index.

ecosystem. Nationwide, agriculture accounts for 62% of water consumption, industry consumes 22%, domestic water takes 14%, and other use 2% (National Bureau of Statistics of China, 2020). With the demand for water resources continuing to grow, the drought afterward brings about serious damages to agricultural production. In China, the average annual crop area affected by drought was 62 million acres at the turn of the century, compared to 28.7 million acres in the 1950's (Ministry of Water Resources, 2010). From January 2009 to April 2010, China endured three severe droughts. The intensity of meteorological droughts in all three disasters reached the level of a 100-years event. Millions of people and livestock had difficulty accessing potable water, the survival of tens of millions of hectares of crops was threatened, and there were far-reaching long-term economic, social and ecological impacts. Subsequently, from 2010 to 2011, drought struck the North China and Huang-Huai-Hai regions again (Ye et al., 2012).

Water resources have a significant impact on whole ecosystems and socioeconomic systems. Many scientists have begun to look across traditional disciplines to explore the interactions between water, vegetation, and nutrients using an ecohydrology perspective (Bonell, 2009). Researchers have emphasized the importance of tracking the movement of water in those water-limited areas. However, cost and logistics impede the availability of monitoring the water resource on a large scale (Rodell and Famiglietti, 2001). In China, hydrological monitoring sites and satellite observations were widely used to monitor water track in a large area. Although researchers can estimate water resources by these methods, the shortcomings of these methods are also evident. These drawbacks include, the monitoring of hydrological condition at a large scale needs a lot of ground observation sites; the integration and preprocessing of such a large amount of data are time-consuming and labor-intensive. When building hydrological models, the total amount of water resources in an area is determined by point sources such as ground-based observations, introducing huge errors. Gravity Recovery and Climate Experiment project, launched on 17 March 2002 by NASA and German Aerospace Center (GLR), is able to measure the changes of Earth's gravity field (Adam, 2002). Scientists are subsequently capable of interpreting these changes in gravity as water movement, whether on the surface or under the ground. Many studies have used representative regions as study areas (northern India, Australia, northern China, etc.) and compared the output of traditional hydrological models to conclude that GRACE data are reliable indicators of local water storage changes (Landerer and Swenson, 2012; Feng et al., 2013; Yang et al., 2014; Cao et al., 2015; Iqbal et al., 2016). Famiglietti et al. (2011) took the central California valley as the study area, finding that GRACE data precisely captured the water storage changes in this area. Wahr et al. (2004) find that both on land and ocean Total Water Storage changes from GRACE data displayed a high consistency with outputs from the hydrological model.

In recent decades, China's grain yield has continued to grow and the pattern of grain production has changed significantly. The center of grain production in China is gradually shifting to the north. Wang et al. (2005) observed that during the entire period of 1990–2005, the grain output center-of-gravity moved

remarkably from the south and east to the north and west of China, and the moving speed was increasing (Zhang et al., 2018). Alone with the water scarcity in northern China in recent years, the shift of grain production centers to the northwest may put more pressure on the water supply in northern China. Exhausting the agricultural potential of northern China too quickly could also bring agricultural products decreasing when the water resource reaches their critical point.

The objectives of this study are to 1) observe the trends of changes in grain production and local water storage at the raster scale using satellite data, and 2) reveal the contradiction between water demand and water supply due to the changing grain production pattern in China. We first introduced the center-of-gravity analysis to explore the trend of CNDVI and TWS at the national scale. Then we discuss the trends of the time series of the two data sets in nine agricultural regions. Finally, we mapped the spatial correlation of these two datasets pixelwise.

# 2 MATERIALS AND METHODS

## 2.1 Study Area

This research focused on mainland China. Mainland China exhibits strong monsoonal and continental climatic characteristics. The topography of China is diverse, with higher elevations in the west and lower elevations in the east. A temperate continental climate dominates the northwest, while a temperate monsoon climate dominates the Northeast. A subtropical monsoon climate is prevalent in southern China, except for the southernmost part of southern China, where a tropical monsoon climate dominates. A highland alpine climate dominates the Qinghai-Tibet Plateau. Most of mainland China is located in the East Asian monsoon region, and there are significant monthly and annual variations in temperature and precipitation.

According to the Comprehensive Agricultural Zoning of China (National Agricultural Zoning Committee, 1981), this study divided mainland China into nine agricultural regions for discussion. These regions have different climatic conditions, soil conditions and farming systems. They are A: Northeast China Plain, B: Northern arid and semi-arid region, C: Huang-Huai-Hai Plain, D: Loess Plateau, E: Qinghai Tibet Plateau, F: Middle-lower Yangtze Plain, G: Sichuan Basin and surrounding regions, H: Southern China, I: Yunnan-Guizhou Plateau. **Figure 1** shows the study area and zoning area. More importantly, these regions face different pressures on water resources. Northwestern China is a relatively water-scarce area compared to the southeast. In these regions, water is a limiting factor in the ecosystem. These areas are classified as water-limited areas.

## 2.2 Data and Preprocessing
### 2.2.1 Gravity Recovery and Climate Experiment Data
In this study, we used the GRCTellus Land grids Level-3 GRACE data product processed by the Jet Propulsion Laboratory (Landerer and Swenson, 2012) to provide estimates of changes in total water storage. The units of Level-3 data are centimeters of equivalent water thickness.

**FIGURE 1 |** Mainland China with Agricultural Zoning [**(A)**: Northeast China Plain, **(B)**: Northern arid and semi-arid region, **(C)**: Huang-Huai-Hai Plain, **(D)**: Loess Plateau, **(E)**: Qinghai Tibet Plateau, **(F)**: Middle-lower Yangtze Plain, **(G)**: Sichuan Basin and surrounding regions, **(H)**: Southern China, **(I)**: Yunnan-Guizhou Plateau].
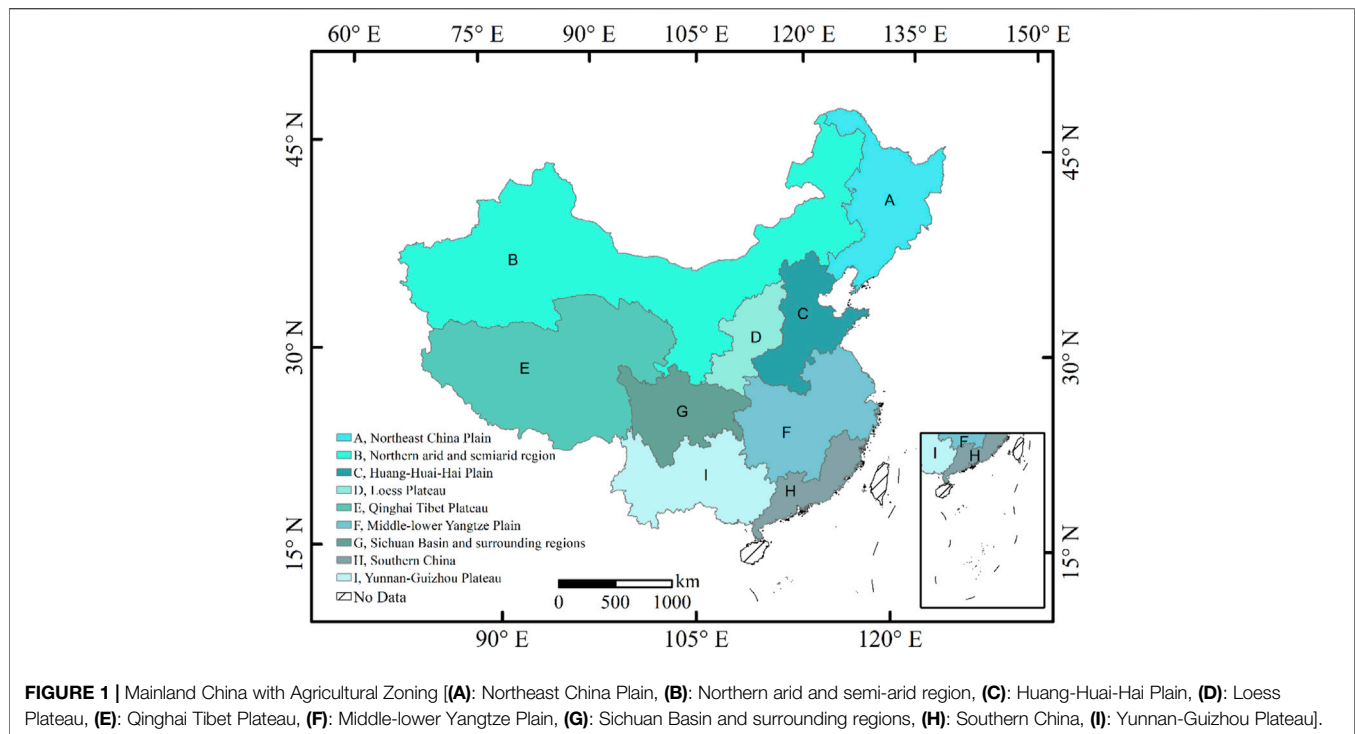
Before calculating the center of gravity for the GRACE data, we applied the following equation to convert the equivalent water thickness provided by the GRACE data to total water storage, for each pixel in the raster of the GRACE data:

$$Q_{TWS} = t_{EWT} \times A, \tag{1}$$

where $t_{EWT}$ is the equivalent water thickness of the pixel and $A$ is the area represented by the same pixel.

Since the spatial resolution of GRACE data is in degree, the area represented by each cell is different at different latitudes, we applied some formulas to simply estimate the area represented by each grid. There is a relatively simple and exact formula for the area of any spherical quadrilateral defined by parallels (latitude) and meridians (longitude). The ellipse can be derived directly by using the basic properties of the ellipse (long axis a and short axis b) rotated about its short axis to produce the ellipsoid.

The formula can be simplified by breaking down the calculation into basic steps. First, the distance between the east-west boundary (meridians $l_0$ and $l_1$) is part of the whole circle and is equal to $q = (l_1 - l_0)/360$ (when the meridian is in degrees). Find the area of the entire slice located between the parallel lines $f_0$ and $f_1$ and multiply it by $q$. Next, we will apply a formula for an elliptical horizontal slice defined by the equator (at $f_0 = 0$) and an ellipse parallel to it at latitude $f = f_1$. The area of the slice between any two latitudes $f_0$ and $f_1$ (located on the same hemisphere) will be the difference between the larger area and the smaller area. Finally, assuming that the model is a true ellipsoid (and not a sphere), the area of such a slice between the equator and a parallel of latitude $f$ is:

**TABLE 1 |** Date with missing GRACE data.

| Year | Months with missing data |
|------|--------------------------|
| 2003 | 6 |
| 2011 | 1, 6 |
| 2012 | 5, 10 |
| 2013 | 3, 8, 12 |
| 2014 | 2, 7, 12 |
| 2015 | 6, 10, 11 |
| 2016 | 4, 9, 10 |

$$\begin{cases} A = \pi \times b^2 \times \left( \dfrac{log\left(\dfrac{zp}{zm}\right)}{2e} \right) + \dfrac{sin(f)}{(zp \times zm)} \\[2ex] zm = 1 - e \times sin(f); \, zp = 1 + e \times sin(f) \\[2ex] e = \sqrt{(1 - (b/a))^2} \end{cases} \tag{2}$$

where $a$ and $b$ are the lengths of the major and minor axes of the generating ellipse, respectively (in WGS84, $a = 6,378,137$ m and $b = 6,356,752.3142$ m); f is the center of latitude.

Due to instrument issues and calibration campaigns, and the GRACE program's implementation of GRACE satellite battery management starting in 2011, part of GRACE data from data centers were missing during the observation period (Rodell et al., 2004; Cooley and Landerer, 2019). **Table 1** shows the index of the month with missing GRACE data during the whole observation period.

As shown in **Table 1**, the dates of missing data do not follow a specific pattern. GRACE data are monthly data and possess significant seasonality. We grouped the data by month and calculate the mean value in each group. We inserted the averages according to months with missing data. After forming a complete set of Monthly GRACE data from June 2003 to December 2016, we calculated the annual average of GRACE data.

### 2.2.2 Normalized Difference Vegetation Index Data and Calculation of Cumulated NDVI

The Normalized Difference Vegetation Index (NDVI) is a normalized index for highlighting vegetation features in images. Many studies have shown that the NDVI can be a helpful tool in measuring the fraction of absorbed photosynthetically active radiation, extracting vegetation classes, or estimating green biomass (Colwell, 1974; Baret and Guyot, 1991; Goward and Huemmrich, 1992; Thenkabail et al., 2000; Ahmed and Akter, 2017). Plant leaf tissue strongly absorbs blue and red light, while it strongly reflects it in the green and infrared bands. From red light to infrared light, the reflection of bare ground is higher, but the increase is slight. The higher the vegetation cover, the smaller the reflection of red light and the greater the reflection in the near-infrared band (NIR). Therefore, NDVI was introduced as a mathematical transformation to enhance the difference between the RED and NIR bands. As a result, researchers can separate land covered by vegetation from other types of land cover. Furthermore, NDVI was defined as:

$$NDVI = [(NIR - Red)/(NIR + Red)], \qquad (3)$$

where NIR indicate the spectral reflectance at the near-infrared and red band separately. Although many studies have found and established the relationship between NDVI and grain yield, these studies have also found that the relationship between NDVI and grain yield varies with different study areas, and therefore the use of time-integrated NDVI values to directly refer to grain yield may be subject to large errors in different regions. Such errors may be caused by local climatic conditions or changes in the type of crops. However, the purpose of this study is to reveal the contradiction between agricultural water use and water availability under the changing grain pattern in China, Responding to crop growth and biomass accumulation through cumulative NDVI. The use of NDVI has some advantages. For example, although the use of NDVI to predict grain yield is not stable, some studies have found that the relationship between NDVI and biomass accumulation in crops is more apparently stable and pronounced (Wang et al., 2005; le Maire et al., 2011). Therefore, crop biomass accumulation is a more appropriate indicator of water consumption in agriculture than yield when revealing water crises under changing food production patterns. CNDVI is also more suitable for this study relative to the crop yield indicator based on field surveys or statistics.

NASA'S Moderate Resolution Imaging Spectroradiometer Vegetation Indices (MODIS VIs) provided consistent spatial time-series information about global vegetation conditions.

The rasterized vegetation index map depicts the temporal and spatial changes of vegetation activity, once every 16 days and every month. To be consistent with the GRACE data, we resampled the NDVI data to 1° × 1°.

Normalized Difference Vegetation Index is widely used to monitor vegetation stress, measuring NDVI throughout a growing season helps to evaluate the effect of continuous phenological and morphological changes on grain yield. To quantify the biomass accumulation by the growth of crops, we introduced the Cumulated Normalized difference vegetation index to this study as an indicator of water consumption for grain production.

Directly predicting grain yields from satellite data has proven to be more difficult. However, some studies have achieved some results using NDVI data (Prasad et al., 2006; Ren et al., 2008; Panek and Gozdowski, 2020). A study by Ren et al. (2008) found that it is more reasonable and accurate to calculate the accumulation of NDVI and use it to predict yields (Lopresti et al., 2015). Based on the assumption that plants grow at temperatures above 10°C, we applied the cumulative temperatures method to the NDVI data. Thus, we found the longest period of the year when the temperature is above 10°C and sum up the NDVI values for that period. This sum calculated by this method was used to characterize the cumulative increase in NDVI of the plant during its growing period. Finally, we extract the cumulated NDVI in cropland by using Land Cover data as masks. NDVI data was provided by NASA's MODIS Satellites. Cropland masks were collected from the EOS CCI land cover datasets. Also, for the correlation test, we subtracted the multiyear average of the same period of TWS data as the baseline for CNDVI to ensure that the two variables were taken the same treatment.

### 2.2.3 Landcover Data

The cropland data were extracted from the land cover maps of The European Space Agency (ESA) CCI projects. The data version is 2.0.7, contains global land cover maps 1992–2015, and 2016 at 300 m spatial resolution (ESA, 2017). CCI-LC maps use the United Nations (UN) Land Cover Classification System (LCCS) to describe the Landcover state with 24 different classes. Bontemps et al. evaluated the accuracy of the 2010 ESA CCI LC product. Using all points interpreted by experts as "definite," either as a single land cover or consisting of multiple mosaics, an overall accuracy of 71.5% was found. Referring to the homogeneous points, the overall accuracy increased to 75.4% (Bontemps et al., 2011). The highest user accuracy values were found in the categories of rainfed farmland, irrigated farmland, broadleaf evergreen forest, urban areas, bare ground, water bodies, and permanent snow and ice. In contrast, the mosaic category of natural vegetation was associated with the lowest user accuracy values as well as the three categories of lichens and mosses, sparse vegetation, and swamp forests. In calculating the center of gravity shift, we used a continuous Land Cover map to extract cropland. In the TWS-CNDVI spatial correlation analysis, the land cover map at the beginning of the observation was used.

## 2.3 Statistical Analysis

### 2.3.1 Center-of-Gravity Method

The concept of center of gravity originated in physics. It is an imagery point in which the force of gravity appears to act. In the Geographic information system, a method of calculating the ideal location for warehousing facilities by calculating the transport costs to each of the outlets to be served by the facility (Chen et al., 2011). The center of gravity model is an essential analytical tool to study the spatial changes of factors in regional development (Wang et al., 2018). As an important tool in spatial analysis, center of gravity method is widely used in population barycenter, economic barycenter and energy barycenter model (Smith and Dicken, 2000; Zhang et al., 2012; Bigot and Klein, 2018). The movement of the center of gravity of factors reflects the spatial trajectory of regional development. The analytical model of the center of gravity constructed in this study is expressed as:

$$
\begin{cases}
X = \dfrac{\sum_{i=1}^{n} G_i X_i}{\sum_{i=1}^{n} G_i} \\[4mm]
Y = \dfrac{\sum_{i=1}^{n} G_i Y_i}{\sum_{i=1}^{n} G_i}
\end{cases}, \tag{4}
$$

where $n$ is the total number of cells in each raster; Point P $(X, Y)$ represents the coordinate of the center of gravity; $G_i$ is the $i$th sample values; $X_i$ and $Y_i$ are the coordinates of the geographic center of the evaluation unit. Next, we calculated the coordinate of the center of gravity for each year. Finally, we plotted the center points' trajectory map to visualize the pattern of changes in GRACE data and Cumulated NDVI data.

### 2.3.2 Pearson Correlation

In statistics, the Pearson product-moment correlation coefficient is used to measure the degree of linear correlation between two sets of variables $X$ and $Y$, with a value between −1 indicates a totally negative linear correlation and 1 represents a totally positive linear correlation.

If $X$ and $Y$ are stationary, the Pearson correlation coefficient is built as follows:

$$
r = \frac{n\left(\sum xy\right) - \left(\sum x\right)\left(\sum y\right)}{\sqrt{\left[n\sum x^2 - \left(\sum x\right)^2\right]\left[n\sum y^2 - \left(\sum y\right)^2\right]}}, \tag{5}
$$

where $r$ is the Pearson correlation coefficient; $x$ and $y$ represent the values in the first and second sets of data separately; $n$ is the total number of data sets.

# 3 RESULTS

## 3.1 The Changes in Water Resources (Total Water Storage) and Cumulated Normalized Difference Vegetation Index Pattern in China

The trajectory of the center of gravity can indicate the tendency of the variable to move in space. **Figure 2A** shows that the center of

gravity of water resources generally moves to the south and east during the observation period. The other side of this occurrence is that TWS data in western and northern China are decreasing. The movement of the center of gravity in the GRACE TWS can be broadly divided into several phases. First, 2004–2008 saw a continuous movement of gravity to the south, followed by a shift to the west from 2009 to 2011. Then, immediately after 2011, the center of gravity began to move significantly to the east, and this trend continued until 2013. After that, from 2013 to 2016, the center of gravity of GRACE data started to move southward.

**Figure 2B** shows the movement of CNDVI's center of gravity from 2003 to 2016. Throughout the observation interval, CNDVI shows the opposite motion trajectory to TWS, from southeast to northwest. However, at each stage, the trajectory of the center of gravity movement of CNDVI does not overlap with that of TWS. In order to make the trajectory of the center of gravity more prominent, we divided the whole interval into several phases. 2003–2006 was the first phase, and 2007–2009 was the second phase when the center of gravity moved more to the west and slightly to the south. After that, the center of gravity continues to move northward from 2009 until 2012. And after that, it continues until the end of the observation period, the center of gravity continues to move sharply to the west and slightly to the south.

Although the interannual trend of the CNDVI center of gravity is not the same as that of TWS's, this fact that the two do not overlap may be due to a variety of reasons, which may include: a delay between changes in grain production and changes in water resources, the cyclic flow characteristics of water that cause agricultural development to affect water resources regionally rather than point-to-point, and changes in water resources that also incorporate the effects of other natural and human activities. **Figure 4** shows the correlation coefficients of GRACE and CNDVI in space. Each pixel contains two sets of data, one set of GRACE data from 2003 to 2016, and CNDVI data for the corresponding period. We matched the two sets of data and calculated the correlation coefficients. For each pixel, the correlation coefficients have large uncertainties. However, when the target is the whole region, the overall trend obtained from the analysis of the correlation coefficients is still credible. The correlation analysis between GRACE data and NDVI data at the spatial scale corroborates the previous analysis more intuitively. The TWS data and CNDVI show the exact opposite relationship in water-limited areas (Northern arid and semi-arid region, Huang-Huai-Hai Plain, Loess Plateau) and other areas where water resources are not a limiting factor.

## 3.2 Total Water Storage and Cumulated Normalized Difference Vegetation Index Trends Within the Nine Agricultural Regions

From January 2002 to December 2016, GRACE satellites observed the changes in water resources all over mainland China. As shown in **Figure 3**, in the Northern arid and semi-arid region of China (Inner Mongolia, Xinjiang, Gansu, and Ningxia province), the Huang-Huai-Hai Plain (Northern China plain), and the Loess Plateau, TWS show a clear trend of annual decline. In Northeast China, GRACE satellites
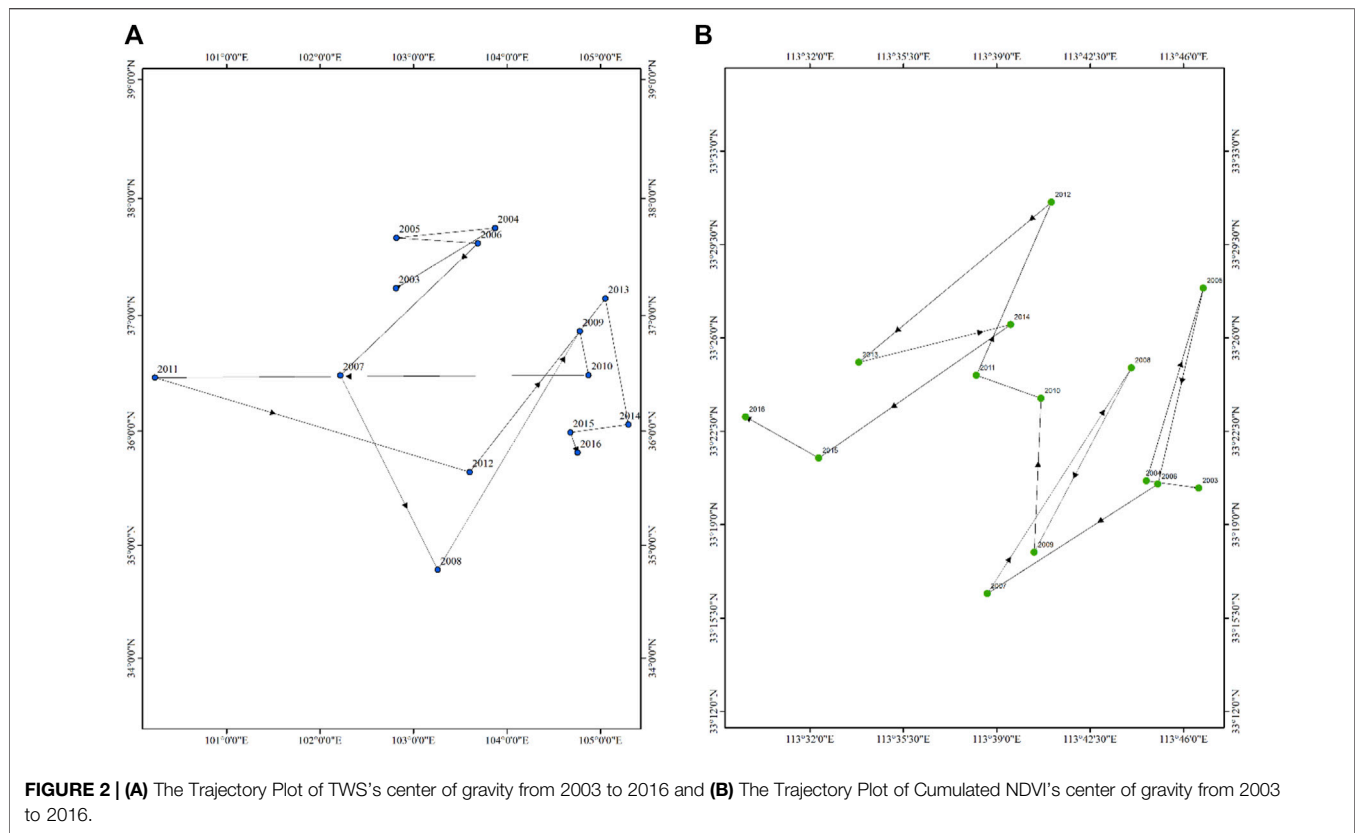
**FIGURE 2 | (A)** The Trajectory Plot of TWS's center of gravity from 2003 to 2016 and **(B)** The Trajectory Plot of Cumulated NDVI's center of gravity from 2003 to 2016.

monitored fluctuations in TWS with three peaks and three troughs throughout the observation period. TWS value of this area reaches a maximum value in 2005, 2010, and 2013, respectively, followed by a rapid decline, reaching its valley in 2008, 2011, and 2015. In the water-limited area, the annual yearly TWS value showed a continuous decline. The data increase in these areas during the first 2 to 3 years of the observation period, and then show an almost continuous decrease during the subsequent observation period. Specifically, the TWS in the northern arid and semi-arid region starts to show a steep decline in 2005, fluctuates between −500 and 0 m$^3$ × 1,000 m$^3$ between 2009 and 2013, and then starts to show a continuous decline again. In other water-limited regions, TWS was stable from 2008 to 2012 and declined continuously during the rest of the period. The overall trend of TWS for the Qinghai-Tibet Plateau is decreasing. Because GRACE TWS Data contains ice, the melting of snow and ice and its inflow into the immediate area will also cause a reduction in TWS. In the southern region, the overall trend of TWS is quite different from that in the north. In and around the Sichuan basin, monthly TWS shows significant interannual variation, but the trend is stable throughout the period. In contrast, in the middle and lower reaches of the Yangtze River plain, southern China, and the Yunnan-Guizhou plateau, TWS remains stable in the early part of the observation period and starts to show a continuous increase around 2010. The annual TWS in the non-water-limited area generally shows an increasing trend. In the south, TWS showed a different trend from the north. TWS showed a growing trend in the middle-lower Yangtze Plain, Sichuan Basin and surrounding regions, Southern China, and Yunnan-Guizhou Plateau. In the middle and lower reaches of the

Yangtze River, TWS increased from −161 m$^3$ × 1,000 m$^3$ at the beginning of the observation to 374 m$^3$ × 1,000 m3 at the end of the observation. The trend line of TWS in the Sichuan basin region shows that the value does not vary much during the observation period, slowly increasing from slightly below the zero line at the beginning to slightly above the zero line at the end. The trends of TWS are similar in South China and the Yunnan-Guizhou plateau, where the value remains relatively small from 2003 to 2010, while showing an increase after this period. The annual TWS value in South China increased from near the zero line to near 270 m$^3$ × 1,000 m$^3$, while the value in the Yunnan-Guizhou plateau was about 512 m$^3$ × 1,000 m$^3$.

**Figure 4** shows the annual trend of CNDVI data with an increasing trend in most agricultural zones of China, except in the Qinghai-Tibet Plateau. During the observation interval, the CNDVI of the Qinghai-Tibet Plateau region showed an increasing yearly trend from 2003 to 2010 and decreased after reaching the peak in 2010. The decreasing trend continued until the end of the observation. Northeast China is an important center of grain production in China. In terms of CNDVI, the value of CNDVI in Northeast China is relatively high. Compared to other regions, although the growth trend in the Northeast is stable, the absolute value of the growth is smaller compared to the Northeast. At the end of the observation period, the growth trend of the CNDVI value in Northeast China was stopped, and its value floated around 7.65/ million. The CNDVI of the Huang-Huai-Hai Plain and Loess Plateau showed similar trends and increased steadily throughout the observation period. However, the base values of the two regions were different, with the CNDVI in the Huang-Huai-Hai Plain
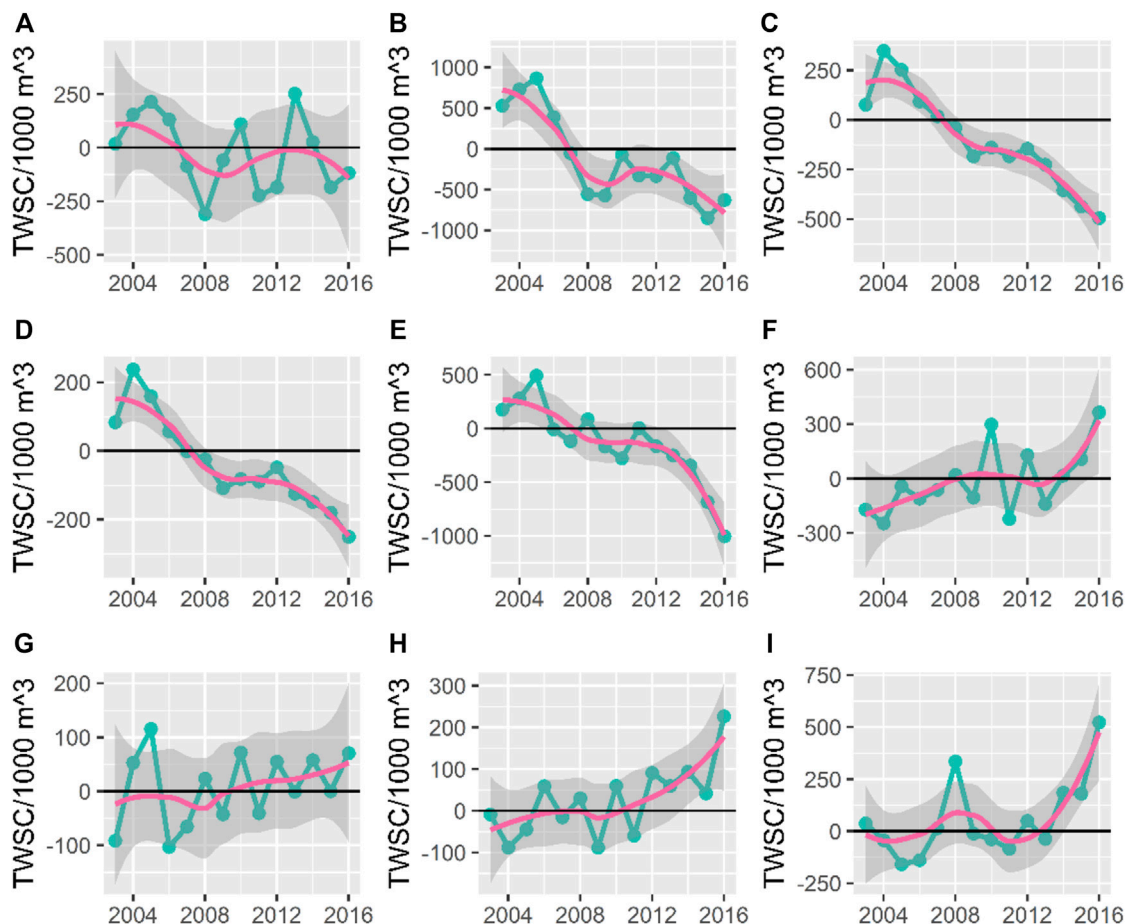
**FIGURE 3** | GRACE time series plot of yearly sum with Trend Line from 2003 to 2016 in nine agricultural regions. [**(A)** Northeast China Plain, **(B)** Northern arid and semi-arid region, **(C)** Huang-Huai-Hai Plain, **(D)** Loess Plateau, **(E)** Qinghai Tibet Plateau, **(F)** Middle-lower Yangtze Plain, **(G)** Sichuan Basin and surrounding regions, **(H)**. Southern China, **(I)** Yunnan-Guizhou Plateau].

increasing from 7.8 million at the beginning to about 8.3 million at the end of the observation period, while the CNDVI in the Loess Plateau increased from 2.3 million to 2.7 million. In the southern part of China, CNDVI generally tends to level off gradually in the early part of the observation and rises in the late part of the observation. For the middle and lower reaches of the Yangtze River, the Sichuan Basin and the Yunnan-Guizhou Plateau, this plateau period occurred between 2008 and 2012. For southern China, CNDVI only stagnated between 2003 and 2008 and then showed the same steady increase until the end of the observation period.

## 3.3 Spaatial Changes of Gravity Recovery and Climate Experiment in Response to Cumulated Normalized Difference Vegetation Index Dynamics

**Figure 5** shows the correlation coefficients of TWS and GRACE. In the Northeast Plain, the correlation coefficients generally fluctuate around 0. In the northern arid and semi-arid region, the part near the Loess Plateau and the northwest border, TWS and CNDVI show a negative correlation, and the correlation

coefficients in the rest of the region are near zero. The central area of the Yellow-Huai-Hai Plain and all parts of the Loess Plateau also show negative correlations between TWS and CNDVI. In the center of the Qinghai-Tibet Plateau region, there is no significant trend in the correlation coefficients. However, on the edges of the region, positive correlations were mainly distributed. In the Sichuan Basin and surrounding area and the middle and lower reaches of the Yangtze River region, the correlation between CNDVI and TWS is not obvious in the north of these two regions, and the correlation coefficients begin to move toward positive correlation as it advances to the south. By the south of China and the Yunnan-Guizhou plateau, these regions have been dominated by positive correlations.

The correlations between TWS and CNDVI showed a clear regional trend. In the water-limited area, the correlations were mainly negative. These areas form a band shape from the central part of the Huang-Huai-Hai Plain in the east to the western boundary of the northern semi-arid region in the west. The negative correlations are mainly spread in this belt area. Another distinct regional trend appears in the south, starting from the southern part of the Sichuan basin and the middle and

**FIGURE 4 |** Yearly CNDVI data Times Series plot with trendline from 2004 to 2016 in nine agricultural subdivisions of China in nine agricultural area [**(A)** Northeast China Plain, **(B)** Northern arid and semi-arid region, **(C)** Huang-Huai-Hai Plain, **(D)** Loess Plateau, **(E)** Qinghai Tibet Plateau, **(F)** Middle-lower Yangtze Plain, **(G)** Sichuan Basin and surrounding regions, **(H)** Southern China, **(I)** Yunnan-Guizhou Plateau].

lower reaches of the Yangtze River region, and covering the whole of southern China and the Yunnan-Guizhou plateau, where positive correlations dominate. Positive correlations also appear in the northern part of the Tibetan Plateau, but the TWS data include the influence of melting snow and ice, and it is unclear whether the trend is due to the influx of melting snow and ice into the region. As can be seen in **Figure 5**, the results of the correlation analysis are consistent with statistical significance in the two regions with significant positive and negative correlations. In the other regions, the correlation analysis could not pass the test. NA values indicate that there is no cropland in the area.

# 4 DISCUSSION

## 4.1 Satellite Data Reveal Spatial and Temporal Variation in Water Resources and Grain Production

The shift in the center of gravity of CNDVI provides evidence of a shift in China's grain production pattern. The absolute value of CNDVI cannot accurately predict grain production, but the direction of change can indicate relative changes in production

patterns. Wang et al. (2018) collected grain production data from the China Statistical Yearbook and field research data, found a similar pattern. From 1996 to 2005, the center of gravity of grain production showed a "northward and westward" trend. The center of gravity moved faster and faster, and according to Wang et al. (2018) estimate, the center of gravity moved from 7.6 km/a in the early period to 41.2 km/a at the end of the observation period (Jieyong and Yansui, 2009). They explain this phenomenon from several aspects. In terms of water resources, drilling of wells to develop groundwater resources has been vigorously developed in the north since the 1980's (Wang et al., 2018). On the other hand, the promotion of agricultural films has caused a much higher replanting index in many northern areas, and many 1-year maturity areas can reach 2-year maturity and 2-year maturity (Ye et al., 2012).

## 4.2 Trends in Cumulated Normalized Difference Vegetation Index and Total Water Storage by Region

The TWS extracted from the GRACE program provided results consistent with Common sense. The GRACE satellite data shows a situation that coincides with the distribution of China's water resources, that is, the total amount of water resources, although

**FIGURE 5 |** Spatial Correlation between TWS and CNDVI with *p*-value under 0.05 [**(A)** Northeast China Plain, **(B)** Northern arid and semi-arid region, **(C)** Huang-Huai-Hai Plain, **(D)** Loess Plateau, **(E)** Qinghai Tibet Plateau, **(F)** Middle-lower Yangtze Plain, **(G)** Sichuan Basin and surrounding regions, **(H)** Southern China, **(I)** Yunnan-Guizhou Plateau].
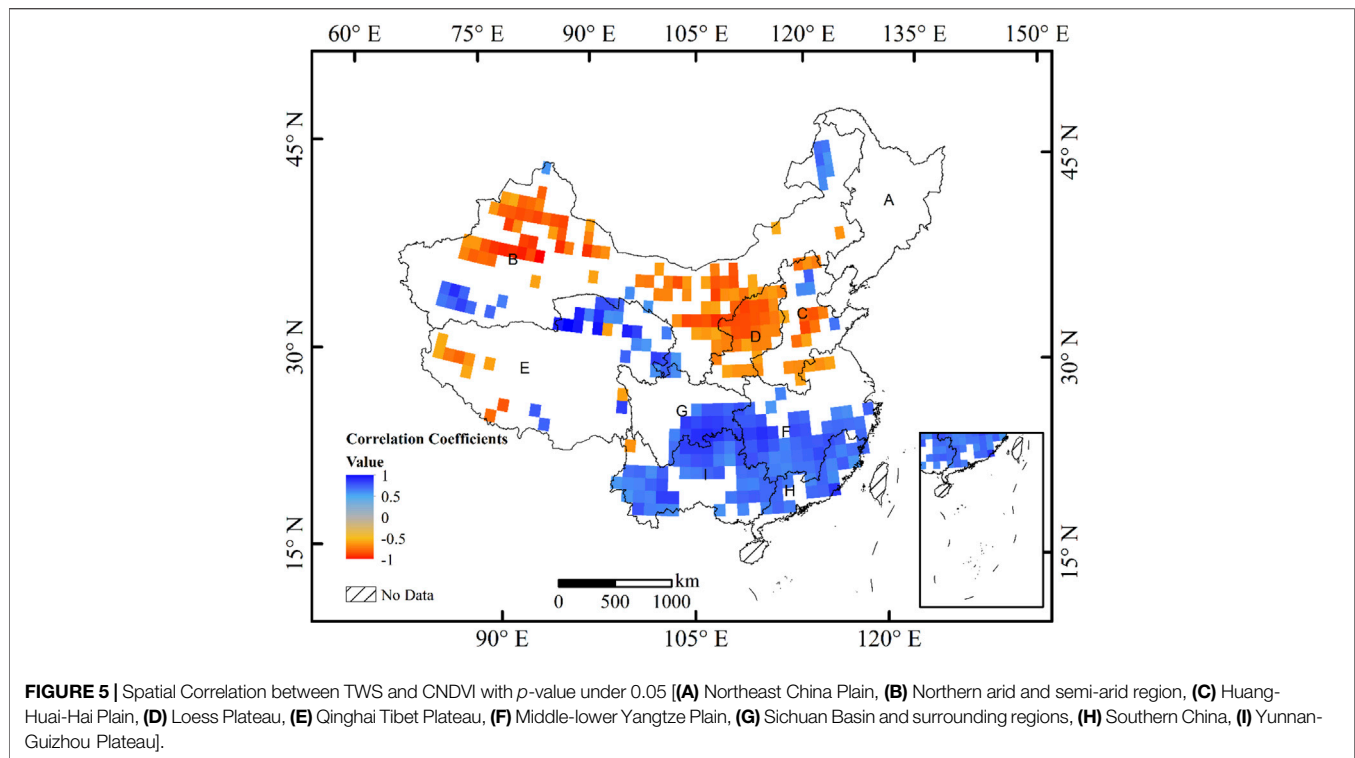
significant, is unevenly distributed in the south and north part of this country. The three regions where the GRACE data shows a significant decline: The North China Plain, the Loess Plateau, and the desert-strewn northwest are precisely the regions where water resources face a considerable shortage. In these regions, where water resources are less distributed, the continuous decline of water resources releases a danger signal. In the water-rich southern and northeastern regions, which are also experiencing rapid socioeconomic development, water resources are not significantly affected. Unlike water resources, all nine agricultural regions showed steady growth in food production, except for the Qinghai-Tibet Plateau region.

Although water resources show large fluctuations during the observation period in the Northeast Plain, there is no significant decrease in CNDVI during the whole period. Combined with the CNDVI data, agricultural activities on water resources are relatively small in the northeastern region in the short term, and it is still a stable grain production center in China. Although there was no significant decrease in TWS data before and after the observation period, Zhang et al. (2018) used the Weather Research and Forecasting (WRF) model to simulate the water balance and assess the impact of agriculture on water resources for each decade from 1910 to 2010 based on a series of interdecadal land use datasets. They found no significant trend in precipitation in the Northeast Plain. However, canopy transpiration and interception evaporation increased and runoff and infiltration decreased. This suggests that agricultural expansion in the region may put significant pressure on this vital food production base in the long term.

The Loess Plateau is the most eroded area in China (Liu and Diamond, 2005). There are four leading causes of soil erosion on the Loess Plateau: topography, soil type, climate, and vegetation. The concentrated rainfall in July, August, and September and the erosion-prone loess have caused severe soil erosion on the Loess Plateau. Soil erosion takes away local water resources not only directly but also indirectly leads to the rapid loss of water resources in this region due to the lack of soil as a carrier. Furthermore, the expansion of agriculture will undoubtedly exacerbate this trend. As more and more land is cleared for agriculture, irrigation water and crop evapotranspiration will increase the water shortage in the region.

The Huang-Huai-Hai Plain is also facing severe water shortages. Groundwater Funnel has been used to describe the increasing water shortage in northern China (Chen et al., 2011). Many researchers have conducted studies on this phenomenon, and the over-exploitation of groundwater is the likely culprit (Changming et al., 2001; Yuan et al., 2004; Zhang et al., 2004). In the Beijing-Tianjin-Hebei region, agriculture accounts for over 70% of total water use (National Bureau of Statistics of China, 2020). The primary cropping system in the region is the winter wheat-summer corn annual rotation (double cropping). The production of winter wheat in the region is increasing year by year. However, in terms of climatic factors, the annual precipitation only meets about 65% of the region's agricultural water needs (Yuan et al., 2004). Further, during the growing period of winter wheat, precipitation is even more scarce and the deficit is mainly supplemented by groundwater. Over-dependence on groundwater water resources and uncontrolled exploitation of groundwater, in turn, destabilize the local water

cycle and accelerate the loss of water resources. Taken together, water resource management in these water-limited areas is unsustainable. Consequently, the growth dynamics of grain production are also unsustainable in the long run.

The Northern arid and semi-arid region, as the name of the region describes, has less annual precipitation than potential evaporation. In the western part of the region, the average annual rainfall in the arid region was between 70 and 100 mm between 1990 and 2010, while in the semi-arid region in the eastern part, the average annual rainfall during the same period was between 300 and 440 mm (National Bureau of Statistics of China, 2020). Grasslands and deserts cover the entire region, and rainfall decreases from east to west (John et al., 2009). Water resources here are also increasingly challenged by GRACE data. In these areas, water resources are clearly a limiting factor for ecosystem development. The average annual available water resource in the region is only 1,275.8 km$^2$, or 4.6% of the national total, with an average annual deficit of at least 36.53 km$^2$ (Xia et al., 2017).

Due to abundant rainfall and rich water reserves, the overall trend of water resources in the south is stable, and even some areas show growth at the end of the observation period compared to the beginning. Natural conditions indicate that these areas still have an enormous potential for grain production.

## 4.3 Potential Risks and Countermeasures Arising From the Changing Pattern of Grain Prodcution

Water, an essential input in agricultural production, can also eventually lead to the suspension of the entire grain production process after it is continuously outflowed from the region. The correlation between TWS and CNDVI releases a potential danger signal. Due to a variety of factors such as cost and uneven economic development, the northern region is beginning to assume a larger share of food production. Such a production pattern is not in line with the water distribution pattern of China. The region, represented by the Huang-Huai-Hai plain, suffers from perennial water shortages and over-exploits groundwater to irrigate farmland. Other water-scarce northern regions are facing similar dilemmas. This situation may eventually lead to the depletion of the agricultural production potential of these regions and, at a certain point, to a significant decrease in grain production in these regions. Kang et al. (2009) found that although crop yield increases with expanded or intensified irrigation, this may increase the rate of environmental degradation. Also they found through modeling that crop yields are more sensitive to precipitation than temperature. Shu et al. (2021) observed a similar water dilemma by analyzing the water footprint of all Chinese provinces. Green water scarcity poses a challenge to agricultural water management in most regions, with important areas for crop export in the north such as the North China Plain, and the Northeast Plain showing high growth in blue, green and gray water footprints. In contrast, in the southwest and southeast, relatively abundant water resources meet the water requirements for crop growth, but green water scarcity limits the long-term development of agriculture (Shu et al., 2021; Zhai et al., 2021).

## 5 CONCLUSION

From the results, GRACE data and CNDVI data exhibit linear correlation in some areas, and this correlation has a clear spatial distribution. In general, TWS and CNDVI are negatively correlated in the western and northern parts of China. In the east and south of China, where water resources are more abundant compared to the North, TWS and CNDVI simultaneously increase steadily and show a positive correlation over the observation period.

The trajectory of center-of-gravity and spatial correlation analysis detected the coupling between changes in grain production patterns and changes in water resources in China at the overall and regional levels, respectively. However, behind the continuous years of grain production increase, there is also a possible crisis. Due to the rapid progressing of urbanization and economic development in the south, agriculture has not developed as fast as in the north. This development reversal and the spatial distribution of water resources have created a contradiction. Compared to the southeast, where rainfall is plentiful, water resources become increasingly scarce as the perspective shifts to the west and north inland. This contradiction lays the groundwork for China's future agricultural development. Whether it is a shift in center of gravity or spatial correlation, the satellite data may reveal the internal-logic changes in China's agricultural development behind the scenes. On the one hand, the uneven distribution of water resources in China has been a nuisance for many years. The pattern of China's food production under the influence of various factors such as climate shows a worrying change.

The endless demand for water from natural bodies of water, including groundwater, to irrigate farmland will sooner or later trigger a water shortage at some point in the future. This will not only force agricultural development in these areas to stagnate but also affect water for domestic and industrial use, ultimately hindering the development of society as a whole. Therefore, policy makers must balance the agricultural development between the north and the south, give full play to the advantages of abundant water resources in the south, and reasonably arrange the spatial pattern of agricultural development. Potential measures include: 1) limiting land reclamation in northern regions; 2) promoting water conservation systems to slow down the exploitation of groundwater resources; 3) promoting agricultural technology innovation, introducing drought-tolerant varieties; appropriately encouraging agricultural reclamation in southern regions.

This study examines the use of satellite data for large scale water resources (including groundwater) and its possible applications. At this stage, satellite data still have some limitations, taking GRACE satellite data as an example, the twin satellite has only collected 18 years of data since it was first launched in 2004, and only up to 18 matched pairs can be generated when performing interannual analysis. Also, due to the low spatial resolution of GRACE's data, only 1° and 0.5° resolutions are available. Two characteristics of GRACE satellite products cause limitations in using this data for use at small scales. Therefore, future research could focus on using data fusion techniques to provide time series of sufficient density to

provide more refined and reliable statistical analysis support for water resources management in an agricultural context.

## DATA AVAILABILITY STATEMENT

The original contributions presented in the study are included in the article/Supplementary Material, further inquiries can be directed to the corresponding author.

## AUTHOR CONTRIBUTIONS

Conceptualization, YF and JW. Methodology, YF and JW. Software, YF. Validation, YF. Formal analysis, YF. Data curation, YF. Writing—original draft preparation, YF. Writing—review and editing, YF and JW. Visualization, YF. Supervision, JW. Project administration, JW. Funding acquisition, JW. All authors have read and agreed to the published version of the manuscript.

## FUNDING

## REFERENCES

Adam, D. (2002). Amazing Grace. *Nature* 416, 10–11. doi:10.1038/416010a

Ahmed, K. R., and Akter, S. (2017). Analysis of Landcover Change in Southwest Bengal Delta Due to Floods by NDVI, NDWI and K-Means Cluster with Landsat Multi-Spectral Surface Reflectance Satellite Data. *Remote Sens. Appl. Soc. Environ.* 8, 168–181. doi:10.1016/j.rsase.2017.08.010

Baret, F., and Guyot, G. (1991). Potentials and Limits of Vegetation Indices for LAI and APAR Assessment. *Remote Sens. Environ.* 35, 161–173. doi:10.1016/0034-4257(91)90009-U

Bigot, J., and Klein, T. (2018). Characterization of Barycenters in the Wasserstein Space by Averaging Optimal Transport Maps. *Esaim Ps.* 22, 35–57. doi:10.1051/ps/2017020

Bonell, M. (2002). Ecohydrology-a Completely New Idea? *Hydrological Sci. J.* 47, 809–810. doi:10.1080/02626660209492984

Bontemps, S., Herold, M., Kooistra, L., van Groenestijn, A., Hartley, A., Arino, O., et al. (2011). Revisiting Land Cover Observations to Address the Needs of the Climate Modelling Community. *Biogeosciences Discuss.* 8, 7713–7740. doi:10.5194/bgd-8-7713-2011

Cao, Y., Nan, Z., and Cheng, G. (2015). GRACE Gravity Satellite Observations of Terrestrial Water Storage Changes for Drought Characterization in the Arid Land of Northwestern China. *Remote Sens.* 7, 1021–1047. doi:10.3390/rs70101021

Changming, L., Jingjie, Y., and Kendy, E. (2001). Groundwater Exploitation and its Impact on the Environment in the North China Plain. *Water Int.* 26, 265–272. doi:10.1080/02508060108686913

Chen, B., Gong, H., Li, X., Lei, K., Zhang, Y., Li, J., et al. (2011). Spatial-temporal Characteristics of Land Subsidence Corresponding to Dynamic Groundwater Funnel in Beijing Municipality, China. *Chin. Geogr. Sci.* 21, 753–764. doi:10.1007/s11769-011-0509-6

Colwell, J. E. (1974). Vegetation Canopy Reflectance. *Remote Sens. Environ.* 3, 175–183. doi:10.1016/0034-4257(74)90003-0

Elahi, E., Khalid, Z., Tauni, M. Z., Zhang, H., and Lirong, X. (2021a). Extreme Weather Events Risk to Crop-Production and the Adaptation of Innovative Management Strategies to Mitigate the Risk: A Retrospective Survey of Rural Punjab, Pakistan. *Technovation*, 102255. In Press. doi:10.1016/j.technovation.2021.102255

Elahi, E., Khalid, Z., and Zhang, Z. (2022a). Understanding Farmers' Intention and Willingness to Install Renewable Energy Technology: A Solution to Reduce the Environmental Emissions of Agriculture. *Appl. Energy* 309, 118459. doi:10.1016/j.apenergy.2021.118459

Elahi, E., Zhang, H., Lirong, X., Khalid, Z., and Xu, H. (2021b). Understanding Cognitive and Socio-Psychological Factors Determining Farmers' Intentions to Use Improved Grassland: Implications of Land Use Policy for Sustainable Pasture Production. *Land use policy* 102, 105250. doi:10.1016/j.landusepol.2020.105250

Elahi, E., Zhang, Z., Khalid, Z., and Xu, H. (2022b). Application of an Artificial Neural Network to Optimise Energy Inputs: An Energy- and Cost-Saving Strategy for Commercial Poultry Farms. *Energy* 244, 123169. doi:10.1016/j.energy.2022.123169

ESA (2017). Land Cover CCI Product User Guide Version 2. Available at: https://maps.elie.ucl.ac.be/CCI/viewer/download/ESACCI-LC-Ph2-PUGv2_2.0.pdf (Accessed November 23, 2021).

Famiglietti, J. S., Lo, M., Ho, S. L., Bethune, J., Anderson, K. J., Syed, T. H., et al. (2011). Satellites Measure Recent Rates of Groundwater Depletion in California's Central Valley. *Geophys. Res. Lett.* 38, L03403. doi:10.1029/2010GL046442

Feng, W., Zhong, M., Lemoine, J.-M., Biancale, R., Hsu, H.-T., and Xia, J. (2013). Evaluation of Groundwater Depletion in North China Using the Gravity Recovery and Climate Experiment (GRACE) Data and Ground-Based Measurements. *Water Resour. Res.* 49, 2110–2118. doi:10.1002/wrcr.20192

Goward, S. N., and Huemmrich, K. F. (1992). Vegetation Canopy PAR Absorptance and the Normalized Difference Vegetation Index: An Assessment Using the SAIL Model. *Remote Sens. Environ.* 39, 119–140. doi:10.1016/0034-4257(92)90131-3

Iqbal, N., Hossain, F., Lee, H., and Akhter, G. (2016). Satellite Gravimetric Estimation of Groundwater Storage Variations over Indus Basin in Pakistan. *IEEE J. Sel. Top. Appl. Earth Obs. Remote Sens.* 9, 3524–3534. doi:10.1109/JSTARS.2016.2574374

Jieyong, W., and Yansui, L. (2009). The Changes of Grain Output Center of Gravity and its Driving Forces in China since 1990. *Resour. Sci.* 31, 1188–1194.

John, R., Chen, J., Lu, N., and Wilske, B. (2009). Land Cover/land Use Change in Semi-arid Inner Mongolia: 1992-2004. *Environ. Res. Lett.* 4, 045010. doi:10.1088/1748-9326/4/4/045010

Kang, Y., Khan, S., and Ma, X. (2009). Climate Change Impacts on Crop Yield, Crop Water Productivity and Food Security - A Review. *Prog. Nat. Sci.* 19, 1665–1674. doi:10.1016/j.pnsc.2009.08.001

Landerer, F. W., and Swenson, S. C. (2012). Accuracy of Scaled GRACE Terrestrial Water Storage Estimates. *Water Resour. Res.* 48, 1–11. doi:10.1029/2011WR011453

le Maire, G., Marsden, C., Nouvellon, Y., Grinand, C., Hakamada, R., Stape, J.-L., et al. (2011). MODIS NDVI Time-Series Allow the Monitoring of Eucalyptus Plantation Biomass. *Remote Sens. Environ.* 115, 2613–2625. doi:10.1016/j.rse.2011.05.017

Liu, J., and Diamond, J. (2005). China's Environment in a Globalizing World. *Nature* 435, 1179–1186. doi:10.1038/4351179a

Lopresti, M. F., Di Bella, C. M., and Degioanni, A. J. (2015). Relationship between MODIS-NDVI Data and Wheat Yield: A Case Study in Northern Buenos Aires Province, Argentina. *Inf. Process. Agric.* 2, 73–84. doi:10.1016/j.inpa.2015.06.001

Ministry of Water Resources (2010). *Bulletin of Flood and Drought Disasters in China 2010*. Beijing: China Water Power Press.

Cooley, S. S., and Landerer, F. W. (2019). "GRACE D-103133 Gravity Recovery and Climate Experiment Follow-on (GRACE-FO) Level-3 Data Product User Handbook," in NASA Jet Propulsion Laboratory (Pasadena, CA: California Institute of Technology).

National Agricultural Zoning Committee (1981). *Comprehensive Agricultural Zoning of China*. Beijing: China Agriculture Press. The map is available at https://www.resdc.cn/data.aspx?DATAID=275.

National Bureau of Statistics of China (2020). *China Statistical Yearbook*. Beijing: China Agriculture Press. Available at http://www.stats.gov.cn/tjsj./ndsj/ (Accessed November 23, 2021).

Panek, E., and Gozdowski, D. (2020). Analysis of Relationship between Cereal Yield and NDVI for Selected Regions of Central Europe Based on MODIS Satellite Data. *Remote Sens. Appl. Soc. Environ.* 17, 100286. doi:10.1016/j.rsase.2019.100286

Prasad, A. K., Chai, L., Singh, R. P., and Kafatos, M. (2006). Crop Yield Estimation Model for Iowa Using Remote Sensing and Surface Parameters. *Int. J. Appl. Earth Observation Geoinformation* 8, 26–33. doi:10.1016/j.jag.2005.06.002

Ren, J., Chen, Z., Zhou, Q., and Tang, H. (2008). Regional Yield Estimation for Winter Wheat with MODIS-NDVI Data in Shandong, China. *Int. J. Appl. Earth Observation Geoinformation* 10, 403–413. doi:10.1016/j.jag.2007.11.003

Rodell, M., and Famiglietti, J. S. (2001). An Analysis of Terrestrial Water Storage Variations in Illinois with Implications for the Gravity Recovery and Climate Experiment (GRACE). *Water Resour. Res.* 37, 1327–1339. doi:10.1029/2000WR900306

Rodell, M., Houser, P. R., Jambor, U., Gottschalck, J., Mitchell, K., Meng, C.-J., et al. (2004). The Global Land Data Assimilation System. *Bull. Amer. Meteor. Soc.* 85, 381–394. doi:10.1175/BAMS-85-3-381

Shu, R., Cao, X., and Wu, M. (2021). Clarifying Regional Water Scarcity in Agriculture Based on the Theory of Blue, Green and Grey Water Footprints. *Water Resour. Manage* 35, 1101–1118. doi:10.1007/s11269-021-02779-6

Smith, M. R., and Dicken, P. (2000). Global Shift: Transforming the World Economy. *Can. J. Sociol./Cahiers Can. de Sociol.* 25, 399. doi:10.2307/3341650

Thenkabail, P. S., Smith, R. B., and De Pauw, E. (2000). Hyperspectral Vegetation Indices and Their Relationships with Agricultural Crop Characteristics. *Remote Sens. Environ.* 71, 158–182. doi:10.1016/S0034-4257(99)00067-X

Wahr, J., Swenson, S., Zlotnicki, V., and Velicogna, I. (2004). Time-variable Gravity from GRACE: First Results. *Geophys. Res. Lett.* 31. doi:10.1029/2004GL019779

Wang, J., Rich, P. M., Price, K. P., and Kettle, W. D. (2005). Relations between NDVI, Grassland Production, and Crop Yield in the Central Great Plains. *Geocarto Int.* 20, 5–11. doi:10.1080/10106040508542350

Wang, J., Zhang, Z., and Liu, Y. (2018). Spatial Shifts in Grain Production Increases in China and Implications for Food Security. *Land use policy* 74, 204–213. doi:10.1016/j.landusepol.2017.11.037

Xia, J., Ning, L., Wang, Q., Chen, J., Wan, L., and Hong, S. (2017). Vulnerability of and Risk to Water Resources in Arid and Semi-arid Regions of West China under a Scenario of Climate Change. *Clim. Change* 144, 549–563. doi:10.1007/s10584-016-1709-y

Yang, Y., Long, D., Guan, H., Scanlon, B. R., Simmons, C. T., Jiang, L., et al. (2014). GRACE Satellite Observed Hydrological Controls on Interannual and Seasonal Variability in Surface Greenness over Mainland Australia. *J. Geophys. Res. Biogeosci.* 119, 2245–2260. doi:10.1002/2014JG002670

Ye, T., Shi, P., Wang, J. a., Liu, L., Fan, Y., and Hu, J. (2012). China's Drought Disaster Risk Management: Perspective of Severe Droughts in 2009-2010. *Int. J. Disaster Risk Sci.* 3, 84–97. doi:10.1007/s13753-012-0009-z

Yuan, G., Luo, Y., Sun, X., and Tang, D. (2004). Evaluation of a Crop Water Stress Index for Detecting Water Stress in Winter Wheat in the North China Plain. *Agric. Water Manag.* 64, 29–40. doi:10.1016/S0378-3774(03)00193-8

Zhai, Y., Zhang, T., Bai, Y., Ji, C., Ma, X., Shen, X., et al. (2021). Energy and Water Footprints of Cereal Production in China. *Resour. Conservation Recycl.* 164, 105150. doi:10.1016/j.resconrec.2020.105150

Zhang, L., Wang, C., Li, X., Zhang, H., Li, W., and Jiang, L. (2018). Impacts of Agricultural Expansion (1910s-2010s) on the Water Cycle in the Songneng Plain, Northeast China. *Remote Sens.* 10, 1108. doi:10.3390/rs10071108

Zhang, Y., Kendy, E., Qiang, Y., Changming, L., Yanjun, S., and Hongyong, S. (2004). Effect of Soil Water Deficit on Evapotranspiration, Crop Yield, and Water Use Efficiency in the North China Plain. *Agric. Water Manag.* 64, 107–122. doi:10.1016/S0378-3774(03)00201-4

Zhang, Y., Zhang, J., Yang, Z., and Li, J. (2012). Analysis of the Distribution and Evolution of Energy Supply and Demand Centers of Gravity in China. *Energy Policy* 49, 695–706. doi:10.1016/j.enpol.2012.07.012

Check for updates

# Tracking Spatio-Temporal Dynamics of Greenhouse-Led Cultivated Land and its Drivers in Shandong Province, China

*Cong Ou and Yongsheng Wang\**

*Institute of Geographic Sciences and Natural Resources Research, Chinese Academy of Sciences (CAS), Beijing, China*

Rapid urbanization and economic development have led the diversified food production and consumption. In this context, as a highly efficient and intensive cultivated land use form, Greenhouse-led cultivated land (GCL) has continuously increased in recent decades worldwide. Previously works have documented the irrational expansion of GCL in challenging the ecological environment and sustainable agricultural development. However, these studies either have been short-term and point-based studies or have not revealed the long-term causes, process and patterns in a large-scale. In this study, long-term annual remote sensing-based and statistical data were used to investigate the spatiotemporal dynamics of GCL and its drivers in Shandong province, China from 1989 to 2018. The results showed that: 1) GCL in Shandong was toward continuous clustering dominated by medium-low and medium densities, showing the same trend as the increase of its total area; 2) GCL with a cumulative duration of more than 15 years and a demolition frequency of less than 0.2 were mainly distributed in the industrial clustering regions and roughly formed a circular expansion pattern around the central mountainous area with the most expansion period appeared in the mid-2010's; 3) Budget expenditure for rural development, local retail sales and average earnings of local farmers were the most important local driving factors of the GCL expansion in Shandong. 4) The competition of external vegetable supply and the consumption demand from Beijing were the main external driving forces of the expansion of GCL in Shandong. These findings can enhance the comprehensive understanding of typical component of "Human-Nature" interaction and support the sustainable development of regional agriculture.

Keywords: greenhouse-led cultivated land, spatiotemporal dynamics, driving factors, long-term period, provincial scale

## 1 INTRODUCTION

With rising need for a balanced food supply within a year and the advancement of agricultural technology in recent decades, the total area of protected agriculture has continuously increased at a rate of close to 20% per year around the world (Jiménez-Lao et al., 2020). In this context, greenhouse-led cultivated land (GCL) has been widely utilized worldwide, with an estimated area of 3.02 million hectares in 2016 (Briassoulis et al., 2016), offering a micro-scale environment to counteract unfavorable natural conditions for agricultural output. Although GCL has revolutionized

extensive farming to intensive farming, changed the form of seasonal food supply, and improved the socio-economic well-being of small-scale farmers (Baudoin and Von Zabeltitz, 2002; González-Yebra et al., 2018; Shi et al., 2022), its rapid global expansion has also posed a number of ecological threats to the local environment, such as soil continuous crop obstacle (Wenshou, 2004), soil biodiversity degradation (Zhang et al., 2015), irrational fertilizer use (Min et al., 2012) or plastic waste (Sica and Picuno, 2007). However, as a typical agricultural component that people interact with natural systems (Liu et al., 2007; Zou et al., 2022), the long-term causes, processes and patterns of GCL still unclear. It is critical to investigate the spatiotemporal dynamics of GCL and its drivers over a long-term period to comprehend the complexity of the typical component of "Human-Nature" interaction and support the sustainable development of agriculture and ecosystem.

According to the results of the Seventh National Census, China's urban population reached 930 million in 2021, up 729 million since the "reform and opening-up" policy was implemented in 1978. In this context, due to government policy support and urban food-consumption demand, GCL in China have rapidly increased from mid-1980, and reached the world's greatest coverage of 1.32 million hectares in 2016. The rapid expansion of GCL in China not only brought some of the above-mentioned environmental issues, but also posed a threat to China's strictest policy of protecting cultivated land and ensuring food security (Liu et al., 2020), as the GCL are always disorderly developed by the autonomous behavior of local farmers in the early stages (Ge et al., 2019), reducing the possibility of restoring grain-planting and the rational rural land use (He and Ma, 2007; Su et al., 2019). Shandong province began to promote GCL for the growing of vegetables in the early 1990s, particularly in Shouguang (a county in Shandong), which is known as "China's cradle of 'Winter-Warm' greenhouse" (Ma et al., 2021). Exploring the spatiotemporal dynamics of GCL and its drivers in Shandong can provide a clear historical picture of the China's remarkable GCL expansion as well as a scientific reference for other protected agriculture developing areas.

Remote sensing technology has been proved its advantages in spatio-temporal explicit monitoring for GCL on different scales when compared to traditional statistics (Jiménez-Lao et al., 2020). Multiple sources of satellite imagery have introduced for GCL mapping, including Landsat TM/ETM+/OLI (Levin et al., 2007; Chaofan et al., 2016), Sentinel-2 MSI (Novelli et al., 2016; Balcik et al., 2019), GF-1/2 (Gao et al., 2018; Li et al., 2020), QuickBird (Agüera et al., 2008; Agüera and Liu, 2009; Carvajal et al., 2010) or WorldView-2 (Koc-San, 2013; Aguilar et al., 2014), etc. Meanwhile, a number of unsupervised methods based on the novel AG-extraction indices, such as the vegetable land extraction index (VI) (Zhao et al., 2004), moment distance index (MDI) (Aguilar et al., 2016), plastic-mulched landcover index (PMLI) (Lu et al., 2014), plastic greenhouses index (PGI) (Yang et al., 2017) and greenhouses detection index (GDI) (González-Yebra et al., 2018), have been proposed to distinguish GCL from other land use types. In order to improve the robustness of such unsupervised methods, previous studies also have adopted the supervised approaches, such as support vector machine (SVM) (Bektas Balcik et al., 2020), random forest (RF) (Lin et al., 2021), artificial neural network (ANN) (Carvajal et al., 2006) and convolutional neural network (CNN) (Sun et al., 2021), to extract the spatial distribution of GCL. Despite the fact that all of these researches performed well and produced a number of accurate GCL maps in various locations and years, only a few studies used the resulting GCL maps to detect spatio-temporal dynamics and driving forces of GCL (Arcidiacono and Porto, 2010; Picuno et al., 2011; Yu et al., 2017; Ou et al., 2020). To our knowledge, a few of these studies have revealed the annual spatiotemporal dynamics of GCL and its drivers over a large-scale and long-term period, which failed to provide a comprehensive and macroscale description of GCL for policymakers.

In this paper, in order to address the aforementioned research gaps, a comprehensive analysis framework that integrated spatial information entropy, kernel density estimation, time-series segmentation sliding algorithm, annual expansion index, geographic detector and granger causality test, was proposed to investigate the spatiotemporal dynamics of GCL and its drivers in Shandong from 1989 to 2018 using long-term annual remote sensing-based and statistical data. The main contributions of this paper were as follows:

- The spatio-temporal dynamics of GCL, including spatial clustering, temporal continuity and expansion trajectory in Shandong were quantified;
- The local driving mechanism between GCL expansion and the change of local economic scale, population growth, transportation conditions, rural infrastructure, consumption demand, farmers' willingness as well as government support in Shandong were detected;
- The external driving mechanism between GCL expansion and the change of the supply and demand of vegetables in external markets in Shandong were clarified.

## 2 MATERIALS AND METHODS

### 2.1 Study Area

Shandong province is located in the eastern coastal region of China (34°22'~38°24'N, 114°47'~122°42'E), with a total area of approximate 157,900 km$^2$ (**Figure 1**). The inland area of Shandong borders the provinces of Tianjin, Hebei, Henan, Anhui, and Jiangsu from north to south and the coastal area of Shandong is surrounded by the Yellow Sea and the Bohai Sea. Its landform can be characterized as a mountain area dominating the south-central part, a plain area dominating the southwest and northwest, and a hill area dominating the east. The study area belongs to a warm temperate monsoon climate zone, with the annual average temperature, ranging from 11 to 14°C and the annual average precipitation, ranging from 550 to 950 mm. Due to such geographical conditions, Shandong has become a major agricultural production province in China, with a cultivated land area of about 7.59 million hectares. In 2019, the total agricultural output value of the province was 547.65 billion yuan and the grain output was 53.57 million tons, ranking second in the country.
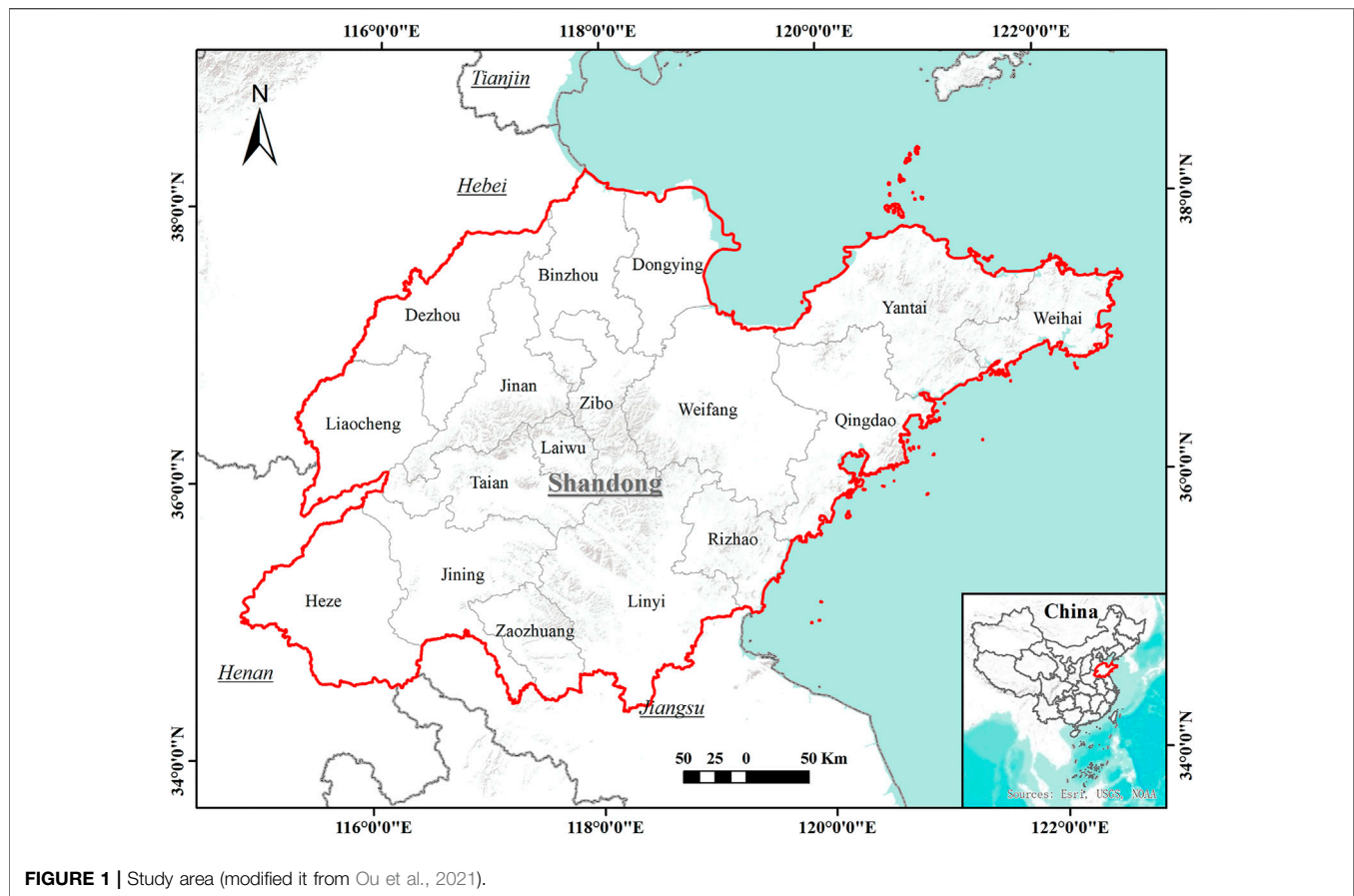
**FIGURE 1** | Study area (modified it from Ou et al., 2021).

Furthermore, Shandong province is not only a major grain producing province, but also an important cash crop producing province in China, with a highest export volume of agricultural products for decades. Particularly in the vegetable-producing industry, Shandong ranked first in the national vegetable supply provinces, with an output of 81.92 million tons, and the planting area of protected vegetables accounting for approximately one-fourth of the planting area of protected vegetables in China.

## 2.2 Data Sources and Processing

A sequential and fine-resolution GCL mapping dataset is the fundamental information for exploring annual spatiotemporal dynamics of GCL and its driving forces. In this study, we used a series of Landsat-derived maps of GCL in Shandong province, China during 1989–2018 with annual temporal resolution and 30 m spatial resolution (Ou et al., 2021). This dataset was developed based on 8,450 Landsat images on the Google Earth Engine (GEE) and an annual remote sensing mapping method of GCL oriented to the provincial area and long-term period, which was the first dataset with accurate and long-term GCL dynamic maps in China. The average User's Accuracy, Producer's Accuracy and F1-score of GCL over 30 years were 96.56%, 86.64%, and 0.911, respectively. This dataset was consistent and comparable over time, which benefits from the same mapping window, feature optimization as well as temporal

consistency correction, could serve as a suitable dataset for more comprehensive characterization of GCL expansion.

In addition, a number of variables were selected for the driven mechanism analysis (for details, **Supplementary Material S1**). The physical aspect included 7 driving variables: elevation (*AVE*), slope (*SLP*), soil type (*ST*), distance to rivers (*DRV*), distance to rural settlements (*DR*), distance to town centers (*DT*) and distance to urban centers (*DU*), which were used to analyze their driving effect on GCL expansion in terms of three relatively stable aspect over a long time period: topography, soil and location. The socioeconomic aspect included 16 driving variables: primary industry added value (*VP*), secondary industry added value (*VS*), tertiary industry added value (*VT*), rural population (*RPOP*), urban population (*UPOP*), road mileage (*RO*), motorway mileage (*MO*), effective irrigation area (*EI*), agricultural machinery (*AM*), rural electricity consumption (*REC*), local retail sales (*LRS*), average earning of local famers (*AE*), budget expenditure for rural development (*BER*), vegetable production in other provinces (*VPO*), total value of agricultural exports (*VAE*) and consumption demand of vegetable in adjacent metropolises (*CDM*), which were used to analyze their driving effect on GCL expansion in terms of seven relatively dynamic aspect over a long time period: economic scale, population growth, transportation conditions, rural infrastructure, consumer demand, farmers' willingness and government support.

**FIGURE 2 |** The Time-series segmentation and sliding algorithm (TSS).
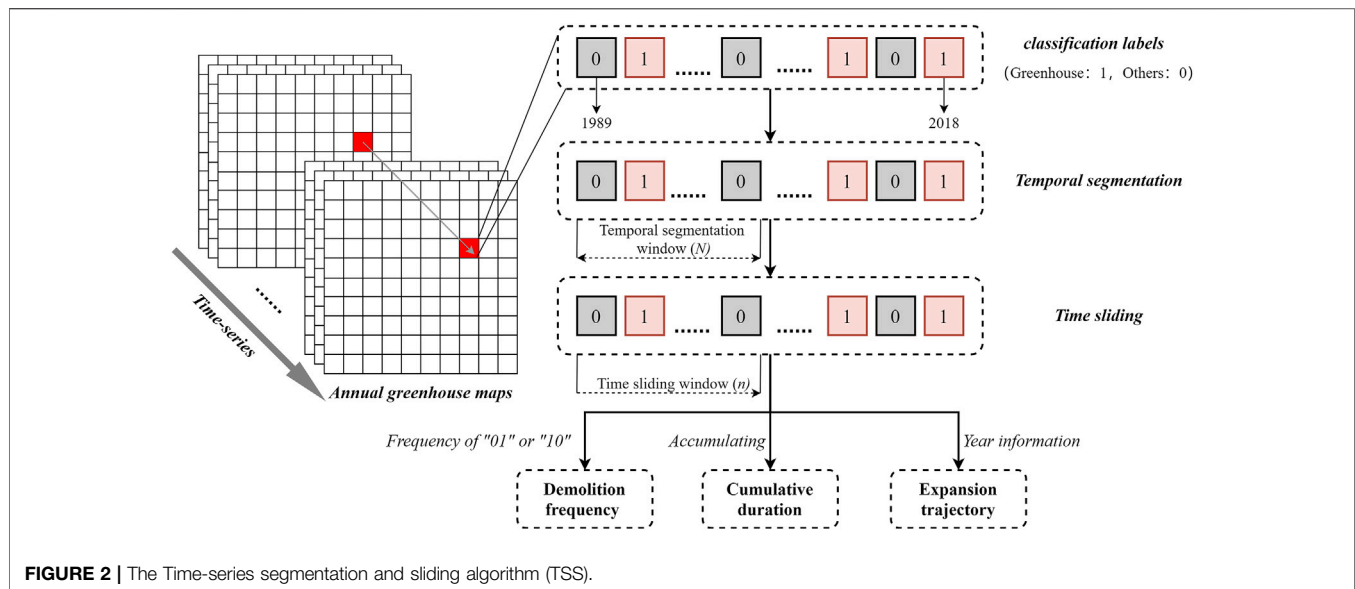
## 2.3 Spatiotemporal Dynamics Analysis
### 2.3.1 Spatial Information Entropy

The spatial information entropy has been widely used in studies such as geography, ecology and life sciences to describe or explain the heterogeneity of data or the distribution of "things" in space due to its ability to characterize the amount of information, uncertainty, heterogeneity and other concepts, in this study we applied it to quantify the global change of GCL clustering in Shandong over the past 30 years, which can be defined as (Leibovici et al., 2014):

$$H(X) = \sum_{i=1}^{I} p(x_i) \log \frac{1}{p(x_i)}$$

where $X$ is the discrete variable containing the corresponding value $x_i$ (in this study is divided into $x_0$ and $x_1$, representing other land use types and GCL, respectively); $p(x_i)$ is the probability mass function (PMF) of $X$, and its result is based on PMF quantifying the average information of $X$. The lower Shannon information entropy value indicates that the spatial distribution of GCL is more clustered, and the higher Shannon information entropy value indicates that the spatial distribution of GCL is more discrete.

### 2.3.2 Kernel Density Estimation

In order to further reflect the spatial heterogeneity of GCL clustering, the density of GCL in each year was classified based on the kernel density estimation (KDE). KDE is a non-parametric test method used to estimate unknown density functions, which has been widely used in natural disasters, public health, industrial spatial layout hotspot analysis and detection, etc. Its calculation formula is as follows (Cai et al., 2013):

$$\hat{f}(x, y) = \frac{3}{nh^2\pi} \sum_{i=1}^{n} \left( 1 - \frac{(x - x_i)^2 + (y - y_i)^2}{h^2} \right)^2$$

where $\hat{f}(x, y)$ is the kernel density of GCL in the grid to be estimated, $h$ is the kernel density estimation bandwidth (set to a 30-year average bandwidth of 42,926 m that guaranteed the comparability of each KDE result over the past 30 years), $x_i$, $y_i$ are the coordinates of the grid centroids to be estimated, $n$ is the number of all sample points within the bandwidth, and $x$, $y$ are the coordinates of the central sample points within the bandwidth.

### 2.3.3 Time-Series Segmentation and Sliding Algorithm

One of the significant advantages of remote sensing-based data is the ability to continuously observe the same area and thus obtain continuous information (Maus et al., 2016). Therefore, we proposed a time-series segmentation and sliding algorithm (TSS) based on the annual remote sensing mapping products of GCL, aiming to analyze the spatiotemporal dynamics of GCL in cumulative duration, demolition frequency and expansion trajectory.

As shown in **Figure 2**, the annual GCL maps were stacked to obtain the classification labels of each pixel from 1989 to 2018, and the temporal label sequences that need to be analyzed were extracted based on the temporal segmentation window N. For the cumulative duration analysis, the cumulative duration of GCL for each pixel at that period can be obtained by accumulating all labels of the segmented sequence. For the demolition frequency analysis, the time sliding window n was further set to 2, and the frequency of "01" or "10" combinations at that period can be obtained by sliding backward from the starting year in steps of 1. For the expansion trajectory analysis, we set the time sliding window n to 1, slide backward from the starting year in steps of 1, and assign the year information to each pixel when "1" appears for the first time.

### 2.3.4 Annual Expansion Index

Regarding the expansion intensity, previous studies have focused on urban expansion as represented by built-up or impervious

areas. However, the major difference between GCL and urban is that urban expansion is generally considered to be irreversible (Li et al., 2015). In terms of GCL, due to the fluctuation of demolition and construction, the information between each year would be lost if the urban expansion intensity calculation rule is followed. Therefore, we proposed an annual expansion index (AEI) based on annual growth to reflect the true expansion intensity over a certain period, which was calculated as follows:

$$AEI = \frac{\sum_{i=1}^{n} GCL_i}{n}$$

where $GCL_i$ represents the annual GCL growth from year $i$ to year $i + 1$ in the specific grid, and $n$ is the study period.

## 2.4 Driven Mechanism Analysis
### 2.4.1 Geodetector
Spatially stratified heterogeneity is a universal characteristic of geographic data, and for geographic data in different layers, if each layer of independent variables has an influence on the dependent variable, its spatial distribution should be similar (Wang et al., 2010). Geodetector is such a statistical method for detecting the spatial heterogeneity and revealing the driving factors behind it based on this assumption (Wang et al., 2016). In this study, we applied the factor detection in Geodetector to explain the local driven mechanism between GCL expansion and the selected variables, which is calculated as follows:

$$q = 1 - \frac{\sum_{h=1}^{L} N_h \sigma_h^2}{N \sigma^2}$$

where L is the total number of stratifications of the dependent variable Y or the independent variables X, $N_h$ and N are the number of units in stratum $h$ and the whole region, respectively, $\sigma_h^2$ and $\sigma^2$ are the variance of the dependent variable Y in stratum $h$ and the whole region, respectively. $q \in [0, 1]$, and the closer the value of q is to 1, the stronger explanatory power of this independent variable for the spatial heterogeneity of the dependent variable (Zhang et al., 2019).

### 2.4.2 Granger Causality Test
Granger causality test is to determine whether a time-series change in one variable is caused by a time-series change in another variable (Freeman, 1983). In this study, we first used the Augmented Dickey-Fuller test (ADF) to test whether the time-series variables were stationary, which is based on the following unit root tests (Krämer, 1998):

$$\Delta X_t = \alpha + \beta_t + \delta X_{t-1} + \sum_{i=1}^{m} \beta_i \Delta X_{t-i} + \epsilon_t$$

where the ADF tests whether the series xt rejects the original hypothesis by judging the estimated value of δ. When δ is less than the critical value of the correlation test, the series Xt is a stationary series, otherwise, the series Xt is a non-stationary series, and a further differential process is required to judge the stationarity of the differenced series.

For variables that are still non-stationary and belong to the same-order of single integer after differencing, further cointegration test based on the Engle-Granger method is required to determine whether there is a long-term stable relationship between the variables, which is conduct by establishing the least squares regression equation as following (Lee and Lee, 2015):

$$Y_t = b_0 + b_1 X_t + \varepsilon_t$$

when ε is less than the critical value of the correlation test, the residual series $\varepsilon_t$ remains a cointegration relationship between variables, otherwise, there is no cointegration relationship between variables in the residual series $\varepsilon_t$.

After testing the stationarity of the variables and the cointegration relationship between the variables, Granger causality tests were carried out on the time-series variables that were stationary and had cointegration relationships, and the following two regression models were estimated:

$$Y_t = \beta_0 + \sum_{i=1}^{m} \beta_i \Delta Y_{t-i} + \sum_{i=1}^{l} \alpha_i X_{t-i} + \mu_t$$

$$X_t = \delta_0 + \sum_{i=1}^{m} \delta_i \Delta X_{t-i} + \sum_{i=1}^{l} \lambda_i Y_{t-i} + \nu_t$$

where the original hypothesis is that $Y_t$ is not the Granger cause of $X_t$ and $X_t$ is not the Granger cause of $Y_t$, and the F-test statistic is performed with the sum of squares of residual $\mu_t$ and the sum of squares of residual $\nu_t$, and if the F statistic is higher than the critical value corresponding to the significance level, the original hypothesis is rejected, which means that there is Granger causality.

# 3 RESULTS

## 3.1 Spatiotemporal Dynamics of Greenhouse-Led Cultivated Land
### 3.1.1 Spatial Clustering
The spatial information entropy was calculated for all years using the annual maps of GCL in Shandong (**Figure 3A**). The unit area entropy value of GCL exhibited a decreasing trend in general, with the maximum value appearing in 1990 and the minimum value appearing in 2017, which can be divided into three stages: 1) from 1989 to 1996, the average unit area entropy value was 0.044; 2) from 1996 to 2005, the average unit area entropy value was 0.036; 3) from 2005 to 2018, the average unit area entropy value was 0.031. It indicated that the spatial clustering of GCL in Shandong over past 30 years was gradually increasing in general, where the highest level of spatial clustering was in 2017 and the lowest was in 1990. Combined with the changes in its total area, it can be seen that entropy value per unit area decreased continuously with the expansion of greenhouses in general, which means that the spatial clustering has a positive synergistic relationship with the change of total area of GCL.

We further explored the spatial heterogeneity of GCL clustering over 30 years by using the KDE method to partition the spatial distribution density (**Figure 3B**). The percentage of low density zones decreased from 96.82% in 1989 to 66.38% in 2018, with a decrease of 30.44% and an average annual decrease of

**FIGURE 3 |** The spatial clustering patterns of GCL: **(A)** the spatial information entropy, **(B)** the spatial distribution density.



**FIGURE 4 |** The cumulative duration patterns of GCL: **(A)** enlarge area A, **(B)** enlarge area B, and **(C)** enlarge area C.
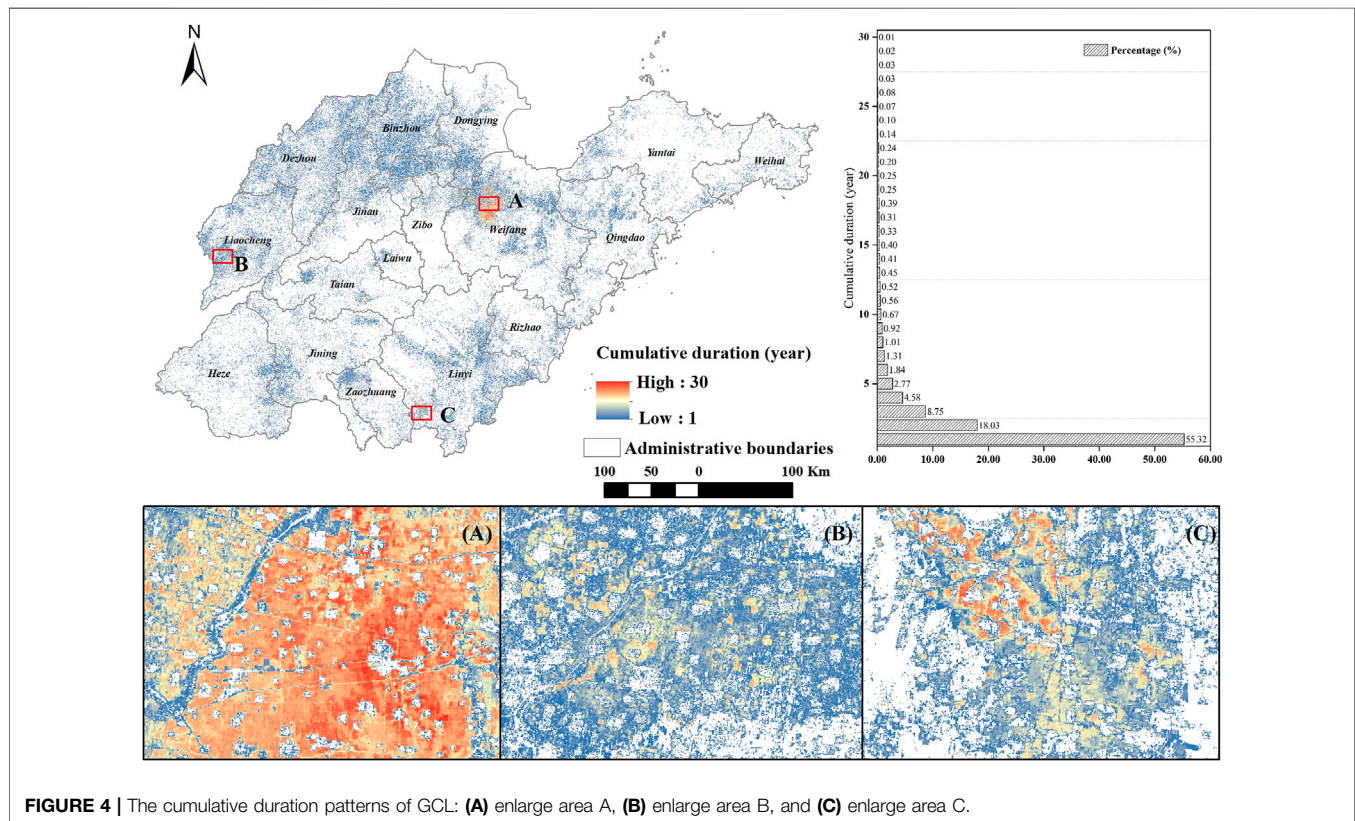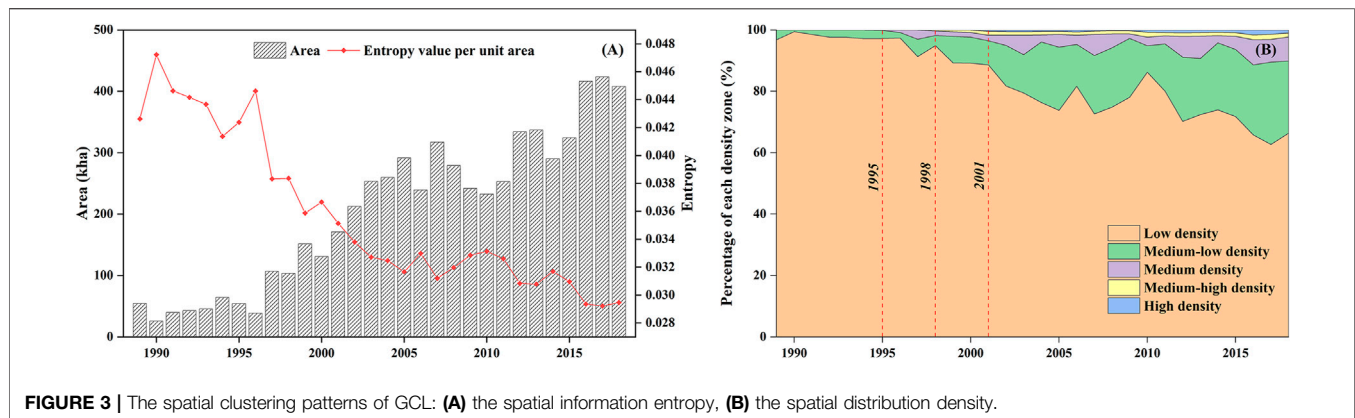
1.05%; the medium-low density zones increased from 0.54% in 1989 to 23.51% in 2018, with an increase of 22.97% and an average annual increase of 0.79%; the medium density zones increased from 0.13% in 1995 to 7.80% in 2018, with an increase of 7.67% and an average annual increase of 0.33%; the medium-high density zones increased from 0.30% in 1998 to 1.36% in 2018, with an increase of 1.06% and an average annual increase of 0.05%; and the high density zones increased from 0.43% in 2001 to 0.95% in 2018, with an increase of 0.47% and an average annual increase of 0.03%. It indicated that despite the GCL expansion in Shandong was toward continuous clustering, but mainly dominated by the medium-low and medium densities.

## 3.1.2 Temporal Continuity

Based on the TSS algorithm, we calculated the cumulative duration of GCL over the past 30 years. As shown in **Figure 4**, GCL with the cumulative duration of 1 year accounted for 55.32% and showed a scattered distribution pattern mainly around the central mountainous area, and when the cumulative duration reached more than 2 years, its percentage rapidly decreased to less than 18.03%. And it can be found that the areas where the cumulative duration of GCL was more than 15 years were mainly distributed in northwestern Weifang, southwestern Linyi and western of Liaocheng, showing a triangular distribution pattern, which is similar to the pattern of the

**FIGURE 5 |** The demolition frequency patterns of GCL: **(A)** enlarge area A, **(B)** enlarge area B, and **(C)** enlarge area C.
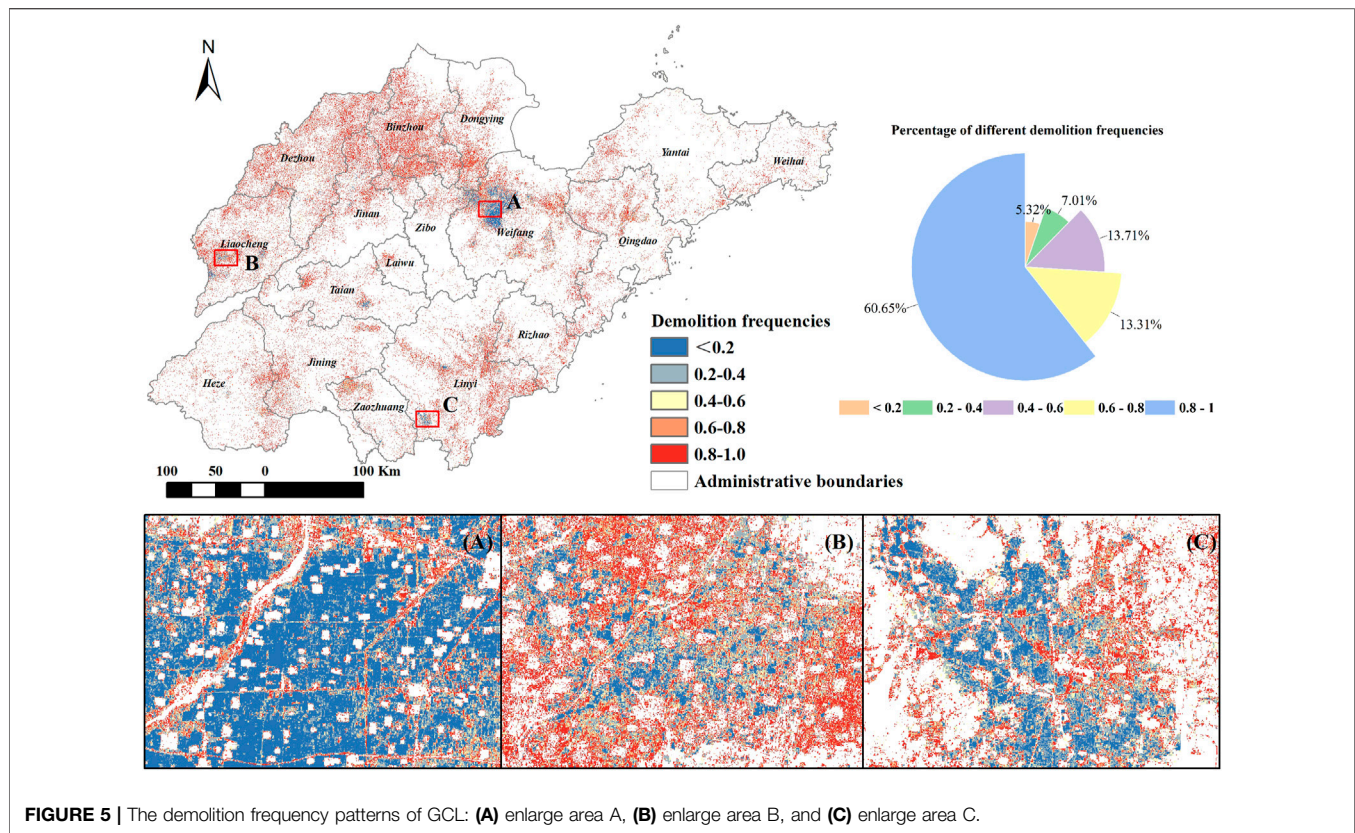
spatial clustering, indicating that the higher level of spatial clustering can extend the cumulative duration of GCL. In addition, it can be seen from the detail enlargements in **Figures 4A–C** that there was a certain spatial continuity in the extension of the cumulative duration.

Then the demolition frequency of GCL over the past 30 years was also calculated based on the TSS algorithm. As shown in **Figure 5**, the demolition frequencies of GCL in the range of 0.8~1.0 accounted for 60.65% during the 30-year period, and showed a scattered distribution pattern mainly around the central mountainous area. The demolition frequencies in the range of 0.6~0.8–0.4~0.6 accounted for about 13%, and when the demolition frequency dropped to 0.4, its percentage decreased rapidly to below 12.33%. At the same time, it can be found that the areas with demolition frequency below 0.2 were mainly distributed in northwestern Weifang, southwestern Linyi and western Liaocheng, which is similar to the patterns of the spatial clustering as well as the cumulative duration, indicating that the higher level of spatial clustering can not only ensure the duration but also the continuity of GCL. In addition, from the detailed enlarged **Figures 5A–C**, it can be seen that there is a certain continuity in the change of demolition frequency, in which the area with low demolition frequency tends to form the area with relatively low demolition frequency around it.

### 3.1.3 Expansion Trajectory

Based on the TSS algorithm, we also identified the year in which GCL first appeared in Shandong province over the past 30 years.

As shown in **Figure 6**, the expansion trajectory of GCL roughly formed a circular expansion pattern around the central mountainous area, among which the expansion trajectories were more disorderly in Dezhou, Jinan, Binzhou and Dongying, and more orderly in Weifang, Liaocheng, Linyi, Zaozhuang and Jining. Combined with its spatial clustering pattern, it can be seen that the expansion trajectories were more orderly in the GCL concentration areas. In terms of each period, in period 2004~2008 and period 2014~2018 accounted for the most percentage of GCL expansion with 25.18% and 20.62%, respectively, followed by period 1999~2003 (18.92%) and period 2009~2013 (18.40%), and the least was period 1989~1993 (7.22%) and period 1994~1998 (9.67%). In addition, from the detail enlarged **Figures 6A–C**, in northwestern Weifang, southwestern Linyi and western Liaocheng showed an obvious pattern of circle outward expansion trajectories.

We further calculated the GCL expansion intensity in the above-mentioned periods at the 1 km grid scale, and classified it into five types: slow expansion, low-speed expansion, medium-speed expansion, high-speed expansion, and rapid expansion based on the natural break method (De Smith et al., 2007). As shown in **Figure 7**, the areas with rapid expansion intensity were mainly located in the northwestern plains represented by Weifang in period 1989~1999 and continued to expand in period 1999~2004, the southern plains represented by Linyi began to appear in the rapid expansion intensity in period 1999~2004 as well. In period 2004~2014, the areas with rapid expansion intensity shrank to the plain areas of northwestern and
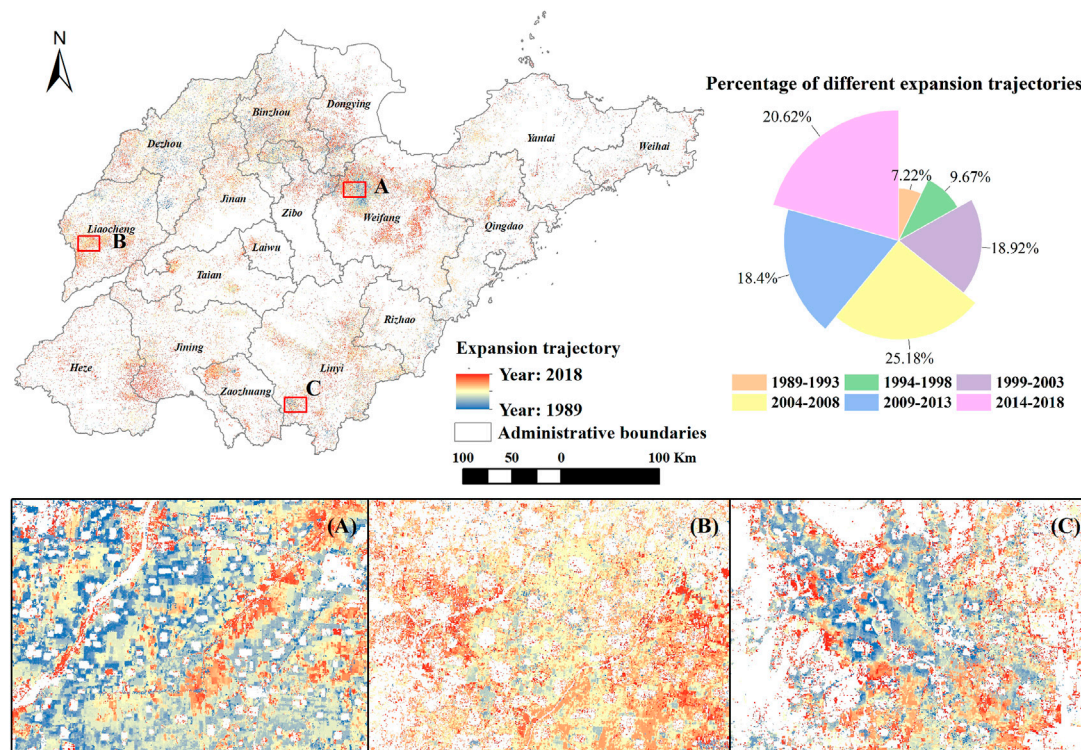
FIGURE 6 | The expansion trajectory patterns of GCL: (A) enlarge area A, (B) enlarge area B, and (C) enlarge area C.
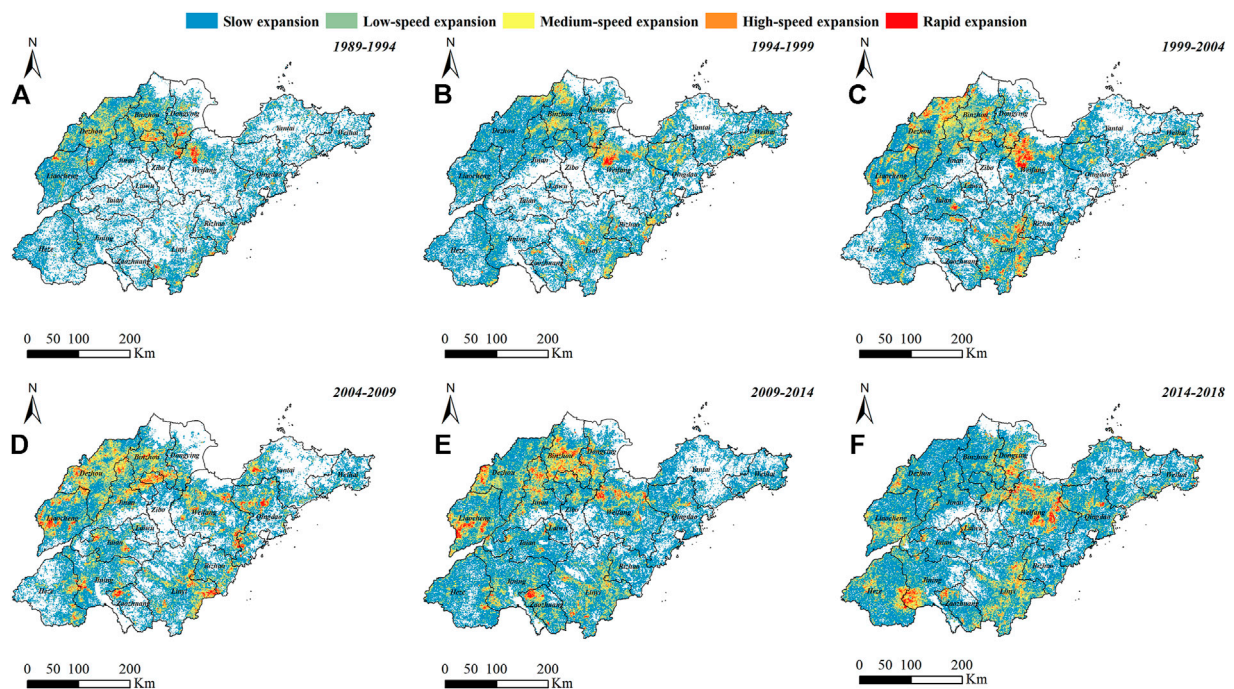


FIGURE 7 | The expansion intensity patterns of GCL at different periods: (A) period 1989–1994, (B) period 1994–1999, (C) period 1999–2004, (D) period 2004–2009, (E) period 2009–2014, (F) period 2014–2018.

**FIGURE 8 |** The local driven mechanism of GCL at different periods: **(A)** factor detection for the local dynamic variables, **(B)** factor detection for the local stable variables.
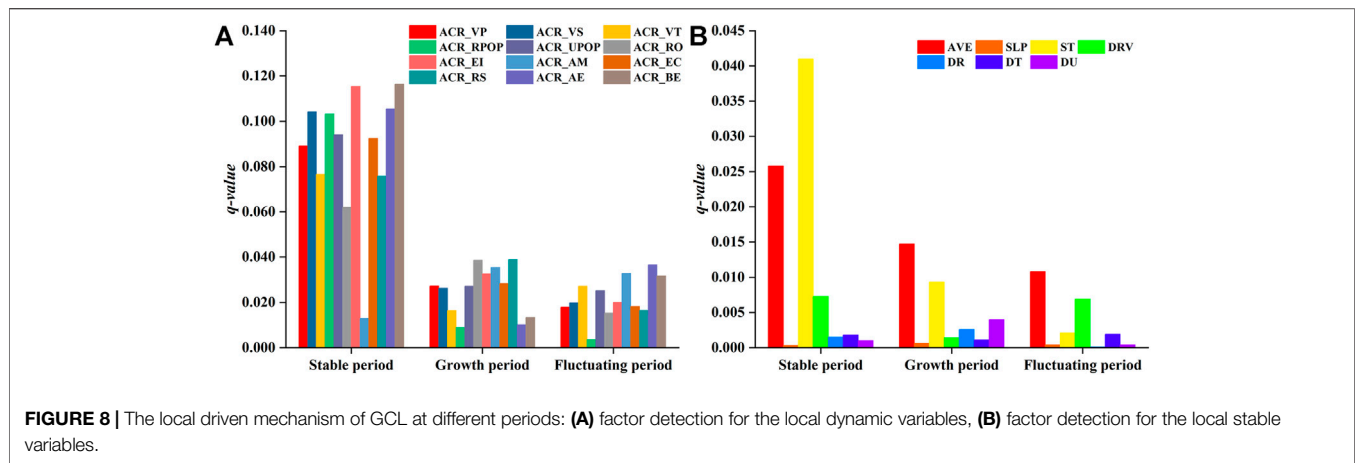
southern Shandong, and appeared in the plain areas represented by Liaocheng in the west. After that, the new areas with rapid expansion intensity appeared in the southeastern of Weifang and the junction of Jining and Heze from 2014 to 2018.

## 3.2 Driven Mechanisms of Greenhouse-Led Cultivated Land

### 3.2.1 Local Driven Mechanism

In order to reveal the differences in the local driven mechanism of GCL at different periods, we first divided the past 30 years into three different periods based on the annual change rate (ACR) of the total area of GCL, which were the stable period (1989~1996, with an ACR of −2.28 kha/year), the growth period (1997~2005, with an ACR of 23.09 kha/year) and the fluctuating period (2006~2018, with an ACR of 14.03 kha/year), respectively. Meanwhile, the ACR of the selected local dynamic variables were calculated and identified as "ACR_XX" within each period. For those local stable variables that vary little over time, were also quantified based on factor detection at different periods.

Regarding the results of factor detection for the local dynamic variables in each period (**Figure 8A**), the top three q-values were ACR_BER (0.1164), ACR_EI (0.1153) and ACR_AE (0.1055) in the stable period, ACR_LRS (0.0389), ACR_RO (0.0386) and ACR_AM (0.0354) in the growth period, and ACR_AE (0.0365), ACR_AM (0.0328) as well as ACR_BER (0.0316) in the fluctuating period. It indicated that 1) budget expenditure for rural development reflecting government support and average earning of local famers reflecting farmers' willingness were both the major driving factors for farmers to promote GCL in the stable as well as the fluctuating period, 2) effective irrigated area reflecting agricultural production conditions only played a major driving role in the stable period, 3) local retail sales reflecting local consumer demand and road mileage reflecting transportation conditions played a key driving role in the growth period.

Regarding the results of factor detection for the local stable variables in each period (**Figure 8B**), the top three q-values

were ST (0.0410), AVE (0.0258) and RIV (0.0073) in the stable period, AVE (0.0147), ST (0.0093) and DU (0.0040) in the growth period, and AVE (0.0108), RIV (0.0069) as well as ST (0.0410) in the fluctuating period. It indicated that 1) elevation and soil type were always the main driving force for GCL expansion in all local stable variables over time, 2) the driving force of the distance to rivers exhibited a significant performance in both the stable and fluctuating periods among the location aspect, 3) compared with elevation, the driving force of slope showed an insignificant performance in all periods.

### 3.2.2 External Driven Mechanism

In order to reveal the driven mechanism of the supply and demand of vegetables in external markets on GCL expansion in Shandong, the following target and explanatory time-series were selected: total area of GCL in Shandong province $(Y)$; vegetable production in Guangxi province $(X_1)$, Hainan province $(X_2)$, Sichuan province $(X_3)$, Hunan province $(X_4)$, Hubei province $(X_5)$, Guangdong province $(X_6)$, Jiangsu province $(X_7)$; Total value of agricultural exports in Shandong province $(X_8)$; consumption demand of vegetable in Beijing $(X_9)$ and Shanghai $(X_{10})$. To eliminate the effects caused by heteroskedasticity of each time-series, which have been treated with logarithm and denoted as "ln $X_n$".

As shown in **Supplementary Material S2**, the ADF values of $Y$, $X_3$, $X_4$, and $X_7$ in the original series were greater than all critical values, indicating that these four original series were non-stationary. The ADF values of $X_1$, $X_2$, $X_5$, and $X_6$ in the original series were less than the critical values at 1% or 5% significance level, indicating that these four original series were stationary. The results of further differencing of each series showed that series $X_2$ was stationary after the second-order differencing and the rest series were stationary after the first-order differencing, which means that the target series $Y$ and the explanatory series $X_1$, $X_3$, $X_4$, $X_5$, $X_6$, and $X_7$ belong to the first-order of single integer after differencing, which satisfied the premise of the cointegration test, while the target series Y and the explanatory series $X_2$ belong to the second-order of single integer after differencing, which also satisfied the

premise of the cointegration test. Further based on the Engle-Granger method, the target series was modeled with each explanatory series to determine whether there was a cointegration relationship between them. As shown in **Supplementary Material S3**, the ADF test statistics between the target series and each explanatory series were all less than the critical values at all significance levels, indicating that there was a cointegration relationship between the target series and each explanatory series, and the Granger causality test between them can be further analyzed.

Therefore, the target series after differencing was selected for Granger causality tests with each explanatory series after the same-order differencing at lag 1, lag 3, and lag 5 (**Supplementary Material S4**). From the perspective of the supply of vegetables in the external markets, vegetable production change in Guangxi, Hainan, Hunan, and Hubei province were a one-way Granger causality of the development of GCL in Shandong province, vegetable production change in Sichuan province was a two-way Granger causality of the development of GCL in Shandong province, and no Granger causality between vegetable production change in Guangdong province and the development of GCL in Shandong. From the perspective of the consumption demand of vegetable in the external markets, vegetable consumption in Beijing was a one-way Granger causality of the development of GCL in Shandong, and no Granger causality between both vegetable consumption in Shanghai as well as abroad and the development of GCL in Shandong.

# 4 DISCUSSION

## 4.1 Significance of Greenhouse-Led Cultivated Land Dynamics in Shandong Over the Past 30 years

Our study revealed that GCL in Shandong was widespread over the past 30 years from 1989 to 2018, involving a total expanded area of 353 kha. In terms of spatial clustering of GCL, the entropy value per unit area of GCL decreased from 0.043 to 0.029 and the spatial distribution of GCL clustering was mainly medium-low and medium densities, which means that despite the GCL expansion in Shandong over the past 30 years was toward continuous clustering, the industrial clustering effect was not evident from the macro level. In terms of temporal continuity of GCL, more than half of GCL with a cumulative duration was 1 year only and more than 60% of GCL with a demolition frequency in range of 0.8~1.0, which means that GCL in most region of Shandong lacked stability except a few industrial clustering regions. In terms of expansion trajectory of GCL, the expansion trajectory of GCL roughly formed a circular expansion pattern around the central mountainous area over the past 30 years and the most expansion period appeared in the mid-2010's, which means that the development of GCL has shown an obvious spatiotemporal heterogeneity in Shandong over the past 30 years. These findings provided a deeper understanding in spatiotemporal dynamics of GCL over a large-scale and long-term period.

## 4.2 Drivers of Greenhouse-Led Cultivated Land Expansion in Shandong Over the Past 30 years

By combining a number of variables involving physical and socioeconomic aspects with the ACR of the total area of GCL, we further explored the local and external driven mechanisms behind rapid GCL expansion in Shandong over the past 30 years. In terms of local driven mechanism, the change of government support and farmers' willingness showed the significant drive forces in both stable and fluctuating period of GCL, the change of agricultural production conditions played a major driving role in the stable period of GCL, and the change of local consumer demand as well as transportation conditions were the dominate driven variables in the growth period of GCL, which means the local driven mechanism behind GCL expansion varied in each period and an effective regulation of its expansion needs to consider the differences of each period. In terms of external driven mechanism, vegetable production change in four provinces showed a great influence on the expansion of GCL in Shandong, the consumption demand of vegetable in Beijing and the expansion of GCL in Shandong were mutually driven, and the consumption demand of vegetable in Shanghai as well as aboard had no significant impact on the expansion of GCL in Shandong, which indicated that the competition of external vegetable supply and the consumption demand from nearby metropolises were the main external driving factor of the expansion of GCL in Shandong over the past 30 years.

## 4.3 Limitations and Future Works

Our results provided a comprehensive and macroscale description of GCL expansion in Shandong province, China over the past 30 years and indicated that the long-term causes, processes and patterns of GCL varied in each period as well as different regions. However, some limitations are worth noting. For instance, we mainly analyzed the spatiotemporal dynamics and driven mechanisms in Shandong province, which is the earliest and largest province in China to promote GCL, considering that GCL has been widely popularized in China and there are differences in the pattern of GCL expansion between in other provinces and Shandong, we will expand the quantitative analysis of the spatiotemporal dynamics and driven mechanisms of GCL at national scale in the follow-up study. In addition, the analysis of driven mechanisms in this study was partially limited by the availability of data, and the micro level information such as farmers' decision-making, terms of trade of GCL products and government subsidy policies were not taken into account. In the future, field research can be carried out to obtain more detailed micro data, so as to realize a more in-depth analysis.

# 5 CONCLUSION

In this study, we proposed a comprehensive analysis framework which oriented to investigate the spatiotemporal

dynamics and driven mechanisms of GCL over a long-term period in a large-scale area. The results showed the following: 1) The spatial clustering of GCL in the area of research during 1989~2018 was gradually increasing in general, which was mainly dominated by medium-low and medium densities. 2) GCL in most region of the area of research lacked stability except a few industrial clustering regions, and the expansion trajectory of GCL roughly formed a circular expansion pattern around the central mountainous area with the most expansion period appeared in the mid-2010's. 3) Local driven mechanism behind GCL expansion varied in each period, and budget expenditure for rural development, local retail sales and average earnings of local farmers were the most important local driving factors of the GCL expansion in Shandong. 4) From the external perspective, the competition of external vegetable supply in Guangxi, Hainan, Hunan as well as Hubei province and the consumption demand from Beijing were the main external driving forces of the expansion of GCL in Shandong. In general, our study quantified a range of spatiotemporal dynamics of GCL and its drivers over a large-scale and long-term period, which puts forwards the potential of earth observations to evaluate the impacts of cultivated land use and management.

# REFERENCES

Agüera, F., Aguilar, F. J., and Aguilar, M. A. (2008). Using Texture Analysis to Improve Per-Pixel Classification of Very High Resolution Images for Mapping Plastic Greenhouses. *ISPRS J. Photogrammetry Remote Sens.* 63 (6), 635–646.

Agüera, F., and Liu, J. (2009). Automatic Greenhouse Delineation from QuickBird and Ikonos Satellite Images. *Comput. Electron. Agric.* 66 (2), 191–200.

Aguilar, M., Bianconi, F., Aguilar, F., and Fernández, I. (2014). Object-based Greenhouse Classification from GeoEye-1 and WorldView-2 Stereo Imagery. *Remote Sens.* 6 (5), 3554–3582. doi:10.3390/rs6053554

Aguilar, M., Nemmaoui, A., Novelli, A., Aguilar, F., and García Lorca, A. (2016). Object-based Greenhouse Mapping Using Very High Resolution Satellite Data and Landsat 8 Time Series. *Remote Sens.* 8 (6), 513. doi:10.3390/rs8060513

Arcidiacono, C., and Porto, S. M. C. (2010). A Model to Manage Crop-Shelter Spatial Development by Multi-Temporal Coverage Analysis and Spatial Indicators. *Biosyst. Eng.* 107 (2), 107–122. doi:10.1016/j.biosystemseng.2010.07.007

Balcik, F. B., Senel, G., and Goksel, C. (2019). "Greenhouse Mapping Using Object Based Classification and Sentinel-2 Satellite Imagery," in 2019 8th International Conference on Agro-Geoinformatics (Agro-Geoinformatics) (IEEE), 1–5.

Baudoin, W., and Von Zabeltitz, C. (2002). Greenhouse Constructions for Small Scale Farmers in Tropical Regions. *Acta Hortic.* 578, 171–179. International Symposium on Design and Environmental Control of Tropical and Subtropical Greenhouses. doi:10.17660/actahortic.2002.578.20

Bektas Balcik, F., Senel, G., and Goksel, C. (2020). Object-based Classification of Greenhouses Using Sentinel-2 MSI and SPOT-7 Images: A Case Study from Anamur (Mersin), Turkey. *IEEE J. Sel. Top. Appl. Earth Obs. Remote Sens.* 13, 2769–2777. doi:10.1109/jstars.2020.2996315

Briassoulis, D., Dougka, G., Dimakogianni, D., and Vayas, I. (2016). Analysis of the Collapse of a Greenhouse with Vaulted Roof. *Biosyst. Eng.* 151, 495–509. doi:10.1016/j.biosystemseng.2016.10.018

Cai, X., Wu, Z., and Cheng, J. (2013). Using Kernel Density Estimation to Assess the Spatial Pattern of Road Density and its Impact on Landscape Fragmentation. *Int. J. Geogr. Inf. Sci.* 27 (2), 222–230. doi:10.1080/13658816.2012.663918

# DATA AVAILABILITY STATEMENT

The original contributions presented in the study are included in the article/**Supplementary Material**, further inquiries can be directed to the corresponding author.

# AUTHOR CONTRIBUTIONS

CO: conceptualization, methodology, and writing—original draft. YW: supervision and funding acquisition.

# FUNDING

# SUPPLEMENTARY MATERIAL

The Supplementary Material for this article can be found online at: https://www.frontiersin.org/articles/10.3389/fenvs.2022.944422/full#supplementary-material

Carvajal, F., Agüera, F., Aguilar, F. J., and Aguilar, M. A. (2010). Relationship between Atmospheric Corrections and Training-Site Strategy with Respect to Accuracy of Greenhouse Detection Process from Very High Resolution Imagery. *Int. J. Remote Sens.* 31 (11), 2977–2994. doi:10.1080/01431160902946580

Carvajal, F., Crisanto, E., Aguilar, F., Agüera, F., and Aguilar, M. (2006). "Greenhouses Detection Using an Artificial Neural Network with a Very High Resolution Satellite Image," in *ISPRS Technical Commission II Symposium* (Vienna: International Society of Photogrammetry and Remote Sensing), 37–42.

Chaofan, W., Jinsong, D., Ke, W., Ligang, M., and Tahmassebi, A. R. S. (2016). Object-based Classification Approach for Greenhouse Mapping Using Landsat-8 Imagery. *Int. J. Agric. Biol. Eng.* 9 (1), 79–88. doi:10.3965/j.ijabe.20160901.1414

De Smith, M. J., Goodchild, M. F., and Longley, P. (2007). *Geospatial Analysis: A Comprehensive Guide to Principles, Techniques and Software Tools.* Matador: Troubador publishing ltd.

Freeman, J. R. (1983). Granger Causality and the Times Series Analysis of Political Relationships. *Am. J. Political Sci.* 27, 327–358. doi:10.2307/2111021

Gao, M., Qunou, J., Yiyang, Z., Wentao, Y., and Mingchang, S. (2018). Comparison of Plastic Greenhouse Extraction Method Based on GF-2 Remote-Sensing Imagery. *J. China Agric. Univ.* 23 (8), 125–134. doi:10.11841/j.issn.1007-4333.2018.08.14

Ge, D., Wang, Z., Tu, S., Long, H., Yan, H., Sun, D., et al. (2019). Coupling Analysis of Greenhouse-Led Farmland Transition and Rural Transformation Development in China's Traditional Farming Area: A Case of Qingzhou City. *Land Use Policy* 86, 113–125. doi:10.1016/j.landusepol.2019.05.002

González-Yebra, Ó., Aguilar, M. A., Nemmaoui, A., and Aguilar, F. J. (2018). Methodological Proposal to Assess Plastic Greenhouses Land Cover Change from the Combination of Archival Aerial Orthoimages and Landsat Data. *Biosyst. Eng.* 175, 36–51.

He, F., and Ma, C. (2007). Development and Strategy of Facility Agriculture in China. *Chin. Agric. Sci. Bull.* 23 (3), 462–465.

Jiménez-Lao, R., Aguilar, F. J., Nemmaoui, A., and Aguilar, M. A. (2020). Remote Sensing of Agricultural Greenhouses and Plastic-Mulched Farmland: An

Analysis of Worldwide Research. *Remote Sens.* 12 (16), 2649. doi:10.3390/rs12162649

Koc-San, D. (2013). Evaluation of Different Classification Techniques for the Detection of Glass and Plastic Greenhouses from WorldView-2 Satellite Imagery. *J. Appl. Remote Sens.* 7 (1), 073553. doi:10.1117/1.jrs.7.073553

Krämer, W. (1998). Fractional Integration and the Augmented Dickey–Fuller Test. *Econ. Lett.* 61 (3), 269–272. doi:10.1016/s0165-1765(98)00194-3

Lee, H., and Lee, J. (2015). More Powerful Engle-Granger Cointegration Tests. *J. Stat. Comput. Simul.* 85 (15), 3154–3171. doi:10.1080/00949655.2014.957206

Leibovici, D. G., Claramunt, C., Le Guyader, D., and Brosset, D. (2014). Local and Global Spatio-Temporal Entropy Indices Based on Distance-Ratios and Co-occurrences Distributions. *Int. J. Geogr. Inf. Sci.* 28 (5), 1061–1084. doi:10.1080/13658816.2013.871284

Levin, N., Lugassi, R., Ramon, U., Braun, O., and Ben-Dor, E. (2007). Remote Sensing as a Tool for Monitoring Plasticulture in Agricultural Landscapes. *Int. J. remote Sens.* 28 (1), 183–202. doi:10.1080/01431160600658156

Li, M., Zhang, Z., Lei, L., Wang, X., and Guo, X. (2020). Agricultural Greenhouses Detection in High-Resolution Satellite Images Based on Convolutional Neural Networks: Comparison of Faster R-CNN, YOLO V3 and SSD. *Sensors* 20 (17), 4938. doi:10.3390/s20174938

Li, X., Gong, P., and Liang, L. (2015). A 30-year (1984-2013) Record of Annual Urban Dynamics of Beijing City Derived from Landsat Data. *Remote Sens. Environ.* 166, 78–90. doi:10.1016/j.rse.2015.06.007

Lin, J., Jin, X., Ren, J., Liu, J., Liang, X., and Zhou, Y. (2021). Rapid Mapping of Large-Scale Greenhouse Based on Integrated Learning Algorithm and Google Earth Engine. *Remote Sens.* 13 (7), 1245. doi:10.3390/rs13071245

Liu, J., Dietz, T., Carpenter, S. R., Alberti, M., Folke, C., Moran, E., et al. (2007). Complexity of Coupled Human and Natural Systems. *science* 317 (5844), 1513–1516. doi:10.1126/science.1144004

Liu, Y., Zou, L., and Wang, Y. (2020). Spatial-temporal Characteristics and Influencing Factors of Agricultural Eco-Efficiency in China in Recent 40 Years. *Land Use Policy* 97, 104794. doi:10.1016/j.landusepol.2020.104794

Lu, L., Di, L., and Ye, Y. (2014). A Decision-Tree Classifier for Extracting Transparent Plastic-Mulched Landcover from Landsat-5 TM Images. *IEEE J. Sel. Top. Appl. Earth Obs. Remote Sens.* 7 (11), 4548–4558. doi:10.1109/jstars.2014.2327226

Ma, A., Chen, D., Zhong, Y., Zheng, Z., and Zhang, L. (2021). National-scale Greenhouse Mapping for High Spatial Resolution Remote Sensing Imagery Using a Dense Object Dual-Task Deep Learning Framework: A Case Study of China. *ISPRS J. Photogrammetry Remote Sens.* 181, 279–294. doi:10.1016/j.isprsjprs.2021.08.024

Maus, V., Camara, G., Cartaxo, R., Sanchez, A., Ramos, F. M., and De Queiroz, G. R. (2016). A Time-Weighted Dynamic Time Warping Method for Land-Use and Land-Cover Mapping. *IEEE J. Sel. Top. Appl. Earth Obs. Remote Sens.* 9 (8), 3729–3739. doi:10.1109/jstars.2016.2517118

Min, J., Zhang, H., and Shi, W. (2012). Optimizing Nitrogen Input to Reduce Nitrate Leaching Loss in Greenhouse Vegetable Production. *Agric. Water Manag.* 111, 53–59. doi:10.1016/j.agwat.2012.05.003

Novelli, A., Aguilar, M. A., Nemmaoui, A., Aguilar, F. J., and Tarantino, E. (2016). Performance Evaluation of Object Based Greenhouse Detection from Sentinel-2 MSI and Landsat 8 OLI Data: A Case Study from Almería (Spain). *Int. J. Appl. earth observation geoinformation* 52, 403–411. doi:10.1016/j.jag.2016.07.011

Ou, C., Yang, J., Du, Z., Liu, Y., Feng, Q., and Zhu, D. (2020). Long-term Mapping of a Greenhouse in a Typical Protected Agricultural Region Using Landsat Imagery and the Google Earth Engine. *Remote Sens.* 12 (1), 55. doi:10.3390/rs12010055

Ou, C., Yang, J., Du, Z., Zhang, T., Niu, B., Feng, Q., et al. (2021). Landsat-Derived Annual Maps of Agricultural Greenhouse in Shandong Province, China from 1989 to 2018. *Remote Sens.* 13 (23), 4830. doi:10.3390/rs13234830

Picuno, P., Tortora, A., and Capobianco, R. L. (2011). Analysis of Plasticulture Landscapes in Southern Italy through Remote Sensing and Solid Modelling Techniques. *Landsc. urban Plan.* 100 (1-2), 45–56. doi:10.1016/j.landurbplan.2010.11.008

Shi, L., Wang, Y., Liu, Y., and Li, Y. (2022). The Poverty Evolution of Typical Countries along the Belt and Road and Implications from China's Poverty Reduction Experiences. *J. Geogr. Sci.* 32 (3), 458–476. doi:10.1007/s11442-022-1953-1

Sica, C., and Picuno, P. (2007). "Spectro-radiometrical Characterization of Plastic Nets for Protected Cultivation," in International Symposium on High Technology for Greenhouse System Management: Greensys2007 801), 245–252.

Su, Y., Li, C., Wang, K., Deng, J., Shahtahmassebi, A. R., Zhang, L., et al. (2019). Quantifying the Spatiotemporal Dynamics and Multi-Aspect Performance of Non-grain Production during 2000-2015 at a Fine Scale. *Ecol. Indic.* 101, 410–419. doi:10.1016/j.ecolind.2019.01.026

Sun, H., Wang, L., Lin, R., Zhang, Z., and Zhang, B. (2021). Mapping Plastic Greenhouses with Two-Temporal Sentinel-2 Images and 1d-Cnn Deep Learning. *Remote Sens.* 13 (14), 2820. doi:10.3390/rs13142820

Wang, J.-F., Zhang, T.-L., and Fu, B.-J. (2016). A Measure of Spatial Stratified Heterogeneity. *Ecol. Indic.* 67, 250–256. doi:10.1016/j.ecolind.2016.02.052

Wang, J. F., Li, X. H., Christakos, G., Liao, Y. L., Zhang, T., Gu, X., et al. (2010). Geographical Detectors-Based Health Risk Assessment and its Application in the Neural Tube Defects Study of the Heshun Region, China. *Int. J. Geogr. Inf. Sci.* 24 (1), 107–127. doi:10.1080/13658810802443457

Wen-shou, H. (2004). Soil Problems and Countermeasure in Facility Agriculture in China. *Soils* 36 (3), 235–242. doi:10.3321/j.issn:0253-9829.2004.03.003

Yang, D., Chen, J., Zhou, Y., Chen, X., Chen, X., and Cao, X. (2017). Mapping Plastic Greenhouse with Medium Spatial Resolution Satellite Data: Development of a New Spectral Index. *ISPRS J. Photogrammetry Remote Sens.* 128, 47–60. doi:10.1016/j.isprsjprs.2017.03.002

Yu, B., Song, W., and Lang, Y. (2017). Spatial Patterns and Driving Forces of Greenhouse Land Change in Shouguang City, China. *Sustainability* 9 (3), 359. doi:10.3390/su9030359

Zhang, L., Liu, W., Hou, K., Lin, J., Song, C., Zhou, C., et al. (2019). Air Pollution Exposure Associates with Increased Risk of Neonatal Jaundice. *Nat. Commun.* 10 (1), 3741–3749. doi:10.1038/s41467-019-11387-3

Zhang, Y., Wang, P., Wang, L., Sun, G., Zhao, J., Zhang, H., et al. (2015). The Influence of Facility Agriculture Production on Phthalate Esters Distribution in Black Soils of Northeast China. *Sci. Total Environ.* 506-507, 118–125. doi:10.1016/j.scitotenv.2014.10.075

Zhao, G., Li, J., Li, T., Yue, Y., and Warner, T. (2004). Utilizing Landsat TM Imagery to Map Greenhouses in Qingzhou, Shandong Province, China. *Pedosphere* 14 (3), 363–369.

Zou, L., Wang, Y., and Liu, Y. (2022). Spatial-temporal Evolution of Agricultural Ecological Risks in China in Recent 40 Years. *Environ. Sci. Pollut. Res.* 29 (3), 3686–3701. doi:10.1007/s11356-021-15927-7

# Soil Organic Carbon Pool and the Production of Goji Berry (*Lycium barbarum* L.) as Affected by Different Fertilizer Combinations Under Drip Fertigation

Fang Wang[1,2], Wenhui Li[1,2], Yanmin Lin[1,2], Xiongxiong Nan[3*†] and Jingjing Yuan[4*†]

[1]College of Geographical Sciences and Planning, Ningxia University, Yinchuan, China, [2]China-Arab Joint International Research Laboratory for Featured Resources and Environmental Governance in Arid Regions, Yinchuan, China, [3]Engineering Research Center of Wolfberry in National Forestry and Grassland Administration, Yinchuan, China, [4]Henan Institute of Metrology, Zhengzhou, China

Goji berries (*Lycium barbarum* L.), widely planted in arid to semi-arid regions, are a functional resource characterized by a homology of medicine and food. Changing extensive water and fertilizer management practices to drip fertigation is one of the most cost-effective ways to achieve the sustainable development of the Goji berry industry. This study explores the effects of different fertilizer combinations on the soil organic carbon pool and *L. barbarum* yield under drip fertigation in Ningxia, northwestern China. A two-year field experiment (2017–2019) was conducted using different levels of drip nitrogen (40, 60, and 80 mg $L^{-1}$) and phosphorus (10, 20, and 30 mg $L^{-1}$) fertigation. Compared with traditional manual fertilization (control), soil organic carbon contents in the 0–20, 20–40, and 40–60 cm layers increased by 33.6–144.4, 39.6–136.8, and 14.0–73.6%, respectively, across all fertigation treatments. With increasing levels of fertigation, the easily oxidizable organic carbon content increased most prominently in the 0–20 cm soil layer and reached the highest value (538 mg $kg^{-1}$) under treatment with 60 mg $L^{-1}$ nitrogen plus 10 mg $L^{-1}$ phosphorus. The microbial biomass carbon contents in the 20–60 cm soil layer was markedly higher under treatment with 60 mg $L^{-1}$ nitrogen plus 30 mg $L^{-1}$ phosphorus compared with other treatments. Fertigation increased the soil carbon pool management index and *L. barbarum* yield. The highest two-year average yield (13,890 kg $ha^{-1}$) was obtained under treatment with 60 mg $L^{-1}$ nitrogen plus 30 mg $L^{-1}$ phosphorus. These findings suggest that drip fertigation with 60 mg $L^{-1}$ nitrogen plus 30 mg $L^{-1}$ phosphorus is the optimal practice for carbon sequestration and sustainable production of *L. barbarum* in arid regions.

**Keywords: arid, drip fertigation, labile carbon, soil management, production**

# INTRODUCTION

Soil organic carbon (SOC) is one of the most important carbon pools in the global carbon cycle. The use of rational management practices, such as irrigation, can increase the carbon pool in global agricultural soil by approximately 0.4–0.9 Pg C year$^{-1}$, with a cumulative increase of 24–43 Pg C over a 50-year period (IPCC, 2007; Qi et al., 2014; Danso et al., 2015). According to its function, turnover time, and chemical attributes, the SOC pool can be divided into labile, slow, and inert fractions. Of these, labile organic carbon (LOC), including dissolved organic carbon (DOC), microbial biomass carbon (MBC), and easily oxidizable organic carbon (EOC), results in most of the dynamic changes in the SOC pool (Demessie et al., 2011; Wang et al., 2014). Although LOC accounts for only a small portion of SOC, it can reflect subtle changes in soil quality before responses of SOC to changes in agricultural management (Wang et al., 2017). As a sensitive indicator, LOC not only responds quickly to cultivation practices, but also plays a vital role in regulating the transformation of soil nutrients (Weil and Magdoff, 2004; Wang et al., 2017). Therefore, it is pivotal to closely monitor the dynamics of soil LOC fractions under agricultural management practices.

Goji berries in the genus *Lycium* (family Solanaceae) are a superior characteristic crop planted widely in the arid to semi-arid regions of Eurasia, Africa, and North and South America (Ili et al., 2020). In Ningxia (an arid region of northwestern China), Goji berry cultivation has become one of the major sources of income. *Lycium barbarum* L. is a unique green woody vegetable commonly found in Ningxia, with a homology of medicine and food. It is distinctly different from traditional Goji berries (*Lycium chinense* Mill.) in terms of cultivation techniques and nutrient requirements (Huang et al., 2003; Lai et al., 2010). Ningxia Province has the least water resources in all of China, with limited amounts of rainfall, surface water, and groundwater. During the *L. barbarum* growing season, irrigation is therefore essential, although it is often excessive, resulting in the unnecessary waste of water resources. Additionally, extensive fertilizer management practices are adopted in most areas of Ningxia, although neither the timing or rate of fertilization nor the type of fertilizer matches the nutrient requirements of *L. barbarum*. These irrational management practices not only cause a serious waste of resources, but also increase the risk of environmental pollution (Li X. H. et al., 2016; Wang, 2016; Wang et al., 2016). In order to achieve sustainable production in the Goji berry industry, cost-effective management practices therefore need to be applied, with the goal of improving soil quality, increasing crop productivity, and enhancing agricultural economic benefits.

Realizing the efficient utilization and protection of water resources is the common key foundation for China to promote the development of low-carbon technologies and environmental protection, cope with global climate change, and achieve the strategic goals of "carbon neutrality." Drip fertigation is a new agricultural technology that integrates irrigation and fertilization to enhance water and fertilizer use efficiency, improve crop yield and quality, and increase economic profits. Drip fertigation has been found to reduce water usage by 40% compared with traditional flood irrigation and by 30% compared with spray irrigation (Danso et al., 2015; EI-Metwally et al., 2021). Furthermore, compared with traditional fertilization, drip fertigation has been found to increase both the yield and nitrogen use efficiency in tomatoes (Xing et al., 2015), while a positive role in terms of soil LOC content was also revealed, resulting in overall effects on soil water distribution and the carbon cycle (Singh and Singh, 1993; Qi et al., 2014). Given its advantages, drip fertigation has therefore become an important agricultural management practice with widespread applications, especially in semi-arid and arid regions (Zhang et al., 2009).

At present, drip fertigation is being gradually introduced into Goji berry cultivation in Ningxia. However, responses of the soil LOC pool to major changes in the fertilization approach in *L. barbarum* fields remain unknown. Additionally, a prerequisite to improving the fertilizer use efficiency and crop yield is the selection of an appropriate rate of fertilization based on the local soil characteristics and specific fertilizer demands. Many studies have document different fertilization rates based on the cultivation of traditional Goji berries or other herbaceous leafy vegetables (Kang et al., 2018), whereas few reports have documented the optimal water and fertilizer management practices for *L. barbarum* cultivation. In particular, the optimal rates of fertilization for drip fertigation in *L. barbarum* fields are unclear.

From the perspective of soil–crop systems, this study investigates the effects of different fertilizer combinations on the SOC pool (especially LOC fractions) and *L. barbarum* yield under drip fertigation. The fertilizer demands of *L. barbarum* grown in the arid region of Ningxia are also clarified during a two-year field experiment. The objectives of this study are to 1) evaluate the effects of different fertigation treatments on SOC sequestration and determine the responses of soil LOC fractions to major changes in the fertilization approach in *L. barbarum* fields and 2) explore the effects of different fertilizer combinations on Goji berry yield and identify the optimal fertilization rate for *L. barbarum* cultivation under drip fertigation. The results could be useful for rational agricultural management and sustainable production of *L. barbarum* in Ningxia and other arid regions.

# MATERIALS AND METHODS

## Field Site Description

This study was conducted at the Goji Berry Demonstration Base (35°25′ N, 106°10′ E) of the Research Center of Engineering Technology for Goji Berry, State Forestry Administration of China. The study area is located in an inland arid region located in northwestern China. It has a warm temperate continental monsoon climate with large diurnal temperature variation. The mean annual temperature, precipitation, and evaporation are 8.5°C, ~180 mm, and ~1883 mm, respectively. The relative humidity is between 45 and 60%, the frost-free period lasts for 160–170 days, and the average annual sunshine duration ranges from 2,800 to 3,000 h. The soil in the study area is classified as aeolian sandy soil according to the US Department of Agriculture Textural Classification System.

**TABLE 1 |** The basic properties of aeolian sandy soil in the experiment site.

| Soil depth (cm) | Bulk density (g cm$^{-3}$) | ECe (μs/cm) | pH | Sand (g kg$^{-1}$) | Silt (g kg$^{-1}$) | Clay (g kg$^{-1}$) | Organic matter (g kg$^{-1}$) | Total nitrogen (g kg$^{-1}$) | Total phosphorus (g kg$^{-1}$) | Available nitrogen (mg kg$^{-1}$) | Available phosphorus (mg kg$^{-1}$) | Available potassium (mg kg$^{-1}$) |
|---|---|---|---|---|---|---|---|---|---|---|---|---|
| 0–20 | 1.41 | 481 | 8.81 | 825 | 105 | 70 | 4.83 | 0.41 | 0.56 | 45 | 13.2 | 66 |
| 20–40 | 1.53 | 394 | 8.63 | 818 | 107 | 75 | 3.76 | 0.34 | 0.60 | 31 | 9.2 | 61 |
| 40–60 | 1.59 | 287 | 8.67 | 766 | 120 | 114 | 3.61 | 0.15 | 0.63 | 20 | 7.9 | 59 |

The basic properties of the 0–60 cm soil profile before the experiment are summarized in **Table 1**.

## Experimental Design

The field experiment was commenced in March 2017 and lasted for 2 years. Six-year-old Goji berry plants (*L. barbarum* cv. Ningqi-9) showing consistent growth were selected from an area planted with spacing of $70 \times 20$ cm and density of 70,000 plants ha$^{-1}$. Based on the growth requirements of *L. barbarum* and the nutrient status of local soil (rich in potassium, **Table 1**), the experiment used a $3 \times 3$ full factorial design with three levels of drip nitrogen fertigation (40, 60, and 80 mg L$^{-1}$; $N_1$–$N_3$, respectively) and three levels of drip phosphorus fertigation (10, 20, and 30 mg L$^{-1}$; $P_1$–$P_3$, respectively). Traditional manual fertilization with nitrogen, phosphorus, and potassium (1,402.5, 292.5, and 132 kg ha$^{-1}$, respectively) was used as a control (CK). The fertilization rates used in the experiment were based on those previously reported for Solanacae crops, fruit, and vegetables in developed countries (e.g., Israel) (Hagin and Sneh, 2003; Wang et al., 2011) in combination with the soil characteristics in the study area. A total of 10 treatments were arranged in a randomized complete design, with three replicates per treatment. The plants of each treatment were grown in $20 \times 5$ m plots with five rows each. In the control treatment, Urea (N 46%), KH$_2$PO$_4$ (K$_2$O 34%, P$_2$O$_5$ 52%), and KNO$_3$ (K$_2$O 46%, N 14%) were divided evenly into five portions based on the annual fertilization rates and applied by broadcasting. One portion was applied in late March 2017 and the other four portions were applied as top-dressing once in mid-May, June, July, and August during the harvest stage, respectively. Annual fertilization rates of nitrogen, phosphorus, and potassium were 1,402.5, 292.5, and 132 kg ha$^{-1}$, respectively. The same fertilization procedure was followed throughout the experiment.

Drip irrigation was carried out in each plot in consistent time periods and using a consistent volume of water. Irrigation was started after the soil thawed in late March and ended before the soil froze in November. In the control treatment, chemical fertilizers were applied by broadcasting. In the fertigation treatment, fertilizer solutions were formulated based on the designed nitrogen and phosphorus concentrations, with a potassium concentration of 40 mg L$^{-1}$. The fertigation device consisted of a water source, a water meter, a hydraulic proportional fertilization pump, a drip irrigation pipe, and a water transmission and distribution pipeline. The proportional fertilization pump had an inlet and outlet diameter of 25 mm, a flow rate of 20–2500 L h$^{-1}$, and a water pressure of 0.02–0.3 MPa. The built-in drip irrigation pipes had a diameter of 16 mm and wall thickness of 0.20 mm with a working pressure of 50–100 kPa, dripper spacing of 0.30 m, and rated flow of 2.0 L h$^{-1}$.

The fertilizer solutions were applied with water through the proportional fertilizer applicator throughout the growing season. Fertigation was initiated when the soil water content dropped to 80% of the field water-holding capacity, with average daily irrigation of 6 mm. Field management practices, such as weeding and pruning, were consistent across treatments.

## Soil Sampling and Analysis

Soil sampling was conducted in all plots after harvest in September 2019. In each plot, soil samples (five each) were taken randomly from depths of 0–20, 20–40, and 40–60 cm. The samples from each depth were mixed thoroughly as composite samples and then transported in an ice box to the laboratory. Each sample was divided into two parts: one part was passed through 1-mm and 0.15-mm sieves after air-drying and manual removal of gravel and plant root residues for analysis of SOC and LOC contents, respectively; the other was passed through a 2-mm sieve and refrigerated for analysis of DOC, MBC, and EOC contents. The basic physicochemical properties of the soil samples were determined following standard testing methods (Bao, 2000). The SOC content was determined using the K$_2$Cr$_2$O$_7$ oxidation–external heating method (Xiong et al., 2016) Soil DOC was extracted by mixing the soil sample with distilled water (1:5, w/v) and then shaking for 1 h on a shaker (25°C, 250 rpm) (Li et al., 2017). The carbon concentration in the extract was measured using a total organic carbon analyzer (Vario TOC; Elementar, Langenselbold, Germany). Furthermore, the MBC and EOC contents were determined using the chloroform fumigation–extraction method (Wang et al., 2010) and KMnO$_4$ oxidation method (Li et al., 2019), respectively.

After stumping in spring, new shoots germinated at the base of the *L. barbarum* plants. Leaf buds were collected when these new shoots reached 15–20 cm long. The sampling region was free of lignification and the sample length was 8–10 cm. Sampling was conducted once every 5 to 7 days on average at fixed points (three points per plot). The area from which all plants were sampled was 10 m long. After collection, the samples were mixed and weighed to estimate the yield of *L. barbarum*.

## Data Analyses

Carbon efficiency, as a sensitive indicator of carbon quality, was used to estimate carbon availability, which was then used to evaluate soil organic matter and soil fertility (Singh and Singh, 1993) as follows:

$$\text{DOC efficiency (\%)} = \text{DOC content/SOC content} \times 100 \quad (1)$$

$$\text{MBC efficiency (\%)} = \text{MBC content/SOC content} \times 100 \quad (2)$$

$$\text{EOC efficiency C (\%)} = \text{EOC content/SOC content} \times 100 \quad (3)$$

**TABLE 2 |** Soil organic carbon contents and labile fractions under different treatments.

| Soil depth (cm) | Treatments | SOC(g kg$^{-1}$) | EOC (mg kg$^{-1}$) | DOC (mg kg$^{-1}$) | MBC (mg kg$^{-1}$) |
|---|---|---|---|---|---|
| 0–20 | CK | 2.77 ± 0.04c | 267 ± 9.80bc | 45 ± 7.42d | 21 ± 1.92e |
| | $N_1P_1$ | 3.70 ± 0.34bc | 452 ± 4.54ab | 69 ± 0.75a | 22 ± 4.83e |
| | $N_1P_2$ | 3.71 ± 0.23bc | 436 ± 22.50b | 57 ± 1.70bc | 44 ± 3.24d |
| | $N_1P_3$ | 4.56 ± 0.06bc | 189 ± 5.17c | 55 ± 0.81c | 56 ± 7.23d |
| | $N_2P_1$ | 4.63 ± 0.61bc | 538 ± 6.25a | 55 ± 1.84c | 70 ± 9.73c |
| | $N_2P_2$ | 6.31 ± 0.22a | 315 ± 9.44bc | 64 ± 4.90ab | 71 ± 6.24c |
| | $N_2P_3$ | 5.01 ± 0.57ab | 398 ± 8.31b | 64 ± 7.71ab | 113 ± 6.43a |
| | $N_3P_1$ | 5.11 ± 0.27ab | 455 ± 23.49ab | 69 ± 3.01a | 98 ± 5.04b |
| | $N_3P_2$ | 5.37 ± 0.28ab | 380 ± 14.74b | 62 ± 1.41abc | 85 ± 13.11b |
| | $N_3P_3$ | 6.77 ± 0.91a | 491 ± 12.95ab | 56 ± 3.31c | 88 ± 10.96b |
| | N | NS | NS | NS | ** |
| | P | NS | NS | * | ** |
| | N × P | * | NS | ** | ** |
| 20–40 | CK | 2.12 ± 0.04c | 203 ± 3.00d | 46 ± 4.47d | 17 ± 1.36e |
| | $N_1P_1$ | 3.91 ± 0.76ab | 329 ± 11.82c | 64 ± 3.86a | 16 ± 0.50e |
| | $N_1P_2$ | 3.07 ± 0.08bc | 226 ± 4.75d | 58 ± 1.51bc | 42 ± 7.50cd |
| | $N_1P_3$ | 3.20 ± 0.06bc | 283 ± 18.34cd | 55 ± 1.71c | 34 ± 5.35d |
| | $N_2P_1$ | 3.08 ± 0.37bc | 276 ± 8.27cd | 46 ± 0.91d | 53 ± 15.14bc |
| | $N_2P_2$ | 2.96 ± 0.44bc | 203 ± 11.60d | 61 ± 3.33ab | 49 ± 11.87bc |
| | $N_2P_3$ | 3.90 ± 0.31ab | 319 ± 17.13c | 50 ± 3.16d | 76 ± 6.93a |
| | $N_3P_1$ | 3.73 ± 0.33ab | 500 ± 37.74a | 56 ± 0.72bc | 60 ± 4.78b |
| | $N_3P_2$ | 5.02 ± 11.25a | 398 ± 18.52b | 45 ± 1.09d | 57 ± 10.51b |
| | $N_3P_3$ | 3.79 ± 0.51ab | 420 ± 21.85ab | 40 ± 0.56e | 40 ± 0.97cd |
| | N | NS | ** | ** | ** |
| | P | NS | NS | ** | NS |
| | N × P | * | NS | ** | ** |
| 40–60 | CK | 1.78 ± 0.20c | 219 ± 2.07d | 49 ± 4.78bc | 11 ± 0.38d |
| | $N_1P_1$ | 2.22 ± 0.09bc | 311 ± 4.40c | 48 ± 3.45bc | 15 ± 0.76cd |
| | $N_1P_2$ | 2.03 ± 0.16bc | 352 ± 1.74c | 36 ± 1.12e | 31 ± 7.82ab |
| | $N_1P_3$ | 2.48 ± 0.01ab | 424 ± 5.49bc | 46 ± 0.54bc | 32 ± 5.41a |
| | $N_2P_1$ | 2.49 ± 0.52ab | 431 ± 7.32bc | 48 ± 2.61bc | 21 ± 5.13c |
| | $N_2P_2$ | 2.15 ± 0.13bc | 385 ± 14.60bc | 50 ± 1.79b | 30 ± 10.21ab |
| | $N_2P_3$ | 2.23 ± 0.15bc | 527 ± 1.61a | 57 ± 0.49a | 33 ± 1.94a |
| | $N_3P_1$ | 2.06 ± 0.06bc | 422 ± 6.51b | 47 ± 0.28bc | 23 ± 9.22bc |
| | $N_3P_2$ | 3.09 ± 0.32a | 446 ± 2.60b | 40 ± 0.67d | 32 ± 3.07a |
| | $N_3P_3$ | 2.11 ± 0.06bc | 377 ± 25.40c | 45 ± 1.95c | 19 ± 2.98cd |
| | N | NS | NS | ** | NS |
| | P | NS | NS | ** | ** |
| | N × P | NS | NS | ** | * |

*The soil organic carbon contents and labile fractions under different fertigation treatments ($N_1$–$N_3$: 40, 60, and 80 mg L−1, respectively; $P_1$–$P_3$: 10, 20, and 30 mg L−1, respectively). SOC, soil organic carbon; EOC, easily oxidized organic carbon; DOC, dissolved organic carbon; MBC, microbial biomass carbon. The values are the means ± SE (standard error) of three replicates, and the different lowercase letters in a row are significantly different at the 0.05 significance level. NS: not significant.*

The carbon pool index (CPI) was used to indicate changes in SOC content caused by each experimental treatment, while the carbon pool activity (CPA) was used to indicate soil carbon instability. The carbon pool activity index (CPAI) was used to indicate carbon loss and its impact on carbon stability, while the carbon pool management index (CPMI) was used to evaluate changes in soil LOC fractions (Shen and Cao, 2000):

$$CPI = SOC\ content\ of\ the\ fertigated\ soil/SOC\ content\ of\ the\ control\ soil \tag{4}$$

$$CPA = LOC\ content/non-labile\ SOC\ content \tag{5}$$

$$CPAI = CPA\ of\ the\ fertigated\ soil/CPA\ of\ the\ control\ soil \tag{6}$$

$$CPMI = CPI \times CPAI \times 100 \tag{7}$$

The sensitivity index (SI) was then used to indicate the sensitivity of soil LOC fractions in response to changes in soil management practices (Liang et al., 2012):

$$SI = LOC\ content\ of\ the\ fertigated\ soil - LOC\ content\ of\ the\ control\ soil/LOC\ content\ of\ the\ control\ soil \tag{8}$$

Statistical analyses were performed using SPSS 22.0 (IBM Corp., Armonk, NY, United States). Two-way analysis of variance, followed by the least significant difference test, was used to compare means between different treatments, and Pearson's correlation coefficients were used to evaluate the relationship between Goji berry yield and soil LOC

fractions. A $p$-value of less than 0.05 was considered statistically significant.

# RESULTS

## Changes in Soil Organic Carbon Content Under Drip Fertigation

Drip fertigation with differing fertilizer combinations had differential effects on the SOC contents of each soil layer (**Table 2**). In the 0–60 cm soil profile, the SOC content tended to decrease with increasing soil depth; meanwhile, compared with the control (1.78–2.77 g kg$^{-1}$), the SOC content in each layer increased under fertigation treatment (2.32–5.02 g kg$^{-1}$). In the 10–20, 20–40, and 40–60 cm soil layers, the SOC contents under fertigation treatment increased by 33.6–144.4, 39.6–136.8, and 14.0–73.6%, respectively.

In the 0–20 cm soil layer, when a medium level (60 mg L$^{-1}$) of nitrogen was applied, the SOC content showed an overall upward trend with increasing phosphorus application, and significant differences were detected between treatments ($p < 0.05$). When medium and high levels (10 and 20 mg L$^{-1}$) of phosphorus were applied, a significant increase in SOC content was observed with increasing nitrogen application. The highest SOC content was observed under $N_3P_3$ treatment (6.77 g kg$^{-1}$), with a considerable increase of 144.4% compared with the control. In the 20–60 cm soil layers, there was an evident plow pan effect on SOC across treatments compared with the 0–20 cm soil layer, with an overall downward trend with increasing soil depth. No significant differences were detected between treatments in terms of SOC content under increasing phosphorus application at the same nitrogen level and vice versa. However, the interaction between nitrogen and phosphorus had a significant effect on SOC content in the 0–40 cm soil layers ($p < 0.05$).

## Contents of Soil Labile Organic Carbon Fractions Under Drip Fertigation

Overall, the EOC content decreased first and then increased with increasing soil depth, while the DOC and MBC contents gradually decreased toward deeper soil depths across all treatments (**Table 2**). In the 0–20 cm soil layer, when the same level of nitrogen was applied, the EOC contents gradually decreased with increasing phosphorus application, although values remained higher than the control except under $N_1P_3$ treatment. Under medium and low levels of phosphorus fertigation, no significant differences in soil EOC content were observed between different nitrogen levels. However, under high phosphorus fertigation, significant increases in the EOC content were observed with increasing nitrogen application ($p < 0.05$). Under a medium level of nitrogen fertigation, soil DOC contents increased significantly with increasing phosphorus application, while under high nitrogen fertigation, DOC contents decreased significantly with increasing phosphorus application, although the values under all three treatments were considerably higher than those of the control ($p < 0.05$). Under medium and low levels of nitrogen fertigation, the MBC contents increased

significantly with increasing phosphorus application ($p < 0.05$), and was highest under $N_2P_3$ treatment, with a substantial increase of 428.6% compared with the control ($p < 0.05$).

Compared with the control, an increase in EOC, DOC, and MBC contents was observed in each soil layer under fertigation treatment (**Table 2**). In the 0–60 cm soil profile, the mean EOC content under fertigation treatment ranged from 328 to 406 mg kg$^{-1}$, while the mean value of the control ranged from 203 to 219 mg kg$^{-1}$. In general, the EOC content in each soil layer showed an overall upward trend with increasing levels of nitrogen and phosphorus, and this was most evident in the 0–20 cm soil layer. The EOC content was significantly higher under $N_2P_1$ treatment (538 mg kg$^{-1}$) than all the remaining treatments, with an increase of 101.74% compared with the control ($p < 0.05$). The increase in DOC content in the 0–20 cm soil layer was most pronounced under $N_1P_1$ treatment, with an increase of 53.35% compared with the control. In the 40–60 cm soil layer, except under $N_2P_2$ and $N_2P_3$ treatments, the DOC content decreased compared with the control. The MBC content also decreased significantly with increasing soil depth under each treatment. In the 20–40 and 40–60 cm soil layers, the MBC contents under $N_2P_3$ treatment (76 and 33 mg kg$^{-1}$, respectively) were significantly higher than those under the remaining treatments, with increases of 349.2 and 199.1% compared with the control, respectively ($p < 0.05$). The interaction between nitrogen and phosphorus had a significant effect on the DOC and MBC contents ($p < 0.05$), but not on the EOC content in the 0–60 cm soil profile.

## Efficiency of Soil Labile Organic Carbon Fractions Under Drip Fertigation

The effects of each fertilizer combination on the efficiency of soil LOC under drip fertigation are shown in **Figure 1**. Overall, the efficiencies of soil EOC and DOC gradually increased with increasing soil depth, while the efficiency of soil MBC tended to decrease with deepening soil depth across all treatments. In the 0–20 cm soil layer, under high levels of nitrogen and phosphorus fertigation, the efficiency of soil EOC did not differ significantly between treatments compared with the control (**Figure 1A**). However, under medium and high levels of fertigation, the efficiency of soil DOC decreased remarkably under fertigation treatment compared with the control ($p < 0.05$, **Figure 1B**). Except under $N_2P_3$ and $N_3P_1$ treatment, the efficiency of soil MBC did not change significantly under fertigation treatment compared with the control (**Figure 1C**).

In the 20–40 cm soil layer, except under $N_3P_1$ treatment, there were no significant differences in the efficiency of soil EOC between the fertigation treatment and control. However, a significant difference in the efficiency of soil DOC was observed ($p < 0.05$). Under a medium level of fertigation, the efficiency of soil MBC increased significantly compared with the control, and the highest value was observed under $N_2P_3$ treatment. In the 40–60 cm soil layer, the efficiency of soil EOC generally increased under fertigation treatment compared with the control. The highest efficiency of soil EOC was achieved

**FIGURE 1** | The efficiency of soil labile organic carbon under different fertigation treatments ($N_1$–$N_3$: 40, 60, and 80 mg L$^{-1}$, respectively; $P_1$–$P_3$: 10, 20, and 30 mg L$^{-1}$, respectively). **(A)** Efficiency of easily oxidized organic carbon; **(B)** Efficiency of dissolved organic carbon; **(C)** Efficiency of microbial organic carbon. Data are the mean ± standard error ($n$ = 3). Different lowercase letters above the column indicate significant difference among treatments at the 0.05 significance level.

under $N_2P_3$ treatment, followed by $N_3P_1$ treatment, with increases of 91.0 and 65.7%, respectively, compared with the control. Under low levels of fertigation, the efficiency of soil DOC significantly differed from the control, while the efficiency of soil MBC increased by 11.7–132.3%. Overall, $N_2P_3$ and $N_1P_2$ treatment resulted in notable increases in the efficiency of soil LOC compared with the control.

## Stability of Soil Labile Organic Carbon (LOC) Fractions Under Drip Fertigation

Compared with the control, the CPI values of total carbon in each soil layer were all greater than 1 under fertigation treatment (**Table 3**). In the 0–20 cm soil layer, CPI was highest under $N_3P_3$ treatment (2.44), while in the 20–60 cm soil layers, the highest CPIs were obtained under $N_3P_2$ treatment (2.37 and 1.74).

Similarly, the CPMI values of soil LOC tended to increase under fertigation treatment compared with the control. In the 0–20 cm soil layer, the CPMI was highest under $N_2P_1$ treatment (206), while in the 20–40 cm soil layer, CPMI values were in the order of $N_3P_1$ > $N_3P_3$ > $N_3P_2$ > $N_1P_1$ > $N_2P_3$ > $N_1P_3$ > $N_2P_1$ > $N_1P_2$ > $N_2P_2$ > control, with highest values under $N_3P_1$ treatment (257). In the 40–60 cm soil layer, the CPMI values tended to increase first and then decrease with increasing nitrogen and phosphorus levels under all treatments, but values remained significantly higher than those of the control, and the highest CPMI was observed under $N_2P_3$ treatment (276).

## Sensitivity of Soil Labile Organic Carbon Fractions Under Drip Fertigation

The SI values of the soil LOC fractions (EOC, DOC, and MBC) under each treatment are presented in **Figure 2**. In general, the SI values of soil DOC and MBC tended to decrease gradually with increasing soil depth, while those of soil EOC showed no clear trend in the soil profile. The SI values of EOC were higher than those of DOC in the 20–40 cm and 40–60 cm soil layers, and except under

$N_1P_1$ treatment, the SI values of MBC were higher than those of EOC and DOC in the entire 0–60 cm soil profile, with the highest value obtained under $N_2P_3$ treatment (348).

## Crop Yield and Economic Profit Under Drip Fertigation

The effects of drip fertigation on *L. barbarum* yield differed between fertilizer treatments (**Table 4**). In 2018, neither the nitrogen level nor the phosphorus level had any significant effect on yield, and the highest yield was obtained under $N_2P_3$ treatment (14,326 kg ha$^{-1}$). After the two-year field experiment, both the nitrogen and phosphorus levels exhibited significant effects on *L. barbarum* yield ($p < 0.01$). Under medium and low levels of nitrogen fertigation, the yield differed significantly between treatments with a high level of phosphorus ($P_3$). Similarly, under medium and low levels of phosphorus fertigation, the yield differed significantly between treatments with a high level of nitrogen ($N_3$). Of the 10 treatments, yield was highest under $N_2P_3$ followed by $N_3P_3$ treatment, with increases of 43.0 and 35.9%, respectively, compared with the control. The two-year average yield of *L. barbarum* from 2018 to 2019 increased under fertigation treatment compared with the control, and was highest under $N_2P_3$ treatment (14,110 kg ha$^{-1}$) followed by $N_3P_1$ treatment (13,577 kg ha$^{-1}$), with increases of 33.2 and 28.2%, respectively. Furthermore, Pearson's correlation analysis revealed that *L. barbarum* yield was significantly correlated with the SOC ($r$ = 0.73, $p < 0.01$) and EOC ($r$ = 0.88, $p < 0.05$) contents.

Compared with the control, fertilizer input was largely reduced under fertigation treatment by 27.4–53.0% (**Table 5**). The output values of *L. barbarum* also increased substantially under fertigation treatment, especially with a high level of phosphorus application combined with low, medium, or high levels of nitrogen ($N_1P_3$, $N_2P_3$, and $N_3P_3$; 32.9, 42.9 and 35.8% increases, respectively). Overall, the output efficiency of *L. barbarum* was highest under $N_2P_3$ treatment.

**TABLE 3 |** Carbon pool management index (CPMI) under different fertigation treatments.

| Soil depth (cm) | Treatment | LOC (mg kg$^{-1}$) | SOC (mg kg$^{-1}$) | CPA | CPAI | CPI | CPMI |
|---|---|---|---|---|---|---|---|
| 0–20 | Control | 267 | 2,771 | 0.11 | 1.00 | 1.00 | 100 |
| | $N_1P_1$ | 452 | 3,699 | 0.14 | 1.31 | 1.34 | 175 |
| | $N_1P_2$ | 436 | 3,712 | 0.13 | 1.25 | 1.34 | 167 |
| | $N_1P_3$ | 189 | 4,556 | 0.04 | 0.41 | 1.64 | 67 |
| | $N_2P_1$ | 538 | 4,630 | 0.13 | 1.23 | 1.67 | 206 |
| | $N_2P_2$ | 315 | 6,311 | 0.05 | 0.49 | 2.28 | 112 |
| | $N_2P_3$ | 398 | 5,013 | 0.09 | 0.81 | 1.81 | 147 |
| | $N_3P_1$ | 455 | 5,114 | 0.10 | 0.92 | 1.85 | 169 |
| | $N_3P_2$ | 381 | 5,367 | 0.08 | 0.72 | 1.94 | 139 |
| | $N_3P_3$ | 491 | 6,767 | 0.08 | 0.74 | 2.44 | 180 |
| | N | NS | NS | | | | |
| | P | NS | NS | | | | |
| | N × P | NS | NS | | | | |
| 20–40 | Control | 203 | 2,116 | 0.11 | 1.00 | 1.00 | 100 |
| | $N_1P_1$ | 329 | 3,910 | 0.09 | 0.86 | 1.85 | 160 |
| | $N_1P_2$ | 226 | 3,069 | 0.08 | 0.75 | 1.45 | 108 |
| | $N_1P_3$ | 283 | 3,198 | 0.10 | 0.91 | 1.51 | 138 |
| | $N_2P_1$ | 276 | 3,080 | 0.10 | 0.92 | 1.46 | 135 |
| | $N_2P_2$ | 203 | 2,957 | 0.07 | 0.69 | 1.40 | 97 |
| | $N_2P_3$ | 319 | 3,895 | 0.09 | 0.84 | 1.84 | 154 |
| | $N_3P_1$ | 500 | 3,730 | 0.15 | 1.46 | 1.76 | 257 |
| | $N_3P_2$ | 398 | 5,023 | 0.09 | 0.81 | 2.37 | 192 |
| | $N_3P_3$ | 420 | 3,789 | 0.12 | 1.17 | 1.79 | 210 |
| | N | ** | NS | | | | |
| | P | NS | NS | | | | |
| | N × P | NS | NS | | | | |
| 40–60 | Control | 219 | 1,776 | 0.14 | 1.00 | 1.00 | 100 |
| | $N_1P_1$ | 311 | 2,217 | 0.16 | 1.16 | 1.25 | 145 |
| | $N_1P_2$ | 352 | 2,031 | 0.21 | 1.49 | 1.14 | 170 |
| | $N_1P_3$ | 424 | 2,477 | 0.21 | 1.47 | 1.40 | 204 |
| | $N_2P_1$ | 431 | 2,489 | 0.21 | 1.49 | 1.40 | 208 |
| | $N_2P_2$ | 385 | 2,147 | 0.22 | 1.55 | 1.21 | 188 |
| | $N_2P_3$ | 527 | 2,233 | 0.31 | 2.20 | 1.26 | 276 |
| | $N_3P_1$ | 422 | 2,064 | 0.26 | 1.83 | 1.16 | 212 |
| | $N_3P_2$ | 446 | 3,093 | 0.17 | 1.20 | 1.74 | 209 |
| | $N_3P_3$ | 377 | 2,113 | 0.22 | 1.54 | 1.19 | 184 |
| | N | NS | NS | | | | |
| | P | NS | NS | | | | |
| | N × P | NS | NS | | | | |

*The carbon pool management index under different fertigation treatments $N_1$–$N_3$: 40, 60, and 80 mg L−1, respectively; $P_1$–$P_3$: 10, 20, and 30 mg L−1, respectively. LOC, labile organic carbon; SOC, soil organic carbon; CPA, carbon pool activity; CPAI, carbon pool activity index; CPI, carbon pool index. The values are the means ± SE (standard error) of three replicates, and the different lowercase letters in a row are significantly different at 0.05 level. NS: not significant.*

# DISCUSSION

## Effects of Different Fertilizer Combinations on Soil Organic Carbon Under Drip Fertigation

As an important component of the soil, SOC plays an essential role in soil fertility and agricultural productivity (Su et al., 2006). Meanwhile, as a vital carbon pool of terrestrial ecosystems, SOC plays a crucial role in balancing the global carbon cycle (Preethi et al., 2013; Qi et al., 2014; Kov et al., 2018). Some studies in the past have explored the effects of irrigation on SOC content and crop yield. Gillabel et al. (2007) found that irrigation can increase SOC content in the 0–20 cm soil layer by about 25% in semi-arid farmland. In addition, Qian et al. (2010) showed that irrigation

has been identified as the management practice with the greatest potential for carbon sequestration, which can increase crop yields by increasing soil carbon input. A previous study revealed a positive correlation between the SOC content and carbon storage under fertigation (Hu et al., 2010). However, due to differing experimental conditions, no unified conclusion has yet been reached with regards to the effects of nitrogen fertilization on the soil carbon pool, especially the LOC fractions, in farmland.

Mockeviciene and Respsiene. (2021) suggested that long-term application of single chemical fertilizers was disadvantageous in maintaining and improving SOC. Furthermore, although nitrogen fertilization can promote the growth of plant roots, it also reduces the soil carbon/nitrogen ratio, thereby increasing the degradation of original organic carbon and fresh organic carbon, causing a reduction in the SOC content. In the present study, compared
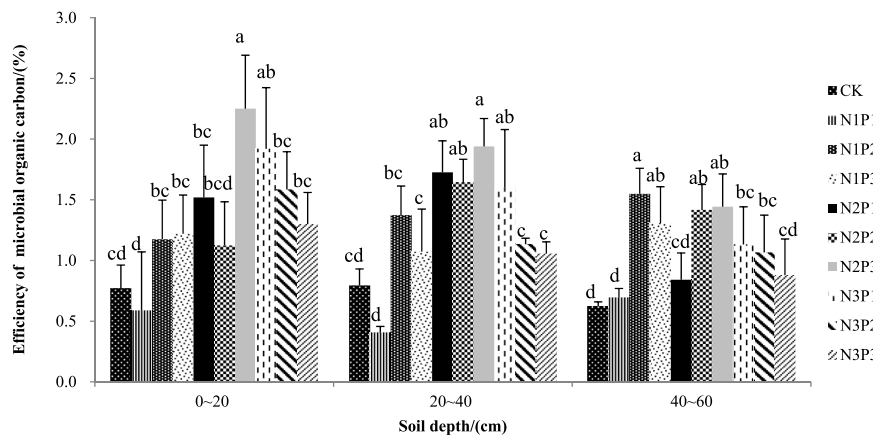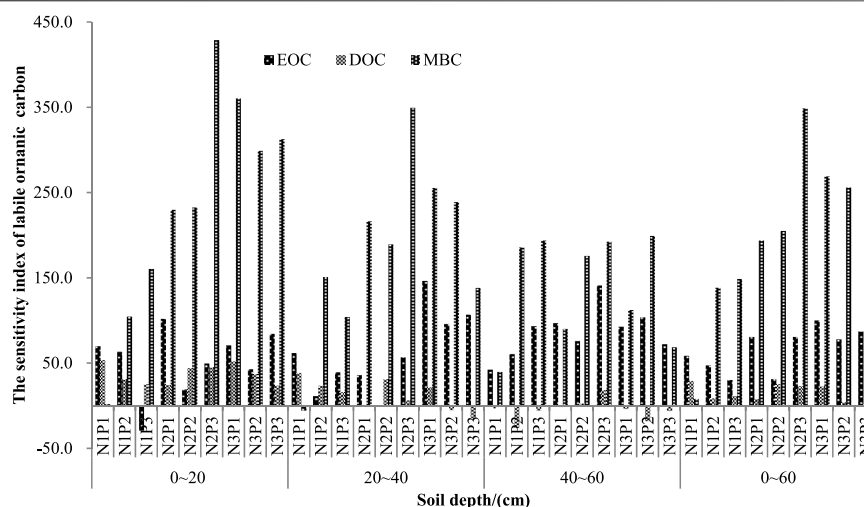
**FIGURE 2 |** The sensitivity index of soil labile organic carbon under different fertigation treatments (N₁–N₃: 40, 60, and 80 mg L$^{-1}$, respectively; P₁–P₃: 10, 20, and 30 mg L$^{-1}$, respectively). EOC, easily oxidized organic carbon; DOC, dissolved organic carbon; MBC, microbial biomass carbon.

**TABLE 4 |** The yields of *L. barbarum* under different fertigation treatments.

| Treatment | Yield (kg hm$^{-2}$) | | Average yield |
|---|---|---|---|
| | 2018 | 2019 | |
| Control | 11,465b | 9,720c | 10,593 |
| N₁P₁ | 12,789ab | 9,930c | 11,360 |
| N₁P₂ | 14,008a | 10,320bc | 12,164 |
| N₁P₃ | 12,586ab | 12,915a | 12,751 |
| N₂P₁ | 12,817ab | 10,635bc | 11,726 |
| N₂P₂ | 12,630ab | 12,090ab | 12,360 |
| N₂P₃ | 14,326a | 13,890a | 14,110 |
| N₃P₁ | 13,969a | 13,185a | 13,577 |
| N₃P₂ | 13,145ab | 12,615a | 12,880 |
| N₃P₃ | 12,674ab | 13,200a | 12,940 |
| N | NS | ** | |
| P | NS | ** | |
| N × P | NS | NS | |

*The yields of* L. barbarum *under different fertigation treatments (N₁–N₃: 40, 60, and 80 mg L−1, respectively; P₁–P₃: 10, 20, and 30 mg L−1, respectively). The values are the means ± SE (standard error) of three replicates, and the different lowercase letters in a row are significantly different at the 0.05 significance level. NS: not significant.*

with traditional fertilization (control), drip fertigation caused an increase in the SOC content of the *L. barbarum* plots, while the degree of increase was dependent on the levels of nitrogen and phosphorus applied. A similar finding was reported by Lin (2019). The cumulative biological carbon sequestration was 7.36–22.41% higher than that of other irrigation modes. Therefore, open-field drip irrigation was considered to be an appropriate water-saving irrigation method to enhance carbon sequestration and emission reduction for farmland (Qiu et al., 2010). Our result also indicates that drip fertigation with nitrogen and phosphorus is more effective than traditional fertilization in increasing the SOC pool in the potassium-rich soil planted with *L. barbarum*.

Because the SOC content tended to decrease with increasing soil depth, the effects of different fertilizer combinations were more pronounced in the 0–20 and 20–40 cm soil layers in the *L. barbarum* plots. The increase in SOC under drip fertigation is thought to be the result of the following mechanisms.

During fertigation, the fertilizer solution, which contains relatively low nutrient concentrations, irrigates the roots in small amounts multiple times, thereby improving nutrient utilization by the plants, reducing nutrient losses, and substantially increasing the fertilizer use efficiency. Accordingly, these factors help optimize the water, air, and heat conditions for soil rhizosphere microorganisms and crop root activity, to some extent facilitating microbial proliferation and organic matter decomposition, thus contributing to the accumulation of SOC.

## Effects of Different Fertilizer Combinations on Soil Labile Organic Carbon Under Drip Fertigation

Soil LOC is composed of EOC, DOC, and MBC (Zhang et al., 2009). Melero et al. (2009) previously reported that EOC is the most sensitive and reliable indicator of the effects of short- and long-term agricultural management practices on soil quality. In the present study, compared with the control, drip fertigation caused an increase in the EOC contents of different soil layers in the *L. barbarum* plots. Meanwhile, under different levels of nitrogen and phosphorus fertigation, the changes in soil EOC content varied with soil depth, similar to previous findings in wheat and corn fields (Aiziguli·Mulati et al., 2012). One plausible reason for this phenomenon is that soil microbial and enzymatic activities were enhanced by drip nitrogen and phosphorus fertigation, in turn accelerating the decomposition of EOC; however, the decomposition rate decreased with increasing soil depth. DOC, on the other hand, is easily affected by soil pH, microbial biomass and activity, and humidity (Zhang et al., 2016). Here, the soil DOC content was also remarkably higher under drip fertigation compared with the control. Overall, therefore,

**TABLE 5 |** Economic profits of *L. barbarum* under different fertigation treatments.

| Treatment | Yield (kg hm$^{-2}$) | Output value (yuan) | N (kg hm$^{-2}$) | P (kg hm$^{-2}$) | K (kg hm$^{-2}$) | Cost input (yuan) | Reduction of fertilizer input (%) | Growth of output value (%) |
|---|---|---|---|---|---|---|---|---|
| Control | 9,720 | 155,520 | 93.50 | 19.5 | 8.8 | 13,722 | 0.00 | 0.00 |
| $N_1P_1$ | 9,930 | 158,880 | 26.13 | 4.37 | 26.2 | 6,443 | 53.04 | 2.16 |
| $N_1P_2$ | 10,320 | 165,120 | 26.13 | 8.73 | 26.2 | 7,360 | 46.36 | 6.17 |
| $N_1P_3$ | 12,915 | 206,640 | 26.13 | 13.10 | 26.2 | 8,280 | 39.66 | 32.87 |
| $N_2P_1$ | 10,635 | 170,160 | 39.20 | 4.37 | 26.2 | 7,285 | 46.91 | 9.41 |
| $N_2P_2$ | 12,090 | 193,440 | 39.20 | 8.73 | 26.2 | 8,202 | 40.23 | 24.38 |
| $N_2P_3$ | 13,890 | 222,240 | 39.20 | 13.10 | 26.2 | 9,121 | 33.53 | 42.90 |
| $N_3P_1$ | 13,185 | 210,960 | 52.27 | 4.37 | 26.2 | 8,126 | 40.78 | 35.65 |
| $N_3P_2$ | 12,615 | 201,840 | 52.27 | 8.73 | 26.2 | 9,043 | 34.09 | 29.78 |
| $N_3P_3$ | 13,200 | 211,200 | 52.27 | 13.10 | 26.2 | 9,963 | 27.40 | 35.80 |

*The economic profits of* L. barbarum *under different fertigation treatments ($N_1$–$N_3$: 40, 60, and 80 mg L$^{-1}$, respectively; $P_1$–$P_3$: 10, 20, and 30 mg L$^{-1}$, respectively).*

fertigation caused a considerable increase in the photosynthetic rate, promoting plant growth and increasing the input of plant litter and root exudates into the soil, thereby increasing the soil DOC content (Wu, 2012; Kennedy et al., 2013).

Soil MBC content is indicative of soil microbial activity and is closely related to soil fertility (Yan et al., 2007); however, the response of soil MBC content to nitrogen fertilization is inconsistent. For example, Yang et al. (2018) revealed a considerable increase in the soil MBC content under fertigation in sugar cane fields. In the present study, the MBC contents in each soil layer tended to increase first and then decrease with increasing levels of nitrogen and phosphorus fertigation, with highest values obtained under $N_2P_3$ treatment. This result suggests that rational application of nitrogen combined with phosphorus fertigation could increase the soil MBC content in the *L. barbarum* field. The application of chemical fertilizers increases the decomposition rate of SOC, reducing the carbon/nitrogen ratio of the soil and improving the soil environment, thereby enhancing soil microbial activity. However, with increasing soil depth, the positive effects of different fertigation treatments on soil MBC content were diminished, with differential changes in the three soil layers.

The CPMI of soil LOC can be used to indicate changes in, and the renewal of, soil quality, reflecting the effects of environmental conditions on SOC and LOC fractions. The level of CPMI sensitively reflects the effects of different fertilization approaches on the dynamics of the soil carbon pool (Xu et al., 2006). In the present study, different levels of nitrogen and phosphorus fertigation increased the CPI and CPMI of soil LOC in all three soil layers, although the effects varied with depth. Yue et al. (2014) also found an increase in the CPMI of the topsoil (0–20 cm) of cotton fields under drip fertigation. This increase suggests that fertigation practice plays a role in improving soil fertility. The increases in the SOC content and LOC fractions are beneficial in terms of the CPMI of organic carbon, thereby increasing the SOC pool. However, after the application of a certain proportion of fertilizers, the CPMI of soil LOC showed no further increases, and instead began to decrease. The optimal fertilization rates under drip fertigation therefore require further investigation in terms of local soil characteristics and the fertilizer demands of specific crops.

The efficiency of soil LOC refers to the ratio of soil LOC to soil SOC. A previous study revealed that the higher the efficiency of

soil LOC fractions, the higher the availability of soil carbon (Li X. Y. et al., 2016). In the present study, compared with the control, both $N_2P_3$ and $N_1P_2$ treatments effectively increased the efficiencies of soil EOC, DOC, and MBC in the *L. barbarum* field. This effect may be attributed to the input of chemical fertilizers, which facilitate microbial activity and thereby accelerate the accumulation of LOC in the soil (Wu, 2012). Moreover, our results also revealed a general decrease in the SI values of soil DOC and MBC with increasing soil depth under all treatments. This suggests that soil DOC and MBC contents reflect the effects of nitrogen and phosphorus fertigation on the LOC fractions in the surface soil. The SI values of MBC were generally higher than those of EOC and DOC in all three soil layers, suggesting that the soil MBC content effectively reflects the effects of fertigation on SOC in the study area.

## Effects of Different Fertilizer Combinations on Goji Berry Yield Under Drip Fertigation

Most farmers use excessive fertilization and irrigation, showing high soil moisture fluctuations and eutrophication (Wang et al., 2021). Drip fertigation not only enables reducing total irrigation water supply and fertilizer application rates, but also decreases nitrogen leaching and $CO_2$ emission (Zhao et al., 2021). It is an environmentally friendly, effective modern agricultural technique that achieves high-quality, high-yielding crop production and efficient resource utilization (Yang et al., 2014). In Ningxia, farmers tend to apply excessive water and fertilizers (mainly nitrogen and phosphorus) during the production and management of *L. barbarum*. The average annual fertilization rates of nitrogen and phosphorus applied by broadcasting are 1,402.5 and 292.5 kg ha$^{-1}$, both of which are much higher than the levels used in fertigation. The excessive use of fertilizers may lead to an unbalanced soil nutrient status, which, in turn, results in relatively low nutrient use efficiency and crop productivity (Zhang et al., 2021; Zhong et al., 2022). Indeed, compared with traditional manual fertilization, the two-year average yield of *L. barbarum* increased under drip fertigation, and the input-output ratio increased by an average of 108.8% in 2019. These results suggest that drip fertigation is a useful practice in Goji berry cultivation,

increasing water and fertilizer use efficiency, as well as the yield and overall income.

The two-year average yield of *L. barbarum* reached its highest value under medium-to-high levels of nitrogen and phosphorus fertigation. Given the significant positive correlations of *L. barbarum* yield and SOC, EOC, and MBC contents, nitrogen and phosphorus fertigation improved the yield of *L. barbarum* by increasing the SOC pool in the study area. Overall, $N_2P_3$ treatment resulted in the highest yield, and this could be attributed to the higher SOC content, LOC fractions, and SI values compared with the remaining treatments. The experimental results suggest that drip fertigation with 60 mg $L^{-1}$ nitrogen fertilizer plus 30 phosphorus fertilizer is the optimal management practice for cultivation of *L. barbarum* in the study area in terms of improving yield and reducing fertilizer costs.

# CONCLUSION

There has been very little, if any, field investigations on the SOC distribution and sequestration potential or optimal water and fertilizer management practices for *L. barbarum* cultivation under drip fertigation with different fertilizer combinations. Based on the two-year experimental study, our data indicate that, compared with traditional manual fertilization, drip fertigation with different fertilizer combinations of nitrogen and phosphorus improved the SOC contents and altered their distribution in the surface and deep soil layers treatments. Especially for the LOC fractions, drip fertigation tended to increase the EOC, DOC, and MBC contents in each soil layer. Additionally, different fertigation treatments increased the changes in soil LOC and the overall yield of *L. barbarum*. On the whole, drip fertigation

with 60 mg $L^{-1}$ nitrogen fertilizer plus 30 mg $L^{-1}$ phosphorus fertilizer is deemed optimal for improving organic carbon sequestration and increasing *L. barbarum* yield in the study area. Long-term comprehensive evaluation is now needed to verify the applicability of this sustainable management practice in the production of *L. barbarum* on arid land in northwestern China and other similar settings.

# DATA AVAILABILITY STATEMENT

The original contributions presented in the study are included in the article/supplementary material, and further inquiries can be directed to the corresponding authors.

# AUTHOR CONTRIBUTIONS

The work was designed by FW, XN, and JY; field work was carried out by XN, FW, and JY; soil physicochemical analyses was performed by FW, WL, and YL; data were analyzed by JY, FW, XN, and WL; the manuscript was drafted by FW and revised by XN and JY.

# FUNDING

# REFERENCES

Aiziguli·MulatiTong, Y. A., Yang, X. L., and Ma, H. Y. (2012). Effect of Different Fertilization on Soil Organic Carbon and its Fraction in Farmland. *Chin. J. Soil Sci.* 43, 1461–1466. doi:10.19336/jcnki.trtb.2012.06.032

Bao, S. D. (2000). *Soil Agricultural Chemical Analysis*. 3rd ed. Beijing: China Agricultural Press, 265–267.

Demessie, A., Singh, B. R., and Lal, R. (2011). Soil Carbon and Nitrogen Stocks under Plantations in Gambo District, Southern Ethiopia. *J. Sustain. For.* 30, 496–517. doi:10.1080/10549811.2010.550547

El–Metwally, I., Geries, L., and Saudy, H. (2021). Interactive Effect of Soil Mulching and Irrigation Regime on Yield, Irrigation Water Use Efficiency and weeds of Trickle-Irrigated Onion. *Archives Agron. Soil Sci.* 68, 1103–1116. doi:10.1080/03650340.2020.1869723

Gillabel, J., Denef, K., Brenner, J., Merckx, R., and Paustian, K. (2007). Carbon Sequestration and Soil Aggregation in Center-Pivot Irrigated and Dryland Cultivated Farming Systems. *Soil Sci. Soc. Am. J.* 71, 1020–1028. doi:10.2136/sssaj2006.0215

Hagin, J., and Sneh, M. A. (2003). *Fertigation Fertilization through Irrigation*. IPI Research Topics No. 23. Basel, Switzerland: International Potash Institute, 72.

Hu, C., Qiao, Y., Li, S.-L., Chen, Y.-F., and Liu, G.-J. (2010). Vertical Distribution and Storage of Soil Organic Carbon under Long-Term Fertilization. *Chin. J. Eco-Agriculture* 18, 689–692. doi:10.3724/SP.J.1011.2010.00689

Huang, G. J., Wang, G. Y., Zhang, D. N., He, R. C., Ma, H. S., and Hu, J. S. (2003). Introduction and Cultivation Techniques of Large Leaf Wolfberry for

Vegetable. *Jiangsu. J. For. Sci. Tech.* 30, 34–35. doi:10.3969/j.issn.1001-7380.2003.04.01310.1023/a:1026392422995

Ilić, T., Dodevska, M., Marčetić, M., Božić, D., Kodranov, I., and Vidović, B. (2020). Chemical Characterization, Antioxidant and Antimicrobial Properties of Goji Berries Cultivated in Serbia. *Foods* 9, 1614. doi:10.3390/foods9111614

IPCC (2007). *Climate Change 2007: Mitigation of Climate Change. Contribution of Working Group III to the Fourth Assessment Report of the Intergovernmental Panel on Climate Change*. Cambridge, UK and New York: Cambridge University Press.

Kang, C., Yang, L., Wang, H., Nan, X. X., Wang, R., and Sun, Q. (2018). Effects of the Ratio of Nitrogen and Phosphorus Concentrations in Drip Fertigation on Yield and Yield Components of Chinese Wolfberry. *J. Irr. Drain.* 37, 26–30. doi:10.13522/j.cnki.ggps.2017.0674

Kennedy, T. L., Suddick, E. C., and Six, J. (2013). Reduced Nitrous Oxide Emissions and Increased Yields in California Tomato Cropping Systems under Drip Irrigation and Fertigation. *Agric. Ecosyst. Environ.* 170, 16–27. doi:10.1016/j.agee.2013.02.002

Kov, R., Camps-Arbestain, M., Calvelo Pereira, R., Suárez-Abelenda, M., Shen, Q., Garbuz, S., et al. (2018). A Farm-Scale Investigation of the Organic Matter Composition and Soil Chemistry of Andisols as Influenced by Land Use and Management. *Biogeochemistry* 140, 65–79. doi:10.1007/s10533-018-0473-7

Lai, Z. F., Zhang, S. P., Wu, S. J., and Lin, G. R. (2010). The Growth Characteristics and Nutritional Quality Analysis to Lycium Chinensis. *Chin. J. Trop. Crops.* 31, 1706–1709. doi:10.1080/00949651003724790

Li, J., Li, H., Zhang, Q., Shao, H., Gao, C., and Zhang, X. (2019). Effects of Fertilization and Straw Return Methods on the Soil Carbon Pool and

CO2 Emission in a Reclaimed Mine Spoil in Shanxi Province, China. *Soil Tillage Res.* 195, 104361. doi:10.1016/j.still.2019.104361

Li, T. K., Guo, Z. L., Kou, C. L., Lv, J. L., Zhang, X. N., and Yang, X. L. (2017). Effects of Extraction Conditions on the Test Results of Soil Dissolved Organic Carbon. *Ecol. Environ. Sci.* 26, 878–1883. doi:10.16258/j.cnki.1674-5906.2017.11.00810.15244/pjoes/65360

Li, X. H., Guo, H. H., Zhu, Z. L., Dong, H. Y., Yang, L. P., and Zhang, X. J. (2016a). Effects of Different Straw Return Modes on Contents of Soil Organic Carbon and Fractions of Soil Active Carbon. *Trans. Chin. Soc. Agric. Eng.* 32, 130–135. doi:10.11975/j.issn.1002-6819.2016.09.018

Li, X. Y., Wang, S. D., Ke, Y., Luo, J. H., Chen, X. Q., and Zhang, X. J. (2016b). Characteristics of Soil Nutrients and Present Situation of Fertilization in the Major Wolfberry Producing Areas of Ningxia. *Agr. Res. Arid. areas.* 34, 113–118. doi:10.7606/j.issn.1000-7601.2016.02.18

Liang, Q., Chen, H., Gong, Y., Fan, M., Yang, H., Lal, R., et al. (2012). Effects of 15 Years of Manure and Inorganic Fertilizers on Soil Organic Carbon Fractions in a Wheat-Maize System in the North China Plain. *Nutr. Cycl. Agroecosyst* 92, 21–33. doi:10.1007/s10705-011-9469-6

Lin, L. M. (2019). Effects of Nitrogen Application and Plant Interaction on Decomposition of Soil Organic Matter. Lanzhou: Lanzhou University. [master's thesis].

Melero, S., López-Garrido, R., Murillo, J. M., and Moreno, F. (2009). Conservation Tillage: Short- and Long-Term Effects on Soil Carbon Fractions and Enzymatic Activities under Mediterranean Conditions. *Soil Tillage Res.* 104, 292–298. doi:10.1016/j.still.2009.04.001

Mockeviciene, I., Repsiene, R., Amaleviciute-Volunge, K., Karcauskiene, D., Slepetiene, A., and Lepane, V. (2021). Effect of Long-Term Application of Organic Fertilizers on Improving Organic Matter Quality in Acid Soil. *Archives Agron. Soil Sci.* 2021, 1–13. doi:10.1080/03650340.2021.1875130

Danso, E., Abenney-Mickson, S., Sabi, E. B., Plauborg, F., Abekoe, M., Kugblenu, Y. O., et al. (2015). Effect of Different Fertilization and Irrigation Methods on Nitrogen Uptake, Intercepted Radiation and Yield of Okra (Abelmoschus Esculentum L.) Grown in the Keta Sand Spit of Southeast Ghana. *Agric. Water Manag.* 147, 34–42. doi:10.1016/j.agwat.2014.07.029

Preethi, B., Poorniammal, R., Balachandar, D., Karthikeyan, S., Chendrayan, K., Bhattacharyya, P., et al. (2013). Long-term Organic Nutrient Managements Foster the Biological Properties and Carbon Sequestering Capability of a Wetland Rice Soil. *Archives Agron. Soil Sci.* 59, 1607–1624. doi:10.1080/03650340.2012.755260

Qi, Y. C., Guo, S. F., Dong, Y. S., Peng, Q., Jia, J. Q., Cao, C. C., et al. (2014). Advances in Research on the Effects of Irrigation on the Greenhouse Gases Emission and Soil Carbon Sequestration in Agro-Ecosystem. *Sci. Agric. Sin.* 47, 1764–1773. doi:10.3864/j.issn.0578-1752.2014.09.011

Qian, Y., Follett, R. F., and Kimble, J. M. (2010). Soil Organic Carbon Input from Urban Turfgrasses. *Soil Sci. Soc. Am. J.* 74, 366–371. doi:10.2136/sssaj2009.0075

Qiu, S. J., Ju, X. T., Ingwersen, J., Qin, Z. C., Li, L., Streck, T., et al. (2010). Changes in Soil Carbon and Nitrogen Pools after Shifting from Conventional Cereal to Greenhouse Vegetable Production. *Soil Tillage Res.* 107, 80–87. doi:10.1016/j.still.2010.02.006

Shen, H., and Cao, Z. H. (2000). Study on Soil C Pool Management Index of Different Farmland Ecosystems. *Acta. Ecol. Sin.* 20, 663–668. doi:10.11849/zrzyxb.1999.03.003

Singh, H., and Singh, K. P. (1993). Effect of Residue Placement and Chemical Fertilizer on Soil Microbial Biomass under Tropical Dryland Cultivation. *Biol. Fert. Soils.* 16, 275–281. doi:10.1007/BF00369304

Su, Y.-Z., Wang, F., Suo, D.-R., Zhang, Z.-H., and Du, M.-W. (2006). Long-term Effect of Fertilizer and Manure Application on Soil-Carbon Sequestration and Soil Fertility under the Wheat-Wheat-Maize Cropping System in Northwest China. *Nutr. Cycl. Agroecosyst* 75, 285–295. doi:10.1007/s10705-006-9034-x

Wang, D., Geng, Z. C., She, D., He, W. X., and Hou, L. (2014). Vertical Distribution of Soil Active Carbon and Soil Organic Carbon Storage under Different Forest Types in the Qinling Mountains. *Ying Yong Sheng Tai Xue Bao* 25, 1569–1577. doi:10.13287/j.1001-9332.20140415.014

Wang, F., Weil, R. R., and Nan, X. (2017). Total and Permanganate-Oxidizable Organic Carbon in the Corn Rooting Zone of US Coastal Plain Soils as Affected by Forage Radish Cover Crops and N Fertilizer. *Soil Tillage Res.* 165, 247–257. doi:10.1016/j.still.2016.08.022

Wang, H., Wang, X. D., and Zhao, S. W. (2011). Distribution of Soil Water and Available Potassium under Drip Fertigation. *Chin. J. Soil Sci.* 42, 27–32. doi:10.19336/j.cnki.trtb.2011.01.006

Wang, K. (2016). Study on Efficient Cultivation Technology of Water and Fertilizer Integration of Lycium Barbarum in Arid Zone of Central Ningxia. Yinchuan: Ningxia University. Master Dissertation [master's thesis]. doi:10.7666/d.Y3109180

Wang, R., Wang, W., Wang, Y. L., Wang, J. T., and Si, G. Y. (2016). Effect of Nitrogen Fertilizer Application on the Accumulation of NPK and Yield for Leaf Wolfberry. *Nor. Hor.* 160–163. doi:10.11937/bfyy.201611042

Wang, Y., Dannenmann, M., Lin, S., Lv, H., Li, G., Lian, X., et al. (2021). Improving Soil Respiration while Maintaining Soil C Stocks in Sunken Plastic Greenhouse Vegetable Production Systems - Advantages of Straw Application and Drip Fertigation. *Agric. Ecosyst. Environ.* 316, 107464. doi:10.1016/j.agee.2021.107464

Wang, Y., Ruan, H. H., Huang, L. L., and Feng, Y. Q. (2010). Soil Labile Organic Carbon of Different Land Use Types in a Reclaimed Land Area of Taihu Lake. *Chin. J. Eco.* 29, 741–748. doi:10.3969/j.issn.1000-2006.2010.05.024

Weil, R. R., and Magdoff, F. (2004). "Significance of Soil Organic Matter to Soil Quality and Health," in *Soil Organic Matter in Sustainable Agriculture*. Editors F. Magdoff and R. R. Weil (Boca Raton: CRC Press), 1–43. doi:10.1201/9780203496374.ch1

Wu, J. (2012). The Effect of Tillage Systems on Organic Carbon Fractions in a Purple Paddy Soil. Chongqing: Southwest University. [master's thesis]. doi:10.5846/stxb201106300981

Xing, Y. Y., Zhang, F. C., Zhang, Y., Li, J., Qiang, S. C., and Wu, L. F. (2015). Effect of Irrigation and Fertilizer Coupling on Greenhouse Tomato Yield, Quality, Water and Nitrogen Utilization under Fertigation. *Sci. Agric. Sin.* 48, 713–726. doi:10.3864/j.issn.0578-1752.2015.04.09

Xiong, D., Shi, P., Zhang, X., and Zou, C. B. (2016). Effects of Grazing Exclusion on Carbon Sequestration and Plant Diversity in Grasslands of China-A Meta-Analysis. *Ecol. Eng.* 94, 647–655. doi:10.1016/j.ecoleng.2016.06.124

Xu, M. G., Yu, R., Sun, X. F., Liu, H., Wang, B. R., and Li, J. M. (2006). Effects of Long-Term Fertilization on Labile Organic Matter and Carbon Management Index (CMI) of the Typical Soils of China. *Plant Nutr. Fert. Sci.* 12, 459–465. doi:10.11674/zwyf.2006.0401

Yan, D., Wang, D., and Yang, L. (2007). Long-term Effect of Chemical Fertilizer, Straw, and Manure on Labile Organic Matter Fractions in a Paddy Soil. *Biol. Fertil. Soils* 44, 93–101. doi:10.1007/s00374-007-0183-0

Yang, X. H., Yan, C. M., Zhang, J. Z., and Shi, W. Q. (2014). The Analysis of Advantages and Disadvantages of Fertigation Technology and Development Strategies in China. *J. Agric.* 4, 76–80. doi:10.3969/j.issn.1007-7774.2014.01.019

Yang, X. Y., Jiang, D. H., Yang, K. R., Huang, Z. G., and Huang, K. (2018). Effects of Water and Fertilizer Integration on Soil Microbial Biomass Carbon, Nitrogen and Enzyme Activities in Sugarcane. *Chin. J. Soil Sci.* 49, 889–896. doi:10.19336/j.cnki.trtb.2018.04.19

Yue, H. J., Tao, R., and Chu, G. X. (2014). Response of Soil Organic Carbon Fraction to Different Ratios of Organic/Inorganic Fertilizer Application in Cotton Field. *Xinjiang Agri. Sci.* 51, 1630–1637. doi:10.6048/j.issn.1001-4330.2014.09.010

Zhang, L., Zhang, W. J., Xu, M. G., Cai, Z. J., Peng, C., Liu, B. R., et al. (2009). Effects of Long-Term Fertilization on Change of Labile Organic Carbon in Three Typical Upland Soils of China. *Sci. Agric. Sin.* 42, 1646–1655. doi:10.3864/j.issn.0578-1752.2009.05.018

Zhang, Q., Li, T., Yin, Y., Ying, H., Cui, Z., and Zhang, F. (2021). Targeting Hotspots to Achieve Sustainable Nitrogen Management in China's Smallholder-Dominated Cereal Production. *Agronomy* 11, 557. doi:10.3390/agronomy11030557

Zhang, X., Sun, N., Wu, L., Xu, M., Bingham, I. J., and Li, Z. (2016). Effects of Enhancing Soil Organic Carbon Sequestration in the Topsoil by Fertilization on Crop Productivity and Stability: Evidence from Long-Term Experiments with Wheat-Maize Cropping Systems in China. *Sci. Total Environ.* 562, 247–259. doi:10.1016/j.scitotenv.2016.03.193

Zhao, Y., Lv, H., Qasim, W., Wan, L., Wang, Y., Lian, X., et al. (2021). Drip Fertigation with Straw Incorporation Significantly Reduces $N_2O$ Emission and N Leaching while Maintaining High Vegetable Yields in Solar Greenhouse Production. *Environ. Pollut.* 273, 116521. doi:10.1016/j.envpol.2021.116521

Zhong, Y. J., Liu, K. L., Ye, C., Huang, S. S., Du, J. X., and Chen, J. Z. (2022). Differential Grain Yields and Soil Organic Carbon Levels between Maize and

Rice Systems of Subtropical Red Soil in Response to Long-Term Fertilizer Treatments. *Eurasian. Soil Sci.* 55, 251–261. doi:10.1134/S1064229322020156

**Publisher's Note:** All claims expressed in this article are solely those of the authors and do not necessarily represent those of their affiliated organizations, or those of the publisher, the editors and the reviewers. Any product that may be evaluated in this article, or claim that may be made by its manufacturer, is not guaranteed or endorsed by the publisher.

# Ecosystem services in Jiangsu province: Changes in the supply and demand patterns and its influencing factors

Yuling Wen[1], Hongbo Li[1,2]*, Xiaolin Zhang[1,2] and Tingyun Li[1]

[1]School of Geography, Nanjing Normal University, Nanjing, China, [2]Jiangsu Center for Collaborative Innovation in Geographical Information Resource Development and Application, Nanjing, China

Revealing the spatial and temporal changing characteristics and key factors driving the relationship between the supply of and demand for ecosystem services (SDES) is paramount for the effective management of regional ecosystems and the rational allocation of natural resources. This study calculated the supply of ecosystem services (ESS) in Jiangsu Province, China, in 2000, 2010, and 2020, and quantitatively evaluated the ecosystem service demand (ESD) in those years by considering land development intensity, population density, and economic conditions. The 'coupling coordination degree and relative development degree' (CDRD) model is introduced to explore the degree of coordination and change in the relationship of supply versus demand of ecosystem services, and then to reveal the impact of various factors on the spatial differentiation characteristics of the SDES. The results show that: 1) the ESS is high in the Taihu Lake Plain, the southwest of Huaihai area and the eastern coastal zone of Jiangsu Province, yet low in the northwest and middle of Huaihai area, and along the Yangtze River Plain. The overall distribution pattern of ESD and the coordinating degree of the SDES is high in the south and north of Jiangsu Province but low in the province's middle. 2) The degree of coordination for the SDES increased from 0.371 to 0.415, and the relationship between supply and demand changed from one of moderate imbalance to one of basic coordination. The imbalance of supply and demand is mainly concentrated in the Lixiahe area, coastal plain area, and middle of the Huaihe River Basin, for which the predominant type is a moderate imbalance−demand lag. Meanwhile, the analysis of influencing factors shows that there is an obvious synergistic effect between different factors. The results of this research could contribute to sustainable ecosystem management and decision-making for the construction of ecological civilization in Jiangsu Province.

# 1 Introduction

Ecosystem services (ES) refer to the environmental conditions and utility for human survival and development as formed and maintained by ecosystems (Daily, 1997). They constitute all the benefits obtained by human beings, directly or indirectly, from an ecosystem (Costanza et al., 1997). Ecosystem service supply (ESS) refers to the ability of an ecosystem to provide specific ecological products and services in a specific time and space (Li et al., 2013). Conversely, ecosystem service demand (ESD) represents the quantity and quality of services required by human society; that is, the quantity and quality of ES consumed or wanted by humans (Wang and Zhou, 2019). The 2005 United Nations Millennium Ecosystem Assessment Report clearly pointed out that human well-being is closely related to changes in natural ES. Therefore, when researching ES, scholars should consider the benefits of "people" from the perspective of human demand while considering its supply capacity (Xie et al., 2008; Ecosystem Assessment, 2005). The research shows that, to a certain extent, the supply–demand relationship of ES can reflect the sustainability of regional social and economic development. The decline in the supply of ecosystem services and the rise in demand in a given region brought about by economic development and urban expansion will exacerbate the conflict between humanity and land in that region (Simonit and Perrings, 2011; Wei et al., 2017). Therefore, using actual human demand and quantitative evaluations of supply capacity and degree of demand for ES, research on the spatio-temporal variability characteristics and driving factors of the supply and demand patterning of ES should be the foundation for formulating a regional sustainable development strategy, which has important academic value and practical significance (Li et al., 2014; Ma et al., 2017; Zhao et al., 2021).

Many scholars have conducted much research investigating the supply and demand of ecosystem services (SDES), involving a variety of ecosystem service types, research perspectives, and scientific methodologies (Burkhard et al., 2012; Geijzendorffer et al., 2015). In the early stage, some studies mostly focused on calculating the quantitative relationship of and differences in temporal and spatial patterns of a single functional demand placed upon the ecosystem; hence, there was little in-depth research on the spatiotemporal distribution of the supply–demand relationship of the overall ES and modeling of that relationship. In recent years, there has been an increasing trend in the literature of paying more attention to the SDES, in which the research content has expanded tremendously and diversified research perspectives and methods are employed (Kroll et al., 2012; Serna-Chavez et al., 2014; Bukvareva et al., 2017; Kramer et al., 2022). When they

study the SDES, some scholars usually select one or more ecosystem services to explore the coupling relationship between their supply and demand characteristics. The research methods used for this mainly include index construction and evaluation, index statistics and analysis, scenario formulation and simulation, and spatial mapping and analysis, among others (Shen et al., 2021; Liu et al., 2019; Zhai et al., 2019; Wu et al., 2020). However, now facing the actual needs of economic and social transformation and eco-environmental protection, scholars in China have begun to shift their attention to the geographical research of ecosystem services and their supply and demand dynamics, which entails the spatial mapping of ESS and ESD and the hot-spot analysis of supply and demand patterns based on GIS data (Li, 2014; Zhang and Fu, 2014; Ou et al., 2018; Li and Zhao, 2022; Liu et al., 2022). In summary, scholars have carried out multi-faceted and multi-scale studies of ecosystem services and their supply–demand relationship. Yet, although research on the SDES has made some progress, some limitations persist in the selection of robust indicators and data acquisition, and the quantitative methodology applies to the SDES needs to be optimized further (Wang et al., 2021).

As one of the most economically developed provinces in China, Jiangsu occupies an important national and international strategic position. With the firm promotion of new urbanization and construction and strengthening of its urban–rural integration and development, Jiangsu Province is now facing mounting pressure on its ecological environment. A series of ecological and environmental problems caused by rapid urbanization, such as the overexploitation of land resources, reduction in area of natural and semi-natural ecological land, and declines in ecosystem service capacity, have become serious obstacles to realizing a new era, one that achieves ecological civilization and sustainable development in Jiangsu Province. In this context, and taking the SDES perspective, the current study analyzes the spatial patterns and changing characteristics of ecosystem service supply, demand, and supply–demand coordination in Jiangsu Province since 2000. Going further, it clarifies the differences in ES supply–demand balances in different research units, and reveals the chief factors influencing spatial heterogeneity in ES. The primary objectives of our study were threefold: 1) to distinguish the changing characteristics of the temporal and spatial pattern of the SDES; 2) to reveal the degree of coupling and coordination of the SDES; and 3) to assess the influencing factors most relevant to the spatial differentiation of the SDES. Our research provides a timely reference for promoting effective ecosystem management and the rational allocation of natural resources, as well as crucial support for policy development related to ecosystem services.
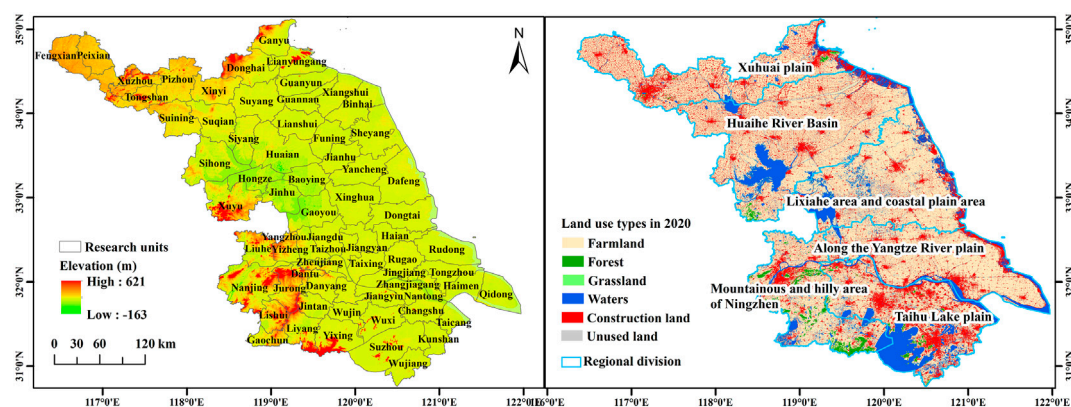
**FIGURE 1**
Geographical location and land use/land cover map of Jiangsu Province, China.

# 2 Materials and methods

## 2.1 Study area

Jiangsu Province is located in the eastern coastal zone of China (30° 45′N ~ 35° 20′N, 116° 18′E ~ 121° 57′E) and has a total area of 107 200 km². The administrative scope of Jiangsu Province includes 13 prefecture level cities, including those of Nanjing, Wuxi, Xuzhou, Changzhou, Suzhou, Nantong, and Lianyungang. It lies in the transition zone between a subtropical zone and warm temperate zone, and has four distinct seasons and moderate rainfall, with an average annual precipitation of ca. 1000 mm. Plains are the predominant terrain in the study area, but low-elevation mountains and hills are found in the southwest and north of Jiangsu Province. The river water system in the territory is well developed, featuring a dense network of rivers and lakes. Further, the Yangtze River crosses the southern part of the study area, and the Beijing-Hangzhou Grand Canal runs through the south and north of Jiangsu Province, whose entire coastline spans is 954 km. By the end of 2020, the resident population of Jiangsu Province stood at 84.7726 million, and its regional gross domestic product (GDP) was 10271.9 billion yuan. Its per capita regional GDP is above the national level, and Jiangsu's comprehensive economic competitiveness puts it ahead of other provinces in China. Based on the administrative divisions published in the 2020 *Jiangsu Statistical Yearbook*, we used county-level administrative regions of Jiangsu Province as the basic research unit. Jiangsu Province has 95 county-level administrative units, consisting of 21 county-level cities, 19 counties, and 55 municipal districts. Because the socio-economic data of some municipal districts could not be obtained, some district level administrative units under the jurisdiction of local cities were merged and integrated, reducing the number of basic research units to 68 (Figure 1).

In the face of rapid socio-economic development and an increasing intensity of territorial space development, the ecological background of Jiangsu Province has been continuously damaged, resulting in the reduction of its ESS. Meanwhile, given the concentration of its population in urban areas, the demand for a good-quality living environment by its residents is increasing daily. Consequently, the supply–demand relationship has become tenser, leading to a series of problems such as supply–demand imbalances in different regions of Jiangsu Province, which seriously affects regional sustainable development and human well-being.

## 2.2 Data sources and preprocessing

Table 1 shows the sources and descriptions of the land use data as well as the pertinent natural and socioeconomic data. Further, by referring to the land use/land cover classification system of the Chinese Academy of Sciences, we divide land use types into six categories: farmland, forest land, grassland, water area, construction land, and unused land (Xiao et al., 2003; Yang and Huang, 2021).

## 2.3 Research methodology

To reveal the spatial and temporal changing characteristics and key factors driving the relationship between the SDES, we performed the following data analysis, for which the main research contents and framework were illustrated in Figure 2.

### 2.3.1 Calculation of ecosystem service supply

Following the work of Costanza et al. (1997) and Xie et al. (2015), this study divided the supply of ecosystem services into four types: supply services, regulation services, support services,

**TABLE 1** The data requirements, sources, and descriptions.

| Data type | Data formats | Sources and descriptions |
|---|---|---|
| 1. Land cover | Digital grids at a 30-m × 30-m resolution | Land use data in 2000, 2010 and 2020 were downloaded from the Zenodo website (https://zenodo.org/) |
| 2. Digital Elevation Model (DEM) | Digital grids at a 90-m × 90-m resolution | Downloaded from the geospatial data cloud website (https://www.gscloud.cn/) |
| 3. Data for net primary productivity (NPP), precipitation, soil conservation, and the Normalized Difference Vegetation Index (NDVI) | Digital grids at a 1000-m × 1000-m resolution | Downloaded from the resource and environment data center of the Chinese Academy of Sciences (http://www.resdc.cn/) |
| 4. Administrative boundary data | Vector data | Taken from Jiangsu geographic information public service platform (http://jiangsu.tianditu.gov.cn/) |
| 5. Data on grain price and grain output per unit area | Excel format | Extracted from the *Jiangsu Statistical Yearbook*, the *China Statistical Yearbook*, and Jiangsu Grain and Material Reserve Bureau (http://lswz.jiangxi.gov.cn/) |
| 6. Population data | Excel format | Derived from the fifth, sixth and seventh national censuses |
| 7. Socio-economic data | Excel format | Extracted from the *Jiangsu Statistical Yearbook*, the *China Statistical Yearbook*, and *Jiangsu County Statistical Yearbook* |



**FIGURE 2**
The analytical framework of this study.
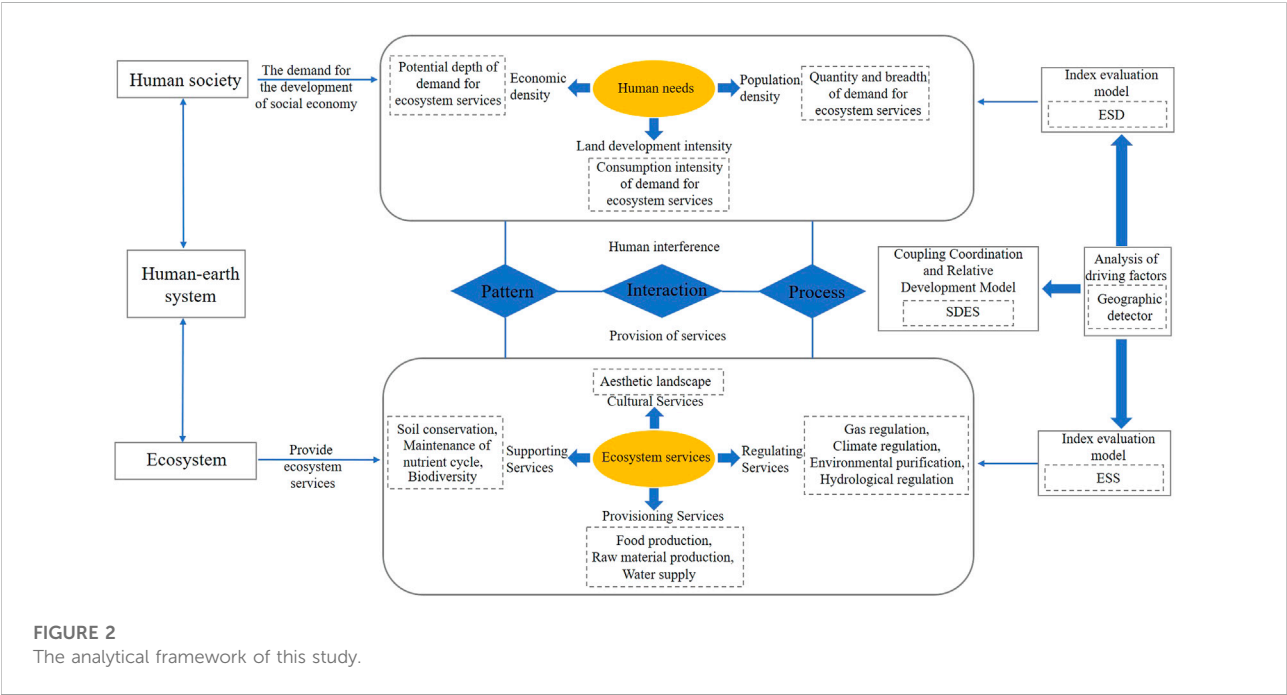
and cultural services. The *supply services* include food production, raw material production, and water resources supply; *regulation services* include gas regulation, climate regulation, environmental purification, and hydrological regulation; *support services* include soil conservation, nutrient cycling, and biodiversity; *cultural services* refer to the provision of aesthetic landscape services. Ecosystem service value (ESV) conveys the supply capacity of ecosystem services (Xiao et al., 2016). Based on the revised ESV equivalence factor table of Jiangsu Province, this paper calculated the ESV per unit area of each research unit to

express its ecosystem service supply capacity (Peng et al., 2017; Wang et al., 2019).

Regarding the calculation process for the equivalent factor table of ESV in Jiangsu Province, it went as follows: the equivalent coefficient in the equivalent table of ESV per unit area in China was corrected by applying the grain yield correction method (Xu et al., 2012). Firstly, according to the data, the average grain output per unit area of Jiangsu Province and the whole country from 2000 to 2020 were 6219.10 kg/hm$^2$ and 5721.88 kg/hm$^2$ respectively; hence, the revised coefficient of equivalence factor for Jiangsu Province is 1.09. Secondly, without human input, the

TABLE 2 Values for coefficients of various land ecosystem services in Jiangsu Province, China (yuan/hm$^2$).

| Primary ecosystem classification | Secondary ecosystem classification | Types of land use | | | | |
|---|---|---|---|---|---|---|
| | | Farmland | Forest | Grassland | Waters | Unused land |
| Provisioning Services | Food production | 4422.44 | 1093.94 | 1200.66 | 3201.77 | 0.00 |
| | Raw material production | 980.54 | 2521.39 | 1780.98 | 920.51 | 0.00 |
| | Water supply | −9108.20 | 2279.96 | 1709.97 | 57859.78 | 0.00 |
| Regulating Services | Gas regulation | 3561.97 | 8297.92 | 6223.44 | 3081.70 | 80.04 |
| | Climate regulation | 1861.03 | 24813.71 | 16469.10 | 9165.06 | 0.00 |
| | Environmental purification | 540.30 | 7217.32 | 5443.01 | 22212.27 | 400.22 |
| | Hydrological regulation | 10434.30 | 26964.01 | 21043.09 | 713580.68 | 209.38 |
| Supporting Services | Soil conservation | 1268.99 | 6157.87 | 4624.51 | 2269.55 | 48.81 |
| | Maintenance of nutrient cycle | 620.34 | 773.76 | 580.32 | 280.15 | 0.00 |
| | Biodiversity | 680.38 | 9191.75 | 6903.82 | 10205.64 | 80.04 |
| Cultural Services | Aesthetic landscape | 300.17 | 4028.89 | 3041.68 | 7564.18 | 40.02 |
| | Total1 | 15562.26 | 93340.52 | 69020.58 | 830341.30 | 858.52 |

economic value provided by natural ecosystems is one-seventh the economic value of food production services provided by the existing farmland per unit area. Thirdly, given the output and sown area of principal grain crops cultivated in Jiangsu Province from 2000 to 2020, and their purchase price in 2020, the economic value of one equivalent factor is 2238.87 yuan/hm$^2$. Then total ESV and single ecosystem service value (ESV$_f$) were calculated this way:

$$ESV = \sum_{i=1}^{n} (A_i \times VC_i) \qquad (1)$$

$$ESV_f = \sum_{i=1}^{n} (A_i \times VC_{fi}) \qquad (2)$$

where ESV is the ecosystem service value (yuan); $i$ is the land use type ($i$ = 1,2,3,..., n), $A_i$ is the area of land type $i$ (hm$^2$); $VC_i$ is the value coefficient of an ecosystem service function of land type $i$ (yuan/hm$^2$); $ESV_f$ is the value of an ecosystem service function $f$ (yuan); $VC_{fi}$ is the value coefficient of ecosystem service function $f$ of land class $i$ (yuan/hm$^2$).

In addition, we selected NPP data, precipitation data, and soil conservation data to further revise the value equivalence factors of ecosystem services (Liu et al., 2020). The calculation formula inorporating NPP, precipitation and soil conservation regulation factors was as follows:

$$A_{ij} = B_{ij} / \bar{B} \qquad (3)$$

where $Bij$ denotes the average annual NPP, average annual precipitation, or average annual soil per unit area of an ecosystem in Jiangsu Province, and $\bar{B}$ is the average annual NPP, average annual precipitation, or average annual soil conservation simulation of an ecosystem in China. The farmland, forest land, grassland, water area, and unused land

as land use types respectively corresponded to the five ecosystems of farmland, forest, grassland, water body, and unused land, according to which the table of ESV coefficient per unit area of Jiangsu Province was finally obtained (Table 2).

## 2.3.2 Calculation of ecosystem service demand

In this study, ecosystem services demand (ESD) is defined as the human consumption of and preference demand for ecosystem services, that is, the number of ecosystem services consumed or wanted by human society (Villamagna et al., 2013). Therefore, to build the ESD model, we selected three indicators: land development intensity, population density, and economic density. Land development intensity represents the percentage of total area of regional land covered with construction, which directly reflects the degree of human activity and interference; the higher its value, the higher the inferred ESD. Population density can directly reflect the ESD. The greater the population density, the greater is the total ESD. Economic density conveys the degree of development of the region and it can indirectly express the level of human preference for enjoying ecosystem services. The stronger the regional economic strength, the higher are the expected ecosystem services. The indicators of population density and economic density vary greatly among some regions. Therefore, here we used the natural logarithm approach in statistics to mitigate the impact of severe fluctuations for the analysis (Han et al., 2021). The calculation formula was as follows:

$$X = Q_i \times \lg P_i \times \lg E_i \qquad (4)$$

where $X$ is the ESD, $Q_i$ is land development intensity, and $Pi$ and $Ei$ respectively denote population density (person/km$^2$) and economic density (10,000 yuan/km$^2$).

TABLE 3 Types and division criteria of coordinated development of supply and demand coupling of ecosystem services.

| Coupling coordination degree | Coupling coordination type | Relative development degree | Types of coupled and coordinated development |
|---|---|---|---|
| $0 \leq D \leq 0.2$ | Severe imbalance | M < 0.5 | Severe imbalance–supply lag |
| | | $0.5 \leq M \leq 1.5$ | Severe imbalance |
| | | M > 1.5 | Severe imbalance–demand lag |
| $0.2 < D \leq 0.4$ | Moderate imbalance | M < 0.5 | Moderate imbalance–supply lag |
| | | $0.5 \leq M \leq 1.5$ | Moderate imbalance |
| | | M > 1.5 | Moderate imbalance–demand lag |
| $0.4 < D \leq 0.6$ | Basic coordination | M < 0.5 | Basic coordination–supply lag |
| | | $0.5 \leq M \leq 1.5$ | Basic coordination |
| | | M > 1.5 | Basic coordination–demand lag |
| $0.6 < D \leq 0.8$ | Moderate coordination | M < 0.5 | Moderate coordination–supply lag |
| | | $0.5 \leq M \leq 1.5$ | Moderate coordination |
| | | M > 1.5 | Moderate coordination–demand lag |
| $0.8 < D \leq 1$ | High coordination | M < 0.5 | High coordination–supply lag |
| | | $0.5 \leq M \leq 1.5$ | High coordination |
| | | M > 1.5 | High coordination–demand lag |

## 2.3.3 Coupling coordination and relative development model

The 'coupling coordination degree' model can characterize the degree of coordinated development between the actual supply of ecosystem services and human demand, and help to gauge whether that relationship is harmonious and consistent (Wang and Tang, 2018). In order to eliminate the dimensional impact of supply and demand, a range standardization was first applied to the original supply and demand data, after which we analyze the coupling and coordination of the SDES. The calculations went as follows:

$$X = \frac{x_i - x_{\min}}{x_{\max} - x_{\min}} \qquad (5)$$

$$C = 2 \times \sqrt{\frac{X_S \times X_D}{(X_S + X_D)^2}} \qquad (6)$$

$$T = \alpha \times X_S + \beta \times X_D \qquad (7)$$

$$D = \sqrt{C \times T} \qquad (8)$$

where $X$ is the supply of or demand for ecosystem services after the range standardization; $x_i$ is the supply or demand of the $i$th research unit; $x_{\max}$ is the maximum value of the whole province and $x_{\min}$ is the minimum value of the whole province; $C$ is the coupling degree; $X_S$ denotes the supply; $X_D$ denotes the demand; $T$ is the comprehensive coordination index of supply and demand; $\alpha$ and $\beta$ are undetermined coefficients. Because the supply and demand of ecosystem services are equally important, we set $\alpha = \beta = 0.5$. The $D$ indicates the degree of supply–demand coupling coordination; where $D \in [0,1]$, with a larger $D$ value indicating better coordination between supply and demand.

Using the equal division method, the coupling coordination degree of the SDES is divided into five intervals (Table 3).

Although the coupling coordination model can reliably capture the internal relationship of the SDES, it cannot reflect the actual gap between supply and demand for a given ES. Therefore, according to Han et al. (2020), this paper introduces the relative development model to measure whether the supply level of ecosystem services is ahead or behind their demand level (Eq. (9)).

$$M = \frac{S_1}{S_2} \qquad (9)$$

where $M$ is the relative development degree; $S_1$ and $S_2$ are respectively the supply and demand of ecosystem services after their range standardization. In the case of $M < 0.5$, the supply–demand relationship is of the supply lag type; when $0.5 \leq M \leq 1.5$, this indicates a net balance in supply and demand; when $M > 1.5$, the supply–demand relationship is of the demand lag type.

## 2.3.4 Geodetector analysis

Geodetector is a statistical analytical method to diagnose the spatial heterogeneity of geographic elements and reveal the driving forces behind it. It can effectively and independently detect the spatial distribution consistency and causality of two variables, and it includes four components: risk detection, factor detection, ecology detection, and interactive detection (Wang et al., 2010; Wang and Xu, 2017). Its core idea is this: the relevant characteristic factors affecting the supply and demand pattern of ecosystem services are heterogeneous in their spatial distribution. If the intensity of a factor is significantly consistent or similar

TABLE 4 Evaluation index of influencing factors and their definitions.

| Factor | Index for the factor | Description of factor | Numbered ID |
|---|---|---|---|
| Natural environmental factors | Average annual temperature | °C | X1 |
| | Annual rainfall | mm | X2 |
| | Elevation | m | X3 |
| | Slope | Vertical height of slope surface/distance in the horizontal direction (%) | X4 |
| | NDVI | Vegetation coverage (%) | X5 |
| | Water network density | Total length of water system in the area/total area of the area (km/km$^2$) | X6 |
| Socio-economic factors | Economic strength | Regional GDP/permanent resident population ($10^4$ yuan/person) | X7 |
| | Industrial structure | Output value of secondary and tertiary industries/regional GDP (%) | X8 |
| | Openness to the outside world | Total import and export volume/regional GDP (%) | X9 |
| | Population attractiveness | Resident population/registered residence population (%) | X10 |
| | Facility supply | Total investment in fixed assets/resident population ($10^4$ yuan/person) | X11 |
| | Consumption level | Total retail sales of social consumer goods/resident population ($10^4$ yuan/person) | X12 |
| | Road density | Area of roads in the region/total area (%) | X13 |

with the spatial distribution of a particular supply and demand pattern, it may be inferred this characteristic factor plays a certain impact on it. The detailed formula is as follows (Eq. (10)):

$$q = 1 - \frac{1}{n\sigma^2} \sum_{h=1}^{L} n_h \sigma_h^2 \qquad (10)$$

where $n$ is the number of geographical units in the study area; $\sigma^2$ is the discrete variance of $Y$ value of the whole region; $h$ is the partitioning of variable $Y$ or factor $X$, with $h = 1,2,3 \ldots L$; $L$ representing the number of partitions; $q$ is the spatial heterogeneity of an index, whose value range is [0,1]. The larger the value of $q$, the stronger the explanatory power of independent variable $X$ for attribute $Y$, and vice versa (Lv et al., 2017).

### 2.3.5 Selection of driving factors

Ecosystem services are under the comprehensive influence of internal and external conditions, including the effects of other ecosystem changes (Fang et al., 2021). According to the relevant literature and actual social-ecological environment background of the study area, we found that the ESS and SDES in Jiangsu Province are primarily affected by natural environment and socio-economic factors, while ESD was mainly impacted by socio-economic factors (Li and Zhang, 2017; Geng et al., 2020; Jing et al., 2022; Zhang et al., 2022). Accordingly, six natural environmental factors—average annual temperature, annual rainfall, elevation, slope, NDVI, and water network density—as well as seven socio-economic factors—economic strength, industrial structure, openness to the outside world, population attractiveness, facility supply, consumption level, and road density—were selected in this paper to simultaneously detect their effects on the spatial differentiation of the ESS and SDES (Dai et al., 2020; Dai et al., 2021). In terms of

natural environmental factors, they are related to climate, topography, vegetation and water systems, which directly determine the ESS and indirectly determine the SDES. From the perspective of socio-economic factors, economic strength, industrial structure and openness to the outside world may be used to assess regional economic development. Population attractiveness, facility supply and consumption level can convey the status of human demand for ES. Road density can reliably characterize the intensity of human exploitation of land: the higher the road density, the greater the demand by people for ecosystem services in the surrounding environment (Dai et al., 2022). Further details can be found in Table 4.

## 3 Results and analysis

### 3.1 Ecosystem service supply: Pattern and change

From the provincial level (Table 5), the ESV of Jiangsu Province in 2000, 2010, and 2020 was respectively 1213.008 billion yuan, 1270.742 billion yuan, and 1150.365 billion yuan, showing a trend of first rising and then falling, with a net negative change of 5.16% from 2000 to 2020. The change of ESV per unit area is consistent with the total ESV, suggesting that among the 3 years, the supply capacity of ecosystem services was strongest in 2010 and weakest in 2020.

According to the natural breakpoint method (Wang et al., 2021; Huang et al., 2018), we divided the ESV per unit area into five levels (Figure 3). Evidently, the high value of ESS over the years is mainly concentrated in the Taihu Plain, in the southwestern of the Huaihai area, and in the eastern coastal zone. Among them, the ESS in Suzhou is the highest, exceeding 46.27 million yuan/km$^2$ over the years; this was followed by

TABLE 5 Changes to the ecosystem service value and demand index in Jiangsu Province, from 2000 to 2020.

| | 2000 | 2010 | 2020 | Change range from 2000 to 2020 (%) |
|---|---|---|---|---|
| ESV ($10^8$ yuan) | 12130.08 | 12707.42 | 11503.65 | −5.16% |
| ESV per unit area ($10^4$ yuan/km$^2$) | 1169.92 | 1225.61 | 1109.51 | −5.16% |
| ES demand index | 0.82 | 1.44 | 2.12 | 158.54% |



FIGURE 3
Distribution pattern of and changes to the ecosystem service supply in Jiangsu Province from 2000 to 2020.
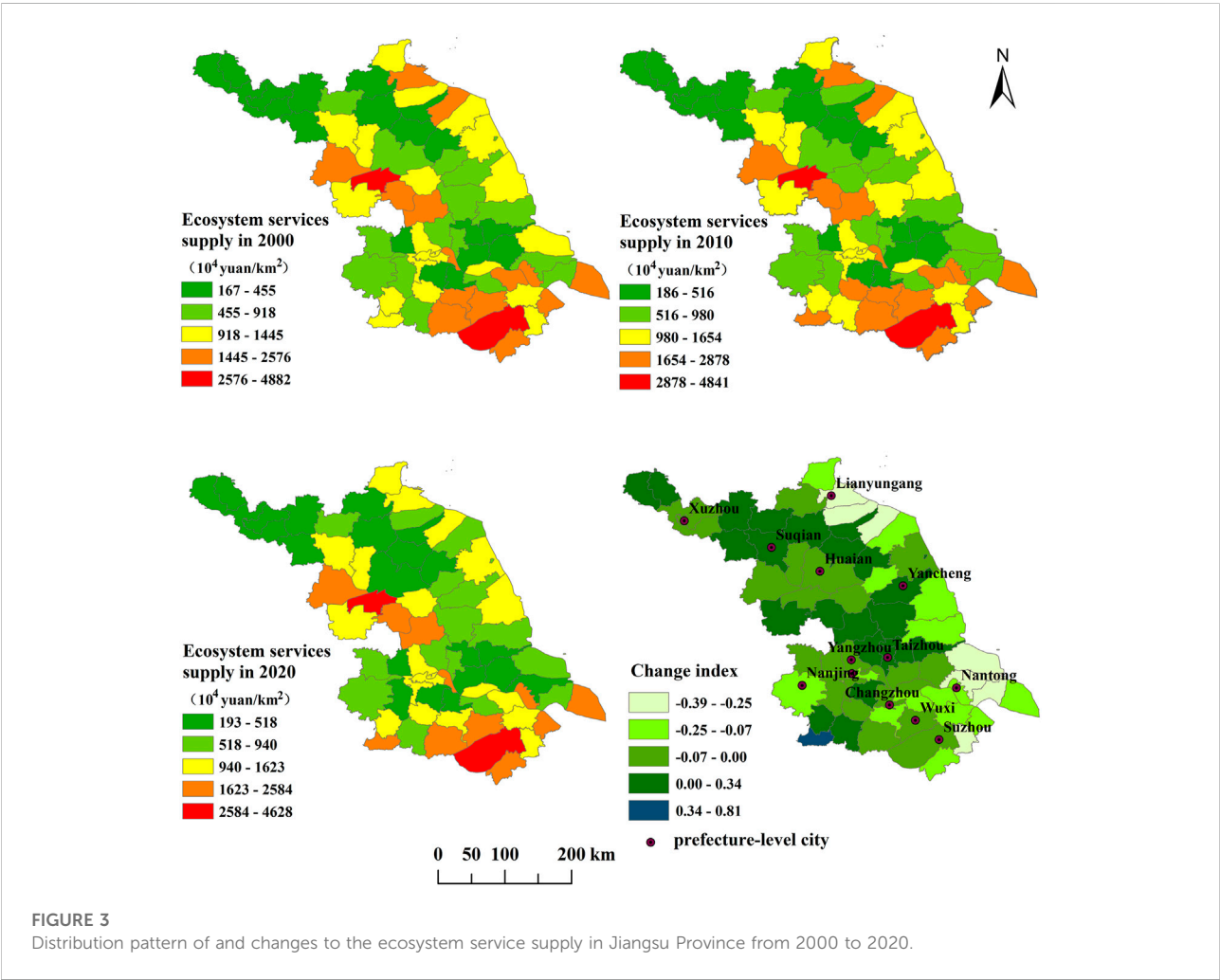
Hongze District, where the ESS has reached more than 38.02 million yuan/km$^2$ over the years. The low value of ESS is mainly distributed in the northwest and middle of Huaihai area and the plain area along the Yangtze River. Among these, the ESS of Fengxian County is the lowest, not exceeding 1.93 million yuan/km$^2$ over the years; likewise, the ESS is also low in Peixian County, Lianshui County, and Hai'an City, at less than 2.24 million yuan/km$^2$.

By calculating the change index of ESS in Jiangsu Province from 2000 to 2020, we could analyze the spatial distribution characteristics of their increases and decreases in ESS. The results show that the ESS in most areas is weakening, and the proportion of research units with reduced supply is 66.18%, these being mainly located in the eastern coastal zone of Jiangsu Province, Southern Jiangsu, and the surrounding areas of Hongze Lake as well as the urban area of Xuzhou. At the same time, there are

**FIGURE 4**

Distribution pattern and changes in ecosystem service demand in Jiangsu Province from 2000 to 2020.
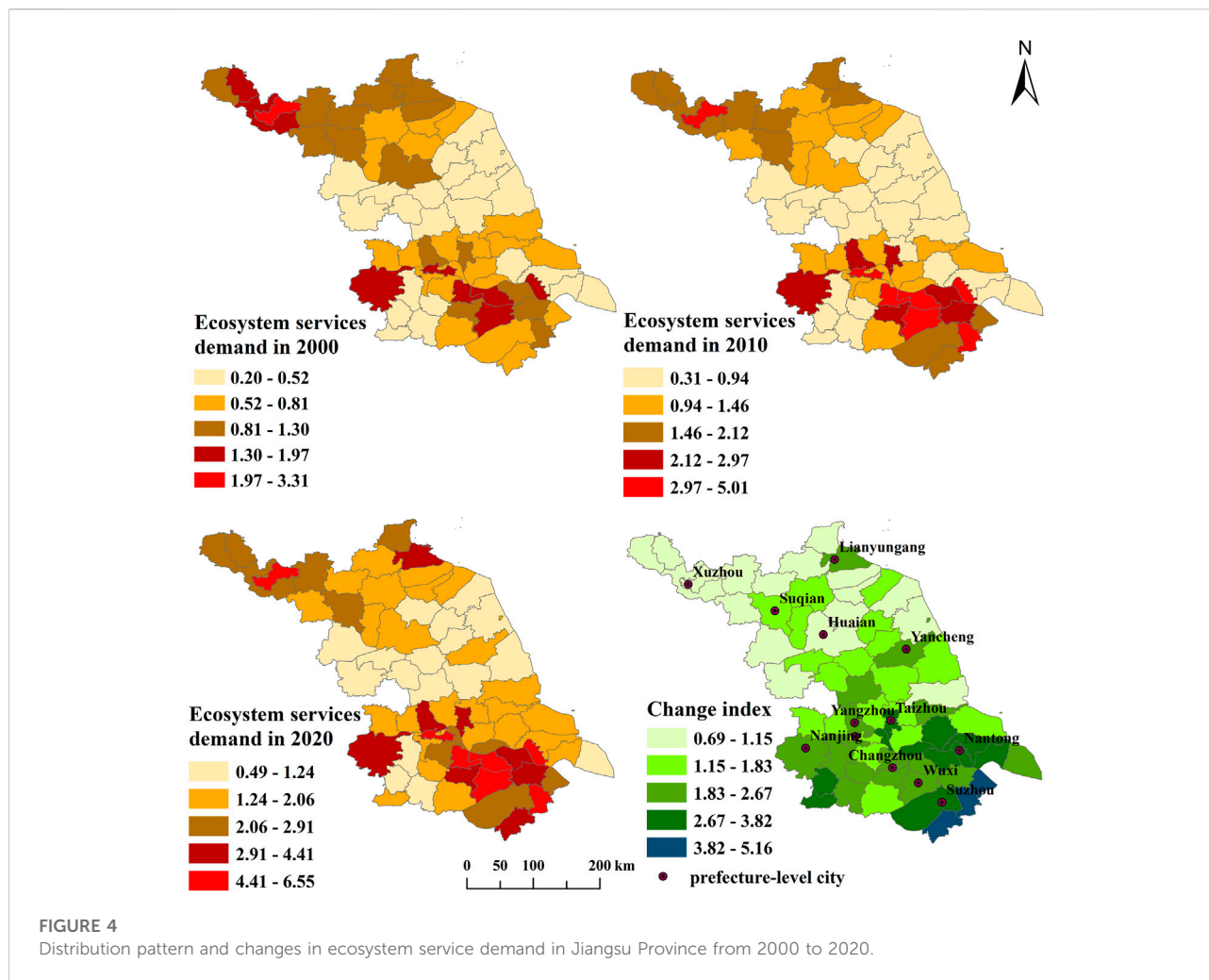
23 research units in which the ESS has increased over time, and these are mainly concentrated in the Xuhuai Plain in the north of Jiangsu Province, Lixiahe Plain in the province's middle, and in the southern part of the Ningzhen mountainous and hilly area.

## 3.2 Ecosystem service demand: Pattern and change

The demand indexes of ecosystem services in Jiangsu Province in 2000, 2010, and 2020 were 0.82, 1.44, and 2.12, respectively, indicating that the ESD in Jiangsu Province rose from 2000 to 2020 (Table 5). Spatially, the overall ESD over time shows a distribution pattern of being high in the north and south whereas it was low in the middle of the province, with obvious signs of clustering (Figure 4). That is, high-value areas for the ESD index are mainly distributed in southern Jiangsu, along the Yangtze River and Xuhuai Plain in Northern Jiangsu. Over time, Xuzhou had the highest level of ESD, followed by Changzhou,

Nantong, Jiangyin, Kunshan, Wuxi, Zhenjiang, Taizhou, Zhangjiagang, and Nanjing. The low-value areas for the ESD index in Jiangsu Province are mainly concentrated in the Huaihe River Basin area, the Lixiahe Plain and coastal plain area, southern part of the Ningzhen mountainous and hilly area, and the eastern part of the Yangtze River Plain. Of them, Hongze District and Jinhu County are distinguished as having the lowest levels of ESD.

According to the change index of ESD, the ESD in different regions has increased by differing magnitudes in the recent 20 years, and the overall growth pattern is best described as a gradient weakening from south to north. Those areas with the most pronounced increase in ESD are Kunshan City, Wujiang District, and Taicang City in southern Jiangsu, where the corresponding change indexes are 5.16, 4.63 and 4.29 respectively. The areas with small increases in ESD are mainly distributed in Northern Jiangsu, among which Guanyun County, Donghai County, and Sihong County have the lowest value for the demand change index, implying that the ESD in

**FIGURE 5**
Distribution patterns in the degree of supply–demand coupling coordination of ecosystem services in Jiangsu Province from 2000 to 2020.
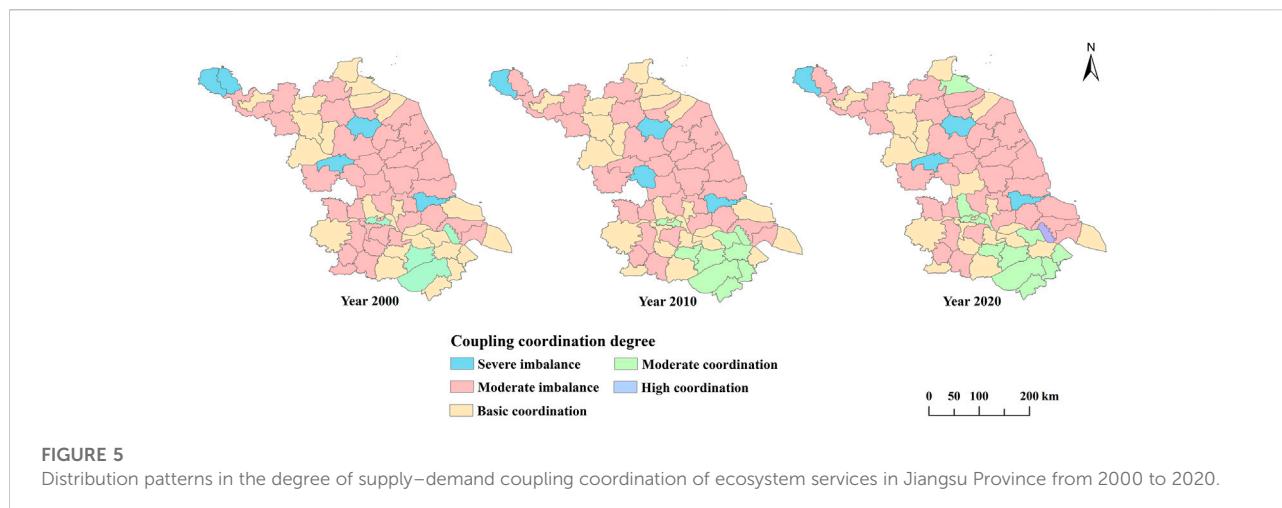
these areas has been relatively stable over the recent 20 years with a slight growth trend discernible.

## 3.3 Analysis of the coupling and coordination between the supply and demand of ecosystem services

From 2000 to 2020, the degree of coupling and coordination of the SDES in Jiangsu Province increased from 0.371 to 0.415, and the overall relationship of the SDES changed from one of moderate imbalance to one of basic coordination. Among the 68 research units (Figure 5), the regions with moderate imbalance and/or basic coordination in the coupling and coordination relationship between supply and demand accounted for the majority. Of these, in 2000, five research units had a serious imbalance between supply and demand, 35 units had a moderate imbalance, 24 units had a basic coordination, and another four had a moderate coordination. By 2020, the number of research units with a severe imbalance decreased to 4, the number having a moderate imbalance decreased to 33, the number featuring a basic coordination decreased to 19, the number distinguished by a moderate coordination increased to 11, and 1 research unit showed high coordination. Considered spatially, the degree of coupling and coordination of the SDES over time is generally high in the north and south of Jiangsu Province and low in its middle. The areas with an imbalance between supply and demand are mainly concentrated and distributed in Lixiahe and the coastal plain area, the middle of Huaihe River Basin area, in the west of the Xuhuai Plain area, and scattered along the borders of the Yangtze River, Taihu Plain area, and Ningzhen hilly area. The areas of supply–demand coordination is interspersed in the north of Jiangsu Province but concentrated in the plain area of Taihu Lake. The degree of supply–demand coordination in the surrounding areas of Taihu Lake and some

areas along the Yangtze River is high, best characterized by moderate coordination.

Based on the above analysis of coupling coordination degree, we then conducted an analysis that also considered the relative development degree (Figure 6). These results uncovered those areas with a serious imbalance of the SDES over the years being mainly located in Feng County, Lianshui County, Hongze District, and Hai'an City. Among them, serious imbalance–supply lag characterized Feng County, Lianshui County, and Hai'an city. Their terrain is flat, the land use type is mainly cultivated land, and certain land use types are lacking, such as water area and forest land that have a high ecosystem service capacity, which renders the supply of ecosystem services far lower than their demand. In contrast, Hongze District is of a different type, the serious imbalance–demand lag. Situated adjacent to Hongze Lake in the West and Baima Lake in the province's east, its ecological base is quite good, the level of economic development is low, and there is little interference from human activities; hence, the demand for ecosystem services is far lower than their supply. In the moderate imbalance category, over the years, the moderate imbalance–supply lag area is found mainly distributed in the middle of the Huaihe River Basin, the west of Xuhuai Plain and in areas along the river. The level of ecological resources in such places is at a disadvantage vis-à-vis the interference level from human activities, so the supply of ecosystem services lags behind their demand. Meanwhile, having a moderate imbalance–demand lag areas are chiefly concentrated in Lixiahe and coastal plain areas, where one finds a dense river network, many lakes, and an excellent ecological background, in addition to prominent ecological functions and a national ecological reserve. Therefore, the value of ecosystem services provided by Xuyi County, Jinhu County, Gaoyou City, Sheyang County, and Dafeng District is high, and the supply level of their ecosystem services surpasses their level of demand. In the basic

**FIGURE 6**
Types of coordinated development in the supply and demand coupling of ecosystem services in Jiangsu Province.
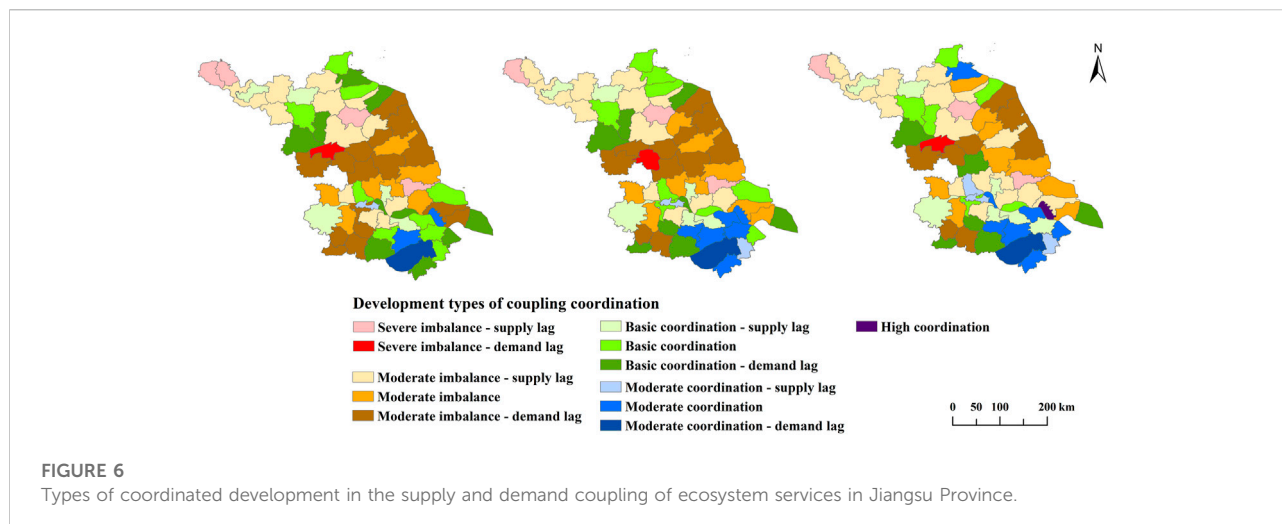
coordination category, those belonging to the basic coordination–supply lag type are mainly the municipal districts of various prefecture level cities. The supply and demand levels of ecosystem services in such areas are high, but supply lags behind demand due to the influence of regional economic development and urban expansion. The supply–demand relationship of ecosystem services in Suzhou-Wuxi-Changzhou area has changed from one of basic coordination in 2000 to one of moderate coordination in 2020, and the coordination relationship is gradually improving. This harbors many rivers and lakes, good hydrothermal conditions and is rich in ecological resources, and therefore the supply of ecosystem services is sufficient. In parallel, the rapid economic development and high population density in this area has led to a very high demand for ecosystem services under the strong interference of human activities. But because of the strong carrying capacity of resources and environment there, a good coordinated relationship between supply and demand still prevails. The supply–demand relationship of ES in the Nantong urban area has changed from medium coordination to high coordination. Over time, the supply and demand levels of ES there have ranked first in the province, though the supply capacity and demand intensity are both increasing, and their degree of coordination is continually improving.

## 3.4 Analysis of factors driving the supply and demand pattern of ecosystem services

To the 68 research units, we applied the 'factor detector' and 'interaction detector' functions of the geodetector model to quantitatively analyze the contribution of driving factors and their interactions, and thereby explore the factors responsible for

the spatial differentiation in ecosystem service supply, demand and supply–demand coordination in Jiangsu Province.

### 3.4.1 Factor detection analysis

From the perspective of supply capacity (Table 6), the factors can be sorted according to their q statistic as follows: X5 (NDVI) > X6 (water network density) > X1 (average annual temperature) > X13 (road density) > X9 (openness to the outside world) > X2 (annual rainfall) > X3 (elevation) > X12 (consumption level) > X7 (economic strength) > X8 (industrial structure) > X10 (population attractiveness) > X11 (facility supply) > X4 (slope). Among them, we find that NDVI, water network density, average annual temperature, and annual rainfall are each significant at the alpha level of 10%, suggesting that these four factors have the highest explanatory contribution. This shows that the driving effect of natural environmental factors upon the supply capacity of ecosystem services is significantly greater than that of socio-economic factors. Therefore, in terms of future ecosystem service management aims and practices, we should strengthen both ecosystem protection and restoration, and implement projects such as forest quality improvement and watershed water ecological health protection, to ensure that ecosystems retain their ability to provide long-term sustainable services.

Regarding the demand intensity, the factors ranked by their q statistic are as follows: X8 (industrial structure) > X10 (population attractiveness) > X9 (openness to the outside world) > X7 (economic strength) > X12 (consumption level) > X11 (facility supply) > X13 (road density). Of these, the explanatory power of industrial structure, population attractiveness, and openness to the outside world for the demand intensity of ES are each more 50%, with all passing the significance test at $p < 0.001$. Therefore, to avoid the excessive consumption of ecosystem services, it is necessary to properly adjust the economic and industrial structure of some regions and

TABLE 6 Detection results of driving factors of ecosystem service supply and demand in Jiangsu Province.

| Driving factors | Ecosystem services supply | | Ecosystem services demand | | The coordination degree of supply and demand | |
| --- | --- | --- | --- | --- | --- | --- |
| | q value | p value | q value | p value | q value | p value |
| X1 | 0.258* | 0.041 | | -- | 0.371* | 0.006 |
| X2 | 0.201* | 0.083 | | -- | 0.313* | 0.008 |
| X3 | 0.191 | 0.259 | | -- | 0.126 | 0.515 |
| X4 | 0.109 | 0.545 | | -- | 0.142 | 0.283 |
| X5 | 0.551* | <0.001 | | -- | 0.564* | <0.001 |
| X6 | 0.280* | 0.024 | | -- | 0.197 | 0.386 |
| X7 | 0.167 | 0.151 | 0.365* | 0.004 | 0.403* | 0.002 |
| X8 | 0.145 | 0.187 | 0.697* | <0.001 | 0.568* | <0.001 |
| X9 | 0.217 | 0.155 | 0.504* | <0.001 | 0.468* | 0.003 |
| X10 | 0.144 | 0.324 | 0.663* | <0.001 | 0.576* | <0.001 |
| X11 | 0.111 | 0.503 | 0.082 | 0.697 | 0.174 | 0.403 |
| X12 | 0.180 | 0.112 | 0.222* | 0.096 | 0.236 | 0.176 |
| X13 | 0.251 | 0.308 | 0.075 | 0.752 | 0.142 | 0.871 |

*significant at $p < 0.1$.



FIGURE 7
Interactions between the driving factors of the supply−demand relationship of ecosystem services.

guide the rational distribution and flows of their populations, so as to achieve a balance between the supply and demand of ecosystem services.

For the coordination degree of the SDES, evidently it was most impacted by X10 (population attractiveness), with a q value of 0.576. It was followed by X8 (industrial structure) > X5 (NDVI) > X9 (openness to the outside world) > X7 (economic strength) > X1 (annual average temperature) > X2 (annual rainfall). These indicators all passed the significance test at $p < 0.01$, which further shows that the spatial differentiation of the coordination degree of the SDES is affected by both natural and socio-economic factors; in general, the latter's explanatory power is greater than the former's. Looking ahead, we should strengthen ecosystem management and the optimal allocation of resources, and strive to alleviate the imbalance between the supply and demand of ecosystem services, to ensure both regional ecological security and sustainable socio-economic development.

### 3.4.2 Interactive detection analysis

The results of interaction detection analysis (Figure 7) revealed that the explanatory power of the interaction between the drivers of the spatial differentiation in the supply, demand, and supply–demand coordination of ES exceeds that of any single factor. Hence, the interaction between any two driving factors will always increase the explanatory power of the spatial differentiation in the supply–demand relationship. The interaction types among the driving factors consist of a nonlinear enhancement type and two-factor enhancement type, of which the former predominates in Jiangsu Province.

Among the interactive detection results for supply capacity, the interactions between NDVI and other factors had the strongest impact on its spatial differentiation. Among them, the explanatory power of NDVI interacting with elevation, slope, annual rainfall, or annual average temperature is highest, whose q values are 0.846, 0.841, 0.827, and 0.811, respectively. Next, we found strong effects of interactions on the spatial differentiation of supply capacity came from annual temperature∩slope (q value = 0.754), annual rainfall∩elevation (q value = 0.773), water network density∩population attractiveness (q value = 0.797), and water network density∩economic strength (q value = 0.794).

From the perspective of demand intensity, the interactions between population attractiveness, industrial structure, openness to the outside world and other factors all strongly impacted the spatial differentiation in demand intensity. Among them, population attractiveness∩facility supply has the greatest impact on the spatial differentiation in demand intensity, given its q value of 0.863. It is followed by industrial structure∩road density (q value = 0.841), industrial structure∩economic strength (q value = 0.810), and industrial structure∩openness to the outside world (q value = 0.791).

For the spatial differentiation in the degree of supply–demand coordination, it was most impact by the interactions between NDVI and other factors. Among these, the explanatory power of NDVI's interaction with elevation, annual rainfall, and industrial structure are each high, with respective q values = 0.873, 0.861, and 0.830. The interaction values between industrial structure and other factors are also large and noteworthy: the q value of industrial structure∩facility supply is 0.785 while that of industrial structure∩water network density is 0.774. The interaction intensity between openness to the outside world, population attractiveness, and other factors are also considerable, in that their explanatory power reaches more than 60%.

Overall, the NDVI and water network density exert a strong influence on the spatial differentiation in ecosystem service supply capacity. The interaction between population attractiveness and facility supply greatly impacts the spatial differentiation in demand intensity. The degree of supply–demand coordination is most significantly affected by the interaction between NDVI, industrial structure, openness to the outside world, population attractiveness, and other factors. Altogether then, the above results show that regional differences in the intensity of human activities underpin spatial heterogeneity in the relationship between supply and demand of ecosystem services. Population aggregation and the expansion of artificial surfaces not only occupy and destroy ecological land, but also lead to an imbalance between supply and demand, namely in the form of high demand for and low supply of ES. Therefore, in the future, we should consider the action characteristics of different driving factors and their interactive enhancement effects, and find reasonable way to develop and utilize precious water and soil resources. We should avoid undue interference from human activities and the joint adverse action of natural and socio-economic factors, to lessen the pressure on balancing the supply and demand of regional ecosystems.

## 4 Discussion

### 4.1 Comparison with other scholarship on supply of and demand for ecosystem services

As both theoretical and methodological research into ESS and ESD continues to expand and deepen, related practical and applied investigations are also being gradually carried out more often. Burkhard et al. (2012) took central Germany as an example, and based on the ecological integrity of biophysical landscape units and the matrix coupling of ecosystem service supply and demand, they used land cover data and socio-economic data assessment and assignment method to unify the ecosystem service supply and demand values into a single unit for quantitative expression. The supply and demand

capacities of ecosystem services for different land types were tabulated, and the spatial distribution of the supply and demand balance was also mapped. Kroll et al. (2012) analyzed the supply and demand characteristics of energy supply, food supply, and water supply services and their spatial distribution patterns along an urban-rural gradient in eastern Germany and proposed a quantitative calculation and spatial visualization method, which is of great significance for coordinating a sustainable regional balance. Based on the spatial differences in ESS and ESD and their balance, some scholars have distinguished different types and levels of control areas and proposed differentiated control strategies, in order to provide practical guidance for regional ecosystem management and territorial space optimization (Li et al., 2020; Sun et al., 2022). In addition, other scholars have also applied the relationship between ESS and ESD to identify source sites or corridors for construction for use in an ecological network, so as to achieve the latter's spatial optimization (Zhang et al., 2019; Rong et al., 2020). Our study assesses the ESS based on the equivalent factor method, measures the ESD using a comprehensive multi-indicator model, reveals the changes in the coordination degree of the SDES, and analyzes the factors influencing their spatial differentiation characteristics. The relationship between supply and demand of ESS in Jiangsu Province is similar to that of the Yangtze River Delta region, Beijing–Tianjin–Hebei region, and Xiamen–Zhangzhou–Quan region (Wu et al., 2018; Li et al., 2020; Hu and Chen, 2021). On the one hand, the ESD is robust in areas with a high level of economic development and high population density; on the other hand, the ESS is weakening in those areas with an increasing intensity of disturbance from human activities. The geodetector-based analysis of drivers showed that natural environmental factors have the greatest influence on ESS, while socio-economic factors most influence ESD and the coordination of SDES, consistent with the findings of Zhao et al. (2021).

## 4.2 Factors influencing the ecosystem services, ecosystem service demand and coordination of supply of and demand for ecosystem services

As a bridge between natural ecosystems and human society, the SDES reflects the complex dynamic linkages between ecosystems and human society (Sun et al., 2019). Changes in ESS, ESD, and the coordination of SDES are jointly influenced by many factors, such as the natural environment, social economy, and so on (Tang et al., 2020). In this respect, we used the analytical method of geodetector to reveal the reasons behind the spatial variation of ESS, ESD and the coordination of SDES in the study area in 2020. We explored correlations between the three aspects of ESS, ESD and the coordination of SDES as well as their influencing factors, which to some extent reflected the internal mechanisms and driving mechanisms of the

supply–demand balance of ecosystem services. For the natural environmental factors, we found that their variability over 20 years was not significant. For example, the variability of factors including average annual temperature, elevation, and water network density is small over time. Therefore, our study did not consider the temporal variability characteristics of the factors influencing ecosystem services, but used the driving factors of 2020 to analyze the spatial variability of ESS, ESD, and the coordination of SDES in 2020 (Zhang et al., 2021). Nor did we consider policy factors due to restrictions in accessing the required data. Further, it is imperative to determine the combined mechanisms of various types of influencing factors in different regions and the levels of differing factors, this represent an important research avenue in the future.

## 4.3 Limitation and further research

This paper only used three indicators, namely population density, economic density, and land development intensity, to characterize the ESD, which may not be able to comprehensively measure the true demand level. In the next research stage, we will consider using scenario formulation and simulation to build a more comprehensive measurement model of ESD. From the spatial scale of this study, we should strengthen research on the supply–demand relationship of ES assessed at different spatial scales. We need to gradually establish a regional and hierarchical governance mechanism for the SDES, and coordinate the supply and demand relationship at different levels in different regions, so as to alleviate the supply/demand imbalances. In tandem, we should seek to ensure the scientificity, continuity, and consistency of supply and demand governance policies of ES at different levels, to thereby maximize the benefits of ES for human society.

## 5 Conclusion

Based on the county-level administrative divisions of Jiangsu Province, and taking its 68 geographical units as the study object, this paper used the revised equivalent factor table to calculate the ESS in 2000, 2010, and 2020. In parallel, the ESD was quantitatively evaluated in combination with the intensity of land development, population density, and economic density. Supported by the coupling coordination degree and relative development degree model, we explored the coordination degree of and change in the supply–demand relationship of ecosystem services, and analyzed the driving factors of the spatial differentiation of that relationship by using geodetector. The main conclusions drawn are as follows:

1) Since 2000, the overall ESS in Jiangsu Province has shown a spatial distribution pattern of being high in the Taihu

Lake Plain area, the southwest of Huaihai area, and the eastern coastal zone of Jiangsu Province, yet low in the northwest and middle of Huaihai area, and along the Yangtze River Plain. 2) The ESD is generally high in the north and south of Jiangsu Province and low in its middle. Furthermore, The ESD in each research unit is increasing albeit not equally so (differing range of values), and overall, the key feature of this trend is that it gradually weakens going from the south to north of Jiangsu Province. 3) The degree of supply–demand coupling and coordination of ES is generally high in both the north and south, but low in the middle of the province. In the recent 20 years, the relationship between supply and demand has improved, and the type of supply–demand coupling and coordination has changed from one of moderate imbalance to one of basic coordination. 4) Through the factor detection and interactive detection analysis of geodetector, we find that the impact of various factors on the supply, demand and coordination of supply and demand of ES are not independent, but rather arise from the synergy of multiple factors. The main factors influencing the ESS capacity are the NDVI and water network density, while those affecting the ESD are industrial structure, population attractiveness, and openness to the outside world. Meanwhile, the main contributing factors to the coordination of the SDES are population attractiveness, industrial structure, and the NDVI.

## Data availability statement

The original contributions presented in the study are included in the article/Supplementary Material, further inquiries can be directed to the corresponding author.

## References

Bukvareva, E., Zamolodchikov, D., Kraev, G., Grunewald, K., and Narykov, A. (2017). Supplied, demanded and consumed ecosystem services: prospects for national assessment in Russia. *Ecol. Indic.* 78, 351–360. doi:10.1016/j.ecolind.2017.03.034

Burkhard, B., Kroll, F., Nedkov, S., and Muller, F. (2012). Mapping ecosystem service supply, demand and budgets. *Ecol. Indic.* 21, 17–29. doi:10.1016/j.ecolind.2011.06.019

Costanza, R., d'Arge, R., de Groot, R., Farber, S., Grasso, M., Hannon, B., et al. (1997). The value of the world's ecosystem services and natural capital. *Nature* 387, 253–260. doi:10.1038/387253a0

Dai, X., Wang, L., Huang, C., Fang, L., and Wang, S. (2020). Spatio-temporal variations of ecosystem services in the urban agglomerations in the middle reaches of the yangtze river, China. *Ecol. Indic.* 115, 106394. doi:10.1016/j.ecolind.2020.106394

Dai, X., Wang, L., Tao, M., Huang, C., Sun, J., and Wang, S. (2021). Assessing the ecological balance between supply and demand of blue-green infrastructure. *J. Environ. Manag.* 288, 112454. doi:10.1016/j.jenvman.2021.112454

Dai, X., Wang, L., Yang, L., Wang, S., and Li, Y. (2022). Predicting the supply–demand of ecosystem services in the yangtze river middle reaches urban

## Author contributions

Conceptualization, YW; formal analysis, YW and HL; funding acquisition, XZ; investigation, YW and HL; methodology, YW; software, YW; supervision, HL, XZ and TL; validation, YW and XZ; writing—original draft, YW; writing—review & editing, HL and TL. All authors have read and agreed to the published version of the manuscript.

## Funding

## Conflict of interest

The authors declare that the research was conducted in the absence of any commercial or financial relationships that could be construed as a potential conflict of interest.

## Publisher's note

agglomeration. *Prog. Phys. Geogr. Earth Environ.* 46, 530–546. doi:10.1177/03091333221074490

Daily, G. C. (1997). *Nature's service: Societal dependence on natural ecosystems.* 4th ed. Washington DC: Island Press, 49.

Ecosystem Assessment, M. (2005). *Ecosystems and human well-being: Biodiversity synthesis.* Washington, D C: Island Press.

Fang, L., Wang, L., Chen, W., Sun, J., Cao, Q., Wang, S., et al. (2021). Identifying the impacts of natural and human factors on ecosystem service in the Yangtze and Yellow River Basins. *J. Clean. Prod.* 314, 127995. doi:10.1016/j.jclepro.2021.127995

Geijzendorffer, I. R., Martin-Lopez, B., Roche, P. K., et al. (2015). Improving the identification of mismatches in ecosystem services assessments. *Ecol. Indic.* 52, 320–331. doi:10.1016/j.ecolind.2014.12.016

Geng, T., Chen, H., Zhang, H., Qin-qin, S., and Di, L. (2020). Spatiotemporal evolution of land ecosystem service value and its influencing factors in Shaanxi province based on GWR. *J. Nat. Resour.* 35, 1714–1727. doi:10.31497/zrzyxb.20200715

Han, Z., Liu, C., Yan, X., et al. (2021). Coupling coordination and matches in ecosystem services supply-demand for ecological zoning management: A case study of dalian. *Acta Ecol. Sin.* 41, 9064–9075.

Han, Z., Zhao, Y., Yan, X., et al. (2020). Coupling coordination mechanism and spatial-temporal relationship between gross ecosystem product and regional economy: a case study of dalian. *Econ. Geogr.* 40, 1

Hu, Q., and Chen, S. (2021). Optimizing the ecological networks based on the supply and demand of ecosystem services in xiamen-zhangzhou-quanzhou region. *J. Nat. Resour.* 36 (2), 342–355. doi:10.31497/zrzyxb.20210206

Jing, H., Liu, Y., He, P., et al. (2022). Spatial heterogeneity of ecosystem services and it's influencing factors in typical areas of the qinghai-tibet plateau: A case study of nagqu city. *Acta Ecol. Sin.* 42 (7), 265

Kramer, K., Bouriaud, L., Feindt, P. H., van Wassenaer, L., Glanemann, N., Hanewinkel, M., et al. (2022). Roadmap to develop a stress test for forest ecosystem services supply. *One Earth* 5, 25–34. doi:10.1016/j.oneear.2021.12.009

Kroll, F., Müller, F., Haase, D., and Fohrer, N. (2012). Rural–urban gradient analysis of ecosystem services supply and demand dynamics. *Land Use Policy* 29, 521–535. doi:10.1016/j.landusepol.2011.07.008

Li, C., and Zhao, J. (2022). Research on spatiotemporal pattern and influencing factors of supply-demand matching in the Yangtze River Delta urban agglomeration." in *Ecological economy*. http://kns.cnki.net/kcms/detail/53.1193.F.20220104.1629.002.html.

Li, R., Li, Y., and Hu, H. (2020). Support of ecosystem services for spatial planning theories and practices. *Acta Geogr. Sin.* 75 (11), 2417–2430.

Li, S. (2014). *Ecosystem service geography*. Beijing: Science Press.

Li, S., Wang, Y., Zhu, W., et al. (2014). Research framework of ecosystem services geography from spatial and regional perspectives. *Acta Geogr. Sin.* 69, 1628.doi:10.11821/dlxb201411004

Li, S., Zhang, C., Liu, J., et al. (2013). The tradeoffs and synergies of ecosystem services: Research progress, development trend, and themes of geography. *Geogr. Res.* 32, 1379–1390.

Li, Z., and Zhang, X. (2017). Spatial differentiation and influencing factors of eco-economic harmony at county level in Jiangsu province. *Res. Soil Water Conservation* 24, 209–215.

Liu, H., Gao, J., Liu, X., et al. (2020). Monitoring and assessment of the ecosystem services value in the national key ecological function zones. *Acta Ecol. Sin.* 40, 1865.doi:10.5846/stxb201903010382

Liu, L., Liu, C., Wang, C., et al. (2019). Supply and demand matching of ecosystem services in loess hilly region: A case study of lanzhou. *Acta Geogr. Sin.* 74, 1921

Liu, Y., Yang, Z., Xu, G., et al. (2022). Correlation between ecosystem services value and human activity intensity based on the four-quadrant model: a case study in the international tourism and culture demonstration area, the south anhui province. *Acta Ecol. Sin.* 42, 1.doi:10.5846/stxb202103030579

Lv, C., Lan, X., and Sun, W. (2017). A study on the relationship between natural factors and population distribution in beijing using geographical detector. *J. Nat. Resour.* 32, 1385. doi:10.11849/zrzyxb.20160707

Ma, L., Liu, H., Peng, J., et al. (2017). A review of ecosystem services supply and demand. *Acta Geogr. Sin.* 72, 127

Ou, W., Wang, H., and Tao, Y. (2018). A land cover-based assessment of ecosystem services supply and demand dynamics in the Yangtze River Delta region. *Acta Ecol. Sin.* 38, 6337

Peng, J., Yang, Y., Xie, P., et al. (2017). Zoning for the construction of green space ecological networks in Guangdong Province based on the supply and demand of ecosystem services. *Acta Ecol. Sin.* 37, 4562. doi:10.5846/stxb201601020007

Rong, Y., Yan, Y., Wang, C., et al. (2020). Construction and optimization of ecological network in Xiong'an New Area based on the supply and demand of ecosystem services. *Acta Ecol. Sin.* 40 (20), 7197. doi:10.5846/stxb202001020016

Serna-Chavez, H. M., Schulp, C. J. E., Van Bodegom, P. M., Bouten, W., Verburg, P., and Davidson, M. (2014). A quantitative framework for assessing spatial flows of ecosystem services. *Ecol. Indic.* 39, 24–33. doi:10.1016/j.ecolind.2013.11.024

Shen, J., Li, S., Liang, Z., Wang, Y. y., and Sun, F. y. (2021). Research progress and prospect for the relationships between ecosystem services supplies and demands. *J. Nat. Resour.* 36, 1909–1922. doi:10.31497/zrzyxb.20210801

Simonit, S., and Perrings, C. (2011). Sustainability and the value of the 'regulating' services: Wetlands and water quality in Lake Victoria. *Ecol. Econ.* 70, 1189–1199. doi:10.1016/j.ecolecon.2011.01.017

Sun, R., Jin, X., Han, B., Liang, X., Zhang, X., and Zhou, Y. (2022). Does scale matter? Analysis and measurement of ecosystem service supply and demand status based on ecological unit. *Environ. Impact Assess. Rev.* 95, 106785. doi:10.1016/j.eiar.2022.106785

Sun, Y., Liu, S., Dong, Y., An, Y., Shi, F., et al. (2019). Spatio-temporal evolution scenarios and the coupling analysis of ecosystem services with land use change in China. *Sci. Total Environ.* 681, 211–225. doi:10.1016/j.scitotenv.2019.05.136

Tang, X., Liu, Y., and Pan, Y. (2020). An evaluation and region division method for ecosystem service supply and demand based on land use and POI data. *Sustainability* 12 (6), 2524. doi:10.3390/su12062524

Villamagna, A. M., Angermeier, P. L., and Bennett, E. M. (2013). Capacity, pressure, demand, and flow: A conceptual framework for analyzing ecosystem service provision and delivery. *Ecol. Complex.* 15, 114–121. doi:10.1016/j.ecocom.2013.07.004

Wang, C., and Tang, N. (2018). Spatio-temporal characteristics and evolution of rural production-living-ecological space function coupling coordination in Chongqing Municipality. *Geogr. Res.* 37, 1100

Wang, J., Li, X., Christakos, G., Liao, Y., Zhang, T., Gu, X., et al. (2010). Geographical detectors-based health risk assessment and its application in the neural tube defects study of the Heshun region, China. *Int. J. Geogr. Inf. Sci.* 24, 107–127. doi:10.1080/13658810802443457

Wang, J., and Xu, C. Geodetector (2017). Instrumental networking and social network building: How horizontal networking and upward networking create social capital. *Acta Psychol. Sin.* 72, 116–134. doi:10.3724/sp.j.1041.2017.00116

Wang, J., Zhai, T., Lin, Y., and Kong, X. (2019). Spatial imbalance and changes in supply and demand of ecosystem services in China. *Sci. Total Environ.* 657, 781–791. doi:10.1016/j.scitotenv.2018.12.080

Wang, J., and Zhou, W. (2019). Ecosystem service flows: Recent progress and future perspectives. *Acta Ecol. Sin.* 39, 4213–4222.

Wang, Y., Xu, X., Zhuang, D., et al. (2021). Evolution of the supply and demand pattern of ecosystem services in Hunan Province. *Chin. J. Ecol.* 40, 3268. doi:10.13292/j.1000-4890.202110.029

Wei, H., Fan, W., Wang, X., Lu, N., Dong, X., Zhao, Y., et al. (2017). Integrating supply and social demand in ecosystem services assessment: A review. *Ecosyst. Serv.* 25, 15–27. doi:10.1016/j.ecoser.2017.03.017

Wu, A., Zhao, Y., shen, H., et al. (2018). Spatio-temporal pattern evolution of ecosystem service supply and demand in beijing-tianjin-hebei region. *J. Ecol. rural Environ.* 34 (11), 968. doi:10.11934/j.issn.1673-4831.2018.11.002

Wu, J., Men, X., Liang, J., et al. (2020). Research on supply and demand equilibrium of ecosystem services in Guangdong Province based on the gini coefficient. *Acta Ecol. Sin.* 40, 6812.

Xiao, Y., Xie, G., and An, K. (2003). The function and economic value of soil conservation of ecosystems in Qinghai-Tibet Plateau. *Acta Ecol. Sin.* 23, 2367–2378.

Xiao, Y., Xie, G., Lu, C., et al. (2016). Involvement of ecosystem service flows in human wellbeing based on the relationship between supply and demand. *Acta Ecol. Sin.* 36, 3096. doi:10.5846/stxb201411172274

Xie, G., Zhang, C., Zhang, L., et al. (2015). Improvement of the evaluation method for ecosystem service value based on per unit area. *J. Nat. Resour.* 30, 1243. doi:10.11849/zrzyxb.2015.08.001

Xie, G., Zhen, L., Lu, C., et al. (2008). Expert knowledge based valuation method of ecosystem services in China. *J. Nat. Resour.* 23, 911.

Xu, L., Xu, X., Luo, T., et al. (2012). Services based on land use: A case study of bohai rim. *Geogr. Res.* 31, 1775

Yang, J., and Huang, X. (2021). The 30 m annual land cover dataset and its dynamics in China from 1990 to 2019. *Earth Syst. Sci. Data* 13, 3907–3925. doi:10.5194/essd-13-3907-2021

Zhai, T., Wang, J., Jin, Z., et al. (2019). Change and correlation analysis of the supply-demand pattern of ecosystem services in the Yangtze River Economic Belt. *Acta Ecol. Sin.* 39, 5414.

Zhang, C., Li, Z., Zeng, H., et al. (2022). Scale effects on ecosystem service trade-off and its influencing factors based on wavelet transform: A case study in the Pearl River Delta, China. *Geogr. Res.* 41 (5), 1279. doi:10.11821/dlyj020210482

Zhang, D., Qu, L., and Zhang, J. (2019). Ecological security pattern construction method based on the perspective of ecological supply and demand: A case study of Yangtze River Delta. *Acta Ecol. Sin.* 39 (20), 7525.. doi:10.5846/stxb201808301854

Zhang, K., Liu, T., Feng, R., and Zhang, Z. (2021). Coupling coordination relationship and driving mechanism between urbanization and ecosystem service value in large regions: a case study of urban agglomeration in yellow River Basin, China. *Int. J. Environ. Res. Public Health* 18 (15), 7836. doi:10.3390/ijerph18157836

Zhang, L., and Fu, B. (2014). The progress in ecosystem services mapping: a review. *Acta Ecol. Sin.* 34, 316.

Zhao, X., Su, J., Wang, J., et al. (2021). A study on the relationship between supply-demand relationship of ecosystem services and impact factors in Gansu Province. *China Environ. Sci.* 41, 4926

Check for updates

# Identification of fragmented cropland in arid and semiarid sandy areas: a case study of horqin left rear banner

Zhiting Sang[1], Jie Liang[1], Huihui Zheng[1], Kaige Wang[1], Yan Xu[1,2]* and Yibin Liu[1]

[1]College of Land Science and Technology, China Agricultural University, Beijing, China, [2]Key Laboratory of Land Quality Ministry of Land and Resources, China Center, Hohhot, China

The sustainable development and utilization of sandy areas in arid and semiarid regions is of strategic importance to ensure both food and ecological security. The unique geographical environment of these areas and uncontrolled exploitation by farmers lead to large amounts of fragmented cropland. Despite government management, the quantity and distribution of these fragmented croplands is unknown, and accurate identification of the region's fragmented croplands can provide data to support the sustainable use of sandy areas. We propose a method for identifying fragmented cropland based on scale transformation. Small-scale fragmented cropland is approximately represented at larger scales, so we apply small-scale high-resolution remote sensing images to identify features and obtain information at a large scale, i.e., the ratio of fragmented cropland area. By correcting the cropland areas identified from low-resolution remote sensing images and using them as the basis for the resulting calculation, more accurate identification can be 1 at a large scale. In this study, this method was applied based on remote sensing images with 0.54 and 30 m resolutions that were acquired during the same period, using Horqin Zuoyihou Banner as the study area. The results showed that (1) there was 13,637.08 hm² of fragmented cropland in Horqin Zuoyihou Banner due to precipitation and terrain topography, mainly in the central and western regions and 2) identification at the sample point scale and plot scale were positively correlated in area and showed a consistent distribution. Therefore, accurate and efficient identification of fragmented cropland can be achieved through scale transformation.

# 1 Introduction

A large amount of fragmented cropland exists in arid and semiarid sandy regions. In addition to natural land fragmentation due to the sandy terrain, the lack of effective regulation and planning has created a large amount of fragmented cropland due to disorderly development and replenishment of cropland (Tan et al., 2006; Zhao, 2011; Jia and Petrick, 2014). Arid and semiarid areas are not only important food production bases in China (Li et al., 2021), but also ecologically fragile areas (Huang et al., 2019; Xu et al., 2021). Facing the dual needs of food security and ecological safety, mapping the amount and distribution of fragmented cropland is the basis for making decisions on the consolidation and removal of cropland (Xiong et al., 2020; Vijay and Armsworth, 2021), and it will also support the sustainable use of sandy areas (Lyu et al., 2020; Wang et al., 2021). The identification of fragmented cropland, which covers a small area but is very common, is limited in many ways, and the quantity and spatial distribution of fragmented cropland are not yet known. Therefore, the efficient and accurate acquisition of information about the quantity and distribution of fragmented cropland on a large scale, as the basis of sustainable use studies and site-specific studies (Wan and Ceng, 2001; Ye et al., 2004; Matton et al., 2015; Lu et al., 2018), is a key issue in land cover identification and is one of the important research directions for research on land cover identification.

Current identification methods for land cover types fall into three broad categories. The first identification method is based on manual mapping and user experience (Zhang et al., 2014; Qu et al., 2021): objects are discriminated based on experience combined with field calibration. This method relies on the empirical knowledge of the researcher, and the identification results have relatively high accuracy but limited applicability and suitability for larger study areas.

The second method is based on existing data processing, which means that results are obtained by processing remote sensing images or existing datasets (Chen Yuanyuan et al., 2012; Ren Yang et al., 2020; Feng et al., 2017; Li et al., 2017; Xiong et al., 2017; Feng et al., 2018). For example, Milbrandt analyzed and summarized data from the USGS 2006 National Land Cover Database to obtain information on the amount and distribution of marginal lands in the United State (Milbrandt et al., 2014). Similarly, Xue used the summary statistics (analysis) tool in ArcGIS 10.1 to calculate the total area of each land type based on the 2000 1 km × 1 km gridded dataset from the Earth System Science Data Sharing Infrastructure (http://www.geodata.cn/) (Xue et al., 2016). Compared with the first method, this approach is not limited in its scope of application. However, the spatial resolution of the images used in large-scale datasets is too low to obtain accurate results when identifying small objects.

The third method uses layer-by-layer screening, that is, in a study area, screening is carried out sequentially one layer at a time by selecting indicators to exclude areas that do not meet search requirements to identify research objects (Du et al., 2020). Fang et al. adopted satellite images with a 30 m resolution to identify marginal land by selecting indicators such as land use type and land cover type and considering environmental impact (Wang and Shi, 2015). Alternatively, Ben et al. used ZY-3 3D land-cover products and the Chinese soil database to exclude land unsuitable for cultivation, conduct screening based on relevant indicators of land quality and crop environment, and finally identify urban marginal land (Zhang et al., 2021). This approach reduces the limitations of the second method, with which results with relatively low accuracy are produced. However, there are still shortcomings when identifying objects with unclear characteristics, which may result in objects being screened out mistakenly.

These findings indicate that results based on manual empirical identification are the most accurate when compared to other identification methods, but this method is limited by the size of the study area that can be addressed. The results achieved by processing existing data address the study area size limitation, but they are still limited by the classification and spatial resolution of the original dataset. For example, when identifying fragmented cropland, original datasets may not contain this land cover type, and the relatively low spatial resolution of the data does not allow the identification of fragmented cropland. Although the layer-by-layer screening method improves on the first two methods, identification of objects with this approach relies on restrictive conditions. Generally, this approach is suitable for identifying relatively obvious characteristics. For example, when identifying an object that is easily confused with other features, such as fragmented cropland, it is difficult to choose a suitable index and establish screening rules for identification.

At present, the identification of fragmented cropland is mainly restricted by the size of the study area, spatial resolution of remote sensing images and feature interpretation characteristics. Methods that provide accurate identification are used in small areas but the remote sensing images used in the methods applied to large areas have low resolution, resulting in less accurate results. Identification based on high-resolution remote sensing images over large scales also faces challenges when identifying features with nonspecific characteristics, such as fragmented cropland.

The main purpose of this study is to explore how to identify fragmented cropland with nonspecific characteristics over a large scale by combining remote sensing images with two resolutions. Specifically, we first select samples in the identification area, which is divided into several sample areas and sample points. Then, we identified areas of fragmented cultivated land by integrating the interpretation of the remote sensing images

with different resolutions at different scales. This study can provide an effective measurement method for the identification of fine-grained cropland in arid and semiarid areas, and provide a valuable reference for other regions and countries in the world.

# 2 Materials and methods

## 2.1 Study area

Horqin Left Rear Banner, Tongliao city, Inner Mongolia Autonomous Region, was selected as the study area. It is located between 121°30′-123°42′E and 42°40′-43°42′N. This area is found at the intersection of the Horqin Sandy and Songliao Plains and the intersection of the East and West Liao Rivers, where there is an alluvial plain accounting for less than 3% of the total area. Except for the alluvial plain at the intersection of the East and West Liao Rivers, the rest of the landform is composed of sand dunes and meadows. Horqin Left Rear Banner is located on the border of the mid-temperate and subhumid areas, with a temperate continental monsoon climate. The spatial distribution of precipitation in the area varies greatly. The average annual precipitation is 414.9 mm, and precipitation amounts large enough to support rain-fed agriculture is usually concentrated from May to September, accounting for approximately 85% of the total annual precipitation. In 2019, the GDP of this region was $12.2 \times 10^9$ RMB, the per capita income of urban residents was 29,025 RMB, the per capita income of rural pastoral areas was 13,671 RMB, and the permanent population amounted to 401,100 people.

In general, the area of Horqin Zuoyihou Banner is large, and the landforms and precipitation in the eastern and western regions of the banner vary greatly. During the research process, it was found that the typical topography and precipitation conditions of Horqin Zuoyihou Banner led to a fine-grained distribution of some cropland in the banner and that there is a large amount of fragmented cropland, making it an ideal study area for this study.

## 2.2 Data

The data used in this study are mainly two contemporaneous remote sensing images of Horqin Left Rear Banner with different resolutions acquired by MapQuest: an image with a 0.54 m resolution acquired in 2021 and a remote sensing image with a 30 m resolution acquired in 2021. The 30 m resolution image was used for supervised classification in ENVI 5.3 to identify the cropland within the sample points and areas, and the 0.54 m resolution image was used for visual interpretation to identify the cropland within the sample points.

## 2.3 Methods

### 2.3.1 Methodological framework

The method described in this paper is the identification of fragmented cropland based on scale transformation (IBST), that is, the distribution of cropland and fragmented cropland at a small scale is used to determine the distribution at a large scale, and the result is calculated based on cropland area weighting by obtaining the total cropland area in a large sample area. The key step is to identify all the cropland (including fragmented cropland) at the large scale and use it as a database for calculation. Therefore, we used the large-scale low-resolution identification data as the basis and adjusted the results according to the difference in the cropland area identified in the images with different resolutions to obtain an estimate of the total cropland at the large scale. We divided this method into three steps: 1) the construction of scale relationships and the establishment of sample points and sample areas, 2) the identification of cropland and fragmented cropland and 3) the calculation of fragmented cropland based on cropland area weighting (Figure 1).

### 2.3.2 Scale relationship construction and sample layout
#### 2.3.2.1 Scale relationship construction

There is some connection between the identification results at large and small scales within a given region (Tobler, 1970; Woodcock and Strahler, 1987; Xu et al., 2011; Wang and Shi, 2015; Wang et al., 2018; Ain and He, 2019), but the conversion between scales needs to be corrected according to the setting (Li et al., 2000; Zhu et al., 2018). We were able to extend patterns observed at smaller scales to larger scales, so the parameter ratio of fragmented cropland (RFC) was introduced to visualize the link between large and small scales, replacing the large scale with the ratio of fragmented cropland obtained from the small scale. Additionally, the parameter area correction coefficient λ was introduced to control the accuracy of the identification according to the setting.

#### 2.3.2.2 Sample layout

To improve the accuracy of identification results over large areas, it is necessary to account for the scale conversion of subregions by establishing sample areas (unit level) and sample points (plot level) (Figure 2A). To reflect the differences and patterns in the distribution and number of recognition results, this method uses a uniform distribution of points to establish samples. The specific steps for establishing sample points and sample areas are as follows (Figure 2B).

After creating a 9 km × 9 km grid for uniform distribution, 144 sample areas covering the grid were selected in the Horqin Left Rear Banner, and a 1 km × 1 km sample point was selected in the center of each sample area. The distribution of identification targets within the sample points represents the distribution within the sample areas where they are located.
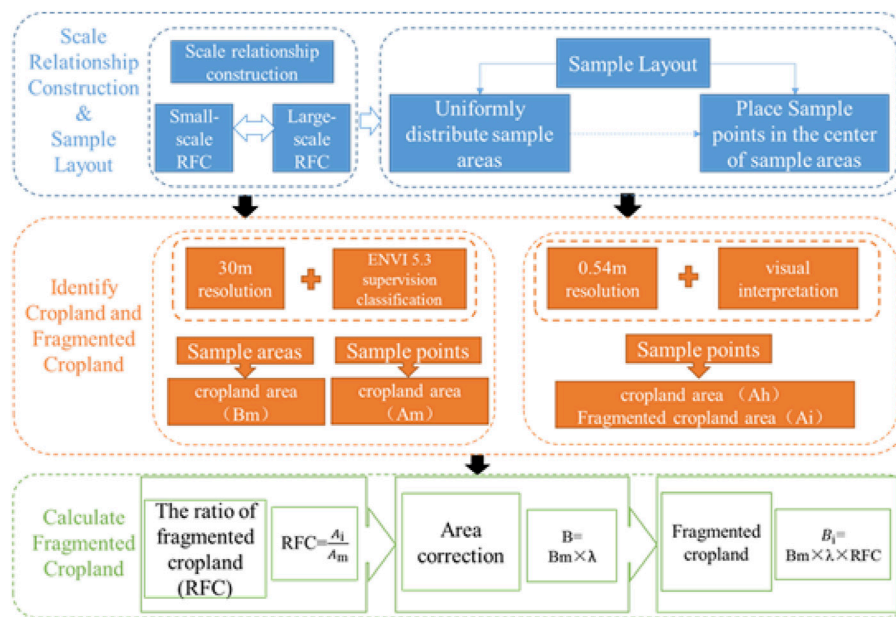
**FIGURE 1**
Research method framework.
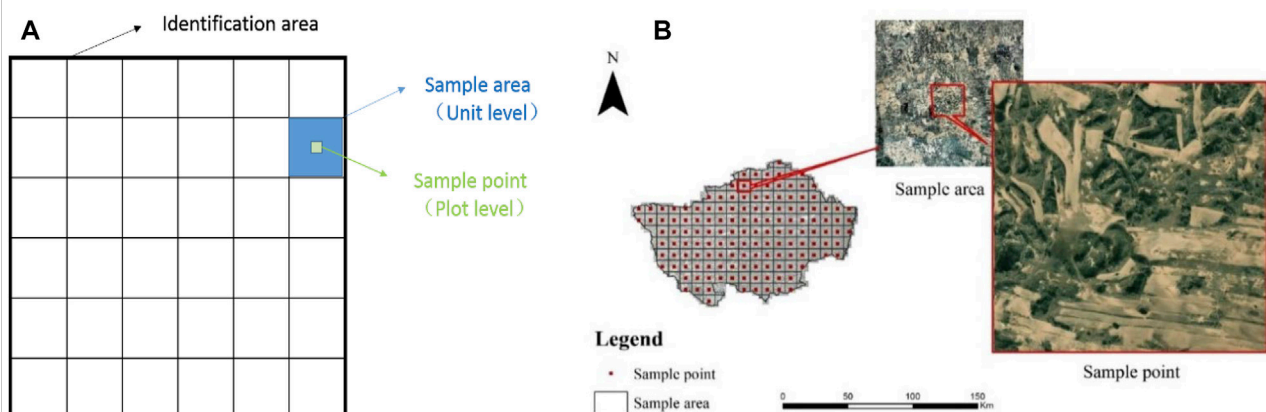


**FIGURE 2**
Diagram of the sample layout. **(A)** Scale construction; **(B)** sample layout.

## 2.3.3 Identification of cropland and fragmented cropland

The main target of identification in this study was fragmented cropland, namely, cropland in woodland, grassland or intermountain zones that is sporadically cultivated. These areas are small (not identifiable in low- and moderate-resolution images but identifiable in high-resolution

images; absolute area <2 ha) and varied in shape (mostly narrow or curved, multilateral, irregular plots). We found that most of the fragmented cropland is located next to large areas of cropland (cropland identified by low- and moderate-resolution images with absolute area ≥2 ha), and the area and distribution of large cropland can be used as a reference for determining the area and distribution of fragmented cropland. Thus, the identification of cropland based on low- and moderate-resolution remote sensing

images at large scales can be used as the basis for scale transformation calculations.

Identification was performed in two steps. The first step was the identification of cropland and fragmented cropland within the sample points using high-resolution imagery. Based on the remote sensing images with a 0.54 m resolution, the areas of cropland and fragmented cropland within the sample points were obtained by visual interpretation. Through this process, we were able to accurately identify the cropland and fragmented cropland within the sample points, and these data were then used to calculate the RFC.

The second step was to identify cropland within the sample points and sample areas using moderate-resolution imagery. Based on the 30 m resolution images, the supervised classification tool in ENVI 5.3 was used to identify the cropland within each sample point and sample area. Through this process, we were able to identify the area of cropland in each sample point and sample area. The area of cropland within each sample point was used to calculate the area correction coefficient λ for the sample area in which it was located, and the area of cropland within the sample area was the basis for the scale transformation.

### 2.3.4 Calculation of fragmented cropland based on cropland area weighting

The calculation of the area of fragmented cropland was divided into three main steps. The first step was to calculate the RFC within each sample point. The RFC is the proportion of fragmented cropland to all the cropland within the sample point. Based on the assumptions of the scale transformation, the RFC within a sample point could be replaced with the RFC within the sample area, thus obtaining the actual RFC within the sample area. The RFC was calculated as

$$RFL = \frac{A_i}{A_h} \tag{1}$$

where Ai is the area of fragmented cropland within the ith sample point identified using the image with a 0.54 m resolution and Ah is the area of all the cropland within the ith sample point identified using the image with a 0.54 m resolution.

The second step is the cropland area correction in each sample area. To correct the cropland area within a sample area, the area correction coefficient λ for that sample area was first obtained. We assume that the difference in image recognition results between the two accuracies at the sample point scale can still be reflected at the sample area scale. Based on this assumption, we constructed the area correction coefficient λi for the ith sample area based on the proportion of the area of large cropland plots (excluding fragmented cropland) identified from the images with two resolutions within the sample points. λi is calculated as

$$\lambda_i = \frac{A_h - A_i}{A_m} \tag{2}$$

where $A_m$ is the area of cropland within the ith sample point identified using remote sensing images with a 30 m resolution.

After obtaining the area correction coefficient of the sample area, we multiplied by the area of cropland within the sample area ($B_m$) to obtain the approximate total cropland area within the sample area (B). B is calculated as

$$B = B_m \times \lambda_i \tag{3}$$

The third step is to calculate the area of fragmented cropland in each sample area and in the study area. By multiplying the approximate total cropland in the sample area by the RFC of the sample area, we obtained the fragmented cropland area of the sample area ($B_i$). $B_i$ is calculated as

$$B_i = B \times \frac{A_i}{A_h} \tag{4}$$

The total area of fragmented cropland in the study area can be obtained by summing the area of fragmented cropland in all the sample areas. C is calculated as

$$C = \sum_{i=1}^{n} B_i \tag{5}$$

where C is the total area of fragmented cropland in the study area.

## 3 Results

### 3.1 Spatial distribution of fragmented cropland in the sample points

Among the 144 sample points selected, 73 did not contain fragmented cropland and these points were mostly distributed in the eastern part of Horqin Left Rear Banner, within a large area of farmland. A total of 71 sample points contained fragmented cropland, and the total area of fragmented cropland in the sample points fluctuated from 0.3056 hm² to 24.3425 h m²; the total area of fragmented cropland in each sample point was 195.9035 hm². Among the sample points, the largest total area of fragmented cropland within the sample points was found in central Horqin Zuoyihou Banner, while the minimum was found in western Horqin Zuoyihou Banner (Figure 3A). Among the sample points containing fragmented cropland, the range of cropland area within a 100 hm² sample point was between 1.83 hm² and 95.75 h m², with the maximum value occurring in south-central Horqin Zuoyihou Banner and the minimum value being found in western Horqin Zuoyihou Banner (Figure 3B). The quantitative distribution of the cropland within the sample points tended to coincide with that of the fragmented cropland.

RFC reflects the degree of fragmentation of cropland in the sample points, and the larger the value is, the more fragmented the cropland in the sample points. RFC was divided into four cases: 1)

**FIGURE 3**
Identification results. **(A)** Area of fragmented cropland in the sample points; **(B)** area of cropland in the sample points; **(C)** RFC for each sample point; **(D)** area of fragmented cropland in the sample areas.
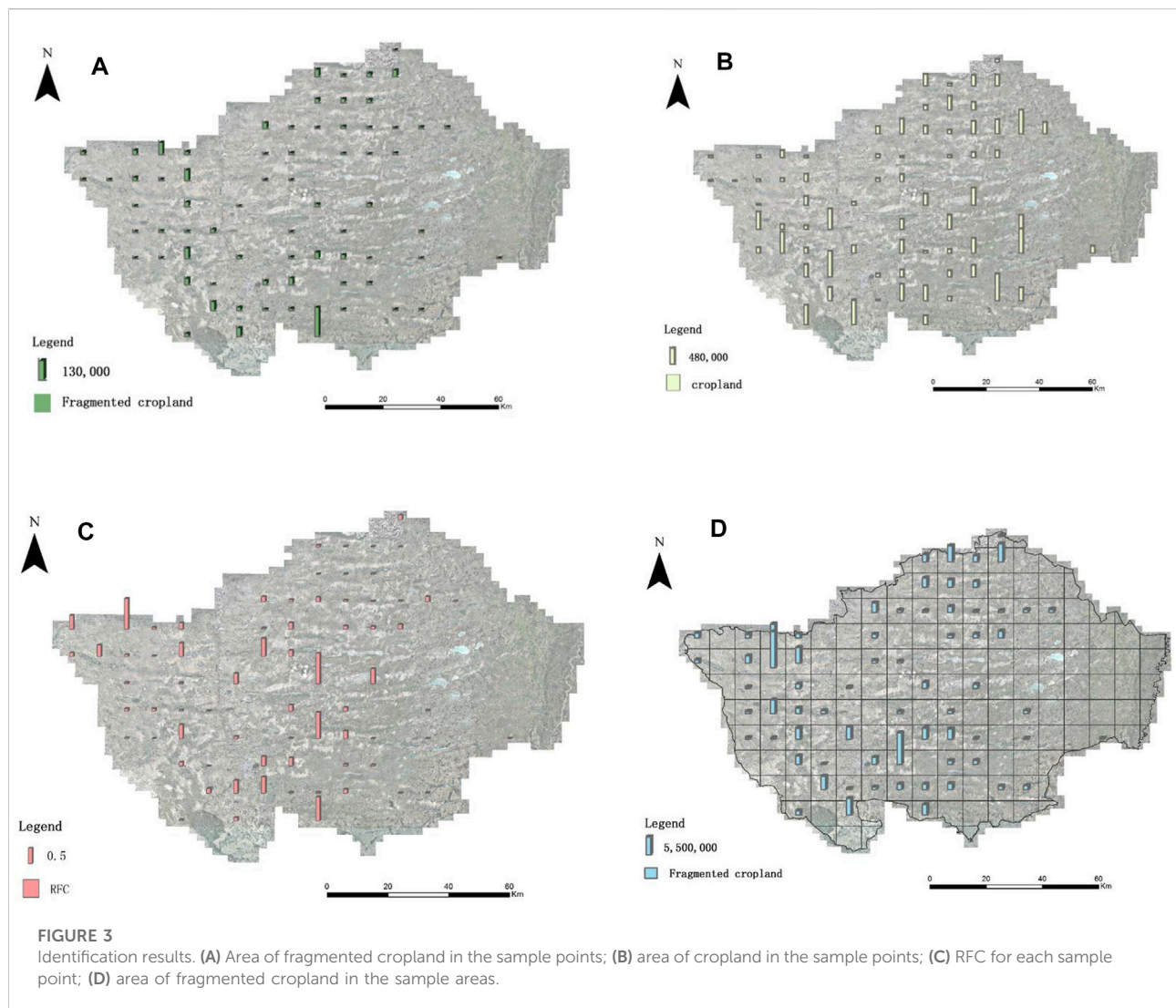
there was no fragmented cropland, RFC was zero, and the percentage of finely fragmented cropland in a total of 73 sample points in Horqin Zuoyihou Banner was zero. 2) Only fragmented cropland was present, and RFC was equal to one; a total of two sample sites had an RFC of 1, and these sites were distributed in western and central Horqin Zuoyihou Banner. 3) In the case of small cropland area, the closer the RFC was to 1, the higher the degree of cropland fragmentation in the sample point; conversely, the closer the RFC was to 0, the lower the degree of cropland fragmentation. 4) In the case of larger cropland areas, the value of RFC was low; nevertheless, the closer the RFC was to 1, the higher the degree of cropland fragmentation in the sample points. Similarly, the closer the RFC was to 0, the lower the degree of cropland fragmentation in the sample points, which mostly occurred in southwestern Horqin Zuoyihou Banner.

Within the sample points where fragmented cropland exists, the RFC ranges between 0.004 and 1, with the highest value occurring in central and western Horqin Zuoyihou Banner and the smallest value occurring in eastern Horqin Zuoyihou Banner (Figure 3C). The RFC ranges from 0.005 to 0.036 in the eastern sample points, from 0.016 to one in the central sample points, and from 0.004 to one in the western sample points in Horqin Zuoyihou Banner. Overall, the degree of fine cropland fragmentation is low in the eastern part of Horqin Zuoyihou Banner and high in the central and western parts of Horqin Zuoyihou Banner.

## 3.2 Distribution of fragmented cropland and its causes

The total area of fragmented cropland in Horqin Zuoyihou Banner is 13,637.08 h m², the area of cropland is 293,145.54 h m², and the fragmented cropland accounts for

4.65% of the cropland area. Currently, most of the fragmented cropland is not in the local governmental and national databases. In this study, a considerable amount of fragmented cropland was identified, and the compiled information on the distribution and quantity of these fragmented croplands provides support for cropland remediation and planning. In the sample area where the sample points with fragmented cropland exist, the total area of fragmented cropland ranges from $11.89\,hm^2$ to $1108.80\,h\,m^2$, and the maximum and minimum values are distributed in the western part of Horqin Zuoyihou Banner (Figure 3D). A comparison of the data revealed that the area of fragmented cropland at the sample points obtained based on the IBST method had a consistent distribution with the sample areas and that there was a positive correlation in quantity.

From east to west, the area and degree of fragmented cropland showed increasing trends, which is mainly caused by the topography of the area and distribution of water resources. The study area is characterized by high terrain in the west and low terrain in the east, and the topography redistributes water and heat so that less fragmented cropland exists in the flatter eastern region and more fragmented cropland exists in the central and western regions, which are interspersed with sand dunes and meadows. In addition, the eastern region is rich in water resources, and there are two rivers used for transit in the region (the Dongliao River and the Xiliao River), so the water resources required for cultivation are sufficient. Therefore, concentrated and continuous cropland is distributed in most of the eastern region, and the amount of fragmented cropland is very limited.

# 4 Discussion

## 4.1 Significance of the identification results

The fragmented cropland in Horqin Zuoyihou Banner accounts for 4.65% of the total cropland. Thus, the fragmented cropland occupies a large part of the cropland resources. The identification results obtained using the IBST method enabled us to determine the distribution and quantity of fragmented croplands, which provides a basis for estimating the carrying capacity of the land, availability of water resources and carrying out land remediation. Currently, arable land resources are limited, and fragmented cropland has become increasingly important in the integration and planning of cropland resources. Information on its quantity and distribution can also support the sustainable development of cropland in arid and semiarid areas with sandy land cover. In these situations, it is extremely important to perform highly precise identification over large areas.

## 4.2 Features and contributions of IBST

The findings of this study show that IBST can efficiently and accurately identify fragmented cropland from a larger study area. To better understand this method, IBST was analyzed from two perspectives: the characteristics of the IBST method and the contribution of the IBST method to the existing identification methods.

### 4.2.1 Features of the IBST method

One of the important features of the IBST method is that it introduces the concept of scale transformation, which enhances recognition efficiency. The accurate identification of the RFC at small scales is upscaled to large scales, simplifying identification at large scales. The second feature is that the IBST method corrects and controls results to improve the accuracy of the identification results. The IBST method introduces the area correction factor λ, which is an important parameter that corrects and controls the results according to the observed situation and improves the accuracy of the identification results.

### 4.2.2 Contributions of the IBST method

The main contribution of this study is to introduce a new identification method using the idea of scale transformation so that the new method can complement existing identification methods. Existing identification methods seldom select identification targets with small areas, large quantities and unclear characteristics over large areas, and IBST provides a new approach to identifying such targets that takes into account efficiency and accuracy. The results of this study showed that this new approach is feasible and that IBST can effectively identify fragmented cropland over a large study area.

# 5 Conclusion

In this study, we applied the IBST method over a large scale and effectively used remote sensing images with two resolutions to create a new approach for the identification of irregular fragmented cropland with unclear characteristics. This article is mainly based on the idea that the patterns observed at small scales can be extended to large scales, and the IBST approach was proposed. We applied this method to Horqin Zuoyihou Banner. First, the study area was divided into 9 km × 9 km sample areas, and a 1 km × 1 km sample point was selected at the center of each sample area. Then, the high-resolution images were used to obtain the area of cropland and fragmented cropland within each sample point, from which the RFC was calculated. The area correction coefficient λ for each sample area was obtained using the difference between the two identification accuracies within the sample point for the results of large areas of cropland (excluding fine cropland). Finally, we corrected

the area of cropland in each sample area obtained from the low-resolution images, calculated the area of fragmented cropland in each sample area by combining the corresponding RFCs, and summed the results to obtain the area of fragmented cropland in the whole study area. We found that the total area of fragmented cropland in Horqin Zuoyihou Banner is 13,637.08 h m$^2$, the area of cropland is 293,145.54 h m$^2$, and the fragmented cropland accounts for 4.65% of the cropland area.

In contrast to existing identification methods, the IBST method is a complement to existing identification methods. IBST is complementary to manual experience-based recognition, enabling the application of visual interpretation to a large study area. It can also improve the accuracy and efficiency of identification by combining existing data processing and layer-by-layer screening recognition methods.

## Data availability statement

The original contributions presented in the study are included in the article/Supplementary Material, further inquiries can be directed to the corresponding author.

## Author contributions

YX and ZS designed the research; ZS wrote the main manuscript text; ZS, JL, and YL performed the data analysis and made figures and tables; ZS, HZ, KW, and YX provided conceptualization, investigation and methodology.

## Conflict of interest

The authors declare that the research was conducted in the absence of any commercial or financial relationships that could be construed as a potential conflict of interest.

## Publisher's note

All claims expressed in this article are solely those of the authors and do not necessarily represent those of their affiliated organizations, or those of the publisher, the editors and the reviewers. Any product that may be evaluated in this article, or claim that may be made by its manufacturer, is not guaranteed or endorsed by the publisher.

## References

Ain, Q., and He, J.-H. (2019). On two-scale dimension and its applications. *Therm. Sci.* 23, 1707–1712. doi:10.2298/tsci190408138a

Chen Yuanyuan, X. J., Li, J., Wang, Q., and Wang, X. (2012). Influence of the varied spatial resolution of remote sensing images on urban and rural residential information extraction. *Resour. Sci.* 34, 159.

Du, J., Quan, Z., Fang, S., Liu, C., Wu, J., Fu, Q., et al. (2020). Spatiotemporal changes in vegetation coverage and its causes in China since the Chinese economic reform. *Environ. Sci. Pollut. Res.* 27, 1144–1159. doi:10.1007/s11356-019-06609-6

Feng, Q., Chaubey, I., Cibin, R., Engel, B., Sudheer, K., Volenec, J., et al. (2018). Perennial biomass production from marginal land in the upper Mississippi river basin. *Land Degrad. Dev.* 29, 1748–1755. doi:10.1002/ldr.2971

Feng, Q., Chaubey, I., Engel, B., Cibin, R., Sudheer, K. P., Volenec, J., et al. (2017). Marginal land suitability for switchgrass, miscanthus and hybrid poplar in the upper Mississippi river basin (UMRB). *Environ. Model. Softw.* 93, 356–365. doi:10.1016/j.envsoft.2017.03.027

Huang, J., Ma, J., Guan, X., Li, Y., and He, Y. (2019). Progress in semi-arid climate change studies in China. *Adv. Atmos. Sci.* 36, 922–937. doi:10.1007/s00376-018-8200-9

Jia, L., and Petrick, M. (2014). How does land fragmentation affect off-farm labor supply: Panel data evidence from China. *Agric. Econ.* 45, 369–380. doi:10.1111/agec.12071

Li, C., Fu, B., Wang, S., Stringer, L., Wang, Y., Li, Z., et al. (2021). Drivers and impacts of changes in China's drylands. *Nat. Rev. Earth Environ.* 2, 858–873. doi:10.1038/s43017-021-00226-z

Li, H., Wu, Y., Huang, X., Sloan, M., and Skitmore, M. (2017). Spatial-temporal evolution and classification of marginalization of cultivated land in the process of urbanization. *Habitat Int.* 61, 1–8. doi:10.1016/j.habitatint.2017.01.001

Li, X., Wang, J., and Strahler, A. (2000). Scale effects and scaling-up by geometric-optical model. *Sci. China Ser. E-Technol. Sci.* 43, 17–22. doi:10.1007/bf02916574

Lu, H., Xie, H., He, Y., Wu, Z., and Zhang, X. (2018). Assessing the impacts of land fragmentation and plot size on yields and costs: A translog production model and cost function approach. *Agric. Syst.* 161, 81–88. doi:10.1016/j.agsy.2018.01.001

Lyu, Y., Shi, P., Han, G., Liu, L., Guo, L., Hu, X., et al. (2020). Desertification control practices in China. *Sustainability* 12, 3258. doi:10.3390/su12083258

Matton, N., Canto, G. S., Waldner, F., Valero, S., Morin, D., Inglada, J., et al. (2015). An automated method for annual cropland mapping along the season for various globally-distributed agrosystems using high spatial and temporal resolution time series. *Remote Sens.* 7, 13208–13232. doi:10.3390/rs71013208

Milbrandt, A. R., Heimiller, D. M., Perry, A. D., and Field, C. B. (2014). Renewable energy potential on marginal lands in the United States. *Renew. Sustain. Energy Rev.* 29, 473–481. doi:10.1016/j.rser.2013.08.079

Qu, Y., Dong, X., Zhan, L., Zhu, W., Wang, S., Ping, Z., et al. (2021), Achieving rural revitalization in China: A suitable framework to understand the coordination of material and social space quality of rural residential areas in the plain. *Growth and change.*

Ren Yang, C. C., Liu, Y., and Hualou, L. (2020). Spatial-temporal characteristics of rural residential land use change and spatial directivity identification based on grid in the bohai rim in China. *Geogr. Res.* 34, 1077.

Tan, S., Heerink, N., and Qu, F. (2006). Land fragmentation and its driving forces in China. *Land Use Policy* 23, 272–285. doi:10.1016/j.landusepol.2004.12.001

Tobler, W. R. (1970). A computer movie simulating urban growth in the detroit region. *Econ. Geogr.* 46, 234. doi:10.2307/143141

Vijay, V., and Armsworth, P. (2021). in Proceedings of the national academy of sciences of the united states of america, *Pervasive Cropland in Protected Areas Highlight Trade-Offs between Conservation and Food Security*, 118.

Wan, G., and Cheng, E. (2001). Effects of land fragmentation and returns to scale in the Chinese farming sector. *Appl. Econ.* 33, 183–194. doi:10.1080/00036840121811

Wang, F., and Shi, X. (2015). Geospatial analysis for utilizing the marginal land in regional biofuel industry: A case study in guangdong province, China. *Biomass Bioenergy* 83, 302–310. doi:10.1016/j.biombioe.2015.10.005

Wang, S., Li, D., Li, T., and Liu, C. (2021). Land use transitions and farm performance in China: A perspective of land fragmentation. *Land* 10, 792. doi:10.3390/land10080792

Wang, X., Yu, D., Wang, C., Pan, Y., Pan, J., Shi, X., et al. (2018). Variations in cropland soil organic carbon fractions in the black soil region of China. *Soil Tillage Res.* 184, 93–99. doi:10.1016/j.still.2018.07.010

Woodcock, C. E., and Strahler, A. H. (1987). The factor of scale in remote sensing. *Remote Sens. Environ.* 21, 311–332. doi:10.1016/0034-4257(87)90015-0

Xiong, J., Thenkabail, P. S., Tilton, J. C., Gumma, M. K., Teluguntla, P., Oliphant, A., et al. (2017). Nominal 30-m cropland extent map of continental africa by integrating pixel-based and object-based algorithms using sentinel-2 and landsat-8 data on google Earth engine. *Remote Sens.* 9, 1065. doi:10.3390/rs9101065

Xiong, X., Hu, M., Wen, N., Liu, L., Xie, J., Lei, F., et al. (2020). Progress and prospect of cultivated land extraction research using remote sensing. *J. Agric. Resour. Environ.* 37, 856–865. (in Chinese).

Xu, L., Zheng, C., and Ma, Y. (2021). Variations in precipitation extremes in the arid and semi-arid regions of China. *Int. J. Climatol.* 41, 1542–1554. doi:10.1002/joc.6884

Xu, N., Zhang, T., Wang, X., and Liu, H. (2011). Soil organic carbon storage changes in yangtze delta region, China. *Environ. Earth Sci.* 63, 1021–1028. doi:10.1007/s12665-010-0778-x

Xue, S., Lewandowski, I., Wang, X., and Yi, Z. (2016). Assessment of the production potentials of miscanthus on marginal land in China. *Renew. Sustain. Energy Rev.* 54, 932–943. doi:10.1016/j.rser.2015.10.040

Ye, G., Jiang, K., and Shi, J. (2004). Study on the consolidation potential of fragmentary land in farmland consolidation——cases study in yong chuan city, wan sheng district, Feng du xian, Wu Shan xian of chong qing city. *China Land Sci.*, 33–38. ISBN 1001-8158. (in Chinese).

Zhang, B., Yang, J., and Cao, Y. (2021). Assessing potential bioenergy production on urban marginal land in 20 major cities of China by the use of multi-view high-resolution remote sensing data. *Sustainability* 13, 7291. doi:10.3390/su13137291

Zhang, B., Zhang, F., Gao, Y., Li, C., and Zhu, F. (2014). Identification and spatial differentiation of rural settlements' multifunction. *Trans. Chin. Soc. Agric. Eng.* 30, 216–224. (in Chinese).

Zhao, K. (2011). Land fragmentation and its quantitative measurement method. *China Land Sci.* 25, 35–39+88. (in Chinese).

Zhu, A., Lu, G., Liu, J., Qin, C., and Zhou, C. (2018). Spatial prediction based on third law of Geography. *Ann. GIS* 24, 225–240. doi:10.1080/19475683.2018.1534890

Check for updates

# Production–living–ecological space transition and its eco-environmental effects based on an improved area-weighted method: A case study of Gangcheng District, a typical industrial base in China

Yanan Wei[1], Yong Zhang[2], Longfei Chen[2], Hongyan Chen[1]*, Xueqiang Zhang[2] and Peng Liu[3]

[1]National Engineering Research Center for Efficient Utilization of Soil and Fertilizer Resources, College of Resources and Environment, Shandong Agricultural University, Taian, China, [2]Shandong Institute of Territorial and Spatial Planning, Jinan, China, [3]Department of Agronomy, Shandong Agricultural University, Taian, China

In the context of rapid social and economic development, it is important to clarify the evolution process of production–living–ecological space (PLES) and its eco-environmental effects on the sustainable utilization of land resources on industrial bases. Based on existing research, it is difficult to accurately measure the differences in eco-environment quality caused by conversions between land-use types in different years. This paper puts forward an improved area-weighted calculation method of the eco-environmental quality index (EQI), combining the land-use transfer matrix and ecological contribution rate to analyze eco-environmental effects on typical industrial bases. The results show that PLES transitions in Gangcheng District from 2009 to 2020 have been mainly from agricultural production and grassland ecology to forest ecology space, from urban living to industrial production space, and from grassland ecology to agricultural production space. This improved method can capture the environmental changes caused by conversions between land-use types in different years. The EQI of agricultural production space increased from 0.373 to 0.388, while the EQI of forest ecology space decreased from 0.810 to 0.739, and the comprehensive EQI increased from 0.441 to 0.470, showing that the eco-environment quality of the study area was improved overall. The conversions of agricultural production and grassland ecology space to forest ecology space were the main factors in improving eco-environment quality, and the conversions of grassland and forest ecology to agricultural production and of agricultural production to industrial production space were the main reasons for the deterioration of eco-environment quality. This paper may contribute to the scientific planning of land-use direction, support the coordination of regional economic and ecological development, and provide case references for similar regions.

# 1 Introduction

During rapid urbanization and industrialization, land-use transitions may directly or indirectly impact regional eco-environments, leading to derived eco-environmental effects (Foley et al., 2005; Lambin and Meyfroidt, 2011; Zhang et al., 2011; Haas and Ban, 2014; Hu et al., 2016; Quintas-Soriano et al., 2016; Allington et al., 2017; Hanaõcek and Rodríguez-Labajos, 2018; Li et al., 2020; Long et al., 2020; Tian et al., 2020). The concept of production–living–ecological space (PLES) was first proposed in the report of the 18th National Congress of the Communist Party of China in 2012 (Hu, 2012), which stressed that "the production space should be intensive and highly efficient, the living space should be moderate and livable, and the ecological space should be unspoiled and beautiful" (Sun et al., 2020; Wang et al., 2020; Fu and Zhang, 2021). Research on land-use transitions and eco-environmental effects from the perspective of PLES is an important basis for optimizing the rational allocation of land resources and for constructing an ecological civilization, which has become a major topic in current research (Li et al., 2016; Liu et al., 2017; Asadolahi et al., 2018; Luo et al., 2018; Hu M. et al., 2019; Hu S. et al., 2019; Lou et al., 2019; Asabere et al., 2020; Tan et al., 2020; Xie et al., 2021; Wang et al., 2022). Eco-environmental quality index (EQI) can quantitatively describe the characteristics of eco-environmental quality and its spatial-temporal evolution, and it has been widely used since its proposal (Dong et al., 2021; Han et al., 2021; Wang Y. et al., 2021).

Research methods for quantitatively describing the relationship between land-use transitions and eco-environmental quality using EQI can be roughly divided into three types. The first method assigns each secondary land-use space a different weight as a unit. Li et al. assigned the secondary space to analyze the characteristics of land-use transitions and their impacts on the eco-environment in the central Guizhou region (Li et al., 2021). Wang et al. assigned the secondary space to explore the characteristics of land-use transitions and their impacts on eco-environmental quality in Yingtan City (Wang R. et al., 2021). This method is easy to assign and simple to construct, but it cannot capture the impacts of various land-use types on eco-environment quality. For example, the forest ecology space consists of woodland, shrubbery and other woodland, which have different impacts on the eco-environment. Therefore, this method cannot accurately quantify the impacts of different land-use types on eco-environment quality.

In the second method, each land-use type is assigned a different ecological weight according to its characteristics and their influence on the eco-environment. The EQI of secondary space is then calculated by the area-weighted method. For example, Hao et al. assigned different weights to each land-use type to explore the response characteristics of land-use change and eco-environment in the farming-pastoral ecotone of China (Hao and Ren, 2009). Gao et al. evaluated the relationship between land-use transition and eco-environment quality in Xining City, Qinghai Province by assigning a different weight to each land-use type and combining it with the transfer matrix (Gao et al., 2019). In contrast to the first method, the second can capture the relationship between land-use type and environmental quality and can meet the needs of a single-year environmental quality assessment. However, this eco-environment effect analysis requires a certain sequence of land use and environmental quality data from different years. The change in land-use area during a certain time series is usually large, and the impact on environmental quality in different years must be reflected.

The third method takes land-use types as assignment units and adopts the area-weighted method in different years to construct the index system. Each land-use type is given a different weight as a unit; taking the area of land-use types in each year into account, the EQI is calculated by an area-weighted method. For example, Kong et al. assigned different land-use types, calculated the average area in 1990, 2000, 2010, and 2018, and then calculated the EQI to measure PLES changes and their eco-environmental effects in China (Kong et al., 2021). To explore the eco-environmental effects of land-use transition in the Beijing–Tianjin–Hebei urban agglomeration, Yang et al. assigned different land-use types, calculated the EQIs for 1985, 1995, 2005, and 2018, and then calculated the average EQI to obtain the final index system (Yang et al., 2020a). Such methods not only reflect the relationships between different land-use types and environmental quality but also reflect the eco-environmental effect caused by land-use change in different years. However, in existing studies, the EQI of the secondary land-use space has been mostly determined by averaging the areas of land-use types in different years. This method can only represent the average impact degree of secondary land-use space on eco-environmental quality over a long time series and cannot accurately describe differences in secondary space in different years.

As the above analysis shows, the first method is simple and convenient but cannot describe the relationship between land-use types and eco-environment quality. The second considers eco-environment quality differences in different land-use types but cannot describe eco-environment quality differences caused by conversions between land-use types in different years. The third method considers eco-environment quality differences of land-use types in different years, combined with the area-weighted method, to meet the requirements of eco-
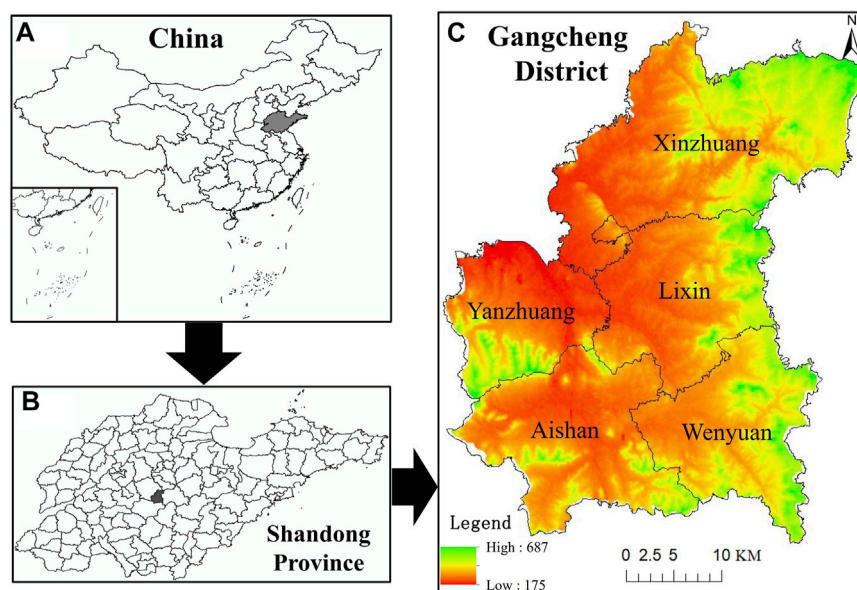
**FIGURE 1**
Location of the study area.

environmental quality assessment in different years. However, in most existing studies, land-use types have been weighted according to the average area in different years, and the conversion of land-use types between different years has led to a change in the area proportion of land-use types in the secondary space. In the same secondary space, the area proportion of land-use types with high EQIs decreases, and the proportion with low EQIs increases, leading the EQI of the secondary space to decrease. Therefore, conversions of land-use types lead the EQI of the secondary space to change in different years. To more accurately and concretely reflect the impact of secondary space on eco-environmental quality in different years, it is necessary to calculate the EQIs of different years, taking the area of land-use types in different years into account.

As an area transforming from old to new, Gangcheng District has prioritized industrial transformation in recent years. The eco-environment effects caused by land-use transitions remain unexplored. Taking the Gangcheng District, a typical industrial base, as an example, this paper proposes an improved area-weighted method according to actual conversions between land-use types in different years and calculates the EQIs of 2009, 2015, and 2020, respectively, by taking land-use types as assignment units. Then, the land-use transfer matrix and ecological contribution rate are combined to quantitatively analyze the eco-environmental effects from 2009 to 2020. This analysis can provide data and decision-making support for the territorial space optimization of industrial bases and for regional sustainable development.

# 2 Materials and methods

## 2.1 Study area

Gangcheng District (117°40′56″-117°58′07″ E, 35°59′32″-36°17′16″ N) is located in the hinterland of Shandong Province, at the eastern foot of Mount Tai, and is under the jurisdiction of Jinan City (Figure 1). It has a total population of 330,000 and a total area of 507 km². The study area is hilly, surrounded by mountains on three sides—east, west, and south—and is open in the middle and the north. The overall terrain from the east, west, and south is tilted toward the center. The area is rich in good-quality mineral resources. Its metal minerals are mainly iron, copper, zinc, aluminum, cobalt, and gold. Its non-metallic minerals are mainly coal, limestone, marble, quartz, and clay. Gangcheng District is an important steel and energy base in Shandong Province. As the only new industrial base named for steel, it is known as the "steel and coal capital." Its steel output accounts for 15% of the province's economy, and the proportion of medium and high quality steel reaches more than 70%.

In recent years, according to its belief in prioritizing industrial transformation and upgrades, Gangcheng District has accelerated its transformation by focusing on the creation of high-quality steel, prefabricated green buildings, new materials, and auto parts, and on other industries. The district has been transformed from a heavy industrial base into a "green steel base." With the important historical opportunity of the Yellow River basin's ecological protection and high-quality

TABLE 1 Production–living–ecological space classification and ecological weight assignment.

| Production–living–ecological space | | Land-use type |
|---|---|---|
| **Primary land-use space** | **Secondary land-use space** | |
| Production space | Agricultural production space | Paddy land (0.30), irrigable land (0.30), dry land (0.30), facilities for agricultural land (0.30), raised path through fields (0.30), orchard (0.65), other garden (0.40) |
| | Industrial production space | Mining lease (0.15), railway land (0.15), highway land (0.15), port land (0.15), country road (0.15), hydraulic construction land (0.15), urban and village road land (0.15), transportation service station land (0.15), industrial land (0.15) |
| | Services and other production space | Scenic spots and special sites (0.15), logistics and warehouse land (0.15), commercial and business facilities land (0.15) |
| Ecological space | Forest ecology space | Woodland (0.95), shrubbery (0.65), other woodland (0.50) |
| | Water ecology space | watershed (0.53), river (0.53), reservoir pond (0.53), ditches (0.53), inland tidal flats (0.53) |
| | Grassland ecology space | Other grass (0.55) |
| | Other ecology space | Naked land (0.05), sandy land (0.05) |
| Living space | Urban living space | Urban land (0.20), organic town (0.20) |
| | Rural living space | Rural residential land (0.20) |

development, Gangcheng District has strived to build a beautiful and modern high-quality steel base.

## 2.2 Data sources and preprocessing

The land-use status data in 2009, 2015, and 2020 comes from the investigation of land-use change. The image data used in the investigation has a resolution of greater than 2.5 m. According to the dominant function principle, referring to the existing commonly used classification criteria (Yu et al., 2017; Zhang et al., 2017), the PLES classification system was constructed by merging land-use types. The land-use types are divided into three main functions: production, living, and ecological spaces. Production space refers to land that provides material products for human beings, including the agricultural, industrial, and service production spaces. Ecological space refers to land that provides ecological services, including forest and grassland ecology space. Living space refers to land for people's living, consumption, leisure, and entertainment, including urban and rural living spaces (Table 1). Referring to the existing research results (Yang et al., 2020b; Hu et al., 2021) and in combination with the actual situation of the study area, weights were assigned to each land-use type in the secondary space to establish the relationship between land-use type and eco-environment quality.

## 2.3 Analysis of land-use characteristics

Based on the PLES classification system, the spatial distribution map of primary land-use space was obtained by merging land-use types in ArcGIS 10.2 software, and the PLES

distribution characteristics for 2009, 2015, and 2020 were analyzed. Then, the quantitative changes in PLES were explored from 2009 to 2020.

## 2.4 Analysis of land-use transition mode

Overlay analyses were conducted on the spatial distribution map using ArcGIS 8 software to make land-use transfer matrixes, which were used to analyze the quantity and direction of land-use spatial transfer and to explore the transition characteristics of the land-use function (Wang and Bao, 1999). The formula is as follows:

$$S_{ij} = \begin{vmatrix} S_{11} & S_{12} & \cdots & S_{1n} \\ S_{21} & S_{22} & \cdots & S_{2n} \\ \cdots & \cdots & \cdots & \cdots \\ S_{n1} & S_{n2} & \cdots & S_{nn} \end{vmatrix},$$

where $S$ is land-use area; $n$ is the number of land-use types; and $i$ and $j$ represent land-use types at the beginning and end, respectively.

## 2.5 Analysis of the spatial-temporal pattern of land-use transition

To analyze the dynamic change characteristics of land-use space, based on the primary land-use spatial distribution maps, the change map of PLES distributions for 2009–2015, 2015–2020, and 2009–2020 was generated using the Erasing Tool in ArcGIS 10.2. Then, the spatial-temporal variation characteristics for different years were analyzed. The spatial distribution change maps were divided

into three parts—constant area, increasing area, and decreasing area—based on the primary land-use space. Finally, the spatial-temporal patterns of land-use transition were obtained.

## 2.6 EQI calculation based on the improved area-weighted method

EQI was used to quantitatively describe the eco-environment quality of different land-use spaces in different years and to portray the overall situation according to the ecological quality and structure proportion in the study area. According to the ecological weight assignment of each land-use type, the EQIs for 2009, 2015, and 2020 were calculated by year using the area-weighted method with the following formula:

$$EQI_t = \sum_{i=1}^{n} LU_x \times C_i / TA,$$

where *EQI* is the eco-environmental quality index of the period *t* in the region; *LU* and *C* are the area and ecological weight of the *i* land-use space in the region during the *t* period, respectively; *TA* is the total land area of the study region; and *N* is the amount of land-use space in the region.

The traditional average area-weighted formula is as follows:

$$EQI_{average} = \sum_{i=1}^{n} LU_x \times C_{average} / TA,$$

where *EQI$_{average}$* is the average eco-environmental quality index in the region; *LU* and *C* are the area and average ecological weights of the *i* land-use space in the region, respectively; *TA* is the total land area of the study region; and *N* is the amount of land-use space in the region.

In the average area-weighted formula, *C* is the average weight of several years, and this weight value can only represent the average impact of land-use type on the eco-environment in this period. In the improved area-weighted formula, *C* is the weight of a particular year, and this weight can specifically reflect the impact of a certain land-use type on eco-environmental quality in a particular year.

## 2.7 Analysis of spatial-temporal characteristics of eco-environmental quality

To analyze spatial-temporal quality characteristics, the EQI of each ecological unit was calculated by the grid method. Different research scales were selected due to the scale dependence of geospatial data, resulting in different conclusions. To obtain the optimal size, land patches were regarded for sampling points. After several tests, referring to the empirical formula (Sudhira et al., 2004), a 150 m × 150 m grid was selected for isometry sampling in

the study area, and 24,700 sample areas were generated. The EQI was quantitatively analyzed by considering the land-use area and eco-environment status of each unit comprehensively. Its expression is:

$$EV(X) = \sum_{i=1}^{n} S_{xi} \times R_i / S_x,$$

where *EV(x)* is the eco-environmental quality index of the *X* ecological unit; *R$_i$* is the ecological weight of the *i*th land-use space; *S$_{xi}$* is the area of the *i*th land-use space in the *x* ecological unit; *S$_x$* is the area of the *X* ecological unit; and *N* is the amount of land-use space in the region.

Then, the results were divided into five levels (Yang et al., 2018) according to the actual situation of the study area: low-quality areas (0<EV ≤ 0.2), medium-low-quality areas (0.2<EV ≤ 0.35), medium-quality areas (0.35<EV ≤ 0.5), medium-high-quality areas (0.5<EV ≤ 0.65), and high-quality areas (0.65 < EV < 1).

## 2.8 Analysis of eco-environmental effects of land-use transition

The ecological contribution rate was used to analyze eco-environmental effects and to measure the impact of each land-use transition on the eco-environment. The ecological contribution rate of land-use transition refers to the change of regional eco-environment quality caused by the change of a certain land-use space. It quantifies the impact of each land-use space conversion on the regional eco-environment. Its calculation formula is as follows:

$$LEI = (LE_1 - LE_0) LA / TA,$$

where *LEI* is the ecological contribution rate of land-use transitions; *LE$_0$* and *LE$_1$* are the EQIs of a certain land-use type in 2009 and 2020, respectively; *LA* is the area of the changed land-use type; and *TA* is the total land area of the study region.

## 3 Results

### 3.1 Land-use characteristics from the perspective of PLES

The distribution map of primary land-use space is shown in Figure 2. Production space accounted for the largest proportion and was widely distributed in the whole region. Ecological space was concentrated in the northeast and southwest of the study area. Living space was the least concentrated in the central and southern urban areas. In terms of the overall change from 2009 to 2020, ecological space increased significantly, from 35 to 41%; living space decreased significantly, from 16 to 8%; and production space remained stable at about 50%.

**FIGURE 2**
Distribution map of the primary land-use space.
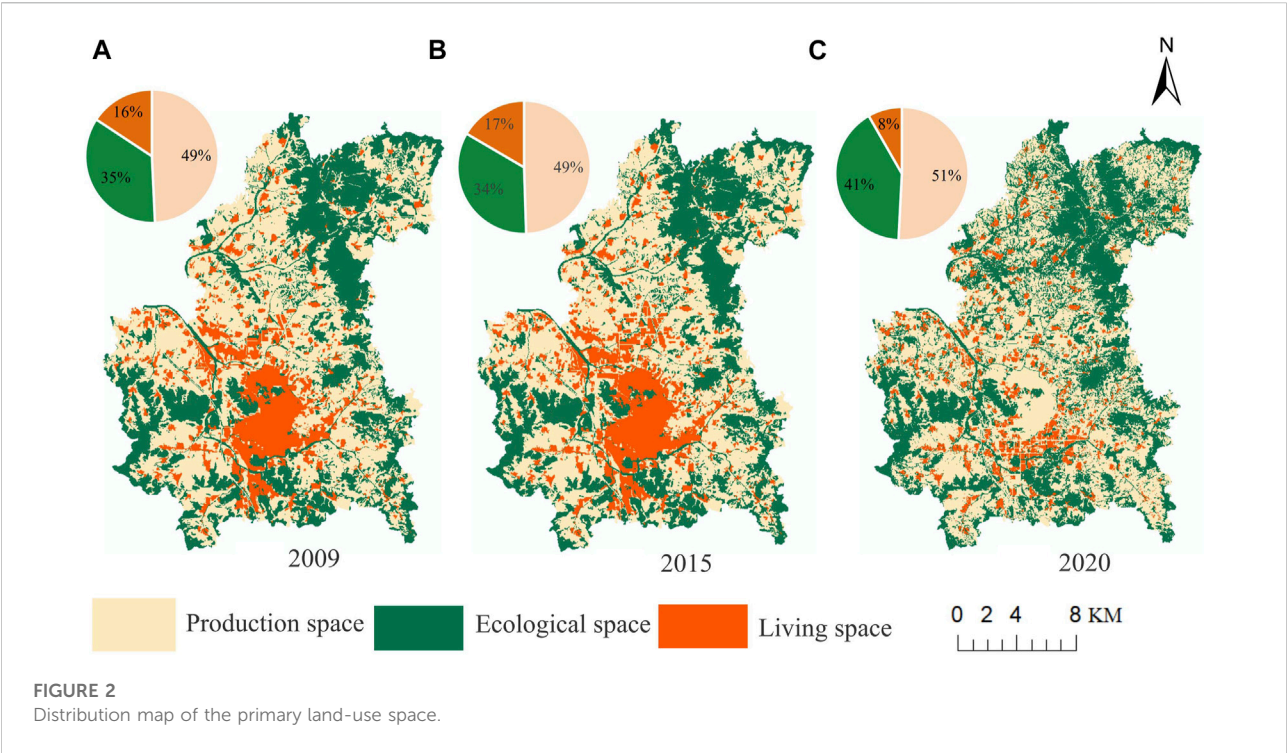
TABLE 2 Transfer matrix of the primary land-use space from 2009 to 2020 (hm²).

|  |  | Final year | | |
|---|---|---|---|---|
|  |  | **Production space** | **Ecological space** | **Living space** |
| Initial year | Production space | *24,407.42* | *7.54* | *534.63* |
|  |  | **18,318.80** | 6,261.32 | 395.44 |
|  |  | <u>**18,390.68**</u> | <u>6,082.30</u> | <u>476.42</u> |
|  | Ecological space | *489.09* | *17,163.80* | *83.54* |
|  |  | 3,352.55 | **13,736.42** | 82.04 |
|  |  | <u>3,705.50</u> | <u>**13,922.25**</u> | <u>108.36</u> |
|  | Living space | *79.26* | *0.00* | *7,884.23* |
|  |  | 4,067.87 | 703.74 | **3,730.79** |
|  |  | <u>3,643.06</u> | <u>696.93</u> | <u>**3,623.49**</u> |

Note: Area counts of persistence on the main diagonal (in bold) and change off the main diagonal from 2009 to 2015 (in italics), 2015–2020 and 2009–2020 (underlined).

## 3.2 Land-use transition mode

### 3.2.1 Land-use transition characteristics and causes from 2009 to 2015

Based on the transfer matrix of primary land-use space (Table 2), from 2009 to 2015, the area conversion from production space to living space was the largest, at 534.63 hm², followed by the area conversion from ecological space to production space, at 489.09 hm². The area of other

land-use space transitions, such as living space to production space and ecological space to living space, was relatively small. Therefore, the land-use transitions from 2009 to 2015 were mainly from production space to living space and from ecological space to production space.

Based on the transfer matrix of secondary land-use space (Table 3), grassland ecology space was transformed into agricultural production space and agricultural production space into urban living space, which was the main transition

TABLE 3 Transfer matrix of the secondary land-use space from 2009 to 2020 (hm²).

| | | Final year | | | | | | | | |
|---|---|---|---|---|---|---|---|---|---|---|
| | | Agricultural production space | Industrial production space | Services and other production space | Forest ecology space | Water ecology space | Grassland ecology space | Other ecology space | Urban living space | Rural living space |
| Initial year | Agricultural production space | *23,183.27* | *21.44* | | *7.54* | | | | *211.63* | *320.86* |
| | | 16,202.19 | 972.63 | 158.34 | 5,545.20 | 388.47 | 105.13 | 2.83 | 62.92 | 300.05 |
| | | 15,937.23 | 1,316.87 | 178.17 | 5,383.33 | 377.22 | 104.78 | 2.83 | 95.11 | 349.01 |
| | Industrial production space | *0.01* | *1,185.52* | | | | | | | *2.14* |
| | | 63.94 | 876.78 | 35.18 | 171.32 | 14.22 | 25.43 | 1.52 | 17.87 | 14.36 |
| | | 61.28 | 852.46 | 34.92 | 167.00 | 13.04 | 25.38 | 1.52 | 17.55 | 14.52 |
| | Services and other production space | | | *17.19* | | | | | | |
| | | 1.50 | 0.61 | 7.64 | 6.08 | 0.18 | 0.94 | | | 0.23 |
| | | 1.50 | 0.61 | 7.64 | 6.08 | 0.18 | 0.94 | | | 0.23 |
| | Forest ecology space | *25.71* | *12.61* | | *8384.73* | | | | *15.06* | *14.01* |
| | | 779.09 | 171.16 | 13.95 | 7,210.72 | 67.17 | 117.47 | 1.29 | 4.22 | 27.01 |
| | | 797.17 | 200.96 | 15.99 | 7,214.47 | 68.50 | 117.53 | 1.29 | 7.13 | 28.88 |
| | Water ecology space | *1.02* | *0.36* | | | *1,693.39* | | | *2.70* | *3.64* |
| | | 45.70 | 78.73 | 3.43 | 122.03 | 1,436.89 | 2.48 | | 1.27 | 2.85 |
| | | 45.76 | 83.97 | 3.55 | 122.50 | 1,437.63 | 3.15 | | 1.61 | 2.92 |
| | Grassland ecology space | *447.76* | *0.26* | | | | *6,646.27* | | *30.65* | *11.37* |
| | | 1839.54 | 233.65 | 24.05 | 2,777.35 | 51.59 | 1,673.11 | 5.26 | 5.95 | 35.65 |
| | | 2,105.61 | 258.63 | 25.17 | 2,940.18 | 62.11 | 1,677.17 | 5.26 | 21.44 | 40.63 |
| | Other ecology space | *1.37* | | | | | | *439.41* | *5.55* | *0.56* |
| | | 119.14 | 39.12 | 4.99 | 201.78 | 3.36 | 32.98 | 32.95 | 0.12 | 4.97 |
| | | 119.75 | 43.95 | 4.99 | 203.15 | 3.36 | 32.98 | 32.95 | 0.12 | 5.62 |
| | Urban living space | | | | | | | | *3,941.11* | |
| | | 95.71 | 2,477.80 | 275.78 | 229.42 | 17.77 | 28.23 | | 519.20 | 565.06 |
| | | 70.42 | 2,301.14 | 264.34 | 213.69 | 17.12 | 24.10 | 5.84 | 487.32 | 557.16 |
| | Rural living space | *78.82* | *0.44* | | | | | | *8.12* | *3,935.00* |
| | | 269.79 | 809.97 | 138.82 | 383.54 | 19.74 | 14.33 | 4.85 | 133.22 | 2,513.30 |
| | | 277.90 | 601.86 | 127.41 | 397.02 | 20.24 | 14.08 | 4.86 | 114.50 | 2,464.52 |

Note: Area counts of persistence on the main diagonal (in bold) and change off the main diagonal from 2009 to 2015 (in italics), 2015–2020 and 2009–2020(underlined).

from 2009 to 2015. Among them, grassland ecology space transferred to agricultural production space was the largest, with an area of 447.76 hm². Grassland was developed and utilized for agricultural production space. In addition, agricultural production space was transformed into urban and rural living spaces, with areas of 211.63 hm² and 320.86 hm², respectively. This was mainly due to urban expansion and to the large-scale mining of mineral resources that occupy a large amount of space. Therefore, the direction of land-use transitions from 2009 to 2015 was mainly from grassland ecology space to agricultural production space and from agricultural production to urban and rural living space.

### 3.2.2 Land-use transition characteristics and causes from 2015 to 2020

Based on the transfer matrix of primary land-use space (Table 2), from 2015 to 2020, the area conversion from production space to ecological space was the largest, at 6,261.32 hm², followed by the conversion from living and ecological space to production space, at 4,067.87 hm² and 3,352.55 hm², respectively. In other land-use spaces, the conversion area from living to ecological space, from production to living space, and from ecological space to living space was relatively small. Therefore, land-use transitions from 2015 to 2020 were mainly from production to ecological space and from living and ecological space to production space.

The transfer matrix of secondary land-use space (Table 3) revealed many obvious changes. Agricultural production space and grassland ecology space transformed into forest ecology space had the largest areas, at 5,545.20 hm², and 2,777.35 hm², respectively. During this period, grassland was developed and utilized as forest land. The adjustment of agricultural structure turned the large area of agricultural production space into forest ecology space. The conversion area between urban living space and industrial production space was also large (2,477.80 hm²) because the land of the Laiwu Iron and Steel Group Co., Ltd. was reclassified from the original urban construction land to industrial land (that is, from living space to production space) in the third National Land Resource Survey. The areas of grassland and forest ecology space transformed into agricultural production space were 1839.54 hm² and 779.09 hm², respectively, while the areas of rural living and agricultural production space transformed into industrial production space were 809.97 hm² and 972.63 hm², respectively. The transitions from grassland and forest ecology space to agricultural production space, and from rural living and agricultural production to industrial production space, were also important directions. Therefore, the transitions from 2015 to 2020 were mainly from agricultural production and grassland ecology to forest ecology space, from urban living to industrial production space, and from grassland ecology to agricultural production space.

### 3.2.3 Land-use transition characteristics and causes from 2009 to 2020

Based on the transfer matrix of primary land-use space (Table 2), from 2009 to 2020, the area conversion from production space to ecological space was the largest, at 6,082.30 hm², followed by the conversion from living and ecological space to production space, which was 3,643.06 hm² and 3,705.50 hm², respectively. In other land-use spaces, the conversion area from living to ecological space, from production to living space, and from ecological space to living space was relatively small. Therefore, land-use transitions from 2015 to 2020 were mainly from production to ecological space and from living and ecological space to production space.

Based on the transfer matrix of secondary land-use space (Table 3), the characteristics of land-use conversion between 2009 and 2020 were similar to those between 2015 and 2020. Agricultural production space and grassland ecology space transformed into forest ecology space had the largest area, 5,383.33 hm², and 2,940.18 hm², respectively. The conversion area between urban living space and industrial production space was also large, 2,301.14 hm². The areas of grassland and forest ecology space transformed into agricultural production space were 2,105.61 hm² and 797.17 hm², while the areas of rural living and agricultural production space transformed into industrial production space were 601.86 hm² and 1,316.87 hm², respectively. The reasons for the transformation are analyzed in Section 3.2.2. Therefore, the direction of land-use transitions from 2009 to 2020 was mainly from agricultural production and grassland ecology to forest ecology space, from urban living to industrial production space, and from grassland ecology to agricultural production space.

## 3.3 Spatial-temporal patterns of land-use transition from 2009 to 2020

According to the land-use transition mode in Section 3.2, the land-use changes in 2009–2015 were not significant compared to 2015–2020. Therefore, this study mainly analyzed the spatial-temporal patterns of land-use transition in 2009–2020. Figure 3 shows the changes in the distribution of PLES in the study area from 2009 to 2020. Overall, living space decreased while production and ecological space increased.

The increasing area of production space was mainly distributed in Xinzhuang Town, on Lixin Street and Aishan Street, which were as follows. 1) West of Lixin Street and east of Aishan Street were the transitions from living space to production space. The reason was that the above-mentioned third National Land Resource Survey reclassified Laiwu Iron and Steel Group Co., Ltd. as industrial land rather than the original urban construction land, that is, from the original living space to production space. 2) Northeast of Xinzhuang Town and

**FIGURE 3**
Change map of production–living–ecological space in distribution.
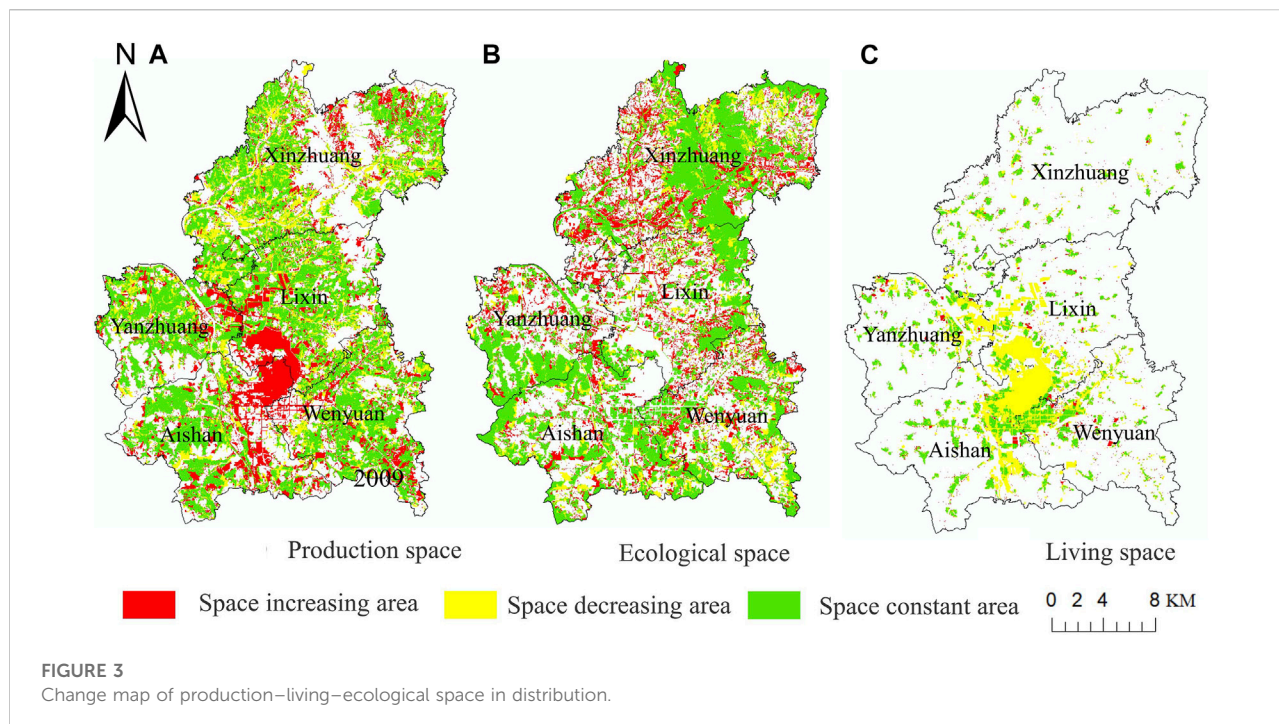
southeast of Wenyuan Street, the ecological space was transformed into production space. This was a transition from grassland and forest ecology space to agricultural production space, as defined by the transition characteristics and cause analysis of secondary space in Section 3.2.3.

The increasing area of ecological space was widely distributed in all streets and towns of Gangcheng District, especially in Xinzhuang Town, and was mainly a transition from production to ecological space. As the previous analysis shows, it was a transition from agricultural production to forest ecology space.

## 3.4 EQI

Table 4 shows the EQI calculated by the improved area-weighted method based on the actual conversions between land-use types in different years. The EQI of forest ecology space was the highest, above 0.7. This was followed by watershed ecology space, grassland ecology space, and agricultural production space, with EQIs ranging from 0.3 to 0.6. The lowest were industrial and mining production space, service and other production spaces, other ecology spaces, urban living space, and rural living space, with EQIs of less than 0.2.

In 2009, 2015, and 2020, the EQI of secondary land-use space changed little, and only the agricultural production space and forest ecology space changed. From 2009 to 2020, the EQI of agricultural production space increased slightly from 0.373 to 0.388, while the forest ecology space decreased from 0.810 to 0.739, a relatively large decrease. Taking agricultural production

space as an example, the reasons for the change of EQI were analyzed. Agricultural production space included irrigated land, dry land, orchards, and other gardens. The change in land-use area led to a change in area proportion. From 2009 to 2020, the decrease in the cultivated land area caused the area proportion of orchards and other gardens in agricultural production space to increase. In other words, the proportion of cultivated land with relatively low EQI (0.3) decreased, and the proportion of orchards (0.65) and other gardens (0.40) with high EQIs increased. Finally, the EQI of the agricultural production space increased.

Based on the annual comprehensive EQI, the variation trend was obtained (Figure 4). The results show that the comprehensive EQI of the study area decreased from 0.441 in 2009 to 0.436 in 2015 and then increased to 0.470 in 2020, showing an initial slight decline and then a sharp rise. The improvement was especially significant from 2015 to 2020. The analysis of land-use transition from 2009 to 2015, in Section 3.2 and Section 3.3, shows that the land-use transition direction was mainly from grassland ecology space into agricultural production and from agricultural production into urban and rural living space. Additionally, the EQI of grassland ecology space was higher than that of agricultural production space and higher than that of urban and rural living space. Although the development and utilization of grassland supplement cultivated land, they had a slight impact on the eco-environment. Although the occupation of cultivated land for construction promoted the development of economy, it had a drastic impact on the eco-environment. The rapid improvement of the comprehensive EQI from 2015 to

TABLE 4 Eco-environment quality index.

| Production–living–ecological land classification | | Eco-environment quality index | | | |
|---|---|---|---|---|---|
| The primary land-use space | The secondary land-use space | 2009 | 2015 | 2020 | Average |
| Production space | Agricultural production space | 0.373 | 0.371 | 0.388 | 0.377 |
| | Industrial production space | 0.150 | 0.150 | 0.150 | 0.150 |
| | Services and other production space | 0.150 | 0.150 | 0.150 | 0.150 |
| Ecological space | Forest ecology space | 0.810 | 0.811 | 0.739 | 0.775 |
| | Water ecology space | 0.530 | 0.530 | 0.530 | 0.530 |
| | Grassland ecology space | 0.550 | 0.550 | 0.550 | 0.550 |
| | Other ecology space | 0.050 | 0.050 | 0.050 | 0.050 |
| Living space | Urban living space | 0.200 | 0.200 | 0.200 | 0.200 |
| | Rural living space | 0.200 | 0.200 | 0.200 | 0.200 |
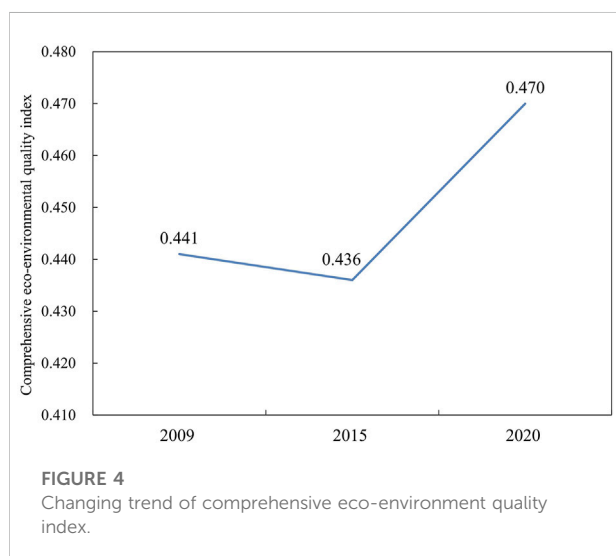


**FIGURE 4**
Changing trend of comprehensive eco-environment quality index.

TABLE 5 Eco-environment quality grades (%).

| Type\ratio | 2009 | 2020 | Change |
|---|---|---|---|
| Low-quality area | 16.93 | 15.31 | −1.62 |
| Medium-low-quality area | 7.52 | 7.52 | 0 |
| Medium-quality area | 44.31 | 36.42 | −7.89 |
| Medium-high-quality area | 14.79 | 16.97 | +2.18 |
| High-quality area | 16.45 | 23.78 | +7.33 |

Overall, the EQI increased significantly from 2009 to 2020, indicating that the study area had the strength to drive breakthroughs in ecological protection, environmental quality improvement, and the adjustment of land-use patterns. But this process also involved the problems of "non-food" and "non-agriculture."

## 3.5 Spatial-temporal characteristics of eco-environment comprehensive quality

The grade tables in 2009 and 2020 (Table 5) show that the overall eco-environment quality of the two periods was relatively consistent, with the medium-quality area taking the highest proportion, about 40%, followed by the high-quality area, about 20%, and the medium-high-quality area and low-quality areas, both about 15%. The medium-low-quality area took the lowest proportion, at 7.52%. However, the proportion of each grade in the two years was different. The spatial distribution map of eco-environment quality levels (Figure 5) shows that the overall distribution was relatively consistent. The medium-high-quality and high-quality areas were mainly distributed east of Xinzhuang Town, Lixin Street, and Wenyuan Street, as well as southwest of Yanzhuang Town. The medium-quality area

2020 was attributed to the main land-use transition direction during this period, which was agricultural production and grassland ecology space transformed into forest ecology space, with a large increase in woodlands and improved eco-environment quality.

The weight only represents the contribution degree of land-use space to the eco-environment. Comprehensive EQI is related not only to the weight of secondary ecological space but also to its area. The EQI of agricultural production space increased slightly, from 0.373 to 0.388, from 2009 to 2020, and the area of agricultural production space decreased. Similarly, the EQI of forest ecology space decreased from 0.810 to 0.739, and the area of forest ecology space increased greatly. Therefore, according to the formula in Section 2.6, the comprehensive EQI increased from 0.441 to 0.470.

**FIGURE 5**
Spatial distribution of the eco-environment quality levels. Note: EV is the eco-environmental quality index of each ecological unit.

was mainly distributed in west of Xinzhuang Town, Lixin Street, Aishan Street, and Wenyuan Street, as well as north of Yanzhuang Town. The low-quality and medium-low-quality areas were mainly distributed west of Lixin Street, northeast of Aishan Street, and north of Yanzhuang Town. The spatial distribution was as follows: the eco-environmental quality of Gangcheng District had significant spatial differentiation, presenting an overall distribution pattern that was high in the periphery and low in the middle.

Comparing the quantity changes in two periods, the proportions of low-quality area, medium-low-quality area, and high-quality area from 2009 to 2020 were essentially the same. The proportion of medium-quality area and high-quality area changed greatly, with the medium-quality area decreasing by 7.89% and the high-quality area increasing by 7.33%. In general, the changes in eco-environmental quality grades from 2009 to 2020 were mainly the decrease in middle-quality area and the increase in high-quality area.

## 3.6 Eco-environmental effects of land-use transition

Based on the ecological contribution rate from 2009 to 2020 (Table 6), the land-use transitions that affected eco-environment

improvement included agricultural production, grassland ecology, rural living, other ecology, urban living, and industrial production, which were all transformed into forest ecology space. Among these, the transitions from agricultural production and grassland ecology into forest ecology space were the main factors, and their ecological contribution proportions were 58.30 and 16.35%, respectively. Therefore, the adjustment of agricultural structure, the development and utilization of grassland, and the conversion from cultivated land and grassland into woodland can greatly improve the eco-environment quality.

From 2009 to 2020, the land-use transitions affecting eco-environment deterioration included the transitions of grassland ecology space and forest ecology space into agricultural production space, and the transitions of agricultural production space, grassland ecology space, forest ecology space and urban living space into industrial production space. Among these, the transitions from grassland and forest ecology space to agricultural production space, and from agricultural production to industrial production space were the main factors, with the ecological contribution proportion of the three at about 20% each, totaling 58.64%. In addition, the transitions from the forest ecology, urban living, and grassland ecology spaces to industrial production space were secondary factors, with the ecological contribution proportions of the three at about 7% each, or 21.42% in total. Therefore, Gangcheng District should

TABLE 6 Main land-use transitions and their eco-environmental contribution rate (hm², %).

| Contribution type | Transition type | Transfer area | Contribution rate | Contribution ratio |
|---|---|---|---|---|
| Improvement | Agricultural production space—Forest ecology space | 5383.33 | 0.03933 | 58.30 |
| | Grassland ecology space—Forest ecology space | 2940.18 | 0.01103 | 16.35 |
| | Rural living space—Forest ecology space | 397.02 | 0.00423 | 6.28 |
| | Other ecology space—Forest ecology space | 203.15 | 0.00277 | 4.10 |
| | Urban living space—Forest ecology space | 213.69 | 0.00228 | 3.38 |
| | Industrial production space—Forest ecology space | 167.00 | 0.00195 | 2.88 |
| | Agricultural production space—Water ecology space | 377.22 | 0.00119 | 1.77 |
| | Rural living space—Agricultural production space | 104.78 | 0.00104 | 1.55 |
| | Total | 9786.38 | 0.06382 | 94.61 |
| Deterioration | Grassland ecology space—Agricultural production space | 2105.61 | 0.00665 | 20.55 |
| | Forest ecology space—Agricultural production space | 797.17 | 0.00661 | 20.42 |
| | Agricultural production space—Industrial production space | 1316.87 | 0.00572 | 17.67 |
| | Forest ecology space—Industrial production space | 200.96 | 0.00262 | 8.09 |
| | Urban living space—Industrial production space | 2301.14 | 0.00227 | 7.02 |
| | Grassland ecology space—Industrial production space | 258.63 | 0.00204 | 6.31 |
| | Agricultural production space—Rural living space | 349.01 | 0.00117 | 3.62 |
| | Agricultural production space—Services and other production space | 178.17 | 0.00077 | 2.39 |
| | Water ecology space—Industrial production space | 83.97 | 0.00063 | 1.95 |
| | Forest ecology space—Grassland ecology space | 117.53 | 0.00060 | 1.86 |
| | Rural living space—Industrial production space | 601.86 | 0.00059 | 1.84 |
| | Total | 8310.90 | 0.02967 | 91.72 |

take this as a reference and avoid the occupation of ecological and living space by production space while guaranteeing production.

In general, the changes in ecological quality from 2009 to 2020 were mainly due to transitions from agricultural and industrial production to grassland and forest ecology space. In addition, the positive contribution rate of agricultural production and grassland ecology space to forest ecology space was greater than was the negative contribution rate of forest and grassland ecology space to agricultural production and agricultural production to industrial production space. Overall, the eco-environment improved from 2009 to 2020. In strengthening its ecological civilization concept under the guidance of a new round of national space planning, Gangcheng District should continue strengthening territorial space control and adjusting land use structure in order to realize the harmonious development of eco-environment protection and social economy.

# 4 Discussion

## 4.1 Effectiveness of the improved method

To verify the effectiveness, the improved area-weighted method was compared with the average area-weighted method, with forest ecology space as an example. The relevant results are shown in Table 8.

Forest ecology space consists of woodland, shrubbery, and other woodland. From 2009 to 2020, the dramatic increase of forest ecology space was due to transitions from agricultural production and grassland ecology space in 2009 into undeveloped forest land in 2020, which belongs to the other woodland category. To assess the actual conversions between land-use types in different years, the improved method was adopted to calculate the EQI. When the area of other woodland increased, the area proportion of other woodland increased while that of woodland and shrubbery decreased in forest ecology space. In other words, the area proportion of other woodland (EQI of 0.50) with relatively low EQI increased, while the area proportions of woodland (EQI of 0.95) and shrubbery (EQI of 0.65) with high EQI decreased. Therefore, the EQI of forest ecology space decreased from 0.81 to 0.77, which indicates that the EQI of forest ecology space in 2020 was lower than in 2009 and 2015.

The average area-weighted method was used to calculate the EQI by taking the mean area of land-use type in different years. The results show that the mean EQI of forest ecology space from 2009 to 2020 was 0.77, indicating that the EQI of forest ecology space was unchanged during this period. Therefore, the average area-weighted method cannot reflect the impact of land-use type conversion on environmental quality in different years, but the improved area-weighted method can describe this difference.

## 4.2 Accuracy of EQI in the study area

According to the actual situation of typical industrial bases and by consulting local experts, this study assigned weights to each land-use type and constructed an index system that conforms to the characteristics of the study area. At the same time, the area-weighted method was improved to calculate the comprehensive EQI of Gangcheng District according to the actual land-use type conversion. The comprehensive EQI decreased from 0.441 in 2009 to 0.436 in 2015, and then increased to 0.470 in 2020, which is consistent with the actual development of the Gangcheng District in the past 10 years. Before 2015, Gangcheng District had vigorously developed steel and other heavy industries to comprehensively promote economic development, but the environment suffered to a certain extent. Since the Central Committee of the Communist Party of China and the State Council issued the Overall Plan for Ecological Civilization System Reform in September 2015, Gangcheng District has actively implemented ecological protection policies and promoted ecological civilization construction. In 2018, a greening campaign was launched to protect and restore mountains, rivers, forests, farmland, lakes, and grasses; focus on industrial transformation; accelerate the shift from old to new drivers of growth; and actively improve the eco-environment. Therefore, the results obtained using the improved area-weighted method proposed in this paper align with the actual situation of the study area. The paper provides specific data references for future land-use structure change and industrial transformation in Gangcheng District and provide technical and case references for exploring the eco-environmental effects of future land-use transformation in other industrial bases.

## 4.3 Applicability of the study

Eco-environmental effect analysis involves complicated factors, and the distribution of ecological resources varies considerably in different regions (Chen et al., 2020; Hu et al., 2021). Different regions are assigned different values, so their comprehensive EQIs are also different from each other. For example, Dong et al. assessed the environmental condition of Gansu Province and found that its comprehensive EQI decreased from 0.2662 in 1980 to 0.2653 in 2000 and then rose to 0.2682 in 2018. The eco-environment of Gansu Province is fragile, and soil erosion and desertification are serious. The final calculated index was relatively low, which reflects the actual situation (Dong et al., 2021). Xiang et al. assessed the environmental quality of Pingshan County in Shijiazhuang City and found that the regional comprehensive EQIs in 2005, 2010, and 2015 were 0.4504, 0.5719, and 0.5800, respectively. Pingshan County is an important water conservation base and an important region for environmental protection and construction.

Consequently, the index was relatively high and consistent with reality (Xiang et al., 2021). As a typical industrial base, the comprehensive EQI in Gangcheng District is higher than that of a typical ecologically fragile area and lower than that of a water conservation base, which is consistent with its macro-regional distribution characteristics and its actual situation. Thus, the comprehensive EQI determined from the analysis well reflects the regional eco-environment level according to the actual situation of the study area.

## 4.4 Shortcomings of the study

Referring to the existing literature and the dominant function principle, this paper constructed the PLES classification system and analyzed land-use transition and its eco-environmental effects from 2009 to 2020. The results were consistent with the actual situation. This classification system is simple, convenient, clear, and easy to understand. A particular land-use type may have multifunctional properties, including both its main and additional functions. For example, arable land has both productive and ecological functions; however, the production function is its main function, and its ecological function is only incidental. Considering the multifunctional properties of the land can be more complicated and may produce slightly different results. With future research, the multi-functionality of land will be considered for classification.

## 5 Conclusion

Based on the spatial-temporal pattern analysis of land-use transition in the study area, this paper put forward an improved area-weighted calculation method for EQI to analyze eco-environmental effects. The results show that the improved method can more specifically describe the impact of conversion between land-use types on environmental quality in different years.

1) From 2009 to 2020, the comprehensive EQI first decreased from 0.441 to 0.436 and then increased significantly to 0.470.
2) On the whole, the eco-environment quality of the study area was improved, mainly because the positive ecological contribution rate of land-use transition was greater than the negative ecological contribution rate. The positive ecological contribution rate was mainly caused by transitions from agricultural production and grassland ecology into forest ecology space; the negative ecological contribution rate was caused by transitions from forest and grassland ecology space into agricultural production space and from agricultural production into industrial production space.
3) Therefore, it is suggested to continue implementing ecological protection policies; protecting the arable land; controlling effectively the expansion of residential, industrial, and mining

land area; and expanding the ecological land area to ensure food security.

The study not only enriches the case of industrial city eco-environmental effect analysis but also provides a reference for future territorial spatial planning and for the high-quality development of industrial bases.

## Data availability statement

The original contributions presented in the study are included in the article/supplementary materials, and further inquiries can be directed to the corresponding author.

## Author contributions

YW: conceptualization, methodology, data analysis, writing of original draft. YZ: investigation, supervision. LC: visualization, investigation. HC: conceptualization, methodology, writing of original draft, funding acquisition. XZ: validation, investigation. PL: funding acquisition.

## Conflict of interest

The authors declare that the research was conducted in the absence of any commercial or financial relationships that could be construed as a potential conflict of interest.

## Publisher's note

All claims expressed in this article are solely those of the authors and do not necessarily represent those of their affiliated organizations, or those of the publisher, the editors and the reviewers. Any product that may be evaluated in this article, or claim that may be made by its manufacturer, is not guaranteed or endorsed by the publisher.

## References

Allington, G. R., Li, W., and Brown, D. G. (2017). Urbanization and environmental policy effects on the future availability of grazing resources on the Mongolian Plateau: Modeling socio-environmental system dynamics. *Environ. Sci. Policy* 68, 35–46. doi:10.1016/j.envsci.2016.11.005

Asabere, S. B., Acheampong, R. A., Ashiagbor, G., Beckers, S. C., Keck, M., Erasmi, S., et al. (2020). Urbanization, land use transformation and spatio-environmental impacts: analyses of trends and implications in major metropolitan regions of Ghana. *Land Use Policy* 96, 104707. doi:10.1016/j.landusepol.2020.104707

Asadolahi, Z., Salmanmahiny, A., Sakieh, Y., Mirkarimi, S. H., Baral, H., and Azimi, M. (2018). Dynamic trade-off analysis of multiple ecosystem services under land use change scenarios: Towards putting ecosystem services into planning in Iran. *Ecol. Complex.* 36, 250–260. doi:10.1016/j.ecocom.2018.09.003

Chen, W., Zhao, H., Li, J., Zhu, L., Wang, Z., and Zeng, J. (2020). Land use transitions and the associated impacts on ecosystem services in the Middle Reaches of the Yangtze River Economic Belt in China based on the geo-informatic Tupu method. *Sci. Total Environ.* 701, 134690. doi:10.1016/j.scitotenv.2019.134690

Dong, J., Zhang, Z., Da, X., Zhang, W., and Feng, X. (2021). Eco-environmental effects of land use transformation and its driving forces from the perspective of "production-living-ecological" spaces: a case study of Gansu province. *Acta eco. Sin.* 41 (15), 5919–5928. doi:10.5846/stxb201908201969

Foley, J. A., DeFries, R., Asner, G. P., Barford, C., Bonan, G., Carpenter, S. R., et al. (2005). Global consequences of land use. *Science* 309, 570–574. doi:10.1126/science.1111772

Fu, J., and Zhang, S. (2021). Functional assessment and coordination characteristics of production, living, ecological function—a case study of henan province, China. *Int. J. Environ. Res. Public Health* 18 (15), 8051. doi:10.3390/ijerph18158051

Gao, Z., Zhang, H., Yang, X., and Song, Z. Y. (2019). Assessing the impacts of ecological-living-productive land changes on eco-environmental quality in Xining City on Qinghai-Tibet Plateau, China. *Sci. Cold Arid Reg.* 11 (3), 194–207. doi:10.3724/SP.J.1226.2019.00194

Haas, J., and Ban, Y. (2014). Urban growth and environmental impacts in jing-jin-ji, the yangtze, river delta and the pearl river delta. *Int. J. Appl. Earth Obs. Geoinf.* 30, 42–55. doi:10.1016/j.jag.2013.12.012

Han, M., Kong, X., Li, Y., Wei, F., Kong, F., and Huang, S. (2021). Eco-environmental effects and its spatial heterogeneity of 'ecological-production-living' land use transformation in the Yellow River delta. *Sci. Geogr. Sin.* 41 (06), 1009–1018. doi:10.13249/j.cnki.sgs.2021.06.010

Hanaõcek, K., and Rodríguez-Labajos, B. (2018). Impacts of land-use and management changes on cultural agroecosystem services and environmental conflicts—a global review. *Glob. Environ. Change* 50, 41–59. doi:10.1016/j.gloenvcha.2018.02.016

Hao, H., and Ren, Z. (2009). Land use/land cover change (LUCC) and eco-environment response to LUCC in farming-pastoral zone, China. *Agric. Sci. China* 8 (1), 91–97. doi:10.1016/s1671-2927(09)60013-4

Hu, F., An, Y., and Zhao, H. (2016). Research on characteristics of ecological environment effect on a "semi-karst" region based on land use transition: A case in central Guizhou province, China. *Earth Environ.* 44 (4), 447–454. doi:10.14050/j.cnki.1672-9250.2016.04.009

Hu, P., Li, F., Sun, X., Liu, Y., Chen, X., and Hu, D. (2021). Assessment of land-use/cover changes and its ecological effect in rapidly urbanized areas—taking pearl river delta urban agglomeration as a case. *Sustainability* 13 (9), 5075. doi:10.3390/su13095075

Hu, M., Li, Z., Wang, Y., Jiao, M., Li, M., and Xia, B. (2019). Spatio-temporal changes in ecosystem service value in response to land-use/cover changes in the Pearl River Delta. *Resour. Conserv. Recycl.* 149, 106–114. doi:10.1016/j.resconrec.2019.05.032

Hu, S., Chen, L., Li, L., Wang, B., Yuan, L., Cheng, L., et al. (2019). Spatiotemporal dynamics of ecosystem service value determined by land-use changes in the urbanization of anhui province, China. *Int. J. Environ. Res. Public Health* 16 (24), 5104. doi:10.3390/ijerph16245104

Hu, J. (2012). *A compilation of documents of the 18th national congress of the communist party of China*. Beijing: People's Publishing House.

Kong, D., Chen, H., and Wu, K. (2021). The evolution of "Production-Living-Ecological" space, eco-environmental effects and its influencing factors in China. *J. Nat. Resour.* 36 (05), 1116–1135. doi:10.31497/zrzyxb.20210503

Lambin, E. F., and Meyfroidt, P. (2011). Global land use change, economic globalization, and the looming land scarcity. *Proc. Natl. Acad. Sci. U. S. A.* 108, 3465–3472. doi:10.1073/pnas.1100480108

Li, C., Xin, G., Yang, C., and Cheng, X. (2016). Land Use and Land Cover Change (LUCC)and its environmental effects of traditional farm area. *J. Southwest Univ. Nat. Sci. Ed.* 38 (5), 139–145. doi:10.13718/j.cnki.xdzk.2016.05.023

Li, Z., Li, M., and Xia, B. (2020). Spatio-temporal dynamics of ecological security pattern of the Pearl River Delta urban agglomeration based on LUCC simulation. *Ecol. Indic.* 114, 106319. doi:10.1016/j.ecolind.2020.106319

Li, L., Yang, L., and Zheng, M. (2021). Study on land use transformation and ecological environment effect in central Guizhou. *Territ. Nat. Resour. Study* 2021 (03), 38–42. doi:10.16202/j.cnki.tnrs.2021.03.010

Liu, J., Liu, Y., and Li, Y. (2017). Classification evaluation and spatial-temporal analysis of 'production-living-ecological' spaces in China. *Geogr. Sci.* 72 (7), 1290–1304. doi:10.11821/dlxb201707013

Long, H., Qu, Y., Tu, S., Zhang, Y., and Jiang, Y. (2020). Development of land use transitions research in China. *J. Geogr. Sci.* 30 (07), 1195–1214. doi:10.1007/s11442-020-1777-9

Lou, P., Fu, B., Lin, X., Bi, L., Ma, R., and Tang, T. (2019). Influence of land use change on ecosystem service value based on GEE in the beijing-tianjin-hebei region from 1998 to 2018. *Environ. Sci.* 40 (12), 5473–5483. doi:10.13227/j.hjkx.201905079

Luo, G., Liao, H., Li, Q., Liao, L., Li, Y., and Fang, A. (2018). A study of land use function transformation based on ecological-production-living spaces and associated eco-environment response: a case study of banan district. *J. Southwest Univ. Nat. Sci. Ed.* 40 (4), 105–113. doi:10.13718/j.cnki.xdzk.2018.04.015

Quintas-Soriano, C., Castro, A. J., Castro, H., and García-Llorente, M. (2016). Impacts of land use change on ecosystem services and implications for human well-being in Spanish drylands. *Land Use Policy* 54, 534–548. doi:10.1016/j.landusepol.2016.03.011

Sudhira, H. S., Ramachandra, T. V., and Jagadish, K. S. (2004). Urban sprawl: metrics, dynamics and modelling using GIS. *Int. J. Appl. Earth Obs. Geoinf.* 5 (1), 29–39. doi:10.1016/j.jag.2003.08.002

Sun, X., Yu, C., Wang, J., and Wang, M. (2020). The intensity analysis of production living ecological land in Shandong province, China. *Sustainability* 12 (20), 8326. doi:10.3390/su12208326

Tan, Z., Guan, Q., Lin, J., Yang, L., Luo, H., Ma, Y., et al. (2020). The response and simulation of ecosystem services value to land use/land cover in an oasis, Northwest China. *Ecol. Indic.* 118, 106711. doi:10.1016/j.ecolind.2020.106711

Tian, F., Li, M., Han, X., Liu, H., and Mo, B. (2020). A production–living–ecological space model for land-use optimisation: a case study of the core tumen river region in China. *Ecol. Modell.* 437, 109310. doi:10.1016/j.ecolmodel.2020.109310

Wang, X., and Bao, Y. (1999). Study on the methods of land use dynamic change research. *Prog. Geogr.* 18, 81–87.

Wang, D., Jiang, D., Fu, J., Lin, G., and Zhang, J. (2020). Comprehensive assessment of production–living–ecological space based on the coupling coordination degree model. *Sustainability* 12 (5), 2009. doi:10.3390/su12052009

Wang, A., Liao, X., Tong, Z., Du, W., Zhang, J., Liu, X., et al. (2022). Spatial-temporal dynamic evaluation of the ecosystem service value from the perspective of "production-living-ecological" spaces: A case study in dongliao River basin, China. *J. Clean. Prod.* 333, 130218. doi:10.1016/j.jclepro.2021.130218

Wang, R., Zhao, X., Guo, X., Ye, Y., Li, Y., and Zhou, Y. (2021). A study on land use transformation and ecological environment effects from the perspective of "production-living-ecological space": a case study of yingtan city, jiangxi province. *Acta Agric. Univ. Jiangxiensis* 43 (3), 681–693. doi:10.13836/j.jjau.2021075

Wang, Y., Wang, Y., Zhang, J., and Wang, Q. (2021). Land use transition and its associated eco- environmental effect: A case study of coastal area in fujian province. *Acta Sci. Circumstantiae* 41 (10), 3927–3937. doi:10.13671/j.hjkxxb.2021.0294

Xiang, X., Li, F., Ouyang, X., Shang, J., and Shao, H. (2021). The production-life-ecological space transformation and ecological effect analysis of Pingshan County. *Hubei Agric. Sci.* 60 (10), 60–63. doi:10.14088/j.cnki.issn0439-8114.2021.10.011

Xie, Z., Li, X., Chi, Y., Jiang, D., Zhang, Y., Ma, Y., et al. (2021). Ecosystem service value decreases more rapidly under the dual pressures of land use change and ecological vulnerability: a case study in zhujiajian island. *Ocean. Coast. Manag.* 201, 105493. doi:10.1016/j.ocecoaman.2020.105493

Yang, Q. K., Duan, X. J., and Wang, L. (2018). Land use transformation based on ecological-production-living spaces and associated eco-environment effects: A case study in the yangtze river delta. *Sci. Geogr. Sin.* 38 (1), 97–106.

Yang, Y., Bao, W., and Liu, Y. (2020a). Coupling coordination analysis of rural production-living-ecological space in the Beijing-Tianjin-Hebei region. *Ecol. Indic.* 117, 106512. doi:10.1016/j.ecolind.2020.106512

Yang, Y., Bao, W., Li, Y., Wang, Y., and Chen, Z. (2020b). Land use transition and its eco-environmental effects in the beijing–tianjin–hebei urban agglomeration: a production–living–ecological perspective. *Land* 9 (9), 285. doi:10.3390/land9090285

Yu, L., Song, A., Zheng, Y., Jian, Q., and Zhang, P. (2017). The ecological-living-industrial land classification system and the analysis of its spatial distribution: case of changli county. *Chin. J. Agric. Resour. Regional Plan.* 38 (2), 89–96. doi:10.7621/cjarrp.1005-9121.20170213

Zhang, Y., Liu, Y., Gu, J., and Ding, Q. (2011). Land use/land cover change and its environmental effects in Wuhan city. *Sci. Geogr. Sin.* 31 (10), 1280–1285. doi:10.13249/j.cnki.sgs.2011.10.016

Zhang, H., Xu, Er., and Zhu, H. (2017). Ecological-living-productive land classification system in China. *J. Resour. Ecol.* 8 (2), 121–128. doi:10.5814/j.issn.1674-764X.2017.02.002

Frontiers in Environmental Science

# The characteristics and influencing factors of change in farmland system vulnerability: A case study of Sanmenxia City, China

Pu Niu[1,2], Yulong Jiang[3], Yongfang Yang[3]* and Li Wang[4]

[1]School of Marxism, Henan University, Kaifeng, Henan, China, [2]Research Institute of Marxism, Henan University, Kaifeng, Henan, China, [3]College of Geography and Environmental Science, Henan University, Kaifeng, Henan, China, [4]Law School of Henan University, Kaifeng, Henan, China

The farmland social-ecological system is an integral part of a regional ecological system, and uses its unique perspective to trace the evolution of vulnerability of the whole ecosystem. Based on the theory of ecosystem vulnerability, the Vulnerability Scoping Diagram (VSD) assessment framework and index system of farmland system vulnerability were constructed by using multi-factor comprehensive analysis, ArcGIS spatial analysis and a factor contribution model. We evaluate the dynamic changes and influencing factors of farmland system vulnerability in Sanmenxia City, aiming to demonstrate the ways in which this vulnerability changes. The results showed a downward trend in the vulnerability of the farmland system in the city over a period of 17 years, from 0.60 in 2000 to 0.36 in 2016. From a spatial perspective, the distribution of vulnerability is uneven in each district and county. The pattern of vulnerability changed from "high in the Middle East-low in the southwest" in 2000 to "high in the Middle East-low in the southeast" in 2016. Population growth, high-speed urbanization, intensity of farmland use, factor input intensity and other human social and economic activities, together with the implementation of regional agricultural policies, have reduced the natural risk impact on the farmland social-ecological system. This is highly significant in revealing the overall evolution process and regional ecosystem mechanisms and informs the discussion on farmland social-ecosystem vulnerability in these representative areas.

KEYWORDS

social-ecological system (SES), farmland system, vulnerability, exposure, sensitivity, adaptive capacity

# 1 Introduction

Farmland is a composite social-ecological system (SES) with the highest degree of human dependence (Neset et al., 2019) and a part of the regional ecosystem (Hagenlocher et al., 2018; Lazzari et al., 2020). The study of farmland SES reveals the evolutionary rules of the overall vulnerability of ecosystems from a particular perspective (Wiréhn et al., 2017; Neset et al., 2019). In recent years, the farmland system has shown two kinds of mutually repelling, ecological service functions. One is that of significantly increasing risk to the farmland system due to disasters, extreme weather and excessive human disturbance (O´ Brien et al., 2004; Bindi and Olesen, 2011), and the other is excessive food, fiber and energy production, which is continuously provided by farmland systems addressing human needs (Fischer et al., 2002; Berry et al., 2006; Kovács et al., 2017; Wiréhn, 2018), showing strong stability. In 2020, as a result of global environmental change, many regions in China suffered natural disasters in the form of floods, geological disasters, hail and typhoons. A total of 138 million people were affected throughout the year, with the affected area of crops reaching 19, 957, 700 $hm^2$; however, the total national grain output in 2020 was 669.49 million tons, an increase of 5.65 million tons on 2019, or 0.9%, reflecting the coexistence of both the vulnerability and stability of the farmland system.

Farmland system stability relates to strategies for both food security and people's livelihoods. To demonstrate the rules for change of farmland system vulnerability, this research addresses the following questions: What is the impact on the regional farmland system and what changes have taken place? What are the factors driving the continuous development of the farmland system? What measures do humans need to take to cope with these changes? From the perspective of regional farmland system vulnerability, using Sanmenxia (Henan Province, China) City as a typical example, this research constructed a Vulnerability Scoping Diagram (VSD) model and established an assessment indicator system for farmland system vulnerability. The research analyzed this vulnerability in three ways, in terms of exposure, sensitivity and adaptive capacity. This research is important for maintaining farmland functions and structure, promoting the sustainable development of agriculture, and maintaining the stability of the ecosystem (Walker and Salt, 2006). Meanwhile, the social-ecological system operates a cascade mechanism, and cross-scale interaction is considered to be the basis of this cascading regime transformation (Pulver et al., 2018; Rocha et al., 2018), therefore, research on the micro-scale ecosystem process provides a valuable reference for the ecosystem over a wider spatial range or a long time period and determines the dynamic process of the system (Peters et al., 2007; Ting et al., 2020).

# 2 Theoretical background and analytical framework

## 2.1 Review of studies of farmland system vulnerability

Social-ecological vulnerability is when individuals or groups in the system cannot cope with pressure interference, which affects the cascade effect of the system and the independent feedback between social and ecological components (Adger, 2000; Adger, 2006; Cinner et al., 2012; Lazzari et al., 2021). The farmland system is part of the composite SES (Wang et al., 2021). In this system, humans, land resources and the environment interact on multiple spatial and temporal scales (Liu et al., 2007; Wilson et al., 2018; Wiréhn, 2018), leading to a system with a dynamic, complex, adaptive nested structure and multiple functional characteristics, which are constantly reshaped by external factors (such as environmental, social, economic, and political changes) and internal factors (e.g., social, economic, political changes, labor availability, production inputs, and other changes in livelihood needs) (Adger, 2006; Rockenbauch and Sakdapolrak, 2017). Such interaction of internal and external factors may unexpectedly disturb the farmland SES (Li and Zander, 2019) and produce feedback effects on social and natural systems (Chen et al., 2019). Therefore, there is some urgency to solve the complexity of the various services of social-ecological, farmland systems and to understand how social and economic services respond to system interventions and the vulnerability challenges this causes, and the need for sustainable management of farmland resources (Wang, 2021).

The farmland system has the dual attributes of agricultural and land resources. The FAO (2021) and the Intergovernmental Panel on Climate Change (IPCC, 2001) pointed out that vulnerability relates to the various risks of food insecurity or malnutrition, including factors that affect people's ability to cope with stress or change, and the degree to which natural or social systems are vulnerable or incapable of coping with the adverse effects of climate change. Existing studies have mainly focused on vulnerability in the fields of climate change and ecosystem services (Cinner et al., 2013; Thiault et al., 2017; Siegel et al., 2019). These studies were mainly concerned with the causes of farming vulnerability due to changes in land use arising from climate change (Jamir, 2013; Bennett et al., 2016) and disaster intrusion (Jinno, 1995; Brugere, 2003; Huang et al., 2012); the dimensions of analysis mainly included system exposure (Pereira, 2012), government and farmer input (Jamir, 2013), infrastructure and industrial sensitivity and other dimensions affecting ecosystem vulnerability (Speranza, 2014; Rogers, 2020), the vulnerability of farmers' production and livelihoods
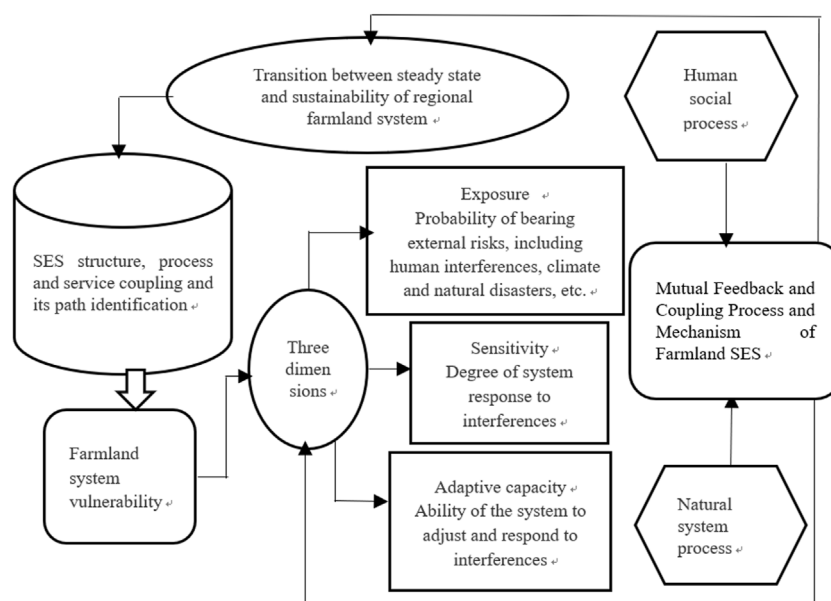
**FIGURE 1**
Vulnerability elements and interrelations of the farmland system.

(Ashley, 2000; Brugere, 2003; Tebbotha, 2019), and the vulnerability of food security and the agricultural industry (Ashley, 2000.; Xie, 2014).

Many theoretical frameworks for vulnerability research have been developed in the past decade, among which Value Sensitive Design (VSD) and Agent Differential Vulnerability (ADV) integrated vulnerability assessment frameworks are widely applied. Acosta-Michlik and Rounsevell (2012) established an ADV framework to elaborate on the complexity and dynamics of human-environmental interactions to predict the degree of ecological vulnerability in different regions. Using the VSD vulnerability framework, Jamir et al. (2013) selected evaluation indicators from exposure, sensitivity and vulnerability to evaluate the vulnerability of farmers in Nagaland, India, and classified the driving factors of this.

In summary, previous studies have been limited to large-scale land and agricultural systems, however, few studies took the farmland system (that intersects the land and agricultural systems) as the object of research. In particular, there was a lack of evaluation and analysis of farmland system vulnerability in typical regions and few studies have focused on the factors that cause this. Therefore, we aimed to reveal the disturbance mechanism of the farmland system in the face of both natural and consequent social disasters, revealing the key factors influencing the development of a more stable and improved farmland system (Salvati et al., 2011), to cultivate and maintain its adaptive capacity and to allow it to be quickly updated and reshaped after any disturbance (Armitage, 2008).

## 2.2 Theoretical framework

With the increase of the degree of risk and uncertainty of the farmland system, the vulnerability framework has become a useful tool for assessing SES vulnerability (Adger, 2006). VSD can address SES problems that are difficult to solve using traditional methods, such as space and time complexity, nonlinearity, feedback loops and uncertainty (Mumby et al., 2014; Pham et al., 2017), and therefore, it is widely applied in system vulnerability assessment. The ADV model focuses on predicting the future, while the VSD model is better at assessing the current situation. Based on the VSD framework proposed by Kienberger (2013), farmland system vulnerability is assessed by its exposure, sensitivity and adaptive capacity. In this section, the literature on the theoretical framework is presented, followed by an introduction to the data sources and research methods. The assessment results of typical cases are then described before the analysis of these results and final conclusions.

### 2.2.1 The conceptual framework of vulnerability

As shown in Figure 1, the basic framework of the VSD model consists of three dimensions: exposure, sensitivity and adaptive capacity. Exposure refers to the degree to which the system may be susceptible to damage and is generally related to the "risk" faced by the system; the degree of exposure depends on the probability of exposure to potential threats to the system and determines the degree of potential loss it faces (Turner et al., 2003; Smit and Wandel, 2006; Perry et al.,

**FIGURE 2**
Location map of Sanmenxia City. (source from: National Earth System Science Data Center of the Chinese Academy, http:www.geodata.cn).
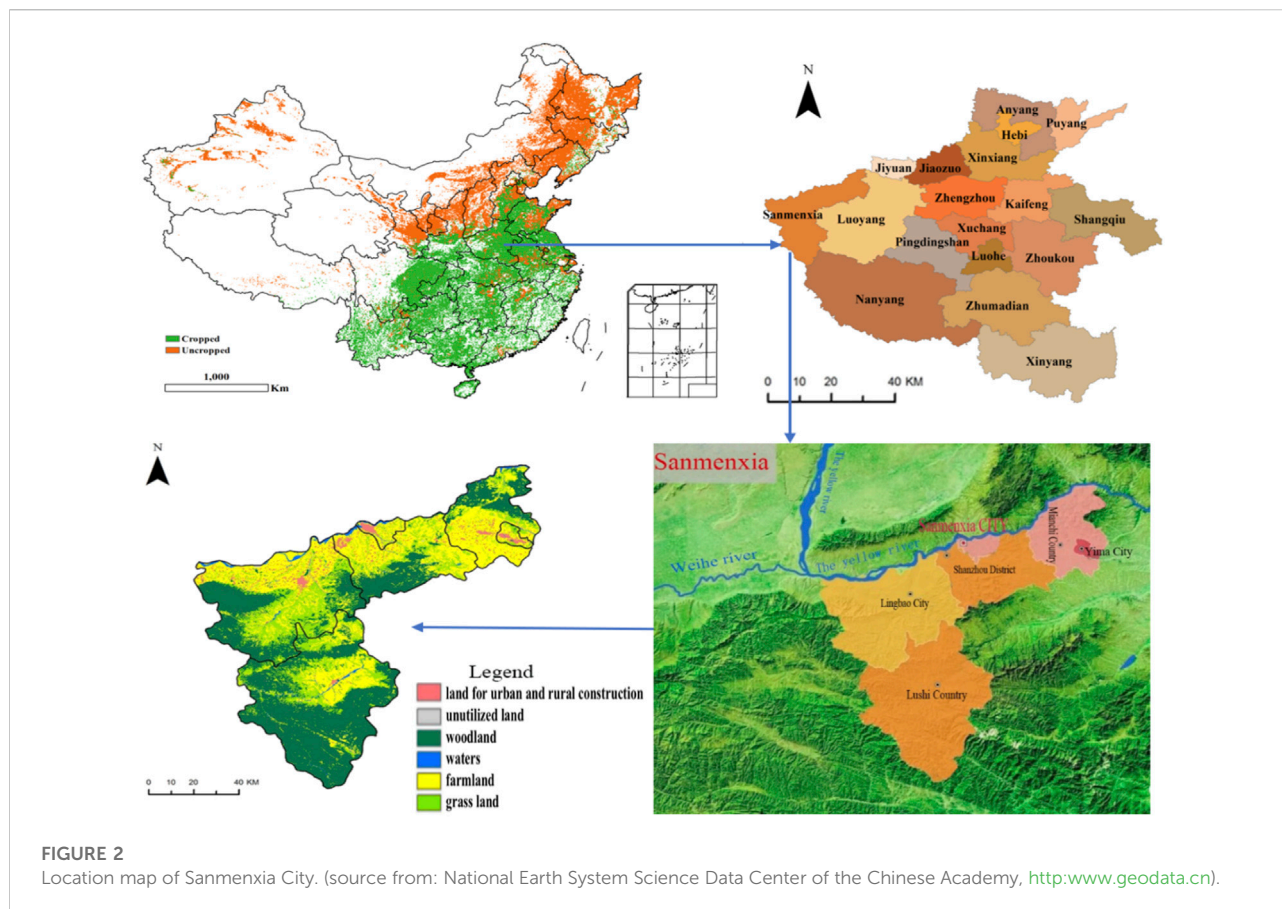
2011). Sensitivity refers to the degree of difficulty for the system to maintain normal operations when it is subjected to external disturbances (Watts and Bohle, 1993), mainly reflecting the system's ability to resist threat; the level of sensitivity depends on the system's stability. Systems with lower sensitivity are less likely to be affected by disturbances and are more likely to maintain normal operations (O'Brien and Leichenko, 2000; O'Brien et al., 2004). Adaptive capacity is the ability of the system to adjust its productive activities and resource management strategies in response to disturbances. It determines the actual loss of the system when it suffers damage, therefore, the lower the adaptive capacity, the lower the actual damage to the system. The system changes, adjusting its state and parameters through its own adaptive capacity and human adaptive behavior, which affects its actual state under exposure pressure and its ability to recover after damage (Folke et al., 2003; Cinner et al., 2009; Bussey et al., 2012; Bennett et al., 2014). The VSD model classifies and displays the vulnerability elements, clearly explaining the relationship between these, and builds a complete assessment framework (Adger, 2006) that provides a theoretical basis for constructing an indicator assessment system and selecting assessment indicators.

## 2.2.2 Relationship between the three dimensions of vulnerability

The vulnerability of the farmland system is the result of the dual impact of the natural environment and human activities due to the intervention of various policies such as farmland utilization, protection and restoration (Walker et al., 2004; Berkes and Ross, 2016). The impact on the natural environment mainly comes from meteorological and geological disasters such as extreme low temperature, frost, drought, and floods (Copeland et al., 2020), in terms of interference to human activity, with the feedback effect of human production and plundering of crops. Increasing crop plundering reduces the return of farmland system production, destroys farmers' intention to retain farmland for planting, and leads to abandonment, pollution and loss of farmland system functions (Cutter, 2016; Siegel et al., 2019). If the dual impact of natural and human activities is positive, it will weaken the vulnerability of the farmland system; if it is negative, it will strengthen its vulnerability and undermine the stable operation of the system (Saja et al., 2019). The sensitivity of the farmland system is its response to exposure; the magnitude and rate of this response reflect the sensitivity degree of the farmland system to disaster intrusion (Copeland et al., 2020). Adaptive capacity captures the ability to respond to and address social and ecological changes by

**FIGURE 3**

Changes in the farmland area of Sanmenxia City. (source from: Sanmenxia Natural Resources Bureau and the Statistical Yearbook of Sanmentxia City from 2000-2017).
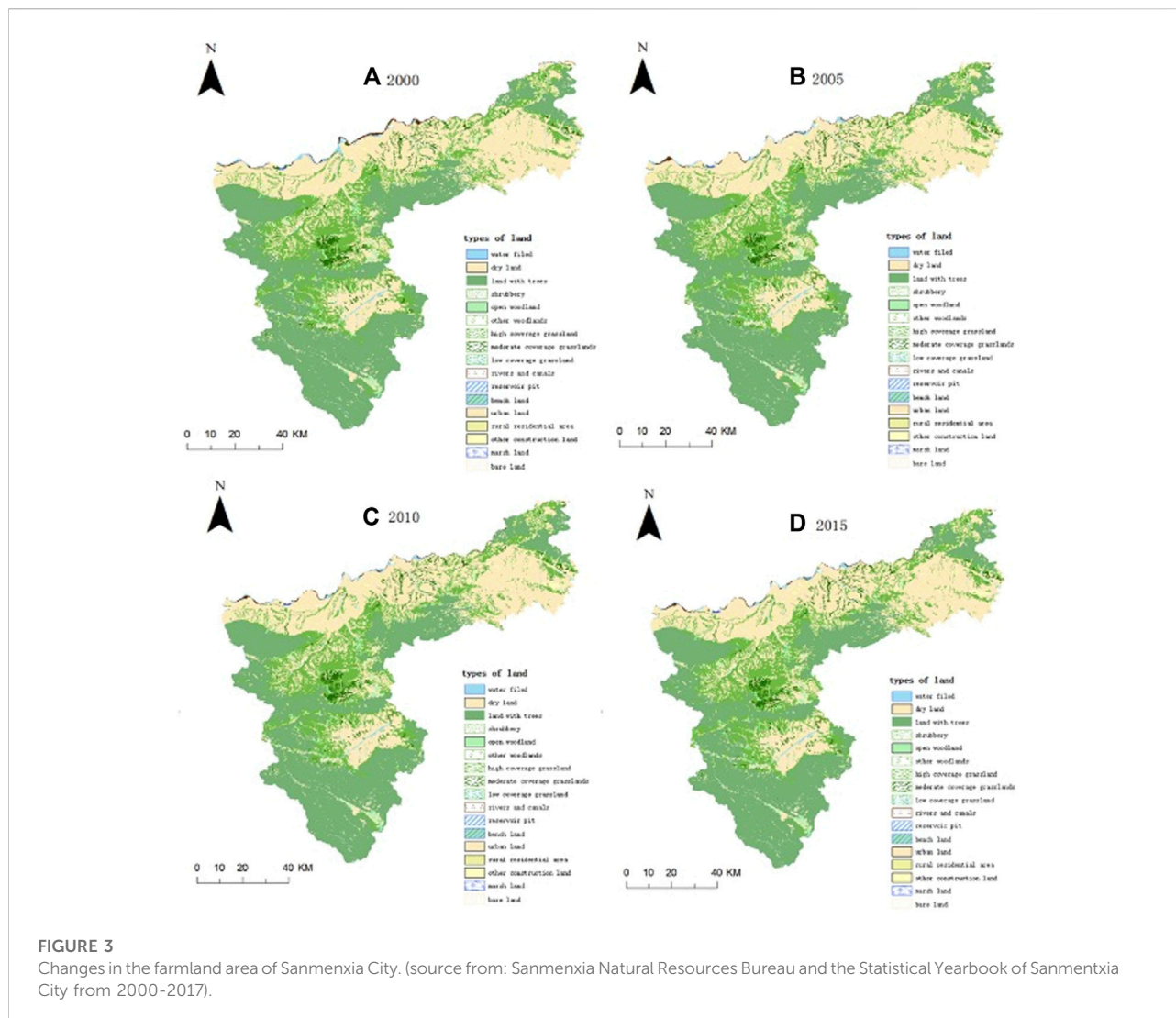
mitigating, coping with and recovering from the potential impact caused by a particular pressure (Thiault et al., 2019). The adaptive capacity of the farmland system can adjust and change the parameters of the potential state and determine the actual loss; the self-organization and adjustment capacity of the farmland system, policy protection and technology upgrades have improved the antagonistic ability of farmland to cope with risks (Lorenz, 2013).

# 3 Materials and methods

## 3.1 Characteristics of the study area

Covering an area of 10,496 km$^2$, Sanmenxia City is located in the western part of Henan Province on the south bank of the Yellow River Delta and is the intersection of the eastern extension of the Qinling Mountains with Funiu Mountain, Xiong'er Mountain and Xiao Mountain. Sanmenxia City has the obvious characteristics of a transition zone. First, located at the intersection of the eastern edge of the Loess Plateau and the Yellow River Delta, it is the transition zone from the Loess Plateau to the alluvial plain. Second, located in the Qinling Mountains (Huai River transition zone), it is a transitional zone from a semi-humid to a semi-arid climate. In terms of the administrative location, Sanmenxia City borders Luoyang City to the east, Weinan to the west, Yuncheng of Shanxi Province to the north across the Yellow River and Nanyang to the south. It is the junction area of Henan, Shaanxi and Shanxi provinces. It is not only the central city of the Yellow River Golden Triangle region but is also a node city along the Belt and Road, so it has an important strategic location. Under the

| District | 2000 | 2005 | 2010 | 2015 |
|---|---|---|---|---|
| Hubin County | 99.53 | 100.89 | 100.19 | 99.98 |
| Mianchi County | 730.97 | 717.09 | 715.47 | 713.77 |
| Lushi County | 682.47 | 681.81 | 681.11 | 681.02 |
| Yima City | 64.61 | 63.36 | 58.99 | 58.99 |
| Lingbao City | 979.59 | 1,011.86 | 1,011.85 | 1,010.36 |
| Shanxian County | 781.62 | 781.74 | 779.44 | 775.41 |
| Sanmenxia City | 3,338.79 | 3,356.75 | 3,349.82 | 3,339.53 |

jurisdiction of Sanmenxia City, there are two districts and four counties, namely, Hubin District, Shanzhou District, Lingbao City, Yima City, Mianchi County, and Lushi County. In 2017, the city's total population was 2,305,500 and regional GDP was 146.081 billion yuan, representing an increase of almost ten times that of 2000. GDP grew steadily in 2000–2018 with an annual growth rate of 13.81%.

## 3.2 Data source

### 3.2.1 Land use data

The remote sensing images of Landsat TM/ETM/OLI 30*30 m provided by the National Earth System Science Data Center of the Institute of Geographical Sciences and Resources of the Chinese Academy of Sciences were the main data source of the study. After image fusion processing, geometric correction, image enhancement and splicing, the remote sensing data of farmland in the years 2000 (Figure 3A), 2005 (Figure 3B), 2010 (Figure 3C), and 2015 (Figure 3D) were obtained using the human-computer interaction visual interpretation method. In combination with the land change survey data provided by Sanmenxia Natural Resources Bureau and the Statistical Yearbook of Sanmenxia City from 2000 to 2017, the farmland utilization data of each county and district were obtained, as shown in Table 1 and Figure 4. The number and transfer direction of farmland change in the periods 2000–2005 (Figure 4A), 2005–2010 (Figure 4B), 2010–2015 (Figure 4C), and 2000–2015 (Figure 4D) were calculated using the transfer matrix, as shown in Figure 5. Due to changes in the quantity of farmland, the per capita farmland area in Sanmenxia City in
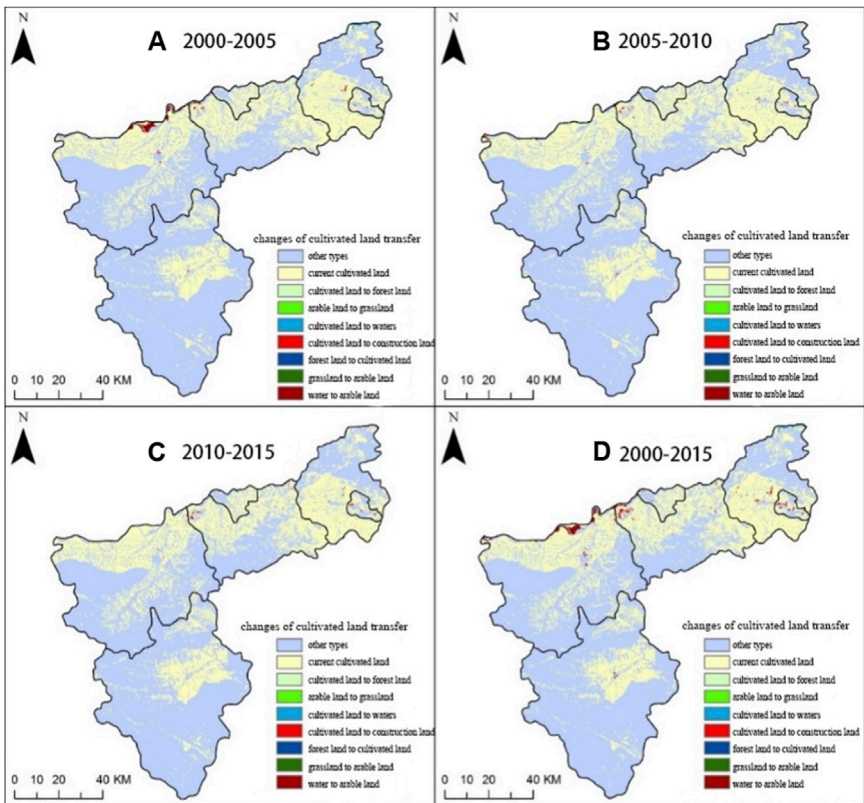


FIGURE 4
Direction of farmland transfer in Sanmenxia City.

FIGURE 5
Changes in the vulnerability of the farmland system in Sanmenxia City.
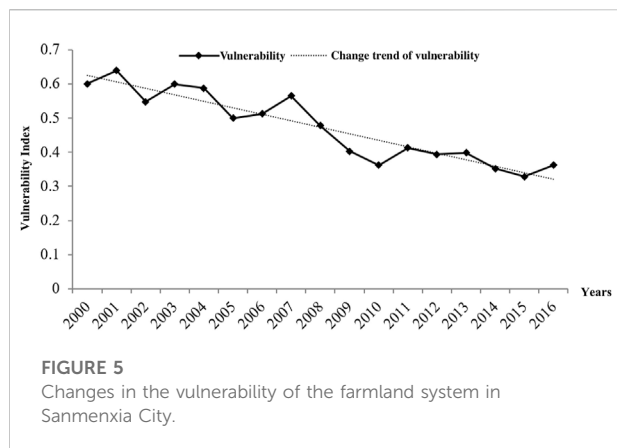
2018 was 0.0762 ha, which was lower than the per capita quantity of 0.0853 ha in Henan Province at the end of 2016 and lower than the per capita farmland area of 0.9667 ha in the whole country.

### 3.2.2 Data collected in the field

We went to Sanmenxia City and the districts and counties under its jurisdiction to collect data and conduct interviews. Sanmenxia Meteorological Bureau provided meteorological observation data and agricultural meteorological disaster data from various meteorological stations for the years 2000–2017. The Agriculture Bureau of Sanmenxia City and its districts and counties provided data on agricultural production, agricultural disasters and disaster prevention for this period. Farmland protection experts from the Sanmenxia Municipal Bureau of Land and Resources and the Agriculture Bureau scored each of the selected indicators.

### 3.2.3 Statistical data

Statistical data was obtained from the Henan Statistical Yearbook, Sanmenxia Statistical Yearbook, Sanmenxia Almanac, and statistical yearbooks of districts and counties of Sanmenxia City, the Land and Resources Bulletin, the Bulletin of Soil and Water Conservation of Henan Province, statistical bulletins, and government work reports of districts and counties of Sanmenxia City in 2000–2017.

## 3.3 Methods

### 3.3.1 Construction of the vulnerability assessment indicator system

The complexity of the farmland system itself makes it difficult to select and construct a farmland system vulnerability assessment system. Since system vulnerability is unobservable and cannot be directly measured (Carpenter, 2005), we used a combination of multiple indicators to characterize three dimensions of system vulnerability, as indicated in Table 2.

### 3.3.1.1 Exposure

The risks faced by the farmland system mainly come from changes in the natural environment and the interference of human social activities. Mean annual temperature and annual rainfall can indicate water and thermal conditions throughout the year, and changes in temperature and precipitation have a crucial impact on crop growth. Annual drought days and torrential rain days reflect the risk probability of agro-meteorological disasters, with the former determined by the soil entropy measurement report, and the latter according to the standard of 30 mm of rainfall within 12 h and 50 mm of rainfall within 24 h. Per capita farmland reflects the change in the amount of farmland; a decrease in the amount of farmland resources threatens food security. Changes in highway density, population density and urbanization reflect the degree of stress on the farmland system caused by social and economic development. Discharge of industrial wastewater may pollute the farmland and affect environmental conditions and crop growth. In addition to the pollution of industrial wastewater, we should also pay attention to the agricultural non-point source pollution caused by the use of pesticides, fertilizers and mulching films. The more of this is used, the greater the threat of pollution to the farmland.

### 3.3.1.2 Sensitivity

Grain yield is an important indicator of measuring the operational status of the farmland system. The more stable the farmland system, the higher the grain yield. The multiple cropping index and reclamation rate reflect the intensity of farmland use. Insufficient use of farmland resources leads to wasted resources, while overdevelopment also leads to problems such as farmland and environmental degradation. The water-soil coordination reflects the irrigation level of the farmland, and an improvement in irrigation capacity can ensure the growth of crops. The forest coverage rate and sewage treatment rate are responses to the ecological environment and pollution threats. The expansion of vegetation coverage can preserve water and soil and improve the quality of the ecological environment. Farmland ecosystem resilience characterizes its ability to maintain the structure and pattern of the ecological environment, namely, the ability of farmland to gradually rebound and recover after disturbance (Lizhen et al., 2010).

### 3.3.1.3 Adaptive capacity

Financial investment in agriculture by government can reflect their efforts to improve agricultural technological innovation and progress. The proportion of financial expenditure on environmental protection reflects the degree of investment in environmental governance. The higher the degree, the better the quality of the ecological environment. Rural

TABLE 2 Assessment indicator system for farmland system vulnerability.

| Target hierarchy | Criterion hierarchy | Indicator hierarchy | Indicator weight | Indicator nature |
|---|---|---|---|---|
| Farmland system vulnerability | Exposure | $X_1$ Mean annual temperature (°C) | 0.021 | − |
| | | $X_2$ Mean annual rainfall (mm) | 0.031 | − |
| | | $X_3$ Annual drought days | 0.063 | + |
| | | $X_4$ Annual torrential rain days | 0.041 | + |
| | | $X_5$ Per capita farmland ($hm^2$) | 0.041 | − |
| | | $X_6$ Highway density ($km/km^2$) | 0.050 | − |
| | | $X_7$ Population density (people/$km^2$) | 0.024 | + |
| | | $X_8$ Urbanization rate (%) | 0.022 | + |
| | | $X_9$ Pesticide load per unit of farmland ($kg/hm^2$) | 0.022 | + |
| | | $X_{10}$ Fertilizer load per unit of farmland ($kg/hm^2$) | 0.013 | + |
| | | $X_{11}$ Mulching film load per unit of farmland ($kg/hm^2$) | 0.022 | + |
| | | $X_{12}$ Wastewater load per unit of farmland ($kg/hm^2$) | 0.035 | + |
| | Sensitivity | $X_{13}$ Grain yield ($kg/hm^2$) | 0.027 | − |
| | | $X_{14}$ Multiple cropping index | 0.023 | + |
| | | $X_{15}$ Reclamation rate (%) | 0.044 | − |
| | | $X_{16}$ Water-soil coordination | 0.088 | − |
| | | $X_{17}$ Forest coverage rate (%) | 0.056 | − |
| | | $X_{18}$ Sewage treatment rate (%) | 0.045 | − |
| | | $X_{19}$ Farmland ecosystem resilience | 0.065 | − |
| | Adaptive capacity | $X_{20}$ Agricultural financial expenditure per unit of farmland ($10^4$ yuan/$hm^2$) | 0.064 | − |
| | | $X_{21}$ Ratio of environmental protection expenditure (%) | 0.019 | − |
| | | $X_{22}$ Total rural income per capita (yuan) | 0.038 | − |
| | | $X_{23}$ Employment level in primary industry | 0.020 | − |
| | | $X_{24}$ Agricultural output value per unit of farmland ($10^4$ yuan/$hm^2$) | 0.018 | − |
| | | $X_{25}$ Number of motor-pumped wells (unit) | 0.055 | − |
| | | $X_{26}$ Agricultural mechanization level | 0.053 | − |

*Note*: + means the indicator has a positive impact on farmland system vulnerability, and − means the indicator has a negative impact on farmland system vulnerability.

income per capita reflects the changes in farmers' income, and increases can promote an improvement in farming levels. The employment level in primary industry reflects the flow of agricultural labor and changes in the industrial structure. Generally, the lower the employment level in primary industry, the less development and use of farmland resources. The number of motor-pumped wells and the general level of agricultural mechanization reflect the degree of agricultural infrastructure and mechanization. The better the farming conditions, the higher the adaptive capacity of the farmland system.

### 3.3.2 Assessment and classification of farmland system vulnerability

In this study, we used the composite index method to assess farmland system vulnerability. The core of this method lies in the construction of the indicator system and the determination of the weight of each indicator. The calculation model is as follows:

$$VI = \sum_{i=1}^{n} P_{ij} W_i \qquad (1)$$

where *VI* denotes the farmland system vulnerability index, $P_{ij}$ is the standardized value of each vulnerability indicator factor, $W_i$ is the weight of the *i*th indicator, *n* is the number of vulnerability indicators; the indicator value of each dimension is calculated by the value of each indicator.

With reference to previous research results and the results of Formula 1, we classified the vulnerability index of the farmland system into five levels from high to low: extreme, severe, moderate, mild and slight, as shown in Table 3. The greater

TABLE 3 Classification of farmland system vulnerability.

| Vulnerability level | Definition | References |
|---|---|---|
| Extreme | The structure of the farmland system is greatly damaged, ecological functions are lost, environment is polluted, and disasters occur frequently and are harmful | Bennett et al., 2016; Barros et al. (2014) |
| Severe | The structural damage of the farmland system is relatively serious, farmland degradation and ecological damage are relatively serious, and disasters occur frequently and have a greater impact on social and economic development | O'Brien et al. (2000); Marull et al. (2007) |
| Moderate | The structure of the farmland system is damaged, the ecological environment is deteriorated, the service functions are destroyed, disasters occur from time to time, and the production activities of farmland are greatly disturbed | Adger, (2006); Speranza et al. (2014) |
| Mild | The structure of the farmland system is relatively complete, the operation is good, and the ecological environment is basically stable. The farmland is slightly disturbed and destroyed, but it has little impact on the production activities of the farmland | Tuler et al. (2008); Wilson et al. (2013) |
| Slight | The structure of the farmland system is complete, the operational status is healthy, the ecological environment is stable, the flow of material and energy is smooth, and the input and output effect of farmland is good | Brklacich et al. (2009); Xutong, (2020) |

the vulnerability index of the farmland system, the higher the vulnerability level.

### 3.3.3 Data processing and determination of indicator weight

#### 3.3.3.1 Data processing

Since the factors influencing farmland system vulnerability are of different units, it is necessary to standardize the data and unify the dimensions. We used the maximum and minimum method to nondimensionalize the original data. The calculation formula is as follows:

Positive indicator:

$$P_{ij} = \frac{X_{ij} - X_{min}}{X_{max} - X_{min}} \qquad (2)$$

Negative indicator:

$$P_{ij} = \frac{X_{max} - X_{ij}}{X_{max} - X_{min}} \qquad (3)$$

where $P_{ij}$ is the standardized value of the indicator, $X_{ij}$ is the original data of the $j$th indicator in the $i$th year, and $X_{max}$ and $X_{min}$ are the maximum and minimum values of the $j$th indicator.

#### 3.3.3.2 Determination of indicator weight

In this study, we used the subjective and objective combined weighting method to determine the weight of each indicator. For objective weighting, we used the entropy method, and for subjective weighting, we used the analytic hierarchy process (AHP).

**3.3.3.2.1 Entropy method.** We constructed a judgment matrix and determined the weight based on the amount of information contained in the indicator data and its effect on

system changes. First, if there are $m$ indicators and $n$ objects to be evaluated, the information entropy of the $j$th indicator is calculated:

$$f_{ij} = \frac{P_{ij}}{\sum_{j=1}^{n} P_{ij}} \qquad (4)$$

where $k = 1/ln\,_m$, $k > 0$; $P_{ij}$ is the standardized indicator value; when $f_{ij} = 0$, let $f_{ij} \ln f_{ij} = 0$.

Next, the effect value $h_j$ of the $j$th indicator is calculated:

$$h_j = 1 - e_j \qquad (5)$$

The weight $W_i$ of the $j$th indicator is calculated:

$$w_i = \frac{1 - H_i}{1 - \sum_{i=1}^{m} H_i} \qquad (6)$$

where $n = 1,2,3 \ldots \ldots$; $0 < w_i < 1 \sum_{j=1}^{m} w_i$, $= 1$.

According to the above calculations, we can obtain the entropy weight of each indicator, and then determine the weight value $w_q$ of the objective weighting method.

**3.3.3.2.2 Determination of factor weight value.** According to the expert scoring, by calculating the maximum eigenvalue $\lambda_{max}$ of the judgment matrix and the corresponding eigenvector $W$, we can obtain the ranking weight of the relative importance of the factors of the same hierarchical level relative to a factor of the previous hierarchical level. The calculation steps are as follows:

Multiply the values in the matrix by rows and calculate the $n$th power of the product, get $W_i$, normalize $W_i$, and obtain $w_i$;

$$\lambda_i = \frac{\sum_{j=1}^{n} a_{ij} w_j}{w_i} \qquad (7)$$

$$\lambda_{max} = \frac{\sum_{i=1}^{n} \lambda_i}{n} \qquad (8)$$

On the basis of single level ranking, calculate the weight value of the previous level factors for the next level to finally obtain the total level of ranking. After calculating all weight vectors, test the consistency of the comparison matrix. Only the determination of the weight passing the consistency test is valid. The consistency coefficient $CR < 0.1$ means that the judgment matrix passes the consistency test. If it fails, the judgment matrix needs to be readjusted until it reaches the satisfactory consistency standard:

$$CI = \frac{\lambda_{max-n}}{n-1} \tag{9}$$

$$CR = \frac{CI}{RI} \tag{10}$$

where $CI$ denotes the consistency coefficient of the judgment matrix and $RI$ is the average random consistency coefficient.

According to the above calculations, on the basis of passing the consistency test, we can obtain the subjective weight value $W_p$ of each indicator.

**3.3.3.2.3 Combined weighting method.** The combined weighting method comprehensively considers the subjective and objective factors and integrates the indicator weights obtained by the objective and subjective weighting methods to obtain the combined weight. In this study, we took the average of the two as the combined weight as follows:

$$W_i = \frac{W_{q+}W_p}{2} \tag{11}$$

where $W_q$ is the weight coefficient obtained by the entropy method, and $W_p$ the weight coefficient obtained by the AHP.

## 3.4 Factor contribution degree model

Identifying the contribution factors influencing vulnerability can assist in further diagnosing the vulnerability mechanism. The stability of the farmland system has an inverse relationship to its vulnerability, in other words, the lower the vulnerability value, the better the operational state of the farmland system. Therefore, using the principle of contribution degree, we improved the obstacle degree model to be a factor contribution degree model, to calculate the contribution value that affects the negative state as follows:

$$D_i = \frac{S_i V_i}{\sum_{i=1}^{n} S_i V_i} \times 100\% \tag{12}$$

$$U_r = \sum D_i \tag{13}$$

$$S_i = W_r \times W_i \tag{14}$$

where $D_i$ is the contribution degree indicating the degree of effect of the $i$th indicator on the vulnerability of the farmland system; $S_i$ is the weight of the $i$th indicator to the overall target; $V_i$ is the

indicator membership degree, namely, the evaluation value of the $i$th indicator; $U_r$ is the contribution degree of the $r$th criterion to the vulnerability; $W_r$ is the weight of the $r$th criterion; and $W_i$ is the weight of the $i$th indicator.

## 4 Evaluation results of the vulnerability of the Sanmenxia City farmland system

### 4.1 Indicator weight results and vulnerability classification

According to the calculation results of the above Formulas 2ormulas –Formulas 12, the weights of the entropy method of Sanmenxia City and its districts and counties are shown in Table 4.

According to the classification criteria for farmland system vulnerability assessment, we divided the vulnerability of the Sanmenxia City farmland system into five levels, as shown in Table 5.

### 4.2 Temporal changes in vulnerability

Using the farmland system vulnerability assessment method, we standardized the original data to obtain standardized values of the vulnerability assessment indicators of the farmland system in Sanmenxia City and its districts and counties. Then, using the vulnerability calculation formula, we calculated its vulnerability in 2000–2017, as shown in Figure 5.

From Figure 4, we can see that in 2000–2017, the overall vulnerability of the farmland system in Sanmenxia City showed a declining trend, decreasing from 0.60 to 0.36, a decrease of 39.7%, with overall vulnerability significantly declining. In 2000–2010, farmland system vulnerability showed a fluctuating downward trend as it was relatively high, and the fluctuations were large. After 2010, vulnerability gradually saw small fluctuations; during this period, the operation of the farmland system was stable, and development occurred. During the past 18 years, the vulnerability level declined from extreme to mild, indicating that the environment has improved greatly, with increases in both its sustainability and resilience.

#### 4.2.1 Changes in exposure
Farmland system exposure characterizes the degree to which farmland is disturbed by external factors. It is not only related to the intensity and frequency of disasters faced by the system, but also is affected by the characteristics of the system and its ability to withstand these disasters. From the perspective of risk stress, the exposure of the farmland system is influenced by the interaction of natural factors such as climate change, meteorological disasters, and human, social and economic

TABLE 4 Weights of indicators of farmland system vulnerability obtained by the combined weighting method.

| Area\indicator | Sanmenxia city | Hubin district | Shanzhou district | Lingbao city | Yima city | Mianchi county | Lushi county |
|---|---|---|---|---|---|---|---|
| $X_1$ | 0.021 | 0.012 | 0.022 | 0.012 | 0.017 | 0.016 | 0.015 |
| $X_2$ | 0.031 | 0.046 | 0.032 | 0.035 | 0.032 | 0.031 | 0.033 |
| $X_3$ | 0.063 | 0.069 | 0.065 | 0.060 | 0.064 | 0.062 | 0.063 |
| $X_4$ | 0.041 | 0.049 | 0.046 | 0.052 | 0.039 | 0.038 | 0.041 |
| $X_5$ | 0.041 | 0.029 | 0.052 | 0.030 | 0.042 | 0.038 | 0.045 |
| $X_6$ | 0.050 | 0.038 | 0.037 | 0.050 | 0.074 | 0.051 | 0.042 |
| $X_7$ | 0.024 | 0.027 | 0.027 | 0.027 | 0.042 | 0.032 | 0.019 |
| $X_8$ | 0.022 | 0.021 | 0.031 | 0.024 | 0.017 | 0.020 | 0.023 |
| $X_9$ | 0.022 | 0.025 | 0.013 | 0.033 | 0.029 | 0.014 | 0.017 |
| $X_{10}$ | 0.013 | 0.017 | 0.016 | 0.020 | 0.027 | 0.014 | 0.016 |
| $X_{11}$ | 0.022 | 0.054 | 0.018 | 0.021 | 0.024 | 0.014 | 0.018 |
| $X_{12}$ | 0.035 | 0.053 | 0.013 | 0.032 | 0.038 | 0.051 | 0.032 |
| $X_{13}$ | 0.027 | 0.029 | 0.037 | 0.029 | 0.019 | 0.044 | 0.026 |
| $X_{14}$ | 0.023 | 0.024 | 0.020 | 0.032 | 0.039 | 0.036 | 0.045 |
| $X_{15}$ | 0.044 | 0.015 | 0.042 | 0.016 | 0.032 | 0.047 | 0.061 |
| $X_{16}$ | 0.088 | 0.077 | 0.087 | 0.079 | 0.070 | 0.078 | 0.071 |
| $X_{17}$ | 0.056 | 0.054 | 0.049 | 0.062 | 0.025 | 0.041 | 0.052 |
| $X_{18}$ | 0.045 | 0.038 | 0.038 | 0.060 | 0.046 | 0.041 | 0.049 |
| $X_{19}$ | 0.065 | 0.036 | 0.063 | 0.037 | 0.052 | 0.067 | 0.082 |
| $X_{20}$ | 0.064 | 0.062 | 0.064 | 0.064 | 0.063 | 0.065 | 0.058 |
| $X_{21}$ | 0.019 | 0.033 | 0.018 | 0.020 | 0.027 | 0.022 | 0.020 |
| $X_{22}$ | 0.038 | 0.045 | 0.038 | 0.042 | 0.039 | 0.034 | 0.035 |
| $X_{23}$ | 0.020 | 0.033 | 0.019 | 0.029 | 0.027 | 0.015 | 0.015 |
| $X_{24}$ | 0.018 | 0.016 | 0.025 | 0.018 | 0.024 | 0.021 | 0.017 |
| $X_{25}$ | 0.055 | 0.058 | 0.058 | 0.057 | 0.051 | 0.054 | 0.055 |
| $X_{26}$ | 0.053 | 0.040 | 0.074 | 0.060 | 0.040 | 0.056 | 0.050 |

TABLE 5 Classification of the farmland system vulnerability of Sanmenxia City.

| Index\classification | Extreme | Severe | Moderate | Mild | Slight |
|---|---|---|---|---|---|
| Index range | >0.6 | 0.5–06 | 0.4–0.5 | 0.3–0.4 | <0.3 |

activities. To a certain extent, human activities can intensify or slow these influences.

From Figure 6, we can see that the overall exposure of the farmland system showed an upward trend, although these changes were not large, increasing from 0.16 in 2000 to 0.21 in 2017, an increase of 31%. The increase in the exposure index of the farmland system indicates that the farmland was more affected by natural and human disturbances, as the environment deteriorated, the risk to it was increased, and its stability was undermined. In 2000–2005, the exposure index declined slightly, although there were small fluctuations; in 2006–2012, the exposure index fluctuated greatly from 0.21 in 2007 to 0.14 in 2010, reaching a peak of

0.23 in 2012; after 2013, the exposure index showed a small declining trend and the farmland system remained at a high exposure level.

## 4.2.2 Changes in sensitivity

Changes in the sensitivity of the farmland system can reflect the damage caused by disasters. Sensitivity is the response to exposure and is mainly influenced by the frequency and amplitude of system interference factors, manifesting in phenomena such as changes in farmland yield and ecological degradation. The level of sensitivity can indicate the stability of the farmland system, as systems with lower sensitivity generally have higher stability.
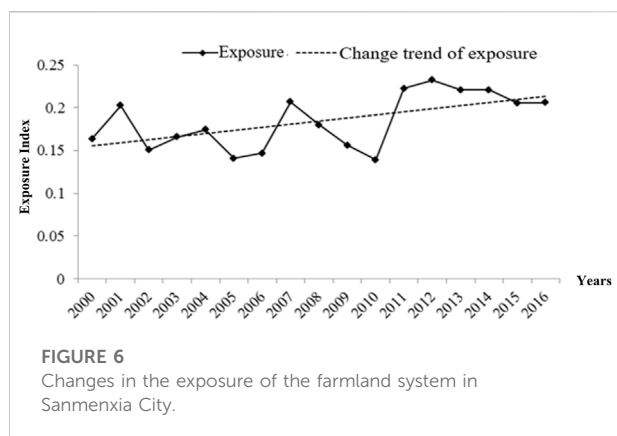
**FIGURE 6**
Changes in the exposure of the farmland system in Sanmenxia City.

In Figure 7, the sensitivity index generally shows a declining trend. In 2000–2017, the sensitivity index declined from 0.22 to 0.06, a decrease of 71%. In 2000–2006, the sensitivity index showed a temporary fluctuation. In 2001 and 2003, it experienced a low growth, but these changes were not large, and it still remained at a high level. In 2007–2012, the sensitivity index dropped sharply, with this decline slowing down after 2013. The changing trend in sensitivity of the farmland system reflects the significant improvements in its stability, with the anti-interference ability also improving.

### 4.2.3 Changes in adaptive capacity

The adaptive capacity characterizes the state and resilience of the farmland system after being disturbed. Changes in adaptive capacity determine the actual loss of farmland in the face of various risks and are mainly affected by the resilience of the farmland itself and human investment in farmland protection. Although sensitivity can describe the state of the system, it focuses on the system stability, while adaptive capacity focuses on the description of the system's resilience and indicates sustainable development.

Figure 8 shows that in 2000–2017, the adaptive capacity index of the farmland system showed a declining trend from 0.29 to 0.1, a decrease of 66%, which suggests that its capacity to withstand pressure to cope with risks was greatly improved. Specifically, in 2000–2010, the adaptive capacity index declined from 0.27 to 0.2, but the decline rate was small, showing that the adaptive capacity of the farmland system during this period improved rapidly; in 2010–2014, the adaptive capacity index rapidly declined; after 2015, it increased, with a large fluctuation that reflected the instability of the adaptive capacity. The lower the adaptive capacity index, the lower the vulnerability index of the farmland system, with a decline in the adaptive capacity index indicating a corresponding increase in resilience.

## 4.3 Analysis of the degree of vulnerability changes

To reveal the regional differences in the vulnerability of the farmland system in the districts and counties of Sanmenxia City, the average value, standard deviation, coefficient of variation and slope of change based on the vulnerability index of the farmland system in each county and district in 2000–2017 were calculated. The average value indicates the average level of farmland system vulnerability during these years. The standard deviation and coefficient of variation reveal the variation of the vulnerability index of the farmland system in the time series of each district and county. The trend slope fits the vulnerability index of the farmland system against time and reflects the degree of vulnerability changes in the time dimension as shown in Figure 9. During this period, Mianchi County had the highest coefficient of variation in the farmland system vulnerability index at 0.251, followed by Lushi County at 0.198, with the lowest being Yima City at only 0.106. Mianchi County and Lushi County had the most significant changes in vulnerability of the farmland system.

## 4.4 Spatial changes in vulnerability

To further explore the changes in vulnerability, we analyzed the spatial differentiation characteristics of the vulnerability of the farmland system in Sanmenxia City's districts and counties. We selected the four time periods of 2000, 2006, 2010 and 2016, and used ArcGIS 10.3 for technical processing. Through data visualization, it is possible to show the spatial changes in vulnerability at the county scale.

From Figure 10, we can see that in 2000, the overall vulnerability of the farmland system was relatively high, and the level of vulnerability was severe. Specifically, the vulnerability of the farmland system in Hubin and Shanzhou Districts in the central region of Sanmenxia City was at an extreme level, Mianchi County in the east was also at an extreme level, with the extreme vulnerability area showing a concentrated and contiguous trend. Lingbao City in the west, Lushi County in the south and Yima City in the east were areas of severe vulnerability.

In 2006, the overall vulnerability level declined. The vulnerability index of the eastern and southern districts and counties was relatively low, with most of them moderate and only Hubin District and Lingbao City being severe. The vulnerability of Shanzhou District and Mianchi County declined from severe to moderate in 2000, representing a significant decline. The vulnerability of Yima City and Lushi County declined from severe to moderate, and Lingbao City remained unchanged at severe.

In 2010, the vulnerability of the farmland system was mostly at a mild level. Apart from Hubin District and Yima City, the

**FIGURE 7**
Changes in the sensitivity of the farmland system in Sanmenxia City.



**FIGURE 8**
Changes in the adaptive capacity of the farmland system in Sanmenxia City.
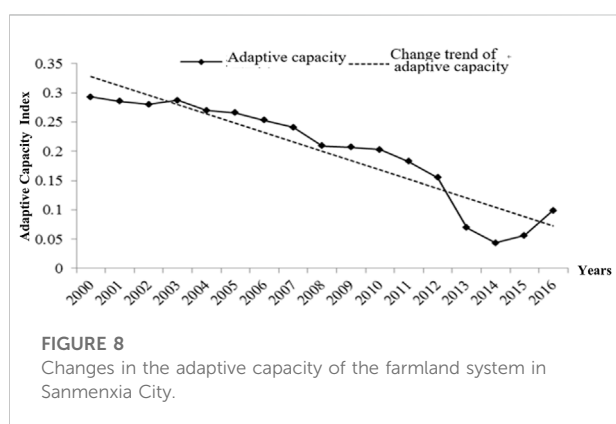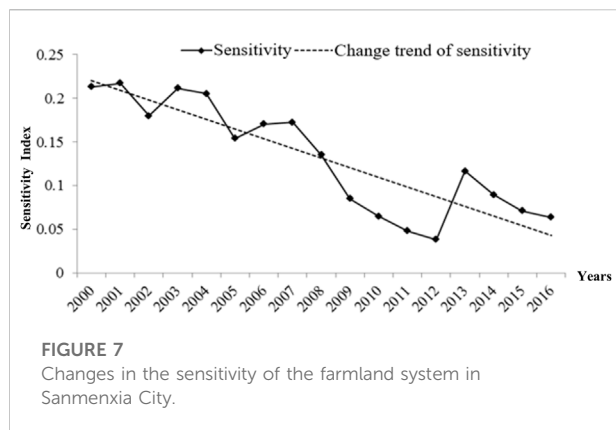
vulnerability of other districts and counties declined. Lingbao City declined from severe in 2006 to mild, and Shanzhou District, Mianchi County and Lushi County declined from moderate to mild. The vulnerability of the farmland system in Sanmenxia City experienced significant changes to the spatial pattern, forming wide ranging low-value vulnerable areas.

In 2016, the spatial difference in vulnerability was more obvious than in 2010, with some areas significantly improved. The western and central regions had relatively high vulnerability levels. Shanzhou District, Lingbao City and Yima City increased from mild to moderate, while Hubin District declined from moderate to mild, and Lushi County in the south changed from mild to slight vulnerability.

## 4.5 Spatial distribution of dominant types - District and county levels

There are two districts and four counties under the jurisdiction of Sanmenxia City. The natural conditions and the level of social and economic development vary greatly between districts and counties; the spatial characteristics of farmland system vulnerability are also different in the various

districts and counties. To further explain the factors that cause these changes in vulnerability, we used the contribution degree model. Using its formula, we calculated the contribution degree of the contribution factors to farmland system vulnerability in each district and county; the sum of the contribution rate of the three dimensions of exposure, sensitivity and adaptive capacity was 100%. Through comparing the contribution degree of the three dimensions of each district and county with that of the Sanmenxia City area, the dimension with the largest difference was found to be the dominant level causing farmland system vulnerability in each district and county to be significantly different from that of the Sanmenxia City area. On the basis of this, it can be judged that there are three main types of the farmland system vulnerability at the county level: exposure dominant (E), sensitivity dominant (S) and adaptive capacity dominant (A). The changes in types of farmland system vulnerability in districts and counties of Sanmenxia City in 2000–2016 are shown in Table 6.

We selected 4 years (2000, 2006, 2010, and 2016) in which to compare the vulnerability dominant types. The results show that Hubin District evolved from type E in 2000 into type A in 2006 and 2010, and then to type S in 2016. This indicates that farmland system vulnerability in Hubin District first evolved from exposure dominant into adaptive capacity dominant, and in recent years, has been significantly influenced by sensitivity. Shanzhou District was type A in 2000, evolving into type E in 2006, 2010, and 2016, indicating that the farmland system in Shanzhou District has been greatly influenced by exposure factors since 2000. The dominant types in Lingbao City were all type E, indicating that exposure had the most significant impact on the vulnerability of the farmland system in Lingbao City. Yima City was type E in 2000, evolving into type A in 2006, and then to type S in 2016, indicating that sensitivity was the dominant factor leading to these changes in vulnerability during this period. Mianchi County was type A in 2000 and type E in 2006, 2010 and 2016, indicating that vulnerability was significantly influenced by exposure factors. Lushi County was type A in 2000 changing to type E in 2010, and to type S in 2016, indicating that changes in sensitivity exerted a major influence on the vulnerability of the farmland system here.

## 5 Discussion

### 5.1 Influencing factors in the vulnerability of the farmland system based on correlation analysis

A bivariate correlation analysis of the vulnerability of the farmland system in Sanmenxia City can reveal its key influencing factors. Using SPSS bivariate correlation analysis, we analyzed the correlation between the 26 indicators in the vulnerability assessment system and the farmland system vulnerability index
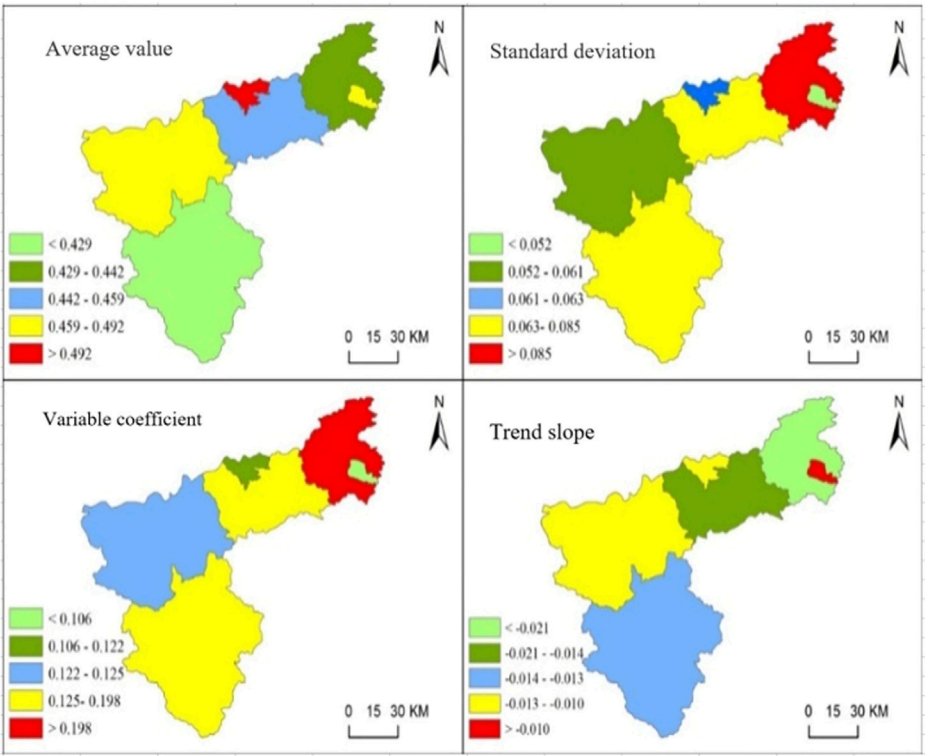
**FIGURE 9**
Degree of vulnerability changes in the farmland system in Sanmenxia City.
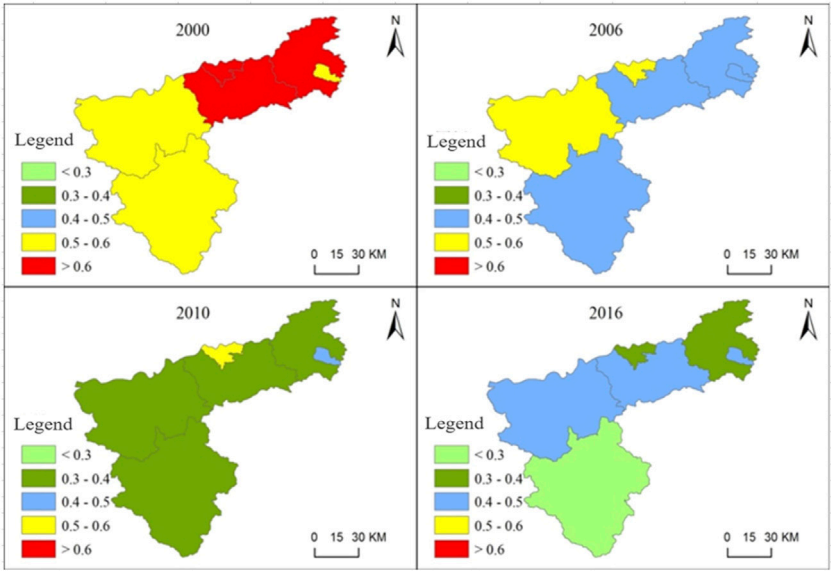


**FIGURE 10**
Spatial changes in vulnerability of the farmland system in Sanmenxia City.

TABLE 6 Changes in dominant types of farmland system vulnerability in districts and counties of Sanmenxia City.

| Area\year | Hubin district | Shanzhou district | Lingbao city | Yima city | Mianchi county | Lushi county |
|---|---|---|---|---|---|---|
| 2000 | E | A | E | E | A | A |
| 2001 | S | E | A | E | E | S |
| 2002 | S | A | E | S | A | A |
| 2003 | S | E | A | A | S | A |
| 2004 | S | E | A | A | E | A |
| 2005 | S | E | E | A | E | A |
| 2006 | A | E | E | A | E | S |
| 2007 | S | E | S | A | A | E |
| 2008 | A | E | E | E | E | E |
| 2009 | A | S | E | S | E | S |
| 2010 | A | A | E | S | E | E |
| 2011 | E | E | S | S | S | S |
| 2012 | E | S | S | S | E | E |
| 2013 | E | E | E | S | S | E |
| 2014 | E | E | S | S | S | E |
| 2015 | E | S | E | E | S | E |
| 2016 | S | E | E | S | E | S |

TABLE 7 Correlation coefficients of vulnerability of the farmland system in Sanmenxia City.

| Correlation factor | Correlation coefficient | Correlation factor | Correlation coefficient | Correlation factor | Correlation coefficient | Correlation factor | Correlation coefficient |
|---|---|---|---|---|---|---|---|
| $X_1$ | −0.134 | $X_8$ | −0.901** | $X_{15}$ | 0.923** | $X_{22}$ | 0.904** |
| $X_2$ | 0.280 | $X_9$ | −0.898** | $X_{16}$ | −0.649** | $X_{23}$ | −0.923** |
| $X_3$ | 0.101 | $X_{10}$ | −0.554* | $X_{17}$ | 0.953** | $X_{24}$ | 0.899** |
| $X_4$ | −0.386 | $X_{11}$ | −0.902** | $X_{18}$ | 0.524* | $X_{25}$ | 0.621** |
| $X_5$ | 0.850** | $X_{12}$ | −0.700** | $X_{19}$ | 0.923** | $X_{26}$ | 0.529* |
| $X_6$ | 0.824** | $X_{13}$ | 0.608** | $X_{20}$ | 0.888** | | |
| $X_7$ | −0.893** | $X_{14}$ | 0.807** | $X_{21}$ | −0.047 | | |

Note: * denotes that the variable is significantly correlated at the 0.05 level (2-tailed); ** indicates that the variable is significantly correlated at the 0.01 level (2-tailed).

of Sanmenxia City to obtain the correlation coefficients of 26 vulnerability variables.

As indicated in Table 7, the changes in the vulnerability of the farmland system were significantly correlated with 16 factors, including $X_5$ (per capita farmland), $X_6$ (highway density), $X_7$ (population density), $X_8$ (urbanization rate), $X_9$ (pesticide load per unit of farmland), and $X_{11}$ (mulching film load per unit of farmland); the changes in the vulnerability of the farmland system in Sanmenxia City were generally correlated with three factors, namely, $X_{10}$ (fertilizer load per unit of farmland), $X_{18}$ (sewage treatment rate), and $X_{26}$ (agricultural mechanization level). Changes in vulnerability had little correlation with five factors, including $X_1$ (mean annual temperature), $X_2$ (mean annual rainfall), and $X_3$ (annual drought days). These indicate that in the Sanmenxia City area, many factors have a high correlation with farmland system vulnerability.

Urbanization, land use intensity and agricultural pollution are major factors influencing farmland system vulnerability. In 2000–2017, Sanmenxia City's farmland system remained in a high exposure state and was subject to relatively high risks, which were mainly due to human interference. According to the correlation coefficient, climatic factors had little correlation with the changes in the vulnerability of the farmland system, while the correlation between population density, urbanization rate, highway density and changes in farmland system vulnerability was relatively high. With the increase in population and the development of the social economy, the demand for food is also increasing. In order to ensure food production, farmers constantly increase the use of pesticides, fertilizers and mulching films, which make farmland pollution worse. The urbanization rate of Sanmenxia City rose from 26.36% to 53.11% during these

18 years. The continuous advancement of urbanization and the increase in urban population led to the rapid expansion of urban construction. Some high-quality farmland around the city is occupied, and the development of road traffic also results in the expansion of construction land on both sides of the road, in turn resulting in an increase in the intensive use of farmland. Therefore, for the farmland system of Sanmenxia City, high exposure is due to the stress of social factors on the farmland, with natural factors having little correlation with this.

The optimization of the farmland use structure and improvements to the ecological environment can reduce the sensitivity of the farmland system. The multiple cropping index, forest coverage rate, and farmland ecosystem resilience are highly correlated with changes in farmland system vulnerability. The multiple cropping index of the farmland in Sanmenxia City has declined over these 18 years from 1.58 to 1.38. The decline in the multiple cropping index shows that the intensity of farmland use in the Sanmenxia area is falling and the quality of farmland is poor. Proper fallowing is conducive to improving the nutrient restoration of farmland and promoting its sustainable use. The reduction in the intensity of farmland use and the improvement in water-soil coordination ensure its sustainable production capacity. The forest coverage rate of Sanmenxia City rose from 36% to 51% during this period. This increase not only improves the ecological environment, but also plays a key role in maintaining water and soil and conserving water resources, which is of utmost importance to the stability of the ecosystem of the city, where there are large mountainous and loess areas.

In 2000–2017, the adaptive capacity of the farmland system gradually fell, which means that actual losses suffered when faced with various risks are decreased. The above analysis indicates that agricultural financial expenditure, rural income per capita, employment levels in primary industries, and agricultural output value have a high correlation with the vulnerability of the farmland system in the Sanmenxia City area. The increase in expenditure by government on agriculture provides advanced equipment and technology for agricultural production and optimizes the use of farmland. From the perspective of farmers, an increase in income from farmland leads to improvements in farming technology, more capital investment in the farmland system, and increases in productivity. The decline in the employment level in primary industries is mainly due to the decline in the rural population, with most young and middle-aged people going out to work. Most of those left behind are elderly and unable to work. The loss of rural labor has caused part of the farmland to be abandoned or left unattended, leading to a waste of farmland resources. The decrease in the number of people engaged in agriculture has impacted on the adaptive capacity of the farmland system.

## 5.2 Influencing factors of farmland system vulnerability

The development of vulnerability theory is already advanced, but there are still few studies on farmland system vulnerability. As a complex SES, the farmland system faces the dual interferences of human activity and natural elements. Since research on these issues is comprehensive, the construction of farmland system vulnerability indicators is inevitably limited. However, this research has the following limitation: when assessing the vulnerability of the farmland system in Sanmenxia City, constructing the indicator system is problematic due to the incompleteness and inaccessibility of some data. For example, it is difficult to obtain continuous data on soil quality and soil erosion conditions that can characterize the transitional characteristics of the Loess Plateau. Consequently, this research does not cover all the variables reflecting the level of ecological vulnerability, and the evaluation results caused by the vulnerability of the farmland system might be different from the actual results.

The dimensions in the social-ecological framework are often spatial or temporal; it is also recognized that supralocal and current events may influence the outcomes of social-economic status (Pulver et al., 2018). In the cross-scale interaction model, the fine-scale process can affect a wide spatial range or a long time period, or the large-scale drivers can interact with the fine-scale to determine the system dynamic process (Peters et al., 2007). Cross-scale interactions are considered to be the basis for the transformation of cascade mechanisms (Rocha et al., 2018) and are increasingly seen to have important implications for ecosystem processes, although the complexity of SES poses significant challenges to understanding these interactions (Ting et al., 2020). This research on the vulnerability of the farmland system in Sanmenxia City area has wider significance for the study of other large-scale farmland systems. Our research has shown that the regional farmland system has the same characteristics of significant vulnerability as the large-scale SES. Although regional small-scale research has particularities and limitations, natural factors with large-scale characteristics, such as temperature, precipitation, drought and floods, have little effect on the vulnerability of the farmland system, indicating that a local balance can be achieved through an adaptive mechanism in the long-term evolution process; human factors are a key process driving these system changes. This result is also consistent with the fact that there have been frequent extreme weather disasters in China in recent years, although food production has not decreased. It should be noted that this paper studies the vulnerability of farmland ecosystems in the study area in a short time span and pays little attention to the interaction between regions and elements. Future studies could feasibly focus on the vulnerability of farmland systems at

different scales and in different regions, in order to explore the cascading regime of cross-scale farmland system interaction. In this case, a dynamic protection mechanism for the farmland SES could provide countermeasures for solving and preventing the issues of sustainable utilization of farmland.

From the above analysis, it is seen that as a complex system, SES has many factors that affect its stability. It is not enough to evaluate the vulnerability of SES. It is clear that the main risks faced by the farmland system in the Sanmenxia City area are due to the pressure caused by rapid social and economic development, while the influence of natural factors is not significant. Avoiding these risks is an effective means of controlling the vulnerability of the farmland system. Thus, when formulating farmland policies, the Sanmenxia municipal government and functional departments should control them from the macro level, ensuring overall awareness, and providing guidance for the formulation of policies in all districts and counties under their jurisdiction.

The results show the feasibility of the evaluation of farmland vulnerability in a fine scale system. First, the index system is constructed. In addition to referring to the relevant research results, our research group also visited Sanmenxia City and the functional departments of counties and districts in July 2016 and March 2017 to collect data and conduct interviews. Experts from Sanmenxia Land Bureau, Agriculture Bureau and the Farmland Protection Bureau were invited to mark the index comparison matrix constructed by AHP. Based on these data and expert interviews, combined with the specific situation of farmland use in Sanmenxia City, the evaluation index system is set. Although this may deviate from existing research results, it is closer to the local situation. Second, the entropy weight method used in this paper is relatively weak in correlation compared with the set pair analysis and pairwise analysis. However, it solves the overall problem of the system. Due to limited space, this paper does not explore further the correlation between indicators. Third, the consistency of land use data is mainly due to the large difference between image interpretation data and annual change data. The indicators in the paper are calculated based on the data integrated in each year, and the calculation results are closer to the actual situation in the study area.

## 6 Conclusion

In this paper, the vulnerability theory and evaluation method are applied to the study of the farmland system, and the VSD research framework of the farmland system is constructed. The results show that:

(1) In 2000–2016, the vulnerability index of the farmland system in Sanmenxia City showed an overall downward trend,

declining from extreme to mild vulnerability. In terms of the three dimensions of farmland system vulnerability, exposure showed an increasing trend, reflecting the fact that both interferences and risks for the farmland system were greater. However, the sensitivity index fluctuated, indicating that the actual loss of the farmland system in dealing with various risks was reduced. The adaptive capacity index showed a declining trend as well, indicating that the ability of the farmland system to withstand stress and deal with risks was greatly improved. Data analysis showed that the increase in the exposure index of the farmland system is much lower than the decrease in the sensitivity and adaptive capacity indexes. Therefore, despite the increase in risks and disturbances, the overall vulnerability of the farmland system still decreases.

(2) In terms of the spatial distribution, the vulnerability of the farmland system in the districts and counties of Sanmenxia City is unevenly distributed as it is higher in the central and western regions and lower in the south. Overall vulnerability shows a declining trend from "high in the central and eastern regions and low in the southwest" in 2000 to "high in the central and western regions and low in the southeast" in 2016.

(3) The main factors influencing the vulnerability of the farmland system in Sanmenxia City are the sensitivity and adaptive capacity of human social and economic activities and the capacity of the farmland system to cope with stress. Population growth and rapid urbanization are the main risk factors for the farmland system in Sanmenxia City, as they place great pressure on the intensity of farmland use. However, the increase in agricultural financial investment and farmers' incomes results in higher agricultural production, farming technology and factor input intensity, so the farmland system becomes less sensitive to the threat of risks. The implementation of regional agricultural policies, changes in agricultural production factors, farming technology inputs, and farming intensity provide support for the stable operation of the farmland system, enabling farmland to be more resilient to risk stress.

## Data availability statement

The raw data supporting the conclusion of this article will be made available by the authors, without undue reservation.

## Author contributions

Conceptualization, PN and YY; methodology, YJ; investigation, LW; writing—original draft preparation, PN; writing—review and editing, YY; visualization, YJ and LW; supervision, YY; project administration, PN and YY; funding

acquisition, PN. All authors have contributed to this version of the manuscript.

## Conflict of interest

The authors declare that the research was conducted in the absence of any commercial or financial relationships that could be construed as a potential conflict of interest.

## Publisher's note

All claims expressed in this article are solely those of the authors and do not necessarily represent those of their affiliated organizations, or those of the publisher, the editors and the reviewers. Any product that may be evaluated in this article, or claim that may be made by its manufacturer, is not guaranteed or endorsed by the publisher.

## References

Acosta-Michlik, L., and Rounsevell, M. (2012). "An agent-based framework for assessing vulnerability futures," in *Assessing vulnerability to global environmental change* (London: Routledge), 168–192. doi:10.4324/9781849770514

Adger, W. N. (2006). Vulnerability. *Glob. Environ. Change* 16, 268–281. doi:10.1016/j.gloenvcha.2006.02.006

Adger, W. N. (2000). Social and ecological resilience: Are they *Prog. Hum. Geogr.* 24 (3), 347–364. doi:10.1191/030913200701540465

Armitage, C. J. (2008). A volitional help sheet to encourage smoking cessation: A randomized exploratory trial. *Health Psychol.* 27 (5), 557–566. doi:10.1037/0278-6133.27.5.557

Ashley, C. (2000). *Applying livelihood approaches to natural resource management initiatives: Experiences in Namibia and Kenya*. London: Overseas Development Institute. Working Paper 134.

Barros, V. R., Field, C. B., and Dokken, D. J. (2014). "Climate change 2014: Impacts, adaptation, and vulnerability. Part B: Regional aspects," in *Contribution of working group II to the fifth assessment report of the intergovernmental Panel on climate change* (Cambridge, United Kingdom and New York: Cambridge University Press), 1267–1326.

Bennett, N. J., Blythe, J., Tyler, S., and Ban, N. C. (2016). Communities and change in the anthropocene: Understanding social-ecological vulnerability and planning adaptations to multiple interacting exposures. *Reg. Environ. Change* 16, 907–926. doi:10.1007/s10113-015-0839-5

Bennett, N. J., Dearden, P., Murray, G., and Kadfak, A. (2014). The capacity to adapt? Communities in a changing climate, environment, and economy on the northern andaman coast of Thailand. *Ecol. Soc.* 19, 5. doi:10.5751/ES-06315-190205

Berkes, F., and Ross, H. (2016). Panarchy and community resilience: Sustainability science and policy implications. *Environ. Sci. Policy* 61, 185–193. doi:10.1016/j.envsci.2016.04.004

Berry, P. M., Rounsevell, M. D. A., Harrison, P. A., and Audsley, E. (2006). Assessing the vulnerability of agricultural land use and species to climate change and the role of policy in facilitating adaptation. *Environ. Sci. Policy* 9, 189–204. doi:10.1016/j.envsci.2005.11.004

Bindi, M., and Olesen, J. (2011). The responses of agriculture in Europe to climate change. *Reg. Environ. Change* 11, 151–158. doi:10.1007/s10113-010-0173-x

Brklacich, M., Chazan, M., and Bohle, H-G. (2009). "Human security, vulnerability, and global environmental change," in *Global environmental change and human security*. Editors R. A. Matthew, J. Barnett, B. McDonald, and K. L. O'Brien (Cambridge: MIT Press), 35–52.

Brugere, C., and Lingard, J. (2003). Irrigation deficits and farmers' vulnerability in Southern India. *Agric. Syst.* 77 (1), 65–88. doi:10.1016/s0308-521x(02)00108-7

Bussey, M., Carter, R. W., Keys, N., Carter, J., Mangoyana, R., Matthews, J., et al. (2012). Framing adaptive capacity through a history–futures lens: Lessons from the south east queensland climate adaptation research initiative. *Futures* 44, 385–397. doi:10.1016/j.futures.2011.12.002

Carpenter, S. R. (2005). Eutrophication of aquatic ecosystems: Bistability and soil phosphorus. *Proc. Natl. Acad. Sci. U. S. A.* 102 (29), 10002–10005. doi:10.1073/pnas.0503959102

Chen, X., Zhang, Q., Peterson, M. N., and Song, C. (2019). Feedback effect of crop raiding in payments for ecosystem services. *Ambio* 48, 732–740. doi:10.1007/s13280-018-1105-0

Cinner, J. E., Fuentes, M., and Randriamahazo, H. (2009). Exploring social resilience in Madagascar's marine protected areas. *Ecol. Soc.* 14, 41. doi:10.5751/es-02881-140141

Cinner, J. E., Huchery, C., Darling, E. S., Humphries, A. T., Graham, N. A. J., Hicks, C. C., et al. (2013). Evaluating social and ecological vulnerability of coral reef fisheries to climate change. *PLoS One* 8, e74321. doi:10.1371/journal.pone.0074321

Cinner, J. E., McClanahan, T. R., Graham, N. A. J., Daw, T. M., Maina, J., Stead, S. M., et al. (2012). Vulnerability of coastal communities to key impacts of climate change on coral reef fisheries. *Glob. Environ. Change* 22, 12–20. doi:10.1016/j.gloenvcha.2011.09.018

Copeland, S., Comes, T., Bach, S., Nagenborg, M., Schulte, Y., and Doorn, N. (2020). Measuring social resilience: Trade-offs, challenges and opportunities for indicator models in transforming societies. *Int. J. Disaster Risk Reduct.* 51, 101799. doi:10.1016/j.ijdrr.2020.101799

Cutter, S. L. (2016). The landscape of disaster resilience indicators in the USA. *Nat. Hazards* 80, 741–758. doi:10.1007/s11069-015-1993-2

FAO (2021). FAO Report on World Food Security and Nutrition in 2021, Available at: https://weibo.com/ttarticle/p/show?id,2021.10.12.

Fischer, G., Velthuizen, V., Shah, H. T., and Nachtergaele, M. M. (2002). *Global agro-ecological assessment for agriculture in the 21st century: Methodology and results*. Laxenburg, Autria: International Institute for Applied Systems Analysis.

Folke, C., Colding, J., and Berkes, F. (2003). "Synthesis: Building resilience and adaptive capacity in social-ecological systems," in *Navigating social-ecological systems: Building resilience for complexity and change*. Editors F. Berkes, J. Colding, and C. Folke (Cambridge; New York: Cambridge University Press), 352–387.

Hagenlocher, M., Renaud, F. G., Haas, S., and Sebesvari, Z. (2018). Vulnerability and risk of deltaic social-ecological systems exposed to multiple hazards. *Sci. total Environ.* 631, 71–80. doi:10.1016/j.scitotenv.2018.03.013

Huang, Y. F., Li, F. Y., Bai, X. M., and Cui, S. (2012). Comparing vulnerability of coastal communities to land use change: Analytical framework and a case study in China. *Environ. Sci. Policy* 23 (23), 133–143. doi:10.1016/j.envsci.2012.06.017

IPCC (2001). *Climate change 2001:impacts, adaptation, and vulnerability[R]*. Cambridge: Cambridge University Press.

Jamir, C., Sharma, N., Sengupta, A., and Ravindranatrh, A. (2013). Farmers' vulnerability to climate variability in Dimapur district of Nagaland, India. *Reg. Environ. Change* 13 (1), 153–164. doi:10.1007/s10113-012-0324-3

Jinno, K. (1995). Risk assessment of a water supply system during drought. *Int. J. Water Resour. Dev.* 11 (2), 185–204. doi:10.1080/07900629550042399

Kienberger, S., Blaschke, T., and Zaidi, R. Z. (2013). A framework for spatio-temporal scales and concepts from different disciplines: The 'vulnerability cube.' *Nat. Hazards (Dordr).* 68 (3), 1343–1369. doi:10.1007/s11069-012-0513-x

Kovács-Hostyánszki, A., Espíndola, A., Vanbergen, A. J., Settele, J., Kremen, C., and Dicks, L. V. (2017). Ecological intensification to mitigate impacts of conventional intensive land use on pollinators and pollination. *Ecol. Lett.* 20 (5), 673–689. doi:10.1111/ele.12762

Li, Q., and Zander, P. (2019). Resilience building of rural livelihoods in PES programmes: A case study in China's loess hills. *Ambio* 49, 962–985. doi:10.1007/s13280-019-01236-4

Lazzari, N., Becerro, M. A., Sanabria-Fernandez, J. A., and Martin-Lopez, B. (2021). Assessing social-ecological vulnerability of coastal systems to fishing and tourism. *Sci. Total Environ.* 784, 147078. doi:10.1016/j.scitotenv.2021.147078

Lazzari, N., Martín-López, B., Sanabria-Fernandez, J. A., and Becerro, M. A. (2020). Alpha and beta diversity across coastal marine social-ecological systems: Implications for conservation. *Ecol. Indic.* 109, 105786. 10.1016/j.ecolind.2019.105786.

Liu, J., Dietz, T., Carpenter, S. R., Alberti, M., Folke, C., Moran, E., et al. (2007). Complexity of coupled human and natural systems. *Science* 317, 1513–1516. doi:10.1126/science.1144004

Lizhen, L., Yuanzeng, Z., Yanmei, Y., Chen, J., Mou, Y., et al. 2010, Regional ecosystem health assessment based on land use pattern: A case of study of zhoushan island. *Acta Ecol. Sin.*, 30, 1, 0245–0252.

Lorenz, D. F. (2013). The diversity of resilience: Contributions from a social science perspective. *Nat. Hazards* 67, 7–24.

Marull, J., Pino, J., Mallarach, M., and Cordobilla, M. J. (2007). A land suitability index for strategic environmental assessment in metropolitan areas. *Landsc. Urban Plan.* 81 (3), 200–212. doi:10.1016/j.landurbplan.2006.11.005

Mumby, P. J., Wolff, N. H., Bozec, Y. M., Chollett, I., and Halloran, P. (2014). Operationalizing the resilience of coral reefs in an era of climate change. *Conserv. Lett.* 7 (3), 176–187. doi:10.1111/conl.12047

Neset, T. S., Wiréhn, L., Opach, T., Glaas, E., and Linnér, B. O. (2019). Evaluation of indicators for agricultural vulnerability to climate change: The case of Swedish agriculture. *Ecol. Indic.* 105, 571–580. doi:10.1016/j.ecolind.2018.05.042

O'Brien, K. L., and Leichenko, R. M. (2000). Double exposure: Assessing the impacts of climate change within the context of economic globalization. *Glob. Environ. change* 10 (3), 221–232. doi:10.1016/S0959-3780(00)00021-2

O'Brien, K. L., Leichenko, R., Kelkar, U., Venema, V., Aandahl, G., Tompkins, H., et al. (2004). Mapping vulnerability to multiple stressors: Climate change and globalization in India. *Glob. Environ. Change* 14, 303–313. doi:10.1016/j.gloenvcha.2004.01.001

Pereira, H. M., Navarro, L. M., and Martins, I. S. (2012). Global biodiversity change: The bad, the good, and the unknown. *Annu. Rev. Environ. Resour.* 37, 25–50. doi:10.1146/annurev-environ-042911-093511

Perry, R. I., Ommer, R. E., Barange, M., Jentoft, S., Neis, B., and Rashid Sumaila, U. (2011). Marine social–ecological responses to environmental change and the impacts of globalization. *Fish. Fish. (Oxf).* 12, 427–450. doi:10.1111/j.1467-2979.2010.00402.x

Peters, D. P. C., Bestelmeyer, B. T., and Turner, M. G. (2007). Cross-scale interactions and changing pattern-process relationships: Consequences for system dynamics. *Ecosystems* 10, 790–796. doi:10.1007/s10021-007-9055-6

Pham, B. T., Khosravi, K., and Prakash, I. (2017). Application and comparison of decision tree-based machine learning methods in landside susceptibility assessment at pauri garhwal area, uttarakhand, India. *Environ. Process.* 4 (3), 711–730. doi:10.1007/s40710-017-0248-5

Pulver, S., Ulibarri, N., Sobocinski, K. L., Alexander, S. M., Johnson, M. L., McCord, P. F., et al. (2018). Frontiers in socio-environmental research: Components, connections, scale, and context. *Ecol. Soc.* 23. doi:10.5751/es-10280-230323

Rocha, J. C., Peterson, G., Bodin, O., and Levin, S. (2018). Cascading regime shifts within and across scales. *Science* 362, 1379–1383. doi:10.1126/science.aat7850

Rockenbauch, T., and Sakdapolrak, P. (2017). Social networks and the resilience of rural communities in the global south: A critical review and conceptual reflections. *Ecol. Soc.* 22, art10. doi:10.5751/es-09009-220110

Rogers, A. D., Aburto-Oropeza, O., Appeltans, W., et al. (2020). *Critical habitats and biodiversity: Inventory, thresholds and governance*. Washington, DC: World Resources Institute.

Saja, A. M. A., Goonetilleke, A., Teo, M., and Ziyath, A. M. (2019). A critical review of social resilience assessment frameworks in disaster management. *Int. J. Disaster Risk Reduct.* 35, 101096. doi:10.1016/j.ijdrr.2019.101096

Salvati, L., Bajocco, S., Ceccarelli, T., Zitti, M., and Perini, L. (2011). Towards a process-based evaluation of land vulnerability to soil degradation in Italy. *Ecol. Indic.* 11 (5), 1216–1227. doi:10.1016/j.ecolind.2010.12.024

Siegel, K. J., Cabral, R. B., McHenry, J., Ojea, E., Owashi, B., and Lester, S. E. (2019). Sovereign states in the Caribbean have lower social-ecological vulnerability to coral bleaching than overseas territories. *Proc. R. Soc. B* 286, 20182365. doi:10.1098/rspb.2018.2365

Smit, B., and Wandel, J. (2006). Adaptation, adaptive capacity and vulnerability. *Glob. Environ. Change* 16, 282–292. doi:10.1016/j.gloenvcha.2006.03.008

Speranza, C. I., Wiesmann, U., and Rist, S. (2014). An indicator framework for assessing livelihood resilience in the context of social–ecological dynamics. *Glob. Environ. Change* 28, 109–119. doi:10.1016/j.gloenvcha.2014.06.005

Tebbotha, M. G. L., Conway, D., and Adger, W. N. (2019). Mobility endowment and entitlements mediate resilience in rural livelihood systems. *Glob. Environ. Change* 54, 172–183.

Thiault, L., Gelcich, S., Cinner, J. E., Lewin, S. T., Chlous, F., and Claudet, J. (2019). Generic and specific facets of vulnerability for analysing trade-offs and synergies in natural resource management. *People Nat. Hob.*, 573–589. doi:10.1002/pan3.10056

Thiault, L., Collin, A., Chlous, F., Gelcich, S., and Claudet, J. (2017). Combining participatory and socioeconomic approaches to map fishing effort in small-scale fisheries. *PLoS One* 12 (5), e0176862. doi:10.1371/journal.pone.0176862

Ting, L., Yuxiang, D., and Zhenhuan, L. (2020). A review of social-ecological system resilience: Mechanism, assessment and management. *Sci. Total Environ.* 723, 138113. doi:10.1016/j.scitotenv.2020.138113

Tuler, S., Agyeman, J., da Silva, P., Roth LoRosso, K., and Kay, R. (2008). Assessing vulnerabilities: Integrating information about driving forces that affect risks and resilience in fishing communities. *Hum. Ecol. Rev.* 15, 171–184.

Turner, B. L., Kasperson, R. E., Matson, P. A., Matson, P. A., Corell, R. W., Christensen, L., et al. (2003). A framework for vulnerability analysis in sustainability science. *Proc. Natl. Acad. Sci. U. S. A.* 100, 8074–8079. doi:10.1073/pnas.1231335100

Walker, B., Holling, C. S., Carpenter, S. R., and Kinzig, A. (2004). Resilience, adaptability and transformability in social–Ecological systems. *Ecol. Soc.* 9 (2), 5.

Walker, B., and Salt, D. (2006). *Resilience thinking: Sustaining ecosystems and people in a changing world*. Washington, D.C., USA: Island Press.

Wang, Y., Zhang, Q., Li, Q., Wang, J., Sannigrahi, S., Bilsborrow, R., et al. (2021). Role of social networks in building household livelihood resilience under payments for ecosystem services programs in a poor rural community in China. *J. Rural Stud.* 86 (8), 208–225. doi:10.1016/j.jrurstud.2021.05.017

Watts, M. J., and Bohle, H. G. (1993). The space of vulnerability: The causal structure of hunger and famine. *Prog. Hum. Geogr.* 17, 43–67. doi:10.1177/030913259301700103

Wilson, G. A., Schermer, M., and Stotten, R. (2018). The resilience and vulnerability of remote mountain communities: The case of Vent, Austrian Alps. *Land Use Policy* 71, 372–383. doi:10.1016/j.landusepol.2017.12.022

Wilson, S., Pearson, L. J., Kashima, Y., Lusher, D., and Pearson, C. (2013). Separating adaptive maintenance (resilience) and transformative capacity of social-ecological systems. *Ecol. Soc.* 18, art22. doi:10.5751/es-05100-180122

Wiréhn, L. (2018). Nordic agriculture under climate change: A systematic review of challenges, opportunities and adaptation strategies for crop production. *Land Use Policy* 77, 63–74. doi:10.1016/j.landusepol.2018.04.059

Wiréhn, L., Opach, T., and Neset, T. S. (2017). Assessing agricultural vulnerability to climate change in the Nordic countries–an interactive geovisualization approach. *J. Environ. Plan. Manag.* 60 (1), 115–134. doi:10.1080/09640568.2016.1143351

Xie, L., Li, Y., and Qian, F. (2014). Analysis on agricultural sensitivity and vulnerability to climate change and countermeasures. *China Popul. Resour. Environ.* 24 (5), 25–30.

Xutong, W., Yongping, W., Bojie, F., Wang, S., Zhao, V., and Moran, E. F. (2020). Evolution and effects of the social-ecological system over a millennium in China's Loess Plateau. *Sci. Adv.* 6, eabc0276. doi:10.1126/sciadv.abc0276

frontiers | Frontiers in Environmental Science

# The spatio-temporal changes of cropping patterns in the black soil area of China: Lessons from Wangkui County

Guoming Du*, Longcheng Yao and Dawei Hou

School of Public Administration and Law, Northeast Agricultural University, Harbin, China

A reasonable planting crop pattern can effectively contribute to maintaining soil fertility and ensuring stable crop growth in the black soil regions of China. This study aimed to analyze the evolution of cropping patterns in Wangkui County between 2002 and 2021. By using ArcGIS and ENVI software, during which visual interpretation was applied, we interpreted three crop rotation cycles based on the classification data of remote-sensing inversion crops for 2002–2005, 2010–2013, and 2018–2021. Our results indicated that maize, rice, and soybean were the three major crops which accounted for a total of 87.02% of the farmland during our study period, while the cropping pattern was dominated by continuous maize cultivation (31.25%), mixed cultivation (29.01%), and continuous maize–soybean cultivation (24.48%). Specifically, the continuous maize cultivation was mainly distributed in the south-central and west-central parts, whereas continuous rice cultivation spread from the northwest to the southwest. In addition, the rice–soybean rotation tended to gather in the southwest and north and spread to the central part, and the rice–maize rotation presented a tendency of radiation diffusion from the county's northwest region to the surrounding areas. This study could provide a practical basis for establishing high-yield and efficient planting models in the black soil areas of China.

## Introduction

China's black soil region is considered one of the most important crop production bases to meet the increasing food demands (Xu et al., 2010). As one of the four predominantly black soil areas in the world, several studies highlighted that the total grain production accounted for one-quarter of China's total crop production (Sinica, 2018). The quantity of commodity grain transferred from the northeast black soil area accounted for one-third of the country. Accordingly, the black soil region in China is the "ballast stone" to maintaining national food security. As the "giant panda in arable land," black soil is the most suitable land for cultivation. The rational use and conservation of black soil is a matter of food security for present and future generations. However, the

high level of exploitation and use over a long period has resulted in soil erosion, water consolidation, salinization, and sandy soil, which has reduced the fertility of black soil in China (Cai, 2019). This situation may threaten the country's food security, ecological environment, and sustainable development. Hence, proper cropping patterns can play crucial roles in improving black soils' physical and chemical properties and increasing their fertility. Crop rotation is a good cropping pattern that coexists with land use and maintenance and coordinates the cultivated land's protection and utilization. Few studies have shown that crop rotation can improve the soil's physical and chemical properties, thus increasing crop yield and economic benefits (Huang et al., 2003). In addition, crop rotation can improve the water-use efficiency of crops (An, 2016; Yang, 2019), conducive to the growth and development of crops. In the strategic context of vigorously advocating the good use and protection of black soil (Wang, 2021) and the implementation of crop rotation and fallow systems (Zhao, 2017), it is of far-reaching significance to explore the types, spatial patterns, distribution patterns, and evolutionary trends of cropping patterns in the black soil areas of Northeast China.

Cropping pattern refers to a standardized way of using arable land or crop cultivation under certain natural and socioeconomic conditions and is a combination of crops in time, space, and plane (Dong, 1999), divided into two patterns of continuous crop and crop rotation (Wu, 2002). As cropping patterns are complex and diverse, scholars have mostly used remote-sensing images to extract spatial information on crops and planting structures (Wang, 2022). For instance, Zhang (2022) constructed a time-series weathering feature set based on the GEE platform and Sentinel-NDVI data to finely identify and map six cropping patterns of five crop types in the Jianghan Plain. In the same context, Su (2013) used the time-series Landsat 8-NDVI to extract the planted area of maize in the fields of Baoding City, Hebei Province. In another research, Foerster et al. (2012) proposed a hierarchical classification method based on spectral–temporal profiles based on each crop type's distinct seasonal, spectral behavior to classify and validate the accuracy of 12 crop types over several consecutive years in a 14,000 km catchment area in Northeastern Germany. El-Magd and Tanton (2003) used multi-stage maximum likelihood supervised classification for satellite sensor data improvement to improve the accuracy of crop identification in irrigated areas. Research on the identification and extraction of cropping patterns is becoming more sophisticated, but there is less research on cropping pattern changes, while research on land-use change is relatively mature.

Regarding the land-use change phenomena, Svoboda et al. (2022) used Sentinel-2 data to analyze the land-use change in the Czech region. Buya et al. (2022) also measured the rate of change of land-use types in Krabi City, Thailand, based on a logistic regression model of built-up land. They had a grid-digitized data structure. Hohensinner et al. (2021) applied a "regressive–iterative GIS reconstruction method" combining historical maps and optical remote-sensing data to explore the long-term evolution of land cover in the Alpine valley. In terms of land-use change prediction and evolutionary analysis, Truong et al. (2022) constructed the MEKOLUC (Mekong Delta Land Use Change) land-use change model to simulate land-use change under the influence of socioeconomic and environmental factors as a means of predicting the resilience of crops to climate impacts and soil salinity in 2030. Jiang et al. (2019) created an integrated LULCC model by integrating a simple global socioeconomic model, a terrestrial ecosystem simulator (TESim), and a land-use allocation model, combining land use, socioeconomic impacts, and ecosystem processes as a means to explore the future land-use dynamics of China under two scenarios. Girma et al. (2022) modeled the land-use cover change in the Gidabo River Basin of the Ethiopian Rift Valley based on a neural network with a cellular automata-Markov chain model to simulate and predict the land change from 1985 to 2050. Overall, land-use change studies have been conducted mainly in terms of the phenomenon of land-use change, the prediction of land-use change, and the analysis of its evolution, providing a rich source of ideas for the analysis of the evolution of cropping pattern types. However, the irreversible character of land-use change is absent in crop conversion, moreover, crop change is reversible and diverse so mapping studies of cropping patterns need a higher temporal resolution to analyze inter-annual or inter-seasonal crop conversion characteristics. It is, therefore, fundamentally feasible to apply the research ideas of land-use change typology to the analysis of the evolution of cropping patterns. Still, it is also necessary to pioneer and innovate practically, given the importance of cropping patterns, to ensure food security and soil health.

Wangkui is one of the typical counties in the black soil region of the Northeast China. Taking Wangkui County as the study area is to provide a scientific basis for the promotion of crop rotation fallow systems in the black soil areas of Northeast China. The data in this study were based on crop classification data from Landsat of Wangkui County for three time periods, 2002–2005, 2010–2013, and 2018–2021. Based on research data, we used geo-information Tupu, information remapping rules, and kernel density estimation to reveal the evolution of cropping patterns in Wangkui County. Our specific objectives were to: *1)* explore the change in land area for each cropping pattern within each rotation cycle in Wangkui County, *2)* analyze the changes in the spatial layout of the pattern, and *3)* describe the influences, potential factors, and regulatory measures for the evolution of cropping patterns.

## Study area

Wangkui County is located in the transition zone between the Songnun Plain and the southwestern edge of the Xiao Hinggan Mountains in the Central Heilongjiang Province, between 126°10′–126°59′E and 46°32′–47°28′N (Zhang, 2022). It is part of Suihua City, Heilongjiang Province, which is one of the typical counties in the black soil region of the Northeast China, as shown in Figure 1. Wangkui County consists of 10 towns, three

**FIGURE 1**
The geographical localization of the study area.
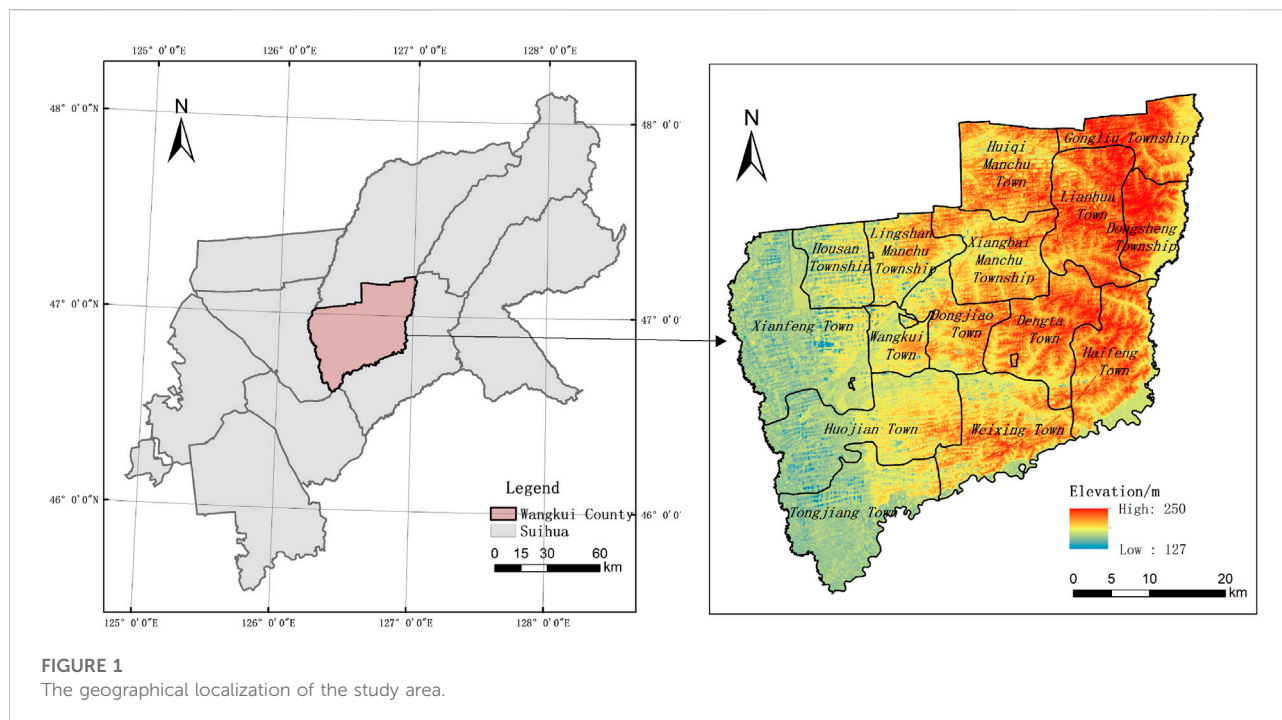
townships, and two ethnic townships. The county's topography is high in the east and low in the west. There are rolling hills, gently sloping rambling hills, and low-lying plains in the county, with an average altitude of 167 m. The climate of Wangkui County belongs to the north temperate continental semi-humid monsoon climate with an average annual temperature of 2.8°C. The average yearly precipitation is 475 mm/year. The county's total area is 2,318 km², of which 1,413.33 km² is arable land with a cultivation rate of 60.97%. The soil types distributed in the district are mainly black soil, black calcium soil, and meadow soil, of which black soil is the main one, accounting for 52.62% of the total arable land area, which is widely distributed in the district. Wangkui County is located in the hinterland of the typical black soil area of Northeast China, with fertile soil suitable for agricultural cultivation (Liu, 2022). The main body of the agricultural operation is mainly farmers, and the crop maturity system is annual, mainly growing soybeans and corn. Wangkui County has a more developed plantation industry. According to the data of the government of Wangkui collected on June 2022 (WWW.HLWANGKUI.GOV.CN), the county sowed 168,000 hm² of grain crops, with a total grain output of 1,081,500 t, accounting for one-seventh of the province's grain output in 2020.

## Materials and methods

### Data sources

Based on the remote-sensing identification methods of crop types and existing studies (Yanjun and Yuhong, 2021),

Landsat7 ETM+ for 2002, 2003, and 2010–2012, Landsat5 TM for 2004 and 2005, and Landsat8 OLI remote-sensing images for 2013 and 2017–2021 in July, August, and September were selected as the main data sources (https://glovis.usgs.gov) (as shown in Table 1). The annual update database of the Third Land Survey with the resolution of 30 m, the vector data of administrative divisions of Wangkui County, and the 30 m resolution DEM data of the county area were used as auxiliary data. The process of data pre-processing mainly refers to image pre-processing of remote-sensing inversion crop classification data using ENVI. The process was as follows: first, the geometric correction of the remote-sensing images was carried out based on the 30 m resolution DEM data of the county, in which the erroneous bands need to be removed before the geometric correction of the landsat7 ETM+ remote sensing images of 2003 and 2010–2012 (Ji Fuhua, 2020). Based on pre-processing methods such as radiometric calibration, atmospheric correction, image fusion, and image mosaic, a mask was created using the county's arable land vector data to crop the remotely sensed images.

The key to the visual interpretation method lies in establishing the interpretation elements, also known as interpretation markers, which can directly reflect the image features with obvious discriminative differences in feature information and are the basis for human–computer interactive interpretation and translation of remote-sensing images. Based on the analysis of the band combination characteristics of Landsat5 TM, Landsat7 ETM+, and Landsat8 OLI, we selected the band combination method that is sensitive to different crops and established a crop classification system for the study area by applying RGB pseudo-color synthesis to different bands of remote-sensing images, mainly

TABLE 1 Remote-sensing image information.

| Landsat images | Year | Imaging time | Resolution ratio/m | Proportion of cloud/% |
|---|---|---|---|---|
| Landsat7 ETM+ | 2002 | 07–06 | 30 | 5.21 |
| Landsat7 ETM+ | 2003 | 08–26 | 30 | 7.63 |
| Landsat5 TM | 2004 | 09–21 | 30 | 4.33 |
| Landsat5 TM | 2005 | 08–07 | 30 | 5.35 |
| Landsat7 ETM+ | 2010 | 09–14 | 30 | 6.16 |
| Landsat7 ETM+ | 2011 | 09–01 | 30 | 0.99 |
| Landsat7 ETM+ | 2012 | 09–19 | 30 | 2.67 |
| Landsat8 OLI | 2013 | 09–30 | 30 | 1.82 |
| Landsat8 OLI | 2017 | 09–09 | 30 | 2.93 |
| Landsat8 OLI | 2018 | 07–10 | 30 | 0.7 |
| Landsat8 OLI | 2019 | 09–15 | 30 | 1.13 |
| Landsat8 OLI | 2020 | 07–15 | 30 | 2.69 |
| Landsat8 OLI | 2021 | 09–04 | 30 | 3.79 |

including rice, maize, soybean, and other crops. The remote-sensing images were then interpreted and deciphered according to the information in the Appendix.

The sample points were selected according to the principle of uniform distribution, and the sample points were mapped according to the cultivation area and spatial distribution on remote-sensing images of different crops to build a crop classification training sample point set. Among them, maize and soybean were the main food crops in the study area, with a wide distribution and a large planting area. One hundred sample points were selected for each crop, randomly divided into 70 training samples and 30 validation samples. Rice and other crops had a smaller area, and each of the 80 sample points was randomly divided into 56 training samples and 24 validation samples. The overall accuracy was 0.91–0.97, with a kappa coefficient of 0.93–0.95, which met the accuracy requirements for general operations. Finally, the "Support Vector Machine Classification" function was used in ENVI to supervise the classification of various crops in Wangkui County from 2002 to 2005, 2010 to 2013, and 2018 to 2021.

## Methodology

### Geo-information Tupu

In land-use change research, geographic information Tupu theory is one of the mainstream research methods which combines the characteristics of the temporal and spatial distribution of features and can clearly express the characteristics of spatial and temporal land-use change. It is conducive to deepening the expression of the inner evolution of land-use change and multiple dimensions. A map has the dual nature of a "graph" and a "spectrum" of elements, with the "graph" visually expressing the spatial distribution characteristics of the elements and the "spectrum" reflecting the process of the elements. "The combination of map and genealogy can show the spatial and temporal evolution of the elements in a comprehensive manner. Drawing on existing research, the formula for calculating the elemental raster cells in geo-information mapping can be expressed as

$$C = 10A + B,$$

where $C$ is the unit attribute value for the change in element type during the study period. $A$ is the element unit attribute value for the previous period, and $B$ is the element unit attribute value for the latter period.

In this article, based on the 12-crop classification raster data from 2002 to 2005, 2010 to 2013, and 2018 to 2021, we first reclassified them in ArcGIS, coding the attribute values of raster cells characterizing rice, maize, soybean, and other features as 1, 2, 3, and 4 respectively, and then used the "map algebra" function in the ArcGIS spatial analysis module to spatially overlay them. The raster data of the three-crop rotation cycles in Wangkui County from 2002 to 2005, 2010 to 2013, and 2018 to 2021 can be obtained by spatial overlaying using the "map algebra" function in the ArcGIS spatial analysis module. The specific calculation formula is as follows:

$$G_1 = 1000Y_{2002} + 100Y_{2003} + 10Y_{2004} + Y_{2005},$$
$$G_2 = 1000Y_{2010} + 100Y_{2011} + 10Y_{2012} + Y_{2013},$$
$$G_3 = 1000Y_{2018} + 100Y_{2019} + 10Y_{2020} + Y_{2021},$$

where $G_1$, $G_2$, and $G_3$ are the coding values of the mapping units that characterize the changes in crop information during the study period. $Y_{2002}$, $Y_{2003}$, $Y_{2004}$, $Y_{2005}$, $Y_{2010}$, $Y_{2011}$, $Y_{2012}$, $Y_{2013}$, $Y_{2018}$, $Y_{2019}$, $Y_{2020}$, and $Y_{2021}$ are the coding values of the mapping units that characterize the crop information for the 12 years: 2002, 2003, 2004, 2005, 2010, 2011, 2012, 2013, 2018, 2019, 2020, and 2021, respectively.

### Information remapping rules

Based on the methodology of geo-information Tupu used by Guo-ming (Guo-ming and Yu, 2022), we used the map algebra

tool in ArcGIS 10.4 to spatially overlay crop classification raster data during the periods stemming from 2002 to 2005, 2010 to 2013, and 2018 to 2021 to obtain crop-change information maps with 255, 256, and 249 class codes for the three-crop rotation cycles, respectively. However, cropping patterns cannot simply be equated with crop change information. They are a further classification and synthesis of the latter. Therefore, both information-mapping units and information-remapping rules were established based on the cropping patterns and the crop's coding characteristics of the crop change (Figure 2). Under these rules, the mapping was reconstructed using the reclassification tool in ArcGIS and can be broadly grouped into seven categories of cropping patterns. Of these, 204, 205, and 198 codes were generated by the overlay of only three crop units, rice, maize, and soybean, within each rotation cycle, and the following can be found:

(1) The coding of a plot with seven crop rotations for at least three consecutive years of rice cultivation in a 4-year period, which was uniformly named "rice continuous cropping pattern," implied that the plot had a significant rice-crop problem.

(2) Codes indicating that a plot had been planted for maize for at least three consecutive years in 4 years, with all three rotation cycles being seven, were unified under the name "maize continuous cropping pattern," which indicated that the plot had a more pronounced barrier to continuous maize crop.

(3) Codes indicating that a plot had been planted for soybeans for at least three consecutive years in 4 years with seven crop rotations, which were uniformly named "soybean continuous cropping pattern," which implied that the plot had a more pronounced problem of soybean crop succession.

(4) A code indicating that a plot was planted to rice and maize in rotation for 4 years, with all three rotation cycles being 10, would be uniformly named "rice–maize rotation," which indicated a form of planting in which rice was dominant and maize was supplementary or maize was dominant. Rice was supplementary in any three consecutive years of a rotation.

(5) A code indicating that a plot had 10 rotations of rice and soybeans over 4 years, all three rotations being unified under the name "rice–soybean rotation pattern," which indicated a form of cultivation in which rice was dominant and soybeans were supplemented or soybeans were dominant. Rice was supplemented in any three consecutive years within a rotation.

(6) The coding of three rotation cycles of maize and soybeans in a plot of land in a 4-year rotation was 10 types, which were uniformly named "maize–soybean rotation pattern." Such patterns indicated that in any three consecutive years of a rotation cycle, maize was the main crop, soybeans were supplemented, and soybeans were the main crop, and maize was supplemented, which was the most widespread traditional crop rotation pattern in Northeast China.

(7) The three crop rotation codes, 204, 205, and 198, which indicated that a plot was planted with other crops for at least one of the 4 years, were named "mixed cropping pattern," which included several cropping patterns such as Chinese hemp crop, water, dry crop, mixed crop rotation, etc. These patterns achieved a certain degree of alternation of the crops.

## Kernel density estimation

The kernel density estimation (KDE) method is to fit the distribution pattern of known data points by estimating the probability density of a randomly distributed point data distribution and obtaining the probability distribution curve of the data without any parameter evaluation model assumptions and has now become one of the mainstream methods for studying the spatial elemental aggregation characteristics of regions. In this article, the kernel density of various cropping pattern plots is calculated to demonstrate the spatial agglomeration characteristics of cropping patterns.

$$f(x) = \frac{1}{nh} \sum_{i=1}^{n} k\left(\frac{x - x_i}{h}\right),$$

where $f(x)$ is the kernel density value; n is the number of known points; $h$ is the bandwidth; $k$ is the kernel function; x is the estimated point coordinate value; and xi is the sample point coordinate value. This article used the kernel density estimation method to measure the spatial clustering characteristics of various types of cultivation pattern plots in Wangkui County. First, the raster of cropping patterns was converted into point elements using the "raster to point" function in ArcGIS. Then, the kernel density values were measured based on these point elements.

# Results

## Analysis of the types of cropping patterns

As can be seen from Figure 3, the cropping pattern in Wangkui County was dominated by maize, soybeans, and rice. Specifically, the sum of the planted areas of rice, maize, and soybeans in Wangkui County accounted for 87.31% of the total during the study period; the inter-year results showed several variations. For instance, in 2002, the land area of soybean represented 67.13%. This result immediately decreased in 2003 and represented 9.43%. This situation seemed the opposite of maize, which recorded 13.84% in 2002 and increased by 70.38% in 2003. The land area of rice was not significant. It gained 12.5% in 2021. This result was the highest for the rice land area during this period.

The areas planted by cash crops such as mixed grains, yams, and hansa were relatively low and stable and thus were uniformly categorized as other crops. The change in acreage for maize and soybeans showed a complementary relationship: when maize
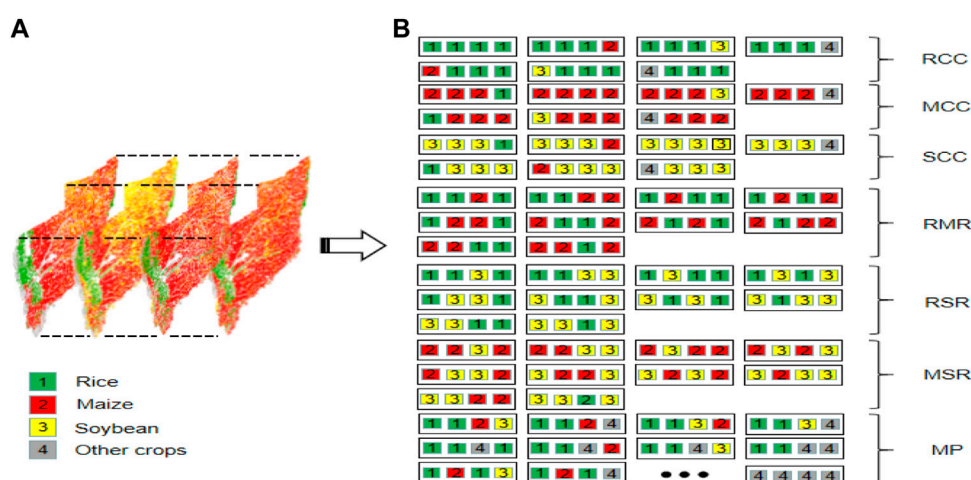
**FIGURE 2**
Information remapping rules. **(A)** Crop classification data during 2017–2021; **(B)** information remapping rules between crop-change information Tupu units and cropping pattern classification system. RCC, rice continuous cropping; MCC, maize continuous cropping; SCC, soybean continuous cropping; RMR, rice–maize rotation; RSR, rice–soybean rotation; MSR, maize–soybean rotation; MP, mixed cropping pattern.



**FIGURE 3**
Change in proportion of crop acreage in Wangkui County, 2002–2005, 2010–2013, and 2018–2021.

increases, soybeans will decrease. Conversely when maize decreases, soybeans will increase. A decrease characterized the change in the acreage of other crops to increase and then decrease over the crop rotation cycles. As the spatial distribution in adjacent years was similar, we visualized them in turning and extreme years (2018, 2019, 2020, and 2021) (Figure 4). Specifically, soybean and maize plots were widely distributed in the county. Their distribution areas were constantly changing and in a "reciprocal advance and retreat" relationship during the 4 years. Rice was concentrated in the western part of the county and was characterized by a banded

distribution along the river valleys, whereas other crops were scattered in the county.

## Spatial patterns of crop rotation at different stages

According to the information remapping rules of the cropping patterns, plots characterizing seven types of cropping patterns in each rotation cycle-crop classification system, including rice continuous-

**FIGURE 4**
Spatial distribution of the crops: rice, maize, soybean and other crops in Wangkui County from 2018 to 2021.



**FIGURE 5**
Evolution of the spatial distribution of the plots of various cropping patterns.
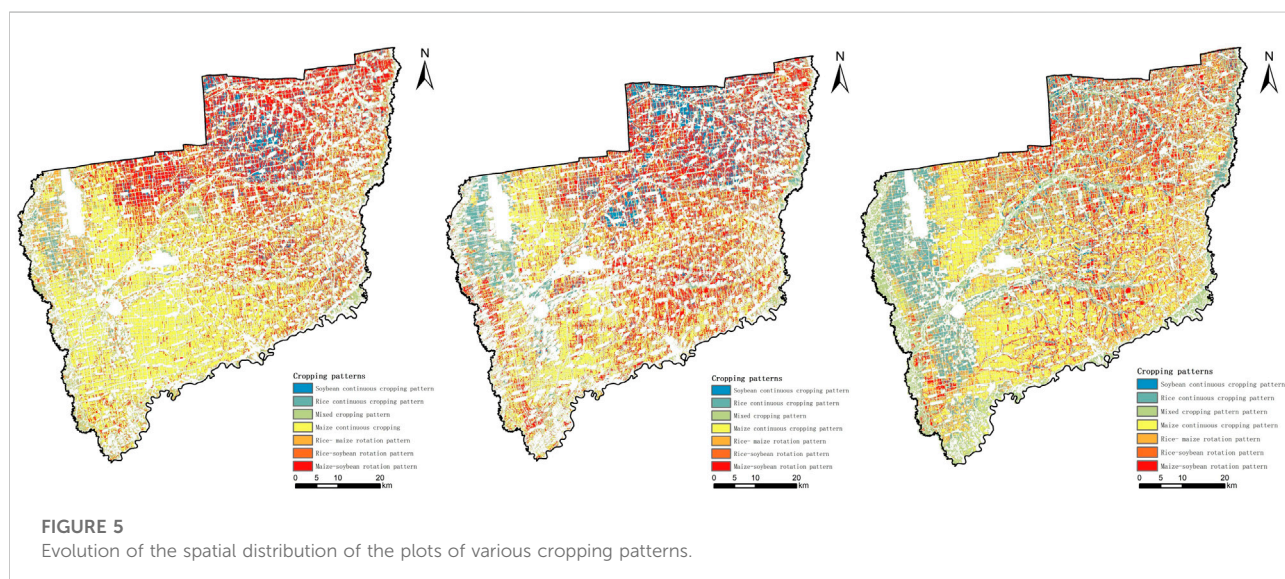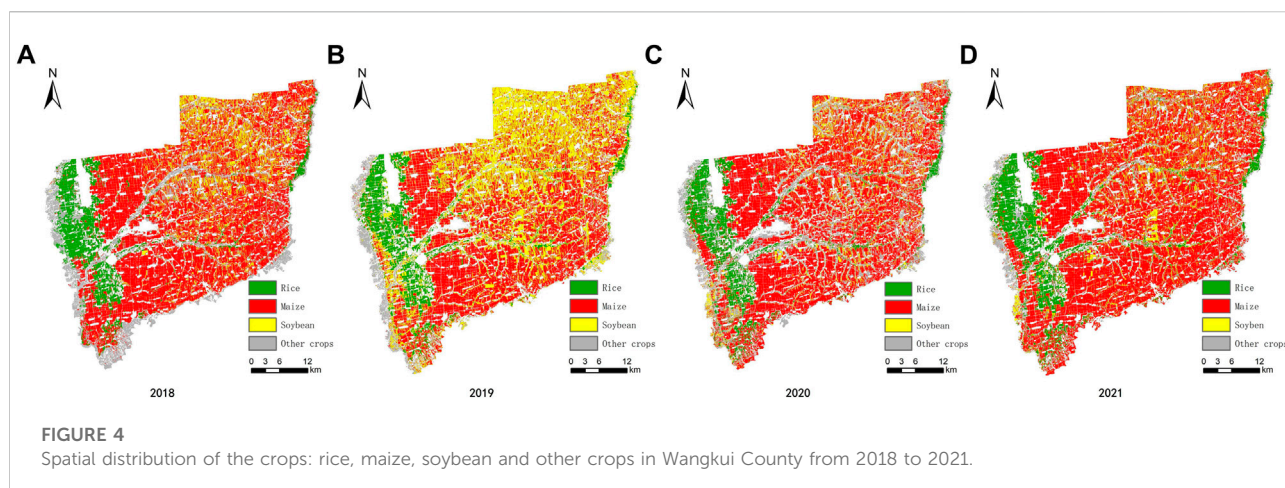
cropping pattern, soybean continuous-cropping pattern, maize continuous-cropping pattern, rice–soybean rotation, rice–maize rotation pattern, maize–soybean rotation pattern, and mixed cropping pattern, were mapped (Figure 5).

Based on the evolution of the cropping patterns and the classification results, the percentage of acreage planted in various cropping rotation cycles in Wangkui County was calculated, as shown in Figure 6.

The main cropping patterns in the black soil area of Wangkui County included maize continuous-cropping pattern, mixed-cropping pattern, maize–soybean rotation pattern, and soybean continuous-cropping pattern, with the total area of the four patterns accounting for 95.28%, 94.66%, and 81.69% in each rotation cycle, respectively. Among them, the maize continuous-cropping pattern was the main one with 39.89%, 29.30%, and 24.56% of the planting area in each rotation cycle. In contrast, the main cropping pattern of rotation was the maize–soybean rotation pattern,

with 25.79%, 32.42%, and 15.22% of the planting area in each rotation cycle, respectively. As the crop rotation cycle progressed, the planted area of the maize–soybean rotation pattern and the soybean continuous-cropping pattern showed a trend of "increasing before decreasing" the planted area of the maize continuous-cropping pattern showed a trend of decrease period by period. The planted land area of the mixed-cropping pattern showed a trend of "decreasing before increasing." The area planted in the rice continuous-cropping pattern, the rice–maize rotation pattern, and the rice–soybean rotation was relatively low and stable.

## Spatial distribution characteristics and evolution of main cropping patterns

This article used the kernel density estimation method to measure the spatial distribution and evolution of the plots of
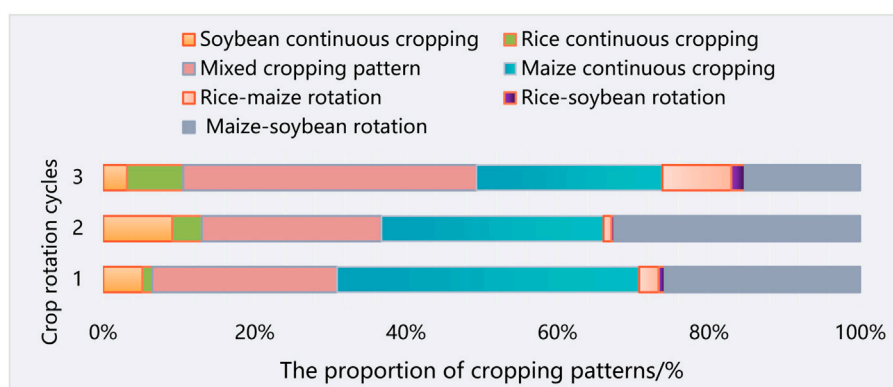
**FIGURE 6**
The proportion of cropping patterns in different crop rotation cycles.
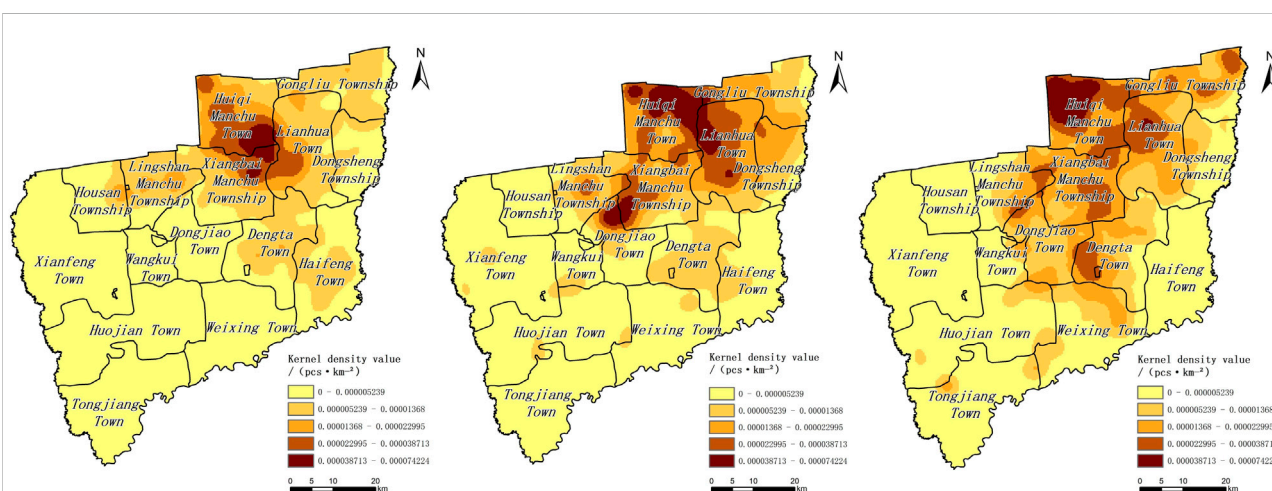


**FIGURE 7**
Spatial distribution characteristics and evolution of soybean continuous-cropping pattern.

various cropping patterns in Wangkui County. The spatial and temporal variations of the various cropping patterns were significant (Figures 7–13).

Among them, the maize continuous-cropping pattern was mainly distributed in the south-central and west-central parts of the county, including Huojian Town, Xianfeng Town, and Housan Township, with a tendency to gather in the east and spread to the northeast. The plots of the mixed-cropping pattern were distributed in the western and northeastern parts of the county in a concentrated and continuous manner, with the characteristics of "local concentration and dispersion" in the county, evolving from the northeast to the southwest; the maize–soybean rotation pattern was widely distributed in the central, eastern, and northern parts of the county, with a trend of spreading from the northeast to the southwest; the soybean continuous cropping pattern was mainly

distributed in the northern part of the county, with Huiqi Manchu Town and Lianhua Town being the most concentrated and evolving in a "north first, then south" trend; the rice continuous-cropping pattern was mainly distributed in Xianfeng Town, with a trend of spreading from the northwest to the southwest of the county; the rice–soybean rotation pattern was mainly distributed in the western, central, and northern parts of the county, with a trend of gathering in the southwest and north and spreading to the center. The rice–maize rotation pattern spread from Xianfeng Town in the northwestern part of the county to the surrounding area. If we compare the spatial distribution with them, it could be seen that there was a certain spatial complementarity between the soybean, maize, and rice continuous-cropping patterns in the evolutionary process; the evolutionary trends of the rice–soybean, rice–maize, and maize–soybean rotation patterns also had the same relationship.

**FIGURE 8**
Spatial distribution characteristics and evolution of maize continuous-cropping pattern.



**FIGURE 9**
Spatial distribution characteristics and evolution of rice continuous-cropping pattern.
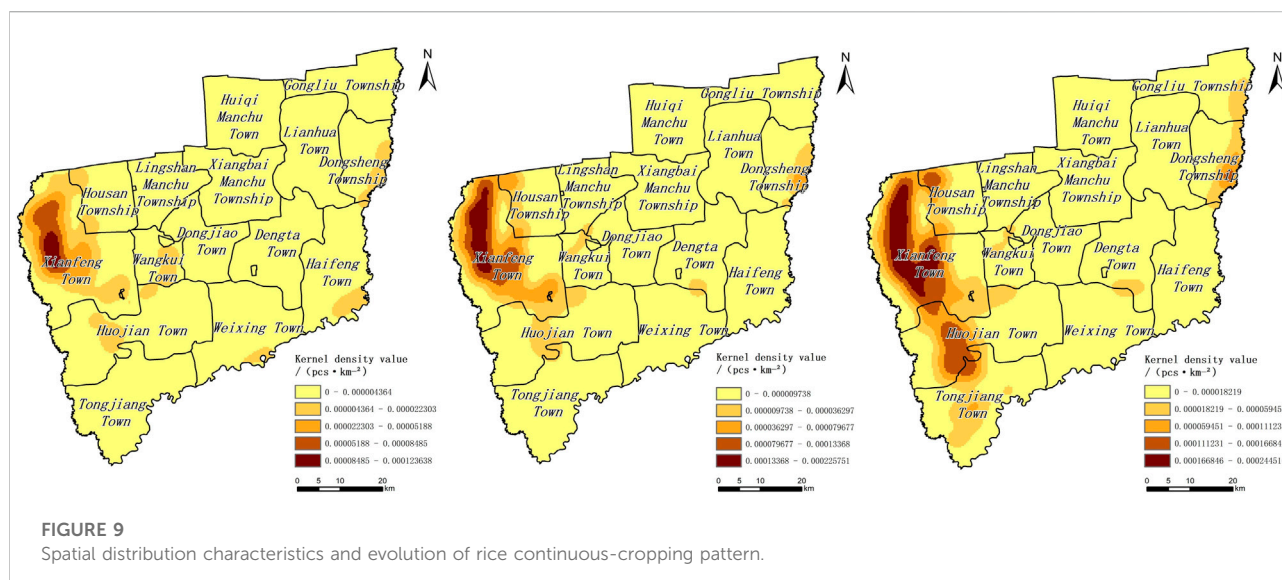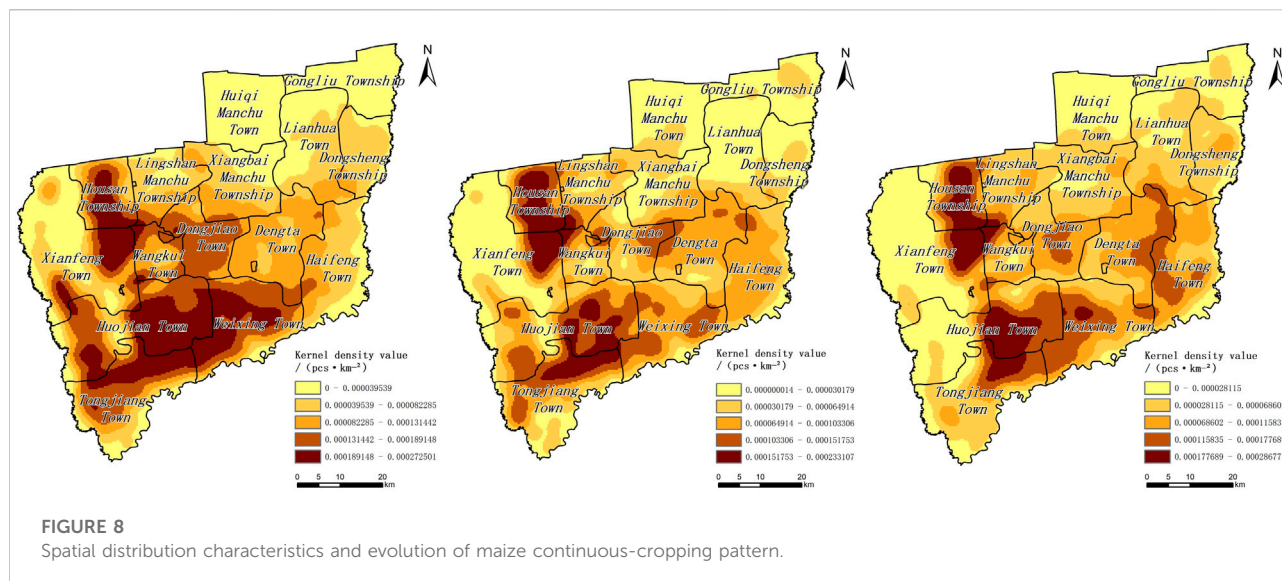
## Discussion

### Factors influencing the evolution of cropping patterns

Various factors influence the formation and evolution of crop cultivation structures. They result from national policies, scientific and technological progress, social demand, economic efficiency, and natural conditions. With the rapid development of social and economic development and the continuous improvement of people's living standards, people's consumption structure of crops and

their ancillary products has changed and they are no longer satisfied with subsistence. Still, they seek not only to live well but also to eat well. The most obvious feature of the marked improvement in the structure and quality of consumption is the continuous decline in the proportion of expenditure on food.

Over the past 30 years, the Engel coefficient of per capita food consumption expenditure of urban households in China has generally shown a declining trend (Gao Jinzhe, 2019). In terms of food consumption trends, as the quality of living standards improves, people's demand for food rations decrease, while the demand for processed foods such as meat, eggs, and milk

**FIGURE 10**
Spatial distribution characteristics and evolution of rice−soybean rotation pattern.



**FIGURE 11**
Spatial distribution characteristics and evolution of rice−maize rotation pattern.
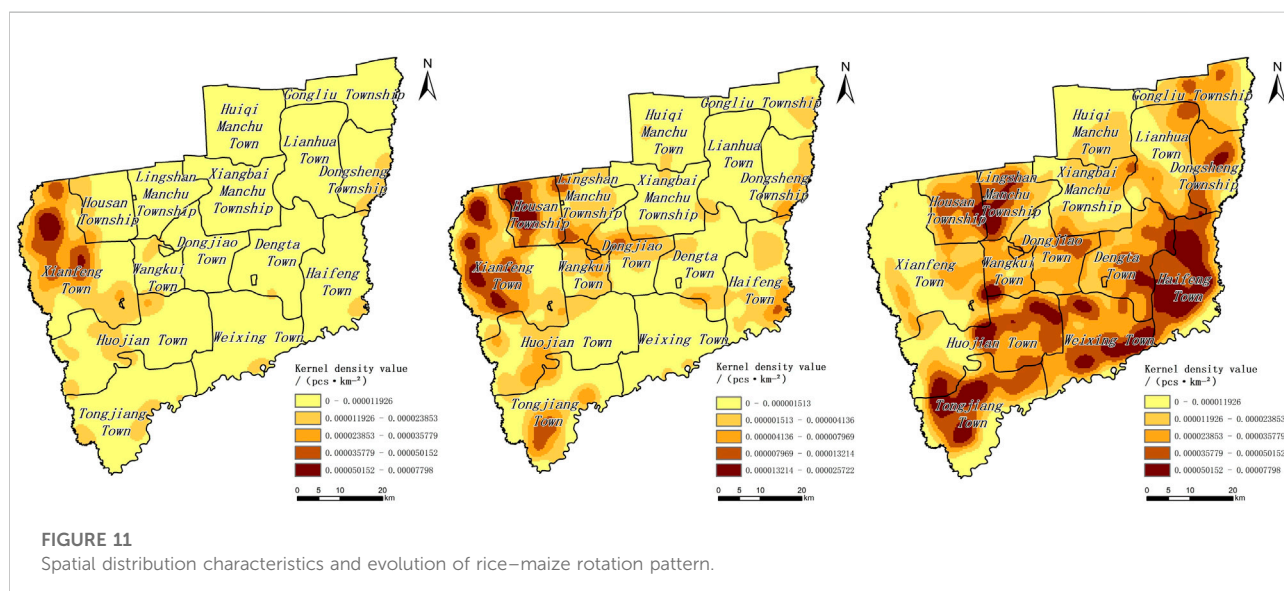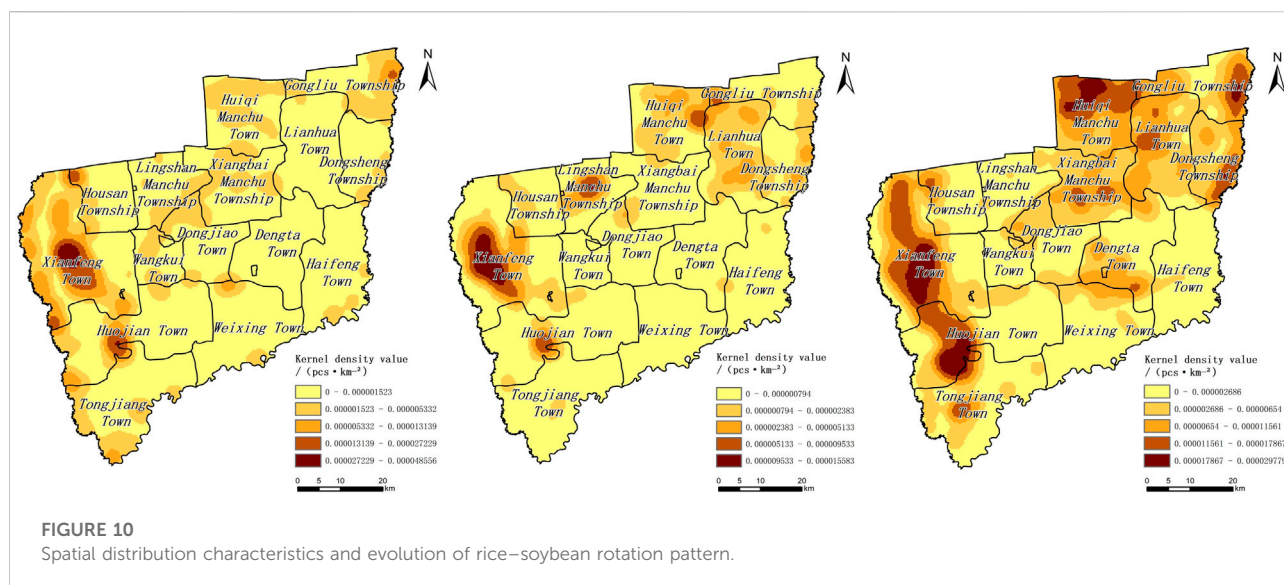
increase, and households in rural China tend to consume higher-quality food as their income increases (Yu and Abler, 2009). Thus, changes in the structure of people's consumption and demand are important factors influencing the cultivation of food crops. In terms of production management practices, the rapid economic growth and rising consumption levels have made it difficult for families to sustain a single farming operation, so the trend is for most migrant workers to move to the cities and for the economy to shift away from a focus on farming (Li, 2019).

The choice of a management-friendly, high-yield, short-cycle cropping pattern is particularly important, and two food crops, maize and soybeans, stood out for their high yields, drought tolerance, and short maturity periods, leading to maize and

soybeans becoming the main food crops in the black soil areas of Northeast China. With the deepening of global integration, the trend of international prices of agricultural products significantly impacts the evolution of the crop rotation model. China's soybeans are highly dependent on imports. High prices curbed the global soybean consumption demand in 2022. Export demand was slowing, with the possibility of a downward revision of export volumes in the future, which in turn will slow the decline in global soybean ending stocks, which will lead to a significant projected increase in the area sown and production of domestically produced soybeans in China. In addition to this, an increase in the yield of a grain crop due to technological progress or increased

**FIGURE 12**
Spatial distribution characteristics and evolution of maize−soybean rotation pattern.



**FIGURE 13**
Spatial distribution characteristics and evolution of mixed-cropping pattern.
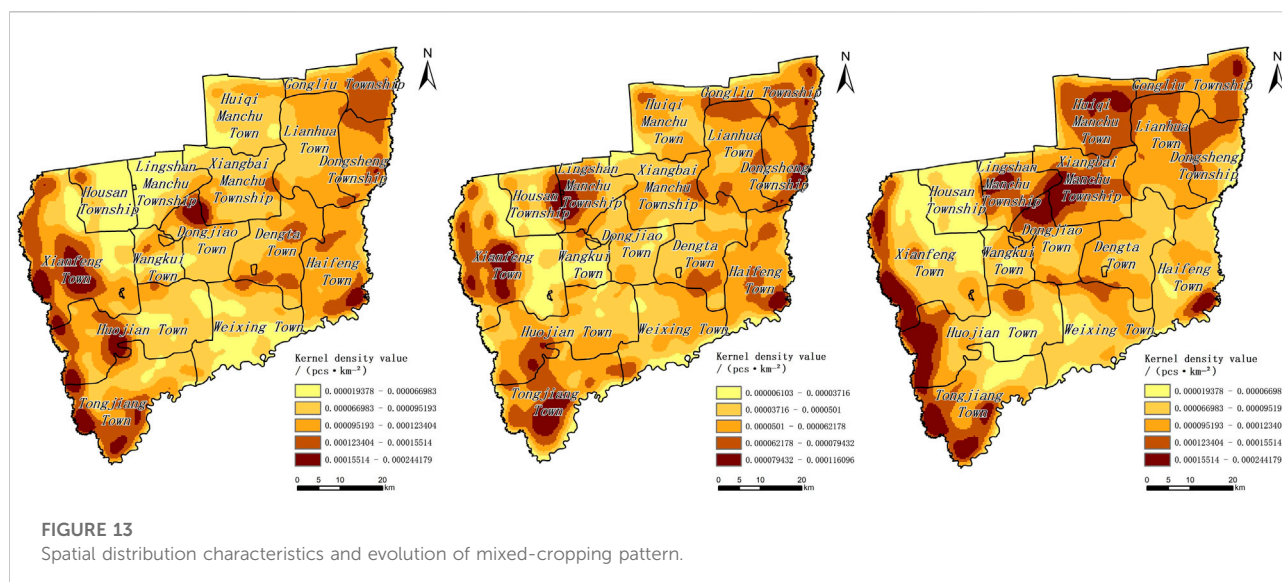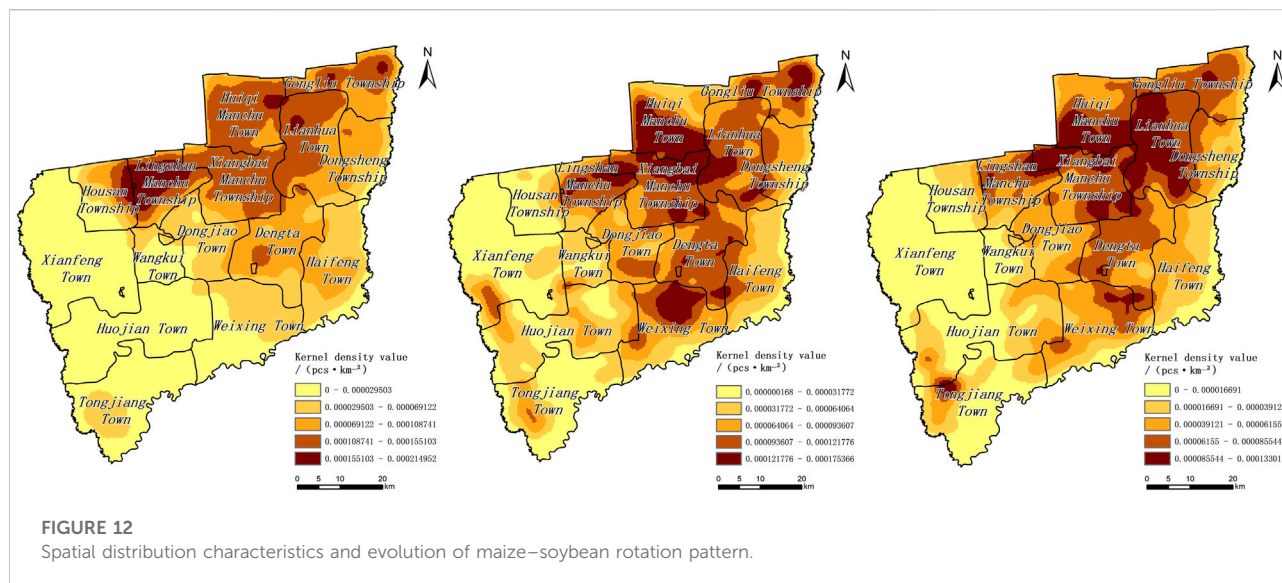
fertilizer application, for example, will lead to a corresponding increase in the share of that grain crop if the planted area remains unchanged (Liu, 2019), which in turn will affect the cropping configuration of the crop rotation pattern.

## Potential impact of the evolution of crop rotation patterns

Crop rotation as a combination of land use and land nourishment has a profound impact on land ecology, food security, and the development of social production. The crop rotation model is based on an organic fit between the phenomena to be studied under the crop rotation system and the laws governing the cultivation of food crops. Since ancient times, China has had a traditional practice of rotating crops on arable land, which helps improve the soil's physical and chemical properties. The successive cultivation of the same crop on the same plot for many years can have a serious impact on the nutrient structure and the physical properties of the soil, which can be remedied to a large extent by replacing crop rotation patterns. At the same time, crop rotation is an important safeguard for the growth and development of crops, as it not only effectively promotes the attenuation of weeds in the field and reduces unnecessary soil nutrient loss but also provides significant protection against plant pathogens and pests (Jalli et al., 2021). The replacement of crop rotation patterns play a significant role in crop yield,

particularly with legumes, increasing soil nitrogen and organic matter content and improving crop yields and the average yield per acre (Huynh et al., 2019). The contradiction between grain storage and supply and demand in China remains acute. Since the 1990s, the cultivation structure of Heilongjiang Province has undergone tremendous changes. The imbalance in the cultivation structure is particularly evident, and there is still an imbalance and failure in allocating cultivated land-use factors. In the context of policies such as the Guiding Opinions on the Structural Adjustment of Maize in the "sickle-curved" areas (The Ministry of Agriculture and Rural Affairs of the People's Republic of China, 2022) and the Pilot Programme for Exploring the Implementation of a Cropland Fallow Crop Rotation System (*Exploring the implementation of a pilot program for arable land rotation fallow system*, 2016), farmers had responded positively to the crop rotation policy, and the change in crop rotation patterns, to some extent, alleviated the imbalance in the structure of the cropland.

## Directions and measures for the regulation of crop rotation patterns

Shifts in crop cultivation systems and improvements in farm management have led to trends in the diversification of total crop yields, acreage, and yields, as well as to different spatial distribution patterns. This study took the cropping patterns of the black soil region of Northeast China as the research object and took the county as the research scale. It described the distribution characteristics and evolution of various cropping patterns in different crop rotation cycles in terms of the evolution of the spatial distribution pattern of cropping patterns in three crop rotation cycles, the spatial evolution of the ratio of the area and quantity of cropping patterns, and the changes in the types of cropping patterns. It then examined the spatial and temporal evolution of the structure of food production in typical counties of the black soil region of Northeast China in recent years. Compared with the first crop rotation cycle (2002–2005), the second cycle (2010–2013) in Wangkui County saw a decrease in the area planted in the maize continuous-cropping pattern and an increase in the area planted in the maize–soybean rotation pattern, probably due to the increase in the price of maize since the national policy of maize storage, which led to the "flooding" of maize in the reclamation area, and the high climatic risk of the cooler areas in northeast China, which produced poor-quality maize and a serious backlog, causing a series of ecological and economic problems in the area due to maize crop rotation. In response, the government has repeatedly advocated the resumption of grain–soybean crop rotation in the northeast China and the development of "one main (maize–soybean rotation-based) and four supplementary" crop rotation and "three-zone crop rotation" models in pilot areas to protect the black soil land (Qiqi, 2021)In the third crop rotation cycle (2018–2021) in Wangkui County, the cropping pattern of the

maize continuous-cropping pattern decreased. The planting area of the rice–soybean rotation increased, probably due to the request to reduce the area of maize and expand the scale of grain–bean rotation in response to the Guiding Opinions on the Structural Adjustment of Maize in the "sickle-curved" areas issued by the Ministry of Agriculture and Rural Affairs in 2015 (The Ministry of Agriculture and Rural Affairs of the People's Republic of China, 2022). During the same period, the cropping patterns of the maize–soybean rotation pattern and the soybean continuous-cropping pattern both showed a decreasing trend, and the planting area accounted for the lowest proportion in each rotation period.

On one hand, this may be because the market price of soybeans has remained low since 2013, and farmers are not willing to plant soybeans. On the other hand, it might be due to the implementation of the national policy of maize storage and various policies to support and subsidize farmers, which, driven by the market, has led to the spatial and temporal evolution of the grain production structure in the black soil areas of Northeast China, with the traditional "soybean–corn" crop rotation pattern being seriously damaged. It can be seen that the configuration and trend of the evolution of cropping patterns are regulated and influenced by policies. A well thought-out, reasonable national agricultural policy has an important influence on the optimization of the industrial structure of the cropping industry and the sustainable use of black land and is also an important regulatory tool for the optimization of the cropping structure of crops. As a typical county in the black soil region of Northeast China, Wangkui County's cropping pattern regulation directions and measures are synchronised with the entire Northeast China black soil region in a broad sense. The regulatory direction and measures for the evolution of its cropping pattern reflect, to a certain extent, the future regulatory direction of the cropping pattern in the black soil area of Northeast China, and are of positive importance for the study of the cropping pattern in the black soil area of Northeast China. However, the shortcoming of this article lies in the long interval between crop rotation cycles, which has a certain impact on the accuracy of the discrimination of the evolution of cropping patterns. In future research, attempts can be made to expand the breadth and depth of research and explore the characteristics of spatial and temporal variations in cropland use at a larger scale.

## Conclusion

During the study period, the sum of the rice, maize, and soybeans acreage in Wangkui County accounted for 87.31% of the total land area. The change in the acreage of corn and soybeans shows a complementary relationship. In another work, corn increased while soybeans decreased, and *vice versa*. The share of rice-planted area was relatively low, and the planted area was more disorderly. Changes in the acreage of other crops showed the characteristics of "decreased, increased, and decreased" in each crop rotation cycle.

The cropping patterns in Wangkui were various. Maize's continuous cropping pattern was the most important and represented 31.25% of the total. This cropping pattern was followed by maize–soybean rotation with 24.48%. In the same context, mixed cropping represented 29.01%. As the crop rotation cycle progressed, the acreage of the maize–soybean rotation pattern and soybean continuous cropping pattern showed an "increasing then decreasing" trend, the acreage of the maize continuous-cropping pattern showed a decreasing trend period by period, and the acreage of the mixed-cropping pattern showed a "decreasing then increasing" trend. The acreage of mixed cropping patterns showed a "decreasing then increasing" trend. The area planted in the rice continuous-cropping pattern, the rice–maize rotation pattern, and the rice–soybean rotation pattern was relatively low and stable.

The spatial and temporal variations of the various cropping patterns were significant. Among them, the maize continuous-cropping pattern evolved with a tendency to gather in the east and spread to the northeast. The mixed-cropping pattern evolved with a tendency to evolve from the northeast to the southwest. The maize–soybean rotation pattern evolved with a trend of spreading from the northeast to the southwest. The soybean continuous-cropping pattern evolved in a "northward and then southward" direction; the rice continuous-cropping pattern spread from the northwestern part of the county to the southwestern part. There was a certain spatial complementarity between the soybean, maize, and rice continuous–cropping patterns in the evolutionary process; the evolutionary trends of the rice–soybean, rice–maize, and maize–soybean rotation patterns also had the same relationship.

## Data availability statement

The original contributions presented in the study are included in the article/Supplementary Material; further inquiries can be directed to the corresponding author.

## Conflict of interest

The authors declare that the research was conducted in the absence of any commercial or financial relationships that could be construed as a potential conflict of interest.

## Publisher's note

All claims expressed in this article are solely those of the authors and do not necessarily represent those of their affiliated organizations, or those of the publisher, the editors, and the reviewers. Any product that may be evaluated in this article, or claim that may be made by its manufacturer, is not guaranteed or endorsed by the publisher.

## References

An, Y. W, S. S. Q. L. S. (2016). Improvement of farmland productivity and water use efficiency bymaize/soybean intercropping. *Horticulture& Seed* 09, 80–83. doi:10.16530/J.CNKI.CN21-1574

Buya, S., Tongkumchum, P., Rittiboon, K., and Chaimontree, S. (2022). Logistic regression model of built-up land based on grid-digitized data structure: A case study of Krabi, Thailand. *J. Indian Soc. Remote Sens.* 50 (5), 909–922. doi:10.1007/s12524-022-01503-0

Cai, H. (2019). The necessity and technical measures of black land conservation. *Agric. Jilin* 18, 72. doi:10.14025/J.CNKI.JLNY.2019.18.042

Dong, W. X. C. Y. (1999). *Plant production*. Beijing: Higher Education Press. Available at: https://xueshu.baidu.com/usercenter/paper/show?paperid=af38b57b0fbceece5b257d43299b2055&site=xueshu_se (Accessed: June 23, 2022).

El-Magd, I. A., and Tanton, T. W. (2003). Improvements in land use mapping for irrigated agriculture from satellite sensor data using a multi-stage maximum likelihood classification. *Int. J. Remote Sens.* 24 (21), 4197–4206. doi:10.1080/0143116031000139791

Exploring the implementation of a pilot program for arable land rotation fallow system (2016). People's daily. Available at: https://kns.cnki.net/kcms/detail/detail.aspx?dbcode=CCND&dbname=CCNDLAST2016&filename=RMRB201606300110

&uniplatform=NZKPT&v=7jTyDE7iKCe8X_G1oM3ZWj61n1JX2lwHWNrsa-kXcenjhD3snFj5D65CdUQNmC2DO_A01fLlgUE%3D.

Foerster, S., Kaden, K., Foerster, M., and Itzerott, S. (2012). Crop type mapping using spectral-temporal profiles and phenological information. *Comput. Electron. Agric.* 89, 30–40. doi:10.1016/j.compag.2012.07.015

Gao Jinzhe, L. C. W. Z. (2019). Analysis of factors affecting per capita food consumption expenditure of urban residents, Market Modernization. Available at: https://kns.cnki.net/kcms/detail/detail.aspx?dbcode=CJFD&dbname=CJFDLAST2019&filename=SCXH201904005&uniplatform=NZKPT&v=96n8CsOoghoSaLe7Eb1iFhSzrXh5CC17Cds9MZ9WTR7RmkcPi8NtXSQu9pxaFa8T (Accessed: June 27, 2022).

Girma, R., Fürst, C., and Moges, A. (2022). Land use land cover change modeling by integrating artificial neural network with cellular Automata-Markov chain model in Gidabo river basin, main Ethiopian rift. *Environ. Challenges* 6, 100419. doi:10.1016/j.envc.2021.100419

Guo-ming, Z. R., and Yu, F. (2022). Analysis of cropping pattern in black soil region of Northeast China based on geo-information Tupu Chinese Journal of Applied Ecology. Available at: https://kns.cnki.net/kcms/detail/detail.aspx?dbcode=CJFD&dbname=CJFDLAST2022&filename=YYSB202203014&uniplatform=

NZKPT&v=
ah886hqBQGgjvGDI4Zblfdyawhp0J9WeSqtS9QO26U9TP8
vo0CbQkBA0uKdt7uhr (Accessed: June 28, 2022).

Hohensinner, S., Atzler, U., Fischer, A., Schwaizer, G., and Helfricht, K. (2021). Tracing the long-term evolution of land cover in an alpine valley 1820–2015 in the light of climate, glacier and land use changes. *Front. Environ. Sci.* 9, 331. doi:10.3389/fenvs.2021.683397

Huang, M., Shao, M., Zhang, L., and Li, Y. (2003). Water use efficiency and sustainability of different long-term crop rotation systems in the Loess Plateau of China. *Soil Tillage Res.* 72 (1), 95–104. doi:10.1016/S0167-1987(03)00065-5

Huynh, H. T., Hufnagel, J., Wurbs, A., and Bellingrath-Kimura, S. D. (2019). Influences of soil tillage, irrigation and crop rotation on maize biomass yield in a 9-year field study in Müncheberg, Germany. *Field Crops Res.* 241, 107565. doi:10.1016/j.fcr.2019.107565

Jalli, M., Huusela, E., Jalli, H., Kauppi, K., Niemi, M., Himanen, S., et al. (2021). Effects of crop rotation on spring wheat yield and pest occurrence in different tillage systems: A multi-year experiment in Finnish growing conditions. *Front. Sustain. Food Syst.* 5, 214. doi:10.3389/fsufs.2021.647335

Ji Fuhua, L. J. W. L. (2020). Ummary of remote sensing algorithm in crop type identification and application based on Gaofen satellite Chinese Journal of Agricultural Resources and Regional Planning. Available at:https://kns.cnki.net/kcms/detail/detail.aspx?dbcode=CJFD&dbname=CJFDLAST2021&filename=ZGNZ202107037&uniplatform=NZKPT&v=lXP1LDpk_N3ADns0EXp_ug2vzDb68XzYhmEe2PIAbFGHwopCUoE8_nGBrKc_e5r_ (Accessed: June 24, 2022).

Jiang, H., Xu, X., Guan, M., Wang, L., Huang, Y., and Liu, Y. (2019). Simulation of spatiotemporal land use changes for integrated model of socioeconomic and ecological processes in China. *Sustain. Switz.* 11 (13), 3627. doi:10.3390/su11133627

Li, B. (2019). Analysis of input behavior and influencing factors of grain farmers in henan province--taikang county as an example, food science and technology and economy. Available at: https://kns.cnki.net/kcms/detail/detail.aspx?dbcode=CJFD&dbname=CJFDLAST2019&filename=LSKJ201907055&uniplatform=NZKPT&v=YP8jHVOkEZCh619h-cC4X80EFGI2RGiuTnZbcn5pQBHzotQ0WuMkJ75qygbpNFDX (Accessed: June 27, 2022).

Liu, L. (2022). Study on the current situation of soil environmental quality of black soil in wangkui County,Heilongjiang province, China energy and environmental protection. Available at: https://kns.cnki.net/kcms/detail/detail.aspx?dbcode=CJFD&dbname=CJFDLAST2022&filename=ZZMT202202024&uniplatform=NZKPT&v=QYFSEn0JpQFBurVVLDX9nO0c64qkjxuYhsjMTkF3Wwo1uurSSVzHBnvJ5eZtAzoT (Accessed: June 28, 2022).

Liu, L. S. W. X. (2019). Spatial-temporal evolution of grain production structure in northeast China, economic geography. Available at: https://kns.cnki.net/kcms/detail/detail.aspx?dbcode=CJFD&dbname=CJFDLAST2019&filename=JJDL20190 5019&uniplatform=NZKPT&v=yfhFpcZHEpV4LUziI_IhQbbTvbk-syJLKSummMJ_3ruWLyEyPRnxCcCkgIx3hIny (Accessed: June 27, 2022).

Qiqi, W. (2021). Rotation between grain and soybean in the cold area of northeast China. AvaliableAt: https://doi.org/10.1038/s41597-021-00827-9.

Sinica, S. G. (2018). Research progress of black soil in northeast China. *Sci. Geogr. Sin.* 38, 1032–1041. doi:10.13249/j.cnki.sgs.2018.07.004

Su, J. F. Z. D. Z. J. M. H. Z. X. (2013). Extraction of maize planting area based on decision tree and mixed-pixel unmixing methods transactions of the Chinese

society for agricultural machinery. Available at: https://kns.cnki.net/kcms/detail/detail.aspx?dbcode=CJFD&dbname=CJFDLAST2015&filename=NYJX201509042&uniplatform=NZKPT&v=tlxPqcgXq6xmTh4xDtc2BNNb9DZUbXct9dEEc-VGd9zAI05puxrRHTxA6_Eth2NH (Accessed: June 23, 2022).

Svoboda, J., Stych, P., Lastovicka, J., Paluba, D., and Kobliuk, N. (2022). Random forest classification of land use, land-use change and forestry (LULUCF) using sentinel-2 data—a case study of Czechia. *Remote Sens.* 14 (5), 1189. doi:10.3390/rs14051189

The Ministry of Agriculture and Rural Affairs of the People's Republic of China (2015) (2022). Guidance of the Ministry of agriculture on the structural adjustment of maize in the 'sickle bend' area , gazette of the Ministry of agriculture and rural Affairs of the People's republic of China. Available at: https://kns.cnki.net/kcms/detail/detail.aspx?dbcode=CJFD&dbname=CJFDLASN2015&filename=GNZB201511002&uniplatform=NZKPT&v=RZYYHKjODzW5ajkn7Y_4wO858rn15J8JsSRlb_ZgLPo9K1ASGnMs5tkakFeshQIH.

Truong, Q. C., Nguyen, T. H., Tatsumi, K., Pham, V. T., and Tri, V. P. D. (2022). A land-use change model to support land-use planning in the mekong Delta (MEKOLUC). *Land* 11 (2), 297. doi:10.3390/land11020297

Wang, J. Y. F. M. (2022). Cropping patterns and farmland landscape at the county level using remote sensing in haihe lowland plain transactions of the Chinese society of agricultural engineering (transactions of the CSAE). Available at: https://kns.cnki.net/kcms/detail/detail.aspx?dbcode=CJFD&dbname=CJFDLAST2022&filename=NYGU202201032&uniplatform=NZKPT&v=__FK__BpVdR6ddBFNLyIhAAzElvyV-39YbZ9clukoX4P43mZw2dwasX_6jgltikr (Accessed: June 23, 2022).

Wang, Y. Y. (2021). Practical exploration and strategy optimization of cultivated land resources in rural China-Focus on black land protection and others. *Hebei Acad. J.* 41 (06), 117–124.

Wu, C. F. O. Z. (2002). Evolution of cropping systems and research progress. *Tillage Cultiv.* 03, 1–5+14. doi:10.3969/J.ISSN.1008-2239.2002.03.001

Xu, X. Z., Xu, Y., Chen, S., Xu, S., and Zhang, H. (2010). Soil loss and conservation in the black soil region of northeast China: A retrospective study. *Environ. Sci. Policy* 13, 793–800. doi:10.1016/j.envsci.2010.07.004

Yang, Z. H. L. L. (2019). Study on soil moisture utilization in different rotation patterns of maize and soybean. *Anhui Agric. Sci. Bull.* 25 (24), 38–40. doi:10.16377/J.CNKI.ISSN1007-7731.2019.24.014

Yanjun, C., and Yuhong, Z. (2021). Filling algorithm for missing pixels in Landsat-7 SLC-off images using no reference images. *Sci. Geogr. Sin.* 41 (07), 1276–1284. doi:10.13249/J.CNKI.SGS.2021.07.018

Yu, X., and Abler, D. (2009). The demand for food quality in Rural China. *Am. J. Agric. Econ.* 91 (1), 57–69. doi:10.1111/j.1467-8276.2008.01159.x

Zhang, W. J. W. (2022). Spatial layout optimization of rural settlements in typical farming areas - a case study of wangkui county, Heilongjiang province, Chinese journal of soil science. Available at: https://kns.cnki.net/kcms/detail/detail.aspx?dbcode=CJFD&dbname=CJFDLAST2022&filename=TRTB202202027&uniplatform=NZKPT&v=mU1dJzawvYTHZ1pKJ9PG3VTjLYMDD2DCLDcl5GSWmrG8OIdvAs8tY69rB_HA0oqm (Accessed: June 28, 2022).

Zhao, T. Y. H. G. (2017). Consideration about exploring pilot program of farmland rotation and fallow system in China. *Ecol. Environ. Sci.* 26 (01), 1–5. doi:10.16258/J.CNKI.1674-5906.2017.01.001

# APPENDIX Crop classification systems in the study area.

| Serial number | Crop type | Swing portfolio | Reading characteristics | Example | Sensors |
|---|---|---|---|---|---|
| 1 | Rice | R: Band_nir<br>G: Band_red<br>B: Band_blue | They are concentrated near river waters, greenish-blue in color during the flooding period, with distinctive field texture characteristics |  | Landsat5 TM<br>Landsat7 ETM+ |
| 2 | Maize | R: Band_nir<br>G: Band_red<br>B: Band_blue | Regular geometric patches with a bright green color at the podding stage, with some tillage texture characteristics |  | |
| 3 | Soybeans | R: Band_nir<br>G: Band_red<br>B: Band_blue | Regular geometric patches with a purplish-red color at the podding stage, with certain tillage texture characteristics Levy |  | |
| 4 | Other crops | R: Band_nir<br>G: Band_red<br>B: Band_blue | Burgundy in color, with a distinctive tillage texture at sowing, showing basic soil characteristics in August |  | |
| 1 | Rice | R: Band_swir1<br>G: Band_nir<br>B: Band_blue | It is concentrated near river waters and has a bright green color during flooding, with distinctive field texture characteristics |  | Landsat8 OLI |
| 2 | Maize | R: Band_swir1<br>G: Band_nir<br>B: Band_blue | Regular geometric patches, mostly lime green in creamy maturity, with some tillage texture characteristics |  | |
| 3 | Soybeans | R: Band_swir1<br>G: Band_nir<br>B: Band_blue | Regular geometric patches with a yellow colour at the podding stage, with some tillage texture characteristics |  | |
| 4 | Other crops | R: Band_swir1<br>G: Band_nir<br>B: Band_blue | Burgundy and reddish-brown with a distinct tillage texture during the sowing period, showing bare soil characteristics in August | <br> | |

frontiers | Frontiers in Environmental Science

# Improvement of a land fragmentation measurement model based on natural surface elements and road network

Lanlan Su[1], Yuluan Zhao[1]*, Mingshun Long[1] and Xiubin Li[2]

[1]College of Geography and Environmental Science, Guizhou Normal University, Guiyang, China, [2]Institute of Geographic Sciences and Natural Resources Research, CAS, Beijing, China

Land fragmentation is one of the most important factors hindering the mechanization and scale of agriculture. To further alleviate the negative impact of arable land fragmentation, a more accurate model for measuring arable land fragmentation is needed. Using 0.1 resolution UAV images and farm survey data, we obtained spatial and tenure data of farming land in Baidu Village through ArcGis and other software, and analyzed the results and correlations of farming plot area, plot shape and plot dispersion indicators in the study area. A road accessibility index that integrates terrain slope and road network is proposed to characterize the dispersion of land parcels for the first time, and is compared with two road accessibility models that do not take into account terrain slope and road network. The results show that the dispersion index of farm plots is the most influential indicator on the fragmentation of farm plots, followed by the area index of farm plots, and finally the shape index of farm plots; the new model of measuring the fragmentation of farm plots based on natural surface elements and road networks is closer to the real situation and more accurate in portraying the degree of fragmentation of farm plots.

## Introduction

With the advancement of economic globalization, the process of world urbanization is accelerating. Currently, about 54% of the world's population lives in urban areas, and this proportion is expected to reach 66% by 2050 (UNDESA, 2014; Masini et al., 2018). The large-scale transfer of agricultural labor to nonagricultural industries increases the opportunity cost of agricultural labor (Kawasaki, 2011). The United Nations predicts that by 2050, the world population is expected to reach 9.3 billion, and the global population will reach 10.1 billion in 2100 (United Nations Population Division, 2011). The continuously growing population, limited arable land resources, and dwindling agricultural population have placed enormous pressure on world food security (Nair, 2014). To provide a maximum guarantee to meet the growing food demand of mankind, it is necessary to improve the intensive utilization of cultivated land. The ability to achieve a

certain scale benefit has become the key to promoting agricultural development and ensuring food security. Land fragmentation (LF) is a prominent feature of cropland use in agricultural production in developing countries, and the supply of cropland for food production is increasingly limited (Niroula and Thapa, 2007; Di Falco et al., 2010). Under the influence of many factors, such as natural environment and social economy, LF in China is serious problem (Tan et al., 2006). LF refers to the phenomenon that a farmer's land resources are scattered and not concentrated (Latruffe and Piet, 2014; Lu et al., 2018). Related studies have focused on the basic plots of farming operations, exploring the essential attributes of the plots and studying the causes of LF (Janus et al., 2016). Also, basic characteristics of LF are included, including the distribution of plots cultivated by farmers, their proximity to households (Niroula and Thapa, 2005), the size of plots cultivated (Lu et al., 2018), the number of plots (Wan and Cheng, 2001), and plot shape (Demetriou et al., 2013).

LF is a pattern of arable land resource utilization that is contrary to the scale of arable land management. This pattern enriches the diversity of agricultural production in China and reduces the risk of agricultural cultivation (Nguyen et al., 1996; Van Hung et al., 2007; Tan et al., 2021). However, there are certain negative effects, and affects the efficient use of land resources and national food security. Disorganized, interspersed, and scattered plot distribution is an important aspect of cultivated plot distribution in China (Qi and Dang, 2018). This distribution can increase commuting costs (Latruffe and Piet, 2014; Wang and Wang, 2010). When the number of plots owned by farmers is large and scattered, the cost of transportation and traveling time from the homestead to each plot will increase (de Garis De Lisle, 2010; del Corral et al., 2011; Niroula and Thapa, 2005). Farmers' traveling time will increase under the influence of terrain slope and distance traveled, which not only causes invariance to material transportation and plot irrigation management but also increases labor input, thus reducing farmers' economic returns (Niroula and Thapa, 2007; Kawasaki, 2010). Considering these conditions, farmers will pay less attention to remote and low-quality plots, and this type of plot often has much higher input costs than net benefits, and farmers will abandon these plots (Carter and Yao, 2002; de Garis De Lisle, 2010; Lu et al., 2018). In addition, LF has a hindering effect on agricultural mechanization and productivity (Blarel et al., 1992; Wan and Cheng, 2001; Ali and Deininger, 2015). In the case of growing maize, late rice, and wheat, the production efficiency decreases by 4%, 15%, and 17% when the degree of cultivated land fineness increases by one unit, respectively (Wan and Cheng, 2001). With the small size of arable plots, farmers need to invest in more labor to increase production value (Lu et al., 2018), and the increase in the number of plots increases the amount of labor invested by farmers. In addition, when plots are small and irregularly shaped, farmers often will not develop advanced agricultural technologies and

may even abandon this land (Van Hung et al., 2007; Gónzalez et al., 2007), which further limits productivity and hinders agricultural modernization.

To mitigate these negative impacts of LF, the Chinese government conducts policy control, and to fully manage the impacts of LF, policy-makers and planners need scientific indicators to measure the extent of LF (Igozurike, 1974; Januszewski, 1968; Simmons, 1964). Based on the definition of land fractionation above, we know that the plot dispersion, plot size, and plot shape indicators ideally should be incorporated into a comprehensive measurement model to accurately measure the degree of LF. Currently there are more accepted ways of evaluating parcel size and parcel shape, among these indicators, plot area uses the Simpson index to combine the number of plots and plot area, which accurately reflects the area characteristics of plots. The plot shape index uses the standard squares and circles as standard measure, which reflects the shape characteristics of the plot to a certain extent. However, there are no accurate indicators for the dispersion of plots in the academic community, the current indicators characterizing the dispersion of farmers' plots include distances, such as the distance from farmers' homesteads to each of their plots as well as the distance between plots. These distances are Euclidean distances or road network distances. Other studies have used farmer's commuting time to reflect the fragmentation of plots (Ge and Zhao, 2019). And calculating the shortest cumulative time from farmers' homesteads to each of their plots through iteration, which is the road accessibility of farmers. It uses commuting time to combine two factors, namely distance and walking speed, to more comprehensively and accurately reflect the dispersion of parcels. Road accessibility refers to the ease of getting from the starting point to the end point (Páez et al., 2012), the two main factors in measuring road accessibility index are walking speed or distance (Hess and Almeida, 2007; Higgins, 2019). Some studies have used Euclidean distance, which ignores the distance of the road networks formed by complex topographic environments (Zhao, 2011; Ge and Zhao, 2019). Alternatively, walking speed was set to the normal human walking speed (5 km/h) and was a constant value (Ge and Zhao, 2019), which was determined under the assumption of a flat walking plane and a constant walking speed of 5 km/h. Although this planar approach is not problematic in a two-dimensional and topographically flat study area, this approach can overestimate (or underestimate) walkability in a topographically diverse environment (Higgins, 2019). Because walking speed and terrain are not constant, in addition to personal ability, time pressure, and other factors, walking speed varies with the slope of the walking environment (Lee et al., 2015; Aghabayk et al., 2021). Figure 1 shows the terrain affects the road accessibility, and road accessibility is much lower in areas with more undulating terrain (Figure 1A) than in areas with flat terrain (Figure 1B). This is especially true in mountainous areas, where the terrain is undulating and the surface is rugged and broken. The slope of the pedestrian
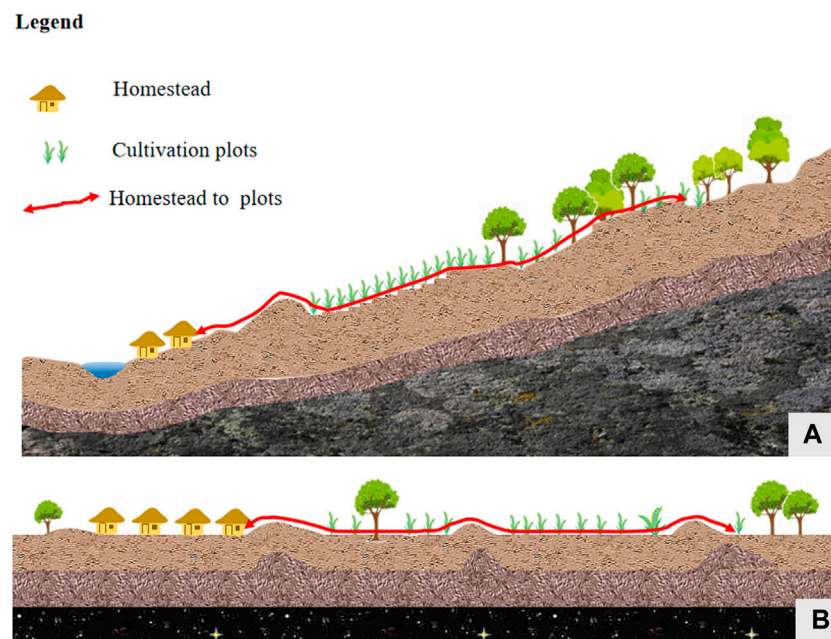
**FIGURE 1**
Schematic diagram of the distribution of homesteads and plots. Figure 1A shows that the road network is affected by the topography in the mountainous areas. Figure 1B shows the road network in a flat terrain.

road has a significant impact on the walking speed of farmers, thus affecting the commuting costs of farmers from their homesteads to their plots. Therefore, use of the LF measurement model without considering the terrain factor is not suitable for mountainous areas.

To address the shortcomings of the LF measurement model, and based on the previous research, we integrated the topographic slope into the measurement model and integrated natural surface elements and road networks to build an LF measurement model that is more realistic and applicable to plain or mountainous areas. We accurately portrayed the degree of fragmentation of cultivated land and provided a basic reference for academic research and policy formulation.

## Materials and methods

### General situation of the research area

The existing measurement model is applicable to the plain areas, which are less spatially heterogeneous. To consider the extent to which the fine fragmentation of mountainous cultivated land is affected by topography, we selected a typical mountainous cultivated area. Baidu Village, Jianhe County, Qiandongnan Prefecture, Guizhou Province, is a typical mountainous village

$(108°47'9\,''E–108°47'30\,''E, 26°4011\,''N–26°40'23\,''N)$ (Figure 2) located on the banks of the Qingshui River. It is 30 km from Nanzhai Town and has two natural villages: the Upper Baidu Village and Lower Baidu Village. Under the jurisdiction of 27 village groups, the village is dominated by the Miao ethnic group. In 2020, the total resident population had reached 1,655. The economy of Baidu Village is mainly agricultural. The village land area is $1241.216\,hm^2$, the total arable land area is $113.407\,hm^2$, the average arable land area is $0.067\,hm^2$, the forestland area is $186.667\,hm^2$, and the per capita forestland area is $0.112\,hm^2$. It is a typical example of the fragmentation of arable land in mountainous areas.

## Research method

### Village and farmer model construction

Rural farmland in China is generally dominated by farm households' contracting and management, and is also affected by village contracting rights, land adjustment, and intra-village transfer, which affect LF to some extent. For this reason, we constructed LF models for farming land at the farm household and village levels, respectively.

The main structure of the farm households model is as follows: we selected the attribute indicators characterizing the
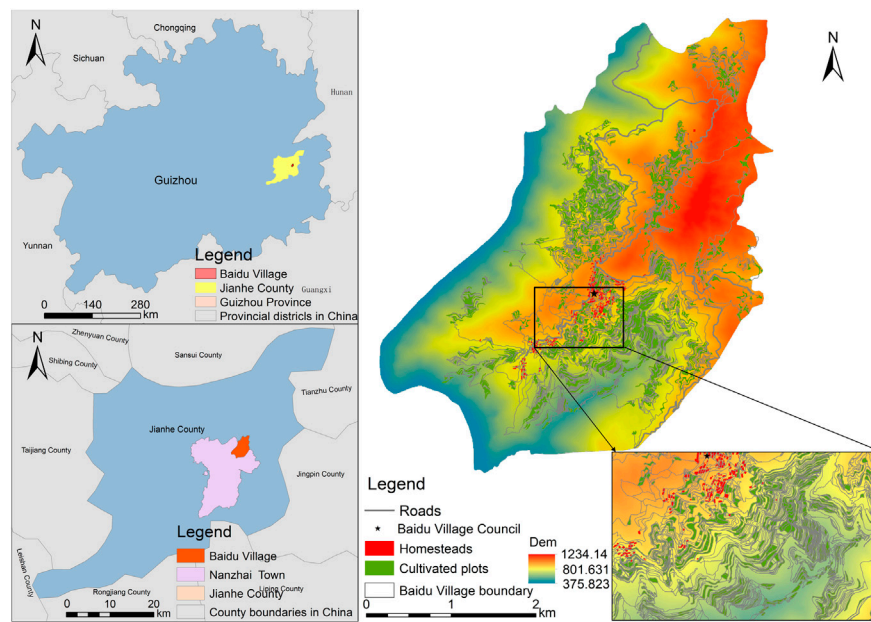
**FIGURE 2**
The study area.

fine fragmentation of farming land for inclusion in the model, calculated the values of each characterizing attribute indicator, and summed the values of each characterizing attribute indicator to obtain the farmer's land fragmentation index (FLFI), according to the following equation:

$$FLFI = \sum_{i=1}^{n} F_i \qquad (1)$$

where Fi represents each indicator of cultivated land fine fragmentation; and n is the number of selected indicators. The range of FLFI is (0, 3), and the larger the value is, the higher the degree of fragmentation of farmers' cultivated land.

The village model is calculated based on the cultivated FLFI of each farming household. The village farmland fragmentation index (VLFI) is the average value of each farming household's FLFI. The formula is as follows:

$$VLFI = \frac{\sum_{j=1}^{m} FLFI_j}{m} \qquad (2)$$

where $FLFI_j$ is the cultivated land fragmentation index of farming household j; and m is the number of farming households in the village. The range of values of VLFI is (0, 3), and the larger the value is, the higher the degree of cultivated land fragmentation in the village.

## Selection of evaluation indicators

The connotation of LF is reflected in the following four aspects: fragmented distribution of arable land plots operated by farmers, relatively large number of plots, relatively small area of individual plots, and irregular shape of plots. Therefore, we constructed a model to determine the degree of fragmentation of cropland according to these four aspects.

1. The plot accessibility index ($F_1$) describes the degree of plot dispersion, labor, and machinery accessibility. Plot dispersion uses commuting time to combine two major factors: network distance and walking speed. Thus, so plot dispersion is measured by the cumulative walking time from the farmer's home base to the shortest network distance from each plot. Farm plot road accessibility index ($F_1$) is the ratio of the plot road accessibility score to the maximum value of the village farm road accessibility score.

$F_1$ of farm plots is calculated as follows:

$$F_1 = \frac{f_1}{f_{1\,max}} \qquad (3)$$

where $f_1$ is the road accessibility score of the plot; and $f_{1max}$ is the maximum road accessibility score in the village.

The plot road accessibility score ($f_1$) is calculated as follows:

$$f_1 = \sum_{k=1}^{q} \frac{S_k}{V} \qquad (4)$$

where q is the number of plots owned by the farmer; $S_k$ is the distance of the road network from the farmer's home base to each of his farming plots k; and V is the walking speed. The larger values of $f_1$ indicate higher commuting costs when the farmer

operates his farming plots, more dispersed plots, and higher fragmentation of farming land.

V is calculated as follows:

By extracting the slope value $\alpha$ between the farmhouse and its plot (Eq. 5), we calculate the walking speed V (km/h) under the influence of slope $\alpha$ (%) (Eq. 6) (Tobler, 1993; Higgins, 2019).

$$\alpha = (h_1 - h_2)/l \times 100\% \tag{5}$$

where $h_1$ and $h_2$ are the maximum elevation difference between the farmer's homestead and the plot; and $l$ is the closest distance from the homestead to the plot.

$$V = 6e^{-3.5|\alpha +0.05|} \tag{6}$$

2. The farmer's plot area index ($F_2$) is the number of plots and plot area that directly affect the farming efficiency and machinery running cost (Lu et al., 2018). We used SI and calculated this index by combining the number of plots and plot area. The farmer's plot area index ($F_2$) is the ratio of the farmer's SI score to the maximum value of the farmer's SI score in the village.

The farm plot area index ($F_2$) is calculated as follows:

$$F_2 = \frac{f_2}{f_{2\,max}} \tag{7}$$

where $f_2$ is the farm household SI score; and $f_{2max}$ is the maximum value of SI score in the village.

The plot area index ($f_2$) is calculated as follows:

$$f_2 = 1 - \frac{\sum_{k=1}^{q} A_k^2}{\left(\sum_{k=1}^{q} A_k\right)^2} \tag{8}$$

where $A_k$ is the area of plot k. The larger the value of $f_2$, the lower the farming efficiency and the higher the degree of fragmentation of cultivated land.

3. The farmers' plot shape index ($F_3$) influences the efficiency of machinery operations (Bettinger et al., 1996). The farmer's plot shape index ($F_3$) is the ratio of the parcel shape score to the maximum village parcel shape score.

The farmer's plot shape index ($F_3$) is calculated as follows:

$$F_3 = \frac{f_3}{f_{3\,max}} \tag{9}$$

where $f_3$ is the parcel shape score; and $f_{3max}$ is the maximum value of the village parcel shape score.

The plot shape index ($f_3$) is calculated as follows:

$$f_3 = \frac{\sum_{k=1}^{q} \frac{C_k}{\sqrt{2\pi A_k}}}{q} \tag{10}$$

where $C_k$ is the perimeter of plot k; and $A_k$ is the area of plot k. The larger the value of $f_3$ is, the lower the efficiency of machinery operation and the higher the degree of fragmentation of the farmer's land.

4. The geographic detector model (Wang and Xu, 2017) was used to analyze the degree of influence of the main influencing factors on the FLFI. Where the q-value is used to represent the degree of factor influence and the q-value is calculated as follows:

$$q = 1 - \frac{\sum_{h=1}^{L} N_h \delta_h^2}{n\delta^2} \tag{11}$$

where h = 1,2..., L is the stratification of variable y or factor x, which is categorical or partition; $N_h$ and N are the number of cells in layer h and the whole area, respectively; and $\delta_h^2$ and $\delta^2$ denote the variance of subregion h and the whole region A, respectively. The range of q is [0,1]. The larger the value of q is, the more pronounced the spatial divergence of the FLFI and the stronger the spatial determination of the independent variable $F_i$ on the FLFI.

## Data source and processing

The data included sample farmer research data and unmanned aerial vehicle (UAV) image data. First, we collected the high-resolution remote sensing image map of Baidu Village with a spatial resolution of 0.1 m by aerial photography with UAV, and the image was pre-processed by ArcGIS10.2 and ENVI5.3 for stitching and correction. Second, Figure 3 shows we extracted the spatial information of house bases, cultivated land, and roads in Baidu Village through visual interpretation: we obtained 171 households, 1,487 plots of cultivated land and 17,442 roads such as main roads and field roads. The extracted homestead and cultivated land plots are numbered separately. We used the Spatial Analysis and Network Analysis tools of ArcGIS to build the road network between the homestead and the cultivated plots in Baidu Village. We performed topology checking and error handling on the road network to realize the spatial connection from the homestead to the cultivated plots and measured the distance of the road network from the farmer's homestead to his cultivated plots. In addition, we calculated the straight-line distance from a farmer's homestead to the farmer's plot using the ArcGIS analysis tool point distance. We obtained the homestead and plot elevation data of Baidu Village using 91 Satellite Map Assistant Software. Through the above work we constructed a spatial information database of cultivated land in Baidu Village.

In 2020, a participatory survey was conducted among village officials and farmers in Baidu Village. Based on a basic understanding of the village situation through interviews with village chiefs and group leaders, a stratified random sample of farmers in different village groups was interviewed, and 171 valid questionnaires were obtained. Through the on-site identification of farmers and questionnaire interviews, we obtained information on the ownership of the completed numbered residential and farmland plots, the composition of the farmers, the current status of farmland utilization, and the input of production materials and labor. We compared the acquired information on the ownership of farmers' residential bases with the corresponding arable land plots and evaluated the utilization of the plots one by one. Combined with the aforementioned spatial information database of cultivated land, we constructed a database of residential bases and cultivated land use tenure and spatial information of farmers in Baidu Village.

**FIGURE 3**
The digitalization process of cultivated land space. **(A–C)** are homesteads, cultivated land, and roads, respectively, and human visual interpretation corresponds to **(A')**, **(B')**, and **(C')**, respectively.
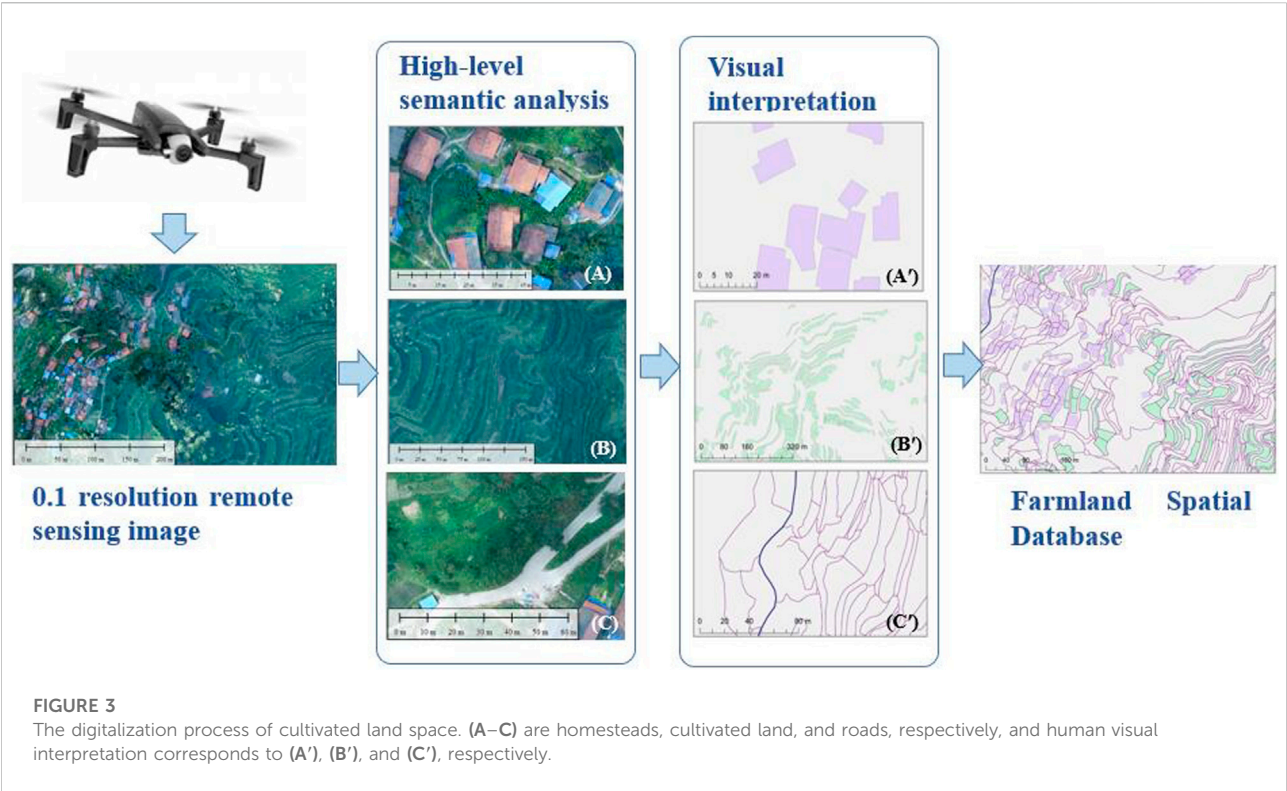
**TABLE 1 Descriptive statistics of farming household survey data.**

| Survey item | Minimum value | Maximum value | Mean value | Standard deviation |
|---|---|---|---|---|
| Plot level/1487 plots | | | | |
| Plot size/hm$^2$ | 0.001 | 0.363 | 0.041 | 0.035 |
| Plot perimeter/m | 10.336 | 883.515 | 132.860 | 89.649 |
| Farmer level/171 households | | | | |
| Farmers farming distance/m | 46.233 | 6004.930 | 1831.696 | 1119.222 |
| Number of farming plots/piece | 2.000 | 23.000 | 8.720 | 4.414 |
| Total arable land of farming households/hm$^2$ | 0.019 | 1.131 | 0.356 | 0.184 |
| Farmers' walking speed/km/h | 0.039 | 5.990 | 3.7098 | 1.529 |
| Farmers cultivate height difference/m | −462.297 | 341.270 | −48.282 | 137.332 |

## Results

### Descriptive statistics of farm household survey data

According to the basic characteristics of the plots of the sample farmers in Baidu Village (Table 1), the scale of farmers' operations is relatively small, the area of plots is small, and the LF is serious. Table 1 shows the average value of the total arable land of farmers was 0.356 hm$^2$ and the smallest farmland area was only 0.019 hm$^2$; the average value of farming plot area was 0.041 hm$^2$ and the smallest plot area was 0.001 hm$^2$; and the average value of farming plot was 8.72, the largest plot was 23, and the smallest plot was 2. In addition, the spatial distribution of arable land varied greatly. The mean value of elevation difference between farmers' homesteads and plots was −48.282 m; the minimum value was −462.297 m, and the maximum value was 341.27 m. The mean value of the road network distance from farmers' homesteads to their plots was 1831.696 m, and the minimum value reached 46.233 m. It was evident that the village did not have a concentrated distribution of home sites and plots, with long distances for farming and high commuting costs.

According to the Tobler function, we know that the walking speed was not directly proportional to the slope (Figure 4); when

**FIGURE 4**
Walking speed and pace by gradient per Tobler (1993) hiking function.
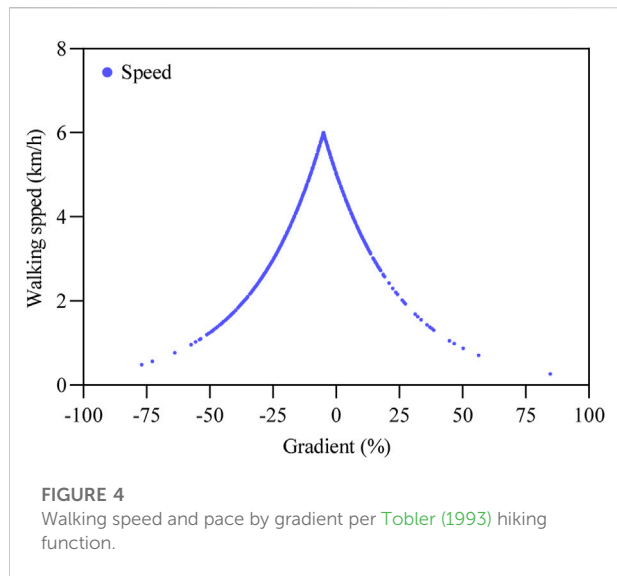
the slope value was less than 0, it is downhill. When the slope was −5%, the walking speed reached a maximum value of 5.999 km/h. When the slope was 0 (i.e., flat), the walking speed was 5 km/h. This result showed that either uphill or downhill slope had an effect on walking speed. Taking the most normal human walking speed, which is 5 km/h on level ground, as the node, walking speed became faster when $−10.136\% < \alpha < 0$, slowed down when $\alpha > 0$, and hindered walking speed when $\alpha < −10.136\%$. Thus, slope

directly affected walking speed and had a significant impact on travel time to work. Considering the slope of the terrain and network distance, the one-way traveling time of commuting from the farmer's homestead to the farming plot (Figure 5) showed that the traveling time of 0.12 h was mostly near the homestead with a comparable slope and closer distance; however, the traveling time increased as the slope between the homestead and the farming plot increased and the distance was longer.

## Land fragmentation of farmer

To quantitatively analyze the relationship between the status quo values of each index and the index of fine fragmentation of farmland, we selected the index of fine fragmentation of farmland in Baidu Village as the dependent variable (y), and selected the accessibility of farm plots ($x_1$), the index of farm plot area ($x_2$), and the index of farm plot shape ($x_3$) as independent variables. We conducted the regression analysis one by one (Figure 6). Each indicator ($x_1$, $x_2$, $x_3$) was linearly and positively correlated with FLFI (y), and the regression coefficients were 1.344, 1.736, and 0.8274. The coefficients of determination R were 0.748, 0.653, and 0.055, the correlation coefficients r were 0.865, 0.808, and 0.236. The two-sided significance test probability $p$ values were less than 0.05. The best fit and the highest correlation were found between the road accessibility index of farm plots and the index of cultivated LF; the correlation between the index of farm plot shape and the index of cultivated LF was lower. The fitted regression equations were as follows:



**FIGURE 5**
Homestead to plot walking time.
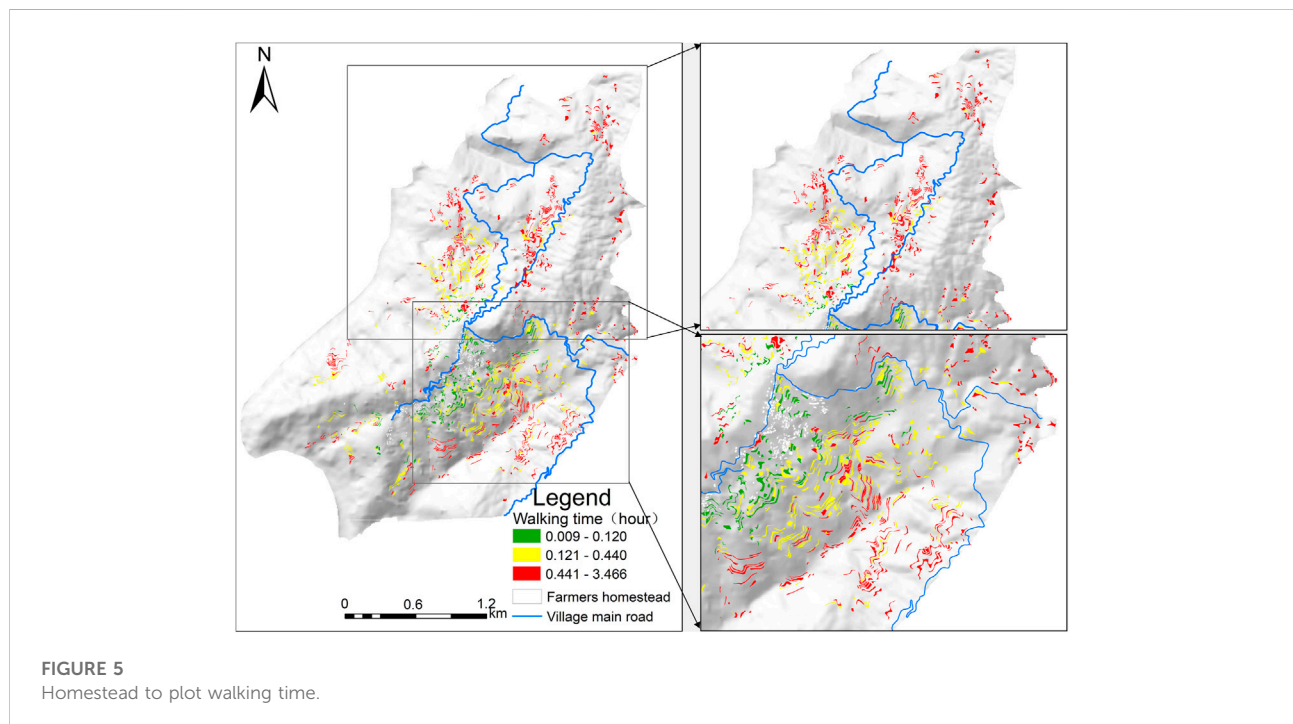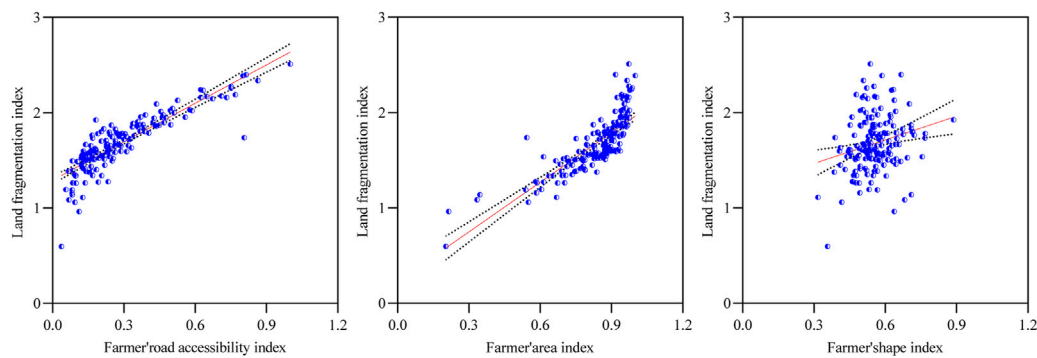
**FIGURE 6**
Correlation analysis on FLFI.
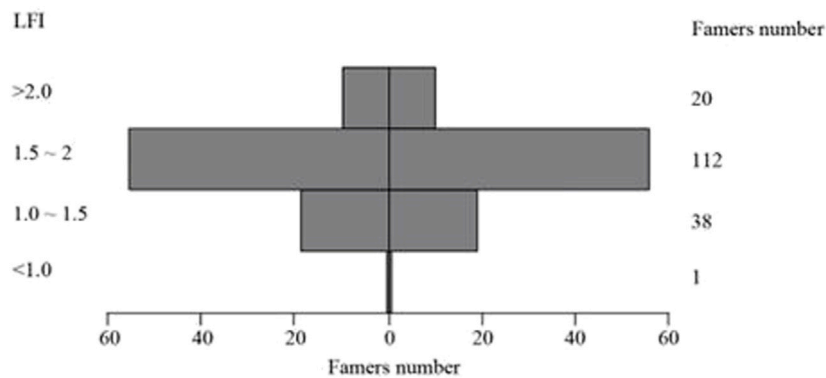


**FIGURE 7**
Correlation analysis on FLFI.

$$y = 1.344x_1 + 1.292 \tag{12}$$

$$y = 1.736x_2 + 0.2276 \tag{13}$$

$$y = 0.8274x_3 + 1.217 \tag{14}$$

We identified the relationship between each evaluation index and FLFI using geographic probes, and the impact measures q of F1, F2, and F3 on FLFI were 0.692, 0.617, and 0.085, respectively. Thus, the road accessibility index of farm plots was the most influential indicator on FLFI, followed by the area index of farm plots, and finally the shape index of farm plots. The results of the correlation analysis and the geographic detector showed no significant differences in the effects of each indicator on FLFI, which indicated that the results of the analysis have good reliability and objectivity.

## Land fragmentation of village

Based on Eq. 2, the VLFI of Baidu Village was 1.678. Equation 1 was used to calculate FLFI (Figure 7) of each farm household in Baidu Village in 2020. With the increase in FLFI, the number of farm households showed an olive shape, increasing first and then decreasing. The cultivated FLFI of farm households was concentrated between 1 and 2, with total 150 households accounting for 87.72% of all farm households, among which 20 households were larger than 2, and only 1 household had FLFI of less than 1.

## Comparative analysis of different plot road accessibility index models

From the correlation analysis and geographic detector synthesis, we concluded that the farm road accessibility index was the dominant factor. To compare the accuracy of the existing F1 index model, we compared the measurement model that considers the natural features of the ground and the road network with the model that does not consider the influence of the terrain and the road network. To make the road accessibility index

**FIGURE 8**
Comparison of the values of the three plot road accessibility indices.
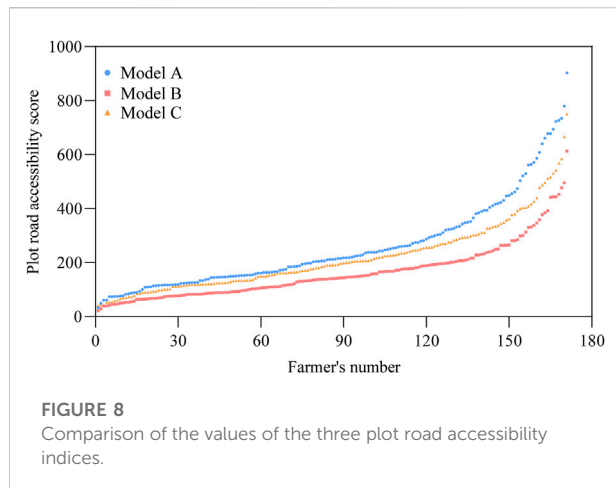
more intuitive to better reflect the convenience of road commuting for farmers, we instead of applying the farmer road accessibility index ($F_1$) normalized by the maximum value, the road accessibility value ($f_1$), which directly reflects commuting time, was used. Three major models were compared and analyzed: Model A refers to the traveling time under the consideration of the terrain and road network distance—that is, the new measurement model proposed in this paper. Model B refers to the traveling time under the consideration of the terrain influence but not the road network distance using the straight-line distance. Model C refers to the traveling time under the consideration of the road network distance but not the terrain influence (Ge and Zhao, 2019).

The results obtained from these three farm-road-accessibility-evaluation models followed a similar trend (Figure 8). Table 2 shows the difference between these three indices was that model A obtained a higher value of 902.790, with a minimum value of 33.38 and a mean value of 258.498. Model B obtained a lower value of 21.83, and its maximum value was also the smaller of the three major models at 612.63, with a mean value of 163.015. The minimum value of model C was greater than models A and B at 41.32, and the maximum value was greater than model B but less than model A at 750.48, with a mean value of 218.479. Therefore, the accuracy of model B for measuring the road accessibility index in mountainous areas was much lower than that of models A and C. In contrast, the lowest values of both model A and model C were found in the same farmer, and model C was 7.94 smaller than model A. The maximum slope

between the cultivated land and the homestead of this farmer was −6.441%, which was located in the downhill direction of the homestead, and the slope was equivalent to a slightly downhill walk, where the speed was slightly higher compared to the flat land (Figure 4). The speed of model A was 95 m/min (Figure 2), and the speed of model C was 83.330 m/min. The speed of model A was greater than that of model C. Model A considered the walking speed under the influence of terrain, whereas the speed of model C was a constant value without considering the influence of terrain. In addition, the difference between the two maximum values of 152.31 appeared in the same farmer (Table 3). This farmer has 21 plots of land, and plot 4 has a large difference between the two models' results. The plot and the farmer's home base slope had a difference of 31.264%, the speed of model A was 1.696 km/h (28.267 m/min), and the speed of model C was a constant value of 83.33 m/min. Model C did not take into account that uphill would slowed down the walking speed and the speed was constant, which was not consistent with the actual situation. Model A was take into account the resistance of road slope to walking, which slowed down the walking speed and greatly increased the traveling time of the farmer. This resistance was enhanced when the distance was larger. The road accessibility index that considered the slope of the terrain and the distance of the road network provided a more accurate portrayal.

According to these results, we found that the road accessibility indicators of models B and C both underestimated the degree of road accessibility. First, the distance of model B was Euclidean distance, which underestimated the distance from the homestead to the plot. Second, the walking speed of model C did not consider the influence of topography, which was limited by the topography in mountainous areas with large topographic relief and directly affected the commuting time of farmers. Therefore, when measuring the degree of LF, the Model A that integrated terrain slope and road network better portrayed the real situation.

## Discussion

In this study, we constructed a new LF measurement model based on topographic slope and road network. This model can more accurately determine the LF of farmers so that decision-makers can accurately implement land management policies. Currently, there are two major perspectives for determining the degree of LF, one is based

**TABLE 2 Results of three road accessibility scenarios.**

| Different road accessibility scenario indices | Minimum value | Maximum value | Average value | Standard deviation |
|---|---|---|---|---|
| Model A | 33.380 | 902.790 | 258.498 | 168.675 |
| Model B | 21.830 | 612.630 | 163.015 | 102.991 |
| Model C | 41.320 | 750.480 | 218.479 | 129.290 |

TABLE 3 Farmer sample data.

| Farmers' plot serial number | Road network distance (m) | Straight line distance (m) | Tillage height difference (m) | Slope (%) | Speed (km/h)[a] | Model A | Model B | Model C |
|---|---|---|---|---|---|---|---|---|
| 1 | 3635.000 | 2588.734 | 184.059 | 7.128 | 3.925 | 55.572 | 39.576 | 46.622 |
| 2 | 1282.760 | 787.446 | −290.213 | −39.646 | 1.785 | 43.129 | 26.476 | 18.394 |
| 3 | 4010.950 | 2850.686 | 134.457 | 4.722 | 4.269 | 56.367 | 40.061 | 51.133 |
| 4 | 1303.250 | 600.950 | 179.320 | 31.264 | 1.686 | 46.371 | 21.382 | 18.640 |
| 5 | 135.189 | 62.141 | 2.911 | 4.690 | 4.274 | 1.898 | 0.872 | 4.622 |
| 6 | 3644.710 | 2474.213 | 172.535 | 6.990 | 3.944 | 55.452 | 37.644 | 46.738 |
| 7 | 3953.600 | 2821.119 | 138.372 | 4.911 | 4.241 | 55.929 | 39.909 | 50.445 |
| 8 | 4158.290 | 2990.590 | 120.954 | 4.048 | 4.371 | 57.075 | 41.047 | 52.901 |
| 9 | 4172.940 | 3006.103 | 116.005 | 3.862 | 4.400 | 56.904 | 40.993 | 53.077 |
| 10 | 3653.450 | 2489.743 | 168.712 | 6.792 | 3.971 | 55.201 | 37.618 | 46.843 |
| 11 | 1954.850 | 1393.415 | −107.800 | −7.760 | 5.448 | 21.531 | 15.347 | 26.459 |
| 12 | 3079.600 | 2159.681 | 235.046 | 10.948 | 3.433 | 53.816 | 37.741 | 39.957 |
| 13 | 1299.220 | 770.802 | −287.779 | −40.245 | 1.747 | 44.609 | 26.465 | 18.591 |
| 14 | 1963.740 | 1395.690 | −107.020 | −7.691 | 5.461 | 21.576 | 15.335 | 26.566 |
| 15 | 1213.030 | 740.013 | −292.381 | −43.010 | 1.586 | 45.881 | 27.990 | 17.557 |
| 16 | 3880.240 | 2804.874 | 151.240 | 5.400 | 4.169 | 55.839 | 40.364 | 49.565 |
| 17 | 4209.610 | 3021.857 | 119.732 | 3.965 | 4.384 | 57.613 | 41.357 | 53.517 |
| 18 | 4042.930 | 2867.322 | 133.568 | 4.663 | 4.278 | 56.700 | 40.213 | 51.517 |
| 19 | 2082.730 | 1393.610 | −79.444 | −5.710 | 5.853 | 21.351 | 14.287 | 27.994 |
| 20 | 2056.220 | 1401.673 | −87.571 | −6.260 | 5.741 | 21.489 | 14.649 | 27.676 |
| 21 | 1555.020 | 1119.350 | −110.675 | 7.128 | 5.048 | 18.483 | 13.304 | 21.661 |

[a]Speed is the walking speed considering the effect of terrain slope and is also the speed of models A and B. The speed of model C is the normal walking speed of human and is a constant value of 5 km/h.



FIGURE 9
Road accessibility index for three different scenarios. (A) indicates a scenario where road network distances and terrain slope are considered, (B) indicates a scenario where straight-line distances and terrain slope are considered, and (C) indicates a scenario where road network distances are considered but terrain slope is not considered.
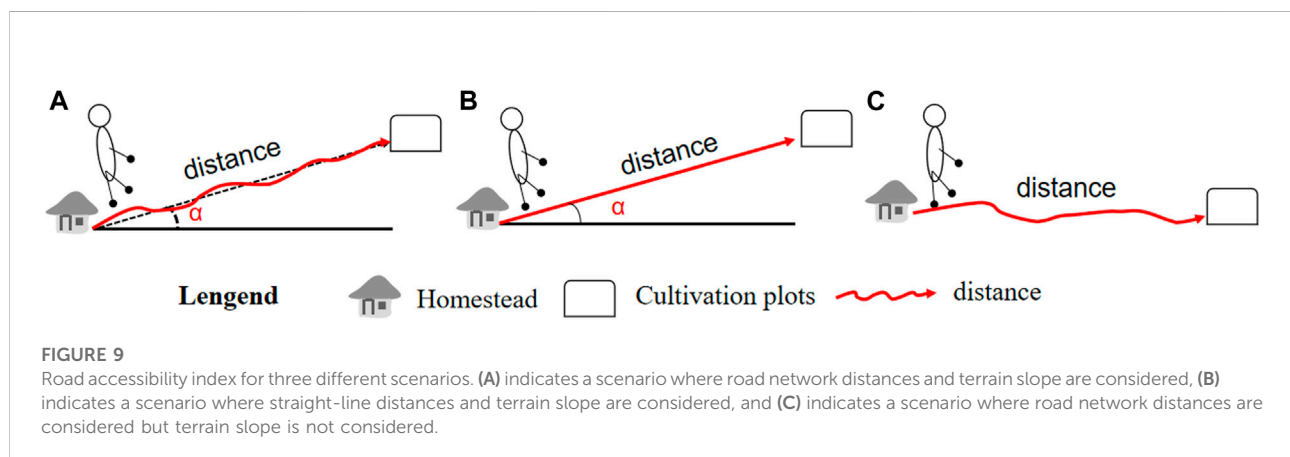
on the mesoscale regional landscape perspective (Liu et al., 2019), which expands the concept of fractionalization to the scale of landscape ecology and focuses on the degree of fragmentation of land use types in surface patches. It ignores the presence of multiple farmer operators in a landscape patch. Another one is based on the micro-scale farmer's perspective and takes the basic unit plot of the

farmer's farming operation as the object of study. Since the main agricultural operators in China are farmers and the land is mainly contracted and operated by farmers, the LF measurement model is more relevant to the actual situation based on the micro-scale farmers' perspective. The current micro-level indicators mainly include the number of parcels, parcel area, shape, and the influence of

the degree of dispersion (Niroula and Thapa, 2005; Demetriou et al., 2013; Lu et al., 2018), through correlation analysis, the results indicate that the indicator of plot dispersion carved using road accessibility is the dominant factor, i.e., the commuting time of the farmer to the homestead, scholars considered the road network distance to break through the error generated by previous studies using straight-line distance (Ge and Zhao, 2019), but did not consider the impact of terrain slope on speed, walking speed of 5 km/h and a constant value, which is not consistent with the actual situation. This study integrates surface natural elements and road network distances to consider walking speed under the influence of topography. Figure 9 shows three different scenarios of road accessibility are compared, Figure 9A shows the scenario considering the terrain slope and the road network, i.e., the scenario presented in this paper. Figure 9B is the scenario considering terrain slope without road network. Figure 9C is the scenario proposed by scholars considering the distance of road network but not the slope of the terrain. The final result indicates that the new measure proposed in this paper further portrays the degree of dispersion of farmers' plots.

To mitigate the effects of LF, in the context of China's strong advocacy of agricultural modernization, mountainous areas have focused on improving agricultural infrastructure, including the construction of farming road networks, such as machine roads. As a result, the costs of farm commuting, material transportation, and machinery running time have decreased and agricultural mechanization and production efficiency have increased. At the same time, when the slope between the homestead and the plot is large and the distance is far away, the input and income costs are integrated, and land transfer and engineering management measures are comprehensively used for plots that have better quality, promoting the moderate-scale operation of agriculture. In this study, to accurately extract the spatial information of farmers' homesteads, plots, and road networks, remote sensing data must have high accuracy, which requires UAV remote sensing images and high-precision satellite images. Thus, understanding how to obtain high-resolution images of large areas must be further explored.

## Conclusions

Decision-makers need an accurate and comprehensive model to quantify LF. We selected three indicators for inclusion in the model: the road accessibility index of farm plots, the area index of farm plots, and the shape index of farm plots. We used resolution of 0.1 m remote sensing images and farm household survey data to build a village road network and constructed a database of farm household residential bases and farmland use tenure and spatial information in Baidu Village. The topography was incorporated into the metrological model, including the calculation of slope and pedestrian walking speed. By obtaining the elevation of the

homestead and the plot, the shortest distance from the farmer's homestead to the corresponding plot, we determined the slope of the homestead and the corresponding plot. By portraying the farmer's walking speed under the slope image, we obtained accurate geospatial data for the model and measured the degree of arable LF in Baidu Village. The results showed that it is necessary to create a road network of house bases and cultivated land in Baidu Village and to calculate the slope perception of pedestrian accessibility. By measuring the degree of cultivated LF while considering the walking speed of farmers with slope, we obtained an effective model to measure cultivated LF.

The LF model generated by the model integrating speed under the influence of road network distance and terrain slope had the following characteristics: it integrated the three core LF factors and was comprehensive; and it was flexible and context-specific, as the model was applicable in both mountainous and plain areas. Applying the model in an empirical study and comparing the results with two existing indicators, the results showed that the existing indicators underestimated (or overestimated) the degree of LF because they ignored the important variable of topographic slope. Therefore, the existing indicators may provide misleading results for decision making. In contrast, we verified that the present model provides a more reliable and robust measure of LF, performing significantly better than existing indices.

## Data availability statement

The original contributions presented in the study are included in the article/Supplementary Material, further inquiries can be directed to the corresponding author.

## Author contributions

YZ: Conceived the research ides. LS: Data curation and writing original draft. ML: Review and editing. XL: Supervision and methodology.

## Funding

## Acknowledgments

## Conflict of interest

The authors declare that the research was conducted in the absence of any commercial or financial relationships that could be construed as a potential conflict of interest.

## Publisher's note

All claims expressed in this article are solely those of the authors and do not necessarily represent those of their affiliated organizations, or those of the publisher, the editors and the reviewers. Any product that may be evaluated in this article, or claim that may be made by its manufacturer, is not guaranteed or endorsed by the publisher.

## Supplementary material

The Supplementary Material for this article can be found online at: https://www.frontiersin.org/articles/10.3389/fenvs.2022.1017599/full#supplementary-material

## References

Aghabayk, K., Parishad, N., and Shiwakoti, N. (2021). Investigation on the impact of walkways slope and pedestrians physical characteristics on pedestrians normal walking and jogging speeds. *Saf. Sci.* 133, 105012. doi:10.1016/j.ssci.2020.105012

Ali, D. A., and Deininger, K. (2015). Is there a farm-size productivity relationship in african agriculture?:evidence from Rwanda. *Land Econ.* 91 (2), 317–343. doi:10.3368/le.91.2.317

Bettinger, P., Bradshaw, G. A., and Weaver, G. W. (1996). Effects of geographic information system vector–raster–vector data conversion on landscape indices. *Can. J. For. Res.* 26, 1416–1425. doi:10.1139/x26-158

Blarel, B., Hazell, P., Place, F., and Quiggin, J. (1992). The economics of farm fragmentation: Evidence from Ghana and Rwanda. *World Bank. Econ. Rev.* 6, 233–254. doi:10.1093/wber/6.2.233

Carter, M. R., and Yao, Y. (2002). Local versus global separability in agricultural household models: The factor price equalization effect of land transfer rights. *Am. J. Agric. Econ.* 84, 702–715. doi:10.1111/1467-8276.00329

de Garis De Lisle, D. (2010). Effects of distance on cropping patterns internal to the farm. *Ann. Assoc. Am. Geogr.* 72, 88–98. doi:10.1111/j.1467-8306.1982.tb01385.x

del Corral, J., Perez, J. A., and Roibas, D. (2011). The impact of land fragmentation on milk production. *J. Dairy Sci.* 94, 517–525. doi:10.3168/jds.2010-3377

Demetriou, D., Stillwell, J., and See, L. (2013). A new methodology for measuring land fragmentation. *Comput. Environ. Urban Syst.* 39, 71–80. doi:10.1016/j.compenvurbsys.2013.02.001

Di Falco, S., Penov, I., Aleksiev, A., and van Rensburg, T. M. (2010). Agrobiodiversity, farm profits and land fragmentation: Evidence from Bulgaria. *Land Use Policy* 27, 763–771. doi:10.1016/j.landusepol.2009.10.007

Ge, Y., and Zhao, Y. (2019). Improvement of farmland fragmentation measurement model based on road network analysis. *Resour. Sci.* 41, 766–774. doi:10.18402/resci.2019.04.13

Gónzalez, X. P., Marey, M. F., and Álvarez, C. J. (2007). Evaluation of productive rural land patterns with joint regard to the size, shape and dispersion of plots. *Agric. Syst.* 92, 52–62. doi:10.1016/j.agsy.2006.02.008

Hess, D. B., and Almeida, T. M. (2007). Impact of proximity to light rail rapid transit on station-area property values in buffalo, New York. *Urban Stud.* 44 (5/6), 1041–1068. doi:10.1080/00420980701256005

Higgins, C. D. (2019). A 4D spatio-temporal approach to modelling land value uplift from rapid transit in high density and topographically-rich cities. *Landsc. Urban Plan.* 185, 68–82. doi:10.1016/j.landurbplan.2018.12.011

Igozurike, M. U. (1974). Land tenure, social relations and the analysis of spatial discontinuity. *Area* 6, 132–135.

Janus, J., Mika, M., Leń, P., Siejka, M., and Taszakowski, J. (2016). A new approach to calculate the land fragmentation indicators taking into account the adjacent plots. *Surv. Rev.* 50, 1–7. doi:10.1080/00396265.2016.1210362

Januszewski, J. (1968). Index of land consolidation as a criterion of the degree of concentration. *Geogr. Pol.* 14, 291–296.

Kawasaki, K. (2010). The costs and benefits of land fragmentation of rice farms in Japan. *Aust. J. Agric. Resour. Econ.* 54, 509–526. doi:10.1111/j.1467-8489.2010.00509.x

Kawasaki, K. (2011). The impact of land fragmentation on rice production cost and input use. *Jpn. J. Rural Econ.* 13, 1–14. doi:10.18480/jjre.13.1

Latruffe, L., and Piet, L. (2014). Does land fragmentation affect farm performance? A case study from brittany, France. *Agric. Syst.* 129, 68–80. doi:10.1016/j.agsy.2014.05.005

Lee, S. H., Goo, S. H., Chun, Y. W., and Park, Y. J. (2015). The spatial location analysis of disaster evacuation shelter for considering resistance of road slope and difference of walking speed by age - case study of seoul, korea. *J. Korean Soc. Geospatial Inf. Syst.* 23, 69–77. doi:10.7319/kogsis.2015.23.2.069

Liu, J., Jin, H., Xu, W., Sun, R., Han, B., Yang, X., et al. (2019). Influential factors and classification of cultivated land fragmentation, and implications for future land consolidation: A case study of Jiangsu Province in eastern China. *Land Use Policy* 88, 104185–104185. doi:10.1016/j.landusepol.2019.104185

Lu, H., Xie, H., He, Y., Wu, Z., and Zhang, X. (2018). Assessing the impacts of land fragmentation and plot size on yields and costs: A translog production model and cost function approach. *Agric. Syst.* 161, 81–88. doi:10.1016/j.agsy.2018.01.001

Masini, E., Barbati, A., Bencardino, M., Carlucci, M., Corona, P., and Salvati, L. (2018). Paths to change: Bio-economic factors, geographical gradients and the land-use structure of Italy. *Environ. Manag.* 61, 116–131. doi:10.1007/s00267-017-0950-0

Nair, P. K. R. (2014). Grand challenges in agroecology and land use systems. *Front. Environ. Sci.* 2, 1. doi:10.3389/fenvs.2014.00001

Nguyen, T., Cheng, E., and Findlay, C. (1996). Land fragmentation and farm productivity in China in the 1990s. *China Econ. Rev.* 7, 169–180. doi:10.1016/s1043-951x(96)90007-3

Niroula, G. S., and Thapa, G. B. (2005). Impacts and causes of land fragmentation, and lessons learned from land consolidation in South Asia. *Land Use Policy* 22, 358–372. doi:10.1016/j.landusepol.2004.10.001

Niroula, G. S., and Thapa, G. B. (2007). Impacts of land fragmentation on input use, crop yield and production efficiency in the mountains of Nepal. *Land Degrad. Dev.* 18, 237–248. doi:10.1002/ldr.771

Páez, A., Scott, D. M., and Morency, C. (2012). Measuring accessibility: Positive and normative implementations of various accessibility indicators. *J. Transp. Geogr.* 25, 141–153. doi:10.1016/j.jtrangeo.2012.03.016

Qi, X., and Dang, H. (2018). Addressing the dual challenges of food security and environmental sustainability during rural livelihood transitions in China. *Land Use Policy* 77, 199–208. doi:10.1016/j.landusepol.2018.05.047

Simmons, A. J. (1964). An index of farm structure, with a Nottinghamsire example. *East Midl. Geogr.* 3, 255–261.

Tan, S., Heerink, N., and Qu, F. (2006). Land fragmentation and its driving forces in China. *Land Use Policy* 23, 272–285. doi:10.1016/j.landusepol.2004.12.001

Tan, S., Heerink, N., Kuyvenhoven, A., and Qu, F. (2021). Impact of land fragmentation on rice producers' technical efficiency in South-East China. *NJAS Wageningen J. Life Sci.* 57, 117–123. doi:10.1016/j.njas.2010.02.001

Tobler, W. (1993). *Three presentations on geographical analysis and modeling: Non- isotropic geographic modeling; speculations on the geometry of geography; and*

*global spatial analysis*. Ncgia Technical Reports. Available at: https://escholarship.org/uc/item/05r820mz.

UNDESA (2014). *World urbanization prospects: The 2014 revision, highlights*. New York: United Nations.

United Nations Population Division (2011). World population prospects: The 2010 revision. Available at: http://esa.un.org/unpd/wpp/index.htm.(Accessed June 18, 2022).

Van Hung, P., MacAulay, T. G., and Marsh, S. P. (2007). The economics of land fragmentation in the north of Vietnam. *Aust. J. Agric. Resour. Econ.* 51, 195–211. doi:10.1111/j.1467-8489.2007.00378.x

Wan, G. H., and Cheng, E. (2001). Effects of land fragmentation and returns to scale in the Chinese farming sector. *Appl. Econ.* 33, 183–194. doi:10.1080/00036840121811

Wang, W. M., and Wang, Q. (2010). *Land use planning: Land use planning*. Beijing: Science Press.

Wang, J. F., and Xu, C. D. (2017). Geodetectors: Principles and prospects. *Acta Geogr. Sin.* 72, 19. doi:10.11821/dlxb201701010

Zhao, K. (2011). Land fragmentation and its quantitative measurement method. *China Land Sci.* 25, 15–31. doi:10.13708/j.cnki.cn11-2640.2011.10.005

# Analysis of spatio-temporal changes and driving forces of cultivated land in China from 1996 to 2019

Jianfeng Li[1,2,3], Jichang Han[1,2,3]*, Yang Zhang[1,2,3], Yingying Sun[1,2,3], Biao Peng[1,2,3], Xiao Xie[1,2,3], Chao Guo[1,2,3] and Huping Ye[4]

[1]Institute of Land Engineering and Technology, Shaanxi Provincial Land Engineering Construction Group Co., Ltd., Xi'an, China, [2]Technology Innovation Center for Land Engineering and Human Settlements, Shaanxi Land Engineering Construction Group Co., Ltd., Xi'an Jiaotong University, Xi'an, China, [3]Shaanxi Provincial Land Engineering Construction Group Co., Ltd., Xi'an, China, [4]State Key Laboratory of Resources and Environmental Information System, Institute of Geographic Sciences and Natural Resources Research, Chinese Academy of Sciences, Beijing, China

Cultivated land is an important prerequisite and guarantee for food production and security, and the change of cultivated land resources in China has always been concerned. National land survey is an effective way to accurately grasp the area and distribution of cultivated land resources. However, due to the differences in technical means and statistical standards at different stages, there are obvious breakpoints among the cultivated land area data of the three land surveys in China, which hinders the in-depth study of the spatio-temporal distribution of cultivated land resources in long-time series. The Autoregressive Integrated Moving Average model is used to reconstruct and mine the cultivated land area data from 1996 to 2019 based on the data of the third land survey in China. The spatio-temporal variation characteristics of cultivated land area are explored by using Geographic Information System spatial analysis, and the driving factors of cultivated land change are analyzed based on Geographical Detector (GeoDetector) from the perspective of social, economic, agricultural and natural. The results show that the area of cultivated land in China decreased continuously from 1996 to 2019, with a sharp decrease from 1996 to 2004 and a slow decrease from 2005 to 2019. From 1996 to 2019, there were obvious spatial differences in the change of cultivated land area in 31 provincial units. From 1996 to 2008, the cultivated land area in 29 provinces showed a downward trend, especially in the central and northern regions such as Shaanxi, Sichuan and Inner Mongolia. From 2008 to 2019, the cultivated land area in the underdeveloped areas of Heilongjiang, Jilin, Liaoning, Xinjiang, Gansu and Tibet increased significantly, while the rest showed a downward trend. Factor detection found that the q values of population, regional gross domestic product grain output, the proportion of the added value of the primary industry and average slope were all more than 0.5, which had an important impact on the change of cultivated land area. The explanatory power of the interaction between factors on the change of cultivated land area is enhanced in different degrees compared with the single factor effect, which is manifested in the enhancement of bilinear or nonlinear enhancement, and the interaction of

different factors promotes the change of cultivated land area. The change of cultivated land area is the result of complex interaction between factors, and is closely related to the land policy in the same period.

# Introduction

Cultivated land is an important prerequisite and guarantee for food production, and food security is an important part of national security (Liu et al., 2018; Wang et al., 2020; Yang et al., 2021). Cultivated land provides the main living guarantee for the rural population and is the main source of living materials for urban residents (Zou et al., 2020). China is a large agricultural country, and cultivated land is the main carrier to maintain population growth (Xu et al., 2021). However, China only has about 0.2 acres of cultivated land per citizen, accounting for less than 40% of cultivated land per citizen in the world (Cui and Shoemaker, 2018). With the development of social economy, the process of urbanization and industrialization in China is constantly advancing, the construction land is expanding rapidly, the cultivated land resources are constantly changing, and the protection of cultivated land is facing great challenges (Zhao et al., 2006; Kong, 2014; Wang et al., 2020). Therefore, much attention has been paid to the change of cultivated land resources in China (Anderson and Strutt, 2014; Liu et al., 2017; Tan et al., 2017). The change of cultivated land is the result of the comprehensive action of multiple factors, which is closely related to economic, social, ecological, political and other factors (Lin and Ho, 2003; Song et al., 2012; Cao Y. et al., 2013). Studying the spatio-temporal change law and influencing factors of cultivated land resources is conducive to comprehensively grasping the current situation of cultivated land use, revealing the driving mechanism of cultivated land change, and providing a scientific basis for rational use of land resources, policy formulation and trend prediction.

Since the 1990s, scholars have begun to study and discuss the changes of cultivated land resources from different perspectives (Deng et al., 2006; Ge et al., 2018; Ramankutty et al., 2018). Relevant research involves cultivated land change (Valbuena et al., 2010), influencing factor (Chen and Wang, 2021), influencing factor model and driving mechanism (He et al., 2005), *etc.* There are two main sources of cultivated land resources data: the data obtained by remote sensing image interpretation or model classification and the official land survey data. The rapid development of remote sensing technology provides long-time dynamic data for the study of cultivated land change. Currently, the widely used remote sensing land use datasets include Global Land Cover Characterization Database (GLCC) (Loveland et al., 2000)、 Global Land Cover 2000 project data (GLC 2000) (Bartholome and Belward, 2005)、University of Maryland

land cover product (UMd) (Hansen et al., 2000)、Global Land Cover Product (GlobCover) (Arino et al., 2007) and GlobeLand30 (Jun et al., 2014). Scholars have studied the spatio-temporal change of cultivated land in China by using remote sensing data (Liu et al., 2003; Xu et al., 2017; Wang et al., 2020). Xu et al. found that from 1990 to 2010, the net increase of cultivated land in China was $1.30 \times 10^6$ ha (Xu et al., 2017). The research results of Wang et al. show that from 1990 to 2000, the area of cultivated land increased by 1.62%, and then continuously decreased during 2000–2015, resulting in a national total growth rate of 0.80% from 1990 to 2015 (Wang et al., 2020). Due to the influence of the spatial-temporal resolution of remote sensing images, the phenomenon of different spectrum of the same object and the same spectrum of foreign objects, as well as the limitations of the algorithm, the accuracy of remote sensing classification in large-scale is generally not high, and there is still a certain gap with the accuracy of the official land survey data (Liu and Xia, 2010; Shao and Lunetta, 2012; Gómez-Chova et al., 2015; Cheng et al., 2020). Since 1996, China has completed three national land surveys. Based on the land survey data, the natural resources bureaus of each province will organize the land change survey every year, and the final summary will be released by the National Bureau of Statistics (NBS). In August 2021, the NBS of China released the data of the third national land survey, which is mainly based on remote sensing images or Unmanned Aerial Vehicle (UAV) images with a resolution better than 1m, combined with professional manual interpretation and field sampling verification to obtain high-precision land use data (Jiang et al., 2022). After statistical analysis, the difference between the cultivated land area of China in the commonly used remote sensing datasets and the data published in the third land survey is more than 10%. Therefore, the official land survey data can more accurately and truly reflect the status of cultivated land resources. However, there are obvious breakpoints in China's cultivated land area data in 2008 and 2018 due to differences in technical means and statistical standards adopted in different stages of the national land survey. Most scholars avoid the transition years with obvious changes in data, and focus on the changes of cultivated land area from 1996 to 2008 and 2009–2018 (Jin, 2014; Tan et al., 2017). At present, there are few studies on the spatio-temporal changes and driving forces of cultivated land area in the whole cycle of three land surveys. The ARIMA model does not depend on external variables and can effectively overcome the problem of insufficient model accuracy caused by external parameters.
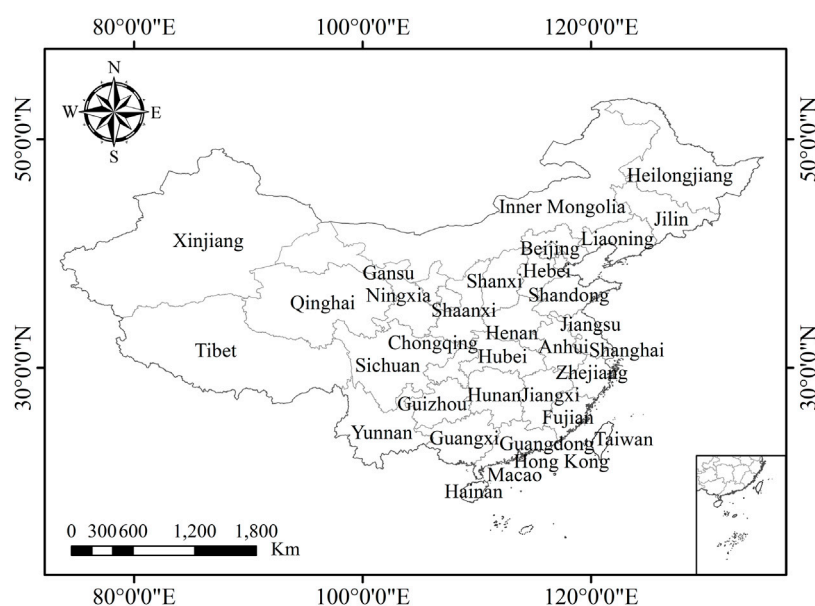
**FIGURE 1**
Location of study area.

The performance of the model has been better than that of the complex structure model in short-term prediction, and has been widely used in the prediction of crop yield, climate change, economic trend and so on (Fattah et al., 2018; Singh and Mohapatra, 2019; Zheng et al., 2020).

Based on the data of the third land survey in China, the ARIMA model is used in this study to reconstruct and mine the cultivated land area data from 1996 to 2019 in order to scientifically grasp the current situation of cultivated land use in different periods. The spatio-temporal change characteristics of cultivated land in China are studied by using GIS spatial analysis. The driving factors of cultivated land change are explored from the social, economic, agricultural and natural dimensions based on GeoDetector to provide scientific support for the intelligent management and precise protection of cultivated land.

## Materials and methods

### Study area

China (Figure 1) is located in eastern Asia, on the west coast of the Pacific Ocean. It starts from the center of the Heilongjiang River near Mohe River in the north and the Zengmu Reef in the Nansha Islands in the south. The land area is 9.6 million km², and the land boundary is more than 20,000 km (Wang et al., 2021). In this study, 31 provinces, cities and autonomous regions except

Taiwan Province, Hong Kong and Macao Special Administrative region were selected as the study area.

## Data

Comprehensively considering the development status of China and the availability of data, and referring to previous literature (Wang et al., 2015; Arowolo and Deng, 2018), 12 indicators related to the change of cultivated land area are selected: 1) social factors: population ($I_1$, unit: $\times10^4$ people); 2) Economic factors: regional GDP ($II_1$, unit: $\times10^8$ yuan), per capita GDP ($II_2$, unit: yuan/person), proportion of added value of primary industry ($II_3$, unit: %), proportion of added value of secondary industry ($II_4$, unit: %), proportion of added value of tertiary industry ($II_5$, unit: %), added value of agriculture, forestry, animal husbandry and fishery ($II_6$, unit: $\times10^8$ yuan); 3) Agricultural factors: grain output ($III_1$, unit: $\times10^4$ tons), total power of agricultural machinery ($III_2$, unit: $\times10^4$ kW); 4) Natural factors: average altitude ($IV_1$, unit: m), terrain relief ($IV_2$, unit: m); average slope ($IV_3$, unit: degrees). The cultivated land resources data come from the website of the Ministry of Natural Resources (http://www.mnr.gov.cn)), and the data related to population and socio-economic development come from the website of the NBS of China (http://www.stats.gov.cn). Table 1 shows the official statistics of China's cultivated land area from 1996 to 2019. Table 2 shows the descriptive statistical characteristics of social, economic and agricultural factors from 1996 to 2019.

TABLE 1 Official statistics of cultivated land area in China from 1996 to 2019.

| Year | Area/×104 hm2 | Year | Area/×104 hm2 | Year | Area/×104 hm2 |
|------|--------------|------|--------------|------|--------------|
| 1996 | 13,003.92 | 2004 | 12,244.43 | 2012 | 13,515.85 |
| 1997 | 12,990.31 | 2005 | 12,208.27 | 2013 | 13,516.34 |
| 1998 | 12,964.21 | 2006 | 12,177.59 | 2014 | 13,505.73 |
| 1999 | 12,920.55 | 2007 | 12,173.52 | 2015 | 13,499.87 |
| 2000 | 12,824.31 | 2008 | 12,177.68 | 2016 | 13,492.10 |
| 2001 | 12,761.58 | 2009 | 13,538.46 | 2017 | 13,488.12 |
| 2002 | 12,593.00 | 2010 | 13,526.83 | 2018 | 13,480.00 |
| 2003 | 12,339.22 | 2011 | 13,523.86 | 2019 | 12,786.19 |

TABLE 2 Descriptive statistical characteristics of social, economic and agricultural factors from 1996 to 2019.

| Factor | Minimum | Maximum | Mean | Standard deviation |
|--------|---------|---------|------|--------------------|
| $I_1$ (×104) | 122,389.00 | 141,212.00 | 132,752.64 | 5,748.05 |
| $II_1$ (×108 yuan) | 71,813.60 | 1,015,986.20 | 406,730.43 | 315,650.85 |
| $II_2$ (yuan/person) | 5,898.00 | 72,000.00 | 29,833.60 | 22,231.92 |
| $II_3$ (%) | 7.00 | 19.30 | 11.23 | 3.57 |
| $II_4$ (%) | 37.80 | 47.60 | 44.33 | 3.04 |
| $II_5$ (%) | 33.60 | 54.50 | 44.44 | 5.92 |
| $II_6$ (×108 yuan) | 14,014.70 | 81,103.90 | 37,792.23 | 22,005.20 |
| $III_1$ (×104 tons) | 43,069.53 | 66,949.15 | 55,420.84 | 8,156.62 |
| $III_2$ (×104 kW) | 38,546.92 | 111,728.07 | 78,943.96 | 23,853.29 |

TABLE 3 Judgment basis of the interaction detector.

| Comparison | Interaction |
|------------|-------------|
| $q(X_1 \cap X_2) < \mathrm{Min}[q(X_1), q(X_2)]$ | Nonlinear weakening |
| $\mathrm{Min}[q(X_1), q(X_2)] < q(X_1 \cap X_2) < \mathrm{Max}[q(X_1), q(X_2)]$ | Single factor nonlinear weakening |
| $q(X_1 \cap X_2) > \mathrm{Max}[q(X_1), q(X_2)]$ | Bilinear enhancement |
| $q(X_1 \cap X_2) = q(X_1) + q(X_2)$ | Independent |
| $q(X_1 \cap X_2) > q(X_1) + q(X_2)$ | Nonlinear enhancement |

Based on the 30-m resolution SRTM DEM data (http://gdex.cr. usgs.gov/gdex), the average elevation, terrain relief and average slope of each province are calculated by Google Earth Engine cloud computing platform (Gorelick et al., 2017).

## ARIMA model

ARIMA is a time series data analysis and prediction model proposed by Box and Jenkins (Gilbert, 2005). Its main principle is to establish a corresponding model to describe or simulate its past behavior from the time series itself, so as to predict and infer the future value. The model can combine the dynamic and persistent characteristics of time series to reveal the relationship between past and present, future and present of time series (Lai and Dzombak, 2020).

The ARIMA(p, d, q) model consists of three parts: AR(p) represents the autoregressive process, that is, the current value of a time series can be expressed as a linear combination of delayed p-period observations; I(d) represents the difference, d is the number of differences required when the time series becomes stationary; MA(q) represents the moving average process, that is,

**FIGURE 2**
Modeling process of ARIMA.
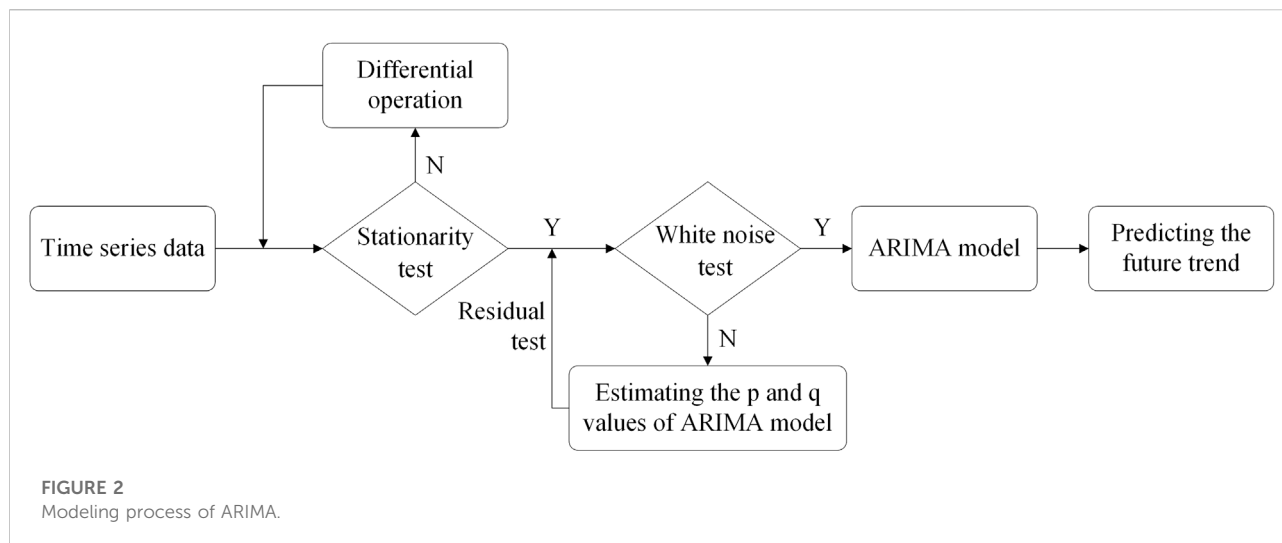
the model value can be expressed as a linear function of the q-order residual term. The expression of the model is as follows:

$$x_t = \phi_0 + \phi_1 x_{t-1} + \ldots + \phi_p x_{t-p} + \varepsilon_t - \theta_1 \varepsilon_{t-1} - \ldots$$
$$- \theta_q \varepsilon_{t-q}, \left( \phi_p \neq 0, \theta_q \neq 0 \right) \qquad (1)$$

Where, $x_t$ is the actual value, $\phi_i$ and $\theta_j$ are coefficients, $p$ is the order of the autoregressive model, $q$ is the moving average order, $\varepsilon_t$ represents the random error at $t$.

Figure 2 shows the modeling process of ARIMA model. Firstly, the stationarity of the time series data is tested. If it is a non-stationary time series, the d-order difference operation is required to convert it into a stationary time series. Then, white noise test is carried out on the data. If it is non-white noise, the best level p and order q are determined by autocorrelation function (ACF) and partial autocorrelation function (PACF) analysis. Finally, the white noise test is performed on the residual. Through the test, the modeling can be established to predict the future trend.

## GeoDetector

GeoDetector is a group of statistical methods to detect spatial differentiation and explain its driving force, including the factor detector, the interaction detector, the risk detector and the ecological detector (Wang et al., 2010). The main principle of the GeoDetector is to assume that the study is divided into several sub-regions. If the sum of the variance of the sub-region is less than the total variance of the region, there is a spatial difference; if the spatial distribution of the two variables tends to be consistent, there is a statistical correlation between the two variables. Geographic detector can evaluate spatial differentiation, detect explanatory factors and analyze the interaction between

variables, and have been widely used in nature, environmental science, human health and other fields (Wang et al., 2010; Cao F. et al., 2013; Liu et al., 2020).

The factor detector is used to detect the spatial differentiation of the dependent variable $Y$ and the explanatory power of a factor $X$ to the dependent variable $Y$, which is measured by the $q$ value. The formula of $q$ is:

$$q = 1 - \frac{\sum_{h=1}^{L} N_h \sigma_h^2}{N \sigma^2} = 1 - \frac{SSW}{SST} \ (h = 1, 2 \ldots) \qquad (2)$$

Where: $L$ is the stratification of variable $Y$ or factor $X$, i.e. classification or partition; $N_h$ and $N$ are the number of units in layer $h$ and the whole area respectively; $\sigma_h^2$ and $\sigma^2$ are the variances of the $Y$ values of the layer $h$ and the whole region respectively, and $SSW$ and $SST$ are the sum of the intra layer variance and the sum of the whole region variance respectively.

The interaction detector is used to evaluate the interaction between factors $X_i$ and $X_j$, reflecting that the explanatory power of the two factors on variable $Y$ is enhanced, weakened or independent. The interaction detector usually first calculates the interpretation force $q(X_1)$ and $q(X_2)$ of the two influence factors $X_i$ and $X_j$ on attribute $Y$, then calculates the value $q(X_1 \cap X_2)$ when they interact, and finally compares $q(X_1)$, $q(X_2)$ and $q(X_1 \cap X_2)$. There are five cases (Table 3).

## Results

### Reconstruction of cultivated land data based on ARIMA model

Figure 3A shows the change trend of cultivated land area in China according to official data. It can be seen from the figure

**FIGURE 3**
**(A)** is the change trend of the original cultivated land area. **(B)** is the change trend of cultivated land area after correction by ARIMA model.
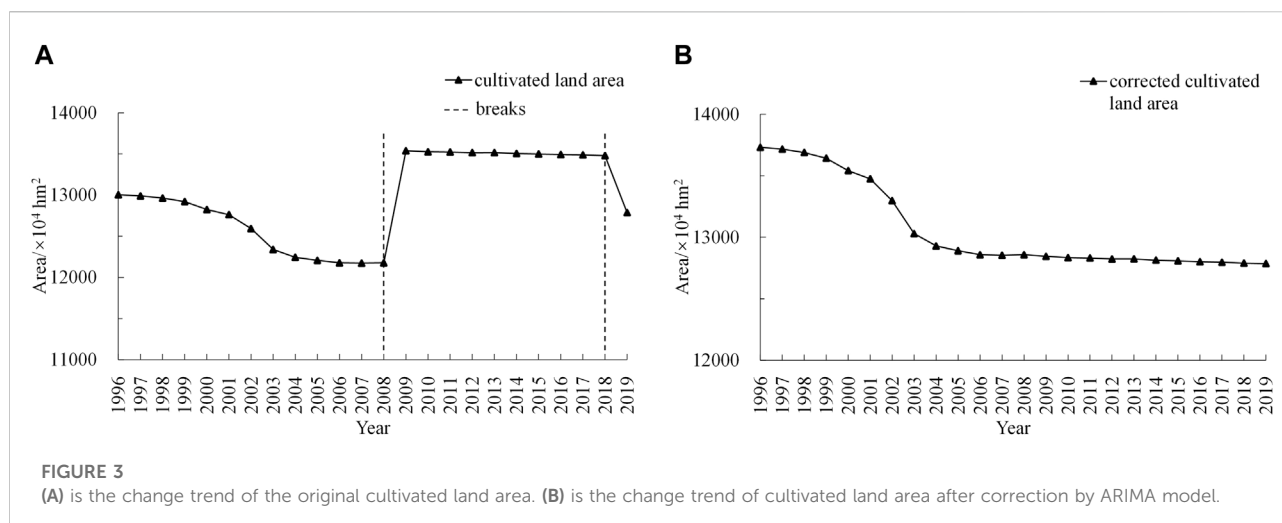
that there are obvious breakpoints in China's cultivated land area data in 2008 and 2018, which is mainly due to the differences in the technical means adopted in different stages of the national land survey. 2008 is the dividing point between the first national land survey and the second national land survey, and 2018 is the dividing point between the second national land survey and the third national land survey. The technical means adopted in the first survey are backward, rely on manual operation, and the result data are stored in paper form, which is not conducive to land change investigation. However, the second survey is completed based on 3S (GIS, RS, GPS) technology, which greatly improves the accuracy and efficiency of land survey, and replenishes the previously uncounted cultivated land area due to underreporting or omission. Therefore, there was a sharp increase in the area of cultivated land in 2009. Compared with the second survey, the third survey is based on satellite images or UAV images with a resolution better than 1m, combined with professional manual interpretation and machine learning, big data and cloud computing technology to further improve the accuracy of the data. The sharp decline in the area of cultivated land in 2019 is mainly due to the elimination of the false positives in the second survey. The two obvious breakpoints make the original cultivated land data lack of coherence and accuracy.

To study the dynamic characteristics of cultivated land area in China from 1996 to 2019, it is necessary to correct the data to improve the rationality and comparability. The cultivated land area data published in the third survey in 2019 were used as the basis for sectional correction based on the ARIMA model. Firstly, the 2009–2018 data were used to predict the 2019 data. After the augmented Dickey–Fuller (ADF) test, it is determined that the data remains stable after the second-order difference. The model was determined to be ARIMA (1,2,0) ($R^2 = 0.922$) after ACF and PACF analysis. The ratio of predicted data to actual data was determined to be 0.9488, and then the data from 2009 to 2018 were corrected. Secondly, the 1996–2008 data were used

to predict the 2009 data. After analysis, ARIMA (1, 2, 0) ($R^2 = 0.908$) was selected as the model, and the ratio between the predicted data and the corrected data was determined to be 1.0543, and then the data from 1996 to 2008 were corrected. Figure 3B shows the change trend of cultivated land area after correction. It can be seen from the figure that the corrected cultivated land data has stronger continuity and integrity, which is conducive to the dynamic analysis of long-time series.

## Characteristics of spatio-temporal variation of cultivated land area in long-time series

As can be seen from Figure 3B, China's cultivated land area showed a continuous decrease from 1996 to 2019. From 1996 to 2004, the cultivated land area showed a sharp decrease trend, with a total decrease of $8.01 \times 10^6$ hm$^2$ and a reduction rate of 5.84%. From 2005 to 2019, the cultivated land area decreased slowly by $8.50 \times 10^5$ hm$^2$, with a reduction rate of 0.66%.

To further analyze the spatial distribution differences of cultivated land from the perspective of provincial units, the ARIMA model was used to reconstruct the cultivated land data of 31 provinces, cities and autonomous regions. Figure 4 shows the amount and rate of change in cultivated land in China from 1996 to 2008 and 2008 to 2019. The change rate is the ratio of the difference between the cultivated land area at the end of the study and the initial stage of the study to the cultivated land area at the initial stage of the study. It can be seen from the figure that there are obvious spatial differences in the change of cultivated land area in 31 provincial units from 1996 to 2019. From 1996 to 2008, the cultivated land area of 29 provincial units showed a downward trend, accounting for more than 90%, especially in Shaanxi, Sichuan, Inner Mongolia and other central and northern regions, with a reduction of more than $1 \times 10^7$ hm$^2$, with a reduction rate of more than 10%. The change rate of

**FIGURE 4**
**(A)** and **(C)** are the amount of changes of cultivated land area in 1996−2008 and 2008−2019, respectively. **(B)** and **(D)** are the change rates of cultivated land area in 1996−2008 and 2008−2019, respectively.
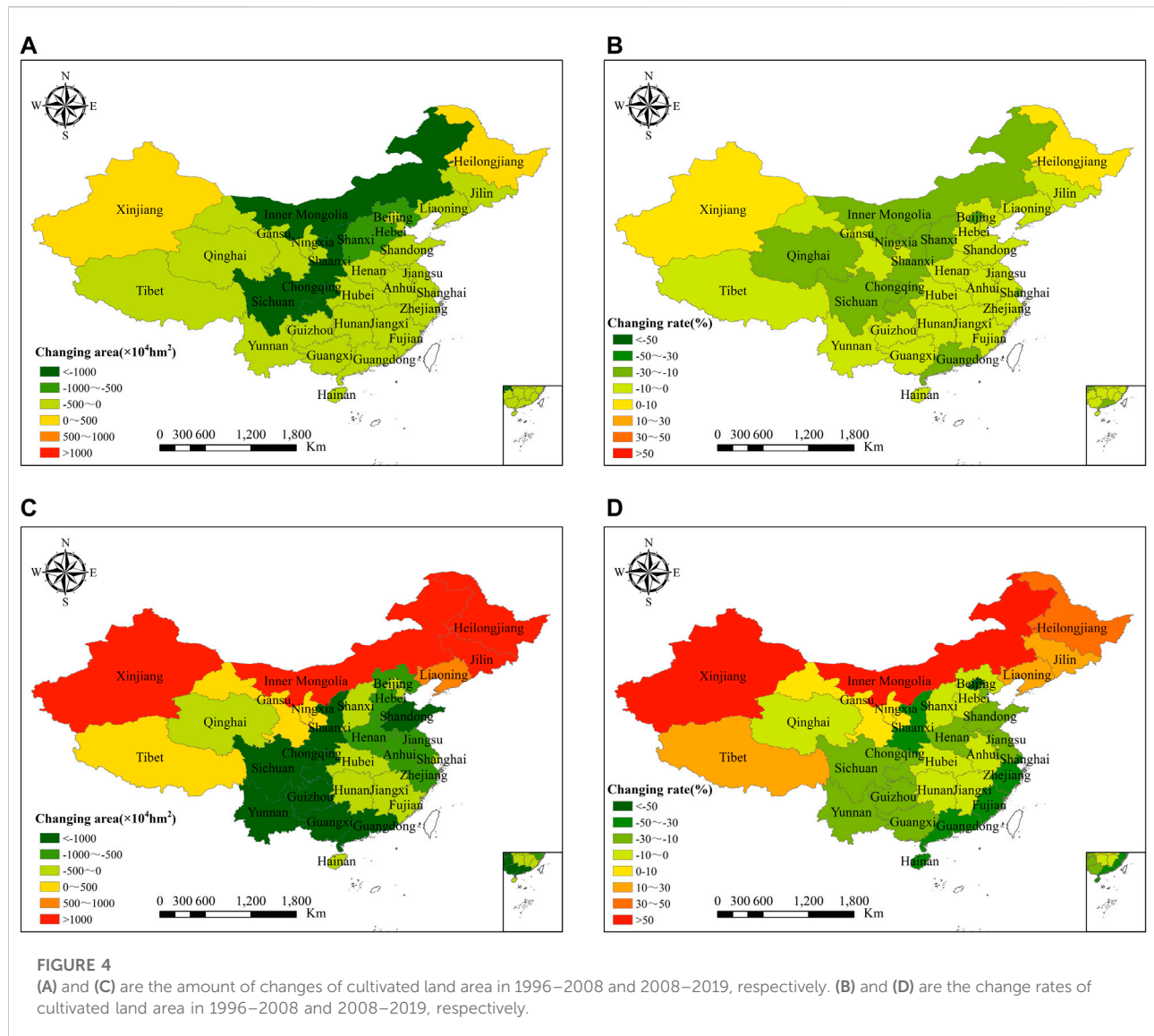
Beijing is the highest, reaching -33%, and the change rate in most areas is maintained at -10–0%. Only Heilongjiang and Xinjiang have seen a small increase in cultivated land area. It can be seen that the rapid progress of industrialization and urbanization has undoubtedly led to the occupation of a large amount of cultivated land. From 2008 to 2019, there are significant differences in cultivated land area changes in different regions. The cultivated land area in underdeveloped areas such as Heilongjiang, Jilin, Liaoning, Inner Mongolia, Xinjiang, Gansu and Tibet has increased significantly, especially in Xinjiang and Inner Mongolia, where the growth rate has exceeded 50%. The other regions showed a downward trend, and the decrease in central and southern provinces exceeded $1 \times 10^7$ hm². In developed regions such as Beijing, Shanghai, Guangdong and Zhejiang, the decline rate exceeded 30%. During this period, China began to implement the cultivated land occupation-compensation balance and cultivated land protection system.

Although the decline rate of cultivated land area slowed down compared with 1996–2008, some provinces still face a severe situation of cultivated land reduction.

## Driving force analysis of cultivated land area change

The factor detector results reflect the explanatory power of each factor on the change of cultivated land area in China, and the results are shown in Figure 5A According to the analysis, the order of explanatory power of each factor on the change of cultivated land area in China is as follows: population ($I_1$) > regional GDP ($II_1$) > grain output ($III_1$) > proportion of added value of the primary industry ($II_3$) > average slope ($IV_3$) > added value of agriculture, forestry, animal husbandry and fishery

**FIGURE 5**
**(A)** is the result of factor detector. **(B)** is the result of the interaction detector.
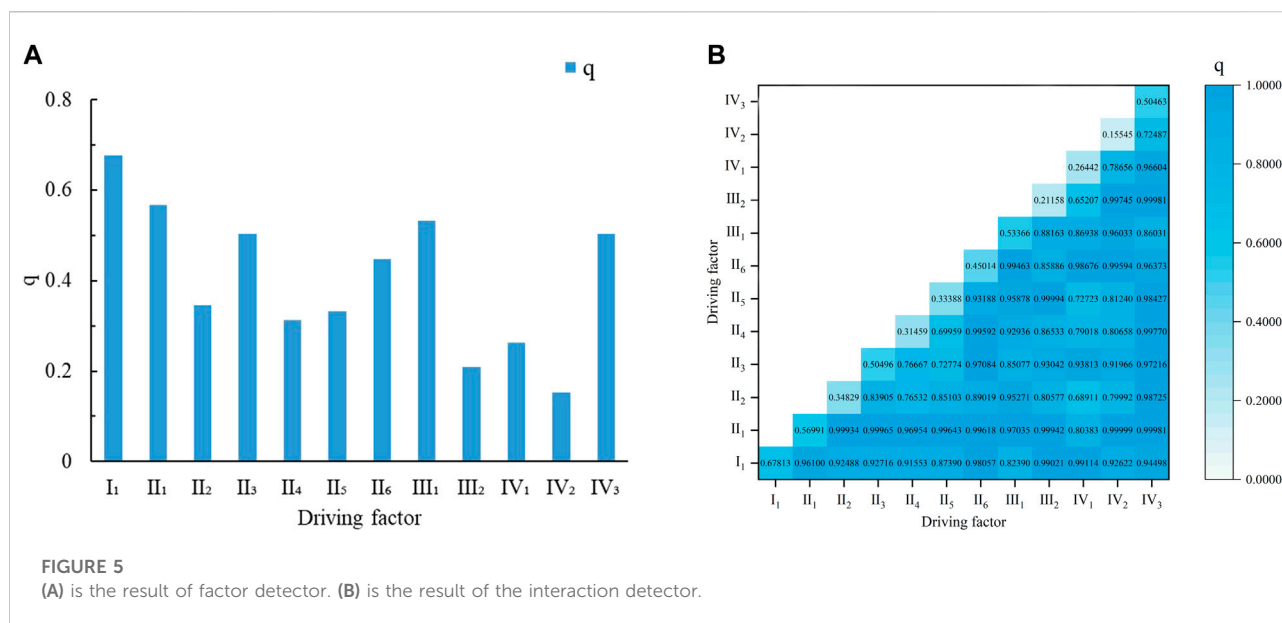
($II_6$) > per capita GDP ($II_2$) > proportion of added value of the tertiary industry ($II_5$) > proportion of added value of the secondary industry ($II_4$) > average altitude ($IV_1$) > total power of agricultural machinery ($III_2$) > terrain relief ($IV_2$). The q values of the five factors, namely population, regional GDP, grain output, the proportion of the added value of the primary industry and average slope, exceeded 0.5, which had an important impact on the change of cultivated land area. With the continuous increase of population and the rapid rise of urbanization rate in China since 1996, the demand for residential land, living land and other construction land has increased sharply, resulting in the pressure of cultivated land being occupied to a certain extent. The regional GDP reflects the level of economic development of the region, and the increase in demand for construction land brought about by economic development is an important reason for the non-agriculturalization of cultivated land. Cultivated land is the most basic material condition of agricultural production, and the change of its quantity and quality will directly affect the grain yield. The qualitative and quantitative changes in the process of economic development are both characterized by the evolution and advancement of the industrial structure, which are mainly manifested in the continuous decline of the proportion of the primary industry and the increase in the proportion of the secondary and tertiary industries. The primary industry generally includes agriculture, forestry, fishing, animal husbandry and gathering. When the economic development enters the industrialization stage, the dominant factors of land use change are the market supply and demand of land products or services and the comparative benefits of land use. The land flows to the more efficient secondary and tertiary industries, and the agricultural land is rapidly non-agricultural. Slope is an

important factor affecting the quality of cultivated land and the safety of cultivation. There is a positive correlation between slope and soil and water loss. With the increase of the slope, the runoff and scouring amount will increase accordingly. In order to control soil erosion and improve the ecological environment, China has implemented the conversion of cultivated land with large slopes to forests. Therefore, the slope has strong explanatory power to the change of cultivated land area.

The interaction detector can reflect the interaction between different types of factors, which is helpful to further study the driving mechanism of cultivated land area change. Figure 5B shows the results of the interaction detector. It can be seen from the figure that the interaction detecor results between factors are both bilinear enhancement or nonlinear enhancement, and there is no independence or weakening. The q value of interaction between different types of factors are significantly larger than that of single factor. The q values of most of the interactions between factors are more than 0.8, accounting for more than 84%. The interaction q value of the average altitude and the total power of agricultural machinery is the smallest, which is close to the maximum value of the single factor q value. The interaction between regional GDP and other factors has a strong explanatory power to the change of cultivated land area, with an average value of more than 0.97. The experimental results show that the explanatory power of the interaction between factors on the change of cultivated land area is enhanced to varying degrees compared with the single factor effect, and the interaction between different factors will have varying degrees of impact on the change of cultivated land area. At the same time, it confirms that the change of cultivated land area is the result of complex interaction between factors.
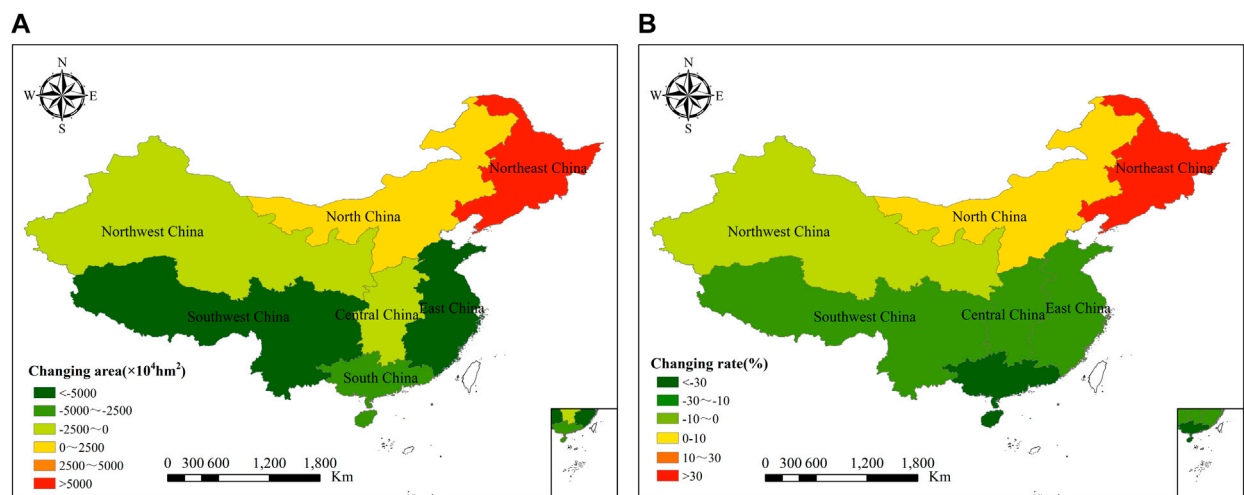
**FIGURE 6**
**(A)** is the amount of changes of cultivated land area in seven geographical regions of China from 1996 to 2019. **(B)** is the change rates of cultivated land area in seven geographical regions of China from 1996 to 2019.



**FIGURE 7**
**(A)** is the factor detector results of cultivated land area change in seven geographical regions of China. **(B)** is the interaction detector results of cultivated land area change in seven geographical regions of China.

## Discussion

### Analysis of driving forces in different geographical regions

China is generally divided into seven geographical regions: North China (Beijing, Tianjin, Hebei, Shanxi, Inner Mongolia), Northeast China (Liaoning, Jilin, Heilongjiang), East China (Shanghai, Jiangsu, Zhejiang, Anhui, Fujian, Jiangxi, Shandong),

South China (Guangdong, Guangxi, Hainan), Central China (Henan, Hubei, Hunan), Southwest China (Chongqing, Sichuan, Guizhou, Yunnan, Tibet) and Northwest China (Shaanxi, Gansu, Qinghai, Ningxia, Xinjiang) (He et al., 2008). Figure 6 shows the amount and rate of change in cultivated land in seven geographical regions of China from 1996 to 2019. As can be seen from the figure, the area of cultivated land decreased in all areas except Northeast and North China from 1996 to 2009. The area of cultivated land in East China and Southwest China decreased greatly, both exceeding

$5 \times 10^7$ hm². The decline rate of cultivated land area in South China is the largest, exceeding 30%. On the other hand, there has been a substantial increase in the Northeast China, with an increase rate of more than 30%.

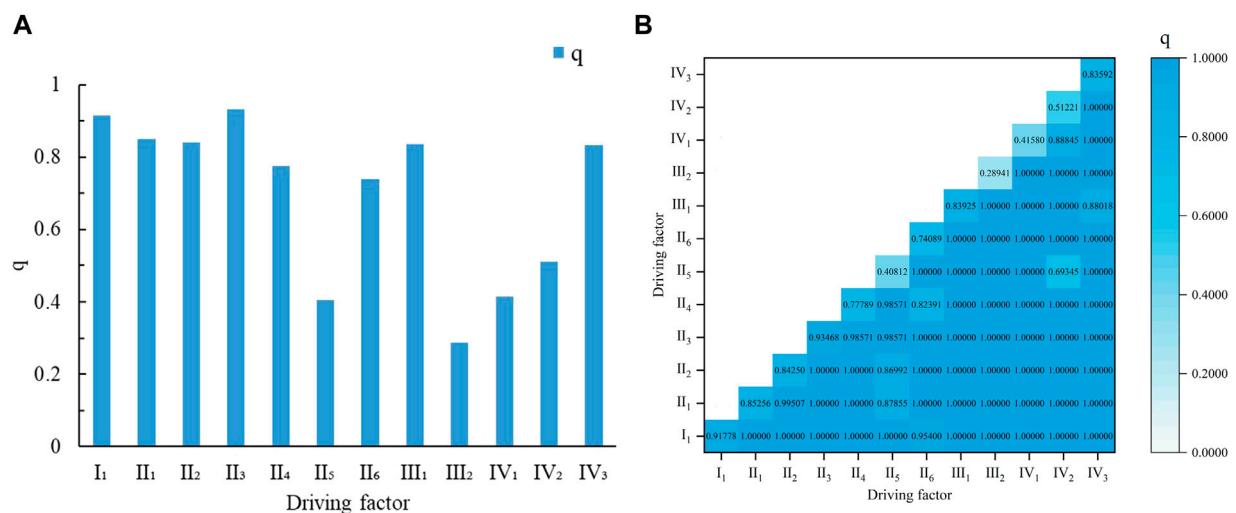Figure 7A shows the factor detector results of cultivated land area change in seven geographical regions of China. It can be seen from the figure that the order of the explanatory power of each factor on the change of cultivated land area in the seven geographical regions of China is: proportion of added value of the primary industry ($II_3$) > population ($I_1$) > regional GDP ($II_1$) > per capita GDP ($II_2$) > grain output ($III_1$) > average slope ($IV_3$) > proportion of added value of the secondary industry ($II_4$) > added value of agriculture, forestry, animal husbandry and fishery ($II_6$) > terrain relief ($IV_2$) > average altitude ($IV_1$) > proportion of added value of the tertiary industry ($II_5$) > total power of agricultural machinery ($III_2$). Except for terrain relief, average altitude, the proportion of added value of the tertiary industry and the total power of agricultural machinery, the q value of other factors exceeded 0.7, which have an important impact on the change of cultivated land area in seven geographical regions of China. The q value of the proportion of added value of the primary industry and the population are both more than 0.9, which has a strong explanatory power to the change of cultivated land area in the seven geographical areas. The q value of the total power of agricultural machinery is the lowest, only 0.289. The total power of agricultural machinery reflects the level of agricultural modernization. The progress of agricultural science and technology has improved the total power of agricultural machinery, promoted the increase of grain yield per unit area and the output rate of cultivated land, thus alleviating the pressure of cultivated land production and food security, but did not directly affect the change of cultivated land area.

Figure 7B shows the interaction detector results of cultivated land area change in seven geographical regions of China. It can be seen from the figure that the interaction detecor results between factors are both bilinear enhancement or nonlinear enhancement, and there is no independence or weakening, which is consistent with the results of provincial cultivated land area. The q values of most of the interactions between factors are 1, accounting for more than 85%. The interaction q value between the proportion of added value of the tertiary industry and the terrain relief is the smallest, which is 0.6935. The average q value of interactive detection of all factors is 0.9839. The results show that the interaction between different factors has a strong explanatory power for the change of cultivated land area in seven geographical regions of China.

## Policy factors of cultivated land area change

Land not only has natural attribute, but also has social-economic attribute (Verburg et al., 2015). For a long time, due to the influence of social, economic, policy and technical means, it is difficult to carry out long-time series analysis of cultivated land resource changes from the perspective of land survey statistics. The existing studies on cultivated land change based on land survey statistics are mainly concentrated in the two periods of 1996–2008 and 2009–2018 (Jin, 2014; Tan et al., 2017). However, there is an obvious gap in accuracy between large-scale cultivated land area data obtained by remote sensing data and land survey data (Manandhar et al., 2009; Liu et al., 2015). In this study, the ARIMA model is used to reconstruct and mine the cultivated land area data from 1996 to 2019, which eliminates the problem of time series data fracture caused by differences in technical means, and improves the rationality and integrity of the data. GIS spatial analysis is used to explore the spatio-temporal change characteristics of cultivated land area based on the corrected data, and the GeoDetector is used to analyze the driving mechanism of cultivated land change from the perspective of single factor and factor interaction. GeoDetector has obvious advantages in explaining the spatial heterogeneity of geographical phenomena, and can make up for the weakness that conventional methods cannot explain the interaction mechanism (Hu et al., 2020; Li et al., 2021; Xiang et al., 2021).

The cultivated land area is not only affected by social, economic, agricultural and natural factors, but also closely related to national policies in the same period (Wang et al., 2012; Wang et al., 2018). Since the 1990s, China has entered a stage of rapid urbanization and industrialization (Liu et al., 2010). Driven by the national macro policy, the demand for construction land increases sharply, which leads to the occupation of a large number of cultivated land resources. Since 1999, in order to control soil erosion and improve the ecological environment, China has implemented the policy of returning farmland to forests, grasslands and lakes, resulting in a further rapid reduction in the area of cultivated land (Bi et al., 2021). In 2004, the government revised the land management law, emphasizing the need to strengthen the protection of cultivated land and implement the balance policy of occupation and compensation, which has played a positive role in the change of cultivated land area (Liu et al., 2014). Under the condition that the balance between occupation and compensation has been strictly implemented for the cultivated land occupied by non-agricultural construction, the main reasons for the reduction of cultivated land area are the adjustment of agricultural structure and land greening. In 2008, China promoted rural reform, improved the strict and standardized rural land management system, and adhered to the strictest cultivated land protection system (Liu et al., 2017). In the new urbanization and Rural Revitalization stage after 2014, China implemented the strictest cultivated land protection system and intensive and economical land use system to optimize the land use structure and improve the land use efficiency (Liu et al., 2017). The implementation of these policies has effectively slowed down the decline of cultivated land.

At present, China is in the "three peaks" period of population, industrialization and urbanization. Social

development is faced with major problems, such as maintaining high-quality green economic development, ensuring ecological construction, protecting cultivated land resources and food security, and achieving the goal of carbon peak and carbon neutralization. At the same time, the international situation is complex and changeable, the epidemic situation of COVID-19 is intertwined with the war, and the food crisis in many countries has intensified. Therefore, the protection of cultivated land resources is facing unprecedented pressure. Looking forward to the future, the protection of cultivated land resources in China should turn to quantity, quality and ecology. On the basis of ensuring the red line of 0.3 billion acres of cultivated land, we should ensure the safety of China's cultivated land resources and food production by increasing land use control and balanced management of cultivated land, improving the incentive mechanism for cultivated land use, adjusting agricultural production methods, increasing investment in agricultural production, optimizing agricultural policies according to local conditions, changing land use patterns and reserving flexible cultivated land.

## Conclusion

Based on the data of three land surveys in China, this study deeply analyzes the reasons for the obvious fracture of cultivated land area data in 2008 and 2018, and uses ARIMA model to reconstruct the cultivated land area data from 1996 to 2019. Combined with GIS spatial analysis and GeoDetector, the spatio-temporal change characteristics and driving factors of cultivated land area are analyzed. The results show that the area of cultivated land in China decreased continuously from 1996 to 2019, with a sharp decrease from 1996 to 2004 and a slow decrease from 2005 to 2019. From 1996 to 2019, there were obvious spatial differences in the change of cultivated land area of 31 provincial units. From 1996 to 2008, the cultivated land area of 29 provincial units showed a downward trend, accounting for more than 90%, especially in the central and northern regions such as Shaanxi, Sichuan and Inner Mongolia. From 2008 to 2019, the cultivated land area in the underdeveloped areas of Heilongjiang, Jilin, Liaoning, Xinjiang, Gansu and Tibet increased significantly, while the rest showed a downward trend. The factor detector found that the q value of the five factors, namely population, regional GDP, grain output, the proportion of the added value of the primary industry and average slope, exceeded 0.5, which had an important impact on the change of cultivated land area. The explanatory power of the interaction between factors to the change of cultivated land area is enhanced in varying degrees compared with that of single factor, which is characterized by bilinear enhancement or nonlinear enhancement. The proportion of interaction q greater than 0.8 is more than 84%, and the interaction of various factors promotes the change of cultivated land area. It can be inferred from the results that the change of cultivated land area is the result of complex interaction between factors, and is closely related to the land policy in the same period.

## Data availability statement

The cultivated land resources data can be downloaded through the website of the Ministry of Natural Resources (http://www.mnr.gov.cn), and population and socio-economic development data can be downloaded free of charge through the website of the National Bureau of Statistics of China (http://www.stats.gov.cn).

## Author contributions

JL contributed by processing the data and wrote the main part of the manuscript. HY contributed to the research design, and gave constructive comments and suggestions. JH, YZ, YS and BP put forward detailed suggestions for the revision of the article, and assisted JL to complete all the experiments. XX and CG contributed to writing and collecting data.

## Funding

## Acknowledgments

## Conflict of interest

JL, JH, YZ, YS, BP, XX and CG are employed by Shaanxi Provincial Land Engineering Construction Group Co., Ltd.

The remaining authors declare that the research was conducted in the absence of any commercial or financial relationships that could be construed as a potential conflict of interest.

## Publisher's note

All claims expressed in this article are solely those of the authors and do not necessarily represent those of their affiliated organizations, or those of the publisher, the editors and the reviewers. Any product that may be evaluated in this article, or claim that may be made by its manufacturer, is not guaranteed or endorsed by the publisher.

## References

Anderson, K., and Strutt, A. (2014). Food security policy options for China: Lessons from other countries. *Food Policy* 49, 50–58. doi:10.1016/j.foodpol.2014.06.008

Arino, O., Gross, D., Ranera, F., Leroy, M., Bicheron, P., Brockman, C., et al. (2007). "GlobCover: ESA service for global land cover from MERIS," in 2007 IEEE international geoscience and remote sensing symposium, Spain, July 23-27, 2007, 2412–2415.

Arowolo, A. O., and Deng, X. (2018). Land use/land cover change and statistical modelling of cultivated land change drivers in Nigeria. *Reg. Environ. Change* 18 (1), 247–259. doi:10.1007/s10113-017-1186-5

Bartholome, E., and Belward, A. S. (2005). GLC2000: A new approach to global land cover mapping from earth observation data. *Int. J. Remote Sens.* 26 (9), 1959–1977. doi:10.1080/01431160412331291297

Bi, W., Wang, K., Weng, B., Yan, D., and Liu, S. (2021). Does the Returning Farmland to Forest Program improve the ecosystem stability of rhizosphere in winter in alpine regions? *Appl. Soil Ecol.* 165, 104011. doi:10.1016/j.apsoil.2021.104011

Cao, F., Ge, Y., and Wang, J.-F. (2013a). Optimal discretization for geographical detectors-based risk assessment. *GIScience Remote Sens.* 50 (1), 78–92. doi:10.1080/15481603.2013.778562

Cao, Y., Bai, Z., Zhou, W., and Wang, J. (2013b). Forces driving changes in cultivated land and management countermeasures in the three gorges reservoir area, China. *J. Mt. Sci.* 10 (01), 149–162. doi:10.1007/s11629-013-2240-5

Chen, L., and Wang, Q. (2021). Spatio-temporal evolution and influencing factors of land use in Tibetan region: 1995–2025. *Earth Sci. Inf.* 14 (4), 1821–1832. doi:10.1007/s12145-021-00627-0

Cheng, G., Xie, X., Han, J., Guo, L., and Xia, G.-S. (2020). Remote sensing image scene classification meets deep learning: Challenges, methods, benchmarks, and opportunities. *IEEE J. Sel. Top. Appl. Earth Obs. Remote Sens.* 13, 3735–3756. doi:10.1109/jstars.2020.3005403

Cui, K., and Shoemaker, S. P. (2018). *A look at food security in China*. Berlin, Germany: Nature Publishing Group.

Deng, X., Huang, J., Rozelle, S., and Uchida, E. (2006). Cultivated land conversion and potential agricultural productivity in China. *Land use policy* 23 (4), 372–384. doi:10.1016/j.landusepol.2005.07.003

Fattah, J., Ezzine, L., Aman, Z., El Moussami, H., and Lachhab, A. (2018). Forecasting of demand using ARIMA model. *Int. J. Eng. Bus. Manag.* 10. doi:10.1177/1847979018808673

Ge, D., Long, H., Zhang, Y., Ma, L., and Li, T. (2018). Farmland transition and its influences on grain production in China. *Land Use Policy* 70, 94–105. doi:10.1016/j.landusepol.2017.10.010

Gilbert, K. (2005). An ARIMA supply chain model. *Manag. Sci.* 51 (2), 305–310. doi:10.1287/mnsc.1040.0308

Gómez-Chova, L., Tuia, D., Moser, G., and Camps-Valls, G. (2015). Multimodal classification of remote sensing images: A review and future directions. *Proc. IEEE* 103 (9), 1560–1584. doi:10.1109/jproc.2015.2449668

Gorelick, N., Hancher, M., Dixon, M., Ilyushchenko, S., Thau, D., and Moore, R. (2017). Google earth engine: Planetary-scale geospatial analysis for everyone. *Remote Sens. Environ.* 202, 18–27. doi:10.1016/j.rse.2017.06.031

Hansen, M. C., DeFries, R. S., Townshend, J. R., and Sohlberg, R. (2000). Global land cover classification at 1 km spatial resolution using a classification tree approach. *Int. J. remote Sens.* 21 (6-7), 1331–1364. doi:10.1080/014311600210209

He, C., Li, J., Wang, Y., Shi, P., Chen, J., and Pan, Y. (2005). Understanding cultivated land dynamics and its driving forces in northern China during 1983-2001. *J. Geogr. Sci.* 15 (04), 387–395. doi:10.1360/gs050401

He, F., Ge, Q., Dai, J., and Rao, Y. (2008). Forest change of China in recent 300 years. *J. Geogr. Sci.* 18 (1), 59–72. doi:10.1007/s11442-008-0059-8

Hu, D., Meng, Q., Zhang, L., and Zhang, Y. (2020). Spatial quantitative analysis of the potential driving factors of land surface temperature in different "centers" of polycentric cities: A case study in Tianjin, China. *Sci. Total Environ.* 706, 135244. doi:10.1016/j.scitotenv.2019.135244

Jiang, Y., Tang, Y.-T., Long, H., and Deng, W. (2022). Land consolidation: A comparative research between europe and China. *Land Use Policy* 112, 105790. doi:10.1016/j.landusepol.2021.105790

Jin, T. (2014). Effects of cultivated land use on temporal-spatial variation of grain production in China. *J. Nat. Resour.* 29 (6), 911–919. doi:10.11849/zrzyxb.2014.06.001

Jun, C., Ban, Y., and Li, S. (2014). Open access to Earth land-cover map. *Nature* 514 (7523), 434. doi:10.1038/514434c

Kong, X. (2014). China must protect high-quality arable land. *Nature* 506 (7486), 7. doi:10.1038/506007a

Lai, Y., and Dzombak, D. A. (2020). Use of the autoregressive integrated moving average (ARIMA) model to forecast near-term regional temperature and precipitation. *Weather Forecast.* 35 (3), 959–976. doi:10.1175/waf-d-19-0158.1

Li, D., Yang, Y., Du, G., and Huang, S. (2021). Understanding the contradiction between rural poverty and rich cultivated land resources: A case study of Heilongjiang province in Northeast China. *Land Use Policy* 108, 105673. doi:10.1016/j.landusepol.2021.105673

Lin, G. C., and Ho, S. P. (2003). China's land resources and land-use change: Insights from the 1996 land survey. *Land Use Policy* 20 (20), 87–107. doi:10.1016/s0264-8377(03)00007-3

Liu, C., Li, W., Zhu, G., Zhou, H., Yan, H., and Xue, P. (2020). Land use/land cover changes and their driving factors in the northeastern Tibetan plateau based on geographical detectors and Google earth engine: A case study in gannan prefecture. *Remote Sens.* 12 (19), 3139. doi:10.3390/rs12193139

Liu, D., Gong, Q., and Yang, W. (2018). The evolution of farmland protection policy and optimization path from 1978 to 2018. *Chin. Rural. Econ.* 12, 37–51.

Liu, D., and Xia, F. (2010). Assessing object-based classification: Advantages and limitations. *Remote Sens. Lett.* 1 (4), 187–194. doi:10.1080/01431161003743173

Liu, J., Liu, M., Zhuang, D., Zhang, Z., and Deng, X. (2003). Study on spatial pattern of land-use change in China during 1995–2000. *Sci. China Ser. D Earth Sci.* 46 (4), 373–384.

Liu, T., Liu, H., and Qi, Y. (2015). Construction land expansion and cultivated land protection in urbanizing China: Insights from national land surveys, 1996–2006. *Habitat Int.* 46, 13–22. doi:10.1016/j.habitatint.2014.10.019

Liu, X., Zhao, C., and Song, W. (2017). Review of the evolution of cultivated land protection policies in the period following China's reform and liberalization. *Land Use Policy* 67, 660–669. doi:10.1016/j.landusepol.2017.07.012

Liu, Y., Fang, F., and Li, Y. (2014). Key issues of land use in China and implications for policy making. *Land Use Policy* 40, 6–12. doi:10.1016/j.landusepol.2013.03.013

Liu, Y., Liu, Y., Chen, Y., and Long, H. (2010). The process and driving forces of rural hollowing in China under rapid urbanization. *J. Geogr. Sci.* 20 (6), 876–888. doi:10.1007/s11442-010-0817-2

Loveland, T. R., Reed, B. C., Brown, J. F., Ohlen, D. O., Zhu, Z., Yang, L., et al. (2000). Development of a global land cover characteristics database and IGBP DISCover from 1 km AVHRR data. *Int. J. remote Sens.* 21 (6-7), 1303–1330. doi:10.1080/014311600210191

Manandhar, R., Odeh, I. O., and Ancev, T. (2009). Improving the accuracy of land use and land cover classification of Landsat data using post-classification enhancement. *Remote Sens.* 1 (3), 330–344. doi:10.3390/rs1030330

Ramankutty, N., Mehrabi, Z., Waha, K., Jarvis, L., Kremen, C., Herrero, M., et al. (2018). Trends in global agricultural land use: Implications for environmental health and food security. *Annu. Rev. Plant Biol.* 69, 789–815. doi:10.1146/annurev-arplant-042817-040256

Shao, Y., and Lunetta, R. S. (2012). Comparison of support vector machine, neural network, and CART algorithms for the land-cover classification using limited training data points. *ISPRS J. Photogrammetry Remote Sens.* 70, 78–87. doi:10.1016/j.isprsjprs.2012.04.001

Singh, S., and Mohapatra, A. (2019). Repeated wavelet transform based ARIMA model for very short-term wind speed forecasting. *Renew. Energy* 136, 758–768. doi:10.1016/j.renene.2019.01.031

Song, X., Ouyang, Z., Li, Y., and Li, F. (2012). Cultivated land use change in China, 1999–2007: Policy development perspectives. *J. Geogr. Sci.* 22 (06), 1061–1078. doi:10.1007/s11442-012-0983-5

Tan, Y., He, J., Yue, W., Zhang, L., and Wang, Q. (2017). Spatial pattern change of the cultivated land before and after the second national land survey in China. *J. Nat. Resour.* 32 (02), 186–197. doi:10.11849/zrzyxb.20160263

Valbuena, D., Verburg, P. H., Bregt, A. K., and Ligtenberg, A. (2010). An agent-based approach to model land-use change at a regional scale. *Landsc. Ecol.* 25 (2), 185–199. doi:10.1007/s10980-009-9380-6

Verburg, P. H., Crossman, N., Ellis, E. C., Heinimann, A., Hostert, P., Mertz, O., et al. (2015). Land system science and sustainable development of the Earth system: A global land project perspective. *Anthropocene* 12, 29–41. doi:10.1016/j.ancene.2015.09.004

Wang, G., Liu, Y., Li, Y., and Chen, Y. (2015). Dynamic trends and driving forces of land use intensification of cultivated land in China. *J. Geogr. Sci.* 25 (1), 45–57. doi:10.1007/s11442-015-1152-4

Wang, J., Chen, Y., Shao, X., Zhang, Y., and Cao, Y. (2012). Land-use changes and policy dimension driving forces in China: Present, trend and future. *Land use policy* 29 (4), 737–749. doi:10.1016/j.landusepol.2011.11.010

Wang, J. F., Li, X. H., Christakos, G., Liao, Y. L., Zhang, T., Gu, X., et al. (2010). Geographical detectors-based health risk assessment and its application in the neural tube defects study of the Heshun Region, China. *Int. J. Geogr. Inf. Sci.* 24 (1), 107–127. doi:10.1080/13658810802443457

Wang, J., Lin, Y., Glendinning, A., and Xu, Y. (2018). Land-use changes and land policies evolution in China's urbanization processes. *Land use policy* 75, 375–387. doi:10.1016/j.landusepol.2018.04.011

Wang, S., Xu, L., Zhuang, Q., and He, N. (2021). Investigating the spatio-temporal variability of soil organic carbon stocks in different ecosystems of China. *Sci. Total Environ.* 758, 143644. doi:10.1016/j.scitotenv.2020.143644

Wang, X., Xin, L., Tan, M., Li, X., and Wang, J. (2020). Impact of spatiotemporal change of cultivated land on food-water relations in China during 1990–2015. *Sci. Total Environ.* 716, 137119. doi:10.1016/j.scitotenv.2020.137119

Xiang, Y., Huang, C., Huang, X., Zhou, Z., and Wang, X. (2021). Seasonal variations of the dominant factors for spatial heterogeneity and time inconsistency of land surface temperature in an urban agglomeration of central China. *Sustain. Cities Soc.* 75, 103285. doi:10.1016/j.scs.2021.103285

Xu, W., Jin, X., Liu, J., and Zhou, Y. (2021). Analysis of influencing factors of cultivated land fragmentation based on hierarchical linear model: A case study of Jiangsu province, China. *Land Use Policy* 101, 105119. doi:10.1016/j.landusepol.2020.105119

Xu, X., Wang, L., Cai, H., Wang, L., Liu, L., and Wang, H. (2017). The influences of spatiotemporal change of cultivated land on food crop production potential in China. *Food Secur.* 9 (3), 485–495. doi:10.1007/s12571-017-0683-1

Yang, Z., Xunhuan, L., and Yansui, L. (2021). Cultivated land protection and rational use in China. *Land Use Policy* 106, 105454. doi:10.1016/j.landusepol.2021.105454

Zheng, A., Fang, Q., Zhu, Y., Jiang, C., Jin, F., and Wang, X. (2020). An application of ARIMA model for predicting total health expenditure in China from 1978–2022. *J. Glob. Health* 10 (1). doi:10.7189/jogh.10.010803

Zhao, Q., Zhou, S., Wu, S., and Ren, K. (2006). Cultivated land resources and strategies for its sustainable utilization and protection in China. *Acta Pedol. Sin.* 43 (04), 662–672. doi:10.11766/200511020420

Zou, L., Liu, Y., Yang, J., Yang, S., Wang, Y., Hu, X., et al. (2020). Quantitative identification and spatial analysis of land use ecological-production-living functions in rural areas on China's southeast coast. *Habitat Int.* 100, 102182. doi:10.1016/j.habitatint.2020.102182

# The impact of agricultural machinery services on cultivated land productivity and its mechanisms: A case study of Handan city in the North China plain

Yan Liu, Xiaoping Shi and Fugang Gao*

China Academy of Resources, Environment and Development & College of Public Administration, Nanjing Agricultural University, Nanjing, China

Studying the impact of agricultural machinery services (AMS) on cultivated land productivity is conducive to scientifically improving agricultural production and has far-reaching significance for ensuring food security. Taking Handan City in the North China Plain as the research context and using a surveyed sample of 1918 farming households, this paper examines the effect of AMS on the productivity of cultivated land using OLS estimation and estimates the average treatment effect on the treated (ATT) using the propensity score matching (PSM) method. The research findings are as follows. 1) AMS has a significantly positive impact on cultivated land productivity, and a heterogeneity analysis finds that the effects are larger for farmers with relatively less cultivated land and the marginal effects decrease as the adoption of AMS increases. 2) In various planting activities, AMS adoption in basic activities (e.g., ploughing, seeding, and harvesting) has positive effects on cultivated land productivity, while AMS adoption in management activities (e.g., fertilizing, irrigation, and pesticide spraying), has no obvious effect on cultivated land productivity. 3) According to the results of ATT, the conversion of non-adopting farmers to adopting AMS would increase cultivated land productivity by 7.6%−12.1%. 4) A mechanism analysis reveals that AMS adoption relieves financial constraints, improves technical efficiency, and increases smallholders' crop yields. These results suggest that AMS has a positive effect on cultivated land productivity and therefore have valuable policy implications for increasing smallholders' access to various types of AMS to improve the productivity of cultivated land in regions dominated by smallholders.

KEYWORDS

agricultural machinery services, cultivated land productivity, smallholders, mechanism identification, the North China plain

# 1 Introduction

Cultivated land productivity is an important indicator for facilitating agricultural production, ensuring food security, and alleviating poverty as well as improving the welfare of farmers (Desiere and Jolliffe 2018; Khan et al., 2019; Zhou and Ma, 2022). In developing countries that have undergone the green revolution and structural transformation (such as China, Thailand, and Myanmar), the rural population has been attracted by increasing wage rates in the urban sector (Belton et al., 2021). A trend towards a gradual shortage of agricultural labor has emerged. Mechanization is an effective labor-saving method, although smallholders have only a limited capacity to acquire and apply machinery as it carries a heavy financial burden and their farms are both small in scale and fragmented (Benin 2015; Adekunle et al., 2016; Qiao 2020; Wang et al., 2020; Mahasuweerachai and Suksawat 2022). In this context, increasing the availability of agricultural machinery may contribute to the viability of smallholder farming and therefore boost cultivated land productivity (Rigg et al., 2016; Takeshima, 2017; Zhang et al., 2017).

China, with 232.1 million farms occupying less than 10 mu (0.67 ha) of cultivated land, has experienced rapid agricultural mechanization during the last few decades (Yu and Zhao, 2009). This trend toward mechanization has relied on the growth of agricultural machinery services (AMS) (Yang et al., 2013; Wang et al., 2020; Qiu et al., 2021; Liu et al., 2022). Some of smallholders' planting activities can be undertaken by mechanized service providers on a much larger scale. For example, Zhang et al. (2017) described harvesting services, a typical AMS offering that utilizes the time lag between regional crop harvesting in China, which can last up to 8 months per year. By tapping into the national machinery services market, AMS may be able to overcome the constraints facing mechanization stemming from the small scale of farms and the fragmentation of cultivated land. This dynamic is not unique to China. Similar services have existed, for example, in Myanmar, Bangladesh, and Thailand in Southeast Asia (Mottaleb et al., 2017; Chaya et al., 2019; Belton et al., 2021), and in Ghana and South Africa in Africa (Benin, 2015; Emmanuel et al., 2016; Lyne et al., 2018).

The contemporary context of AMS gives rise to two major themes in the mechanization literature. First, the role of AMS in enhancing machine availability for smallholders and the determinants of AMS adoption (Yang et al., 2013; Lyne et al., 2018; Justice and Biggs 2020; Belton et al., 2021). Second, the impact of AMS on overcoming the shortage of family labor in agricultural production (Zhang et al., 2017), reducing the cost of agricultural production (Tang et al., 2018), and increasing crop income and household welfare (Wang et al., 2016; Mi et al., 2020). AMS adoption is also associated with the farm size adjustment and off-farm employment decisions of rural households (Ji et al., 2012; Qiu et al., 2021; Qian et al., 2022). Considering the effects of AMS on agricultural inputs and

outputs, it follows that it may also affect cultivated land productivity. To date, although the potential impact of AMS adoption on cultivated land productivity has been mentioned in some studies (e.g., Justice S and Biggs S; Qiu et al., 2022), few studies examined how AMS may affect cultivated land productivity.

The objective of this paper is therefore to understand whether AMS improves cultivated land productivity and to examine its potential impact mechanisms, which have broader implications for farmers' welfare and national food security. The results of this study will help to reveal the impacts and obstacles to increasing cultivated land productivity in the presence of AMS. China is a new frontier for AMS research and the results may be of general relevance to other developing countries where AMS has emerged and agricultural systems are dominated by smallholders. The North China Plain is used as the research context in this paper considering that it is dominated by smallholders and its plain terrain is suitable for mechanization. In fact, AMS has been developed for decades in this area. This paper estimates the impact of AMS adoption on agricultural production in general and in different planting activities (e.g., ploughing, seeding, fertilizing, pesticide spraying, irrigation, and harvesting) in particular on arable land productivity, and estimates the average treatment effect on the treated (ATT). We collected our data through face-to-face interviews. The potential mechanisms of the impact of AMS on cultivated land productivity, such as the inputs of labor, capital, and technology, are further examined.

Our study extends the findings of previous studies and contributes to the literature on several fronts. First, our research focuses on the effect of AMS on cultivated land productivity at the micro-level by taking smallholders as the research sample. Despite evidence that mechanization affects cultivated land productivity (e.g., Ito, 2010; Zhou and Ma, 2022), the potential effects of AMS have been neglected in the existing literature. The adoption of AMS, as a market service purchase decision, represents neither an agricultural investment nor the acquisition of a household asset, but may allow smallholders to access mechanization that may have previously been held out of reach by financial constraints or small farm size. In addition, this paper provides implications for ensuring food security and promoting agricultural production, both of which remain serious challenges in many developing counties.

Second, this paper provides insights into AMS, including its adoption rate in general as well as that in various planting activities. Basic services include ploughing, seeding, and harvesting, and management services include fertilizing, spraying, and irrigation. As such, we follow the existing studies in measuring the overall adoption of AMS and adopt other, more detailed measures based on this. Meanwhile, this paper analyzes the heterogeneous impact of different types of AMS and estimates the ATT, which can provide a more targeted reference for policy-makers.
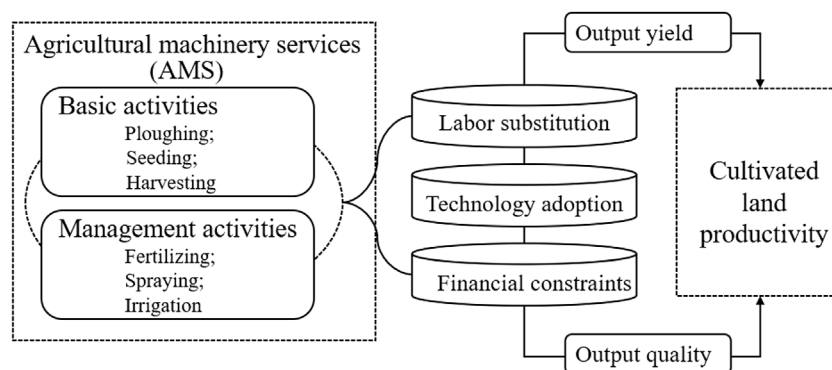
**FIGURE 1**
Conceptual framework of the impact of AMS on cultivated land productivity.

Finally, this study develops a conceptual framework for understanding the underlying mechanisms between AMS adoption and cultivated land productivity that includes factors such as agricultural labor substitution, financial constraints, technological improvements, and output quality and quantity enhancement and empirically tests these mechanisms. This extends upon the existing research and provides more detailed information with which to explain the pathways of the effects of AMS on agricultural production.

The rest of this paper proceeds as follows. Section 2 illustrates the conceptual framework. Section 3 introduces the data sources and describes the identification strategy. The results are presented and analyzed in Section 4. Section 5 concludes and suggests policy implications.

## 2 Conceptual framework

The essential elements of farming are land, labor, capital, and technology. For developing countries, the contributions of AMS are mainly reflected by its capacity to relieve the input constraints of agricultural labor, capital, and technology (Yang et al., 2013; Benin, 2015; Tang et al., 2018). In this study, we analyze the effect of AMS on cultivated land productivity through these mechanisms. Figure 1 depicts a simplified framework of potential mechanisms and illustrates how AMS adoption affects cultivated land productivity.

The first mechanism highlights the impact of AMS on cultivated land productivity by alleviating the constraints caused by agricultural labor shortages. The rising wage rate and the wage gap between rural and urban sectors have attracted increasingly rural labor migration, which has resulted in the agricultural labor pool shrinking and aging over time (Ji et al., 2012; Yamauchi, 2016; Min et al., 2017; Yu et al., 2021). Input constraints on the quantity and quality of agricultural labor may lead to extensive farming

operations and lagging technology adoption, and ultimately reduce cultivated land productivity. AMS, as an available source of mechanization for smallholders, can reduce labor drudgery and alleviate agricultural labor shortages at a relatively lower cost than hired labor and/or purchased machinery (Tang et al., 2018; Daum and Birner, 2020; Qiao, 2020). As such, the adoption of AMS can reduce or compensate for the loss of cultivated land productivity due to agricultural labor shortages.

The second mechanism focuses on the impact of AMS on the application of agricultural technology. The adoption of specialized agricultural techniques, such as deep soil ploughing, straw returning, and soil formula fertilization, often requires specific types of machinery (Shikuku, 2019; Zhou et al., 2020; Yu et al., 2021). Smallholders are constrained by factors such as access to information and capital as well as the limited size of cultivated land, and their adoption of new technologies is often slow and/or limited as a result (Tan et al., 2006; Zhang et al., 2017). AMS provides mechanized operations and acts as a transmitter of agricultural technology (Mi et al., 2020; Yu et al., 2021). As such, AMS may lead to technological improvement *via* the substitution of agricultural labor by mechanization as well as through the use of specialized machinery. In this way, AMS can facilitate the adoption of agricultural technologies and improve the technical efficiency of smallholders and thus potentially increase cultivated land productivity (Pfeiffer et al., 2009; Kousar and Abdulai, 2016).

The third mechanism refers to the effect of AMS on financial constraints in agriculture. Various types of AMS can relieve the financial burden of purchasing machinery. Most agricultural machines have strong asset specificity; that is, they cannot easily be adapted for other purposes. Purchasing multiple complex and specified agricultural machines would require smallholders to assume a prohibitively heavy financial burden (Yu et al., 2021). Moreover, the mechanisms for labor-saving and adopting new

technologies can separately reduce the cost per unit of cultivated land or the unit output yield. Therefore, the adoption of AMS may relieve smallholders' financial constraints and allow them to secure the capital inputs needed to increase their cultivated land productivity (Ma and Abdulai, 2016).

In light of the aforementioned mechanisms, AMS adoption may allow smallholders to secure essential inputs for agricultural production, reduce financial constraints and productivity loss due to agricultural labor shortages, and increase productivity through technology improvements. These effects manifest in terms of increased crop yield and/or quality. For example, the adoption of deep soil ploughing as a soil improvement measure may contribute to improving yield and/or output quality and thus improve cultivated land productivity (Pfeiffer et al., 2009; Kousar and Abdulai 2016). We therefore hypothesize that the adoption of AMS can increase cultivated land productivity.

Due to the unique characteristics of each planting activity, AMS adoption may have different effects in different activities. For example, a mechanized harvesting service allows farmers to reduce labor inputs as well as relieve financial constraints as they are not required to purchase the harvester. However, sprayers are relatively cheaper than harvesters, and AMS for pesticide spraying mainly substitutes labor rather than financial input. We divide planting activities into basic activities and crop management activities based on their characteristics. The former includes ploughing, seeding, and harvesting, all of which are essential and the mechanization of which relies on relatively expensive large machinery such as tractors and harvesters. The latter concerns fertilizing, spraying, and irrigation. Farmers may engage in these activities a variable number of times during planting, and their mechanization is largely based on the use of small machinery. As an example, the frequency of pesticide spraying depends on seasonal pest conditions, and the required sprayer is relatively inexpensive. In terms of the intensity of the labor input required for the different planting activities, basic activities often require intense physical input, while management can be done by older workers who are relatively less physically capable.

Considering the differential impact of AMS adoption in basic and management activities on capital constraints and labor input intensity, it follows that smallholder that predominantly use family labor are more likely to adopt AMS in basic activities and thus be more affected by it overall. Therefore, we hypothesize that AMS adoption in basic activities has a larger impact on cultivated land productivity than AMS adoption in management activities.

# 3 Materials and methods

## 3.1 Data source

The data used in this study were obtained from a rural household survey conducted in the North China Plain. This survey was conducted in February 2018 through face-to-face interviews in collaboration with Nanjing Agricultural University and China Agricultural University. With the assistance of computer-assisted personal interviewing techniques, we used an open-source software, ODK, to design the questionnaire and collect rich data (such as photos, GPS location and agricultural production data). It provides detailed information on the input and output of agricultural production in 2017 as well as the basic characteristics of rural households and villages.

Handan city, a prefecture-level city in Hebei Province, is set as a case study area in the North China Plain. The topography in Handan city is diverse, the west of which is the mountain and the hill (46%), while the east is the plain (54%). We selected four adjacent counties in the northeast, including Feixiang, Jize, Qiu, and Quzhou. The locations are shown in Figure 2. These four counties share some key characteristics which could help focus on our key research questions. First, they are all plain topography and are dominated by smallholders. Second, the majority of farmers grow double-season crops that consist of winter wheat and summer maize. Third, AMS has been developed for a few decades. (Liu et al., 2022). Moreover, these four counties differ in distance from Handan city center and then imply the variance in off-farm employment and AMS, which is necessary for the empirical identification. Therefore, the study area is representative of the North China Plain, which not only reduces the concerns about inconsistent results caused by agricultural production conditions, but also provides the necessary variation in key explanatory variables.

A multi-stage random sampling method was used in these four adjacent counties. Most townships in these four counties were selected as surveyed regions[1], and the townships were divided into three groups according to the number of villages in the township (i.e., 1–10, 11–20, and >20 villages). From each of these three groups, two, four, or six villages were randomly selected. In each of the selected villages, 16 households were randomly selected from a list of household heads. In total, 2080 households were randomly chosen from 130 villages. We used a sample of 1918 of those households that engaged in farming. The majority of the farmers in this area grow double crops, including winter wheat and summer maize. The composition of the sample is shown in Supplementary Appendix.

## 3.2 Variable definitions and descriptive analysis

The dependent variable for cultivated land productivity is measured as output per unit of cultivated land area. This is consistent with many existing studies (e.g., Martey et al., 2019; Zhou and Ma., 2022). In our study area, farmers usually grow more than one crop. To ensure consistent estimates of cultivated land productivity among the sampled households, we took the logarithm of the total value of maize and wheat per mu (15 mu = 1 ha).

**FIGURE 2**
Geographical location of the study area.
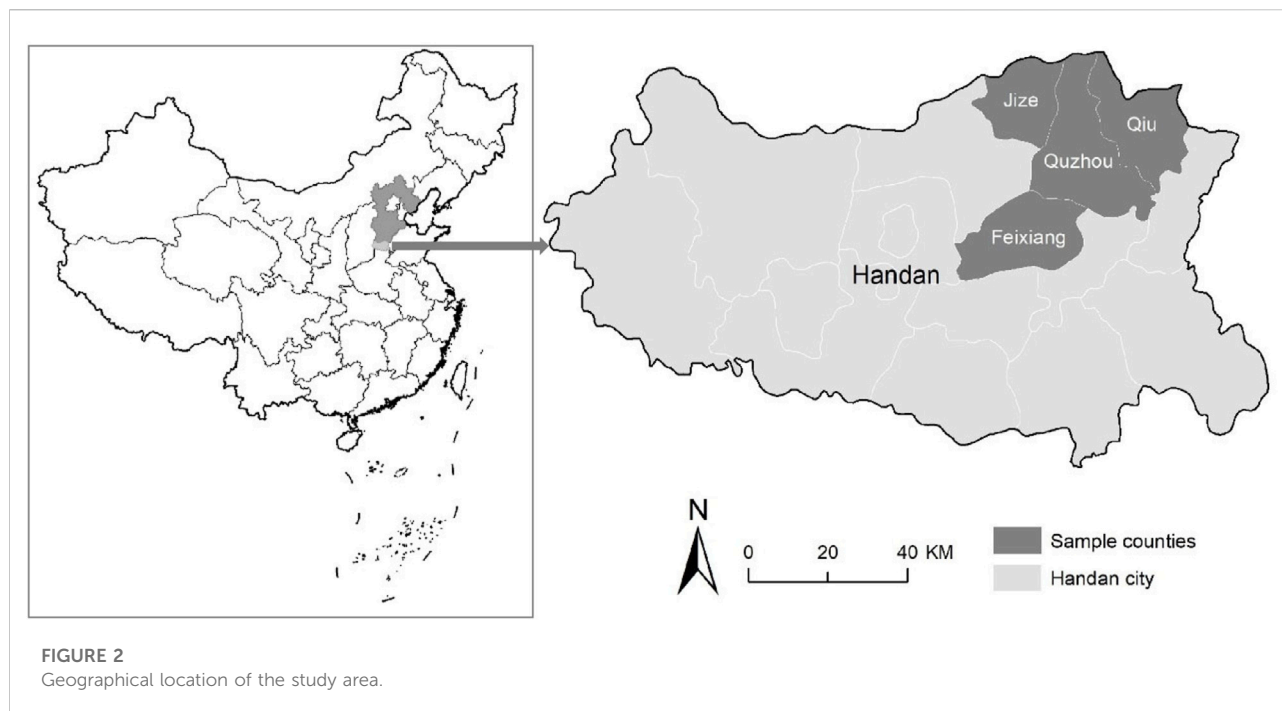
In this study, the treatment variable refers to farmers' AMS adoption status. The treatment and non-treatment groups are classified as adopters and non-adopters based on their adoption of AMS. This is consistent with many studies that have focused on the impact of AMS on farm size adjustment, agricultural income, and the welfare of rural households (e.g., Chaya et al., 2019; Mi et al., 2020; Qian et al., 2022). Crop cultivation encompasses a variety of activities, such as ploughing, seeding, fertilizing, spraying, irrigation, and harvesting, which, in the study area, may require mechanization in the cultivation of wheat and maize. Thus, to identify the different effects of AMS in various planting activities, the treatment groups can be divided according to AMS adoption in general as well as that in each planting activity.

As described in Chapter 2, we divide planting activities into basic activities and crop management activities based on the characteristics of each. The overall proportion of AMS adoption in basic activities is relatively high (i.e., 86.9%–92.5%; see Table 1) and has been largely mechanized, while the average proportion of AMS adoption in crop management activities, which are generally performed manually or through the use of owned machines, is relatively low and ranges from 1.1% to 13.7% (also see Table 1). The obvious difference in the adoption rate between basic and management activities is consistent with the theoretical analysis in Section 2. As such, this study seeks to examine the impact of AMS adoption on cultivated land productivity, including overall adoption, adoption in different types of services, and adoption in each planting activity.

Drawing upon the work of Takeshima (2017), Baiyegunhi et al. (2019), Amoozad-Khalili et al. (2020), Zhou and Ma (2022), this study adds control variables in three categories that describe the characteristics of the household head, family, and village. The variables in the household head category include age, gender, education (in years), participation in agricultural training, off-farm experience, and membership in village cadres. Family-level variables include household size, contract land area, the net change in cultivated land area through land rental, main soil type of cultivated land, number of tractors owned, and the availability of loans. The variables in the village category include distance to the nearest township, the total number of households, and the total area of arable land. Detailed definitions and descriptive statistics for the above variables are presented in Table 1. To detect the collinearity, we tested for the degree of multicollinearity amongst the independent variables. The mean VIF (Variance inflation factors) for the independent variables was 2.42. Therefore, there was no significant multicollinearity amongst the independent variables.

## 3.3 Estimation strategy

As mentioned above, this study is interested in assessing the impact of AMS on cultivated land productivity. We begin by estimating the relationship between AMS adoption and cultivated land productivity at the household level. The specified equation is set as follows:

**TABLE 1 Variable definitions and summary statistics.**

| Variable | Definition | Mean | S.D. |
|---|---|---|---|
| **Dependent variables** | | | |
| Land productivity | Total output value of cultivated land (RMB/mu), log | 7.464 | 0.203 |
| **Independent variables** | | | |
| AMS ratio | Percentage of planting activities adopted AMS (%) | 42.07 | 14.67 |
| Basic services | 1, if any basic activities (ploughing, seeding, harvesting) adopted AMS | 0.947 | 0.224 |
| Ploughing | 1, if AMS was adopted in ploughing activity; 0, otherwise | 0.869 | 0.337 |
| Seeding | 1, if AMS was adopted in seeding activity; 0, otherwise | 0.925 | 0.263 |
| Harvesting | 1, if AMS was adopted in harvesting activity; 0, otherwise | 0.885 | 0.319 |
| Management services | 1, if any management activities (fertilizing, spraying, irrigation) used AMS | 0.208 | 0.406 |
| Fertilizing | 1, if AMS was adopted in fertilizing activity; 0, otherwise | 0.137 | 0.344 |
| Spraying | 1, if AMS was adopted in spraying activity; 0, otherwise | 0.011 | 0.104 |
| Irrigation | 1, if AMS was adopted in irrigation activity; 0, otherwise | 0.092 | 0.289 |
| **Control variables** | | | |
| **Household head** | | | |
| Age | Age of the household head (years) | 57.550 | 10.300 |
| Gender | 1, if the household head is male; 0, if female | 0.943 | 0.232 |
| Education | Number of years of education of the household head (years) | 6.981 | 3.589 |
| Village leader | 1, if the household is a village cadre; 0, otherwise | 0.314 | 0.464 |
| Training | 1, if the household participated in agricultural training; 0, otherwise | 0.063 | 0.243 |
| Off-farm | 1, if the household has held an off-farm job; 0, otherwise | 0.105 | 0.307 |
| **Family** | | | |
| Household size | Number of household members | 4.752 | 2.207 |
| Contract land | Area of contracted land (mu) | 7.224 | 4.117 |
| Rented land | Area of rented-in land from land rental market (mu) | 0.880 | 3.972 |
| Soil type[a] | Main soil types of arable land cultivated by family | 1.950 | 0.897 |
| Tractor | Number of tractors owned by household | 0.143 | 0.386 |
| Credit | 1, if a loan can be obtained from banks; 0, otherwise | 0.198 | 0.399 |
| **Village** | | | |
| Township distance | Village distance to the nearest township (km) | 12.719 | 7.368 |
| Household number | Total number of households in the village | 306.070 | 191.319 |
| Village cultivated land | Total size of village arable land (mu) | 1840.884 | 955.747 |

Note: 6.18 RMB, 1 dollar (2018).[a] 1 = sandy soil; 2 = loamy soils; 3 = clay; 4 = others.
Data source: Authors' survey.

$$Y_i = \alpha_0 + \alpha_1 AMS_i + \alpha_2 \boldsymbol{X}_i + \sigma T_i + \mu_i \qquad (1)$$

where $Y_i$ represents the dependent variable for household $i$ (i.e., cultivated land productivity) measured as the logarithm of output value per unit area of cultivated land. $AMS_i$ is a set of variables on the AMS adoption of household $i$ that includes the AMS adoption rate in total planting activities and that in different activities, including basic and management activities. $\boldsymbol{X}_i$ controls the characteristics of the household head, family, and village, which also affect land productivity. $T_i$ is a series of dummy variables at the township level to control for differences across townships (e.g., agroclimate) . $\mu_i$ is the error term. Because the dependent variable in this paper (i.e., cultivated land productivity) is a continuous variable, the OLS estimator is suitable for Eq. 1.

Because farmers are not randomly assigned into the groups of those who adopt AMS and those who do not, the adoption of AMS by rural households may be self-selective and thus the OLS estimator in Eq. 1 may be biased (Takeshima, 2017; Khan et al., 2019). To achieve an unbiased estimation of the impact of AMS adoption on cultivated land productivity, we should first address the selection bias. Several solutions have been used in the existing studies to solve the self-selection problem, such as the Heckman selection model, Endogenous switching regression, and the instrumental variable method. However, all such approaches face challenges in identifying appropriate instrumental variables (Mendola, 2007; Zhang et al., 2020). In this study, AMS involves a range of adoption variables related to the total planting process and to different planting activities. It is challenging to find suitable instrumental variables that affect

the AMS adoption in the ploughing, seeding, irrigation, fertilizing, pesticide spraying, and harvesting activities while not directly affecting cultivated land productivity.

Following Dehejia and Wahba (2002) and Zhang et al. (2020), this study uses a statistical matching approach to estimate the average treatment effect on the treated (ATT). In particular, the matching method matches AMS adopters and non-adopters that have similar observable attributes. The matching estimator will have a consistent treatment effect when the dependent variable is independent of AMS adoption (Mendola, 2007). To estimate the average treatment effect of AMS on land productivity, for each rural household $i$, $Y_{io}$ and $Y_{i1}$ represent the outcomes for treated and untreated groups (i.e., the cultivated land productivity of AMS adopters and non-adopters), respectively. For a rural household, the treatment effect of AMS adoption on cultivated land productivity can be derived from $E(Y_{i1} - Y_{i0})$. Because the treatment is exclusive, it is impossible to observe the cultivated land productivity of non-adoption for those who actually adopt AMS. Similarly, for non-adopters of AMS, we could not observe their cultivated land productivity if they adopt AMS. Using the counterfactual framework proposed by Rosenbaum and Rubin (1983) to randomize the non-random data, this study estimates the counterfactual probabilities for the treatment and control groups. To estimate the impact of AMS adoption on cultivated land productivity, we use a matching method to calculate the ATT, which we estimate by the following equation:

$$ATT = E[(Y_{i1} - Y_{i0})|T = 1] \qquad (2)$$

where $T$ represents a binary variable for treatment status and takes the value of 1 if household $i$ in the treated group is an AMS adopter and 0 otherwise. Matching methods usually assume ignorability, common support selection on observables, or confoundedness (Dehejia and Wahba, 2002; Imbens and Wooldridge, 2008). This implies that the differences in land productivity between the treatment and control groups after matching are uniquely attributed to the treatment attributes and that the matched observations assigned to the treated group are random (Uematsu and Mishra, 2012).

Propensity score matching (PSM) is employed to match the AMS adopters to non-adopters with similar characteristics and to ensure that dissimilar households and outliers will have little or no influence on the treatment effects (Rosenbaum and Rubin, 1985). As a commonly used matching estimate in treatment effect analysis, PSM has been widely used in the agricultural economics literature (e.g., Mendola, 2007; Imbens and Wooldridge, 2008; Uematsu and Mishra, 2012; Mishra et al., 2017). It is popularly used as a non-experimental method to estimate ATT for specific program participation or technology adoption (Smith and Todd, 2005; Caliendo and Kopeinig, 2008; Mi et al., 2020). For example, Zhang et al. (2020) used PSM to estimate the effect of land rental market participation on the labor productivity of rural households. PSM is a non-parametric

type of estimate without any specific functional forms or distribution assumptions (Imbens and Wooldridge, 2008). With the matched sample, ATT can be estimated directly by comparing outcomes between the treated and untreated groups (Austin, 2011). In this study, the control group is a sample of farm households that do not adopt AMS but have similar characteristics to those that do. We construct a near-random counterfactual dataset to compare the impact of AMS on cultivated land productivity.

The shortcoming of the PSM approach is that it cannot eliminate the selection bias caused by unobservable factors. If an unobservable factor simultaneously affects both the observations assigned to the treated group and the outcome variable, a hidden bias may arise to which matching estimation is not robust (Rosenbaum, 2002). For example, a farmer's agricultural ability is difficult to observe, although it may affect both AMS adoption and cultivated land productivity. In recognition of this, a sensitivity analysis of the robustness of the estimates is conducted to determine how strongly unobservable factors affect AMS adoption. We estimate a critical odds ratio as proposed by Rosenbaum and Rubin (1983) and Rosenbaum (2002) and followed by studies such as Khan et al. (2019) and Zhang et al. (2020).

# 4 Results

## 4.1 OLS estimation results

### 4.1.1 Main results

The estimated results of Eq. 1 are reported in Table 2. In column (1), the estimated coefficient of AMS is positive and statistically significant. The results show that the adoption rate of AMS increases cultivated land productivity when controlling for the characteristics of the household head, family, and village. A similar positive relationship between mechanization and land productivity was found by Paudel et al. (2019) in Nepal, and Zhou and Ma (2022) in China. This result is consistent with the hypothesis that the adoption of AMS has a positive impact on cultivated land productivity and implies that AMS can play an active role in promoting agricultural production and ensuring food security.

In addition to AMS, several control variables have a significant effect on cultivated land productivity. Specifically, the coefficients on the years of education and the membership in the village cadre of household heads are positive and significant. These are in line with existing studies that have found that the efficiency of household agricultural production is related to the capacity of the household head (Khan et al., 2019; Zhou et al., 2019; Zhang et al., 2020). Moreover, loan availability has a significant and positive impact on cultivated land productivity, thus indicating that the less financial

TABLE 2 OLS regression for the effect of AMS on cultivated land productivity.

| | Full sample | Farm size | | AMS ratio | |
|---|---|---|---|---|---|
| | | [0,50] | (50,100] | [0,50] | (50,100] |
| | (1) | (2) | (3) | (4) | (5) |
| AMS ratio | 0.002*** | 0.003*** | 0.002*** | 0.004*** | -0.000 |
| | (0.001) | (0.001) | (0.001) | (0.001) | (0.002) |
| Age | 0.000 | 0.000 | 0.000 | 0.000 | -0.000 |
| | (0.000) | (0.001) | (0.001) | (0.001) | (0.001) |
| Gender | 0.005 | −0.012 | 0.044 | 0.000 | 0.037 |
| | (0.020) | (0.024) | (0.036) | (0.022) | (0.043) |
| Education | 0.003* | 0.004** | 0.000 | 0.003* | 0.003 |
| | (0.001) | (0.002) | (0.002) | (0.002) | (0.003) |
| Village leader | 0.029** | 0.008 | 0.047* | 0.023 | 0.037 |
| | (0.014) | (0.019) | (0.025) | (0.018) | (0.027) |
| Training | 0.026* | 0.034 | 0.025 | 0.034** | -0.047 |
| | (0.015) | (0.023) | (0.021) | (0.017) | (0.042) |
| Off-farm | −0.002 | −0.011 | 0.010 | −0.006 | 0.015 |
| | (0.010) | (0.016) | (0.016) | (0.013) | (0.020) |
| Household size | 0.003* | 0.004 | 0.003 | 0.004* | −0.003 |
| | (0.002) | (0.003) | (0.003) | (0.002) | (0.005) |
| Contract land | 0.002* | 0.005 | 0.004** | 0.001 | 0.006** |
| | (0.001) | (0.004) | (0.002) | (0.001) | (0.002) |
| Rented land | 0.000 | 0.001 | 0.001 | 0.001 | −0.001 |
| | (0.001) | (0.009) | (0.001) | (0.002) | (0.002) |
| Soil type | 0.008 | 0.003 | 0.017** | 0.009 | 0.011 |
| | (0.006) | (0.008) | (0.008) | (0.007) | (0.011) |
| Tractor | 0.014 | 0.009 | 0.017 | 0.012 | 0.041 |
| | (0.015) | (0.030) | (0.016) | (0.016) | (0.033) |
| Credit | 0.047*** | 0.032* | 0.064*** | 0.050*** | 0.014 |
| | (0.010) | (0.017) | (0.014) | (0.012) | (0.024) |
| Township distance | −0.001 | 0.001 | −0.003** | −0.002 | −0.002 |
| | (0.001) | (0.002) | (0.002) | (0.001) | (0.003) |
| Household number | −0.000 | −0.000 | −0.000 | −0.000 | 0.000 |
| | (0.000) | (0.000) | (0.000) | (0.000) | (0.000) |
| Village cultivated land | 0.000 | 0.000 | 0.000 | 0.000 | -0.000 |
| | (0.000) | (0.000) | (0.000) | (0.000) | (0.000) |
| Township FE | Yes | Yes | Yes | Yes | Yes |
| Constant | 7.372*** | 7.266*** | 7.246*** | 7.251*** | 7.255*** |
| | (0.052) | (0.064) | (0.079) | (0.055) | (0.126) |
| F test | 8.74*** | 2.46*** | 3.48*** | 4.00*** | 2.20*** |
| R² | 0.105 | 0.125 | 0.140 | 0.120 | 0.243 |
| Observations | 1918 | 967 | 951 | 1596 | 322 |

Note: The standard errors clustered at village level are shown in parentheses. *, **, and *** denote $p < 0.10$, $p < 0.05$, and $p < 0.01$, respectively.
Data source: Authors' survey.

constraints, the higher possibility that farmers can increase land productivity. The village-level variables are not significant, most likely because the township fixed effect controls for most regional differences.

### 4.1.2 Heterogeneity analysis results

In columns (2) to (5) of Table 2, we explore the heterogeneity of the impact of AMS adoption on cultivated land productivity to deepen our understanding of this relationship. First, the sample is

**TABLE 3** OLS regression for the effect of AMS on cultivated land productivity by planting activity.

**Dependent variable: Cultivated land productivity**

| | (1) | (2) | (3) | (4) | (5) | (6) | (7) | (8) |
|---|---|---|---|---|---|---|---|---|
| Basic services | 0.109*** | | | | | | | |
| | (0.038) | | | | | | | |
| Plaughing | | 0.076*** | | | | | | |
| | | (0.019) | | | | | | |
| Seeding | | | 0.101*** | | | | | |
| | | | (0.032) | | | | | |
| Harvesting | | | | 0.121*** | | | | |
| | | | | (0.027) | | | | |
| Management services | | | | | −0.016 | | | |
| | | | | | (0.000) | | | |
| Spraying | | | | | | −0.018 | | |
| | | | | | | (0.012) | | |
| Irrigation | | | | | | | −0.090 | |
| | | | | | | | (0.060) | |
| Fertilizing | | | | | | | | −0.005 |
| | | | | | | | | (0.014) |
| Controls | Yes | Yes | Yes | Yes | Yes | Yes | Yes | Yes |
| Township FE | Yes | Yes | Yes | Yes | Yes | Yes | Yes | Yes |
| *F* test | 9.02*** | 8.58*** | 9.34*** | 8.48*** | 7.81*** | 7.70*** | 7.53*** | 7.69*** |
| $R^2$ | 0.091 | 0.092 | 0.093 | 0.111 | 0.078 | 0.079 | 0.080 | 0.078 |
| Observations | 1918 | 1918 | 1918 | 1918 | 1918 | 1918 | 1918 | 1918 |

Note: The standard errors clustered at the village level are shown in parentheses. *, **, and *** denote $p < 0.10$, $p < 0.05$, and $p < 0.01$, respectively.
Data source: Authors' survey.

divided into two subsamples based on the median farm size, with columns (2) and (3) reporting the results of AMS adoption for farmers operating relatively smaller and larger farms. We find that AMS is more effective in increasing the cultivated land productivity among farmers with relatively small farms. Considering that smallholders usually operate fragmented plots and lack collateral, it is likely that they face financial constraints. As a result, it is more difficult for smallholders to access mechanization through machinery ownership, which is the standard method of mechanization (Tan et al., 2006; Wang et al., 2020). Furthermore, AMS can offer smallholders easier access to mechanization in various planting activities and thus has a greater effect on cultivated land productivity among farmers with relatively small farms. This finding is largely consistent with that of Zhou and Ma (2022) that small farms are more beneficial to land productivity through mechanization.

We separate the sample into observations with below-median and above-median AMS adoption rates for separate analyses. The estimated results are reported in columns (4) and (5). We find that households in the lower adoption rate group benefit more from AMS in terms of cultivated land productivity. In contrast, the coefficient for the higher adoption rate group is not significant. These results imply

that the marginal effects of AMS adoption decrease as the rate of AMS adoption increases.

### 4.1.3 Effects of AMS adoption in different planting activities

Table 3 presents the estimated results of the adoption of AMS in different activities. The results in columns (1) to (4) reveal that the general adoption rate of AMS for basic activities and the specific adoption in the ploughing, seeding, and harvesting activities have significant and positive effects on land productivity at the 1% significance level. The effects of AMS adoption in basic activities on cultivated land productivity are between 7.6 and 12.1%. In contrast, columns (5) to (8) show that the adoption of AMS in management activities has no significant effect on cultivated land productivity. Combined with the reality that the rate of AMS adoption in management activities is very low compared to that in basic activities (see Table 1), the difference in the impact on cultivated land productivity between management and basic activities may be partly explained by the following two reasons. Machinery used in management activities (e.g., pumps) is less expensive than that used in basic activities (e.g., tractors), thus smallholders rely more on AMS in basic activities. And the agricultural labor force used

TABLE 4 Average treatment effect of AMS adoption on land productivity by PSM.

| | Nearest neighbors | Mean outcome | | Treatment effect | |
|---|---|---|---|---|---|
| | | Treated | Controls | ATT | |
| AMS adoption | 1 | 7.471 | 7.292 | 0.179** | (0.047) |
| | 2 | 7.471 | 7.303 | 0.168*** | (0.044) |
| | 3 | 7.471 | 7.308 | 0.163*** | (0.044) |
| Basic activities | 1 | 7.468 | 7.296 | 0.172*** | (0.047) |
| | 2 | 7.468 | 7.296 | 0.172*** | (0.045) |
| | 3 | 7.468 | 7.303 | 0.164*** | (0.044) |
| Plaughing | 1 | 7.473 | 7.365 | 0.108*** | (0.030) |
| | 2 | 7.473 | 7.365 | 0.108*** | (0.030) |
| | 3 | 7.473 | 7.368 | 0.105*** | (0.028) |
| Seeding | 1 | 7.469 | 7.338 | 0.131*** | (0.041) |
| | 2 | 7.469 | 7.341 | 0.128*** | (0.038) |
| | 3 | 7.469 | 7.349 | 0.119*** | (0.038) |
| Harvesting | 1 | 7.476 | 7.335 | 0.141*** | (0.036) |
| | 2 | 7.476 | 7.354 | 0.122*** | (0.033) |
| | 3 | 7.476 | 7.355 | 0.121*** | (0.032) |
| Management activities | 1 | 7.456 | 7.466 | −0.010 | (0.017) |
| | 2 | 7.456 | 7.470 | −0.013 | (0.015) |
| | 3 | 7.456 | 7.475 | −0.019 | (0.014) |
| Fertilizing | 1 | 7.446 | 7.471 | −0.025 | (0.020) |
| | 2 | 7.446 | 7.473 | −0.027 | (0.018) |
| | 3 | 7.446 | 7.473 | −0.027 | (0.017) |
| Spraying | 1 | 7.377 | 7.392 | −0.015 | (0.087) |
| | 2 | 7.377 | 7.422 | −0.045 | (0.073) |
| | 3 | 7.377 | 7.451 | −0.074 | (0.070) |
| Irrigation | 1 | 7.470 | 7.491 | −0.021 | (0.024) |
| | 2 | 7.470 | 7.488 | −0.018 | (0.019) |
| | 3 | 7.470 | 7.488 | −0.018 | (0.018) |

Note: ATT, the average treatment effect on the treated; The standard errors are shown in parentheses. *, **, and *** denote $p < 0.10$, $p < 0.05$, and $p < 0.01$, respectively.
Data source: Authors' survey.

by smallholders is often the residual family labor force after off-farm migration, which has a low opportunity cost and allows for the engagement in management activities that are relatively less physically demanding. The above results are therefore consistent with the hypothesis in the theoretical analysis that AMS adoption in basic activities has a larger impact on cultivated land productivity than AMS adoption in management activities.

## 4.2 Average treatment effects on the treated

Table 4 presents the results of the ATT of AMS on cultivated land productivity. We use the nearest neighbors matching method, and the radius matching method and kernel matching method are performed for comparison (see Supplementary Appendix). In particular, the households that

adopt AMS in general, basic, and management activities are compared separately to the counterfactual households that do not adopt AMS. The results reveal a significant and positive impact of AMS adoption in general and basic activities as well as in each individual activity in basic services on cultivated land productivity. Since the dependent variable is in logarithmic form, the estimated results of ATT suggest that the overall adoption of AMS increases cultivated land productivity by between 16.3% and 17.9%. Furthermore, the AMS adoption in basic activities in general and in each individual activity increase land productivity by 10.3%–17.2%. However, the adopters of AMS in management activities are not significantly different from non-adopters in terms of cultivated land productivity.

Based on the results in Table 4, it can be concluded that in the absence of selection bias, cultivated land productivity for rural households who adopt AMS is significantly higher than that for non-adopters. This finding is similar to those of the studies that

previously found a significant and positive effect of agricultural technology adoption on cultivated land productivity (e.g., Asfaw et al., 2012; Khonje et al., 2015; Zhou and Ma, 2022). In addition, the above results are also consistent with the results of the OLS estimation in Table 3 and support our first hypothesis. Given the consistency between the OLS and PSM results, it is convincing to use the ATT results of PSM to interpret the economic significance of the effect of AMS on cultivated land productivity, as well as to use the results of OLS regression to compare the effects among different groups mentioned above.

A Rosenbaum bounds sensitivity analysis is used to assess the presence of unobserved factors when the key assumption is relaxed by a quantifiable increase in uncertainty (Rosenbaum, 2002). The measurement of the critical value of hidden bias, Γ, is expressed in terms of the odds ratio of differential treatment. The magnitude of hidden bias, which would make the finding of a positive and significant effect of AMS adoption on cultivated land productivity questionable, should be higher than one[2]. At each Γ, we calculate the lower and upper hypothetical significance levels, which represent the bound on the significance level of the ATT in cases of endogenous self-selection into the treatment group. From the results of Rosenbaum's sensitivity in Supplementary Appendix, a hidden bias of Γ between 2.0 and 2.1 is required to declare that the finding of a positive effect of AMS adoption on cultivated land productivity is false. This small Γ suggests that the results of the ATT estimation can be trusted.

## 4.3 Mechanism test of the effect of AMS adoption on cultivated land productivity

Our analysis in the previous section demonstrates that AMS adoption increases cultivated land productivity both in general and in basic planting activities. This study also examines the heterogeneity in this effect across farm sizes and rates of AMS adoption. While limitations in the available data prevent us from revealing all possible mechanisms that link AMS adoption to cultivated land productivity, we consider the main mechanisms discussed in the conceptual framework (i.e., those shown in Figure 1), namely, labor substitution, technology improvement, financial constraints, and output yield and quality. The mechanism variables are defined and summarized in Supplementary Appendix.

The first mechanism is *via* the effect of AMS adoption on agricultural labor input. Column (1) of Table 5 shows that increasing the rate of AMS adoption has a negative effect on the amount of agricultural labor input needed by smallholders, although the coefficient is not significant.

We speculate that the potential reasons for this insignificant result may be as follows. First, the labor force used by smallholders is usually the residual labor, that is, unable to obtain off-farm employment opportunities. In such a situation, even if AMS could reduce the input intensity of agricultural labor, this component of the household labor force may still engage in agriculture. Second, the adoption of AMS may result in the expansion of farm sizes, as found by Qian et al. (2022). Those households may then not be able to reduce the total amount of family labor needed for agriculture. Third, AMS adoption varies by planting activity, and activities for which AMS adoption is relatively weak generally rely on manual labor.

The second mechanism (i.e., technological improvement) is motivated by the idea of mechanization and has been cited in the literature as a mechanism for technological adoption. Because the adoption of AMS for different planting activities may involve different agricultural technologies that are not necessarily directly comparable with each other, we use technical efficiency as a more comparable measure of technological progress. We expect the adoption of AMS to improve the technical efficiency of adopters. As in previous studies (e.g., Villano and Fleming 2006; Michler and Shively 2015; Ma et al., 2017), we estimate technical efficiency using stochastic frontier analysis. In column (2) of Table 5, we find that AMS adoption has a significant and positive effect on technical efficiency. This is largely consistent with the existing studies that find that mechanization enhances technological improvement at the household level in Iran, Bangladesh, and parts of rural China (Hormozi et al., 2012; Zhou et al., 2019; Vorita et al., 2021).

The third mechanism is the effect of AMS on alleviating financial constraints. Financial constraints have been an important obstacle to smallholders purchasing agricultural machinery, adopting new technologies, and investing in agriculture. Given their lack of collateral, inter-farmer borrowing is the main method through which they alleviate financial constraints. In this paper, the number of times farmers borrowings from other villagers in the past 5 years is used to measure financial constraints. As the results in column (3) of Table 5 show, a rising adoption rate of AMS significantly reduces the frequency of borrowings from other villagers. This result is consistent with the theoretical analysis of Yu et al. (2021).

Increases in land productivity may be the result of quantity and/or quality improvements (i.e., increases in output yields and/or selling prices). Columns (4) and (5) show that the AMS adoption rate has a positive effect on crop yield, although there is no significant effect on selling price. Our results reveal that AMS adoption can increase the output yield per unit area of cultivated land. The insignificant coefficient on selling price can be partly explained by the low bargaining power of smallholders in agricultural markets, which makes selling prices relatively

---

2 Readers who are interested in the Rosenbaum sensitivity test are advised to read Rosenbaum (2002) and Diprete and Gangl (2004) for a detailed understanding of the method.

TABLE 5 Mechanism analysis: the effect of AMS on potential mechanisms, OLS.

| | Labor input | Technical efficiency | Financial constrains | Output yield | Selling price |
|---|---|---|---|---|---|
| | (1) | (2) | (3) | (4) | (5) |
| AMS ratio | −0.003 | 0.0004* | −0.016*** | 0.003*** | −0.0004 |
| | (0.002) | (0.0002) | (0.006) | (0.000) | (0.0003) |
| Controls | Yes | Yes | Yes | Yes | Yes |
| Township FE | Yes | Yes | Yes | Yes | Yes |
| $F$ test | 33.97*** | 8.89*** | 4.71*** | 9.37*** | 4.63*** |
| $R^2$ | 0.321 | 0.086 | 0.056 | 0.116 | 0.102 |
| Observations | 1918 | 1888 | 1918 | 1918 | 1918 |

The standard errors clustered at village level are shown in parentheses. *, **, and *** denote $p < 0.10$, $p < 0.05$, and $p < 0.01$, respectively.
Data source: Authors' survey.

exogenous to smallholders (Rutten, et al., 2017; Pingali et al., 2019).

# 5 Conclusions and policy implications

The importance of AMS for improving smallholders' access to mechanization and the need for mechanization to boost agricultural production and ensure food security have been greatly highlighted in the existing studies. However, few studies consider the effect of AMS, as a new mechanization source, on cultivated land productivity. In response to this gap, this study investigates the broad impact of AMS adoption and the adoption of AMS in various production activities on cultivated land productivity, and further identifies the mechanisms of those impacts. In the context of the North China Plain and based on the survey data of 1918 smallholders, this study uses OLS estimation as its basic results and PSM to address self-selection bias and estimate the average treatment effect on the treated (ATT).

The results of the OLS estimation show that AMS increases cultivated land productivity, especially for farmers with relatively small farms and relatively low AMS adoption rates. Moreover, we find that the adoption of AMS in basic activities (e.g., ploughing, seeding, and harvesting) significantly increases cultivated land productivity, while the adoption of AMS in management activities (e.g., spraying, irrigation, and fertilizing) has no obvious effect on land productivity. In addition, the results of PSM show that the adoption of AMS both in general and in basic activities increases cultivated land productivity by between 10.5% and 17.9%. Furthermore, we find that technological improvement, easing of financial constraints, and increasing yields are important mechanisms through which AMS affects cultivated land productivity.

Our findings have important implications for promoting agricultural modernization and ensuring food security. First, this study finds that AMS adoption can increase cultivated land productivity and suggests that improved adoption of AMS by smallholders can facilitate agricultural production.

Second, the findings from the mechanism analysis suggest that AMS adoption can be an effective pathway for alleviating financial constraints, promoting technological improvement, and increasing crop yields. The existence of these mechanisms implies that there will be a complementary relationship between the extension of AMS and the support policies of the agricultural credit as well as the agricultural technology systems.

There are a few limitations that should be taken into account in interpreting and generalizing the results of this study. First, this study was conducted in a plain area dominated by smallholders with a similar crop structure, while for the other areas of rural China where the topography and crop structure are more diverse, the results may need some caveats. Future research should examine whether the effects of AMS on cultivated land productivity vary with topography and crop structure. Second, this study mainly examines the cultivated land productivity of smallholders. In recent years, however, the Chinese government has actively encouraged the development of farmer cooperatives and agricultural companies. These new actors in Chinese agriculture may also be providers of AMS. Taking these developments into account may provide a complete picture of the relationship between AMS and cultivated land productivity.

# Data availability statement

The raw data supporting the conclusions of this article will be made available by the authors, without undue reservation.

# Author contributions

YL: substantial contributions to conception and design, data collection, analysis data, drafting the paper; XS: project administration and revising the paper critically for important intellectual content; FG: contributions to conception and design and revising the draft.

# Funding

This work was supported by National Natural Science Foundation of China (No. 72173065), 111 Project (No. B17024), Outstanding (Blue) Teaching Team Project of JiangSu Province, and the China Scholarship Council (No.201806850051).

# Conflict of interest

The authors declare that the research was conducted in the absence of any commercial or financial relationships that could be construed as a potential conflict of interest.

# Publisher's note

All claims expressed in this article are solely those of the authors and do not necessarily represent those of their affiliated organizations, or those of the publisher, the editors and the reviewers. Any product that may be evaluated in this article, or claim that may be made by its manufacturer, is not guaranteed or endorsed by the publisher.

# Supplementary material

The Supplementary Material for this article can be found online at: https://www.frontiersin.org/articles/10.3389/fenvs.2022.1008036/full#supplementary-material

# References

Adekunle, A., Osazuwa, P., and Raghavan, V. (2016). Socio-economic determinants of agricultural mechanisation in Africa: A research note based on cassava cultivation mechanisation. *Technol. Forecast. Soc. Change* 112, 313–319. doi:10.1016/j.techfore.2016.09.003

Amoozad-Khalili, M., Rostamian, R., Esmaeilpour-Troujeni, M., and Kosari-Moghaddam, A. (2020). Economic modeling of mechanized and semi-mechanized rainfed wheat production systems using multiple linear regression model. *Inf. Process. Agric.* 7 (1), 30–40. doi:10.1016/j.inpa.2019.06.002

Asfaw, S., Shiferaw, B., Simtowe, F., and Lipper, L. (2012). Impact of modern agricultural technologies on smallholder welfare: Evidence from Tanzania and Ethiopia. *Food policy* 37 (3), 283–295. doi:10.1016/j.foodpol.2012.02.013

Austin, P. C. (2011). An introduction to propensity score methods for reducing the effects of confounding in observational studies. *Multivar. Behav. Res.* 46 (3), 399–424. doi:10.1080/00273171.2011.568786

Baiyegunhi, L. J. S., Majokweni, Z. P., and Ferrer, S. R. D. (2019). Impact of outsourced agricultural extension program on smallholder farmers' net farm income in Msinga, KwaZulu-Natal, South Africa. *Technol. Soc.* 57, 1–7. doi:10.1016/j.techsoc.2018.11.003

Benin, S. (2015). Impact of Ghana's agricultural mechanization services center program. *Agric. Econ.* 46 (S1), 103–117. doi:10.1111/agec.12201

Belton, B., Win, M. T., Zhang, X., and Filipski, M. (2021). The rapid rise of agricultural mechanization in Myanmar. *Food Policy* 101, 102095.

Caliendo, M., and Kopeinig, S. (2008). Some practical guidance for the implementation of propensity score matching. *J. Econ. Surv.* 22 (1), 31–72. doi:10.1111/j.1467-6419.2007.00527.x

Chaya, W., Bunnag, B., and Gheewala, S. H. (2019). Adoption, cost and livelihood impact of machinery services used in small-scale sugarcane production in Thailand. *Sugar Tech.* 21 (4), 543–556. doi:10.1007/s12355-018-0651-x

Daum, T., and Birner, R. (2020). Agricultural mechanization in Africa: Myths, realities and an emerging research agenda. *Glob. Food Secur.* 26, 100393. doi:10.1016/j.gfs.2020.100393

Dehejia, R., and Wahba, S. (2002). Propensity score-matching methods for non-experimental causal studies. *Rev. Econ. Stat.* 84 (1), 151–161. doi:10.1162/003465302317331982

Desiere, S., and Jolliffe, D. (2018). Land productivity and plot size: Is measurement error driving the inverse relationship? *J. Dev. Econ.* 130, 84–98. doi:10.1016/j.jdeveco.2017.10.002

DiPrete, T. A., and Gangl, M. (2004). 7. Assessing bias in the estimation of causal effects: Rosenbaum bounds on matching estimators and instrumental variables estimation with imperfect instruments. *Sociol. Methodol.* 34 (1), 271–310. doi:10.1111/j.0081-1750.2004.00154.x

Emmanuel, D., Owusu-Sekyere, E., Owusu, V., and Jordaan, H. (2016). Impact of agricultural extension service on adoption of chemical fertilizer: Implications for rice productivity and development in Ghana. *NJAS Wageningen J. Life Sci.* 79, 41–49. doi:10.1016/j.njas.2016.10.002

Hormozi, M. A., Asoodar, M. A., and Abdeshahi, A. (2012). Impact of mechanization on technical efficiency: A case study of rice farmers in Iran. *Procedia Econ. Finance* 1, 176–185. doi:10.1016/s2212-5671(12)00021-4

Imbens, G. W., and Wooldridge, J. M. (2008). Recent developments in the econometrics of program evaluation. *J. Econ. Literature* 47 (1), 5–86. doi:10.1257/jel.47.1.5

Ito, J. (2010). Inter-regional difference of agricultural productivity in China: Distinction between biochemical and machinery technology. *China Econ. Rev.* 21 (3), 394–410. doi:10.1016/j.chieco.2010.03.002

Ji, Y., Yu, X., and Zhong, F. (2012). Machinery investment decision and off-farm employment in rural China. *China Econ. Rev.* 23 (1), 71–80. doi:10.1016/j.chieco.2011.08.001

Justice, S., and Biggs, S. (2020). The spread of smaller engines and markets in machinery services in rural areas of South Asia. *J. Rural Stud.* 73, 10–20. doi:10.1016/j.jrurstud.2019.11.013

Khan, M. F., Nakano, Y., and Kurosaki, T. (2019). Impact of contract farming on land productivity and income of maize and potato growers in Pakistan. *Food Policy* 85, 28–39. doi:10.1016/j.foodpol.2019.04.004

Khonje, M., Manda, J., Alene, A. D., and Kassie, M. (2015). Analysis of adoption and impacts of improved maize varieties in eastern Zambia. *World Dev.* 66, 695–706. doi:10.1016/j.worlddev.2014.09.008

Kousar, R., and Abdulai, A. (2016). Off-farm work, land tenancy contracts and investment in soil conservation measures in rural Pakistan. *Aust. J. Agric. Resour. Econ.* 60 (2), 307–325. doi:10.1111/1467-8489.12125

Liu, Y., Heerink, N., Li, F., and Shi, X. (2022). Do agricultural machinery services promote village farmland rental markets? Theory and evidence from a case study in the north China plain[J]. *Land Use Policy* 122, 106388. doi:10.1016/j.landusepol.2022.106388

Lyne, M. C., Jonas, N., and Ortmann, G. F. (2018). A quantitative assessment of an outsourced agricultural extension service in the Umzimkhulu District of KwaZulu-Natal, South Africa. *J. Agric. Educ. Ext.* 24 (1), 51–64. doi:10.1080/1389224x.2017.1387159

Ma, W., and Abdulai, A. (2016). Does cooperative membership improve household welfare? Evidence from apple farmers in China. *Food Policy* 58, 94–102. doi:10.1016/j.foodpol.2015.12.002

Ma, X., Heerink, N., Feng, S., and Shi, X. (2017). Land tenure security and technical efficiency: New insights from a case study in northwest China. *Environ. Dev. Econ.* 22 (3), 305–327. doi:10.1017/s1355770x1600036x

Mahasuweerachai, P., and Suksawat, J. (2022). Incentives for mechanized cane harvesting in Thailand: A choice experiment. *J. Asian Econ.* 78, 101434. doi:10.1016/j.asieco.2021.101434

Martey, E., Kuwornu, J. K., and Adjebeng-Danquah, J. (2019). Estimating the effect of mineral fertilizer use on Land productivity and income: Evidence from Ghana. *Land Use Policy* 85, 463–475. doi:10.1016/j.landusepol.2019.04.027

Mendola, M. (2007). Agricultural technology adoption and poverty reduction: A propensity-score matching analysis for rural Bangladesh. *Food Policy* 32 (3), 372–393. doi:10.1016/j.foodpol.2006.07.003

Mi, Q., Li, X., and Gao, J. (2020). How to improve the welfare of smallholders through agricultural production outsourcing: Evidence from cotton farmers in Xinjiang, Northwest China. *J. Clean. Prod.* 256, 120636. doi:10.1016/j.jclepro.2020. 120636

Michler, J. D., and Shively, G. E. (2015). Land tenure, tenure security and farm efficiency: Panel evidence from the Philippines. *J. Agric. Econ.* 66 (1), 155–169. doi:10.1111/1477-9552.12082

Min, S., Waibel, H., and Huang, J. (2017). Smallholder participation in the land rental market in a mountainous region of Southern China: Impact of population aging, land tenure security and ethnicity. *Land Use Policy* 68, 625–637. doi:10.1016/ j.landusepol.2017.08.033

Mishra, A. K., Khanal, A. R., and Mohanty, S. (2017). Gender differentials in farming efficiency and profits: The case of rice production in the Philippines. *Land Use Policy* 63 (63), 461–469. doi:10.1016/j.landusepol. 2017.01.033

Mottaleb, K. A., Rahut, D. B., Ali, A., Gérard, B., and Erenstein, O. (2017). Enhancing smallholder access to agricultural machinery services: Lessons from Bangladesh. *J. Dev. Stud.* 53 (9), 1502–1517. doi:10.1080/00220388.2016. 1257116

Paudel, G. P., Kc, D. B., Justice, S. E., and McDonald, A. J. (2019). Scale-appropriate mechanization impacts on productivity among smallholders: Evidence from rice systems in the mid-hills of Nepal. *Land Use Policy* 85, 104–113. doi:10.1016/j.landusepol.2019.03.030

Pfeiffer, L., López-Feldman, A., and Taylor, J. E. (2009). Is off-farm income reforming the farm? Evidence from Mexico. *Agric. Econ.* 40 (2), 125–138. doi:10. 1111/j.1574-0862.2009.00365.x

Pingali, P., Aiyar, A., Abraham, M., and Rahman, A. (2019). "Linking farms to markets: Reducing transaction costs and enhancing bargaining power," in *Transforming food systems for a rising India* (Cham: Palgrave Macmillan), 193–214.

Qian, L., Lu, H., Gao, Q., and Lu, H. (2022). Household-owned farm machinery vs. outsourced machinery services: The impact of agricultural mechanization on the land leasing behavior of relatively large-scale farmers in China. *Land Use Policy* 115, 106008. doi:10.1016/j.landusepol.2022.106008

Qiao, F. (2020). The impact of agricultural service on grain production in China. *Sustainability* 12 (15), 6249. doi:10.3390/su12156249

Qiu, T., Choy, S. T. B., and Luo, B. (2022). Is small beautiful? Links between agricultural mechanization services and the productivity of different-sized farms[J]. *Appl. Econ.* 54 (4), 430–442. doi:10.1080/00036846.2021.1963411

Qiu, T., Shi, X., He, Q., and Luo, B. (2021). The paradox of developing agricultural mechanization services in China: Supporting or kicking out smallholder farmers? *China Econ. Rev.* 69, 101680. doi:10.1016/j.chieco.2021.101680

Rigg, J., Salamanca, A., and Thompson, E. C. (2016). The puzzle of East and Southeast Asia's persistent smallholder. *J. Rural Stud.* 43, 118–133. doi:10.1016/j. jrurstud.2015.11.003

Rosenbaum, P. R. (2002). *Observational studies*. 2nd ed. New York: Springer.

Rosenbaum, P. R., and Rubin, D. B. (1985). Constructing a control group using multivariate matched sampling methods that incorporate the propensity score. *Am. Statistician* 39 (1), 33–38. doi:10.2307/2683903

Rosenbaum, P. R., and Rubin, D. B. (1983). The central role of the propensity score in observational studies for causal effects. *Biometrika* 70 (1), 41–55. doi:10. 1093/biomet/70.1.41

Rutten, R., Bakker, L., Alano, M. L., Salerno, T., Savitri, L. A., and Shohibuddin, M. (2017). Smallholder bargaining power in large-scale land deals: A relational perspective. *J. Peasant Stud.* 44 (4), 891–917. doi:10.1080/03066150.2016.1277991

Shikuku, K. M. (2019). Information exchange links, knowledge exposure, and adoption of agricultural technologies in northern Uganda. *World Dev.* 115, 94–106. doi:10.1016/j.worlddev.2018.11.012

Smith, J. A., and Todd, P. E. (2005). Does matching overcome LaLonde's critique of non-experimental estimators? *J. Econ.* 125 (1-2), 305–353. doi:10.1016/j. jeconom.2004.04.011

Takeshima, H. (2017). Custom-hired tractor services and returns to scale in smallholder agriculture: A production function approach. *Agric. Econ.* 48 (3), 363–372. doi:10.1111/agec.12339

Tan, S., Heerink, N., and Qu, F. (2006). Land fragmentation and its driving forces in China. *Land Use Policy* 23 (3), 272–285. doi:10.1016/j.landusepol. 2004.12.001

Tang, L., Liu, Q., Yang, W., and Wang, J. (2018). Do agricultural services contribute to cost saving? Evidence from Chinese rice farmers. *China Agric. Econ. Rev.* 10, 323–337. doi:10.1108/caer-06-2016-0082

Uematsu, H., and Mishra, A. K. (2012). Organic farmers or conventional farmers: Where's the money? *Ecol. Econ.* 78, 55–62. doi:10.1016/j.ecolecon. 2012.03.013

Villano, R., and Fleming, E. (2006). Technical inefficiency and production risk in rice farming: Evidence from central luzon Philippines. *Asian Econ. J.* 20 (1), 29–46. doi:10.1111/j.1467-8381.2006.00223.x

Vortia, P., Nasrin, M., Bipasha, S. K., and Islam, M. (2021). Extent of farm mechanization and technical efficiency of rice production in some selected areas of Bangladesh. *GeoJournal* 86 (2), 729–742. doi:10.1007/s10708-019-10095-1

Wang, X., Yamauchi, F., Huang, J., and Rozelle, S. (2020). What constrains mechanization in Chinese agriculture? Role of farm size and fragmentation. *China Econ. Rev.* 62, 101221. doi:10.1016/j.chieco.2018.09.002

Wang, X., Yamauchi, F., Otsuka, K., and Huang, J. (2016). Wage growth, landholding, and mechanization in Chinese agriculture. *World Dev.* 86, 30–45. doi:10.1016/j.worlddev.2016.05.002

Yamauchi, F. (2016). Rising real wages, mechanization and growing advantage of large farms: Evidence from Indonesia. *Food Policy* 58, 62–69. doi:10.1016/j.foodpol. 2015.11.004

Yang, J., Huang, Z., Zhang, X., and Reardon, T. (2013). The rapid rise of cross-regional agricultural mechanization services in China. *Am. J. Agric. Econ.* 95 (5), 1245–1251. doi:10.1093/ajae/aat027

Yu, X., Yin, X., Liu, Y., and Li, D. (2021). Do agricultural machinery services facilitate land transfer? Evidence from rice farmers in sichuan Province, China. *Land* 10 (5), 466. doi:10.3390/land10050466

Yu, X., and Zhao, G. (2009). Chinese agricultural development in 30 years: A literature review. *Front. Econ. China* 4 (4), 633–648. doi:10.1007/s11459-009-0034-y

Zhang, J., Mishra, A. K., Zhu, P., and Li, X. (2020). Land rental market and agricultural labor productivity in rural China: A mediation analysis. *World Dev.* 135, 105089. doi:10.1016/j.worlddev.2020.105089

Zhang, W., Cao, G., Li, X., Zhang, H., Wang, C., Liu, Q., et al. (2016). Closing yield gaps in China by empowering smallholder farmers. *Nature* 537 (7622), 671–674. doi:10.1038/nature19368

Zhang, X., Yang, J., and Thomas, R. (2017). Mechanization outsourcing clusters and division of labor in Chinese agriculture. *China Econ. Rev.* 43, 184–195. doi:10. 1016/j.chieco.2017.01.012

Zhou, X., and Ma, W. (2022). Agricultural mechanization and land productivity in China. *Int. J. Sustain. Dev. World Ecol.* 29, 530–542. doi:10.1080/13504509.2022. 2051638

Zhou, X., Ma, W., Li, G., and Qiu, H. (2020). Farm machinery use and maize yields in China: An analysis accounting for selection bias and heterogeneity. *Aust. J. Agric. Resour. Econ.* 64 (4), 1282–1307. doi:10.1111/1467-8489.12395

Zhou, Y., Shi, X., Heerink, N., and Ma, X. (2019). The effect of land tenure governance on technical efficiency: Evidence from three provinces in eastern China. *Appl. Econ.* 51 (22), 2337–2354. doi:10.1080/00036846.2018.1543941

# Simulation of citrus production space based on MaxEnt

Zhengyu Lin[1,2]\*, Chunyan Chen[1], Yuanli Liu[1], Guanghui Liu[3], Peng He[2], Guitang Liao[4], Wenbo Gao[1], Ji Cao[1] and Zhouling Shao[1]

[1]Institute of Agricultural Information and Rural Economy, Sichuan Academy of Agricultural Science, Chengdu, China, [2]College of Resources, Sichuan Agriculture University, Chengdu, China, [3]Chengdu Land and Resources Information Center, Chengdu, China, [4]College of Resources and Environment, Chengdu University of Information Technology, Chengdu, China

Crop production space is the most important part of land use system, and spatial simulation has always been the key task of land science. Crop production space is affected by many factors on different spatio-temporal scales, which leads to the complexity of simulation models. The existing simulation models also have the limitations of lack of human factors, large simulation area and excessive reliance on expert experience. Sichuan Province is a typical area of Citrus spatial expansion in China, so it is of great practical significance to carry out spatial regulation. From the comprehensive perspective of nature and humanity, this research uses MaxEnt, ArcGIS, Orcale, SQL to design a spatial regulation method (CSSM) for citrus, predict the citrus production space in Sichuan Province in 2025, and put forward regulation suggestions. The results showed that the citrus spatial simulation method better reflects the comprehensive effect of natural and human factors on crop space, and realizes the research on the regulation of single crop production space. The dominant environmental variables affecting citrus production in Sichuan are input of production factors, society, climate and terrain. Human activities play a leading role. The suitable environment for citrus production in Sichuan is: elevation ≤500m, annual average temperature ≥16.5 °C, aspect are northeast, southwest and northwest, supported by preferential policies, the input of Citrus fertilizer in the county is ≥ 500t, the input of Citrus labor in the county is ≥ 5,000, the input of Citrus pesticide in the county is ≥ 12.5t, and the technical progress represented by unit yield is 750−7000 t/km[2]. The suitable space for citrus production in Sichuan are mainly located in Zigong, Nanchong, Ziyang, Neijiang, Meishan, Leshan, Yibin and Luzhou. The government should choose a positive low growth scenario to stabilize the citrus area in Sichuan at 3533 km[2] in 2025, and form a major citrus production area in Meishan, Ziyang, Neijiang, Chengdu, Nanchong and Yibin.

KEYWORDS

land use, crops suitability, maximum entropy model(MaxEnt), multi-scenario simulation, citrus

# 1 Introduction

Crop production space is the most extensive and important part of land use system (Ramankutty et al., 2008; Volk and Ewert, 2011; Tang et al., 2015). It is the spatial expression of crop type and production distribution (Tang et al., 2010). Crop spatial simulation is not only an important task of agricultural land system research, but also an industrial policy problem faced by government departments. Therefore, it has always been the research focus of land science (Liu and Chen, 2002). The purpose of crop spatial simulation is to arrange crops in the most suitable space as far as possible, form a relatively centralized regional layout, realize the optimization of agricultural land system, and obtain the best comprehensive benefits (Tang et al., 2015).

The land use change simulation model has formed SD, Markov, CA, clue, flus and their coupling models (Verburg et al., 2002; Genga et al., 2017; Mamanis et al., 2021; Zhang et al., 2021). This kind of simulation is based on driving factors, utilization needs, regional constraints and conversion order, and realizes top-down or bottom-up change simulation on different space-time scales. However, this kind of research only realizes the simulation of the primary type of agricultural land and construction land, but fails to realize the spatial simulation of the internal crop types of agricultural land, and because the simulation area is too large, it is difficult to guide the practice at the samll-scale of county (town) and even villages. Land ecological suitability evaluation (LESE) based on GIS is often used in spatial simulation. This kind of method is based on the response of crop physiological growth to the natural environment, selects representative indicators from climate, terrain and soil, identifies and divides suitable space, and realizes spatial regulation on different scales (Neamatollahi et al., 2012; Bagherzadeh and Daneshvar, 2014; Li et al., 2015; Wotlolan et al., 2021). However, this kind of method also has two limitations. The first is to ignore social and economic factors and reduce the scientificity of the results. The most suitable space is the result of agricultural land adapting to changes in natural and human factors, including natural suitability and human suitability (Lin et al., 2020). The natural environment determines the basic pattern of crop production space, and makes the natural suitable space become the initial gathering area of crops (Li et al., 2012). With the development of society, economy, science and technology, human factors have become an important inducement to cause spatial changes. The spatial heterogeneity of labor, farmers' behavior, production costs, consumption, policy and technological progress on different spatial and temporal scales has an increasingly strong impact on spatial changes (Xiang et al., 2014; Zhang and Zhang, 2016; Wang and Qi, 2018). Spatial change has changed from natural driving to common driving of nature and humanity (Lin et al., 2021). Second, it is difficult to determine the representative indicators and their thresholds. Crop growth is affected by many variables. The dominant variables affecting the spatial change of crop production in different regions are different, and the threshold of the same variable affecting the spatial change in the same region also has time differences (Zabihi et al., 2015; Mokarram and Mirsoleimani, 2018; Tercana and Dereli, 2020). Therefore, the determination of representative indicators and their thresholds is often affected by subjective experience and regional differences.

Species distribution model (SDM) provides a new idea for crop spatial simulation. According to the relationship between species distribution and eco-environmental characteristics, SDM does not need to have rich prior knowledge of species ecological characteristics. Now it has been widely used in potential distribution (Yang et al., 2013; Qin et al., 2017). A series of ecological statistical models based on ArcGIS have been widely used, such as MaxEnt (Phillips et al., 2006), BIOCLIM (Beaumont et al., 2005), ENFA (hengl et al., 2009), GARP (Stockwell and Peters, 1999). More than 1,000 studies since 2006 show that MaxEnt model has been proved to have the best prediction ability and accuracy (Wisz et al., 2008; Merow et al., 2013). MaxEnt model has achieved good results in the suitability zoning of rice, wheat, corn, potato and other crops and the assessment of the response to environmental and major climate factors (Khalil et al., 2021; Khubaib et al., 2021; Yu et al., 2022). MaxEnt model can not only consider the impact of natural variables such as climate, terrain and soil, but also consider the impact of non natural variables such as labor force and land use (Galletti et al., 2013; Yi et al., 2016; Gu et al., 2018; Cao et al., 2021; Yang et al., 2022). The change of environment and human activities has obvious uncertainty and complexity (Zhang et al., 2016; Yang et al., 2022). MaxEnt model shows applicability in coupling analysis of natural environment and human activities (Tan et al., 2019; Nyairo and Machimura, 2022), which is conducive to understanding the comprehensive impact of environment and human activities on agricultural production. Supported by Geographic Information System (GIS), MaxEnt model provides a good method for crop spatial distribution and agricultural land structure optimization.

This work uses MaxEnt, ArcGIS, Oracle, SQL to design the citrus spatial simulation method (CSSM). CSSM comprehensively considers natural and human factors, uses MaxEnt to calculate the distribution probability of citrus production, simulates the production space with the distribution probability as the standard through Oracle and SQL, and carries out empirical research on the spatial layout of citrus production in Sichuan Province of China in 2025, in order to provide a new method for the simulation of agricultural land system.

# 2 Study area and data source

## 2.1 Study area

Sichuan Province located in the southwest of China (26°03′–34°19′ N, 92°21′–108°12′ E), is the transitional area
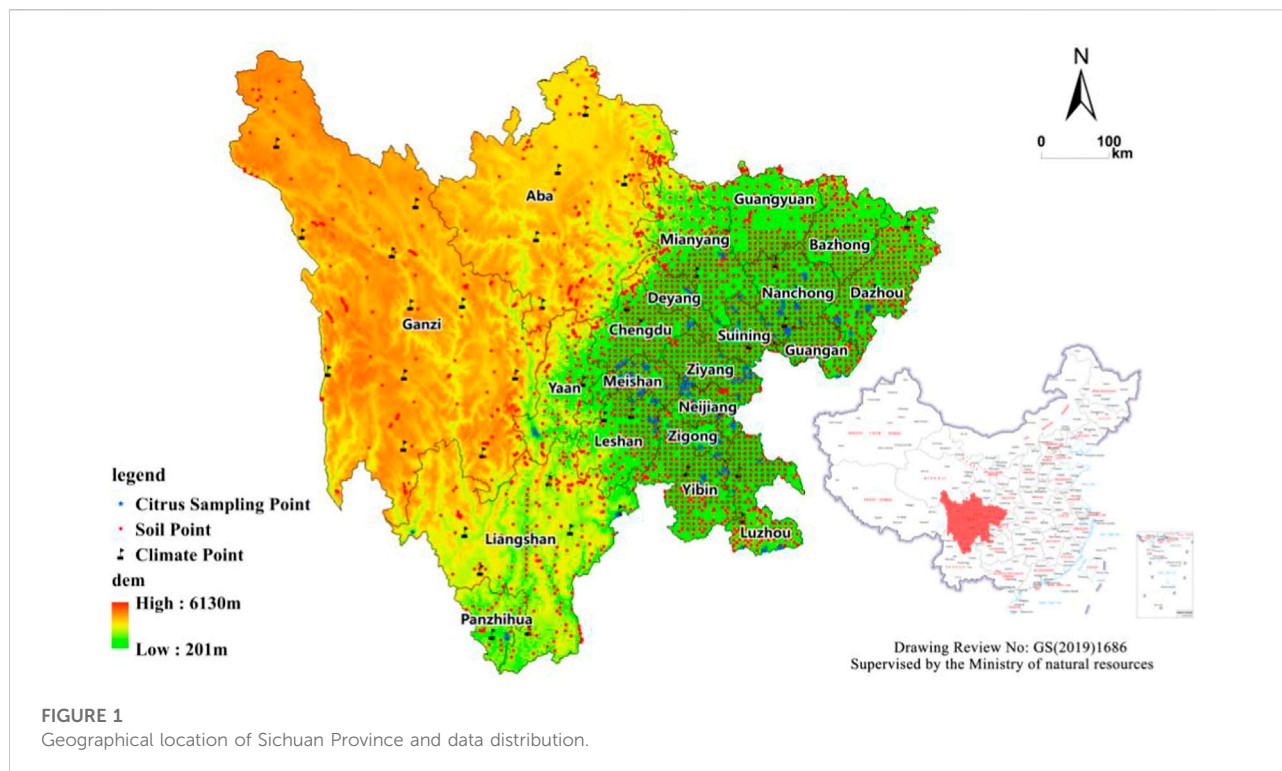
**FIGURE 1**
Geographical location of Sichuan Province and data distribution.

between the Qinghai-Tibet Plateau and the middle-lower Yangtze Plain (Figure 1). The western part is a plateau area, with an elevation of more than 4000m; The eastern part is the hilly plain area of the basin, with an elevation of 1,000–3,000 m. The climate types of Sichuan Province are diverse, including the mid-subtropical humid climate area in the basin, the subtropical semi humid climate area in the mountains of Southwest Sichuan, and the alpine climate area in the plateau of Northwest Sichuan. Since the reform and opening up, China's citrus production space has expanded rapidly, and has become the world's largest citrus producer. The planting area reached $2.83 \times 10^4 \, km^2$ in 2020 (Rural social and Economic Investigation Department of the National Bureau of statistics of China, 2021), and citrus has become an important land cover type in southern China. The citrus production in Sichuan Province has been in the forefront for a long time. In 2020, the citrus area in Sichuan reached 3,389 km². Since 2000, the production space has expanded by 1837 km²(Rural social and Economic Investigation Department of the National Bureau of statistics of China, 2021), which is a typical area of Citrus spatial expansion. At present, citrus has formed Chengdu Plain production area, South Sichuan production area and Northeast Sichuan production area in Sichuan. Compared with the production space and suitable space, the production area has far exceeded the high suitable area, and there is a reality of transferring to the middle and low suitable space. It is urgent to carry out spatial regulation, reduce the supply and demand risks faced by the citrus industry, and

promote the sustainable development of the citrus industry (Lin et al., 2019).

## 2.2 Data source and preprocessing

### 2.2.1 Data source

This study uses a large number of public data provided by national (provincial and municipal) data platforms, mainly including climate, topography, land and socio-economic data (Table 1).

### 2.2.2 Pretreatment of environmental variables

According to the existing research conclusions, 35 environmental variables of seven types affecting the distribution of citrus production were selected (Table 2) (Li and Xie, 2003; Zhang and Zhang, 2016; Su et al., 2017; Lin et al., 2019; Lin et al., 2021). Variable 1) to Variable 12) are the average annual values from 1980 to 2015 obtained from the daily meteorological data of 42 meteorological stations calculated by MATLAB (Figure 1). Variable 13) to Variable (20) are obtained by potassium dichromate volumetric method, potentiometric method, semi micro Kjeldahl method, spectrophotometry, hydrofluoric acid digestion method and hydrometer speed measurement method. Variable 24) to Variable 34) are the average value of county from 1980 to 2015 calculated by using the

TABLE 1 Datasets used in this study.

| Data name | Period | Data sources |
|---|---|---|
| Climatic data | | |
| Daily meteorological dataset of basic meteorological elements of China National Surface Weather Station | 1951–2017 | China National Meteorological Information Center (http://data.cma.cn) |
| Topographic data | | |
| Elevation (SRTM 90m) | 2000 | Resource and environment science data center of Chinese Academy of Sciences (http://www.resdc.cn) |
| Land data | | |
| Nutrient data set of soil testing and formula fertilization in Sichuan Province | 2008–2010 | Sichuan Provincial Department of agriculture and Rural Affairs |
| Land use/land cover data | 2020 | Resource and environment science data center of Chinese Academy of Sciences (http://www.resdc.cn) |
| Socio economic data | | |
| Administrative division | 2010 | National Geomatics Center of China (http://www.webmap.cn) |
| Population、GDP | 1981–2016 | Sichuan statistical yearbook |
| Road | 1981–2016 | Sichuan statistical yearbook |
| Disposable income of residents | 1981–2016 | Sichuan statistical yearbook |
| Area and output (Citrus, Grain) | 1981–2016 | Sichuan Rural Statistical Yearbook |
| Pesticides | 1981–2016 | Sichuan Agricultural statistical yearbook |
| Fertilizer | 1981–2016 | Sichuan Agricultural statistical yearbook |
| Rural laborers | 1981–2016 | Sichuan Agricultural statistical yearbook |
| Effective irrigation area | 1981–2016 | Sichuan Agricultural statistical yearbook |
| Distribution data | | |
| Global Biodiversity Information Facility | | http://www.gbif.org |

corresponding formula. The time smoothing method is used to supplement the missing data in a few counties. Variabl 35) is a dummy variable, 51 counties that implement industrial support policies are 1, and the rest are 0. The administrative divisions of Sichuan Province have been adjusted for many times. In order to ensure the consistency of data, the administrative boundaries in 2010 are taken as the benchmark and merged into 181 counties. Using ArcGIS 10.2 software to unify the boundary of all environmental variables, the coordinate system was WGS_1984_UTM_Zone_48N, the resolution was 1 km × 1 km, and data were converted to the ASCII format required by MaxEnt software.

### 2.2.3 Distribution data processing

There are two sources of Citrus distribution data. The longitude and latitude of the main citrus producing areas in Sichuan were obtained by handheld GPS positioning. Other distribution data are queried and supplemented by the Global Biodiversity Information Facility (http://www.gbif.org), and invalid records and duplicate records are removed. Sampling bias will lead to MaxEnt over fitting, thereby reducing the prediction ability of the model (Phillips et al., 2009). In this study, SDMtoolbox was used for spatial screening of sampling points, and one distribution point was reserved in 1 km × 1 km pixels, and 191 sampling points were finally obtained (Figure 1).

## 3 Research methods

### 3.1 Method framework

#### 3.1.1 Probability model

CSSM simulates citrus production space with distribution probability, and MaxEnt is an important model tool of CSSM. The maximum entropy model is a mathematical method for unbiased inference of unknown distribution based on limited known information. The theory holds that, without external force, things always strive for the maximum freedom under constraint conditions. Under known conditions, things with the maximum entropy are most likely to be close to their true state (Jaynes, 1957). MaxEnt model requires two types of data. The first is the geographical location of known crop distribution, which is expressed in the form of longitude and latitude coordinates. The second is the environmental variable within the predicted spatial range (Phillips et al., 2006). The distribution of crops is affected by environmental variables. In the sample data set composed of environmental variables and crop distribution, the introduction of environmental variables will affect the distribution probability and amount of information. MaxEnt model obtains the prediction model according to the geographical coordinates of the known distribution points of species and the environmental variables of the species distribution area, and then uses the optimal model to simulate the possible distribution of the target species in the

TABLE 2 Calculation formula and raster processing of environment variables.

| No | Type | Variable | Calculation formula | Raster processing |
|---|---|---|---|---|
| 1 | Climate | Annual sunshine hours | Sum of daily sunshine hours | IDW |
| 2 | | Annual average temperature | (Sum of daily average temperature) ÷ (Days) | MR + Residual IDW |
| 3 | | Florescence average temperature | (Sum of daily average temperature from April to may) ÷ (Days) | MR + Residual IDW |
| 4 | | Average temperature in July | (Sum of daily average temperature in July) ÷ (Days) | MR + Residual IDW |
| 5 | | Average temperature in January | (Sum of daily average temperature in January) ÷ (Days) | MR + Residual IDW |
| 6 | | Annual temperature range | (Average temperature in July)—(average temperature in January) | IDW |
| 7 | | ≥0 °C accumulated temperature | the sum of daily mean temperatures above 0 °C in 1 year | MR + Residual IDW |
| 8 | | ≥10 °C accumulated temperature | the sum of daily mean temperatures above 10 °C in 1 year | MR + Residual IDW |
| 9 | | summer ≥38 °C duration days | Cumulative days with the highest temperature ≥38 °C from July to September | IDW |
| 10 | | Frost free period | Days between the last frost day and the first frost day | IDW |
| 11 | | Annual precipitation | Sum of daily precipitation | Ordinary kriging |
| 12 | | Annual average air humidity | (Sum of daily air humidity) ÷ (Days) | MR + Residual IDW |
| 13 | Soil | Organic matter | Potassium dichromate volumetric method | Ordinary kriging |
| 14 | | pH | Potentiometric determination | Ordinary kriging |
| 15 | | Total N | Semi micro Kjeldahl method | Ordinary kriging |
| 16 | | Total P | Spectrophotometry | Ordinary kriging |
| 17 | | Total k | Hydrofluoric acid digestion method | Ordinary kriging |
| 18 | | Clay | Hydrometer speed measurement method | Ordinary kriging |
| 19 | | Silt | Hydrometer speed measurement method | Ordinary kriging |
| 20 | | Sand | Hydrometer speed measurement method | Ordinary kriging |
| 21 | Topography | Slope | — | Spatial Analyst Tools |
| 22 | | aspect | — | Spatial Analyst Tools |
| 23 | | elevation | — | Spatial Analyst Tools |
| 24 | Production | Land input | (Citrus area) ÷ (Agricultural land area) | Feature To Raster |
| 25 | | Labor input | Labor input × (Citrus area) ÷ (Agricultural land area) | Feature To Raster |
| 26 | | Fertilizer input | Fertilizer input× (Citrus area) ÷ (Agricultural land area) | Feature To Raster |
| 27 | | Pesticide input | Pesticide input× (Citrus area) ÷ (Agricultural land area) | Feature To Raster |
| 28 | | Irrigation input | Irrigation input× (Citrus area) ÷ (Agricultural land area) | Feature To Raster |
| 29 | Economics | Urbanization | (total population - rural population) ÷ Total population | Feature To Raster |
| 30 | | Economic feedback | (Output value of secondary and third industry)÷(Total output value) | Feature To Raster |
| 31 | | Food security | (Grain output)÷ (Total population) | Feature To Raster |
| 32 | Market | Traffic | (Highway mileage) ÷ (Total area) | Feature To Raster |
| 33 | | consumption | Disposable income of urban residents | Feature To Raster |
| 34 | Sociology | technical progress | (Citrus yield) ÷ (Citrus area) | Feature To Raster |
| 35 | | Policy | The county implementing the supporting policy is 1, otherwise it is 0 | Feature To Raster |

MR: multiple regression; IDW: inverse distance weighting.

target area, and selects the distribution with the largest entropy from the distribution that meets the conditions as the optimal distribution (Elith et al., 2006; Phillips et al., 2006; Merow et al., 2013). The maximum entropy algorithm is a constrained optimization algorithm, which is simply described as: when the output of $x$ is known to be $y$, for the given training data set and characteristic function $f_i(x, y)$, where $i = 1,2,..., n$, MaxEnt solves the equation as follows (Yang et al., 2022):
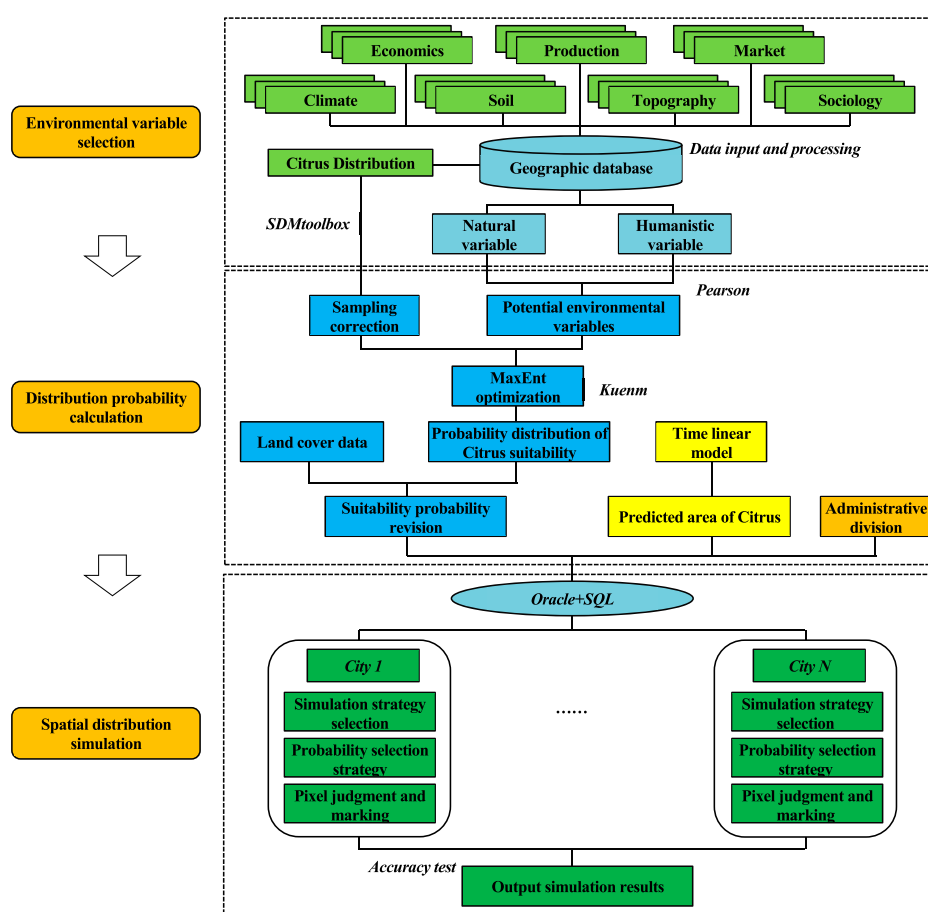
**FIGURE 2**
Research framework of CSSM.

$$\max_{pec} H(P) = -\sum_{x,y} \tilde{P}(x)P(y|x)logP(y|x),$$
$$s.t. E_P(f_i) = E_{\tilde{P}}(f_i), i = 1, 2, \cdots, n, \qquad (1)$$
$$\sum_y P(y|x) = 1,$$

Where $H(P)$ is the conditional entropy, $P(y|x)$ is the conditional probability distribution assumption, $\tilde{P}(x)$ is the empirical distribution, and $E_P(f_i)$ represents the expectation of the characteristic function of the empirical distribution. Lagrangian multiplier method is used to transform the original constrained optimization problem into a dual unconstrained optimization problem.

### 3.1.2 Main steps

CSSM includes three steps: environmental variable selection, distribution probability calculation, and spatial distribution simulation (Figure 2). The first step is to use ArcGIS to unify the data structure, spatial resolution and geographic coordinates of various environmental variables, and establish a geographic

information database. Then, Pearson correlation analysis was carried out on environmental variables to screen out the potential environmental variables that drive the spatial changes of citrus production. The second step is to calculate the distribution probability of citrus on the basis of MaxEnt parameter optimization, and revise it with land cover data. Use the prediction model to obtain the future citrus planting area. The third step is to select the simulation strategy according to the discrimination conditions to judge and mark the pixels suitable for citrus production one by one. When the threshold is reached, stop labeling, output all labeled pixels, and get the most suitable citrus production space. This step is implemented by SQL and Oracle.

## 3.2 Environment variable selection

In order to avoid the error caused by the over fitting of the model caused by the multicollinearity of environmental variables, and to retain the ecological significance of different

TABLE 3 Potential environmental variables affecting the spatial distribution of citrus production.

| Type | Potential environment variable | Code | Factor meaning |
|---|---|---|---|
| Climate | Annual sunshine hours | Sun | Sunshine is conducive to the growth of branches, leaves and flower buds, and improves the fruit setting rate, fruit coloring and acidity. Suitable threshold: 1200–1500 h |
| | Annual average temperature | Ta | Citrus likes warm and humid climate, and temperature is the decisive factor of Citrus Distribution and growth. Suitable threshold: 16.5°C–23 °C |
| | Annual temperature range | Tad | Too high or too low is not conducive to citrus production, so Tad is used to evaluate the average temperature change range |
| | summer ≥38 °C duration days | Sta38d | When the temperature is higher than 38 °C, high temperature heat damage occurs, and the growth of citrus trees stops completely |
| | Annual precipitation | Pre | The uneven distribution of rainfall in Sichuan Province has a great impact on the growth and quality of citrus, and the appropriate threshold is 1,000–2000 mm |
| Soil | Organic matter | Om | Improve the physical and chemical properties of soil and affect the yield and quality of citrus |
| | pH | Ph | PH affects the dissolution of mineral nutrients, and the appropriate threshold is 5–6.5 |
| | Total P | Tk | Phosphorus can reduce fruit acidity and improve solid acid ratio |
| | Total k | Tk | Potassium can increase single fruit weight and soluble solid content, and reduce fruit cracking |
| | Clay | Clay | Affect soil porosity, change soil water and gas content, and indirectly affect citrus growth |
| | Silt | Silt | Affect soil porosity, change soil water and gas content, and indirectly affect citrus growth |
| Topography | Slope | Slope | The drainage and ventilation of hillside land are good, and it is easy to form an inversion layer, which is conducive to the growth of citrus |
| | Aspect | Aspect | Aspect affects citrus yield and quality through light and precipitation |
| | Elevation | Dem | Elevation affects citrus growth through temperature |
| Production | Labor input | Lab | Reflect the situation of Citrus workers in the county |
| | Fertilizer input | Fer | Reflect the fertilization of Citrus in the county |
| | Pesticide input | Pes | Reflect the pesticide application of Citrus in the county |
| Economics | Urbanization | Ur | Reflect the land and labor environment faced by county citrus production |
| | Economic feedback | Neo | Reflect the supporting capacity of county economy for citrus production |
| | Food security | Gra | Reflect farmers' land selection behavior in the decision-making of planting grain or citrus |
| Market | Traffic | Traf | Reflect the market circulation of Citrus in the county |
| | Consumption | Cons | Reflect the willingness and ability of Citrus consumption |
| Sociology | Technical progress | Sci | Reflect the popularity of advanced technology and varieties of citrus |
| | Policy | Pol | Reflect the impact of industrial policies on citrus production |

types of variables on the distribution of citrus as much as possible (Elith et al., 2011), this study conducted Pearson on the same type of environmental variables, and retained the variables with R < 0.75. Among the variables with R > 0.75, select a variable closely related to citrus distribution or convenient for model interpretation to participate in the prediction. Finally, 24 variables were identified as potential environmental variables (Table 3).

## 3.3 Distribution probability calculation

### 3.3.1 Model optimization

The parameter optimization of MaxEnt helps to improve the prediction accuracy of the model. The most important parameters

are feature class (FC) and regulation multiplier (RM) (Radosavljevic and Anderson, 2014). MaxEnt provides five feature types: linear (L), quadratic (Q), hinge (H), product (P), and threshold (T), which can produce 31 feature class. RM parameter is set to 0.1–4, with an increase of 0.1 each time, a total of 40 regulation multiplier. Kuenm toolkit of R is used to optimize 1,240 parameter combinations. Among all candidate combinations, select the parameter combination with statistical significance, omission rate ≤5%, and delta. AICc = 0 for modeling (Warren and Seifert, 2011). The results show that the parameter combination when FC = h and RM = 4 is the optimal model. MaxEnt settings are as follows: ① sampling points are randomly divided into training samples (75%) and verification samples (25%). ② Select random seed. ③ The repetition type is subsample. ④ Take the average of 10 calculations as the final result.
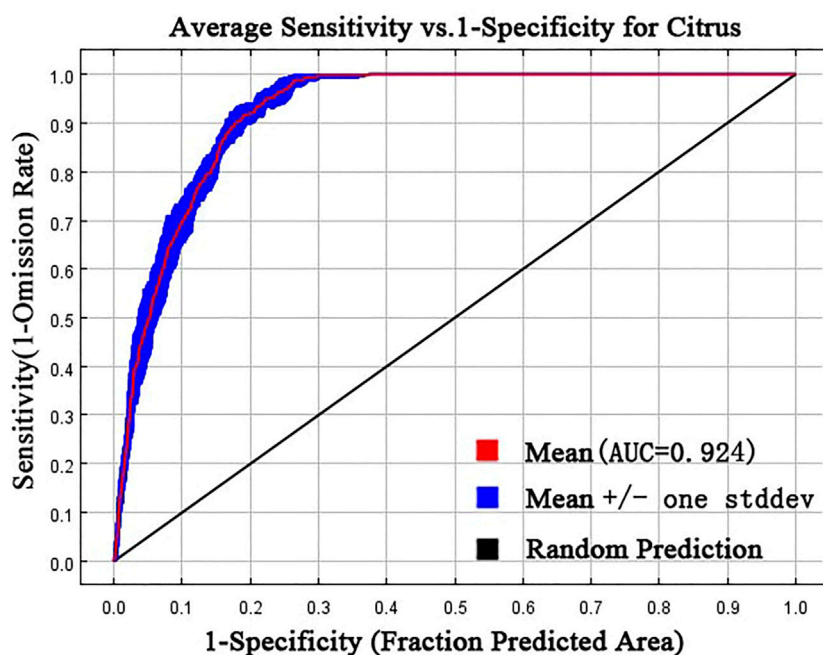
**FIGURE 3**
ROC curve and AUC value of MaxEnt.

### 3.3.2 Model accuracy

The MaxEnt model uses the receiver operating characteristic (ROC) curve to evaluate the accuracy of the analysis results for fitness area. The ROC curve takes the false positive rate as the abscissa and the true positive rate as the ordinate. The area value enclosed by the curve and abscissa is area under curve (AUC), and an AUC value between 0.5 and 0.6 is unqualified, 0.6–0.7 poor, 0.7–0.8 fair, 0.8–0.9 good, and 0.9–1.0 excellent. (Swets, 1988). The closer the AUC was to 1, the better the model performance was. In this study, the average AUC of 10 repeated runs is 0.924, and the standard deviation is 0.008 (Figure 3), indicating that the accuracy of the model is reliable.

### 3.3.3 Probability revision

The result of MaxEnt is the suitable distribution probability (P), and P range is 0–1. The closer the $p$-value is to 1, the more suitable the citrus production distribution is (Ma and Sun, 2018). Limited by land cover, the distribution probability results need to be revised according to the land cover type, and the probability distributed in water, construction land, grassland and unused land should be deleted.

## 3.4 Spatial distribution simulation

### 3.4.1 Area prediction

In the future, whether citrus in Sichuan Province will show spatial expansion or spatial contraction is facing great

uncertainty. Different research results show different development expectations. The Sichuan provincial government has formulated the citrus industry development plan and proposed to maintain the citrus area at 3333 km$^2$ by 2025. According to this calculation, the average annual growth rate of Citrus area in Sichuan must reach 3.26%. The research results of China's Agricultural Outlook report (2020–2029) show that the expansion of China's fruit planting area is limited in the next 10 years, with an average annual growth rate of about 0.77% (Market early warning Expert Committee of the Ministry of agriculture and rural, 2020). Wang (Wang and Qi, 2018) used the panel data from 2005 to 2015 to quantitatively calculate the comparative advantage index of the main citrus producing areas in China. The results showed that the citrus advantage in Sichuan was in a downward trend, with a growth rate of -0.79% to -2.78%. According to the above conclusions, this study takes 2020 as the base year, and sets four scenarios of average annual growth rate, positive high growth (3.26%), positive low growth (0.77%), negative low growth (-0.79%), negative high growth (-2.78%), using a time linear model to predict the citrus planting area in Sichuan Province in 2025 (Table 4).

### 3.4.2 Model strategy

Taking the provincial predicted area ($Q_y$), provincial suitable area ($Q_x$), municipal predicted area ($S_{n,y}$) and municipal suitable area ($S_{n,x}$) as the discrimination conditions, four simulation strategies are set (Figure 4). The discriminant condition and

TABLE 4 Predicted area of Citrus in Sichuan Province under different scene in 2025.

| City | Planting area in 2020 (km$^2$) | Predicted area in 2025 (km$^2$) | | | |
|---|---|---|---|---|---|
| | | Positive low growth | Positive high growth | Negative low growth | Negative high growth |
| Chengdu | 336.80 | 349.97 | 395.40 | 323.70 | 292.52 |
| Zigong | 187.80 | 195.14 | 220.47 | 180.50 | 163.11 |
| Panzhihua | 3.50 | 3.64 | 4.11 | 3.36 | 3.04 |
| Luzhou | 161.50 | 167.81 | 189.60 | 155.22 | 140.27 |
| Deyang | 50.10 | 52.06 | 58.82 | 48.15 | 43.51 |
| Mianyang | 72.50 | 75.33 | 85.11 | 69.68 | 62.97 |
| Guangyuan | 27.10 | 28.16 | 31.81 | 26.05 | 23.54 |
| Suining | 26.50 | 27.54 | 31.11 | 25.47 | 23.02 |
| Neijiang | 250.80 | 260.61 | 294.43 | 241.05 | 217.82 |
| Leshan | 125.60 | 130.51 | 147.45 | 120.72 | 109.09 |
| Nanchong | 341.50 | 354.85 | 400.91 | 328.22 | 296.60 |
| Meishan | 600.80 | 624.29 | 705.33 | 577.44 | 521.80 |
| Yibing | 303.50 | 315.37 | 356.30 | 291.70 | 263.59 |
| Guangan | 129.60 | 134.67 | 152.15 | 124.56 | 112.56 |
| Dazhou | 177.10 | 184.02 | 207.91 | 170.21 | 153.81 |
| Yaan | 45.40 | 47.18 | 53.30 | 43.63 | 39.43 |
| Bazhong | 37.80 | 39.28 | 44.38 | 36.33 | 32.83 |
| Ziyang | 471.50 | 489.93 | 553.53 | 453.17 | 409.51 |
| Aba | 0.00 | 0.00 | 0.00 | 0.00 | 0.00 |
| Ganzi | 1.20 | 1.25 | 1.41 | 1.15 | 1.04 |
| Liangshan | 38.50 | 40.01 | 45.20 | 37.00 | 33.44 |
| Total | 3,389.10 | 3,521.61 | 3,978.73 | 3,257.33 | 2,943.49 |

simulation strategy are implemented by Oracle and SQL. Before discrimination, the suitable probability raster is converted into points, and then spatially connected with the municipal administrative division data, so as to obtain the city name, distribution probability and predicted area fields of each point, and import them into Oracle to establish a table file. Select the corresponding strategy to store the table file according to the discrimination conditions. The simulation process of the four strategies is as follows: Strategy 1: ① take the city as the unit, sort the raster pixels one by one according to the probability from high to low. ② Take $S_{n,x}$ as the threshold, mark the raster pixels one by one according to the probability from high to low, until all raster pixels are marked, and the simulation ends. Strategy 2: ① refer to step 1 of strategy 1. ② For cities with $S_{n,y} < S_{n,x}$, take $S_{n,y}$ as the threshold, mark the suitable raster pixels one by one according to the probability from high to low, until the marked raster pixels area is greater than or equal to $S_{n,y}$, and repeat the simulation until (n-m) cities are simulated. ③ For cities with $S_{n,y} \geq S_{n,x}$, first refer to step 2 of strategy one; Secondly, calculate the difference ($S_m$) between the predicted area and the suitable area, and take it as the threshold, mark the suitable raster pixels that have not been marked one by one within the provincial scope according to the probability from high to low, until the
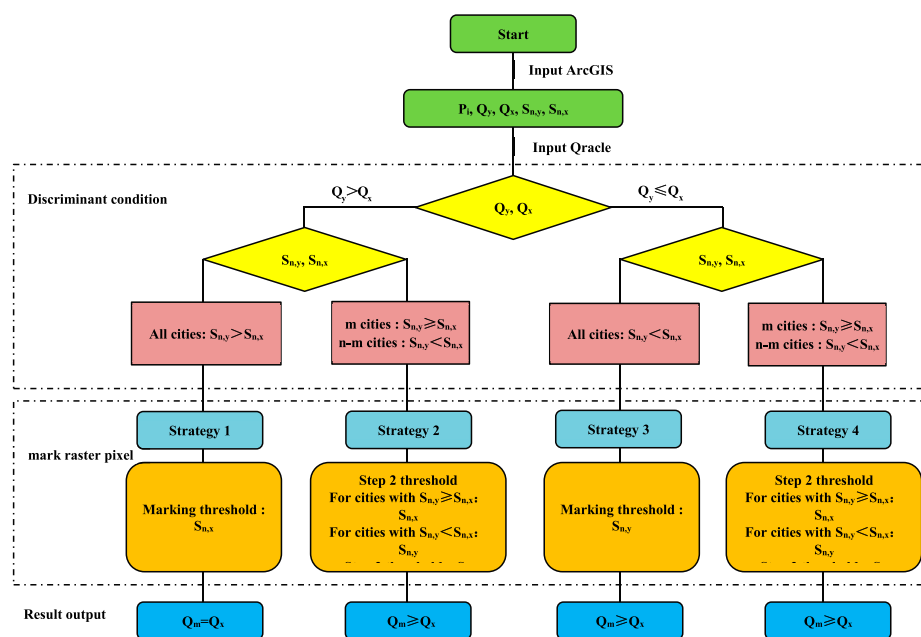
marked suitable raster pixels area is greater than or equal to $S_m$, and end the simulation. Strategy 3: ① refer to step 1 of strategy 1. ② Take $S_{n,y}$ as the threshold, mark the suitable raster pixels one by one according to the probability from high to low, until the area of the marked suitable raster pixels is greater than or equal to $S_{n,y}$, and the simulation ends after all city simulations are completed. Strategy 4: refer to strategy 2.

$Q_y$ is the provincial predicted area. $Q_x$ is provincial suitable area. $Q_m$ is the provincial simulated area. $S_{n,y}$ is the predicted area of city n. $S_{n,x}$ is the suitable area of the city n. n is the number of cities. m is the number of cities with $S_{n,y} \geq S_{n,x}$. n-m is the number of cities with $S_{n,y} < S_{n,x}$. $S_m$ is the sum of the difference between the predicted area and the suitable area of all city with $S_{n,y} \geq S_{n,x}$

# 4 Results and analysis

## 4.1 Analysis of environmental variables

The contribution of 24 potential environmental variables to the distribution of citrus production is calculated according to the Jackknife method (Table 5). The percent contribution (PC) of pesticide input (pes, 62.1%), fertilizer input (fer, 14.26%), policy

**FIGURE 4**
Discrimination conditions and thresholds of strategies.

(pol, 6.93%), annual average temperature (ta, 5.56%) and labor input (lab, 4.06%) ranked in the top 5, with a cumulative contribution rate of 92.91%. The permutation importance (PI) of annual average temperature (ta, 46.88%), pesticide input (pes, 29.32%), aspect (aspect, 8.44%), technical progress (sci, 4.89%) and fertilizer input (fer, 4.46%) ranked in the top 5, with a cumulative contribution rate of 93.99%. In the regularization training gain (RTGO) using this factor alone, the average annual temperature (ta) and pesticide input (pes) are 1.2, and the elevation (dem), fertilizer input (fer) and labor input (lab) are 1.19, 1.18 and 1.16 respectively, indicating that these environmental variables have more effective information than other variables. Therefore, the main environmental variables that affect the distribution of citrus production are production factors (pesticide input, fertilizer input, labor input), social factors (policy, technological progress), climate factors (annual average temperature), topography factors (aspect, elevation). The response curve of environmental factors can further clarify the relationship between Citrus Distribution Probability and environmental variables. It is generally believed that when the distribution probability is >0.5, the corresponding environmental variable value is conducive to species distribution (Wang et al., 2020). Natural environment suitable for citrus production in Sichuan Province is (Figure 5): elevation ≤500m, annual average temperature ≥16.5 °C, and the aspect is relatively suitable in Northeast, Southwest and

Northwest. Human environment suitable for distribution is: with the support of citrus policy, the input of citrus fertilizer in the county is ≥ 500t, the input of citrus labor in the county is ≥ 5,000, the input of citrus pesticides in the county is ≥ 12.5t, and the technical progress represented by unit yield is 750–7000 t/km$^2$.

## 4.2 Citrus distribution probability in sichuan

According to the land use/land cover classification system monitored by remote sensing in China (Liu and Buhe, 2000), China's land use control policies and citrus planting habits in Sichuan Province, citrus production can only be in garden and dryland. Therefore, retain the probability of distribution on garden and dryland, and eliminate the probability of distribution on paddy field, grassland, water, unused land and urban and rural (industrial and mining, residential) construction land, and finally obtain the probability of Citrus Distribution in Sichuan Province (Figure 6). The number of pixels of citrus distribution probability is 77,906, including 34,360 pixels with $p < 0.3$, 20,520 pixels with P (0.3–0.5), 21,863 pixels with P (0.5–0.7), 1,163 pixels with $p > 0.7$, the minimum value is 0.003, and the maximum value is 0.893.

TABLE 5 Various parameters of the main environmental variables of Citrus.

| Code | PC/% | PI/% | RTGO | RTGW | TGo | TGw | AUCo | AUCw |
|---|---|---|---|---|---|---|---|---|
| pes | 62.1 | 29.32 | 1.20 | 1.40 | 1.34 | 1.56 | 0.90 | 0.92 |
| fer | 14.26 | 4.46 | 1.18 | 1.41 | 1.34 | 1.54 | 0.90 | 0.92 |
| pol | 6.93 | 1.26 | 0.70 | 1.41 | 0.96 | 1.54 | 0.82 | 0.92 |
| ta | 5.56 | 46.88 | 1.20 | 1.35 | 1.35 | 1.52 | 0.90 | 0.92 |
| lab | 4.06 | 1.92 | 1.16 | 1.42 | 1.31 | 1.56 | 0.90 | 0.92 |
| slope | 3.90 | 0.75 | 0.70 | 1.42 | 0.87 | 1.56 | 0.85 | 0.92 |
| aspect | 1.51 | 8.44 | 0.03 | 1.40 | 0.02 | 1.55 | 0.52 | 0.92 |
| dem | 0.70 | 0.00 | 1.19 | 1.42 | 1.33 | 1.56 | 0.90 | 0.92 |
| sci | 0.49 | 4.89 | 0.58 | 1.41 | 0.64 | 1.55 | 0.77 | 0.92 |
| cons | 0.35 | 0.09 | 0.03 | 1.42 | 0.12 | 1.55 | 0.68 | 0.92 |
| pre | 0.05 | 0.95 | 0.58 | 1.42 | 0.68 | 1.55 | 0.79 | 0.92 |
| om | 0.04 | 0.35 | 0.78 | 1.42 | 0.83 | 1.56 | 0.81 | 0.92 |
| tp | 0.02 | 0.47 | 0.43 | 1.42 | 0.67 | 1.56 | 0.82 | 0.92 |
| clay | 0.01 | 0.11 | 0.45 | 1.42 | 0.56 | 1.56 | 0.81 | 0.92 |
| pH | 0.01 | 0.02 | 0.17 | 1.42 | 0.21 | 1.56 | 0.72 | 0.92 |
| gra | 0.00 | 0.00 | 0.29 | 1.42 | 0.38 | 1.56 | 0.74 | 0.92 |
| neo | 0.00 | 0.09 | 0.16 | 1.42 | 0.21 | 1.56 | 0.64 | 0.92 |
| silt | 0.00 | 0.00 | 0.02 | 1.42 | 0.05 | 1.56 | 0.57 | 0.92 |
| sta38days | 0.00 | 0.00 | 0.74 | 1.42 | 0.82 | 1.56 | 0.83 | 0.92 |
| sun | 0.00 | 0.00 | 0.83 | 1.42 | 1.10 | 1.56 | 0.88 | 0.92 |
| tad | 0.00 | 0.01 | 0.21 | 1.42 | 0.28 | 1.56 | 0.71 | 0.92 |
| tk | 0.00 | 0.00 | 0.06 | 1.42 | 0.09 | 1.56 | 0.54 | 0.92 |
| traf | 0.00 | 0.00 | 0.87 | 1.42 | 0.98 | 1.56 | 0.86 | 0.92 |
| ur | 0.00 | 0.00 | 0.01 | 1.42 | 0.02 | 1.56 | 0.57 | 0.92 |

PC, is percent contribution; PI, is permutation importance; RTGO, is the regularization training gain using the factor alone; RTGW, is the regularization training gain using other factors; TGw, is the test gain using other factors; TGO, is the test gain using the factor alone; AUCo, is the area under the working characteristic curve of the subjects using the variable alone; AUCw, is the area under the receiver operating characteristic curve using other factors.

Most areas of Sichuan province are unsuitable areas ($p < 0.3$), low suitable areas ($0.30 \leq p < 0.50$) are mainly distributed in Suining, Deyang and Mianyang, medium suitable areas ($0.50 \leq p < 0.70$) are distributed in Neijiang, Meishan, Ziyang, Nanchong, Zigong, Yibin and Guang'an, and high suitable areas ($p > 0.7$) are in Neijiang, Ziyang and the south of Nanchong. In addition, in Dazhou and Zigong, high suitability areas are scattered.

## 4.3 Spatial regulation of citrus production in sichuan

In this study, the predicted area of Citrus in Sichuan Province in 2025 is less than the appropriate grid area of Citrus ($Qy \leq Qx$), and the predicted area of all cities is less than the appropriate grid area of Citrus ($Sn,y < Sn,x$), so Strategy three simulation is selected. The spatial pattern of citrus production in the four scenarios is similar. The production space is concentrated in Central Sichuan, relatively concentrated in Meishan, Ziyang, Neijiang,

Chengdu, Nanchong and Yibin, and scattered in Deyang, Mianyang, Dazhou, Luzhou, Leshan, Liangshan and Panzhihua (Figure 7). In different scenarios, the relative error between the simulated area and the predicted area of citrus production space is 0.28%–0.39%.

Using ArcGIS spatial analyst statistics, the spatial simulation data of citrus production in each city are obtained (Table 6). In the positive low growth scenario, the citrus planting area in Sichuan will reach 3533 km² in 2025, an increase of 143.90 km² compared with 2020, and the total spatial expansion will increase by about 4.25%. Meishan (24.20 km²) is the only city with an increase of more than 20km², and five cities with an increase of 10–20 km² are Ziyang (18.5 km²), Nanchong (13.50 km²), Chengdu (13.20 km²), Yibin (12.50 km²) and Neijiang (10.20 km²). In the positive high growth scenario, the citrus production area in Sichuan in 2025 was 3990km², an increase of 600.90 km² compared with 2020, and the total spatial expansion increased by 17.73%. There are 11 cities with an increase of more than 20km², of which Meishan has the largest increase (105.20 km²). In the negative low growth scenario, the
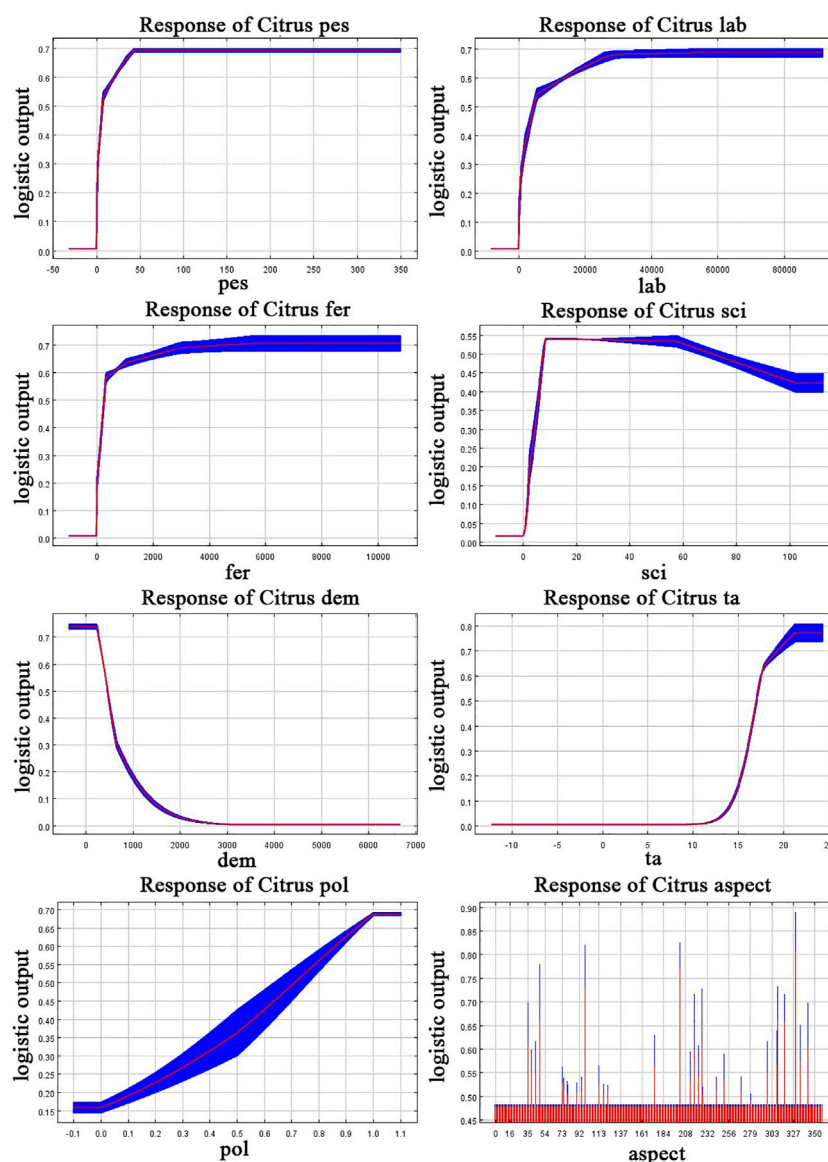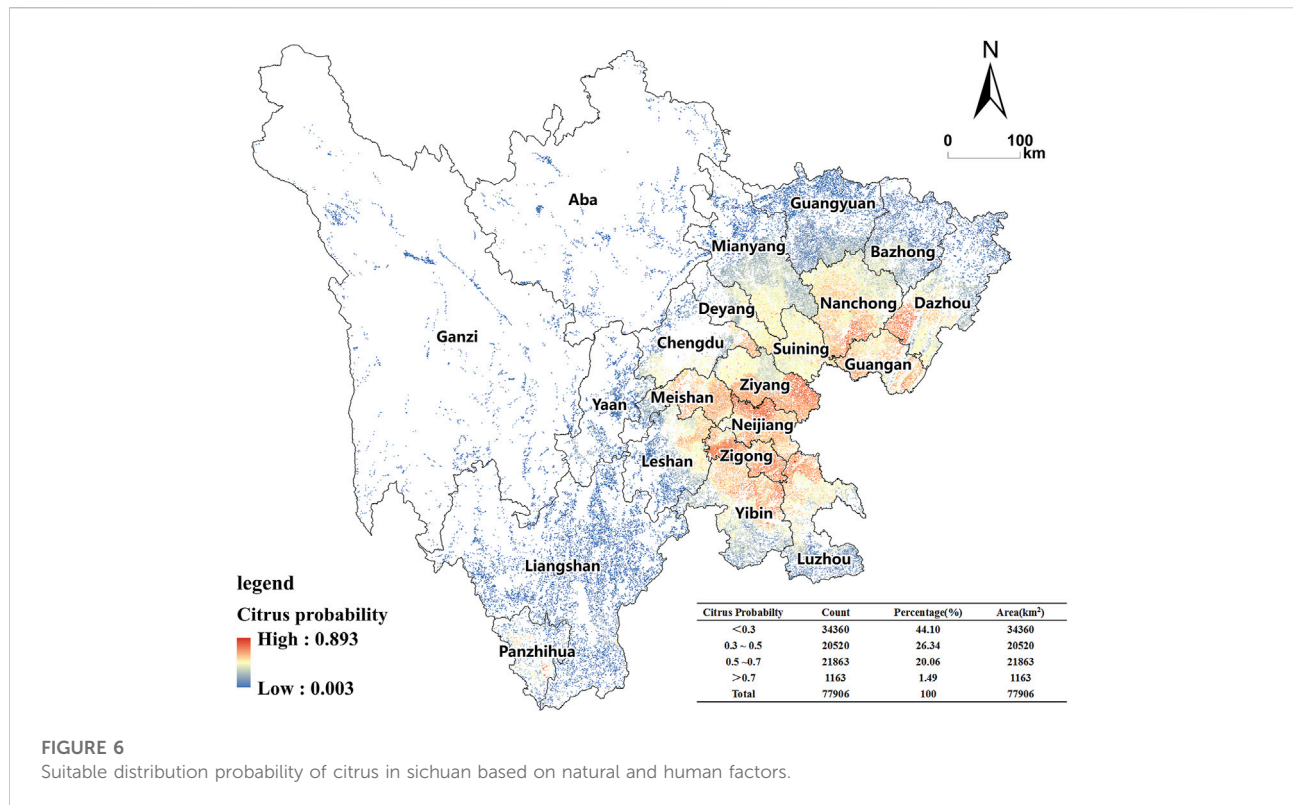
**FIGURE 5**
Response curves of existence probability of Citrus.

citrus production area in Sichuan will be 3270 km² in 2025, a decrease of 119.10 km² compared with 2020, and the total space needs to be reduced by 3.51%. Only Meishan (22.80 km²) has a reduction of more than 20km², and there are four cities with a reduction of 10–20km², which are Ziyang (17.50 km²), Chengdu (12.80 km²), Nanchong (12.50 km²) and Yibin (11.50 km²). In the scenario of negative high growth, the citrus planting area in Sichuan will reach 2954 km² in 2025, which will be reduced by 435.10 km² compared with 2020. There are nine cities with a reduction of more than 20km², of which Meishan has the largest reduction (78.80 km²).

# 5 Discussion

## 5.1 Applicability of MaxEnt model

MaxEnt model is a highly complex machine learning model. Like other distribution models, the basic assumption of modeling is that the study area has undergone systematic or random unbiased sampling (Phillips et al., 2009). However, samples are often taken from easily accessible areas, such as along roads and rivers, orchards and farms. Therefore, due to the influence of sampling deviation, AUC may overestimate the ability to evaluate the model (Veloz, 2009). 87% of the

**FIGURE 6**
Suitable distribution probability of citrus in sichuan based on natural and human factors.

previous MaxEnt model studies used data that are easy to cause sampling deviation (Yackulic et al., 2013). Spatial filtering is often used to correct sampling bias, that is, only a limited number of sites are retained within a certain distance (Syfert et al., 2013; Radosavljevic and Anderson, 2014). The difficulty of spatial screening method is the setting of spatial spacing, which should be consistent with the variation degree of environmental variables on the spatial scale (Anderson, 2012; Shcheglovitova and Anderson, 2013). There are few studies on the sampling interval of citrus sample points. In the existing research on national scale and regional scale, the space spacing of 1 km² shows good accuracy (Lu et al., 2012; Yan et al., 2021). Therefore, this study refers to their method and reserves one distribution point in 1 km × 1 km pixel to reduce sampling deviation.

The MaxEnt model provides a set of default parameters for modeling. The distribution model under the default parameters is sensitive to the test data and prone to over fitting. Therefore, the optimization of model parameters is crucial to improve the prediction accuracy and reliability of results (Syfert et al., 2013). In this study, Feature Class and Regulrzation Multiplier are used to constrain the complexity of the model (Cobos et al., 2019), and the combination of parameters when AICc is 0 is selected for modeling. The results show that when AICc is the smallest, AUC value is the largest, which is consistent with Anderson's research (Anderson and Gonzalez, 2011). At the same time, in recent

research, Xian used MaxEnt model to simulate the spatial distribution of citrus based on nine environmental factors, with AUC values ranging from 0.888 to 0.973 (Xian et al., 2022). The average AUC of this study is 0.924 ± 0.008, which is similar to that of the study, indicating good model performance.

## 5.2 Dominant environmental variables

The results show that elevation, annual average temperature and aspect are important natural factors affecting citrus production in Sichuan. This finding is basically consistent with Tercan's research results. Based on ArcGIS multi criteria evaluation spatial decision support system, Tercan found that temperature is the most important variable affecting citrus production and distribution in Antalya province of Turkey, followed by elevation (Tercana and Dereli, 2020). Mokarram's research on the suitability of citrus land in Fars Province Iran, also shows that temperature, elevation and aspect are important factors affecting the distribution of citrus production (Mokarram and Mirsoleimani, 2018). In this study, soil had little influence on citrus distribution, with PC and PI tending to 0 and RTGO less than 1. However, Likhar's assessment on the suitability of citrus production in Nagpur, Maharashtra, showed that soil particle structure, pH and soil fertility also significantly affected the
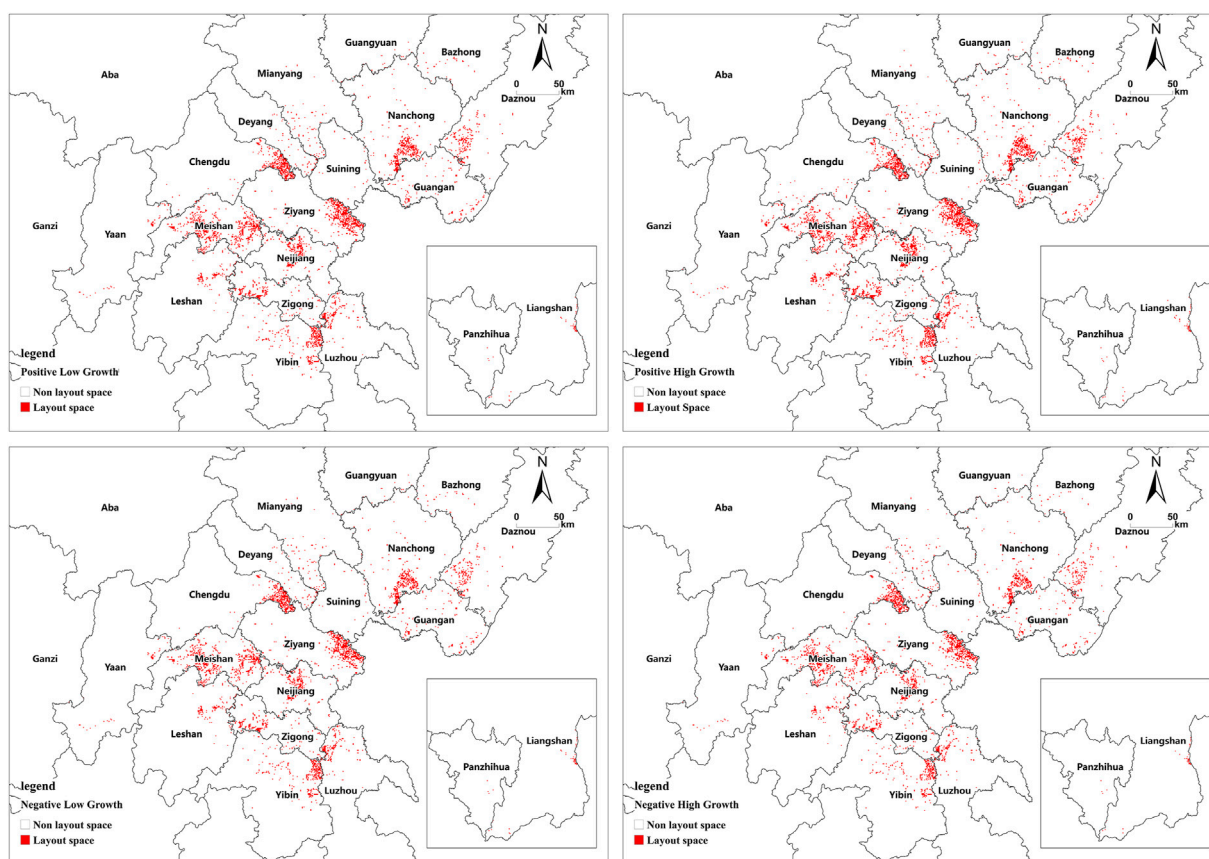
**FIGURE 7**
Simulation of spatial distribution of citrus production in Sichuan under different scenarios.

distribution of citrus production, which is different from this study (Likhar and Prasad, 2011). The reasons may be as follows: ① It may be caused by the spatial scale effect of variables. Most of the citrus distribution sampling points in this study are located in plain and hilly areas. The soil environmental variables in this area have obvious homogeneity, and their dispersion is small (Table 7). ② The production and management level of farmers in Sichuan Province has gradually improved, especially since 2005, with the promotion of soil testing and formulated fertilization technology, the spatial difference of soil variables has been reduced.

Crop production space has dual characteristics of nature and society, and is the result of interaction of many factors such as nature, economy, market and society. In the process of transformation from tradition to modernity, the constraint of natural environment on the formation of comparative advantage of crops has been greatly weakened, and the impact of economic and social activities has been increasing. In most existing studies, only climate factors are used to establish models (Kogo et al., 2019; Khalil et al., 2021; Khubaib et al., 2021), which reduces the scientificity and guidance of spatial regulation of crop production. In this study, both the natural environment and human activities are integrated into the model. The results show that the contribution rate of human activities (88.19%) is higher than that of the natural environment (11.81%), and pesticides (62.1%), fertilizers (14.26%), policy support (6.93%) and labor force (4.06%) are the top four leading environmental variables. The results show that with the support of production factors and financial policies, the constraints of natural environment on Sichuan citrus production space are decreasing, and human activities have become the dominant factor.

## 5.3 Citrus suitable space and production optimization

The research results show that the citrus suitable area in Sichuan ($p > 0.5$) covers an area of 8,549.21km², of which Zigong (1,698.13 km²), Nanchong (1,571.26 km²), Ziyang (1,211.25 km²), Neijiang (1,035.58 km²), Meishan (559.54 km²), Leshan (435.92 km²), Yibin (370.86 km²) and Luzhou (361.10 km²) are the main distribution areas. This is because

TABLE 6 Spatial regulation results of citrus production in Sichuan Province in different scenarios.

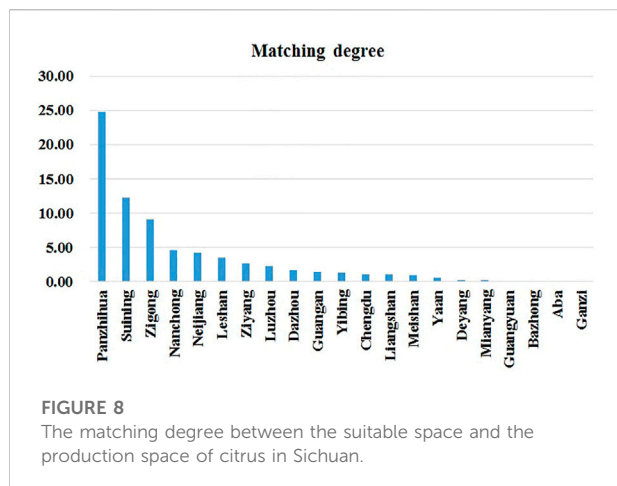| City | Positive low growth (km²) | | Positive high growth (km²) | | Negative low growth (km²) | | Negative high growth (km²) | |
|---|---|---|---|---|---|---|---|---|
| | Simulated area | Regulation quantity | Simulated area | Regulation quantity | Simulated area | Regulation quantity | Simulated area | Regulation quantity |
| Chengdu | 350.00 | 13.20 | 396.00 | 59.20 | 324.00 | (12.80) | 293.00 | (43.80) |
| Zigong | 196.00 | 8.20 | 221.00 | 33.20 | 181.00 | (6.80) | 164.00 | (23.80) |
| Panzhihua | 4.00 | 0.50 | 5.00 | 1.50 | 4.00 | 0.50 | 4.00 | 0.50 |
| Luzhou | 168.00 | 6.50 | 190.00 | 28.50 | 156.00 | (5.50) | 141.00 | (20.50) |
| Deyang | 53.00 | 2.90 | 59.00 | 8.90 | 49.00 | (1.10) | 44.00 | (6.10) |
| Mianyang | 76.00 | 3.50 | 86.00 | 13.50 | 70.00 | (2.50) | 63.00 | (9.50) |
| Guangyuan | 29.00 | 1.90 | 32.00 | 4.90 | 27.00 | (0.10) | 24.00 | (3.10) |
| Suining | 28.00 | 1.50 | 32.00 | 5.50 | 26.00 | (0.50) | 24.00 | (2.50) |
| Neijiang | 261.00 | 10.20 | 295.00 | 44.20 | 242.00 | (8.80) | 218.00 | (32.80) |
| Leshan | 131.00 | 5.40 | 148.00 | 22.40 | 121.00 | (4.60) | 110.00 | (15.60) |
| Nanchong | 355.00 | 13.50 | 401.00 | 59.50 | 329.00 | (12.50) | 297.00 | (44.50) |
| Meishan | 625.00 | 24.20 | 706.00 | 105.20 | 578.00 | (22.80) | 522.00 | (78.80) |
| Yibing | 316.00 | 12.50 | 357.00 | 53.50 | 292.00 | (11.50) | 264.00 | (39.50) |
| Guangan | 135.00 | 5.40 | 153.00 | 23.40 | 125.00 | (4.60) | 113.00 | (16.60) |
| Dazhou | 185.00 | 7.90 | 208.00 | 30.90 | 171.00 | (6.10) | 154.00 | (23.10) |
| Yaan | 48.00 | 2.60 | 54.00 | 8.60 | 44.00 | (1.40) | 40.00 | (5.40) |
| Bazhong | 40.00 | 2.20 | 45.00 | 7.20 | 37.00 | (0.80) | 33.00 | (4.80) |
| Ziyang | 490.00 | 18.50 | 554.00 | 82.50 | 454.00 | (17.50) | 410.00 | (61.50) |
| Aba | 0.00 | 0.00 | 0.00 | 0.00 | 0.00 | 0.00 | 0.00 | 0.00 |
| Ganzi | 2.00 | 0.80 | 2.00 | 0.80 | 2.00 | 0.80 | 2.00 | 0.80 |
| Liangshan | 41.00 | 2.50 | 46.00 | 7.50 | 38.00 | (0.50) | 34.00 | (4.50) |
| Total | 3,533.00 | 143.90 | 3,990.00 | 600.90 | 3,270.00 | (119.10) | 2,954.00 | (435.10) |

Brackets represent negative values.

TABLE 7 Descriptive statistics of soil environmental variables of Citrus sampling points in plain and hilly areas.

| Soil variables | Range | Minimum | Maximum | Mean | Standard deviation |
|---|---|---|---|---|---|
| Organic matter | 1891 | 1,352 | 3,243 | 1930.78 | 460.109 |
| pH | 26 | 54 | 80 | 67.81 | 7.845 |
| Total nitrogen | 91 | 84 | 175 | 120.95 | 20.697 |
| Total phosphorus | 39 | 59 | 98 | 75.08 | 9.125 |
| Total potassium | 412 | 1723 | 2,135 | 1994.09 | 100.662 |
| Clay | 37 | 36 | 73 | 50.28 | 4.220 |
| Silt | 8 | 14 | 22 | 18.15 | 1.187 |
| Sand | 35 | 11 | 46 | 31.79 | 3.443 |

the natural and social conditions in the above areas meet the requirements of citrus production. The elevation is within 1000m, the annual average temperature is 16–18 °C, the social economy is relatively developed, the rural laborers is relatively rich, and the level of fertilizer and pesticide input is high. For example, Meishan, as a typical area, has about 13.39×10⁴ workers engaged in citrus planting, and the input of chemical fertilizer

and pesticide for citrus production is $1.53 \times 10^4$t and 455.79t, and the input level of production factors is in the forefront of the province.

The optimization of crop production space is to maximize the efficiency of resource allocation and realize the transfer of agricultural production to high-yield, efficient and stable regions (Wang et al., 2018; Li et al., 2020). Driven by interests, although

FIGURE 8
The matching degree between the suitable space and the production space of citrus in Sichuan.

technological progress has reduced the constraints of the natural environment on crop production distribution, the natural environment still determines the basic space of crop distribution (Rurinda et al., 2020). This means that arbitrarily expanding the scale of crop production will inevitably increase the cost of natural transformation, leading to increased costs of agricultural products and greater pressure on the environment. Therefore, we must respect the natural environment and minimize the impact of human activities. The citrus production space in Sichuan has experienced long-term expansion, and there is a reality that it has been distributed to low suitability areas, or even unsuitable areas. The matching result between the production space and the suitable space shows (Figure 8) that the production area in Liangshan (0.99), Meishan (0.93), Ya'an (0.53), Deyang (0.13) and Mianyang (0.07) has exceeded the suitable area. The matching degree in Panzhihua (24.79), Suining (12.28), Zigong (9.04), Nanchong (4.60), Neijiang (4.13) and Leshan (3.47) is relatively large, which still has a certain potential space. At present, the development of China's citrus industry has shifted from quantity growth to quality improvement, and the growth rate of planting area has decreased. Therefore, Sichuan should not expand the citrus space scale at a high speed. It should choose a positive low growth scenario, stabilize the citrus area at 3,533 km$^2$, and focus on optimizing the citrus production space. The government should speed up the elimination and transformation of low yield, low quality and low efficiency citrus orchards, encourage companies and farmers to increase production input, improve land quality, improve water conservancy facilities, production roads and trading markets, and build standardized and large-scale citrus production bases. Strengthen the training, demonstration and promotion of new varieties and technologies. Through the optimization of production space, the main citrus production areas can be formed in Meishan, Ziyang, Neijiang, Chengdu, Nanchong, Yibin.

## 5.4 Limitations and uncertainties

Based on MaxEnt model, this study constructed the citrus spatial simulation method (CSSM), which better reflects the comprehensive effect of natural and human factors on crop space, and realizes the regulation simulation of single crop production space. However, the study found that the method is not perfect, mainly in the following aspects: ① Crop production space is affected by many factors, including crop physiological and ecological factors, as well as many complex environmental factors and human activities, such as extreme weather events, heavy metal pollution, sales prices, import and export trade, it is difficult to include all aspects of the impact in the model. ② Citrus distribution points have an impact on MaxEnt. MaxEnt calculates the suitable distribution probability, generally taking the current position as the distribution variable. When simulating the distribution of citrus production in the future, the influence of the actual distribution points in the future may be ignored, resulting in systematic errors. The longer the citrus planting time, the more prominent the path dependence of citrus planting. Therefore, when sampling the distribution of citrus in this study, try to select citrus producing areas with planting years ≥30a to reduce the impact of the actual distribution points in the future. ③The environmental variables in CSSM are all based on the average value of many years, ignoring the time change of environmental variables, which makes the prediction results of the model have certain limitations. In the next step, the predicted value of environmental variables can be used to calculate the distribution probability to improve the accuracy of the model. Despite these limitations, the CSSM method has successfully mapped the spatial distribution of citrus in Sichuan Province under four different scenarios for the first time. The results obtained have certain reference value for guiding the spatial optimization of citrus production in Sichuan Province and the adjustment of crop structure.

## 6 Conclusion

This study uses MaxEnt, ArcGIS, Oracle, SQL to build citrus spatial simulation method (CSSM) to simulate the spatial distribution of citrus production in Sichuan Province under different scenarios in 2025. The following conclusions are drawn: 1) The main environmental variables affecting the distribution of citrus production in Sichuan are production factors (pesticide input, fertilizer input, labor input), social factors (policy, technological progress), climate factors (annual average temperature), Topographic factors (aspect, elevation). 2) Driven by production factors and financial policies, the constraints of natural environment on Sichuan citrus production space are gradually reducing, and human activities play a leading and decisive role. 3) Citrus suitable space in

Sichuan are mainly distributed in Zigong, Nanchong, Ziyang, Neijiang, Meishan, Leshan, Yibin and Luzhou. 4) The government should choose a positive low growth scenario to stabilize the citrus area in Sichuan at 3533 km$^2$ in 2025. Through the optimization of production space, the main citrus production areas are formed in Meishan, Ziyang, Neijiang, Chengdu, Nanchong and Yibin.

## Data availability statement

The original contributions presented in the study are included in the article/supplementary material, further inquiries can be directed to the corresponding author.

## Author contributions

ZL, CC, YL, and GL conceived and designed the CSSM. PH, GL, and WG collected the data and analyzed the data. JC and ZS helped the language correction; ZL wrote the paper.

## Conflict of interest

The authors declare that the research was conducted in the absence of any commercial or financial relationships that could be construed as a potential conflict of interest.

## Publisher's note

All claims expressed in this article are solely those of the authors and do not necessarily represent those of their affiliated organizations, or those of the publisher, the editors and the reviewers. Any product that may be evaluated in this article, or claim that may be made by its manufacturer, is not guaranteed or endorsed by the publisher.

## References

Anderson, R. P., and Gonzalez, I, Jr. (2011). Species-specific tuning increases robustness to sampling bias in models of species distributions: An implementation with Maxent. *Ecol. Model.* 222 (15), 2796–2811. doi:10.1016/j.ecolmodel.2011.04.011

Anderson, R. P. (2012). Harnessing the world's biodiversity data: Promise and peril in ecological niche modeling of species distributions. *Ann. N. Y. Acad. Sci.* 1260, 66–80. doi:10.1111/j.1749-6632.2011.06440.x

Bagherzadeh, A., and Daneshvar, M. R. M. (2014). Qualitative land suitability evaluation for wheat and barley crops in khorasan-razavi province, northeast of Iran. *Agric. Res.* 3 (2), 155–164. doi:10.1007/s40003-014-0101-2

Beaumont, L., Hughes, L., and Poulsen, M. (2005). Predicting species distributions: Use of climatic parameters in BIOCLIM and its impact on predictions of species' current and future distributions. *Ecol. Model.* 186 (2), 251–270. doi:10.1016/j.ecolmodel.2005.01.030

Cao, Z., Zhang, L., Zhang, X., and Guo, Z. (2021). Predicting the potential distribution of hylomecon japonica in China under current and future climate change based on maxent model. *Sustainability* 13 (20), 11253. doi:10.3390/su132011253

Cobos, M. E., Peterson, A. T., Barve, N., and Osorio-Olvera, L. (2019). kuenm: an R package for detailed development of ecological niche models using Maxent. *Peerj* 7, e6281. doi:10.7717/peerj.6281

Elith, J., Graham, C. H., Anderson, R. P., Dudı´k, M., Ferrier, S., and Guisan, A. (2006). Novel methods improve prediction of species'distributions from occurrence data. *Ecography* 29 (2), 129–151. doi:10.1111/j.2006.0906-7590.04596.x

Elith, J., Phillips, S. J., Hastie, T., Dudik, M., Chee, Y. E., and Yates, C. J. (2011). A statistical explanation of MaxEnt for ecologists. *Divers. Distrib.* 17 (1), 43–57. doi:10.1111/j.1472-4642.2010.00725.x

Galletti, C. S., Ridder, E., Falconer, S. E., and Fall, P. L. (2013). Maxent modeling of ancient and modern agricultural terraces in the Troodos foothills, Cyprus. *Appl. Geogr.* 39 (4), 46–56. doi:10.1016/j.apgeog.2012.11.020

Genga, B., Zhengb, X., and Fua, M. (2017). Scenario analysis of sustainable intensive land use based on SD model. *Sustain. Cities And Soc.* 29, 193–202. doi:10.1016/j.scs.2016.12.013

Gu, C. J., Zhang, Y. L., Liu, L. S., Li, L. H., and Zhang, B. H. (2018). Comprehensive evaluation of the suitability of agricultural land in Myanmar. *J. Resour. Ecol.* 9 (6), 609–621. doi:10.5814/j.issn.1674-764x.2018.06.004

Hengl, T., Sierdsema, H., Radovic, A., and Dilo, A. (2009). Spatial prediction of species' distributions from occurrence-only records: Combining point pattern analysis, ENFA and regression-kriging. *Ecol. Model.* 220 (24), 3499–3511. doi:10.1016/j.ecolmodel.2009.06.038

Jaynes, E. T. (1957). Information theory and statistical mechanics. *Phys. Rev.* 106 (2), 620–630. doi:10.1103/PhysRev.106.620

Khalil, T., Asad, S. A., Khubaib, N., Baig, A., Atif, S., and Umar, M. (2021). Climate change and potential distribution of potato (<i&gt;Solanum tuberosum&lt;/i&gt;) crop cultivation in Pakistan using Maxent. *AIMS Agric. Food* 6 (2), 663–676. doi:10.3934/agrfood.2021039

Khubaib, N., Asad, S. A., Khalil, T., Baig, A., Atif, S., and Umar, M. (2021). Predicting areas suitable for wheat and maize cultivation under future climate change scenarios in Pakistan. *Clim. Res.* 83, 15–25. doi:10.3354/cr01631

Kogo, B. K., Kumar, L., Koech, R., and Kariyawasam, C. S. (2019). Modelling climate suitability for rainfed maize cultivation in Kenya using a maximum entropy (MaxENT) approach. *Agron. (Basel).* 9 (11), 727. doi:10.3390/agronomy9110727

Li, B., Zhang, F., Zhang, L. W., Zhang, J. F., Jin, Z. F., and Gupta, D. K. (2015). Comprehensive suitability evaluation of tea crops using GIS and a modified land ecological suitability evaluation model. *Pedosphere* 22 (1), 122–130. doi:10.1016/S1002-0160(11)60198-7

Li, E. L., Pang, A. C., and Zhu, J. G. (2012). Analysis of the evolution path and mechanism of China's agricultural agglomeration and geographic pattern. *Geogr. Research* 31, 885–898. doi:10.11821/yj2012050012

Li, M., Fu, Q., Singh, V. P., Liu, D., Li, T., and Zhou, Y. (2020). Managing agricultural water and land resources with tradeoff between economic, environmental, and social considerations: A multi-objective non-linear optimization model under uncertainty. *Agric. Syst.* 178, 102685. doi:10.1016/j.agsy.2019.102685

Li, Z. L., and Xie, D. T. (2003). A review of relationship between citrus growth and environment. *Chin. Agric. Sci. Bull.* 19, 181–189. doi:10.3969/j.issn.1000-6850.2003.06.058

Likhar, C. K., and Prasad, J. (2011). Productivity and suitability assessment of orange (Citrus reticulata)-growing soils in Nagpur. *Indian J. Agric. Sci.* 81 (6), 500–505. doi:10.5958/0974-0228.2016.00007.4

Lin, Z. Y., Chen, Q., Deng, L. J., Li, X., He, P., Liao, G. T., et al. (2021). Evaluation of morphological and phytochemical characteristics of Mesona chinensis populations in southern China. *Plant Prod. Sci.* 41, 374–387. doi:10.1080/1343943x.2020.1847667

Lin, Z. Y., Chen, Q., Deng, L. J., Li, X., He, P., and Xiong, Y. (2019). Response of suitable distribution of citrus in Sichuan Province to climate change. *Chin. J. Eco-Agriculture* 27, 845–859. doi:10.13930/j.cnki.cjea.180983

Lin, Z. Y., Deng, L. J., Chen, Q., Chen, C. Y., Liu, Y. L., and Chen, Z. (2020). Analysis on change of citrus production patterns and driving factors in sichuan province. *Southwest China J. Agric. Sci.* 33, 2591–2604. doi:10.16213/j.cnki.scjas.2020.11.027

Liu, J. Y., and Buhe, A. (2000). Study on spatial-temporal feature of modern land-use change in China: Using remote sensing techniques. *Quat. Sci.* 20, 229–239. doi:10.3321/j.issn:1001-7410.2000.03.003

Liu, Y. S., and Chen, B. M. (2002). The study framework of land use/cover change based on sustainable development in China. *Geogr. Research* 21, 324–330. doi:10.11821/yj2002030007

Lu, N., Jing, Y., Lloyd, H., and Sun, Y.-H. (2012). Assessing the distributions and potential risks from climate change for the sichuan jay (perisorelis internigrans). *Condor* 114 (2), 365–376. doi:10.1525/cond.2012.110030

Ma, B., and Sun, J. (2018). Predicting the distribution of stipa purpurea across the Tibetan plateau via the MaxEnt model. *BMC Ecol.* 18, 10. doi:10.1186/s12898-018-0165-0

Mamanis, G., Vrahnakis, M., Chouvardas, D., Nasiakou, S., and Kleftoyanni, V. (2021). Land use demands for the CLUE-S spatiotemporal model in an agroforestry perspective. *Land* 10 (10), 1097. doi:10.3390/land10101097

Merow, C., Smith, M. J., and Silander, J. A., Jr (2013). A practical guide to MaxEnt for modeling species' distributions: What it does, and why inputs and settings matter. *Ecography* 36 (10), 1058–1069. doi:10.1111/j.1600-0587.2013.07872.x

Mokarram, M., and Mirsoleimani, A. (2018). Using Fuzzy-AHP and order weight average (OWA) methods for land suitability determination for citrus cultivation in ArcGIS (Case study: Fars province, Iran). *Phys. A Stat. Mech. its Appl.* 508, 506–518. doi:10.1016/j.physa.2018.05.062

Neamatollahi, E., Bannayan, M., Jahansuz, M. R., Struik, P., and Farid, A. (2012). Agro-ecological zoning for wheat (Triticum aestivum), sugar beet (Beta vulgaris) and corn (Zea mays) on the Mashhad plain, Khorasan Razavi province. *Egypt. J. Remote Sens. Space Sci.* 15 (1), 99–112. doi:10.1016/j.ejrs.2012.05.002

Nyairo, R., and Machimura, T. (2022). Potential effects of climate and human influence changes on range and diversity of nine fabaceae species and implications for nature's contribution to people in Kenya. *Climate* 8 (10), 109. doi:10.3390/cli8100109

Phillips, S. J., Anderson, R. P., and Schapire, R. E. (2006). Maximum entropy modeling of species geographic distributions. *Ecol. Model.* 190 (3-4), 231–259. doi:10.1016/j.ecolmodel.2005.03.026

Phillips, S. J., Dudik, M., Elith, J., Graham, C. H., Lehmann, A., and Leathwick, J. (2009). Sample selection bias and presence-only distribution models: Implications for background and pseudo-absence data. *Ecol. Appl.* 19, 181–197. doi:10.1890/07-2153.1

Qin, A., Liu, B., Guo, Q., Bussmann, R. W., Ma, F., and Jian, Z., (2017). Maxent modeling for predicting impacts of climate change on the potential distribution of Thuja sutchuenensis Franch., an extremely endangered conifer from southwestern China. *Glob. Ecol. And Conservation* 10, 139–146. doi:10.1016/j.gecco.2017.02.004

Radosavljevic, A., and Anderson, R. P. (2014). Making better MAXENT models of species distributions: Complexity, overfitting and evaluation. *J. Biogeogr.* 41 (4), 629–643. doi:10.1111/jbi.12227

Ramankutty, N., Evan, A. T., Monfreda, C., and Foley, J. A. (2008). Farming the planet: 1. Geographic distribution of global agricultural lands in the year 2000. *Glob. Biogeochem. Cycles* 22 (1), B1003. doi:10.1029/2007gb002952

Rural social and Economic Investigation Department of National Bureau of Statistics (2021). *China rural statistical yearbook.* Beijing, China: China Statistics Press.

Rurinda, J., Zingore, S., Jibrin, J. M., Balemi, T., Masuki, K., and Andersson, J. A., (2020). Science-based decision support for formulating crop fertilizer recommendations in sub-Saharan Africa. *Agric. Syst.* 180, 102790. doi:10.1016/j.agsy.2020.102790

Shcheglovitova, M., and Anderson, R. P. (2013). Estimating optimal complexity for ecological niche models: A jackknife approach for species with small sample sizes. *Ecol. Model.* 269, 9–17. doi:10.1016/j.ecolmodel.2013.08.011

Stockwell, D., and Peters, D. (1999). The GARP modelling system: Problems and solutions to automated spatial prediction. *Int. J. Geogr. Inf. Sci.* 13 (2), 143–158. doi:10.1080/136588199241391

Su, T. T., Zhou, X. B., Xu, M. C., Wu, T. H., Gao, A. X., and Shi, X. J. (2017). Study on nutrient status of citrus orchard soil in chongqing. *Soils* 49, 897–902. doi:10.13758/j.cnki.tr.2017.05.007

Swets, J. A. (1988). Measuring the accuracy of diagnostic systems. *Science* 240 (4857), 1285–1293. doi:10.1126/science.3287615

Syfert, M. M., Smith, M. J., and Coomes, D. A. (2013). The effects of sampling bias and model complexity on the predictive performance of MaxEnt species distribution models. *Plos One* 8 (2), e55158. doi:10.1371/journal.pone.0055158

Tan, J., Li, A., Lei, G., and Xie, X. (2019). A SD-MaxEnt-CA model for simulating the landscape dynamic of natural ecosystem by considering socio-economic and natural impacts. *Ecol. Model.* 410, 108783. doi:10.1016/j.ecolmodel.2019.108783

Tang, H. J., Wu, W. B., Yang, P., Zhou, Q. B., and Chen, Z. X. (2010). Recent progresses in monitoring crop spatial patterns by using remote sensing technologies. *Sci. Agric. Sin.* 43, 2879–2888. doi:10.3864/j.issn.0578-1752.2020.14.006

Tang, H. J., Wu, W. B., Yu, Q. Y., Xia, T., Yang, P., and Li, Z. G. (2015). Key research priorities for agricultural land system studies. *Sci. Agric. Sin.* 48, 900–910. doi:10.3864/j.issn.0578-1752.2015.05.08

Tercana, E., and Dereli, M. A. (2020). Development of a land suitability model for citrus cultivation using GIS and multi-criteria assessment techniques in Antalya province of Turkey. *Ecol. Indic.* 117, 106549. doi:10.1016/j.ecolind.2020.106549

Veloz, S. D. (2009). Spatially autocorrelated sampling falsely inflates measures of accuracy for presence-only niche models. *J. Biogeogr.* 36 (12), 2290–2299. doi:10.1111/j.1365-2699.2009.02174.x

Verburg, P., Soepboer, W., Veldkamp, A., Limpiada, R., Espaldon, V., and Mastura, S. S. A. (2002). Modeling the spatial dynamics of regional land use: The CLUE-S model. *Environ. Manag.* 30 (3), 391–405. doi:10.1007/s00267-002-2630-x

Volk, M., and Ewert, F. (2011). Scaling methods in integrated assessment of agricultural systems—state-of-the-art and future directions. *Agric. Ecosyst. Environ.* 142 (1/2), 1–5. doi:10.1016/j.agee.2010.10.014

Wang, L. K., and Qi, C. J. (2018). Research on the compa rative advantage and its influencing factors of in Chinese citrus main producing region —empirical analysis based on interprovincial panel data. *Chin. J. Agric. Resour. Regional Plan.* 39, 121–128. doi:10.7621/cjarrp.1005-9121.20181117

Wang, Q., Fan, B. G., and Zhao, G. H. (2020). Prediction of potential distribution area of Corylus mandshurica in China under climate change. *Chin. J. Ecol.* 39, 3774–3784. doi:10.13292/j.1000-4890.202011.014

Wang, Q., Li, S. q., He, G., Li, R. r., and Wang, X. f. (2018). Evaluating sustainability of water-energy-food (wef) nexus using an improved matter-element extension model: A case study of China. *J. Clean. Prod.* 202, 1097–1106. doi:10.1016/j.jclepro.2018.08.213

Warren, D. L., and Seifert, S. N. (2011). Ecological niche modeling in maxent: The importance of model complexity and the performance of model selection criteria. *Ecol. Appl.* 21 (2), 335–342. doi:10.1890/10-1171.1

Wisz, M. S., Hijmans, R. J., Li, J., Peterson, A. T., Graham, C. H., and Guisan, A. (2008). Effects of sample size on the performance of species distribution models. *Divers. Distrib.* 14, 763–773. doi:10.1111/j.1472-4642.2008.00482.x

Wotlolan, D. L., Lowry, J. H., Wales, N. A., and Glencross, K. (2021). Land suitability evaluation for multiple crop agroforestry planning using GIS and multi-

criteria decision analysis: A case study in Fiji. *Agrofor. Syst.* 95 (8), 1519–1532. doi:10.1007/s10457-021-00661-3

Xian, Y. y., Liu, G. l., and Zhong, L. m. (2022). Will citrus geographical indications face different climate change challenges in China? *J. Clean. Prod.* 356, 131885. doi:10.1016/j.jclepro.2022.131885

Xiang, Y., Qi, C. J., and Lu, Q. (2014). The comparative advantage and its influencing factors of citrus production in hubei province. *Econ. Geogr.* 34, 134–139. doi:10.15957/j.cnki.jjdl.2014.11.021

Yackulic, C. B., Chandler, R., Zipkin, E. F., Royle, J. A., Nichols, J. D., and Grant, E. H. C., (2013). Presence-only modelling using MAXENT: When can we trust the inferences? *Methods Ecol. Evol.* 4 (3), 236–243. doi:10.1111/2041-210x.12004

Yan, H. y., He, J., Xu, X. c., Yao, X. y., Wang, G. y., and Tang, L. g., (2021). Prediction of potentially suitable distributions of codonopsis pilosula in China based on an optimized MaxEnt model. *Front. Ecol. Evol.* 9, 773396. doi:10.3389/fevo.2021.773396

Yang, S. l., Wang, H. m., Tong, J. p., Bai, Y., Alatalo, J. M., and Liu, G., (2022). Impacts of environment and human activity on grid-scale land cropping suitability and optimization of planting structure, measured based on the MaxEnt model. *Sci. Total Environ.* 836, 155356. doi:10.1016/j.scitotenv.2022.155356

Yang, X. Q., Kushwaha, S. P. S., Saran, S., Xu, J., and Roy, P. S. (2013). Maxent modeling for predicting the potential distribution of medicinal plant, Justicia adhatoda L. in Lesser Himalayan foothills. *Ecol. Eng.* 51, 83–87. doi:10.1016/j.ecoleng.2012.12.004

Yi, Y. j., Cheng, X., Yang, Z. F., and Zhang, S. H. (2016). Maxent modeling for predicting the potential distribution of endangered medicinal plant (*H. riparia* Lour) in Yunnan, China. *Ecol. Eng.* 92 (7), 260–269. doi:10.1016/j.ecoleng.2016.04.010

Yu, X., Tao, X., Liao, J., Liu, S. c., Xu, L., and Yuan, S., (2022). Predicting potential cultivation region and paddy area for ratoon rice production in China using Maxent model. *Field Crops Research* 275 (1), 108372. doi:10.1016/j.fcr.2021.108372

Zabihi, H., Ahmad, A., Vogeler, I., Said, M. N., Golmohammadi, M., and Golein, B. (2015). Land suitability procedure for sustainable citrus planning using the application of the analytical network process approach and GIS. *Comput. Electron. Agric.* 117, 114–126. doi:10.1016/j.compag.2015.07.014

Zhang, C., Wang, P., Xiong, P., Li, C., and Quan, B. (2021). Spatial pattern simulation of land use based on flus model under ecological protection: A case study of hengyang city. *Sustainability* 13 (8), 10458. doi:10.3390/su131810458

Zhang, Y., Dong, S. k., Gao, Q. z., Liu, S. l., Zhou, H. k., and Ganjurjav, H. (2016). Climate change and human activities altered the diversity and composition of soil microbial community in alpine grasslands of the Qinghai-Tibetan Plateau. *Sci. Total Environ.* 562, 353–363. doi:10.1016/j.scitotenv.2016.03.221

Zhang, Y. W., and Zhang, S. Y. (2016). Study on citrus production's spatial distribution, changes and influencing factors in central delta area. *Research Agric. Mod.* 37, 687–693. doi:10.13872/j.1000-0275.2016.0068

# Frontiers in Environmental Science

Explores the anthropogenic impact on our natural world

An innovative journal that advances knowledge of the natural world and its intersections with human society. It supports the formulation of policies that lead to a more inhabitable and sustainable world.

## Discover the latest Research Topics

See more →

**Frontiers**

Avenue du Tribunal-Fédéral 34
1005 Lausanne, Switzerland
frontiersin.org

**Contact us**

+41 (0)21 510 17 00
frontiersin.org/about/contact



🔹 frontiers

Frontiers in
Environmental Science

🔹 frontiers | Research Topics